Titre: Title:	Experimental measurement, mathematical description, and machine learning prediction of the mechanical properties of waste rocks for mine haul roads
Auteur: Author:	Shengpeng Hao
Date:	2021
Type:	Mémoire ou thèse / Dissertation or Thesis
Référence: Citation:	Hao, S. (2021). Experimental measurement, mathematical description, and machine learning prediction of the mechanical properties of waste rocks for mine haul roads [Thèse de doctorat, Polytechnique Montréal]. PolyPublie. https://publications.polymtl.ca/9479/

POLYTECHNIQUE MONTRÉAL

affiliée à l'Université de Montréal

Experimental measurement, mathematical description, and machine learning prediction of the mechanical properties of waste rocks for mine haul roads

SHENGPENG HAO

Département de génie civil, géologique et des mines

Thèse présentée en vue de l'obtention du diplôme de *Philosophiæ Doctor*

Génie minéral

November 2021

POLYTECHNIQUE MONTRÉAL

affiliée à l'Université de Montréal

Cette thèse intitulée:

Experimental measurement, mathematical description, and machine learning prediction of the mechanical properties of waste rocks for mine haul roads

présentée par **Shengpeng HAO**

en vue de l'obtention du diplôme de *Philosophiæ Doctor*

a été dûment acceptée par le jury d'examen constitué de :

Pooneh MAGHOUL, président or présidente

Thomas PABST, membre et directeur or directrice de recherche

Benoît COURCELLES, membre

Biao LI, membre externe

DEDICATION

Learning without thought is labour lost; thought without learning is perilous.

学而不思则罔，思而不学则殆。

- *Confucius* 孔子 (551-479 BCE)

ACKNOWLEDGEMENTS

I am deeply grateful to my supervisor Professor Thomas Pabst for his constant support, valuable guidance, and inspiration during this research. I am fortunate to have had the opportunity of learning from him during my studies at Polytechnique Montreal. I greatly appreciate his advice, encouragement, and guidance which made possible the completion of this dissertation.

I would like to thank Professor Li Li and Mamert Mbonimpa for their time and evaluation of the pre-doctoral report during the Comprehensive Examination. Many thanks also to Professor Poonech Maghoul, Benoît Courcelles, and Biao Li for being the members of my graduate thesis committee.

It would have been impossible to even come this far without the help from Noura EI-Harrak and Patrick Berneche who are technicians at Mining Laboratory. My special thanks go to Noura who taught me to conducting laboratory tests (e.g., Proctor, GS, and Sieving), and helped me to manage the tested materials and repair the laboratory apparatuses. I am also thankful to Patrick for his help and valuable suggestions for my laboratory work (especially triaxial tests). Also, many thanks go to Samuel Chénier and Eric Turgeon (technicians at Geotechnique Laboratory) for their help and suggestions about CBR tests. I also very much appreciate all my colleagues and friends from the Research Institute on Mines and the Environment (RIME) for their cooperation, help, advice and kindness.

I acknowledge the financial support from Fonds de recherche du Québec-Nature et Technologies (FRQNT) and the industrial partners of RIME UQAT-Polytechnique.

Finally, and the most importantly, I would like to thank my family for their consistent love and support. I am deeply indebted to them for all that they have done for me during my life.

RÉSUMÉ

Les opérations minières peuvent générer de grandes quantités de roches stériles, lesquelles sont souvent entreposées en surface, dans des haldes généralement construites à proximité des sites de production. Cependant, la gestion et la restauration des haldes à stériles peuvent s'avérer complexes en raison notamment de leur grande taille et des risques d'instabilités géochimiques et géotechniques. La valorisation des stériles pour la construction de routes minières peut donc être une alternative intéressante au stockage en surface, tant sur le plan économique qu'environnemental. Le réseau routier sur un site minier est en effet un élément critique et vital du processus de production, et il a un impact direct et significatif sur la productivité et les coûts. Les propriétés mécaniques des stériles sont des paramètres essentiels pour améliorer la conception des routes de transport de la mine, mais les résultats et informations sur les propriétés mécaniques des roches stériles de mines en roches dures sont relativement limitées. De plus, les outils de conception et les méthodes de mesure ont généralement été développés pour des applications civiles, et leur applicabilité aux routes minières (qui sont souvent soumises à une charge de trafic significativement différente de celle des autoroutes) reste incertaine.

L'objectif principal de ce projet était donc d'évaluer les propriétés mécaniques des roches stériles soumises au chargement des camions miniers afin d'améliorer la conception des routes minières. L'applicabilité des normes et des méthodes expérimentales au laboratoire ainsi que des modèles mathématiques aux stériles a été évaluée. L'effet des propriétés de base et des facteurs climatiques sur les propriétés mécaniques des stériles a été quantifié. Des modèles d'apprentissage automatique ont été développés au moyen de différents algorithmes afin de prédire les propriétés mécaniques des stériles.

Un grand nombre d'essai CBR et triaxiaux, de différentes dimensions et sous différents types de contraintes, ont été réalisés dans cette étude. Les niveaux de contrainte proposés dans les normes existantes (p.ex. AASHTO T307 et EN 13286) était significativement plus faibles que les contraintes attendues sur les sites miniers puisque ces normes ont été développées pour le design

des autoroutes. Des conditions expérimentales différentes et des chemins de contraintes plus élevés ont donc été proposés et appliqués dans cette étude afin de représenter les conditions typiques causées par des camions miniers extra-lourds.

Les essais CBR dynamiques ont été proposés comme une alternative efficace aux essais triaxiaux dynamiques afin d'estimer le comportement de déformation résiliente et permanente des stériles. Les résultats ont montré que l'impact de la fréquence de chargement et de la forme d'onde dans les essais CBR dynamique était limité, tandis que le module équivalent mesuré augmentait de manière significative avec la contrainte. L'équation et le modèle développés pour les essais CBR dynamiques se sont avérés fiables pour décrire la rigidité et la déformation permanente des stériles.

Le rapport optimal gravier/sable des stériles broyés se situait entre 1 et 1,5 et a contribué à obtenir un module de résilience et une résistance au cisaillement plus élevés, ainsi qu'une déformation permanente plus faible. Une augmentation de la teneur en fines a, au contraire, entraîné la diminution du module d'élasticité et de la déformation permanente mais aussi une augmentation significative de la résistance au cisaillement. Le rapport gravier/sable optimal des stériles non broyés avec une taille de particule maximale de 60 mm était d'environ 5 et le taux de déformation permanente a augmenté de manière significative lorsque la taille maximale des particules a été réduite à 25 mm. Une augmentation de l'énergie de compactage a entraîné une diminution significative de la déformation permanente des stériles ; les stériles d'une granulométrie maximale de 60 mm, d'un rapport gravier/sable de 5 et d'une teneur en fines de 5 % ont montré une résistance au cisaillement plus élevée.

Les cycles de gel-dégel ont entraîné une réduction du module d'élasticité et de la résistance au cisaillement, et une augmentation de la déformation permanente. Une plus grande teneur en eau pendant les cycles de gel-dégel a également entraîné une augmentation significative de la déformation permanente. Les résultats ont également montré que les cycles mouillage-séchage pouvaient contribuer à augmenter la rigidité, le CBR et la déformation permanente des stériles broyés.

Le modèle M_R-θ et le modèle MEPDG sont apparus fiables pour décrire le comportement du module de résilience des stériles sous différentes conditions de contraintes. Le modèle de Rahman et Erlingsson (étendu à l'aide d'une approche d'écrouissage) était bien adapté pour décrire l'accumulation de déformation permanente avec le nombre de cycles de chargement causés par la succession de nombreux chemins de contraintes. Des modèles de prédiction des coefficients k_1, k_2, a et b, exprimés en fonction des propriétés physiques de base et des facteurs climatiques, ont également été proposés afin de prédire le module de résilience et la déformation permanente des stériles. Les modèles proposés pourraient être utilisés pour prédire les propriétés mécaniques des stériles sur le terrain, mais devraient être améliorés en utilisant davantage de résultats d'essais et ainsi étendre leur capacité de généralisation.

Différents algorithmes d'apprentissage automatique, y compris la régression linéaire multiple (MLR), la machine à vecteurs de support (SVM), les k plus proches voisins (KNN), l'arbre de décision (DT), la forêt aléatoire (RF), le réseau de neurones à rétropropagation (BPNN) et la neuroévolution des topologies d'augmentation (NEAT) ont été utilisées pour développer des modèles de prédiction du CBR, du module de résilience et de la déformation permanente des stériles broyés à partir des propriétés de base des matériaux. Huit propriétés (densité sèche, énergie de compactage, teneur en fines, taille maximale des particules, C_C, C_U, D_{10} et D_{60}) ont été sélectionnées comme variables d'entrée pour les modèles CBR, et le nombre de cycles de chargement, la pression de confinement et la contrainte de déviation ont été ajoutés comme variables d'entrée supplémentaires pour les modèles de module de résilience et de déformation permanente. L'architecture optimale des modèles d'apprentissage automatique a été déterminée par l'étude des hyperparamètres. Une étude comparative a montré que les modèles DT, RF et BPNN permettaient d'obtenir de meilleurs résultats pour le CBR, le module de résilience et la déformation permanente, respectivement.

Les résultats présentés dans cette thèse devraient contribuer à donner aux exploitants miniers des indications générales pour sélectionner et préparer les stériles à utiliser dans la construction de

routes minières. Les recommandations proposées pourraient améliorer les performances à court et à long terme des routes minières et réduire les besoins d'entretien, et ainsi diminuer la consommation de carburant, améliorer la durée de vie des composants des véhicules (en particulier les pneus), augmenter la productivité et réduire les coûts d'exploitation.

ABSTRACT

Mining operations can generate large amounts of waste rocks, which are often stored on the surface, in piles, close to production sites. However, the management and reclamation of waste rock piles can be challenging because of their large size and the risks for geochemical and geotechnical instabilities. The valorization of waste rocks for the construction of mine haul roads is an attractive alternative to surface disposal, both economically and environmentally. The mine haul road network is, indeed, a critical and vital component of the production process, which directly and significantly impacts mine productivity and costs. Waste rock mechanical properties are critical parameters to improve mine haul roads design, but the relevant research on the mechanical properties of waste rocks from hard rock mine are relatively limited. Also, design tools and measurement methods were usually developed for civil applications, and their applicability to mine haul roads (which are subjected to significantly different traffic loading compared to highways) remains uncertain.

The main objective of this project was therefore to evaluate the mechanical properties of waste rocks under mining truck loading to improve the design of mine haul roads. The applicability of laboratory test standards and methods, and of mathematical regression models to waste rocks was assessed. The effect of basic properties and climatic factors on the mechanical properties was quantified. Machine learning models for predicting the mechanical properties of waste rocks were also developed using different algorithms.

A large number of CBR and triaxial tests, of various dimensions and with different load types, were carried out in this study. The stress levels proposed in the existing laboratory tests standards (e.g., AASHTO T307 and EN 13286) were significantly lower than the stress state within mine haul roads since these standards were initially developed for the highway design. High stress levels were therefore proposed and applied in this study to represent the typical stress conditions caused by extra heavy mining trucks.

Repeated load CBR tests appeared to be an effective alternative to repeated load triaxial tests to estimate resilient and permanent deformation behavior of waste rocks. Results showed that the impact of loading frequency and waveform in repeated load CBR tests was limited, while the measured equivalent modulus increased significantly with contact stress. The developed equation and model for repeated load CBR tests were reliable to describe the stiffness and permanent deformation of waste rocks, respectively.

The optimum gravel-to-sand ratio of crushed waste rocks was between 1 and 1.5 and contributed to provide higher resilient modulus and shear strength, and lower permanent strain. An increase in fines content could, to the contrary, result in the decrease of resilient modulus and permanent strain but also to significant increase of shear strength. The optimum gravel-to-sand ratio of uncrushed waste rocks with 60 mm of maximum particle size was around 5 and the permanent strain rate increased significantly when the maximum particle size was decreased to 25 mm. An increasing of compaction effort resulted in a significant decrease in permanent strain of waste rocks; waste rocks with 60 mm of maximum particle size, a gravel-to-sand ratio of 5, and 5% of fines showed higher shear strength.

Freeze-thaw cycles resulted in a reduction of the resilient modulus and shear strength, and an increase of the permanent deformation. A greater water content during freeze-thaw cycles also resulted in a significant increase of the permanent deformation. Results also showed that wetting-drying cycles could contribute to increase the stiffness, CBR, and permanent deformation of crushed waste rocks.

M_R-θ model and MEPDG model appeared reliable to describe the resilient modulus behavior of waste rocks under different stress conditions. Rahman and Erlingsson model (extended using time hardening approach) was well adapted to fit the accumulation of permanent strain with number of loading cycles caused by numerous stress paths. Coefficient prediction models (k_1, k_2, a, and b), expressed as a function of basic physical properties and climatic factors, were also developed to predict the resilient modulus and permanent strain of waste rocks. The proposed models could be

used to predict the mechanical properties of waste rocks in the field, but would need to be improved using more test results to extend their generalization capacity.

Different machine learning algorithms, including multiple linear regression (MLR), support vector machine (SVM), k-nearest neighbors (KNN), decision tree (DT), random forest (RF), backpropagation neural network (BPNN), and neuroevolution of augmenting topologies (NEAT), were therefore used to develop prediction models for CBR, resilient modulus, and permanent deformation of crushed waste rocks based on experimental data. Eight properties (dry density, compaction energy, fines content, maximum particle size, C_C, C_U, D_{10}, and D_{60}) were selected as input variables for CBR models, and number of loading cycles, confining pressure, and deviator stress were chosen as the input variables for the resilient modulus and permanent deformation models. The optimum architecture of machine learning models was determined through hyperparameters study. A comparison study showed that the DT, RF, and BPNN models provided better results for CBR, resilient modulus, and permanent deformation, respectively.

The results presented in this thesis should contribute to give mine operators general indications to select and prepare waste rocks to be used in haul road construction. The proposed recommendations could improve the short and long-term performance of haul roads and reduce the need for maintenance, and therefore decrease fuel consumption, improve vehicle component lifetime (especially tires), increase productivity and reduce operation costs.

TABLE OF CONTENTS

LIST OF TABLES

LIST OF FIGURES

LIST OF SYMBOLS AND ABBREVIATIONS

Symbols

a	Rahman and Erlingsson model parameter (-)
b	Rahman and Erlingsson model parameter (-)
BR	binder ratio (-)
c'	effective cohesion (kPa)
CBR	California Bearing Ratio (%)
C_C	coefficient of curvature (-)
C_U	coefficient of uniformity (-)
D_{10}	size at which 10% of particles pass the sieve (mm)
D_{30}	size at which 30% of particles pass the sieve (mm)
D_{60}	size at which 60% of particles pass the sieve (mm)
D_{max}	maximum particle size (mm)
DR	dust ratio (-)
e	super-elevation applied (m/m width of road)
$E_{equ.}$	equivalent modulus (kPa)
f	saturation factor (-)
FC	fines content (%)
G	gravel percentage (%)
GS	gravel-to-sand ratio (-)
G_s	specific gravity (-)

h	specimen height (mm)
h_m	matric suction (m)
k_1	regression coefficient (-)
k_2	regression coefficient (-)
k_3	regression coefficient (-)
k_4	regression coefficient (-)
LL	liquid limit (%)
L_δ	Huber loss (-)
m	slope of the Mohr-Coulomb failure line (-)
MDD	maximum dry density (kg/m^3)
M_R	resilient modulus (MPa)
N	number of loading cycles (-)
N_i^{eq}	equivalent loading cycles (-)
$N_{i\text{-}1}$	total number of loading cycles at the end of (i-1)th stress path (-)
P2	percentage of material passing 2.0 mm sieve (%)
P475	percentage of material passing the 4.75 sieve (%)
p_a	the reference stress/atmospheric pressure (100 kPa)
PI	plasticity index (%)
PL	plasticity limit (%)
p_{max}	the maximum applied hydrostatic stress (kPa)
q_{max}	the maximum applied deviator stress (kPa)

q_u	unconfined compression strength (kPa)
R	minimum curve radius (m)
R^2	coefficient of determination (-)
s	the intercept of the Mohr-Coulomb failure line (-)
S	sand percentage (%)
SM_R	summary resilient modulus (MPa)
S_r	degree of saturation (%)
U_{min}	coefficient of lateral friction supply
V	vehicle speed (km/h)
α	Rahman and Erlingsson model parameter (-)
γ_{dmax}	maximum dry unit weight (-)
ε_p	permanent strain (-)
ε_p^{3000}	the accumulated permanent strain measured at the 3000th loading cycles (-)
ε_p^{5000}	the accumulated permanent strain measured at the 5000th loading cycles (-)
ε_r	recoverable axial strain (-)
θ	bulk stress (kPa)
θ_w	volumetric water content (%)
ρ_d	dry density (kg/m^3)
σ_1	major principal stress (kPa)
σ_{1f}	major principal stress at failure (kPa)
σ_{1max}	the peak axial stress (kPa)

σ_3	minor principal stress (kPa)
σ_c	confining pressure (kPa)
σ_d	deviator stress (kPa)
σ_H	horizontal (or lateral) stresses applied on the specimen (kPa)
σ_p	plunger stress (kPa)
σ_V	vertical stresses applied on the specimen (kPa)
u	vertical elastic deformation of materials under plunger (mm)
τ	shear strength (kPa)
τ_{oct}	octahedral shear stress (kPa)
v	Poisson's ratio of tested material (-)
v_0	vehicle speed (m/s)
ϕ	specimen diameter (mm)
ϕ'	the effective stress angle of internal friction (°)
Ψ	shape parameter (-)
w	gravimetric water content (%)
w_0	initial gravimetric water content (%)
w_f	final gravimetric water content (%)
w_{opt}	optimum water content (%)

Abbreviations

AASHTO	American Association of State Highway and Transportation Officials

ANFIS	adaptive neuro-fuzzy inference system
ANN	artificial neural network
AMD	acid mine drainage
BPNN	backpropagation neural network
CCBE	covers with capillary barrier effects
CND	contaminated neutral drainage
CWR	crushed waste rocks
DCP	dynamic cone penetrometer
DM	days between last maintenance and minimum cycle defect
DSMIN	minimum defect score in maintenance cycle
DT	decision tree
ESWL	equivalent single wheel load
EWT	elevated water table
FCF	fuel consumption for favorable grades
FCU	fuel consumption for unfavourable grades
FOS	factor of safety
FWD	falling weight deflectometer
GEP	gene expression programming
GA	genetic algorithm
GC	grading coefficient
GR	road grade

GVW	gross vehicle mass
HSL	high stress level
HSLM	high stress level for mining engineering
KNN	k-nearest neighbors
LFWD	light falling weight deflectometer
LSCT	linear strain conversion transducer
LSL	low stress level
LSSVM	least square support vector machine
LVDT	linear variable differential transformer
MAE	mean absolute error
MAS	maximum axial stress
MEPDG	Mechanistic-Empirical Pavement Design Guide
ML	maintenance labour costs
MLR	multiple linear regression
MOD	modified compaction effort
MOD 81	compaction effort with 81 blows per layer
MSE	mean squared error
NEAT	neuroevolution of augmenting topologies
PFWD	portable falling weight deflectometer
PSD	particle size distribution
RF	random forest

RMSE	root mean squared error
RT-MMS	real-time maintenance management system
RR	rolling resistance
SP	shrinkage product
SR	store-and-release covers
STD	standard compaction effort
SVM	support vector machine
SVR	support vector regression
TW	truck tyre wear
USBM	United States Bureau of Mines
USCS	Unified Soil Classification
UVW	unladen vehicle mass
VOC	vehicle operating cost
WRI	waste rock inclusion
XRD	X-ray diffraction

LIST OF APPENDICES

CHAPTER 1 INTRODUCTION

1.1 Description of the problem

Mining operations generate large amounts of waste rocks, low grade ore materials which are often stored on the surface, in piles, close to production sites. Waste rock piles are typically large structures which can exceed 300 m in height, and can cover more than 500 million m^2 in area (McCarter 1990). Waste rock piles generally show important segregation and hydrogeological and geochemical properties can be significantly heterogeneous because of spatial variability of mineralogy, particle size and porosity (Fala et al. 2012; Amos et al. 2015). Geotechnical and geochemical risks associated with waste rock piles management represent a great challenge for mining compagnies, with potentially huge impact on life, property, health, and environment (Sheets and Bates 2008; Adamczyk 2016).

The valorization (i.e., the reuse) of waste rocks for the construction of mine haul roads is an attractive alternative to surface disposal, both economically and environmentally. The mine haul road network is, indeed, a critical and vital component of the production process, which directly and significantly impacts mine productivity and costs (Thompson et al. 2019). The length of haul roads can be 10 to 40 km on some surface mine sites and therefore require a lot of materials for their construction (Thompson and Visser 2003). The poor performance of mine haul roads can result in the increase of road maintenance and vehicle operating costs. The materials used for construction have a significant influence on the performance of haul roads, but finding appropriate materials can sometimes be difficult (Thompson et al. 2019), and borrowing the required materials in the vicinity of the mine can also have significant environmental impacts. Waste rocks are an interesting alternative to natural materials and their mechanical properties usually make them quite suitable for such applications. In practice, waste rocks have been used for haul roads construction in many years and on many mine sites (Tannant and Regensburg 2001). However, waste rocks are, as mentioned previously, highly heterogeneous and variable, and must therefore be carefully

selected to ensure a good performance of the road and minimize costs. For example, waste rocks used for wearing course should not contain to many fines to reduce dust generation, but should also contain enough fines to maintain adequate binding characteristic (Thompson and Visser 2007). Selection and/or preparation of waste rocks for haul road construction consist therefore in defining optimal properties to answer various and sometimes opposing objectives.

Mine haul roads are typical low-volume and short-service-life roads, and the empirical design method is therefore often used in the field (Tannant and Regensburg 2001; Thompson et al. 2019). California Bearing Ratio (CBR) design method is one of the commonly used methods in practice. However, this method cannot guarantee the adequate road performance since it cannot account for influence factors such as climatic effects and traffic information during the haul road design. Mechanistic design for haul roads is therefore also needed to ensure the road performance. In the mechanistic design procedure, the mechanical properties, such as shear strength, resilient modulus, and permanent deformation, are generally used to compute pavement response under traffic loading. However, experimental studies on the mechanical properties of waste rocks are scarce. The laboratory equipment for the measurement of waste rock properties is very specific (and therefore often rare) because of the wide range of particle sizes. Coarse-grained waste rocks require specialized laboratory equipment since the corresponding sample and apparatus size should increase significantly. However, the usual laboratory apparatus is generally designed for fine-grained materials such as sands and clays. Also, the testing of the mechanical properties is usually complex and costly. Repeated load triaxial tests are usually used to evaluate the resilient modulus and permanent deformation of pavement materials, but these tests usually consist of numerous stress paths and more than ten thousand loading cycles, and are therefore very time-consuming. Also, the preparation of triaxial specimens is generally complex especially for loose and angular waste rocks. From an engineering perspective, predictive models would therefore be very useful to evaluate the resilient modulus and permanent deformation behavior of waste rocks. Some mathematical models were proposed to describe the mechanical behavior of pavement materials

under traffic loading (Lekarp et al. 2000b, 2000a). However, the applicability of the existing models to waste rocks from hard rock mines need be assessed. Different techniques such as machine learning therefore can be used to develop prediction models for waste rocks.

Moreover, the existing approaches and standards for laboratory tests were initially developed for fine-grained soils and aimed at civil engineering applications (such as highways), and they may therefore not be applicable to waste rocks and mine haul roads because of the entirely different particle size and traffic loading imposed by extreme heavy mining trucks. For example, AASHTO T307 standard (2017) procedures was developed for evaluating resilient modulus of pavement soils. As a consequence, the stress level applied in AASHTO T307 is significantly lower than that observed in haul roads due to extra heavy mining trucks (with payload capacity regularly increasing and around 450 mt these days) (Thompson et al. 2019). The applicability of available testing standards to mine haul roads is therefore uncertain, and should therefore be verified, and, if necessary, adapted.

Several physical factors (e.g., density, gradation, water content, material type, and particle shape) can influence the mechanical properties of waste rocks (Lekarp et al. 2000a, 2000b). The effect of physical factors on mechanical properties can change with the type of materials (Brown and Selig 1991; Kolisoja 1997; Lekarp et al. 2000a, 2000b) and can therefore not be directly extrapolated from other studies on different materials. The effect of physical factors of waste rocks therefore should be specifically quantified. In addition to physical properties, environmental factors such as freeze-thaw and wetting-drying cycles can also affect the mechanical properties of pavement materials (Gullà et al. 2006; Ling et al. 2015). However, most of the relevant studies focus on fine-grained materials or subgrade materials for highways. Many Canadian mines being located in cold climates, the impact of environmental factors on the mechanical properties of waste rocks should be studied to improve the design of mine haul roads. This has become even more critical following climate change and the lengthening of mine life span which often exceed several decades these days.

1.2 Research question

How do the physical properties and climatic conditions affect waste rocks mechanical properties and can influence the efficiency and durability of haul roads? This question was addressed considering that the mechanical properties of waste rocks can be influenced by the physical properties (e.g., gradation, compaction, and water content) and climate factors (freeze-thaw and wetting-drying cycles).

1.3 Research objectives

The main objective of this research was to investigate the mechanical properties, and establish guidelines to optimize the selection of waste rocks to improve the performance of haul roads. Specific objectives of this project research included:

1. Assess the applicability of the existing laboratory test approaches or standards developed for civil engineering to waste rocks and mine haul roads.
2. Evaluate the suitability of repeated load CBR test as an alternative to repeated load triaxial test for estimating the stiffness and permanent deformation of waste rocks.
3. Assess the effect of gravel-to-sand ratio and fines content on the mechanical properties of waste rocks, and propose the optimum gradation for haul roads.
4. Assess the effect of maximum particle size, compaction effort, and water content on the mechanical properties of waste rocks.
5. Assess the impact of freeze-thaw and wetting-drying cycles on the variation of waste rocks mechanical behavior with time.

6. Evaluate the applicability of existing models for fitting resilient modulus and permanent deformation of waste rocks.
7. Develop prediction models for the mechanical properties of waste rocks using machine learning.

Note: This project focused on non-acid generating waste rocks from hard rock mines only. Waste rocks produced by coal mines have completely different properties and cannot be related to the material tested in this research. Also, sulfide bearing and potentially acid generating waste rocks should not be used in haul road because they would be directly exposed to atmospheric conditions and oxidation.

1.4 Thesis outline

Chapter 2 presents a detailed literature review of waste rocks management and valorization, design of mine haul roads, and waste rocks mechanical properties. Chapter 3 describes the tested materials and laboratory methodology used in this research. The applicability of existing standard protocol of repeated load triaxial test to waste rocks in mine haul roads was assessed, and repeated load CBR test was also evaluated to estimate the stiffness and permanent deformation behavior of waste rocks in Chapter 4 and 5. Chapter 6 discusses the effect of gravel-to-sand ratio and fines content on the resilient modulus, shear strength, and permanent deformation of crushed waste rocks; the optimum gravel-to-sand ratio and fines content was also proposed to optimize the gradation of crushed waste rocks used in mine haul roads. More laboratory tests were carried out to study the effect of the physical factors (including maximum particle size, gradation, compaction energy, and water content) on the mechanical properties of uncrushed (coarse-grained) waste rocks in Chapter 7. In addition to these physical factors, the effect of environmental factors, i.e., freeze-thaw and wetting-drying cycles, on the mechanical properties (CBR, shear strength, stiffness, and permanent deformation) was also evaluated using repeated load CBR and triaxial tests in Chapter 8. The measured resilient modulus and permanent deformation of waste rocks presented in Chapter 4, 5,

6, 7, and 8 were fitted using existing regression models. Different machine learning algorithms were assessed for predicting CBR, resilient modulus, and permanent deformation of crushed waste rocks, and the optimum prediction models were developed in Chapter 9 and 10. Finally, Chapter 11 and 12 summarize the main results of this research and proposes some recommendations for future work.

1.5 Main contributions and originality of the thesis

The main contribution of this study was to provide a better understanding of the mechanical behaviour of waste rocks under mining traffic loading. The knowledge acquired through this doctoral project will be helpful to maximize the valorization of waste rocks in mine haul roads while improving their performance and durability.

1. High stress levels were proposed for laboratory tests to represent the typical stress state in mine haul roads caused by extreme heavy mining trucks. Repeated load CBR test, as a relatively simple laboratory test, was applied in this project, and the corresponding fitting models were developed to estimate the stiffness and permanent deformation of waste rocks.

2. The effect of physical properties (gradation, compaction, and water content) and climatic factors (freeze-thaw and wetting-drying cycles) on the mechanical properties of waste rocks was quantified in the laboratory, and the measured mechanical behaviour was also described using mathematical models. The experimental results could provide a better understanding on the mechanical characterization of crushed and uncrushed waste rocks and the scale effect in the extrapolation of medium scale laboratory tests. The findings were also beneficial to the selection and preparation of waste rocks for haul road design in the field.

3. The machine learning models were developed for predicting the CBR, resilient modulus, and permanent deformation of waste rocks. The model architectures were determined by evaluating the hyperparameters effect on the model performance.

4. Several machine learning algorithms (i.e., multiple linear regression MLR, k-nearest neighbors KNN, decision tree DT, random forest RF, support vector machine SVM, backpropagation neural network BPNN, and neuroevolution of augmenting topologies NEAT) were applied and compared for predicting the mechanical properties of waste rocks, and the optimum algorithms for CBR, resilient modulus, and permanent deformation were determined.

CHAPTER 2 LITERATURE REVIEW

2.1 Management and valorization of waste rocks

A mine is an excavation in the earth from which profitable ores and minerals are extracted. The ore can be extracted from an open pit mine, or an underground mine. Waste rocks are low grade ore materials, and they are typically produced in large quantities from both underground and open pit mining.

The particle size distribution of waste rocks generally ranges from clay-size to boulders fractions (Figure 2.1(a)), from 0.001 to 1000 mm (Figure 2.1(b)) (Gamache-Rochette 2004; Wickland and Wilson 2005; James et al. 2013; Smith et al. 2013; Amos et al. 2015). Generally, nearly 50% of waste rocks in weight are gravel size (Leps 1970; Williams and Walker 1983). The coefficient of uniformity ($C_U = D_{60}/D_{10}$) of waste rocks is typically greater than 20 (Maknoon 2016). The bulk density of waste rocks measured in the field can vary between 1600 and 2200 kg/m^3, while the specific gravity of waste rock particles can range from 2.6 to 4.8 and more (Maknoon 2016). The saturated hydraulic conductivity of mine waste rocks varies widely because of the variability of particle sizes. The saturated hydraulic conductivity increases with the average particle size of waste rocks, but typically varies between 10^{-2} m/s for igneous/metamorphic rocks and 10^{-5} m/s for clayey basaltic andesite (Morin 1991).

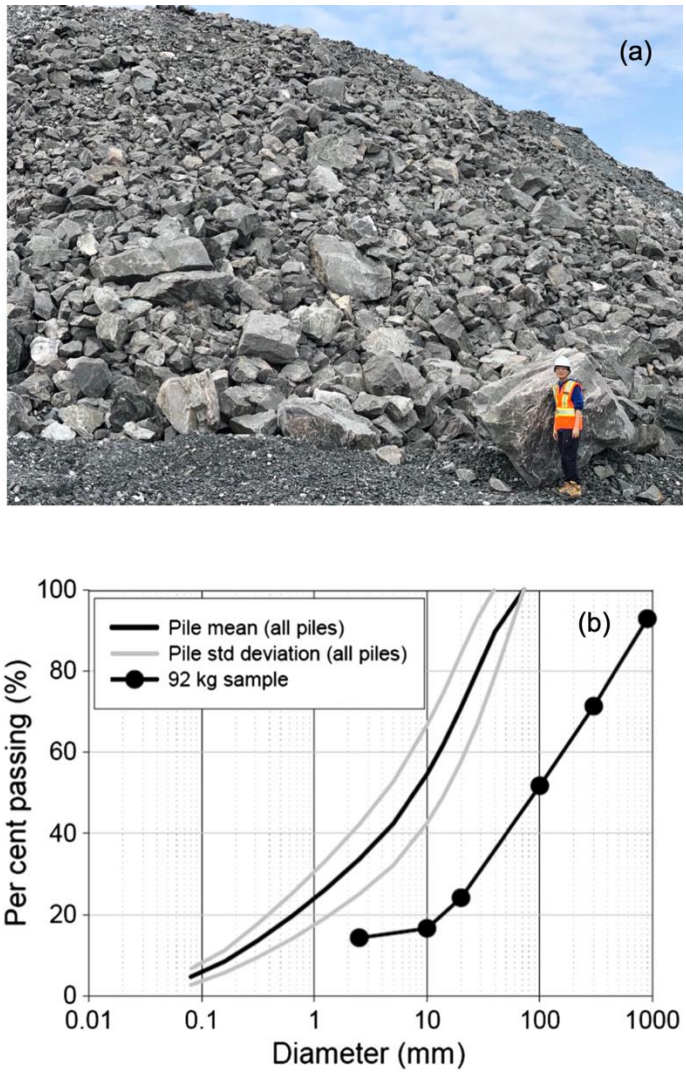

Figure 2.1: Typical particle size of waste rocks; (a) waste rocks at Canadian Malartic Mine, the particle size showed significant heterogeneity with some fine particles (< 2 mm) in the top layers while the particle size at the bottom of the pile can exceed 1.5 m; (b) the mean and standard deviation particle size distributions (< 50 mm) of waste rocks from different piles, and a larger-scale (92 kg) particle size measurement of waste rocks for size fraction < 900 mm at Diavik Diamond Mine in Canada (Smith et al. 2013).

Waste rocks are generally stored on the surface, in piles (or dumps), close to the production sites

(Blowes 1997; Bian et al. 2009; Aubertin 2013). Waste rock piles are usually constructed using end dumping, push dumping, free dumping, and drag line spoiling (McLemore et al. 2009). The selection of disposal technique depends on the site conditions, economic considerations and environmental policy (Blowes 1997; Aubertin 2013). The piles are typically large-scale structures which can exceed 300 m in height and several dozens of hectares in area (McCarter 1990). Generally, waste rock piles show important segregation and hydrogeological and geochemical properties can be significantly heterogeneous because of spatial variability of mineralogy, particle size and porosity, and disposal method (Fala et al. 2012; Amos et al. 2015).

Geotechnical instabilities of waste rock piles, including internal and surface erosion, sliding along the side slopes, and foundations instabilities, are among the main challenges faced by the industry (Aubertin, 2013). Slope failures of waste rocks piles may have a huge impact on life, property, health, and on the environment (Sheets and Bates 2008; Adamczyk 2016). The stability of waste rock piles is a complex problem, which can be affected by many factors such as the properties of waste rocks, the geometry of the piles, the foundation conditions, pore pressures, and climatic conditions (Hustrulid et al. 2001; Blight 2009; McLemore et al. 2009; Poisson et al. 2009; Aubertin 2013). The instability risks during the operation and after mine closure can be minimized by, for example, building the pile using benches with height smaller than 25 m (at least 2 benches), compacting and inclining the surface of each bench (5% slope or more), and maintaining the overall slope of the pile below 26° (Aubertin 2013; Maknoon and Aubertin 2020).

Waste rock piles are also exposed to potential environmental risks as well as geochemical instabilities. Waste rock piles containing reactive minerals (such as sulfides) may generate acid mine drainage (AMD) or contaminated neutral drainage (CND) (Fala et al. 2012; Aubertin 2013; Aubertin et al. 2016). AMD is typically produced from the oxidation of sulfidic minerals, such as pyrite and pyrrhotite in contact with oxygen and water, and is characterized by low pH (Skousen et al. 2017) and high concentrations of dissolved sulphates, iron and metals (Blowes et al. 1994;

Aubertin 2013). CND may also develop from the oxidation of sulfidic minerals, but the pH of the leachate remains close to neutrality while the concentration of sulfate, metals, and metalloids can be high (Aubertin 2013; Amos et al. 2015). The reclamation of waste rock piles is complex because the required lifetime of reclamation can be very long (even indefinite; Vick, 2001), which presents a major environmental risk and financial liability for the mining industry (Wickland and Wilson 2005; Seal II and Shanks III 2008; Amos et al. 2015; Aubertin et al. 2016). Waste rock piles management therefore can be complex, costly, and environmentally hazardous (Aubertin et al. 2016).

Other avenues and techniques were recently developed to improve management and valorization of waste rocks, such as in cover systems (Pabst 2011; Aubertin et al. 2016), waste rock inclusions in tailings impoundments (James and Aubertin 2012), mine backfill (Li et al. 2019), and mine haul roads (Thompson et al. 2019). The valorization of waste rocks for the construction of mining facilities contributes to decrease the amounts of materials that need to be borrowed in the environment, therefore decreasing environmental footprint and promoting circular economy (Wilson et al. 2006; James et al. 2013; Ferdosi et al. 2015a).

2.1.1 Valorization in cover systems

Waste rocks can be used in cover systems, such as covers with capillary barrier effects (CCBE), store-and-release (SR) covers, or single-layer covers coupled with an elevated water table (EWT) (Christensen and O'Kane 2005; Pabst 2011; Aubertin et al. 2016; Gorakhki and Bareither 2017; Kalonji-Kabambi et al. 2020a, 2020b).

CCBE are an efficient approach to control AMD production from mine waste disposal sites (Bussière et al. 2007; Aubertin 2013), especially for relatively humid climates. The objective of the CCBE is to limit oxygen migration by creating capillary barrier effects (Bussière et al. 2003;

Bussière et al. 2007). The capillary barrier phenomenon can appear when a fine-grained material is placed in contact with a coarse-grained material above the water table. Waste rocks can be used for the construction of the coarse-grained layers because it is coarse, relatively permeable, and with a low air entry value (Bussière et al. 2007; Pabst 2011; Kalonji-Kabambi et al. 2017; Kalonji-Kabambi et al. 2020b, 2020a). Recent studies have also shown that reactive waste rock could be used in the bottom capillary break layer (Larochelle et al., 2019).

SR covers can be used to control water percolation to reactive mineral wastes. A homogeneous cover system layer with a well-graded texture and with sufficient storage capacity can be used to retain water during the wet season, and release a significant portion of water to the atmosphere by evaporation and transpiration during dry periods (Christensen and O'Kane 2005; Gorakhki and Bareither 2017). Waste rocks are usually not suitable as a stand-alone SR cover, but compacted waste rocks (with reduced hydraulic conductivity) can be placed on the surface of tailings, at the base of the SR cover system, to form a capillary barrier effect (Christensen and O'Kane 2005). The cost associated with SR covers is typically lower than conventional covers that constructed using low-permeability soils and/or impermeable geomembranes (Albright et al. 2010).

Single layer cover with EWT is an alternative approach to the water cover technique, and aims to maintain tailings saturated to limit oxidation (Dagenais et al. 2006). A cover built with a coarse-grained material favors infiltration and limits water evaporation (Dobchuk et al. 2013; Pabst et al. 2017). Waste rocks could be used as a protection layer to limit evaporation (Dagenais et al. 2006).

2.1.2 Valorization in waste rock inclusions

Mine waste co-disposal consists in disposing simultaneously or in alternate layers waste rocks and tailings in the same surface storage facility. Tailings usually have low permeability and slow consolidation rates, and impoundments can face long term stability issues related to low shear

strength (Wickland and Wilson 2005; Wickland et al. 2006). Co-disposing waste rocks and tailings can improve the hydro-geotechnical properties of the mixture (typically with higher strength and lower hydraulic properties) (Wickland and Wilson 2005; Bussière 2007a). Waste rock inclusions (WRI) are an alternative co-disposal technique to the mixing or layering approaches (L.Bolduc and Aubertin 2014; Saleh-Mbemba et al. 2019). The construction of tailing impoundments with WRI consists in placing waste rocks linear inclusions within the tailings storage facilities and at the base of the impoundment, to act as a drainage layer and columns and to compartmentalize the impoundment into several cells (Bussière 2007a; James et al. 2013; James et al. 2017).

WRI can contribute to improve physical and chemical stability of the tailings, favor their drainage, increase their mechanical strength, facilitate the rehabilitation of the site, reduce AMD generation rate of waste rocks and reduce the volume of waste rocks that need to be stored in piles (Bussière 2007a; James et al. 2013). WRI can also significantly improve the seismic performance and stability of a tailings impoundment because of the higher stiffness and shear strength of waste rocks (James and Aubertin 2012; Ferdosi et al. 2015b, 2015a; James et al. 2017).

2.1.3 Valorization in mine backfill

Underground mining can lead to severe surface subsidence (Gray 1990). Waste rocks are widely used (together with other types of mine wastes) to fill underground stopes (Yang 2016; Sun et al. 2018) and goafs in longwall mining coal mines (Pappas and Mark 1993; Li et al. 2019) to control surface subsidence.

Waste rocks filled in stopes, usually called rockfill, have a limited ground support capability and self-standing height in the absence of binder (Hassani and Archibald 1998). Rockfill is generally used where no requirements for side and base exposures such as working floors (Yang 2016). Rockfill with binders can provide active support for the extraction of adjacent stopes (Hassani and

Archibald 1998; Sun et al. 2018). The binders generally consist of Portland cement, slag, and fly ash (Li and Aubertin 2003; Yang 2016). The efficiency of rockfill is also influenced by the gradation of waste rocks, filling method, raise dip and length, free fall height, and stope geometry (Yu 1989; Farsangi 1996; Yang 2016).

Waste rocks are also used to build barricades (or bulkheads) to retain backfill in stopes. Compared to the traditional barricades constructed using bricks, concrete blocks, and reinforced shotcrete, waste rock barricades are significantly simpler, faster, and lower cost (Yang et al. 2017). In addition, this type of barricades is easier to dismantle for ore recovery (Yang et al. 2017).

2.1.4 Valorization in mine haul roads

Finally, waste rocks are also often used to build mine haul roads because of their hardness, durability, low rolling resistance, easy accessibility and relatively low cost (Arulrajah et al. 2012; Thompson et al. 2019).

In open pit mines, the mine haul road network is a critical and vital component of the production process. Mine haul road length varies widely from mine to mine. Temporary haul road length ranges from 0.5 km to 10 km, while the length of permanent haul roads varies from 1.3 km to 14 km (Tannant and Regensburg 2001). Mine haul roads are generally subjected to extra heavy vehicle loading. For example, mining trucks size and capacity have grown significantly during the last few decades, with payload capacity increasing to 450 mt, and tire pressure sometimes exceeding 1000 kPa ("Belaz-7571 series"). In comparison, the gross vehicle weight limit of three axles straight truck for highway is 24.25 mt in Canada which is much lower than mining trucks (Woodrooffe 2010). Haul roads therefore need high strength and stiffness capacity.

The performance of haul roads can significantly affect the mine productivity and costs. Operations safety, productivity, and equipment longevity are dependent on well-designed, constructed and

maintained haul roads (Thompson et al. 2019). The selection of waste rocks for haul road construction should be commensurate with safety, operational, environmental and economic considerations (Thompson et al. 2019). For example, waste rocks should not contain weathered rock, clay or soil, to be used in base layer construction, but should rather be blocky, hard material, with less than 20% fines (Thompson 2015). For wearing course, waste rocks should not be too fine otherwise it may be slippery and dusty, and too unbound, or it will produce loose stones, raveling and, in both cases, rapidly increasing rolling resistance and operational risks once the road is trafficked (Thompson 2011c). More details about the design of mine haul roads are presented in the following section.

2.2 Mine haul road design

The design of mine haul roads typically involves geometric, structural, functional, and maintenance designs (Tannant and Regensburg 2001; Thompson et al. 2019). The present research was more particularly related to the structural and functional design of haul roads.

2.2.1 Geometric design

Geometric design of mine haul roads involves both vertical and horizontal plane of roads, berm walls, and drainage (Thompson et al. 2019). Geometric layout of mine haul rods should allow the vehicles to operate up to the design speed, but since the same roads are used to for laden and unladen haulage, the laden travel times should also be minimized using appropriate geometric alignment, whilst accepting compromise (generally in the form of speed limits) on the unladen return haul (Thompson et al. 2019).

Stopping distance requirements are a critical component of the geometric design, which has a significant impact on the operational safety of mine haul road (Tannant and Regensburg 2001). The ISO 3450 standard typically gives 114 m stopping distance at 10% downgrade at 50 km/h and 73 m at 40 km/h, which satisfy most mine ramp road designs where rear-dump trucks are used (Thompson et al. 2019). Stopping distance also depends on the type of wearing course material, moisture, climatic conditions, type of tyre, inflation pressures, load and vehicle speed (Tannant and Regensburg 2001). For example, a greater stopping distance should be considered for wet roads, poor and slippery road surface, spillage and sub-standard tyres. The sight distance of a driver should be equal to or greater than the stopping distance of the vehicle, and the horizontal and vertical curves of a road should be planned accordingly (Figure 2.2).

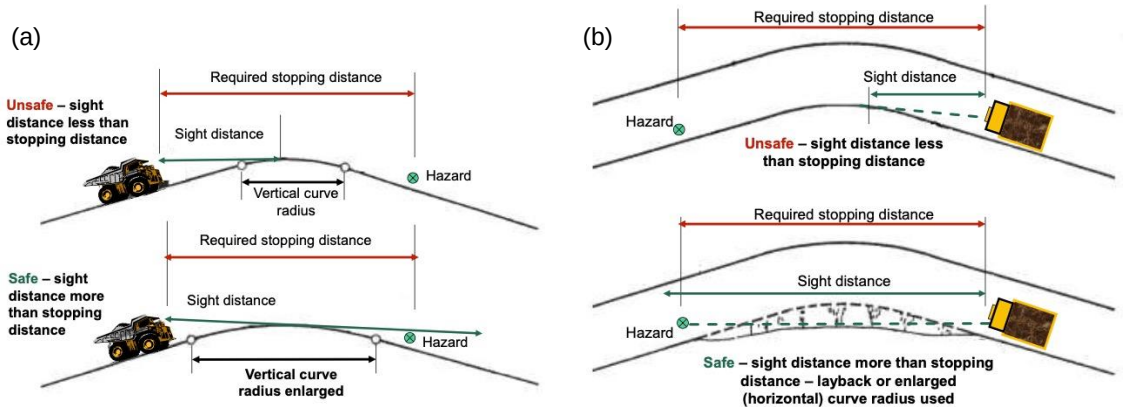

Figure 2.2: Sight distances for (a) vertical curve and (b) horizontal curve (Thompson et al. 2019).

The width of a haul road must allow safe vehicle manoeuvrability and maintain road continuity. In most cases, a straight stretch of road should be 3 to 4 times width of the truck, excluding shoulders, berms and drains (Tannant and Regensburg 2001).

Horizontal curves should be designed to ensure that all vehicles can safely negotiate the curve at a given speed, which should consider sight distance and minimum turning radius. The minimum

curve radius can be calculated from the following equation (Thompson et al. 2019):

$$R = \frac{v_0^2}{127(U_{min} + e)} \quad 2.1$$

Where R: minimum curve radius, m; U_{min}: coefficient of lateral friction supply; v_0: vehicle speed, m/s; e: super-elevation applied, m/m width of road. Super-elevation of a curve is required to reduce the centrifugal forces on the truck when it run through the corner.

Grades generally vary between 0 and 12% on long roads and may approach 20% on short roads. Most haul roads grades in the field varied between 6% and 10% (Thompson et al. 2019).

A drainage ditch is excavated on each side of the road, and the depth is typically 0.5 m lower than the top of the subgrade. The slope of the sides of the ditch should not be steeper than 3H:1V (Thompson et al. 2019).

2.2.2 Structural design

The objective of structural design is to allow haul roads to carry the imposed loads without excessive deformation of the pavement, and avoid excessive maintenance (Thompson and Visser 1996).

A haul road cross-section can be broadly divided into subgrade, subbase, base, and wearing (surface) course (Figure 2.3) (Tannant and Regensburg 2001). The thickness of subbase and base layer are generally 1 to 2 m, but the subbase thickness can be up to 10 m when a higher road elevation is required. The wearing course is generally 0.3 to 1 m in thickness. The pavement must limit the strains in the subgrade, and the upper layers must protect the underlying layers. Vertical compressive strains induced in a pavement by heavy wheel loads decrease with depth, so the stiffest materials are usually placed on top (Thompson and Visser 1996; Kumar 2000). In general, applied load, subgrade strength, structural thickness and layer strengths mainly control the structural

performance of a haul road (Thompson and Visser 1996, 1997b, 1997a).

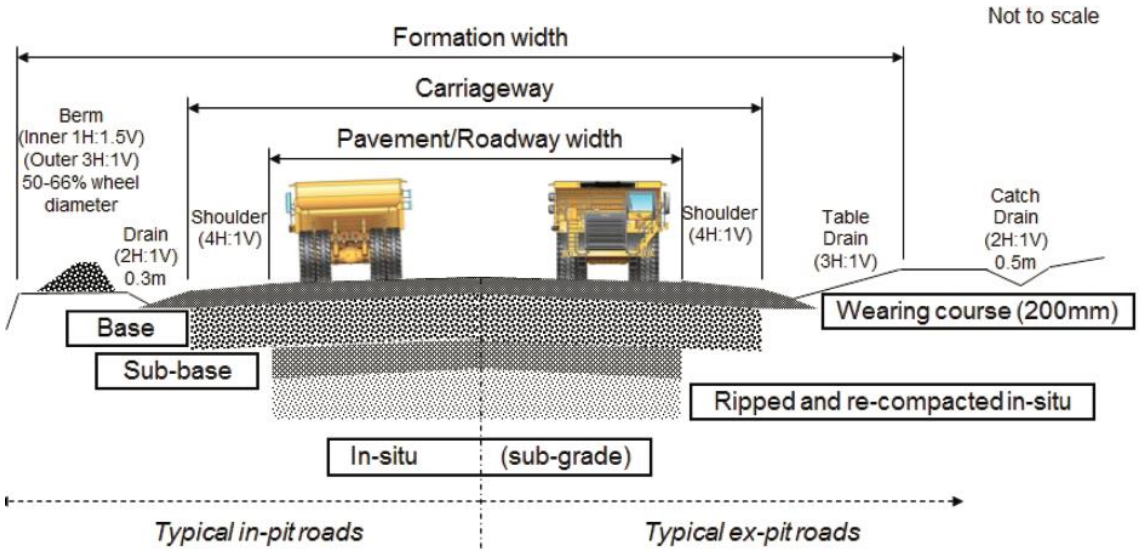

Figure 2.3: The typical cross-section of mine haul roads (in-pit and ex-pit roads), the road layers include subgrade, subbase, base, and wearing (surface) course (Thompson et al. 2019).

Historically, the structural-design techniques for haul roads consisted of placing several layers of granular materials over in-situ materials, and adding more layers to provide adequate strength as excessive deterioration occurred (Thompson and Visser 1996). This method heavily relies on the available experience from previous road construction, and it is therefore difficult to ensure the adequate haul road performance. California Bearing Ratio (CBR) method and mechanistic design method were therefore proposed to better design mine haul roads.

California Bearing Ratio (CBR) method

California Bearing Ratio (CBR) method was first used for haul roads by the United States Bureau of Mines (USBM) (Thompson and Visser 1996). CBR method is widely used in practice because

it is a simple and straight forward design method based on the Boussinesq semi-infinite single layer theory, which assumes a constant elastic modulus for different materials in the pavement (Kumar 2000).

In CBR method, surface layer must have higher CBR than underlying layers, and the change in CBR should not be too abrupt (Thompson 2011a). The layer thickness can be determined using CBR curve chart (Figure 2.4), or calculated (Thompson 2010, 2011a):

$$Z_{\mathrm{CBR}}=\frac{9.81t_w}{p}\left[0.104+0.331e^{(-0.0287t_w)}\right]\left[2\times10^{-5\left(\frac{\mathrm{CBR}}{p}\right)}\right]\left[\left(\frac{\mathrm{CBR}}{p}\right)^{-\left(0.415+p\times10^{-4}\right)}\right] \quad 2.2$$

Where t_w: truck wheel load (metric tons); p: tire pressure, kPa; Z_{CBR}: layer thickness, m.

When the equivalent single wheel load (ESWL) is used to estimate wheel load (to account for the tandem rear axle), the layer thickness Z_{ESWL} (m) can be calculated using the following equation (Thompson 2010, 2011a):

$$Z_{\mathrm{ESWL}}=Z_{\mathrm{CBR}}+\left[0.184+\left(0.086\mathrm{CBR}+\frac{17.76\mathrm{CBR}}{t_w}\right)\right]^{-1} \quad 2.3$$

CBR design chart that relate pavement, base and subbase thickness to truck wheel load and CBR values was also developed, such as the USBM CBR design chart (Figure 2.4). The thickness of mine haul roads can be estimated for various wheel loads generated by typical 6-wheeled rear-dump trucks together with the bearing capacities of various soil types defined by the Unified Soil Classification (USCS) and the American Association of State Highway and Transportation Officials (AASHTO) systems (Thompson et al. 2019).

CBR design method is particularly simple and useful to estimate the total cover thickness needed over the subgrade material. However, CBR design method is not applicable to design the multilayered roads with a base layer of selected waste rocks (Thompson 2011b). Also, this method does not account for the properties of the wearing course material, the service life of haul roads and traffic volumes. Also, CBR was originally designed for paved roads and surfaces for airfields,

and is less applicable to unpaved roads, especially haul roads which experience different wheel geometry and construction materials from highways (Thompson and Visser 1996, 1997b, 1997a). CBR method tends to result in under-design in most cases, but may be over-conservative for haul roads with very short designed life (Tannant and Regensburg 2001).

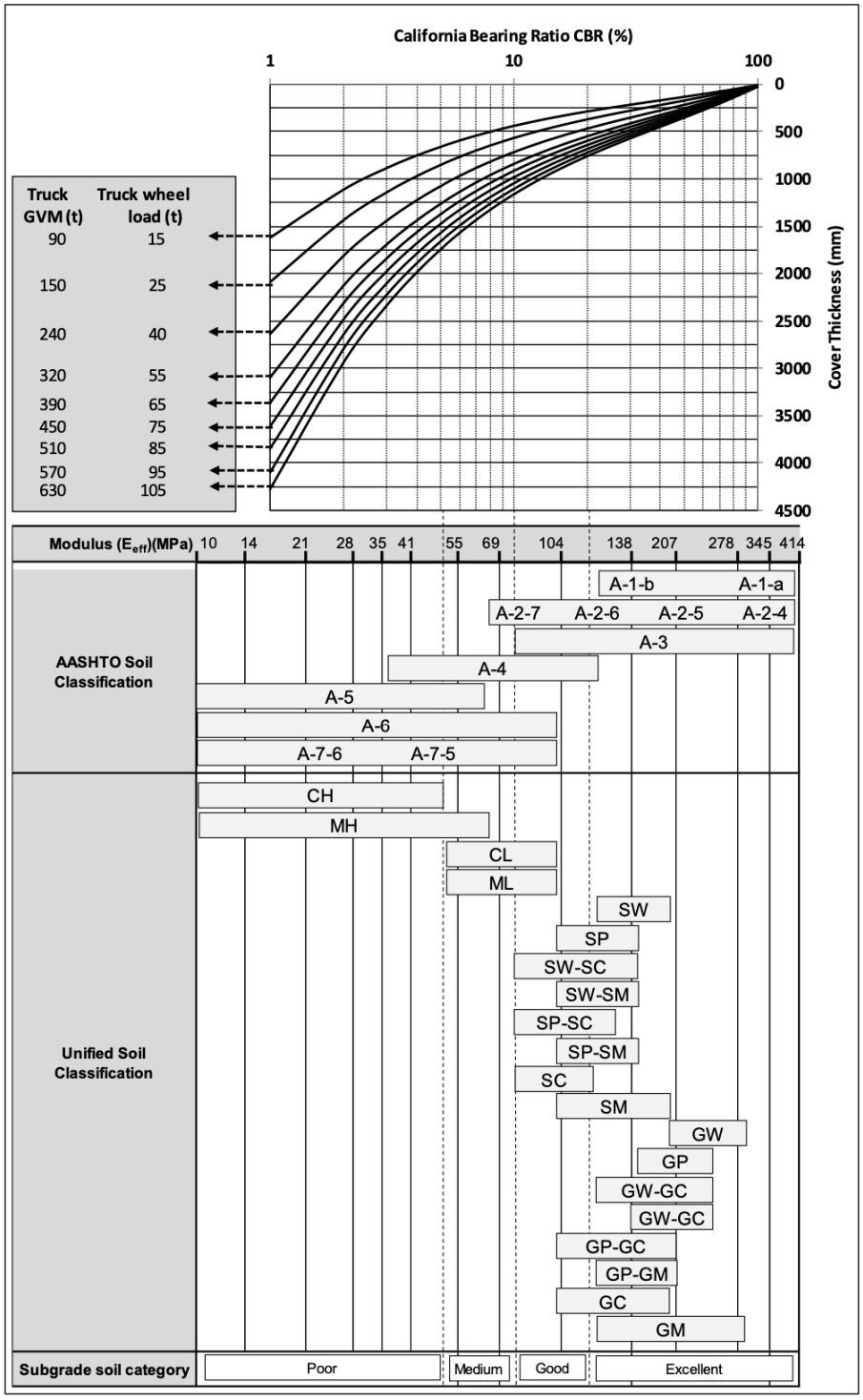

Figure 2.4: United States Bureau of Mines (USBM) CBR design chart for mine haul roads (Thompson 2019).

Mechanistic design method

The mechanistic method (including linear and nonlinear elastic modelling), relies on mechanistically derived data to which empirical procedures are applied, therefore extending the applicability of the technique (Thompson and Visser 1996, 1997b, 1997a).

Mechanistic method, based on a theoretical elastic multi-layer system model of road layers, is more accurate than CBR for multi-layer haul roads (Kumar 2000; Thompson 2011c). Unbound aggregate and subgrade layers can show nonlinear and stress-dependent behavior (usually represented by resilient modulus) under traffic loading (Tutumluer 1995; Lekarp et al. 2000a). Unbound aggregate typically exhibits stress-hardening behavior, while subgrade soil tends to exhibit stress-softening behavior (Pyo 2012). For mechanistic method, resilient modulus of pavement materials is therefore generally used for computing the vertical strains in a haul road (Thompson 2011b). This method is usually applied using software or numerical codes to calculate layers thickness such as ELSYM5, MePADS, CIRCLY6, Finite Difference Method (e.g. FLAC), and Finite Element Method (e.g. ANYSIS and ABAQUS) (Chen et al. 1995; Pyo 2012; Thompson 2015).

Two design criteria are used in mechanistic design method, namely the factor of safety (FOS) (the ratio of ultimate available shear strength to actual working shear stress) for the two uppermost layers, and the vertical elastic compressive strain for road layers. The vertical strain criterion usually correlates well with structural performance of the haul road (Morgan et al. 1994; Thompson 1996; Kumar 2000; Paige-Green 2007), while the FOS criterion is not always applicable since the applied stresses are significantly lower than the ultimate strength of the different layers (Thompson and Visser 1996, 1997b). The vertical strain limit depends on the design lifetime of the road and the traffic density, and can be calculated using the following equations:

$$E_s = 21600/N^{0.28} \quad \text{(Knapton 1989)} \tag{2.4}$$

$$E_s = 80000/N^{0.27} \quad \text{(Tannant and Regensburg 2001)} \tag{2.5}$$

Where E_s: allowable strain limit (micro strain); N: number of load repetitions.

The critical strain limit is typically around 1500 micro-strain at the top of the subgrade (Morgan et al. 1994) and 2000 micro-strains at the road surface (Thompson et al. 2019). More accurate strain values can be determined according to the category of road to be built and the associated operating life and traffic volumes (Figure 2.5).

Mechanistic design method is more accurate than the CBR method for designing mine haul roads since it directly takes into account the different material properties, number of loaded trucks, and designed life of haul roads (Thompson and Visser 2000a; Tannant and Regensburg 2001; Thompson 2010). However, the mechanical properties of waste rocks including shear strength and resilient modulus are necessary for this method, indicating the application of this method needs more advanced laboratory or field tests than CBR test.

Haul Road Category	Typical Description	Range of maximum permissible vertical elastic strains (μstrains)	
		Traffic volumes > 100kt/day	Traffic volumes < 100kt/day
CATEGORY I	Permanent life-of-mine high traffic volume main hauling roads and ramps in- and ex-pit. Operating life >20 years	900	1500
CATEGORY II	Semi-permanent medium- to high traffic volume ramp roads in- and ex-pit. Operating life >10 years	1500	2000
CATEGORY III	Shorter-term medium- to low-volume in-pit bench access, ex-pit dump, or ramp roads. Operating life; • <5 years (@ > 50kt/day) • <10 years (@ <50kt/day)	2000	2500

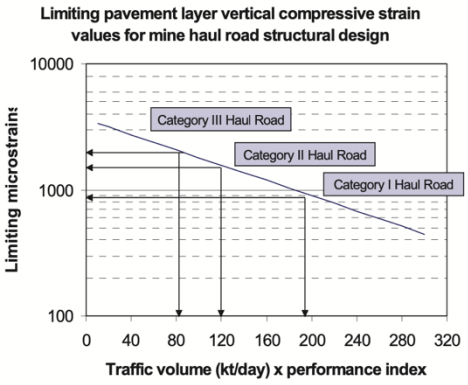

Maximum permissible vertical strains can also be determined from (*kt/day x performance index*) where performance index is defined as;

1 Adequate but fairly maintenance intensive
2 Good with normal maintenance interventions
3 Outstanding with low maintenance requirements

Figure 2.5: Haul road classification and associated mechanistic structural design limiting strain criteria (Knapton 1989).

2.2.3 Functional design

Functional design refers to the ability of a haul road to provide an economic and safe ride. Trafficability is dictated to a large degree by the choice, application, and maintenance of locally available wearing course materials (Thompson and Visser 1996, 1997b, 2000b). Road geometrics, climate and traffic volumes also influence the performance of the wearing course. Poor functional performance induces poor ride quality, excessive dust, increased tire wear and damage and an accompanying loss of productivity, which all induce an increase in overall vehicle operating and maintenance costs (Thompson and Visser 1997a).

The wearing course faces the greatest weathering and highest dynamic loads because of truck travels (Kaufman and Ault 1977; Kumar 2000; Thompson 2011c). Usual wearing course materials for haul roads include compacted gravel, crushed stone, asphaltic concrete, roller compacted concrete, and stabilized earth (Tannant and Regensburg 2001). Asphaltic concrete offers a high coefficient of road adhesion and creates a smooth surface that reduces dust problems. However, asphalt offers little resistance to development of ice or snow glaze, and the high cost of asphaltic road wearing course severely restricts its applicability to haul roads which have a relatively short life. Stabilized earth usually cannot create a sufficient haul road wearing course, but it can significantly reduce the quantity of base material required.

Waste rocks are an interesting alternative to construct haul roads because of the relatively low cost, high strength, and availability. Compared to other valorization methods, the large haul road network can consume more waste rocks, which can greatly relieve the pressure of waste rocks management in the field. However, it needs relatively frequent maintenance, and waste rocks may require screening or crushing. Also, it can generate dust problems in dry weather, or because of frost action (fines>10%) (Kaufman and Ault 1977; Tannant and Regensburg 2001). Generally, wearing course is constructed with fine gravel (<19 mm) with closely controlled grading to avoid dust problems while maintaining proper binding characteristic of the material. Grading and plasticity parameters can be used to predict the functional performance of a wearing course material. For example, a specification for haul road wearing course materials has been proposed and used in South Africa (Thompson and Visser 2000b) based on a parametric relationship suggested in Transport Recommendations for Highways (TRH 20). The specification is based on the parameters of shrinkage product (SP) and grading coefficient (GC), and it recommends that GC and SP should range from 25 to 32, and from 95 to 130, respectively. A defect score progression model, based on traffic, maintenance and wearing course material interactions, also has been developed to calculate the functional performance of a particular wearing course material (Thompson and Visser 2013):

$$LDDD=1.261+DM(0.000121\cdot CBR\cdot KT-0.02954\cdot GC+0.009824\cdot SP\cdot DR) \quad 2.6$$

$$LDDI=1.7929+D[0.002276\cdot KT+GC(0.01029\cdot DR-0.010887)] \quad 2.7$$

$$DSMIN=37.9164+12.7093\cdot M-0.15799\cdot KT+1.3836\cdot GC-0.08752\cdot SP \quad 2.8$$

Where LDDD: rate of defect score decreases immediately following last maintenance cycle; LDDI: rate of defect score increases; DSMIN: minimum defect score in maintenance cycle; KT: average daily tonnage hauled (kt); WM: wearing course material type; P075: percentage of material passing 0.075 mm sieve; DR: Dust ratio; PI: plasticity index; CBR: 100% modified California Bearing Ratio of wearing course material; GC: grading coefficient; P2 is percentage of material passing 2.0 mm sieve; P475 is percentage of material passing the 4.75 sieve; SP: shrinkage product; PL: plasticity limit; D: days since last maintenance; DM: days between last maintenance and minimum cycle defect; DSMIN: minimum defect score in cycle.

However, only one mechanical property (i.e., CBR) is considered in this defect model for predicting the performance of waste rocks for wearing course. Other mechanical properties, such as shear strength, stiffness (or resilient modulus), and permanent deformation, also affect the road performance (Atkinson 1992; Tannant and Regensburg 2001; Douglas 2016; Thompson et al. 2019). Moreover, climatic conditions affect the physical and mechanical properties of waste rocks, and then impact the selection of waste rocks for haul roads. For example, in wet climate, fines should be less than 10% to prevent muddy and slippery conditions when wet. In drier climates, fines should exceed 5% to prevent raveling or loosening of wearing course aggregates (Thompson 2015). On the other hand, excessive fines in drier climates can lead to dust problems (Thompson and Visser 2013). Therefore, the prediction of road defect and selection of waste rocks should take more indexes into account.

2.2.4 Maintenance design

Maintenance design concerns the optimal frequency of wearing course maintenance commensurate with minimum vehicle operating and road maintenance costs (Figure 3.7) (Thompson and Visser 2000a). The maintenance design is complementary to the structural and functional designs (Thompson and Visser 1996, 1997b). The optimum maintenance frequency for a haul road can be determined using the maintenance management system (MMS) (Thompson and Visser 2000a).

Road roughness is the principal measurement of pavement condition that can be directly related to both vehicle operating costs and the frequency of maintenance activities and is therefore the basis of the MMS. The progression model is a function of wearing course material parameters, traffic volumes and maintenance interval (Thompson and Visser 1997a, 2000a, 2013).

Predictive models for Rolling resistance (RR) progression and Vehicle operating cost (VOC) were developed to minimize total road costs and can be written (Thompson and Visser 2013):

$$RDS=RDSMIN+\left[\frac{RDSMAX-RDSMIN}{1+e^{Dg}}\right] \quad 2.9$$

$$LDRDI=1.768+0.001D(2.69KT-72.75PI-2.59CBR-9.35GC+1.67SP) \quad 2.10$$

$$RDSMIN=31.1919-0.05354SP-0.0152CBR \quad 2.11$$

$$RDSMAX=7.6415+0.4214KT+0.3133GC+0.4952RDSMIN \quad 2.12$$

Where RDS: roughness; RDSMIN: minimum roughness defect score immediately following last maintenance cycle; RDSMAX: maximum roughness defect score; LDRDI: rate of roughness defect score increase; RR: rolling resistance, N/kg; RRMIN: minimum rolling resistance at RDS=0; LDRRI: rate of increase in rolling resistance from RRMIN; V: vehicle speed, km/h.

Vehicle operating and road maintenance cost models:

$$FCU=1.02+\left[UVMV(296TRU+4.5V)+LGVMV\left(246TRU+0.027V^{2}\right)\right]\times10^{-5} \quad 2.13$$

$$FCF=-3.575+UVM(0.092-0.016DV)+0.0017LGVM \quad 2.14$$

$$TW=0.098+0.0015RDS+0.002|GR| \quad 2.15$$

$$\frac{P}{VP}=(67.28+2.31RDS)H^{0.375} \quad 2.16$$

$$ML=220\left(\frac{P}{VP}\right)^{0.45} \quad 2.17$$

Where FCU: Truck fuel consumption (mL/s) for unfavourable (against the load) grades; FCF: Truck fuel consumption (mL/s) for favorable (with the load) grades; TW: Truck tyre wear (tyres consumed per 1000 km for a 6 wheeled truck); P: Truck parts cost (per 1000 km); VP: Truck replacement value ($\times 10^{-5}$); ML: Maintenance labour costs (per 1000 km); L: Truck loading (laden is 1, unladen is 0); DV: Truck drive type (electric wheel motors is 1, mechanical drive is 0); GVW: Truck gross (laden) vehicle mass, t; UVW: Truck unladen vehicle mass, t; TRU: Total resistance (against the load), %; GR: Road grade, %; H: Truck age (total operating hours $\times 10^{-3}$).

MMS are effective to predict maintenance frequency of a haul road, but for complex mine road networks where material is sourced and hauled from a large and highly variable number of loading points, the MMS can become onerous for the road maintenance design (Thompson et al. 2003). The real-time maintenance management system (RT-MMS) is therefore often considered a more effective approach to mine road network maintenance management. Since most large mines operate trucks with on-board diagnostic data collation, road condition can be monitored on a real-time basis through on-board vibration signature analysis. The defect locations and type and road rolling resistance can then be monitored and repaired on a real-time basis (Thompson et al. 2003).

The literature review on haul road design indicates that CBR and resilient modulus of waste rocks are necessary input parameters for the CBR and mechanistic design method, respectively. Shear strength of waste rocks is another critical geotechnical property influencing the stability of haul

roads (Tannant and Regensburg 2001; Long et al. 2011; Arulrajah et al. 2014; Byun et al. 2020). Shear strength is therefore generally used in the mechanistic design method to calculate the factor of safety (FOS) (Thompson et al. 2019). The permanent deformation behavior of waste rocks is directly related to rutting, one of the most common deteriorations in flexible pavements (Erlingsson 2012). Excess rutting can decrease the driving quality and safety because of hydroplaning and reduced skid resistance of the haul road surface (Rahman and Erlingsson 2015a; Salour and Erlingsson 2017). The critical properties of waste rocks, i.e., CBR, resilient modulus, shear strength, and permanent deformation, should be studied to improve the structural and functional design, and to decrease the maintenance frequency of mine haul roads. The following sections therefore reviews these mechanical properties of waste rocks.

2.3 Shear strength of waste rocks

Shear strength is the maximum shearing resistance of a granular material along its failure plane. Shear strength of waste rocks is one of the critical geotechnical properties influencing the performance of haul roads (Tannant and Regensburg 2001; Long et al. 2011; Byun et al. 2020). Waste rocks are considered cohesionless, and their effective stress shear strength envelope therefore passes through the origin of the Mohr stress diagram (Duncan et al. 2014). The angle of internal friction of waste rocks varies between 21° and 62° depending on the material properties such as gradation, dry density, and water content (more details see below section 2.3.2) (Aubertin 2013).

The shear strength of saturated materials is usually interpreted by extending Terzaghi's effective stress concept to the Mohr-Coulomb failure criterion using the following equation:

$$\tau = c' + (\sigma - u_w) \tan \phi' \qquad 2.18$$

Where τ: shear strength, kPa; ϕ': the effective stress angle of internal friction, °; c': the effective stress cohesion intercept of waste rocks, kPa; σ-u_w: the effective normal stress on the failure plane, kPa.

Bishop (1959) developed a model extending the principle of effective stress to unsaturated soils by introducing a variable χ related to the degree of saturation, and which varies between 0 for dry state and 1 for saturated state:

$$\tau=c'+[(\sigma-u_a)+\chi(u_a-u_w)]\tan\phi' \quad 2.19$$

Fredlund et al. (1978) modified Bishop (1959) model by considering the shear strength contribution caused by suction τ_{us}:

$$\tau=c'+(\sigma-u_a)\tan\phi'+\tau_{us} \quad 2.20$$

2.3.1 Measurement of shear strength

Shear strength testing methods can be divided into forced (direct shear) and free shear plane (indirect shear) tests. Direct shear methods usually use instruments with linear or rotary shear kinematics such as direct shear box test and shearing grouser test, while indirect shear methods are usually based on soil compression such as triaxial compression test and cone penetrometer test (Stefanow and Dudziński 2021).

Direct shear box test is one of the simplest shear tests to conduct. The specimen is sheared along a direct plane and the confining pressure is equal to the normal pressure (ASTM D6528 2017). The size of shear boxes (length×width×height) in laboratory typically ranges from 60×60×20 mm to 300 × 300 × 150 mm (Bagherzadeh-Khalkhali and Mirghasemi 2009). Large-scale direct tests (600×600×400 mm) were also developed in the field to fit large size particles (Xu et al. 2011).

Triaxial test is more complex than direct shear test but also provides more information such as pore

water pressure and effective stress. Compared to direct shear test, the shear failure plane of triaxial test is not predetermined, and the stress distribution on the failure plane is uniform. The triaxial test specimen is enclosed by rubber membrane and a confining pressure is applied prior to and during shearing. The specimen is subjected to an increasing vertical stress and will ultimately fail at an angle approximately equal to the angle of internal friction. Triaxial tests typically include consolidated drained (ASTM D7181 2020), consolidated undrained (ASTM D4767 2020), and unconsolidated undrained (ASTM D2850 2015) tests. The shear strength of materials is significantly affected by the specimen size, the specimen height to maximum particle size and the specimen diameter to maximum particle size ratios are generally greater than 50 and 6, respectively (Jewell and Wroth 1987; Cerato and Lutenegger 2006; ASTM D4767 2020; Deiminiat et al. 2020). However, the usual triaxial test instruments for soils are generally smaller than 100 mm in diameter, which limits the applicability of these instruments to waste rocks. Large-scale triaxial testing equipment was developed to accommodate coarse-grained particles, for example, Indraratna et al. (1998) and Zhang et al. (2020) used 300 mm diameter×600 mm high specimen to measure the shear strength of ballast, Lee et al. (2017) used 500×900 mm, 700×1200 mm, and 900×1650 mm triaxial cells to measure the shear strength of ballast, and Ovalle et al. (2014) used 250×375 mm and 1000×1500 mm triaxial cells to measure the shear strength of waste rocks with 40 and 160 mm of maximum particle size, respectively (Figure 2.5). The applied confining pressure for large-scale triaxial test can exceed to 1 to 10 MPa (Ovalle et al. 2020). In this study, a series of triaxial tests with 150×300 mm and 300×600 mm specimen size was carried out on waste rocks to study the shear strength.

Figure 2.6: Large-scale triaxial test apparatus; (a) 1000 mm diameter and (b) 250 mm diameter (Ovalle et al. 2014). The tested materials were rock aggregates with maximum particle size 40 mm and 160 mm and uniformity coefficient 2.

2.3.2 Factors affecting shear strength

Several factors can affect the shear strength of waste rocks, such as density, particle size, particle shape, particle size distribution, mineralogy, and water content (Williams and Walker 1983; Yazdanjou et al. 2008; Duncan et al. 2014; Alshameri et al. 2016).

Density plays an important effect on the shear strength of waste rocks, and the angle of internal friction generally increases with density (Duncan et al. 2014). Marsal (1973) found that the variation of angle of internal friction caused by density is 3° to 4° at 65 kPa of normal stress, and it decreases to 1.5° at 3.45 MPa. Al-Hussaini (1983) and Holtz and Gibbs (1957) also reported similar findings for crushed basalt rocks and gravelly soils.

Literature is sometimes contradictory regarding the effect of particle size on shear strength. Shear

strength tends to increase with the maximum particle size according (Bala and Bishnoi 2016), while Marachi et al. (1972) argued that shear strength decreased with the maximum particle size and Roner (1985) found that the influence of maximum particle size on the shear strength of quartzite ballast was negligible. It was suggested that the shear strength increases as the particle size increases to a critical diameter, above which no significant variation would occur (Ionescu 2004). Particle shape also has an impact on shear strength. Higher angularity particles usually provide a strong interlocking effect, which results in a higher angle of internal friction (Holtz and Gibbs 1956). However, angularity particles may also lead to poor compaction and higher deformations (Pike 1973).

The shear strength is typically higher for well-graded granular materials than for uniformly graded materials (Ionescu 2004). Smaller particles can fill voids between larger particles in well-graded waste rocks, which results in a denser packing state that brings a greater resistance to shear. The shear strength is generally higher for waste rocks with a higher coefficient of uniformity (Marsal and La Rosa 1976; Rico et al. 1977). On the other hand, excessive fines in aggregates may cause a significant reduction in shear strength although the corresponding coefficient of uniformity increases in this case (Kalcheff 1974). The shear strength of waste rocks is mostly affected by the frictional resistance of gravel particles when they represent more than 70% in waste rocks weight. If gravel content is below 40%, the shear strength of waste rocks is mostly controlled by the frictional resistance of the sand particles. When the gravel content is between 40 and 70%, the shear strength is controlled by the frictional resistance provided by both the gravel and sand particles in the mixtures (Vallejo 2001).

Shear strength of waste rocks is also controlled by particle crushing (Bala and Bishnoi 2016). For example, Ovalle and Dano (2020) reported that particle breakage tended to increase with particle size and caused a slight decrease of shear strength for coarse waste rocks with 40 to 160 mm maximum particle size.

Water content in waste rocks is typically around residual and therefore quite low (Ferry et al. 2002). Therefore, in general water does not transmit suction effectively to the particle contact point and increases in suction will not necessarily result in a significant increase of shear strength. A decrease in shear strength is, however, possible for low suctions when waste rocks desaturate rapidly (Vanapalli et al. 1996). An increasing degree of saturation could significantly reduce the strength of loose waste rocks, but had a negligible effect on the shear strength of compacted waste rocks (Williams and Walker 1983).

Climatic factors can also affect the shear strength of waste rocks. Freeze-thaw cycles generally result in a decrease of shear strength (Aldaood et al. 2016; Lu et al. 2019), depending on environmental factors and material properties such as the availability of water (Yong et al., 1985), cooling rate (Broms and Yao, 1964), particle size distribution, and fines content (Liu et al., 2016; Zhang et al., 2017). The frost expansion of pore water can also lead to a redistribution of particles and porosity, therefore altering the mechanical properties of the material (Aldaood et al. 2016; Ishikawa et al. 2019; Lu et al. 2019).

2.4 California Bearing Ratio (CBR) of waste rocks

California bearing ratio (CBR) is the one of the most used parameters in road design (also see section 2.2.2). CBR is an easy and reliable measurement of the relative resistance of pavement materials to uniaxial penetration (ASTM D1883 2016). The suitability and stability of construction materials is usually evaluated using CBR, also for haul roads. For example, the CBR of waste rocks used for the construction of wearing course of mine haul roads should be greater than 80% (Thompson et al. 2019).

2.4.1 Measurement of CBR

The laboratory CBR test was developed by the California Division of Highways in the 1920s, and then approved by American Society for Testing and Material (ASTM) in 1961 (Shi et al. 2017). CBR test has been widely used to evaluate the strength of subgrade, subbase, and base materials (less than 19 mm), to evaluate the bearing capacity of various soil structures such as earth dams, road fillings, highways, and mine haul roads. The CBR value is expressed as the ratio (multiplied by 100) of the unit load on the piston required to penetrate 2.5 mm and 5.1 mm of the test material to the unit load required to penetrate material of well-graded crushed stone (ASTM D1883 2016). The diameter of standard CBR mold and piston is 152.4 mm and 49.63 mm, respectively (Figure 2.7). The compacted specimen is penetrated by the piston at a constant rate of 1.3 mm/min. The CBR tests can be performed on soaked and unsoaked soil samples (ASTM D1883 2016). Laboratory CBR tests were carried out on crushed waste rocks in this study.

The field CBR test (ASTM D4429 2004) can be used to verify laboratory CBR test results. Field CBR test uses a loading jack to force a piston into the investigated material. The jack is loaded against dead weights or a heavy piece of equipment such as a loaded dump truck (Sayida et al. 2019) and the test can therefore be cumbersome to conduct. Also, the results of the laboratory and field CBR test may show differences depending on the material type, water content, and dry density (Kurnaz and Kaya 2019). The in-situ CBR values of soils also can be determined using Dynamic Cone Penetrometer (DCP), which is lighter and less costly than field CBR test (Zumrawi 2014).

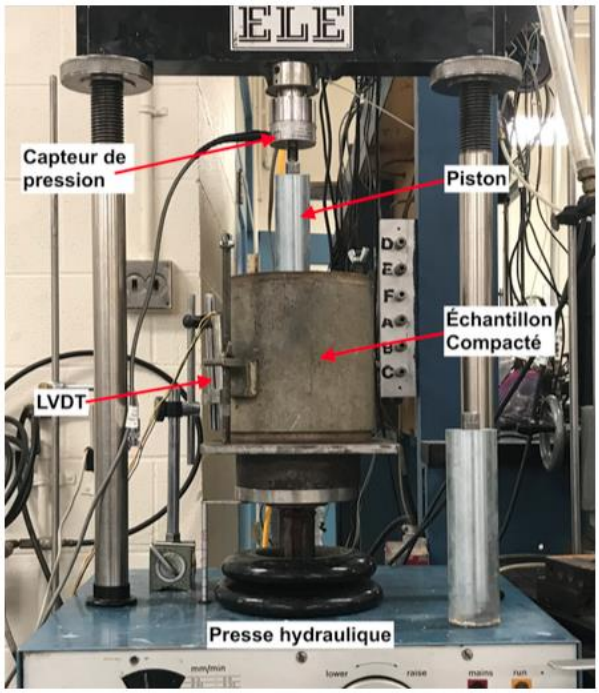

Figure 2.7: Laboratory CBR test setup (Laverdière 2019). The tested materials were crushed waste rocks, and the diameter of CBR mold and piston was 152.4 mm and 49.63 mm, respectively.

2.4.2 Factors affecting CBR

CBR depends on many factors such as maximum dry density, optimum moisture content, liquid limit, plastic limit, plasticity index, soil types, permeability, and soaking condition (Talukdar 2014).

CBR typically increases with compaction effort and dry density (Lakshmi et al. 2016; Laverdière 2019; Al-Obaydi et al. 2021). CBR also generally increases with particle size (Patel and Desai 2010; ul Rehman et al. 2015; Yao et al. 2016; Laverdière 2019). However, CBR also can decrease as particle size increases if the fines content is too small (Salam et al. 2018). In this case, fines are not sufficient to fill voids which remain empty, therefore decreasing CBR of granular materials. Typically, fines content above 12% are sufficient to limit this effect (Salam et al. 2018).

Fines content can significantly impact the CBR, for example, Laverdière (2019) suggested that the

CBR of waste rocks is maximum for a fines content of approximately 10%. Other research studies also showed that the optimum fines content regarding CBR comprised between 8 and 10% when unbound granular material had over 35% gravel (Siswosoebrotho et al. 2005; Farias et al. 2018). The grain-to-grain contact of coarser material that offers a structural strength can, however, become less effective for fines content greater than the optimum, leading to a decrease of CBR (Yoder and Witczak 1991).

Finally, CBR also decreases with moisture content, and soaked CBR of soils with large fines content may decrease compared to unsoaked samples (Razouki and El-Janabi 1999; Talukdar 2014). The presence of excessive water would reduce the effective strength and soften the connectors of filler (fines) (Aiban and Mohammed 2002). On the other hand, CBR tends to reach the maximum at around optimum water content because of the higher dry density (Laverdière 2019).

2.4.3 Predictive models for CBR

CBR test can be time consuming because representative soil samples should be collected from the location selected and then remolded at field dry density and water content. Also, preparing soaked CBR sample can take about a week (Bassey et al. 2017). Several CBR prediction models based on easily determinable parameters, such as dry density, water content, coefficient of uniformity, and particle size distribution, were therefore developed (Kin 2006; Ferede 2010). The applied dataset is generally divided into training and testing dataset, and the training dataset is used to optimize the hyperparameters while the testing dataset is used to evaluate the accuracy of the developed machine learning models. In general, around 80% and 20% of the dataset can be used for the training and testing, respectively, when the total dataset is large enough (Taskiran 2010; de Souza et al. 2020; Tenpe and Patel 2020). If the total dataset is relatively small, around 70% and 30% of the dataset can be used as the training and testing dataset, respectively (Ghorbani and Hasanzadehshooiili 2018; Kaloop et al. 2019; Oskooei et al. 2020).

However, most of the available models were proposed for fine-grained subgrade soils (Gregory and Cross 2007; Lakshmi et al. 2016; Bassey et al. 2017; Katte et al. 2019; Sreelekshmypillai and Vinod 2019), and they are not applicable to waste rocks because of the quite different physical and mechanical properties. CBR predictive model for coarse-grained pavement materials documented in the National Cooperative Highway Research Program (2001) of United States of America through the "Guide for Mechanical-Empirical Design of New and Rehabilitated Pavement Structures" is one of the most cited models, and D_{60}, diameter at 60% passing from grain size distribution is used as predictor in this model. However, only one physical property is considered in this model, which limits its prediction accuracy to waste rocks since other properties also affect CBR (see above section 2.4.2):

$$\mathrm{CBR}=28.09D_{60}^{2} \tag{2.21}$$

Rehman et al. (2017) also proposed two models to predict the CBR of coarse-grained materials based on the coefficient of uniformity C_U and maximum dry density MDD (pcf). However, the limited number of predictors and small developing data (41 samples) would limit the prediction accuracy to new materials, i.e., waste rocks in this study:

$$\mathrm{CBR_s}=0.7C_U+8.5 \tag{2.22}$$

$$\mathrm{CBR_s}=0.7C_U+0.045\mathrm{MDD}+3.4 \tag{2.23}$$

Machine learning, as an analytical alternative to conventional statistical method, is also used to develop the predictive models for CBR, and these models often have a higher prediction accuracy than conventional regression models (Erzin and Turkoz 2016; Kurnaz and Kaya 2019; Tenpe and Patel 2020) (Table 2.1). The selected input features for the machine learning models are different, but they typically are the basic soil properties, such as gravel content, sand content, fines content, liquid limit, plasticity index, water content, and dry density. Although these machine learning models showed reliable prediction accuracy ($R^2 > 0.9$) in the literature, their applicability to waste rocks is uncertain because of the different material properties (e.g., gradation and mineralogy) or

they are difficult to replicate since some critical information about these models is lacking in the literature (e.g., the layer's weights and bias of the neural network). The algorithm backpropagation neural network (BPNN) is generally used to develop the machine learning models in the literature. The architecture of BPNN is an important factor that can influence its computational efficiency and prediction accuracy (Pan et al. 2019). However, the determination of the BPNN architecture mainly depends on trial and error methods based on the network performance, which is time-consuming and increases the workload. Other common algorithms, such as k-nearest neighbors (KNN), decision tree (DT), and random forest (RF), therefore should be evaluated for the development of CBR predictive models for waste rocks.

Table 2.1: Examples of machine learning models used for predicting CBR reported in the literature. BPNN is usually used in most studies, and the basic physical properties are generally used as input features. These models were developed for different materials from subgrade soils to base materials.

References	Technic	Input	No. of datasets	Material	R^2
Tenpe and Patel (2020)	BPNN	G, S, PI, w_{opt}, γ_{dmax}	389	Subgrade soil	0.89
de Souza et al (2020)	BPNN	G, S, silt, clay, color	1790	Subgrade soil	0.997
Ghorbani and Hasanzadehshooiili (2018)	BPNN	lime, microsilica, curing days, curing conditions	90	Lime and microsilica	0.99
Erzin and Turkoz (2016)	BPNN	G_s, C_U, C_C, ρ_d, w, Q, Fel, Ca, C, A	61	Sands	0.939
Varghese et al. (2013)	BPNN	ρ_{dmax}, w_{opt}, PL, LL	112	Fine-grained soils	0.93
Taskiran (2010)	BPNN, GEP	LL, PI, ρ_d, w_{opt}, P#200, S, G	151	Base and subbase material	0.91

Where BPNN: backpropagation neural network; GEP: gene expression programming; ρ_d: dry density, kg/m^3; w: gravimetric water content, %; LL: liquid limit, %; PI: plastic index, %; P#200: percentage of soil particles passing through #200sieve, %; w_{opt}: optimum water content, %; G: gravel percentage, %; S: sand percentage, %; γ_{dmax}:

maximum dry unit weight, -; G_s: specific gravity, -; C_U: coefficient of uniformity, -; C_C: coefficient of curvature, -.

2.5 Resilient modulus of waste rocks

The low stiffness of waste rock layers of haul roads can result in poor trafficability under wet weather, churning, and excessive deformation (Thompson et al. 2019). The poor pavement performance increases the road maintenance costs and vehicle operating costs. Resilient modulus is a parameter generally used to characterize unbound granular material stiffness (Lekarp et al. 2000a), and is typically used in mechanistic design method to compute pavement response under traffic loading (Thach Nguyen and Mohajerani 2016). Resilient modulus of pavement materials is defined as the ratio of the repeated axial deviator stress to the recoverable axial strain, as shown in the following equation (AASHTO T307 2017):

$$M_R = \frac{\sigma_d}{\varepsilon_r} \tag{2.24}$$

Where M_R: resilient modulus, MPa; σ_d: deviator stress, MPa; and ε_r: recoverable axial strain, -.

2.5.1 Measurement of resilient modulus

The common method for characterizing the resilient behavior of unbound granular materials is the repeated load triaxial test conducted in the laboratory (EN 13286 2004; AASHTO T307 2017). AASHTO T307 (2017) standard provides two stress levels to simulate the stress conditions in base and subbase and subgrade materials of highways, respectively. For subgrade soils, the applied confining pressure and deviator stress ranges between 13.8 and 41.4 kPa, and between 13.8 and

68.9 kPa, respectively. For base/subbase soils, the applied confining pressure and deviator stress ranges between 20.7 and 137.9 kPa, and between 20.7 and 275.8 kPa, respectively. Each stress path is generally applied at least 100 cycles to obtain the representative resilient modulus. A repeated axial cyclic stress, load duration (0.1 s), and cyclic duration (1.0 to 3.1 s) is generally applied to a cylindrical specimen during repeated load triaxial tests, and the haversine-shaped load from is usually used to simulate the traffic loading. EN 13286 standard (2004) also proposed two stress levels (low and high) to evaluate the resilient behavior of unbound mixtures. The confining pressure in this standard ranges from 20 to 150 kPa, while the deviator stress varies from 30 to 475 kPa for high stress level, and from 20 to 300 kPa for low stress levels. However, the proposed stress levels in these two standards are significantly lower than the stress state in mine haul roads.

The specimen diameter to maximum particle size is generally greater than 5, and the specimen height should be at least 2 times the diameter (AASHTO T307 2017). However, the usual repeated load triaxial test instruments for soils are generally smaller than 150 mm (300 mm in height) in diameter, which limits the applicability of these instruments to coarse-grained waste rocks. Generally, the particles greater than 25.4 mm shall be scalped off prior to testing with 150 mm diameter of specimen. Some larger apparatuses have been developed in recent years to measure the resilient behavior of coarse-grained aggregates, and the diameter and height sizes increase to 300 and 600 mm, respectively (Nair and Latha 2012, 2015; Cao et al. 2021). In this study, repeated load triaxial tests with both 150 mm and 300 mm specimen diameter were carried out on waste rocks to study the resilient modulus

Repeated load triaxial tests are, however, complex, time consuming, and costly, especially considering the short-service-life of mine haul roads. Repeated load CBR tests were therefore proposed as an alternative to indirectly evaluate resilient behavior of pavement materials (Molenaar 2008). The principle of repeated load CBR test is similar to the standard CBR test, except that cyclic loading is applied (Molenaar 2008; ASTM D1883 2016). Resilient modulus determined

using repeated load CBR tests are typically greater than using repeated load triaxial tests (Araya 2011). An "equivalent modulus" ($E_{equ.}$) was therefore proposed to normalize the repeated load CBR test results and compare them to the triaxial resilient modulus (Opiyo 1995; Molenaar 2008). Several equivalent modulus equations were developed based on elastic theory and regression fitting (Table 2.2). A series of repeated load CBR tests were conducted on crushed waste rocks, and the applicability of existing equivalent modulus equations to waste rocks was also assessed in this study.

Table 2.2: Equivalent modulus equations for repeated load CBR test.

Equation	Description	References
$E_{equ.}=\frac{1.797(1-\nu^{0.889})\sigma_p r}{u^{1.098}}$	No friction	Opiyo (1995)
$E_{equ.}=\frac{1.375(1-\nu^{1.286})\sigma_p r}{u^{1.086}}$	Full friction	Opiyo (1995)
$E_{equ.}=\frac{1.513(1-\nu^{1.104})\sigma_p r}{u^{1.012}}$	Without strain gauges	Araya (2011)
$E_{equ.}=\frac{0.144(\sigma_V-2\nu\sigma_H)}{u}$	With strain gauges	Araya (2011)

Where $E_{equ.}$: equivalent modulus, kPa; σ_p: plunger stress, equal to total plunger load/plunger area, kPa; u: vertical elastic (resilient) deformation of materials under plunger, mm; ν: Poisson's ratio of tested material, -; σ_V and σ_H: vertical and horizontal (or lateral) stresses applied on the specimen, kPa.

Plate load test is widely used in the field to evaluate the stiffness of pavement systems (ASTM D1195 1997; Alshibli et al. 2005). The test consists of applying a static load in uniform increments on a circular plate (usually 305 mm in diameter) resting on the pavement surface and measuring

the corresponding deflections, and the load is usually transmitted to the plate via a hydraulic jack acting against a reaction frame (Alshibli et al. 2005).

Falling weight deflectometer (FWD) is a deflection testing device operating on the impulse loading principle, and it has been used extensively to assess the resilient modulus of pavement layer in the field (Mehta and Roque 2003). The portable (or light) falling weight deflectometer (PFWD or LFWD) is one of the recent in-situ non-destructive testing devices that has been developed to measure the pavement stiffness (Alshibli et al. 2005). The working principle of PFWD is similar with FWD, but it is easy to use, portable and easy to transport, quick to perform the test and analysis, which gives quick results and relatively cheap compared to the conventional FWD equipment (George et al. 2009). In addition to PFWD, GeoGauges, also known as the stiffness gauge, is a portable device capable of performing simple and robust measurements of the in situ stiffness and elastic modulus of pavement soils (Alshibli et al. 2005).

2.5.2 Factors affecting resilient modulus

A number of factors such as stress conditions, gradation, density, particle shape, and freeze-thaw cycles can affect resilient modulus (Lekarp et al. 2000a). It is important for design purposes to study how the resilient modulus varies with the influencing factors.

The resilient response of waste rocks significantly dependents on the applied stress levels. The resilient modulus increases considerably with an increase in confining pressure and sum of principal stresses (Witczak 2004; Ba et al. 2013). The effect of confining pressure is more significant than deviator stress on resilient modulus (Uthus 2007).

Resilient modulus generally increases with density (Lekarp et al. 2000a; Yao et al. 2016), and the resilient modulus of dense uniform materials is generally higher than loose materials (Robinson 1974). The increasing in density could result in significant increase in the number of particle

contacts, which would decrease the deformation in particle contacts and increase the resilient modulus (Kolisoja 1997). The effect of density on resilient modulus is more significant for a partially crushed aggregate than a fully crushed aggregate (Hicks and Monismith 1971).

Gradation of waste rocks is a key factor that affects the resilient modulus (Duong et al. 2016; Hatipoglu et al. 2020). Well-graded aggregates generally provide higher stiffness (Xiao et al. 2012; Xiao and Tutumluer 2017). However, the resilient modulus of aggregates with uniformly gradation may be slightly higher than that of well-graded one (Thom and Brown 1988), as well-graded materials can hold water in pores, which decreases the stiffness (Plaistow 1994). The gravel-to-sand ratio is a practical and easy-to-use criterion which is often used to optimize aggregate gradations (Xiao et al., 2012). The aggregate with around 1.5 of gravel-to-sand ratio shows higher density and resilient modulus when the maximum particle size is 19 mm (Xiao et al. 2012; Xiao and Tutumluer 2017). Fines content is another important factor influencing the resilient modulus of aggregates, the increasing of fines content can increase the resilient modulus because the more voids are filled (Thom and Brown 1988; Kamal et al. 1993), but excessive fines could decrease the stiffness (Hicks and Monismith 1971; Mishra and Tutumluer 2012).

Resilient modulus generally increases with the maximum particle size of aggregates (Kolisoja 1997). The major part of a load applied on aggregates is transmitted by particle queues, and when the load is transmitted via coarser particles, the smaller number of particle contacts results in less total deformation and consequently higher stiffness (Kolisoja 1997).

Water content or degree of saturation can affect the resilient modulus of waste rocks (Lekarp et al. 2000a), and the resilient modulus generally decreases with growing saturation level, and it may decrease significantly as complete saturation is approached (Lekarp et al. 2000a; Gudishala 2004). Cyclic loading may result in the development of positive pore water pressure for saturated materials, which would reduce the effective stress and deformation resistance, and consequently reduce the stiffness of materials (Araya 2011). The resilient modulus of fine graded materials is more sensitive

to water content than coarse graded materials (Sweere 1990).

Waste rocks with angular to subangular shaped particles generally show better load spreading properties and a higher resilient modulus (Lekarp et al. 2000a). On other hand, the resilient modulus of natural gravel with rounded particles is higher than that of crushed materials at the same density level, and one of the possible reasons is that rounded gravel particles are easier to rearrange and to reach a more stable structure (Janoo and Bayer II 2001).

Freeze-thaw cycles can lead to waste rocks degradation, and even a small number of freeze-thaw cycles may lead to a significant reduction in resilient modulus (Bozyurt et al. 2013). The effect of freeze-thaw cycles on resilient modulus is more significant when larger percentage of fine particles are in aggregates (Simonsen et al. 2002). Dense materials tend to dilate under freeze-thaw cycles, while loose materials are densified under freeze-thaw cycles and may show an increase in resilient modulus (Liu et al. 2018).

2.5.3 Descriptive models

Several mathematical procedures for describing the stress dependence of resilient modulus using various stress variables were developed. A great majority of the models found are based on simple curve-fitting procedures, using the data from laboratory repeated load triaxial tests.

One approach in dealing with the effect of stress on resilient modulus is the expression of resilient modulus as a function of the sum of the principal stresses, or bulk stress, which is known as two-parameter model or M_R-θ model (Seed et al. 1967):

$$M_R=k_1\theta^{k_2} \text{ or } M_R=k_1\left(\frac{\theta}{p_a}\right)^{k_2} \quad 2.25$$

Where k_1 and k_2: regression constants; p_a: the reference stress/atmospheric pressure (100 kPa); θ: the bulk stress, $\theta=\sigma_1+\sigma_2+\sigma_3=\sigma_1+2\sigma_3=3\sigma_3+\sigma_d$, kPa.

M_R-θ model assumes a constant Poisson's ratio, which is then used to calculate radial strain. However, Poisson's ratio is not a constant and varies with applied stresses, so this model may not always be reliable (Lekarp et al. 2000a). The major limitation of the M_R-θ model is that it does not account for shear stresses and shear strains during loading (Uzan 1985). Also, M_R-θ model is not capable of predicting volumetric strain and dilative behavior of granular materials under repeated triaxial loading (Senadheera et al. 1995).

Uzan (1985) developed a separate three-parameter model for granular materials that accounts for both confining pressure and deviator stress:

$$M_R=k_1\left(\frac{\theta}{p_a}\right)^{k_2}\left(\frac{\sigma_d}{p_a}\right)^{k_3} \quad 2.26$$

Where k_1, k_2, and k_3: regression coefficients; σ_d: deviator stress, kPa. Uzan model is reliable to describe the resilient modulus behavior of dense-graded materials (Uzan 1985).

Uzan model was modified by replacing the deviator stress term with an octahedral shear stress term. The bulk stress and octahedral shear stress terms in the model are normalized using atmospheric pressure (Witczak and Uzan 1988):

$$M_R=k_1 p_a\left(\frac{\theta}{p_a}\right)^{k_2}\left(\frac{\tau_{oct}}{p_a}\right)^{k_3} \quad 2.27$$

Where τ_{oct}: the octahedral shear stress, deviator stress, $\tau_{oct}=(\sqrt{2}/3)(\sigma_1-\sigma_3)$, kPa; k_1, k_2, and k_3: regression coefficients.

The Mechanistic-Empirical Pavement Design Guide (MEPDG) (NCHRP 2004) proposed a modified version of the Witczak and Uzan model (1988) to characterize the resilient modulus of the unbound base, sub-base, and subgrade layers, as follows:

$$M_R=k_1 p_a\left(\frac{\theta}{p_a}\right)^{k_2}\left(\frac{\tau_{oct}}{p_a}+1\right)^{k_3} \quad 2.28$$

Huurman (1997) proposed a four-parameter model based on M_R-θ model, and the model takes into account principal stresses:

$$M_R=k_1\left(\frac{\sigma_3}{p_a}\right)^{k_2}\left[1-k_3\left(\frac{\sigma_1}{\sigma_{1f}}\right)^{k_4}\right] \quad 2.29$$

Where k_1, k_2, k_3, and k_4: regression coefficients; σ_1: major principal stress, kPa; σ_3: minor principal stress, kPa; σ_{1f}: major principal stress at failure, kPa. This model is reliable to describe the resilient behavior of unbound granular materials at high stress level that close to failure, but it cannot describe an increment of resilient modulus with an increasing deviator stress but far from failure (Araya 2011).

The resilient modulus of unbound aggregates is not only stress-dependent but also moisture-dependent. One resilient model employing an environmental factor to represent the moisture dependence was proposed in the current mechanistic-empirical pavement design (AASHTO 2008):

$$\log\frac{M_R}{M_{Ropt}}=a+\frac{b-a}{1+exp\left[\ln\frac{-b}{a}+k_m\cdot(S-S_{opt})\right]} \quad 2.30$$

Where M_{Ropt}: resilient modulus at reference condition; a: minimum of $\log(M_R/M_{Ropt})$; b: maximum of $\log(M_R/M_{Ropt})$; k_m: regression parameter; S-S_{opt}: variation of degree of saturation, expressed in decimal.

Other resilient modulus models have been proposed considering the saturation factor and the matric suction to reflect the moisture dependence (Lytton 1996; Gu et al. 2014):

$$M_R=k_1P_a\left(\frac{\theta-3\theta_w f h_m}{P_a}\right)^{k_2}\left(\frac{\tau_{oct}}{P_a}\right)^{k_3} \quad 2.31$$

Where θ_w: volumetric water content; h_m: matric suction in the aggregate matrix; f: saturation factor, $1\le f\le 1/\theta_w$. The matric suction h_m should be determined in discriminating different moisture contents.

These models are widely used to describe the resilient modulus of pavement materials in the literature. The applicability of these models to waste rocks was evaluated, and M_R-θ model and MEPDG model were used to fit the measured resilient modulus of waste rocks in this study.

2.5.4 Predictive models

The measurement of resilient modulus in the laboratory or field are generally complex, time consuming, and costly. The coarse-grained waste rocks increase the measurement difficulty since the particular instruments are needed in this case. The resilient modulus prediction models would be beneficial to reduce costs and ensure optimal pavement performance. Several prediction models were proposed to estimate the resilient modulus of waste rocks based on relatively simple properties such as CBR, LFWD modulus, and dynamic cone penetration index DCP.

AASHTO (1984) proposed a model to estimate the resilient modulus based on CBR of pavement materials:

$$M_R=17.63\mathrm{CBR}^{0.64} \tag{2.32}$$

Two models similar with AASHTO model were also developed based on CBR, and these models are widely used for mine haul roads design (Thompson et al. 2019):

$$M_R=21.1\mathrm{CBR}^{0.64} \quad (\mathrm{CBR}<15) \tag{2.33}$$

$$M_R=19\mathrm{CBR}^{0.68} \quad (\mathrm{CBR}>15) \tag{2.34}$$

Gudishala (2004) proposed three models to estimate resilient modulus based on Geogauge modulus, LFWD modulus, and dynamic cone penetration index DCP of base course and subgrade materials:

$$M_R=20.3(E_{GEO})^{0.54} \tag{2.35}$$

$$M_R=73.3(E_{LFWD})^{0.25} \tag{2.36}$$

$$M_R=425.4(\mathrm{DCP})^{-0.25} \tag{2.37}$$

All these models are expressed as a simple power function, but the in-situ or laboratory CBR or DCP tests are still needed. They were developed through fitting limited data, which can affect the prediction accuracy to waste rocks. Also, resilient modulus is a stress-dependent property rather than a constant (see section 2.5.2 and 2.5.3), so these regression models cannot predict the resilient modulus behavior of waste rocks under different stress conditions.

Machine learning is also used to develop the predictive models for resilient modulus based on physical properties and stress conditions in recent years (Table 2.3). Different machine learning algorithms including BPNN, SVR, GA, and ANFIS were used to develop the predictive models. The machine learning models typically have reliable prediction accuracy ($R^2 > 0.85$) for different materials (from subgrade soils to base aggregates). The prediction performance is influenced by the number of used datasets, and the bigger dataset generally can better train and test the machine learning models. However, the applicability of these models to waste rocks is uncertain because of the different minerology.

Table 2.3: Some machine learning models for predicting resilient modulus for different pavement materials reported in the literature, different algorithms, input features, and number of datasets were used for these models.

References	Technic	Input	No. of datasets	Material	R^2
Oskooei et al. (2020)	BPNN	BR, DR, SR, OMC, q_u, σ_c, σ_d	645	Recycled aggregates	0.96
Ghorbani et al. (2020b)	BPNN	γ_d, w, q_c, f_s	124	Cohesive subgrade soils	0.99
Ghorbani et al. (2020a)	ANN-GA	LL, PI, P#200, w_{opt}, w, S_r, qu, σ_3, σ_d	283	Cohesive subgrade soils	0.97
Ghorbani et al. (2020b)	BPNN, SVR	N_{FT}, σ_3, σ_d, Mat	150	Demolition wastes	0.997
Kaloop et al. (2019)	BPNN, LSSVM	RCM, θ/p_a, τ/p_a	128	Construction and demolition waste	0.887
Ren et al. (2019)	BPNN	PI, γ_{dmax}, w, No., σ_c, σ_d	2120	Subgrade soil	0.90
Saha et al. (2018)	BPNN	P#3/8, P#200, PL, PI, w_{opt}, γ_{dmax}, TMC, g_s, Ψ	779	Plastic and nonplastic base materials	0.90
Sadrossadat et al. (2016)	ANFIS	P#200, LL, PI, w_{opt}, w, S_r, q_u, σ_3, σ_d	418	Cohesive Ohio soils	0.973

Kim et al. (2014)	BPNN	P#10, #40, #60, #200, Clay, Swell, Shrink, ρ_{dmax}, w_{opt}, LL, PI, EI, σ_1, σ_3, θ	27	Subgrade soils	0.86
Nazzal and Tatari (2013)	ANN-GA	P#4, P#40, w, P#200, w_{opt}, ρ_d, LL, ρ_{dmax}	-	Subgrade soils	0.92
Park HI et al. (2009b)	BPNN	ρ_{dmax}, C_U, P#200, σ_3, σ_d	272	subgrade soils and subbase materials	0.982

Where BPNN: backpropagation neural network; ANN: artificial neural network; GA: genetic algorithm; SVR: support vector regression; LSSVM: least square support vector machine; ANFIS: adaptive neuro-fuzzy inference system; BR: binder ratio, -; q_u: unconfined compression strength, kPa; σ_c: confining pressure, kPa; σ_d: deviatoric stress, kPa; ρ_d: dry density, kg/m^3; w: gravimetric water content, %; q_c: cone tip resistance, -; f_s: sleeve friction resistance, -; LL: liquid limit, %; PI: plastic index, %; P#4, #10, #40, #60, #200, and #3/8: percentage of soil particles passing through #4, #10, #40, #60, #200, and #3/8 sieve, respectively, %; w_{opt}: optimum water content, %; S_r: degree of saturation, %; G: gravel percentage, %; S: sand percentage, %; FC: fines content, %; γ_{dmax}: maximum unit dry weight, -; RCM: recycled clay masonry; No.: number of F-T cycles, -; g_s: gradation scale parameter, -: Ψ: shape parameter, -; G_s: specific gravity, -; C_U: coefficient of uniformity, -; C_C: coefficient of curvature, -; Q, Fel, Ca, C, and A: the proportions of quartz, feldspar, calcite, corund, and amorphous minerals, respectively; EI: erosion index, -; θ: bulk stress, kPa.

2.6 Permanent deformation of waste rocks

The permanent deformation of waste rocks can be caused by compaction, crushing and material migration under traffic loading (Tholen 1980; Lekarp 1999). The development of permanent deformation in unbound granular materials typically consists of two phases (Erlingsson et al. 2017). The permanent strain increases rapidly with loading cycles in the initial phases. This phase is usually characterized as post-compaction, which is accompanied by densification of the material, reduction in pore volume and volumetric change of the material (Werkmeister et al. 2004; El-Basyouny et al. 2005). In the second phase, the deformation rate becomes more or less constant and is dominated by volume change (Werkmeister et al. 2004). The shakedown concept is typically used to describe the behavior of pavement materials under repeated loading (Werkmeister et al. 2001; Werkmeister et al. 2004). Based on the shakedown theory, the evolution of permanent strain

with loading cycles can be classified into three categories (A, B or C). Werkmeister (2003) suggested the following criteria to define the shakedown boundaries based on the repeated load triaxial test results, which have been adopted in the European standard *Cyclic Load Triaxial Test for Unbound Mixtures* (EN 13286 2004). The shakedown categories of unbound granular materials depend on the applied stress levels (Werkmeister et al. 2004):

Range A (plastic shakedown): $(\varepsilon_p^{5000}-\varepsilon_p^{3000})<0.045\times10^{-3}$

Range B (plastic creep): $0.045\times10^{-3}<(\varepsilon_p^{5000}-\varepsilon_p^{3000})<0.4\times10^{-3}$

Range C (incremental collapse): $(\varepsilon_p^{5000}-\varepsilon_p^{3000})>0.4\times10^{-3}$

Where ε_p^{5000} and ε_p^{3000}correspond to the accumulated permanent strains measured at the 5000^{th} and 3000^{th} loading cycles during the repeated load triaxial tests.

In range A, the post-compaction is completed, and the material becomes stable with no further permanent strain after a finite number of load applications. In range B, the permanent strain rate decreases with the number of loads and progressively becomes very low and nearly constant. Yet, the permanent strain continues to accumulate but at a very slow rate. In range C, the permanent strain decreases very slowly compared to ranges A or B, and permanent strain continues to accumulate with load applications, ultimately leading to failure (Werkmeister 2003; EN 13286 2004; Werkmeister et al. 2004). The shakedown categories are often used in pavement analysis and design (Collins and Boulbibane 1998, 2000; Tao et al. 2010). For highway engineering, materials falling in range A can be used provided the total accumulated strain is sufficiently small, materials in range B may be permitted for a limited number of load cycles (e.g. short term roads) while materials in range C are not authorized (Werkmeister et al. 2004). However, the applicability of shakedown theory and the corresponding criteria to haul roads need further investigations because of the specificities of haul roads, such as high stress levels, low-volume traffic, short-service-life, and relatively low running speed of mining trucks.

2.6.1 Measurement of permanent deformation

Permanent deformation of pavement materials are generally measured using multistage repeated load triaxial tests (EN 13286 2004). The specimen is exposed to a series of consecutive stress paths of varying magnitudes to determine the maximum stress levels which should not be exceeded to avoid the development of excessive permanent deformations (EN 13286 2004). Applied stress levels in repeated load triaxial tests should cover the stress range to which the material will be subjected in the field (EN 13286 2004). There are two sets of stress levels (low stress level LSL and high stress level HSL) proposed in EN 13286-7 standard, the stress levels are divided into five sequences, with each sequence containing 5 or 6 stress paths with a constant confining pressure and different deviator stresses. Each stress path is applied for at least 10000 cycles. However, these two stress levels are developed for highways, and they are significantly lower than the stress states observed in mine haul roads.

The repeated load triaxial test apparatus shall be able to apply the required cyclic loading to a cylindrical specimen with a diameter larger than 5 times the maximum particle size of the material, and a height twice the diameter (EN 13286 2004). The usual specimen diameter is lower than 150 mm because of the limitation of test instruments. Few studies developed larger repeated load triaxial testing apparatus to measure the permanent deformation behavior of coarse-grained specimens, such as 300 mm in diameter and 600 mm in height (Nair and Latha 2012, 2015; Cao et al. 2021). In this study, a series of multistage repeated load triaxial tests with 150 mm and 300 mm specimen diameter were carried out on waste rocks to evaluate the permanent deformation behavior.

The most traditional technique for measuring rut depth (permanent deformation) in the field is the straightedge method (Wang 2005). This method is simple and accurate if proper technique is used, but it is time-consuming and difficult to perform especially with limited traffic control (Hoffman and Sargand 2011). The mechanical profilometer or transverse profile beam also can be used for

measuring pavement surface permanent deformation in the field (Hoffman and Sargand 2011). This method can level each profile in a series to produce an interpolated, three-dimensional pavement profile (Hoffman and Sargand 2011). Laser rut measurement system can give immediate and accurate transverse profiles used for the detection and characterization of pavement rutting (Wang 2005; Hoffman and Sargand 2011). The measured rutting measurement data can be viewed in real time, and this test method can be carried out at a normal traffic speed (Wang 2005; Hoffman and Sargand 2011).

Heavy vehicle simulator, one type of accelerated pavement tests, can be used to evaluate the performance (including permanent deformation) of full-scale pavements in an accelerated manner, which can fill the important gap between mechanistic-empirical design models using laboratory materials testing characterization and real, long-term pavement performance monitoring and analysis data (Du Plessis et al. 2018).

2.6.2 Factors affecting permanent deformation

Lekarp (2000b) summarized the research on permanent deformation, and it was reported that permanent deformation of granular materials is affected by several factors such as stress condition, number of loading cycles, water content, density, and gradation.

Stress condition is one of the most important factors affecting the permanent behaviour of granular materials (Lekarp et al. 2000b). Permanent strain generally increases with deviator stress, while it decreases as confining pressure increases (Morgan 1966). The permanent deformation of waste rocks is also directly related to the ratio of deviator stress to confining pressure (Lashine et al. 1971; Brown and Hyde 1975). Some studies tried to explain the permanent deformation using the ultimate shear strength, and the static failure line was considered as a boundary for permanent deformation (Gidel et al. 2001; Korkiala-Tanttu 2005). However, Lekarp and Dawson (1998) argued that

ultimate shear strength and stress levels that cause sudden failure were of no interest for the accumulation of permanent strain, since failure in granular materials under repeated loading was a gradual process and not a collapse as in static failure tests.

The development of permanent deformation of granular materials is a gradual process with number of loading cycles, and the significance of number of loading cycles has been mentioned in the literature. The rate of increasing of permanent strain of waste rocks decreases significantly after a certain number of loading cycles, and an equilibrium state can be established in this case (Brown and Hyde 1975). This stabilization of granular materials generally can be achieved at low stress levels, while high stress levels can result in a continuous increasing of permanent strain (Barksdale 1972).

Water content also can affect permanent deformation, and a high degree of saturation could result in high pore pressure and low effective stress, and consequently low permanent deformation resistance (Barksdale 1972; Lekarp et al. 2000b). An increase in water content may result in a large increase of permanent strain even without generation of excess pore water pressure because of the lubricating effect of water in granular materials (Thom and Brown 1988). The increase of permanent deformation caused by wetting was also observed in the field (Maree et al. 1982).

Permanent deformation resistance generally increases with density (Lekarp et al. 2000b). The increase of compaction effort can result in significant decrease of permanent deformation (Allen 1973). The effect of density on permanent deformation may be more significant for angular aggregates than rounded aggregates since rounded aggregates have higher initial density for the same compaction effort (Holubec 1969).

The uniform grading waste rocks without compaction generally have lower permanent deformation, while the effect of gradation on permanent deformation is limited when the materials are heavily compacted (Thom and Brown 1988). The permanent deformation could increase as the fines content increases (Thom and Brown 1988). Waste rocks with sharp particle edges or angular

particles are generally tended to have more grain abrasion, and thus high resistance to permanent deformation, while rounded particles tended to slip easily (Janoo 1998; Araya 2011).

The climate conditions also can affect the permanent deformation behaviour of waste rocks. Permanent deformation generally increases gradually with the number of freeze-thaw cycles, and the first several cycles have the greatest impact (Li et al. 2013; Lu et al. 2019). The unbound granular materials at high water content subjected to freeze-thaw cycles may fail after thousands of loading cycles (Bilodeau et al. 2011).

2.6.3 Descriptive models

Several models were proposed in the literature to describe the permanent strain of unbound granular materials. These models are usually expressed as a function of number of loading cycles and other parameters such as deviator stress and mean bulk stress. Different modeling techniques from the literature and their mathematical expressions are reviewed in this section.

Barksdale (1972) carried out a comprehensive study of the permanent behavior of base course materials using repeated load triaxial tests. Barksdale found that the accumulated permanent strain is proportional to the logarithm of the number of loading cycles and proposed the lognormal model:

$$\varepsilon_p = a + b\log(N) \tag{2.38}$$

Where ε_p: permanent strain, -; a and b: regression coefficients, -; N: number of loading cycles, -.

Sweere (1990) studied the long-term permanent response of granular materials after 10^6 loading cycles using repeated load triaxial tests. It was found that the lognormal model cannot fit the test results well, and Sweere proposed a log-log model for many loading cycles:

$$\varepsilon_p = aN^b \tag{2.39}$$

Wolff and Visser (1994) performed a series of full-scale heavy vehicle simulator tests to study the

permanent behavior after several million loading cycles. The test results showed that the permanent deformation can be divided into two phases, i.e., the initial phase of up to 1200000 loading cycles with rapid development of permanent deformation and constantly diminishing rate of increase. Sweere model failed to give a reliable fitting of permanent strain in this case, and Wolff and Visser developed a different stress-strain model with three regression coefficients *a*, *b*, and *c*:

$$\varepsilon_p=(cN+a)(1-e^{-bN}) \tag{2.40}$$

Barksdale model, Sweere model, and Wolff and Visser model are relatively simple because these models only relate the permanent strain to the number of loading cycles. stress condition is one of the most important factors influencing the permanent behavior of granular materials (Lekarp et al. 2000b), but these models do not take it into account, which may limit their applicability for fitting permanent strain caused by different stress paths. Some models were therefore proposed to combine the influence of the number of loading cycles and stress conditions on permanent strain (Gidel et al. 2001; Korkiala-Tanttu 2005; Rahman and Erlingsson 2015a), and these models are essentially improvements over previous models (Erlingsson and Rahman 2013).

Gidel et al. (2001) proposed a model that combines the stress conditions, shear strength parameter, and the number of loading cycles:

$$\varepsilon_p=\varepsilon^0\left(1-\left(\frac{N}{100}\right)^{-B}\right)\left(\frac{L_{max}}{p_a}\right)^{u}\left(m+\frac{s}{p_{max}}-\frac{q_{max}}{p_{max}}\right)^{-1} \tag{2.41}$$

Where ε^0, B, and u: regression material parameters, -; p_{max} and q_{max}: the maximum applied hydrostatic stress and deviator stress, respectively, kPa; p_a: the reference stress, 100 kPa; m and s: the slope and the intercept of the Mohr-Coulomb failure line in the mean bulk stress p - deviator stress q space, respectively, and they are determined using static triaxial tests; L_{max} in the model can be calculated using the following equation:

$$L_{max}=\sqrt{p_{max}^2+q_{max}^2} \tag{2.42}$$

Korkiala-Tanttu (2005) developed a model to describe the development of permanent strain using a power law function of the number of loading cycles. The impact of stress condition on permanent strain is taken into account in this model by introducing the shear stress ratio:

$$\varepsilon_p = CN^b \frac{R}{A-R} \quad 2.43$$

Where C and b: regression parameters, -; A: the maximum theoretical shear stress ratio, and it is recommended to be 1.05; R is the shear stress ratio defined as follows:

$$R = \frac{q}{q_f} \quad 2.44$$

$$q_f = mp + s \quad 2.45$$

Rahman and and Erlingsson (2015a) proposed a model that directly takes into account the effect of stress condition on permanent strain by introducing the term S_f:

$$\varepsilon_p = aN^{bS_f} S_f \quad 2.46$$

Where a and b: regression parameters associated with the material, and the term S_f describes the effect of stress condition on permanent strain, and it is expressed as:

$$S_f = \frac{(q/p_a)}{(p/p_a)^{\alpha}} \quad 2.47$$

Where α: a parameter determined using regression analysis, and it is generally recommended to be 0.75.

However, the permanent deformation models mentioned above were initially developed to fit permanent strain of a single stress path in repeated load triaxial tests. The models can be extended using time hardening approach to fit the accumulated permanent strain measured by multistage repeated load triaxial tests. Time hardening approach has been widely used for fitting accumulated permanent strain through considering the effect of stress history (Lytton et al. 1993; Zhou et al. 2010; Erlingsson and Rahman 2013; Mohammadinia et al. 2020; Li et al. 2021). More details about

the application of time hardening approach for permanent deformation models can be found in section 3.6. The applicability of these models (extended using time hardening approach) to waste rocks was evaluated, and the Rahman and Erlingsson model was particularly used to fit all the measured permanent deformation data in this study.

2.6.4 Predictive models

Multistage repeated load triaxial tests can be time consuming, sophisticated, and expensive, especially when up to 30 stress paths are used, each applied for 10000 cycles (EN 13286 2004; Saberian et al. 2020). Waste rocks also require larger and more specific equipment to accommodate larger particles and greater stresses (Mishra et al. 2013; Qian et al. 2014; Sun et al. 2014). Conducting lots of permanent deformation tests may result in delay in the progress of the project and lead to escalation of the project cost. However, the prediction of permanent deformation is a very complex process and the development of prediction model based on the laws of geomechanics is very difficult because of highly heterogeneous nature of aggregate particles and testing environments (Ullah et al. 2020). Therefore, there are very few prediction models available that is expressed as a function of easily determinable parameters. The common used method is to calibrate the regression parameters of the descriptive models (see section 2.6.3) by fitting test results, and then using them to extrapolate the permanent deformation of soils subjected to different stress conditions and loading cycles (Rahman and Erlingsson 2015a; Erlingsson et al. 2017; Zhang, Peng, et al. 2020). However, this prediction method still needs to conduct some permanent deformation tests, and the accuracy of this method heavily relies on the fitted experimental data.

Machine learning method is therefore used to develop prediction models for permanent deformation (Ullah et al. 2020). Artificial neural network (ANN) is the most common used algorithm in the literature, for example, Ghorbani et al. (2020a) developed an artificial neural network model for predicting permanent strain of demolition wastes. The machine learning models

usually exhibit reliable prediction accuracy. However, the materials used in the literature are different from waste rocks, which prevents a direct application of the machine learning models to waste rocks in this study.

2.7 Knowledge frontiers

The shear strength, CBR, resilient modulus, and permanent deformation are important properties for the mine haul road design (section 2.2.2). However, the literature review presented above has shown that relevant research on the mechanical properties of waste rocks from hard rock mine is relatively limited, especially for mine haul roads that are subjected to significantly different traffic loading compared to highways. The present project therefore focused on the measurement (in the laboratory), the description, and the prediction of the mechanical properties of waste rocks for mine haul roads. Also, the existing laboratory test procedures and standards (sections 2.5.1 and 2.6.1) were evaluated and modified to better apply to waste rocks. The impacting factors on the mechanical properties of waste rocks were also quantified. The results of this study will be helpful to complement and specify the abundant literature summarized above, and more precisely to understand the mechanical behaviour of waste rocks under heavy mine truck loading, to improve the performance of mine haul roads, and to valorise waste rocks in such infrastructures.

CHAPTER 3 EXPERIMENTAL METHODOLOGY

3.1 Sampling and origin of waste rocks

Canadian Malartic Mine is an open pit gold mine located in the Abitibi region, in Quebec province, Canada. Mining operations produce large quantities of waste rocks, and the waste rocks have been used to build the mine haul roads at this mine. Waste rocks are also crushed because the original waste rock particles can exceed 1 m which limits its valorization in practice. A total of 1.5 tons (4 barrels) of waste rocks were sent to Polytechnique Montreal in August 2019. The received materials were categorized into two groups, i.e., 2 barrels were crushed waste rocks with 25 mm maximum particle size and 2 barrels were uncrushed waste rocks with 60 mm maximum particle size. Received waste rocks were wet and heterogeneous, and were therefore first dried (at room temperature, using fans) and sieved into different portions for their storage and the preparation of homogeneous samples in the laboratory. The crushed and uncrushed waste rocks are generally used to construct the wearing course and base/subbase course, respectively (Figure 3.1).

Particle shape index test, mineralogy test, specific gravity, and modified Proctor test were carried out on crushed waste rocks to determine the basic physical properties. CBR tests (standard and repeated load) and triaxial tests (monotonic and repeated load) were conducted on crushed waste rocks to evaluate the applicability of test approaches and standards, and the effect of gradation and climatic factors on the mechanical properties (CBR, shear strength, stiffness, and permanent deformation). Large-scale triaxial tests (monotonic and repeated load) were carried out on uncrushed waste rocks to study the mechanical properties of coarse-grained materials, and the effect of maximum particle size, gradation, compaction effort, and water content.

Figure 3.1: Mine haul roads at Canadian Malartic Mine (2019); the wearing course was constructed using crushed waste rocks and the base course was constructed using uncrushed waste rocks.

3.2 Characterization of waste rocks

3.2.1 Particle size distribution

The particle size distribution curves of both crushed and uncrushed waste rock samples were determined using sieving (ASTM C136/C136M, 2019) (Figure 3.2). The mesh sizes of the sieves used were 0.075 mm, 1.19 mm, 2 mm, 2.38 mm, 3.36 mm, 4.75 mm, 8 mm, 9.5 mm, 14 mm, 19 mm, 25 mm, and 40 mm.

Crushed waste rocks contained around 69% of gravel (> 4.75 mm), 27% of sand (< 4.75 mm) and 4% of fines (< 0.075 mm), and were therefore classified as a poorly graded gravel (GP) (USCS;

(ASTM D2487 2017). Particles larger than 19 mm accounted for around 5% in weight in crushed waste rocks. The D_{10} and C_U of crushed waste rocks were 0.4 mm and 25.5, respectively.

Uncrushed waste rocks were composed of 80% of gravel, 15% of sand and 5% of fines, and they were also classified as a poorly graded gravel corresponding to the symbol GP. The D_{10} and C_U of uncrushed waste rocks were 0.7 mm and 38.6, respectively.

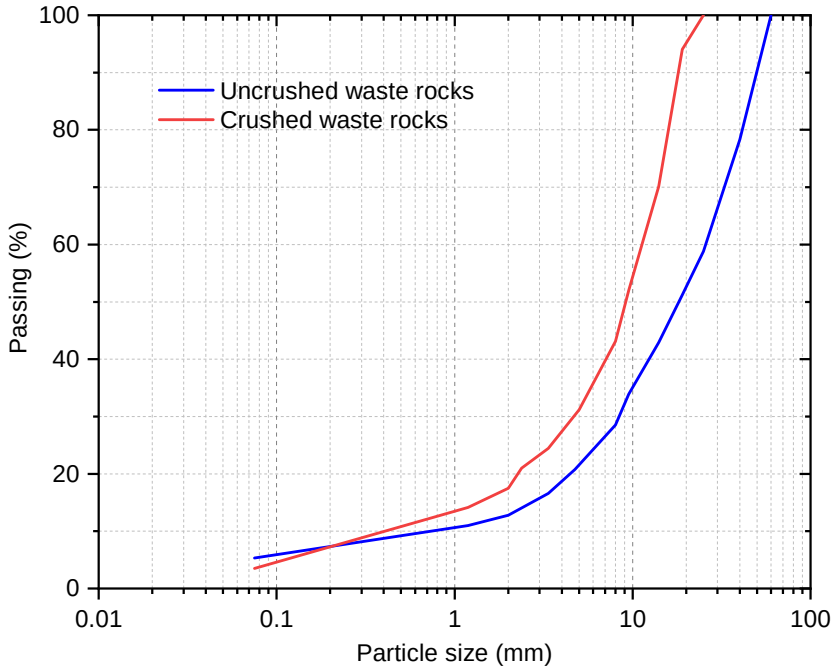

Figure 3.2: Particle size distributions of crushed and uncrushed waste rocks, and the maximum particle size for crushed and uncrushed waste rocks were 25 mm and 60 mm, respectively.

3.2.2 Particle shape

The Elongation index and Flakiness index of coarse particles (> 6.3 mm) were measured using length gauge and thickness gauge according to IS 2386 standard (IS 2386 1963). The elongation index represents the percentage by weight of particles whose greatest dimension (i.e., length) is

greater than 1.8 times the mean dimension (mean sieve size). The flakiness index corresponds to the percentage by weight of particles whose smallest dimension (i.e., thickness) is less than 0.6 times the mean dimension (mean sieve size). The measured Elongation index and Flakiness index of crushed waste rocks were 38.56±1.62% and 34.95±2.08%, respectively.

3.2.3 Mineralogy

The mineralogy of the crushed waste rocks was measured using X-ray diffraction (XRD; Bruker A.X.S. Advance D8 at UQAT laboratory). Three samples were prepared and analyzed. Waste rocks were mainly composed of quartz (23-28%), albite (34-43%), muscovite (10-12%), chlorite (6-8%), corundum (5-8%), and diopside (5-8%). Waste rocks also contained a small fraction of sulfides (1% of pyrite) but were considered non-acid generating because of the presence of a significant buffering capacity (Tremblay and Hogan 2001; Golder 2019). The detailed test results can be found in APPENDIX A.

3.2.4 Specific gravity

The specific gravity of crushed waste rock particles smaller and larger than 4.75 mm was measured using ASTM C127 (2015) and ASTM D854 (2014) standards, respectively. The measured specific gravity of particles larger and smaller than 4.75 mm was 2.71 and 2.75, respectively. The water absorption of particles larger than 4.75 mm was also estimated during the specific gravity test, and it was 0.41%.

3.2.5 Compaction properties

The moisture-density relationship of crushed waste rocks was measured using modified effort Proctor compaction tests (ASTM D1557-12e1, 2012). Particles larger than 19 mm were removed (sieved) to accommodate the sample to the 152.4 mm diameter Proctor mold. The maximum attainable degree of saturation was around 85%; above, water would leak out of the sample during compaction. The optimum water content was 5.6%, for a corresponding maximum dry density of 2334 kg/m^3 (Figure 3.3).

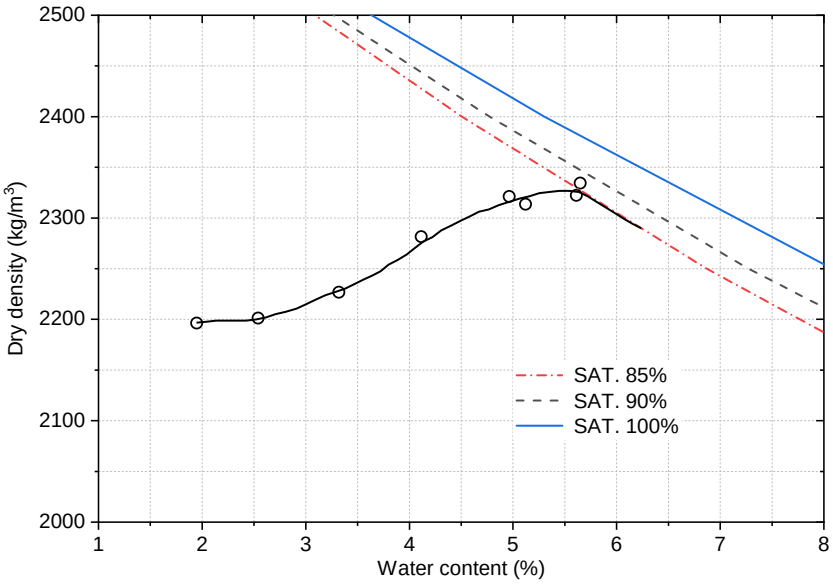

Figure 3.3: The modified Proctor test results (moisture-density relationship) for crushed waste rocks; the optimum water content and maximum dry density was 5.6% and 2334 kg/m^3, respectively.

3.3 California Bearing Ratio (CBR) tests

3.3.1 Standard CBR tests (ASTM D1883)

CBR tests were conducted using a 100 kN loading frame. A 50 kN load cell, located under the frame beam, was used to measure applied load, and a 50 mm linear variable differential transformer (LVDT) was used to measure displacements (Figure 3.4). A 49.63 mm diameter circular plunger penetrated a compacted specimen of 152.4 mm diameter and 127 mm height. The penetration rate of plunger was maintained constant at 1.3 mm/min. The tests continued until 10 mm of penetration or until the load limit of the equipment was reached (with a minimum of 5.08 mm penetration). The stress corresponding to a penetration of 5.08 mm was then compared to the standard value 10 MPa given in the ASTM D1883 standard (2016) to determine the CBR of crushed waste rocks.

In this research, four CBR tests were carried out to evaluate the effect of wetting-drying cycles on CBR value of crushed waste rocks. The particles larger than 19 mm were removed (sieved) to accommodate the CBR mold size (diameter = 152.4 mm). All the CBR specimens were prepared with 4% of initial gravimetric water content, and using modified compaction effort (ASTM D1883 2016). Specimens were subjected to 0, 5, 10, and 15 wetting-drying cycles. One wetting-drying cycle corresponded to the immersion of the specimen in water (allowing the free access of water to the top and bottom of specimens) at room temperature (20 ℃) for 72 hours followed by drying at room temperature using a fan for 72 hours. The specimens were subjected to a surcharge load of 4.54 kg during wetting-drying cycles. Swelling during wet-dry cycles was recorded. More details about these CBR tests can be found in Chapter 8.

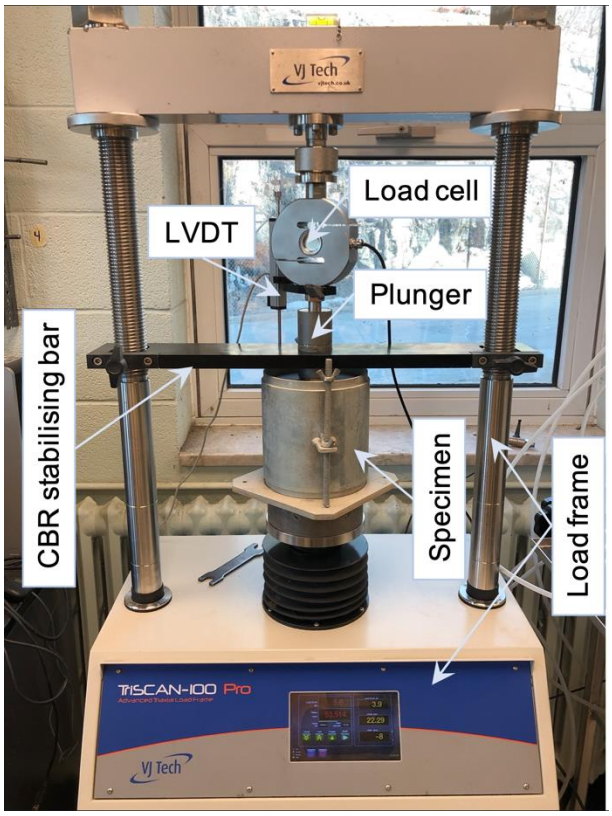

Figure 3.4: CBR test apparatus in Research Institute of Mines and Environment (RIME); it consists of a loading frame, linear variable differential transformer (LVDT), load cell, plunger (or piston), stabilizing bar, and a waste rock specimen.

3.3.2 Repeated load CBR test

Repeat load CBR tests were carried out using the same apparatus (including the plunger and mold) as the standard CBR tests (section 3.3.1) to estimate stiffness and permanent deformation of crushed waste rocks (Figure 3.4). The vertical deformation was considered equal to the vertical displacement of the plunger during loading and unloading and measured by the LVDT. The axial vertical load was measured using the load cell. Repeated load CBR tests were performed in the load-controlled mode. A total of 39 repeated load CBR tests were carried out in this project.

Stiffness (equivalent modulus): the stiffness of crushed waste rocks was evaluated using 32

repeated load CBR tests. Two sets of cyclic loading sequences were defined for repeated load CBR tests to study the stiffness of crushed waste rocks, i.e., a low stress level (LSL) sequence developed for civil engineering (highways) (AASHTO T307 2017) and a high stress level (HSL) specifically developed in this study to represent mining engineering applications (mine haul roads) more realistically (Table 3.1). The LSL cyclic loading sequences were based on the AASHTO T307 standard procedures developed for repeated load triaxial tests (AASHTO T307 2017), and the HSL cyclic load sequences were based on the typical stress levels observed on mine haul roads. A total of 100 cycles were applied for each stress path. The tested specimens were prepared with different initial gravimetric water contents (2%, 3%, 4%, 5%, 6%, 7%, and 8%) to investigate the impact of dry density on stiffness (Table 3.2). Different compaction energies were also used to prepare specimens, i.e., standard effort (STD), 600 kN-m/m^3 (ASTM D698 2012) and modified effort (MOD), 2700 kN-m/m^3 (ASTM D1557 2012). An alternative compaction method (MOD 81) was also used in this study. MOD 81 compaction used a modified effort hammer (44.48 N), but with 81 blows per layer (instead of 56 blows; the rest of the test being identical to ASTM D1557-12e1 (2012). The objective of MOD 81 was to simulate a higher compaction energy (3905 kN-m/m^3) which was more representative of field conditions. The influence of contact stress on tested stiffness was studied by using 2%, 5%, 10%, and 15% of maximum axial stress (Table 3.2). The impact of loading frequency on measured stiffness of crushed waste rocks was studied by using different loading frequency 0.1, 0.3, 0.5, and 0.7 Hz for repeated load CBR tests. Two types of loading waveforms, i.e., haversine waveform and square waveform, were used to investigate the effect of loading waveforms on measured stiffness. Soaking and drying specimens were also prepared and tested to evaluate the stiffness corresponding to the most unfavorable field conditions in situ. The soaking and drying specimens were prepared using modified compaction effort. More details about these tests can be found in Chapter 4.

Table 3.1: Cyclic loading sequences (including different maximum axial stress MAS) used for repeated load CBR tests. Low stress level (LSL) and high stress level (HSL) correspond to the stress state for highways and mine haul roads, respectively.

LSL		HSL	
Stress path	MAS, kPa	Stress path	MAS, kPa
1	100	1	200
2	300	2	700
3	500	3	1200
4	700	4	1700
5	900	5	2200
6	1100	6	2700
		7	3200
		8	3700
		9	4200
		10	4700
		11	5200

Table 3.2: Properties of repeated load CBR tests specimens. SC: stress conditions; *w*: initial water content; Fre.: loading frequency; LW: loading waveform; CS: contact stress; LSL: low stress level; HSL: high stress level; CE: compaction effort; MOD: modified compaction effort; STD: standard compaction effort; MOD 81: compaction effort with 81 blows per layer; H: haversine waveform; S: square waveform.

No.	SC	*w* (%)	Fre. (Hz)	CS (%)	CE	LW	Duplicates
1	LSL	4	0.3	2	MOD	H	2
2	LSL	4	0.3	5	MOD	H	1
3	LSL	4	0.3	10	MOD	H	3
4	LSL	4	0.1	10	MOD	H	2
5	LSL	4	0.3	15	MOD	H	3
6	LSL	4	0.3	10	MOD	S	2
7	LSL	4	0.5	10	MOD	H	2
8	LSL	4	0.7	10	MOD	H	2
9	LSL	2	0.3	10	MOD	H	1
10	LSL	3	0.3	10	MOD	H	1
11	LSL	5	0.3	10	MOD	H	1
12	LSL	6	0.3	10	MOD	H	1

13	LSL	7	0.3	10	MOD	H	1
14	LSL	8	0.3	10	MOD	H	1
15	LSL	4	0.3	10	STD	H	1
16	LSL	4	0.3	2	MOD	S	1
17	LSL	4	0.3	10	MOD 81	H	1
18(soaked)	LSL	4	0.3	10	MOD	H	1
19(dried)	LSL	4	0.3	10	MOD	H	1
20	HSL	4	0.3	10	MOD	H	3
21	HSL	4	0.3	15	MOD	H	1

Permanent deformation: the permanent deformation behavior of crushed waste rocks was evaluated using three repeated load CBR tests. In these tests the maximum axial plunger stress varied from 100 to 4000 kPa. Specimens were compacted using modified effort 2700 kN-m/m^3 (ASTM D1883 2016) and with an initial gravimetric water content of 4%. Each stress path was applied either 6000, 3000 or 1000 times, to evaluate the permanent deformation behavior of crushed waste rocks. More details about permanent deformation tests can be found in Chapter 5.

Effect of wetting-drying cycles: the effect of wetting-drying cycles on stiffness and permanent deformation was also investigated using four repeated load CBR tests. Four specimens were prepared to evaluate the effect of wetting and drying cycles. Specimens were prepared with an initial gravimetric water content of 4%, and using modified compaction effort (ASTM D1883, 2016). The wetting and drying process was same as for standard CBR tests, i.e., the immersion of the specimen in water (allowing the free access of water to the top and bottom of specimens) at room temperature (20 ℃) for 72 hours followed by drying at room temperature using a fan for 72 hours. The specimens were subjected to 0, 5, 10, and 15 wetting and drying cycles. More details about these tests can be found in Chapter 8.

3.4 Triaxial tests

3.4.1 Monotonic triaxial test

Consolidated drained monotonic triaxial tests were carried out to measure the shear strength (peak deviator stress) of crushed waste rocks (ASTM D7181 2020). Monotonic triaxial tests were conducted following repeated load triaxial tests, so these tests were post-cyclic monotonic triaxial tests. The unpaved mine haul roads are compacted extremely in the field because of the traffic loading of heavy mining trucks. Post-cyclic monotonic triaxial tests are therefore considered appropriate to evaluate the realistic shear strength of waste rocks in haul roads. Triaxial tests were carried out using a 100 kN loading frame and 1000 kPa stress controllers. A 50 kN load cell and a 50 mm LVDT completed the setup (Figure 3.5). Specimens were 150 mm in diameter and 300 mm in height, and the waste rock particles larger than 19 mm were removed. All the specimens were prepared using modified compaction effort (2700 kN-m/m^3) (ASTM D1557 2012). Specimens were sheared at a constant axial rate of 0.015 mm/sec, and the deviator stress was recorded during shear process. A total of 23 crushed waste rocks specimens were prepared and tested to determine the Mohr-Coulomb envelope, and to assess the effect of gradation and freeze-thaw cycles on the shear strength of crushed waste rocks.

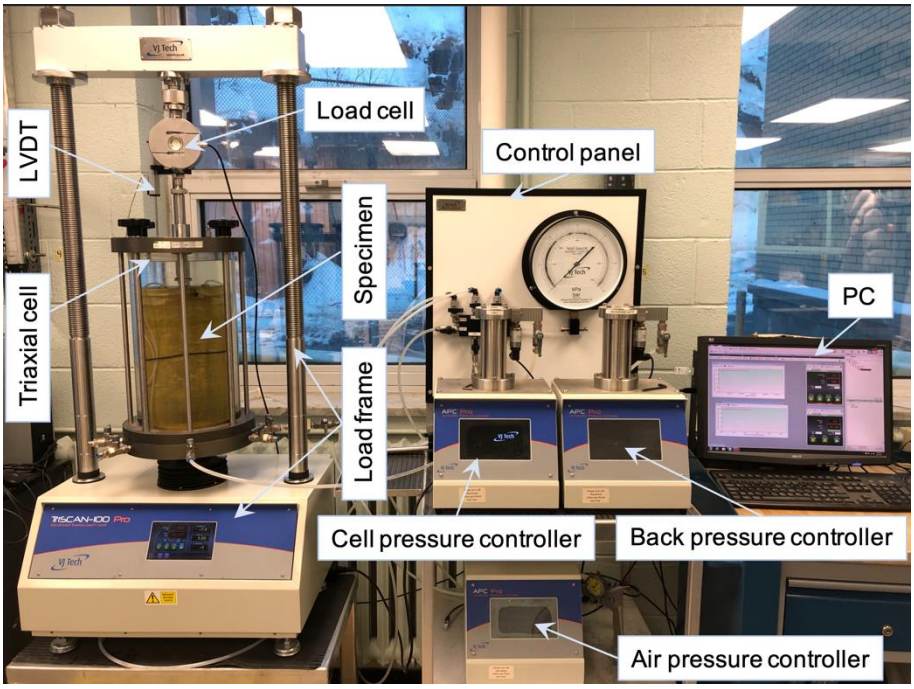

Figure 3.5: Triaxial test setup used in RIME; it consists of a loading frame, linear variable differential transformer (LVDT), load cell, triaxial cell, pressure controllers, a waste rock specimen, and a computer.

Mohr-Coulomb envelope: six monotonic triaxial tests were conducted under different confining pressures (i.e. 50 (duplicate), 100, 135, 200, and 300 kPa) to determine the Mohr-Coulomb envelope. The testing specimens were prepared at 4% initial gravimetric water content. More details about these six tests can be found in Chapter 5.

Effect of gradation: nine monotonic triaxial tests were conducted to study the effect of gradation on shear strength of crushed waste rocks under 50 kPa of confining pressure. The specimens for these nine tests were prepared at an initial gravimetric water content of 4%. Specimens' gradations were different, and the gravel-to-sand ratio and fines content were altered. Specimens' properties are summarized in Table 3.3. More details about these tests can be found in Chapter 6.

Table 3.3: Physical properties of crushed waste rocks specimens for various gradations; ρ_d: dry density; D_{max}: maximum particle size; C_U: coefficient of uniformity; C_C: coefficient of curvature; D_{60}: 60% of the soil particles are finer than this size; D_{30}: 30% of the soil particles are finer than this size; D_{10}: 10% of the soil particles are finer than this size; PG: percentage of gravel; PS: percentage of sand; GS: gravel-to-sand ratio; FC: fines content.

No.	ρ_d	D_{max}	C_U	C_C	D_{60}	D_{30}	D_{10}	PG	PS	GS	FC
	kg/m^3	mm	-	-	mm	mm	mm	%	%	-	%
1	2108	4.75	16.92	0.98	2.2	0.53	0.13	0	96.25	0	3.75
2	2259	19	23.53	2.88	4.0	1.4	0.17	32.08	64.17	0.5	3.75
3	2299	19	39.47	3.09	7.5	2.1	0.19	48.13	48.13	1.0	3.75
4	2276	19	36.00	3.48	9.0	2.8	0.25	57.75	38.5	1.5	3.75
5	2211	19	27.63	4.42	10.5	4.2	0.38	67.08	29.17	2.3	3.75
6	2190	19	23.00	5.26	11.5	5.5	0.5	72.19	24.06	3.0	3.75
7	2240	19	76.92	12.31	10.0	4.0	0.13	66.21	28.79	2.3	5.0
8	2311	19	40.00	5.18	10.0	3.6	0.25	64.12	27.88	2.3	8.0
9	2304	19	237.50	20.632	9.5	2.8	0.04	61.33	26.67	2.3	12.0

Effect of freeze-thaw cycles: eight monotonic triaxial tests were carried out to study the effect of freeze-thaw cycles on shear strength of crushed waste rocks under 50 kPa confining pressure. The eight specimens were prepared using modified compaction effort and were subjected to different freeze-thaw cycles (0-16). One freeze-thaw cycle consisted in placing a specimen in a temperature-controlled freezer with a constant temperature of -20 ℃ for 24 hours, and then moving it to a room with a temperature of 20 ℃ for 24 hours. A temperature of -20 ℃ is common in the literature (Tian et al. 2019; Zou et al. 2020) and was also considered representative of field conditions in

Canada. Tests information is summarized in Table 3.4 and more details can be found in Chapter 8.

Table 3.4: Physical properties of specimens subjected to different freeze-thaw cycles; w_0: initial gravimetric water content.

No.	No. of freeze-thaw cycles	w_0 (%)	Dry density (kg/m^3)
1	0	4	2217
2	2	4	2220
3	4	4	2225
4	7	4	2226
5	10	4	2230
6	16	4	2226
7	10	2	2226
8	10	5	2223

3.4.2 Repeated load triaxial test

Repeated load triaxial tests were carried out using the same apparatus as the monotonic triaxial tests. The objective was to evaluate the resilient modulus and permanent deformation of crushed waste rocks under drained conditions (Figure 3.5). The tests were conducted using haversine loading pulses with no rest period and with a 0.2-0.3 Hz loading frequency. A total of 22 repeated load triaxial tests were carried out on crushed waste rocks in this study.

Effect of stress levels on resilient modulus: two repeated load triaxial tests were conducted to evaluate the effect of stress levels on the resilient modulus of crushed waste rocks (AASHTO T307 2017). Two stress levels, i.e., low stress level (LSL) and high stress level (HSL) simulated the stress conditions in highways and mine haul roads, respectively. LSL and HSL testing sequences consisted of a succession of combinations of axial and confining stresses. LSL testing sequence was based on AASHTO T307 standard (2017), which was initially proposed for highway design. The maximum axial stress in LSL was varying from 20.7 to 275.8 kPa and confining pressure was

between 20.7 and 137.9 kPa (Table 3.5). The stress level proposed in AASHTO T307 protocol was, however, significantly lower than the tire pressure of haul trucks expected on mine sites (often around 1000 kPa ("Electric drive mining truck 960e-2k"). HSL stress combinations of axial and confining stresses were therefore proposed in this study to evaluate the resilient behavior of crushed waste rocks under conditions more representative of heavy haul trucks (Table 3.5). In HSL, the maximum axial stress and confining pressure were between 80 and 2000 kPa, and between 100 and 1000 kPa, respectively. A total of 100 cycles were applied for each stress path (except during the conditioning stress path which was made of 500 cycles), with a haversine shaped loading pulse and a frequency of 0.3 Hz, for both LSL and HSL tests. Two specimens were prepared for LSL and HSL tests using modified compaction effort (2700 kN-m/m^3) and an initial gravimetric water content of 4%. The resilient modulus was defined and calculated as the ratio of the cyclic deviator stress to the recoverable axial strain (AASHTO T307 2017). More details about these tests can be found in Chapter 4.

Table 3.5: Low stress level (LSL) and high stress level (HSL) testing sequences for repeated load triaxial tests; the cyclic loading parameters include confining pressure (CP), maximum axial stress (MAS), and cyclic stress (CYS).

LSL					HSL				
No.	CP	MAS	CYS	CS	No.	CP	MAS	CYS	CS
	(kPa)					(kPa)			
0	103.4	103.4	93.1	10.3	1	100	80	72	8
1	20.7	20.7	18.6	2.1	2	100	150	135	15
2	20.7	41.4	37.3	4.1	3	100	200	180	20
3	20.7	62.1	55.9	6.2	4	300	240	216	24
4	34.5	34.5	31.0	3.5	5	300	450	405	45
5	34.5	68.9	62.0	6.9	6	300	600	540	60
6	34.5	103.4	93.1	10.3	7	500	400	360	40
7	68.9	68.9	62.0	6.9	8	500	750	675	75
8	68.9	137.9	124.1	13.8	9	500	1000	900	100

9	68.9	206.8	186.1	20.7	10	700	560	504	56
10	103.4	68.9	62.0	6.9	11	700	1050	945	105
11	103.4	103.4	93.1	10.3	12	700	1400	1260	140
12	103.4	206.8	186.1	20.7	13	900	720	648	72
13	137.9	103.4	93.1	10.3	14	900	1350	1215	135
14	137.9	137.9	124.1	13.8	15	900	1800	1620	180
15	137.9	275.8	248.2	27.6	16	1000	800	720	80
					17	1000	1500	1350	150
					18	1000	2000	1800	200

Effect of stress levels on permanent deformation: three repeated load triaxial tests were conducted to evaluate the effect of stress levels on the permanent deformation of crushed waste rocks (EN 13286 2004). Three different stress levels, i.e., low stress level (LSL), high stress level (HSL), and high stress level for mining (HSLM), were used for this study (Table 3.6). LSL and HSL are proposed in European Standard 13286 (2004), which consist of five sequences, and each sequence contains 5 or 6 stress paths with a constant confining pressure and different deviator stresses (Table 3.6). A total of 10000 loading cycles were applied for each stress path. HSLM was specifically defined in this study to represent typical stress conditions within mine haul roads. HSLM was divided into 4 sequences, and each of these sequences contained 4 stress paths characterized by a constant confining pressure but different deviator stresses (Table 3.6). The confining pressure and deviator stress ranged from 80 to 550 kPa, and from 100 to 1500 kPa, respectively. In total, 6000 loading cycles were applied for each stress path in HSLM tests. The number of cycles was smaller than in the standard since mine haul roads are typically low-volume roads. The three specimens were prepared using modified compaction effort (2700 kN-m/m^3) with an initial gravimetric water content of 4%. More details about these three tests can be found in Chapter 5.

Table 3.6: Stress levels with different confining stress σ_3 and deviator stress σ_d for repeated load

triaxial tests; LSL and HSL are prescribed by the European Standard (EN 13286 2004), and HSLM was defined in this study for mining applications (see text for details).

Sequence 1		Sequence 2		Sequence 3		Sequence 4		Sequence 5	
σ_3, kPa	σ_d, kPa	σ_3, kPa	σ_d, kPa	σ_3, kPa	σ_d, kPa	σ_3, kPa	σ_d, kPa	σ_3, kPa	σ_d, kPa
LSL									
20	20	45	60	70	80	100	100	150	100
20	40	45	90	70	120	100	150	150	200
20	60	45	120	70	160	100	200	150	300
20	80	45	150	70	200	100	250	150	400
20	100	45	180	70	240	100	300	150	500
20	120	45	210	70	280	100	350	150	600
HSL									
20	50	45	100	70	120	100	200	150	200
20	80	45	180	70	240	100	300	150	300
20	110	45	240	70	320	100	400	150	400
20	140	45	300	70	400	100	500	150	500
20	170	45	360	70	480	100	600	150	600
20	200	45	420	70	560				
HSLM									
80	100	200	300	350	400	550	600		
80	200	200	500	350	700	550	900		
80	300	200	700	350	1000	550	1200		
80	400	200	900	350	1300	550	1500		

Effect of gradation: the effect of gradation on resilient modulus and permanent deformation was studied using nine additional repeated load triaxial tests. These repeated load triaxial tests used the same specimens with the monotonic triaxial tests for the gradation study, and the information of specimen preparation can be found in section 3.4.1 and Table 3.3. More details about these nine tests can be found in Chapter 6.

Effect of freeze-thaw cycles: the effect of freeze-thaw cycles on the resilient modulus and permanent deformation was evaluated using eight repeated load triaxial tests. These repeated load triaxial tests used the same specimens with the monotonic triaxial tests for the effect of freeze-thaw

cycles, and the information of specimen preparation can be found in section 3.4.1 and Table 3.4. More details about these eight tests can be found in Chapter 8.

3.5 Large-scale triaxial tests

3.5.1 Monotonic triaxial test

Large-scale post-cyclic monotonic triaxial tests were carried out on 600 mm high and 300 mm diameter uncrushed (coarse-grained) waste rock samples. These tests were consolidated drained tests for the evaluation of shear strength (peak deviator stress) (ASTM D7181 2020). The testing apparatus mainly consisted of a load frame (250 kN), a triaxial cell (2000 kPa), a load cell (100 kN), a linear strain conversion transducer (LSCT, 100 mm of measurement range), and a cell pressure controller (2000 kPa), a back pressure controller (2000 kPa) (Figure 3.6). The load cell and LSCT was used to record the axial load and axial deformation, respectively. The cell pressure controller was used to maintain the confining pressure as applied during triaxial tests. A hammer was especially designed for compacting the large waste rock samples in this study. The hammer was made of a 5 kg rammer dropped from a height of 1 m, and the diameter of the baseplate surface was 160 mm. The compaction energy produced by one blow of this hammer was 2.5 times the energy caused by modified Proctor hammer (ASTM D1557 2012). The samples were sheared at a constant axial rate of 0.02 mm/sec under a constant confining pressure of 50 kPa, and the deviator stress was recorded during the shear process.

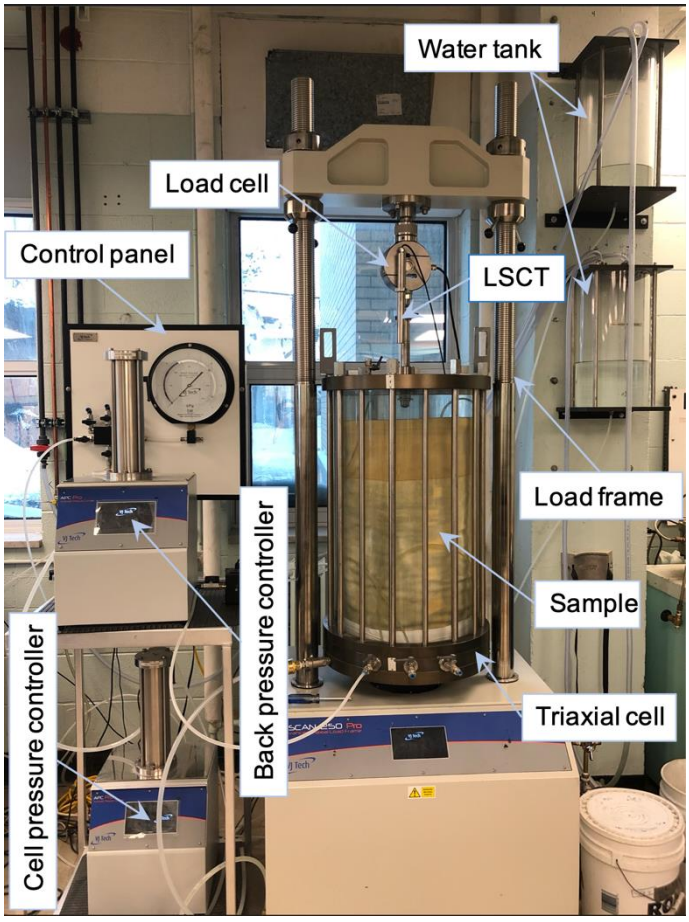

Figure 3.6: Large-scale triaxial test setup in RIME; it consists of a loading frame, linear strain conversion transducer (LSCT), load cell, triaxial cell, pressure controllers, water tank, and a waste rock specimen.

A total of 12 large-scale monotonic triaxial tests were carried out to study the effect of maximum particle size, gravel-to-sand ratio, fines content, compaction effort, and water content on shear strength of coarse-grained waste rocks. All the waste rock samples were prepared with five layers of 12 cm, each compacted with 31 (180 kJ/m^3), 62 (360 kJ/m^3), or 93 (540 kJ/m^3) blows of the hammer corresponding different compaction effort. The maximum particle size was 25, 40, and 60 mm, respectively. The fines content and gravel-to-sand ratio varied from 0% to 5% and 10%, and varied from 1 to 3, 5, and 8, respectively. The influence of water content on mechanical

properties of waste rock samples was investigated by using 1%, 2%, and 4% of initial gravimetric water content to prepare the samples. The information of tested specimens is summarized in Table 3.7. More details about the large-scale monotonic triaxial tests can be found in Chapter 7.

Table 3.7: The tested waste rock samples and the corresponding physical properties including dry density ρ_d (kg/m^3), D_{10} (mm), D_{30} (mm), D_{60} (mm), coefficient of curvature C_C (-), coefficient of uniformity C_U (-), compaction effort C (kJ/m^3), maximum particle size D_{max} (mm), gravel-to-sand ratio GS (-), fines content FC (%), and water content w (%).

No.	ρ_d	D_{10}	D_{30}	D_{60}	C_C	C_U	C	D_{max}	GS	FC	w
	kg/m^3	mm	mm	mm	-	-	kJ/m^3	mm	-	%	%
1	2008	0.7	8.5	27	3.8	38.6	360	60	5	5	2
2	1990	0.25	5.7	18	7.2	72.0	360	40	3.7	6.8	2
3	2115	0.1	3.7	10	13.7	100.0	360	25	2.5	9	2
4	2061	0.17	2.2	9	3.2	52.9	360	60	1	5	2
5	2037	0.25	5	22	4.5	88.0	360	60	3	5	2
6	1939	1.8	9.5	28	1.8	15.6	360	60	8	5	2
7	1932	2.5	9.5	28	1.3	11.2	360	60	5	0	2
8	2023	0.075	7	25	26.1	333.3	360	60	5	10	2
9	1876	0.7	8.5	27	3.8	38.6	180	60	5	5	2
10	2018	0.7	8.5	27	3.8	38.6	540	60	5	5	2
11	2004	0.7	8.5	27	3.8	38.6	360	60	5	5	1
12	2017	0.7	8.5	27	3.8	38.6	360	60	5	5	4

3.5.2 Repeated load triaxial test

Large-scale repeated load triaxial tests were carried out to investigate the effect of maximum particle size, gravel-to-sand ratio, fines content, compaction effort, and water content on resilient modulus and permanent deformation of uncrushed waste rocks. These tests were conducted under drained conditions. The repeated load triaxial test apparatus was same with the monotonic triaxial tests. A total of four successive stress paths were applied on waste rock samples with increasing

deviator stresses and confining pressures (Table 3.8). The confining pressure varied from 45 to 150 kPa and the deviator stress ranged from 120 to 320 kPa. Each stress path was applied for 3000 cycles with a frequency of 0.025 Hz with no rest period. All tests were performed in a stress-controlled mode using haversine loading pulses. The axial deformation and load were recorded during repeated load triaxial tests, and the resilient modulus (the ratio of deviator stress to recoverable axial strain; (AASHTO T307 2017)) and permanent strain were then calculated for each cycle. A total of 12 repeated load triaxial tests were conducted. These repeated load triaxial tests used the same specimens with the large-scale monotonic triaxial tests on uncrushed waste rocks, and the information of specimen preparation can be found in section 3.5.1 and Table 3.7. More details about the large-scale repeated load triaxial tests can be found in Chapter 7.

Table 3.8: Stress paths applied in large-scale repeated load triaxial tests; σ_3: confining pressure, kPa; σ_d: deviator stress, kPa.

Stress path	1	2	3	4
σ_3, kPa	45	70	100	150
σ_d, kPa	120	160	200	320

A total of 112 laboratory tests (including CBR and triaxial tests) were conducted to measure the CBR, shear strength, stiffness, and permanent deformation of crushed and uncrushed waste rocks from Canadian Malartic Mine. All the laboratory tests information in this project is summarized in Table 3.9, including the test type, specimen size, tested materials, number of tests, and the corresponding Chapter that the test results are presented.

Table 3.9: Summary of the laboratory tests on crushed and uncrushed waste rocks in this project; ϕ: specimen diameter, mm; h: specimen height, mm.

Test type	Specimen size ($\phi \times h$)	Material	No.	Chapter
Standard CBR	152.4×127 mm	Crushed	4	8
Repeated load CBR	152.4×127 mm	Crushed	39	4, 5, and 8
Monotonic triaxial	150×300 mm	Crushed	23	5, 6, and 8
Repeated load triaxial	150×300 mm	Crushed	22	4, 5, 6, and 8
Large-scale monotonic triaxial	300×600 mm	Uncrushed	12	7
Large-scale repeated load triaxial	300×600 mm	Uncrushed	12	7

3.6 Regression model fitting

M_R-θ model (Eq. 2.25 in section 2.5.3) and MEPDG model (Eq. 2.28 in section 2.5.3) were used to fit the measured resilient modulus of waste rocks by minimizing the coefficient of determination R^2 calculated on the resilient modulus, and the model coefficients were calibrated. The fitting results were presented in Chapter 4, 6, 7, and 8. The correlations between the model coefficients and gradation and climatic factors were also investigated, which could be used to estimate the resilient modulus of waste rocks in the field (see Chapter 6 and 8).

The applicability of the descriptive models of permanent deformation (in section 2.6.3) to waste rocks was evaluated in Chapter 5. Gidel et al. model (2001) (Eq. 2.41 and 2.42 in section 2.6.3) and Korkiala-Tanttu model (2005) (Eq. 2.43, 2.44, and 2.45 in section 2.6.3) and Rahman and Erlingsson model (2015a) (Eq. 2.46 and 2.47 in section 2.6.3) were used to fit the measured permanent deformation of waste rocks since these models are more suitable to describe coarse-grained materials strain at different stress conditions (Rahman and Erlingsson 2015b; Erlingsson et al. 2017). These models relate the permanent strain to number of loading cycles and stress

condition. However, Gidel et al. model, Korkiala-Tanttu model, and Rahman and Erlingsson model were initially proposed for single stress path repeated load triaxial tests and must be modified to describe multistage repeated load triaxial tests. Time hardening was proposed to consider the stress history effect caused by previous loading stress paths. The approach consists in introducing the equivalent loading cycles N_i^{eq} (Lytton et al. 1993; Zhou et al. 2010; Erlingsson and Rahman 2013; Mohammadinia et al. 2020; Li et al. 2021) which is calculated based on the current *i*th stress condition and the accumulated permanent strain achieved by previous stress paths. The total number of loading cycles N is then modified as $(N\text{-}N_{i\text{-}1}+N_i^{eq})$ in which $N_{i\text{-}1}$ is the total number of loading cycles at the end of the previous (*i*-1)th stress path. In the present study, Gidel et al. (2001), Korkiala-Tanttu (2005), and Rahman and Erlingsson (2015a) models were modified to include time hardening. Model coefficients were calibrated on experimental data using the method of least squares, and the error between experimental and predicted accumulated permanent strains was assessed using coefficient of determination R^2. The fitting accuracy of these models was presented and compared in Chapter 5. Rahman and Erlingsson model (extended using time hardening approach) was used to fit the accumulated permanent strains of crushed waste rocks with different gradations (Chapter 6), strains of crushed waste rocks subjected to climatic factors (Chapter 8), and strains of uncrushed waste rocks with different physical properties (Chapter 7).

3.7 Machine learning (more details are given in Chapter 9 and 10)

Machine learning method was used to develop prediction models for CBR, resilient modulus, and permanent deformation of crushed waste rocks based on the experimental data, and these models were developed using Python in this project. Seven different types of algorithms were used and compared to develop machine learning models for predicting CBR, resilient modulus, and permanent deformation of crushed waste rocks, namely multiple linear regression (MLR), k-

nearest neighbors (KNN), decision tree (DT), random forest (RF), support vector machine (SVM), backpropagation neural network (BPNN), and neuroevolution of augmenting topologies (NEAT). The principle of these algorithms can be found in Chapter 9 and 10. The correlations between basic parameters (including material physical properties and applied stress conditions) and the mechanical properties of crushed waste rocks were investigated to determine the input variables for the machines learning models. Particularly, Pearson correlation coefficient r analysis was conducted to determine the input variables for the CBR prediction models. The input variables were normalized using the Z-Score normalization method (Jain et al. 2005):

$$X_i^* = \frac{X_i - \mu}{\sigma} \tag{3.1}$$

Where X_i^*: the normalized input values; X_i: the experimental input values; μ: the mean value of the input variable; and σ: the standard deviation of the input variable.

The normalized data were then split between a training dataset and a testing dataset (to verify the generalization capability of the trained machine learning models). In this study, 70-80% of the total experimental data were selected randomly for the training dataset (for the training and validation of the machine learning models), while the remaining 20-30% data were used as the testing dataset (to test the developed machine learning models).

The prediction performance of machine learning models was assessed using coefficient of determination (R^2, Eq. 3.2), mean squared error (MSE, Eq. 3.3), mean absolute error (MAE, Eq. 3.4), and Huber loss L_δ (Eq. 3.5). These metric functions are widely used to assess the prediction accuracy of machine learning models for regression tasks (Zhang and Goh 2013; Kang et al. 2019; Meyer 2019; Gupta et al. 2020; Zheng 2020; Lee et al. 2021). A value of R^2 closer to 1 means a better performance (Fan et al. 2019). MSE value is always positive, and it is ideal to be close to zero (Chen 2010; Chollet 2018; Vidal and Kristjanpoller 2020). MAE value is always positive, and the smaller the value of MAE is, the better the model performs. Huber loss combines analytical tractability of MSE and outlier-robustness of MAE (Yi and Huang 2017; Sun et al. 2020).

$$R^2 = 1 - \frac{\sum_{i=1}^{n} (y_i^* - y_i)^2}{\sum_{i=1}^{n} (y_i - \bar{y})^2} \quad 3.2$$

$$\text{MSE} = \frac{1}{n}\left[\sum_{i=1}^{n} (y_i - y_i^*)^2\right] \quad 3.3$$

$$\text{MAE} = \frac{1}{n}\left(\sum_{i=1}^{n} |y_i - y_i^*|\right) \quad 3.4$$

$$L_\delta = \begin{cases} \frac{1}{2}(y_i - y_i^*)^2, & \text{if } |y_i - y_i^*| \leqslant \delta \\ \delta |y_i - y_i^*| - \frac{1}{2}\delta^2, & \text{otherwise} \end{cases} \quad 3.5$$

Where n: number of data sets; y_i and y_i^*: the experimental and predicted values of the i^{th} output, respectively; and $\bar{y}$: the mean of the experimental values. The given constant δ in Huber loss controls the transitions from a quadratic function (for small values of $|y_i - y_i^*|$) to an absolute value function (when the value of $|y_i - y_i^*|$ exceeds δ) (Huber 1973, 1992).

The hyperparameters study was also conducted to determine the optimum architecture of machine learning models. The hyperparameters study included the effect of the number of neighbors in KNN model, the maximum DT depth, the number of estimators in RF model, and the number of hidden neurons and hidden layers in BPNN model on the prediction accuracy. More details about the machine learning models can be found in Chapter 9 and 10.

CHAPTER 4 ARTICLE 1: ESTIMATION OF RESILIENT BEHAVIOR OF CRUSHED WASTE ROCKS USING REPEATED LOAD CBR TESTS

Shengpeng Hao and Thomas Pabst

This article has been published online in *Transportation Geotechnics* in February 2021.

Abstract: Crushed waste rocks (CWR), generated from mining operations, have been widely used for the construction of mine haul roads because of their low-cost, high-strength, and availability. Resilient modulus is a necessary input to mechanistic design for mine haul roads, but its determination usually requires advanced and complex equipment such as repeated load triaxial (RLT) test. Repeated load CBR (RLCBR) tests are simpler and more often available, and were therefore investigated in this study to estimate CWR resilient behavior under low and high stress levels. RLCBR equivalent modulus calculated using various equations were validated using RLT resilient modulus. The M_R-θ model showed good representation and prediction of CWR resilient behavior under both low and high stress levels. A new equation was also proposed to predict more precisely the equivalent modulus of CWR based on RLCBR tests. Results showed that the impact of loading frequency and waveform was limited, while the measured equivalent modulus increased significantly with contact stress (especially when contact stress < 10%). The effect of dry density and soaking on equivalent modulus was negligible, but specimen drying resulted in a marked increase of the equivalent modulus. The good agreement between RLCBR equivalent modulus and RLT resilient modulus indicates that RLCBR tests could be an effective alternative to RLT tests to estimate resilient behavior of CWR used in mine haul roads.

Keywords: Crushed waste rock, Mine haul roads, Resilient modulus, Repeated load CBR test, Equivalent modulus.

4.1 Introduction

Waste rocks are low grade ore materials produced by mining operations to access ore. Waste rocks are often stored on the surface, in piles, close to production sites. Management and reclamation of waste rocks piles can be challenging because of their large size and the risks for geochemical and geotechnical instabilities (Aubertin 2013). The reuse (or valorization) of waste rocks for roads construction is therefore an attractive alternative to surface disposal, both economically and environmentally (Thompson et al. 2019). Most mines already use crushed waste rocks (CWR) for the construction of haul road wearing courses because of their hardness, durability, low-cost and availability (Thompson et al. 2019).

Mine haul roads are typically unpaved flexible roads, and the design, construction and maintenance of the road surface or wearing course is critical to trafficability (Tannant and Regensburg 2001). Potholes, rutting, and settlement are the major symptoms of haul road deterioration, and are mainly caused by precipitation, runoff, heavy traffic volume, spring breakup, vehicle spillage, and poor compaction (Tannant and Regensburg 2001). More specially, the low stiffness of wearing course layers can result in poor trafficability under wet weather, churning, and excessive deformation (Thompson et al. 2019). The deterioration can result in reduced pavement performance and increase of road maintenance costs and vehicle operating costs. However, haul roads design methods are often empirical and rely heavily on local experience (Thompson et al. 2019). However, such empirical approaches cannot account for the influence factors such as pavement materials properties, climatic effects, and traffic information during the haul road design. Mechanistic design for unpaved haul roads is therefore needed. Resilient modulus is a parameter generally used to characterize unbound granular material stiffness (Lekarp et al. 2000a) and can be defined as (AASHTO T307 2017):

$$M_R = \frac{\sigma_d}{\varepsilon_r} \tag{4.1}$$

Where M_R: resilient modulus [MPa]; σ_d: deviator stress [MPa]; and ε_r: recoverable axial strain

[-].

Resilient modulus is typically used in mechanistic design methods to compute pavement response under traffic loading (Thach Nguyen and Mohajerani 2016). Waste rocks resilient behavior is characterized by non-linear behavior under external loading imposed by vehicles and is highly stress sensitive (Lekarp et al. 2000a; Coronado et al. 2016). Various models were proposed to describe the stress dependence of resilient modulus as a function of confining pressure, deviator stress, and/or bulk stress, and most constitutive models usually comprise two or three constant parameters evaluated empirically (Lekarp et al. 2000a).

The resilient behavior of soil and aggregate materials is usually obtained using repeated load triaxial (RLT) tests in the laboratory (AASHTO T307 2017). RLT tests are, however, complex, time consuming, and costly, especially considering the short-service-life of mine haul roads. Conventional RLT tests were also developed for civil roads, such as public highways, rather than mine haul roads which are subjected to extra heavy vehicle loading. For example, haul trucks size and capacity have grown significantly during the last few decades, with payload capacity increasing to 450 mt, and tire pressure sometimes exceeding 1000 kPa ("Belaz-7571 series"). In comparison, the gross vehicle weight limit of three axles straight truck for highway is 24.25 mt in Canada which is much lower than mining trucks (Woodrooffe 2010).

Repeated load CBR (RLCBR) tests were therefore proposed as an alternative to indirectly evaluate resilient behavior of fine-grained materials (i.e., sand and black cotton clay) (Molenaar 2008). The principle of RLCBR test is similar to the standard CBR test, except that cyclic loads are applied (Molenaar 2008; ASTM D1883 2016).

The research for RLCBR test technique is relatively limited, especially regarding the impact of frequency, waveform, and contact stress on test results. For instance, the contact stress (or load) is usually set to a relatively low value to maintain a positive contact between the specimen and the plunger, and to simulate the weights of overlying layers. Some studies also set contact stress to

zero to minimize the influence of contact stress (Molenaar 2008; Bhattacharjee and Bandyopadhyay 2015). Other researchers set it to 0.1 to 0.3 MPa (Araya et al. 2010; Molenaar et al. 2011), 0.1 kN (Haghighi et al. 2017), 10 kPa (Sas et al. 2012; Sas and Gluchowski 2013), or 10% of the maximum plunger load (Sparsha et al. 2016) to ensure the plunger remains stable during the cyclic loading and unloading. The differences between test setups makes it difficult to compare the RLCBR results from different research.

Resilient modulus determined using RLCBR are typically greater than using RLT tests (Araya 2011). An "equivalent modulus" ($E_{equ.}$) was therefore proposed to normalize the RLCBR test results and compare them to the RLT resilient modulus (Opiyo 1995; Molenaar 2008). Several equivalent modulus equations were developed based on elastic theory and regression fitting (Table 4.1). However, these equations were developed for low stress levels, and mainly for lateritic soil and fine-textured metamorphic rock.

Table 4.1: Equivalent modulus equations for RLCBR test. $E_{equ.}$: equivalent modulus [kPa]; σ_p: plunger stress, equal to total plunger load/plunger area [kPa]; u: vertical elastic (resilient) deformation of materials under plunger [mm]; v: Poisson's ratio of tested material [-]; σ_V and σ_H: vertical and horizontal (or lateral) stresses applied on the specimen [kPa].

No.	Name	Description	Equation	Reference
1	NF	No-Friction	$E_{equ.}=\frac{1.797(1-v^{0.889})\sigma_p r}{u^{1.098}}$	(Opiyo 1995)
2	FF	Full-Friction	$E_{equ.}=\frac{1.375(1-v^{1.286})\sigma_p r}{u^{1.086}}$	(Opiyo 1995)
3	WOSG	Without Strain Gauges	$E_{equ.}=\frac{1.513(1-v^{1.104})\sigma_p r}{u^{1.012}}$	(Araya 2011)
4	WSG	With Strain Gauges	$E_{equ.}=\frac{0.144(\sigma_V-2v\sigma_H)}{u}$	(Araya 2011)

The aim of this study was therefore to estimate the resilient behavior of CWR under low and high stress levels by using RLCBR and RLT tests. The stress state of RLCBR specimens was estimated using transfer functions, and the applicability of existing equivalent modulus equations under low and high stress levels was evaluated by comparing the calculated equivalent modulus to the RLT resilient modulus. A modified equation was also proposed to estimate the equivalent modulus of CWR under low and high stress levels. The effects of cyclic loading frequency, contact stress, and waveform, and of specimen properties (dry density, soaking, and drying) on CWR equivalent modulus were also investigated. In addition to the wearing course of haul roads (Thompson et al. 2019), CWR also can be used for the construction of base layers for public roads (Barksdale 1984; Titi and Matar 2018), and other structures at mine sites such as waste rock inclusions within tailings impoundments (Ferdosi et al. 2015a). Determine the resilient modulus of CWR could also be useful for all these different applications.

4.2 Materials and methods

4.2.1 Material sampling and characterization

The tested CWR material was obtained from Canadian Malartic Mine, an open pit gold mine located in the Abitibi region, in Quebec province, Canada. Uncrushed waste rocks were used for the construction of the base layer and crushed waste rocks for the wearing course. The CWR was representative of the material typically used for haul road surface layer construction at the mine. The particles larger than 19 mm were removed (sieved) because of the limitation of specimen size in the CBR mold (diameter = 152.4 mm) (ASTM D1883 2016).

The particle size distribution (PSD) was measured in the laboratory using sieving (ASTM C136/C136M 2019) (Figure 4.1(a)). The material had a very small amount (around 3.7%) of fines

(< 75 microns). It was a poorly graded gravel with 3.72% fines and was classified as GP (ASTM D2487 2017).

Proctor compaction tests were carried out on CWR material using modified effort (ASTM D1557 2012) (Figure 4.1(b)). The optimum water content was 5.6% corresponding to a maximum density $\rho_d = 2334$ kg/m^3. The maximum attainable degree of saturation of CWR specimens was 85%; above, water would leak out from the mold. Specific gravity of particles under and over 4.75 mm was determined (ASTM D854 2014, C127 2015). X-ray diffraction (XRD) tests were conducted to determine the CWR mineralogy. The CBR of this CWR was around 115% under modified compaction effort with 5.5% initial gravimetric water content (Laverdière 2019), which met the strength requirement for haul road wearing courses (> 80%, (Thompson et al. 2019)).

The basic properties of CWR, i.e. mineralogy, specific gravity, water absorption, optimum water content, maximum dry density, shape index, coefficient of uniformity, coefficient of curvature, grading coefficient, dust ratio, and CBR are summarized in Table 4.2.

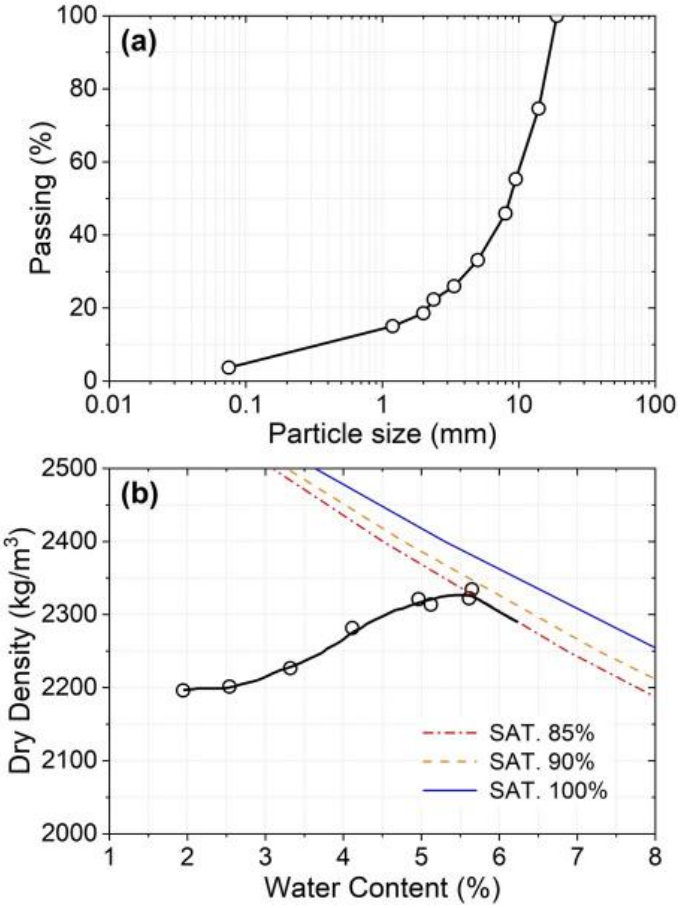

Figure 4.1: (a) Particle size distribution of tested crushed waste rocks, and (b) Proctor test results.

Table 4.2: (a) Mineralogy of tested CWR in this study, (b) Geotechnical properties of CWR. [a]: particle size < 4.75 mm; [b]: particle size > 4.75 mm; coefficient of uniformity $C_U = D_{60}/D_{10}$ and coefficient of curvature $C_C = D_{30}^2/(D_{60}\times D_{10})$; the CBR value was measured under modified compaction effort with 5.5% initial gravimetric water content.

(a)

Mineralogy	Proportion	Mineralogy	Proportion
Quartz	26.08±2.46%	Diopside	6.50±1.34%
Albite	38.74±4.30%	Anhydrite	2.42±0.48%
Muscovite	10.87±1.42%	Pyrite	1.08±0.15%
Chlorite	7.12±0.97%	Rutile	1.18±0.79%

Corundum	6.80±1.33%

(b)

Properties	Values	Standard/Reference
Specific gravity [a]	2.75	(ASTM D854 2014)
Specific gravity [b]	2.71	(ASTM C127 2015)
Water absorption [b]	0.41%	
Elongation index	38.56±1.62%	(IS 2386 1963)
Flakiness index	34.95±2.08%	
Optimum water content	5.6%	(ASTM D1557 2012)
Maximum dry density	2334 kg/m^3	
Coefficient of uniformity	7.98	(ASTM D2487 2017)
Coefficient of curvature	2.21	
Grading coefficient	25.6	(Thompson et al. 2019)
Dust ratio	0.47	
CBR	115%	(ASTM D1883 2016; Laverdière 2019)

4.2.2 RLCBR tests

RLCBR tests were carried out using a loading frame (100 kN), stress controllers (1000 kPa), a load cell (50 kN), a linear variable differential transformer (LVDT), and a PC, to estimate resilient behavior of CWR material (Figure 4.2(a)). The vertical deformation during RLCBR tests was considered equal to the vertical displacement of the plunger during loading and unloading and measured by a LVDT. The axial vertical load was measured using a 50 kN capacity external load cell. A standard CBR mold (diameter: 152.4 mm and height: 178 mm, including a 51 mm compaction collar), and a plunger of 49.63 mm diameter were used to prepare and penetrate the CWR specimens. Tests were performed in the load-controlled mode.

Two sets of cyclic loads sequences, i.e., low stress level (LSL) for civil engineering (highways) and high stress level (HSL) for mining engineering (mine haul roads), were defined for RLCBR tests (Table 4.3). A total of 100 cycles were applied for each load sequence, and the contact stress was 10% of the maximum axial stress. The LSL cyclic load sequences were based on the AASHTO

T307 standard procedures developed for RLT tests (AASHTO T307 2017), and the HSL cyclic load sequences were based on the typical stress levels observed on mine haul roads.

Table 4.3: Low stress level (LSL) and high stress level (HSL) testing sequences for RLCBR tests. The cyclic loading parameters include maximum axial stress (MAS), cyclic stress (CYS), and contact stress (CS).

LSL				HSL			
No.	MAS (kPa)	CYS (kPa)	CS (kPa)	No.	MAS (kPa)	CYS (kPa)	CS (kPa)
1	100	90	10	1	200	180	20
2	300	270	30	2	700	630	70
3	500	450	50	3	1200	1080	120
4	700	630	70	4	1700	1530	170
5	900	810	90	5	2200	1980	220
6	1100	990	110	6	2700	2430	270
				7	3200	2880	320
				8	3700	3330	370
				9	4200	3780	420
				10	4700	4230	470
				11	5200	4680	520

Araya et al. (2012) developed a set of transfer functions to estimate the vertical and horizontal (or lateral) stresses, Poisson's ratio and elastic modulus (i.e. WSG equation in Table 4.1) of the tested specimen based on linear elastic theory. These functions were developed based on the assumption that the granular material under the plunger is carrying most of the load, thus the stress and strains along the central axis are considered as representative of the bulk specimen. The transfer functions depend on plunger stress, vertical plunger deformation and lateral strain. However, the measurement of the lateral strain is complex and limits the application of these transfer functions. Therefore, the original transfer functions were modified to estimate the vertical and horizontal stress based on plunger stress and Poisson's ratio (Eq. 4.2, 4.3). The ratio of horizontal to vertical

stress was a linear function of Poisson's ratio (Eq. 4.4). The bulk stress (Eq. 4.5) then could be calculated based on Eq. 4.3 and 4.4, and was used for the model fitting (M_R-θ model) in this study.

$$\sigma_H=0.363\nu\sigma_p e^{(0.072/\upsilon)} \quad 4.2$$

$$\sigma_V=0.368\sigma_p \quad 4.3$$

The ratio of horizontal stress to vertical stress, α, was obtained by:

$$\alpha=0.986\nu e^{(0.072/\upsilon)}\approx 0.9617\upsilon+0.0919 \ (R^2 = 0.9996) \quad 4.4$$

Then the bulk stress was calculated as follows:

$$\theta=(0.7078\upsilon+0.4356)\sigma_p \quad 4.5$$

The Poisson's ratio of granular material is typically between 0.3 and 0.5 (Tannant and Regensburg 2001). A value $\nu = 0.35$ is often considered representative of granular material such as waste rocks (Thompson and Visser 1997b; Tannant and Regensburg 2001; Laverdière 2019) and was therefore considered to calculate the equivalent modulus in this study.

The cyclic loading caused by moving vehicles can generally be represented by a square waveform close to the pavement surface, and a haversine or triangle waveform deeper (Hu et al. 2010). In this study, both haversine and square shaped load pulses were used to simulate traffic loading (Figure 4.2(b)).

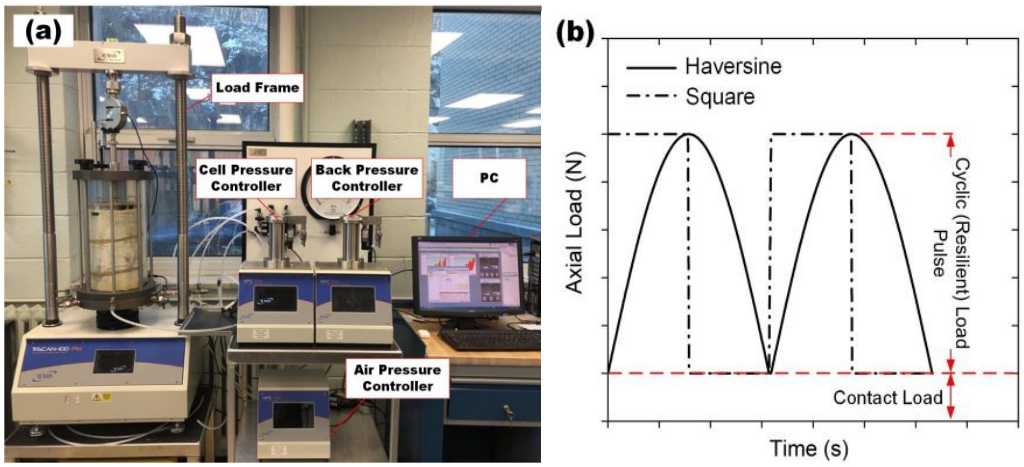

Figure 4.2: (a) RLT and RLCBR tests setup; (b) haversine and square shaped load pulses used in RLCBR tests; the total load applied to the specimen included the contact (constant) and cyclic (resilient) loads.

Different cyclic loading frequencies (0.1, 0.3, 0.5, and 0.7 Hz) and different contact stress (2%, 5%, 10%, and 15% of maximum axial stress) were applied during RLCBR tests to investigate their effect on the measured equivalent modulus.

The vertical deformation was recorded during RLCBR tests, and the average elastic (resilient) deformation of the last five loading cycles of each stress sequence was used to calculate the equivalent modulus.

4.2.3 Specimen preparation

The CWR specimens for RLCBR tests were prepared with different initial gravimetric water contents (2%, 3%, 4%, 5%, 6%, 7%, and 8%) to investigate the impact of dry density on equivalent modulus. Different compaction energies were also used to prepare RLCBR specimens, i.e., standard effort (STD), 600 kN-m/m^3 (ASTM D698 2012) and modified effort (MOD), 2700 kN-m/m^3 (ASTM D1557 2012). An alternative compaction method (MOD 81) was also used in this

study. MOD 81 compaction used a modified effort hammer (44.48 N), but with 81 blows per layer (instead of 56 blows; the rest of the test being identical to ASTM D1557-12e1). The objective was to simulate a higher compaction energy (3905 kN-m/m^3) which was more representative of field conditions where compaction is achieved using heavy haul trucks.

Soaking and drying specimens were also prepared and tested to evaluate the RLCBR equivalent modulus corresponding to the most unfavorable field conditions in situ. The soaking and drying specimens were prepared using modified compaction effort. A 4.54 kg of surcharge weights was placed on the compacted CWR specimen during soaking and drying. The mold and weights were immersed in water allowing the free access of water to the top and bottom of the specimen at room temperature (around 20°C). The specimen was soaked for four days (i.e. 96 hours) according to the ASTM D1883 Standard (2016). The water level was maintained constant, and the swelling of the soaked specimen was recorded. In practice, no swell was observed during soaking. The compacted CWR specimen was dried in oven at a uniform temperature of 110°C for one day (i.e. 24 hours). The mass of specimen was determined after 16 hours of drying, and then placed it into the oven for another 8 hours. The mass of specimen after 16 and 24 hours were compared to ensure the specimen dried completely.

In total, 32 RLCBR tests (including duplicates) were carried out with different loading features and specimen properties (Table 4.4).

Table 4.4: Summary of RLCBR tests carried out in this study. SC: stress conditions; *w*: initial water content; Fre.: loading frequency; LW: loading waveform; CS: contact stress; LSL: low stress level; HSL: high stress level; CE: compaction effort; MOD: modified compaction effort; STD: standard compaction effort; MOD 81: compaction effort with 81 blows per layer; H: haversine waveform; S: square waveform.

No.	SC	*w* (%)	Fre. (Hz)	CS (%)	CE	LW	Duplicates

1	LSL	4	0.3	2	MOD	H	2
2	LSL	4	0.3	5	MOD	H	1
3	LSL	4	0.3	10	MOD	H	3
4	LSL	4	0.1	10	MOD	H	2
5	LSL	4	0.3	15	MOD	H	3
6	LSL	4	0.3	10	MOD	S	2
7	LSL	4	0.5	10	MOD	H	2
8	LSL	4	0.7	10	MOD	H	2
9	LSL	2	0.3	10	MOD	H	1
10	LSL	3	0.3	10	MOD	H	1
11	LSL	5	0.3	10	MOD	H	1
12	LSL	6	0.3	10	MOD	H	1
13	LSL	7	0.3	10	MOD	H	1
14	LSL	8	0.3	10	MOD	H	1
15	LSL	4	0.3	10	STD	H	1
16	LSL	4	0.3	2	MOD	S	1
17	LSL	4	0.3	10	MOD 81	H	1
18(soaked)	LSL	4	0.3	10	MOD	H	1
19(dried)	LSL	4	0.3	10	MOD	H	1
20	HSL	4	0.3	10	MOD	H	3
21	HSL	4	0.3	15	MOD	H	1

Compaction energy and initial water content had a direct influence on the dry density of RLCBR specimen. For example, the dry density increased from 2196 to 2334 kg/m^3 (around +6%) when the water content increased from 1.9% to 5.6% (Figure 4.3). The final water content after RLCBR tests was always measured and was typically slightly lower than the initial water content. It increased about 9%, i.e., from 2039 to 2227 kg/m^3, when the compaction energy increased from STD (600 kN-m/m^3) to MOD (2700 kN-m/m^3). The increase of dry density was, however, insignificant when the compaction energy increased from MOD to MOD 81 (3905 kN-m/m^3). The minimum and maximum dry densities of CWR specimen for RLCBR tests in this study were 2039 and 2334 kg/m^3, respectively.

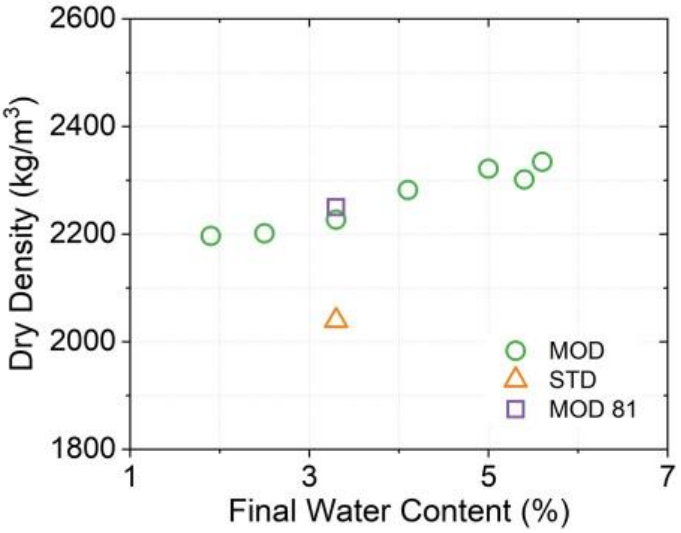

Figure 4.3: Dry density of RLCBR specimens for different final water contents (1.9%, 2.5%, 3.3% 4.1%, 5.0%, 5.4%, and 5.6%) and compaction efforts (STD, MOD, and MOD 81).

4.2.4 RLT test

The RLT tests were conducted under drained conditions on 300 mm high and 150 mm diameter specimens. The tests were carried out using the same test apparatus than for RLCBR tests (Figure 4.2(a)). A low (LSL) and a high (HSL) stress levels were employed for RLT tests. The LSL and HSL testing sequences consisted of a succession of combinations of axial and confining stresses (Table 4.5).

AASHTO T307 standard was employed for LSL testing sequence. This standard was initially proposed for highway design, with a maximum axial stress varying from 20.7 to 275.8 kPa and confining pressure from 20.7 to 137.9 kPa.

The stress level applied in AASHTO T307 protocol is, however, significantly lower than the tire pressure of haul trucks, e.g., around 1000 kPa ("Electric drive mining truck 960e-2k"). HSL stress combinations of axial and confining stresses were therefore also proposed in this study to evaluate

the resilient behavior of CWR material under heavy haul trucks (Table 4.5). The maximum axial stress and confining pressure were between 80 and 2000 kPa, and between 100 and 1000 kPa, respectively, which could cover the range of stress variation in the field, even for the heavier mining truck (e.g., BELAZ 75710 with 450 mt of payload capacity). A total of 100 repetitions were employed for each cyclic loading sequence (except the conditioning stress path with 500 cycles), with a haversine shaped loading pulse and a frequency of 0.3 Hz, for both LSL and HSL RLT tests.

RLT specimens were prepared using modified compaction effort (2700 kN-m/m^3), and this high compaction energy could minimize the effect of the rapid accumulation of vertical permanent strain. Specimens were prepared with an initial gravimetric water content w = 4%.

The RLT resilient modulus was calculated as the average ratio of the deviator stress and the recoverable axial strain (Eq. 4.1) for the last five loading cycles of each stress sequence.

Table 4.5: Low stress level (LSL) and high stress level (HSL) testing sequences for RLT tests; the cyclic loading parameters include confining pressure (CP), maximum axial stress (MAS), cyclic stress (CYS), contact stress (CS), and number of loading cycles.

LSL					HSL				
No.	CP	MAS	CYS	CS	No.	CP	MAS	CYS	CS
	(kPa)					(kPa)			
0	103.4	103.4	93.1	10.3	1	100	80	72	8
1	20.7	20.7	18.6	2.1	2	100	150	135	15
2	20.7	41.4	37.3	4.1	3	100	200	180	20
3	20.7	62.1	55.9	6.2	4	300	240	216	24
4	34.5	34.5	31.0	3.5	5	300	450	405	45
5	34.5	68.9	62.0	6.9	6	300	600	540	60
6	34.5	103.4	93.1	10.3	7	500	400	360	40
7	68.9	68.9	62.0	6.9	8	500	750	675	75
8	68.9	137.9	124.1	13.8	9	500	1000	900	100
9	68.9	206.8	186.1	20.7	10	700	560	504	56
10	103.4	68.9	62.0	6.9	11	700	1050	945	105

11	103.4	103.4	93.1	10.3	12	700	1400	1260	140
12	103.4	206.8	186.1	20.7	13	900	720	648	72
13	137.9	103.4	93.1	10.3	14	900	1350	1215	135
14	137.9	137.9	124.1	13.8	15	900	1800	1620	180
15	137.9	275.8	248.2	27.6	16	1000	800	720	80
					17	1000	1500	1350	150
					18	1000	2000	1800	200

4.3 Test results

4.3.1 RLCBR test results

The vertical resilient deformation of CWR under the plunger was recorded continuously during RLCBR tests. The resilient deformation increased with increasing maximum axial stress (plunger stress) in all cases (Figure 4.4). For example, for the LSL RLCBR tests with 0.3 Hz, haversine waveform, 10% contact stress, 4% initial water content, and MOD compaction effort, the resilient deformation increased from around 0.0252 to 0.0657 mm (±0.008 mm) when the maximum axial stress increased from 100 to 1100 kPa (Figure 4.4(a)). For the HSL RLCBR tests with the same loading features and specimen properties with LSL RLCBR tests, the resilient deformation increased from around 0.0363 to 0.1664 mm ($\pm$ 0.027 mm) with the maximum axial stress increasing from 200 to 5200 kPa. The deviation of deformation caused by the duplicates increased from around 0.003 to 0.027 mm with the maximum axial stress increasing from 200 to 5200 kPa (Figure 4.4(b)).

Further investigation of the effect of loading features and specimen properties on test results was conducted based on equivalent modulus in Section 4.4.

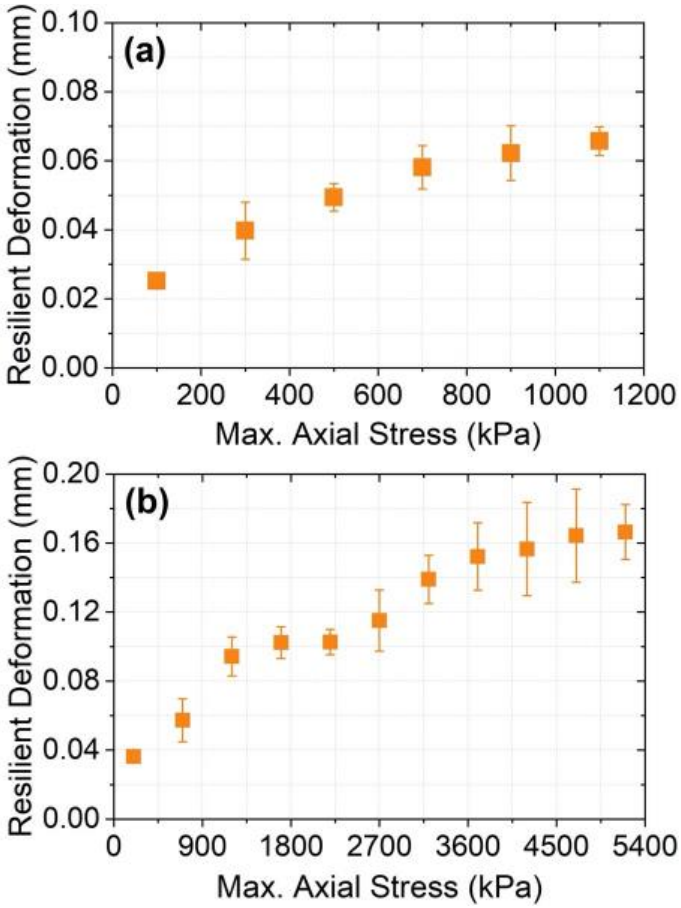

Figure 4.4: Measured resilient deformation during RLCBR tests under (a) low stress level and (b) high stress level, the deviation of deformation was caused by the duplicates.

CWR specimens were characterized after compaction and RLCBR tests, and compared to the original material properties (before the tests). Results showed some differences in the grain size distribution (Figure 4.5). The proportion of coarse particles (14-19 mm) decreased between 3 and 8%, depending on compaction energy. The decrease was more pronounced for higher compaction energies (-8% for MOD 81 compaction) than for small energies (-4% for STD compaction). On the other hand, the fine content (< 0.075 mm) increased, by up to 7% for MOD 81. Compaction and cyclic loads therefore appeared to have crushed some of the coarse particles (> 14 mm), which is relatively common in such tests (Cetin et al. 2014).

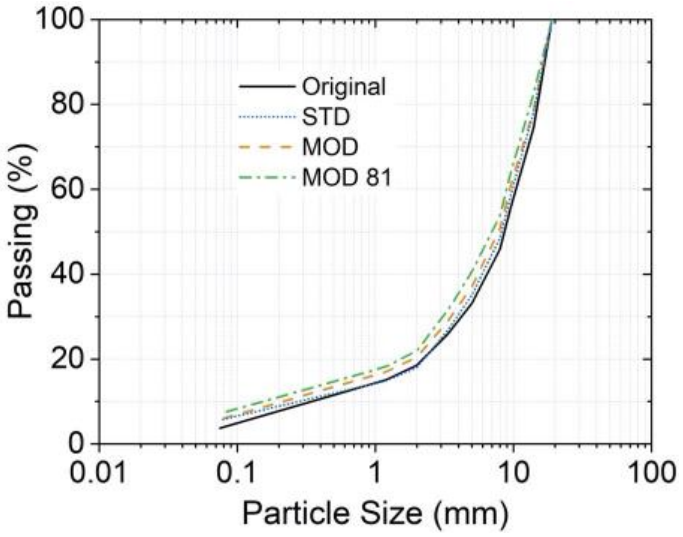

Figure 4.5: Particle size distribution of CWR specimens before and after RLCBR tests.

4.3.2 RLT Resilient modulus

CWR resilient modulus was assessed using RLT tests under both LSL and HSL conditions. Measured resilient modulus tended to increase significantly with increasing bulk stress (Figure 4.6). The resilient modulus of CWR material under high stress condition was significantly higher than for low stress conditions. For example, for LSL RLT test, the resilient modulus increased from around 137 to 455 MPa as the bulk stress increased from 82.8 to 689.5 kPa. For HSL RLT tests, the resilient modulus increased from 313 to 1238 MPa when the bulk stress increased from 380 to 5000 kPa. The increase of resilient modulus with bulk stress was non-linear, and the increasing rate decreased as the bulk stress increased. For example, for LSL RLT test the increase of resilient modulus was around 120 MPa when the bulk stress increased from 120 to 340 kPa, but 85 MPa when the bulk stress increased from 210 to 410 kPa. HSL RLT tests showed a similar trend.

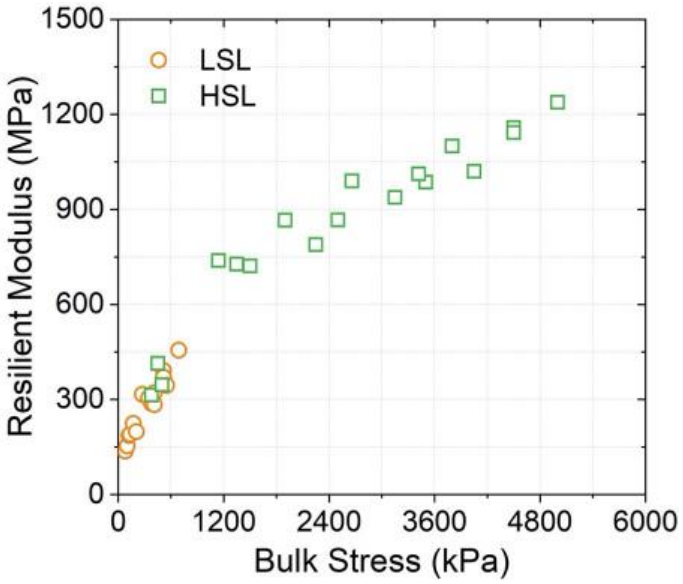

Figure 4.6: CWR resilient modulus measured by RLT tests under low (LSL) and high (HSL) stress levels.

4.4 Calibration of equivalent modulus

4.4.1 Model fitting of resilient modulus

The stress dependency of CWR resilient modulus was analyzed using different models (Dunlap 1963; Seed et al. 1967; Moossazadeh and Witczak 1981; Uzan 1985; Witczak and Uzan 1988; Pezo and Hudson 1994; Ni et al. 2002). The M_R-θ model appeared to be the most suitable for the tested material. This model was proposed by Seed et al. (1967) for fine-grained subgrade soils, granular based materials, and bituminous surface courses, and can be written:

$$M_R = k_1 p_a \left(\frac{\theta}{p_a}\right)^{k_2} \quad 4.6$$

Where k_1, and k_2: regression coefficients; θ: bulk stress [kPa]; and p_a: atmospheric pressure (100 kPa).

The M_R-θ model is widely accepted, and is considered accurate as long as stresses remain below the static failure condition (Elliott and David 1989).

The parameters (k_1 and k_2) of M_R-θ model were fitted (or calibrated) for both LSL and HSL RLT tests by minimizing the coefficient of determination R^2 calculated on the resilient modulus (Figure 4.7(a), (b)). The coefficient of determination was higher than 0.9 for both LSL and HSL RLT tests, which is deemed acceptable.

The calibrated M_R-θ model parameters (k_1 and k_2) for LSL and HSL tests were slightly different (Figure 4.7(a), (b)) and the resilient modulus predicted using HSL fitting curve was generally greater than that predicted by LSL fitting curve for bulk stress < 6000 kPa (Figure 4.7(c)). Usually, the tire pressure of mining trucks can reach 1000 kPa ("Electric drive mining truck 960e-2k"), so the bulk stress in haul roads can vary between 1000 and 3000 kPa. Therefore, the resilient modulus prediction model (e.g. M_R-θ model in this paper) calibrated from LSL RLT testing results (AASHTO T307 2017) tended to underestimate the resilient behavior of CWR material used in mine haul roads, as CWR exhibited some “stiffening” with increasing stress levels.

Predicted resilient modulus should be zero when the bulk stress is zero, based on the fitted model (Figure 4.7(c)) but it seemed to be different based on Figure 4.7(a), (b). Capillarity (or matric suction) is a typical reason for non-null resilient modulus (Tian et al. 1998; Ekblad and Isacsson 2006). However, in this case, the measured pore water suction during the RLT test did not exceed 8 kPa, and the effect of capillarity on the resilient modulus was therefore deemed limited in this study. The use of two membranes (0.3 mm and 0.6 mm thick) could have increased the cyclic loading resistance of the specimens (Henkel and Gilbert 1952; Evans and Seed 1987; Evans et al. 1992).

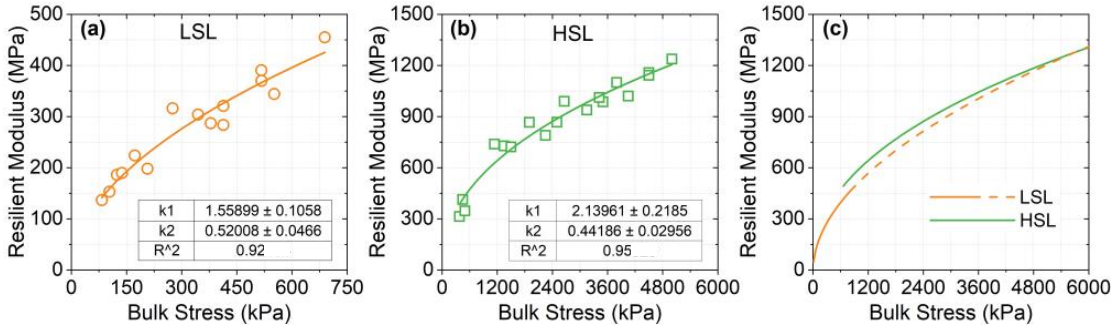

Figure 4.7: Fitting curves of M_R-θ model for CWR resilient moduli under (a) low stress level (LSL) and (b) high stress level (HSL); (c) comparison of calibrated (fitted) curves for LSL and HSL conditions, the dashed line represents the extrapolation of resilient modulus.

4.4.2 Calculation and validation of equivalent modulus

The CWR equivalent modulus was determined from RLCBR tests using existing equivalent modulus equations reported in the literature (Table 4.1). These equations are based on the resilient deformation and plunger stress recorded during the RLCBR tests.

The calculated equivalent moduli were compared to RLT resilient moduli (Figure 4.8, 4.9). The objective was to evaluate the applicability of the different equations in Table 1 to CWR material. The equivalent moduli were also fitted using M_R-θ model (Eq. 4.6). The bulk stress of RLCBR specimen was calculated based on the maximum axial stress (plunger stress) and Poisson's ratio (0.35) (Eq. 4.5). For this validation, the RLCBR tests with 4% initial water content, 10% contact stress, 0.3 Hz frequency, haversine waveform, and MOD compaction effort were selected, so the loading features and specimen properties were the same as for RLT tests.

For LSL RLCBR tests, the equivalent modulus increased from around 100 to 600 MPa as the bulk stress increased from 50 to 650 kPa. The M_R-θ model was able to describe relatively well the equivalent moduli calculated by different equations, with a regression coefficient R^2 always greater than 0.85 (Figure 4.8). The equivalent moduli calculated by WOSG equation were relatively lower

(around -75 MPa) than with other equations. The equivalent modulus computed with the WOSG equation seemed more accurate, i.e., closer to RLT resilient modulus, for LSL RLCBR tests. Indeed, the fitting curves seemed coincide (Figure 4.8(d)). The model parameters (k_1 and k_2) for the equivalent moduli calculated by WOSG equation (1.488 and 0.571, respectively) were the closest to the ones estimated for the resilient moduli (1.559 and 0.520, respectively).

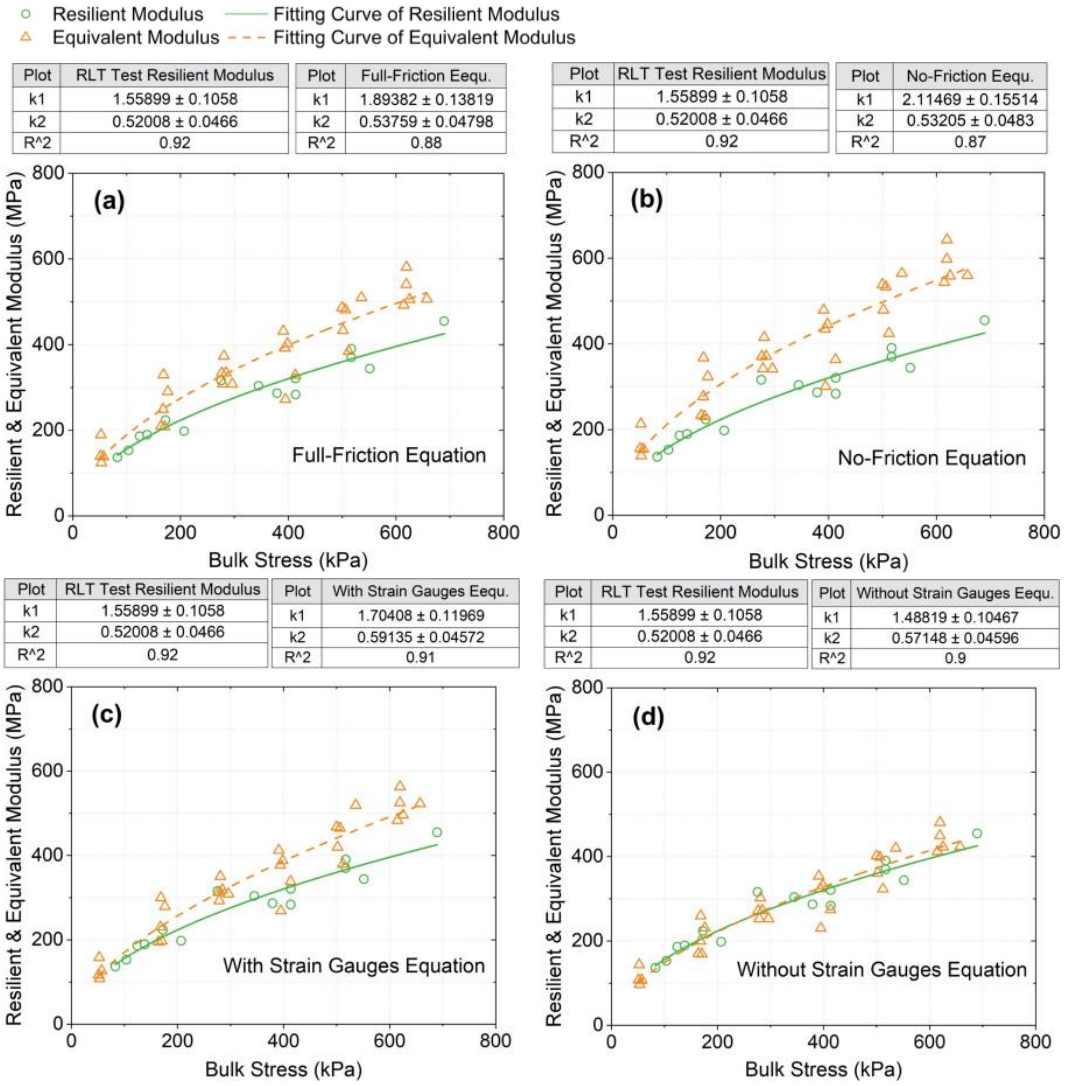

Figure 4.8: Comparison of RLCBR equivalent moduli and RLT resilient moduli under low stress level (LSL). (a) Full-Friction (FF) equation (Opiyo 1995), (b) No-Friction (NF) equation (Opiyo

1995), (c) With Strain Gauges (WSG) equation (Araya 2011), and (d) Without Strain Gauges (WOSG) equation (Araya 2011). Fitting curves (M_R-θ model) with corresponding parameters (k_1 and k_2) and coefficient of determination R^2 are also shown.

The same approach was used to compare equivalent moduli and resilient moduli for HSL condition. The equivalent modulus calculated for HSL RLCBR tests showed similar trend than the LSL tests, but the values reached were higher (up to 1100 MPa). The equivalent modulus increased from around 200 to 1100 MPa when the bulk stress increased from 135 to 3550 kPa (Figure 4.9). All the equivalent modulus equations gave relatively accurate results (i.e. were close to RLT resilient moduli). The M_R-θ model could fit all the equivalent moduli satisfactorily ($R^2 > 0.9$). The NF equation performed relatively better, with a maximum difference of moduli smaller than 50 MPa. The model parameters (k_1 and k_2) were also closer to resilient moduli (Figure 4.9(b)). The NF equation was therefore deemed more reliable to calculate equivalent modulus from HSL RLCBR tests in this study. For HSL RLCBR tests, WOSG equation showed underestimation in equivalent modulus (around -100 MPa) (Figure 4.9(d)).

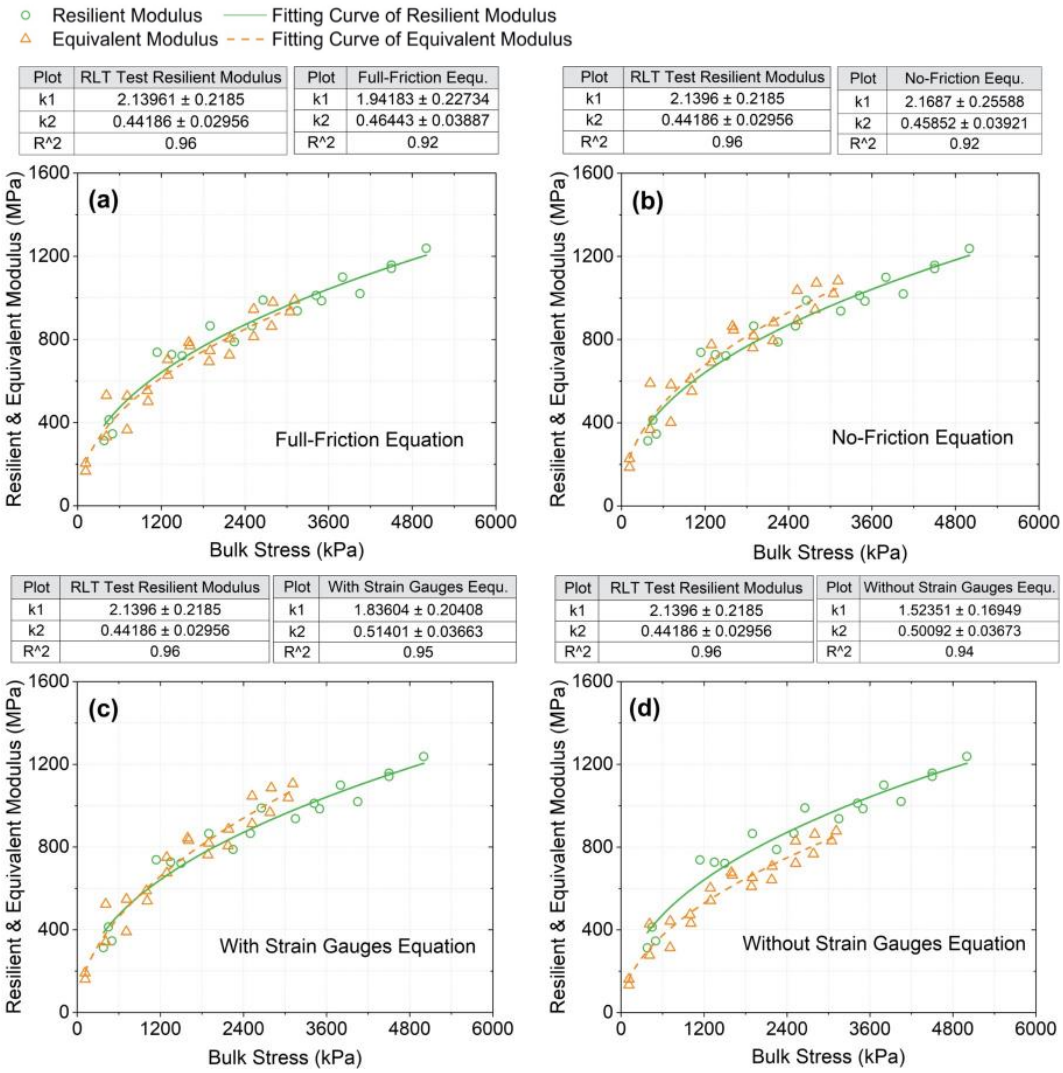

Figure 4.9: Comparison of RLCBR equivalent moduli and RLT resilient moduli under high stress level (HSL). (a) Full-Friction (FF) equation (Opiyo 1995), (b) No-Friction (NF) equation (Opiyo 1995), (c) With Strain Gauges (WSG) equation (Araya 2011), and (d) Without Strain Gauges (WOSG) equation (Araya 2011). Fitting curves (M_R-θ model) with corresponding parameters (k_1 and k_2) and coefficient of determination R^2 are also shown.

4.4.3 Development of a new equivalent modulus equation

The FF, NF, and WOSG equivalent modulus equations (Table 4.1) had the same general form, i.e.

they were a function of plunger stress σ_p and vertical resilient deformation u. This form was developed from elastic theory (Araya 2011) and can be generalized to:

$$E=\frac{k_1(1-\nu^{k_2})\sigma_p r}{u^{k_3}} \quad 4.7$$

A new equivalent modulus equation for CWR was therefore developed here using the same form as Eq. 4.7. The Poisson's ratio ($\nu = 0.35$) and the radius of plunger ($r = 24.815$ mm) were fixed. The values of k_1, k_2 and k_3 in the new equation were determined from a fitting procedure based on the resilient moduli predicted by M_R-θ model for LSL and HSL RLCBR tests. The new equivalent modulus equation could therefore be expressed as follows:

$$E_{equ.}=\frac{2.432(1-\nu^{2.630})\sigma_p \cdot r}{u^{0.766}} \quad 4.8$$

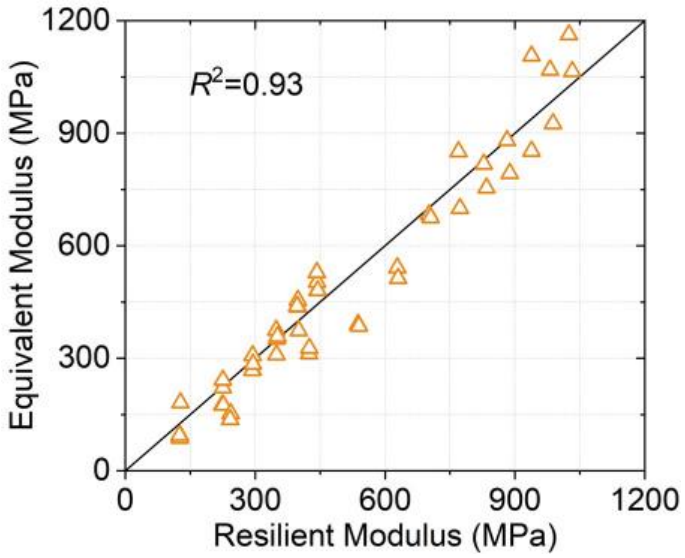

Figure 4.10: Comparison of equivalent modulus calculated by new equation and resilient modulus predicted by M_R-θ model under both low and high stress levels.

This new equation seemed reasonably reliable to calculate equivalent modulus for both LSL and HSL RLCBR tests with a satisfactory coefficient of determination ($R^2 = 0.93$) (Figure 4.10). The

values of parameters k_1, k_2 and k_3 in this new equation were different from existing equations in Table 4.1, with k_1 and k_2 being relatively higher while k_3 was lower than that in previous equations.

4.4.4 Effect of loading features and specimen properties

The equivalent moduli of all RLCBR tests were calculated using the new equation (Eq. 4.8). RLCBR loading features (contact stress, frequency, and waveform) and specimen properties (dry density, soaking, and drying) all had an effect on the equivalent modulus and were further investigated (Figure 4.11). The equivalent modulus increased linearly with maximum axial stress for all tests.

CWR equivalent modulus was sensitive to contact stress for both LSL and HSL conditions (Figure 4.11(a), (b)), and increased with increasing contact stress. For example, the average equivalent modulus for a contact stress of 15% was 23% greater (i.e. +50 MPa) than a contact stress of 2% (Figure 4.11(a)). For HSL tests, the average increase of equivalent modulus was 12% as the contact stress increased from 10% to 15% (Figure 4.11(b)). The equivalent modulus seemed to be more sensitive to contact stress when it was lower than 10% of the maximum axial stress. This value of 10% is also the contact stress recommended for RLT tests to maintain a positive contact between the cap and the specimen and to simulate the weight of overlying materials (AASHTO T307 2017).

The effect of frequency on equivalent modulus of CWR material appeared to be neglectable, with an average variation caused by the change of frequency (between 0.1 and 0.7 Hz) less than 25 MPa (Figure 4.11(c)). This was consistent with previous research carried out on crushed limestone (Boyce et al. 1976). Some reported that the resilient modulus could increase slightly when the frequency increased to 3.3 Hz (Seed et al. 1965) but the variation of frequency used this study (from 0.1 to 0.7 Hz) was too limited to confirm these observations for CWR. Also, usually, low frequencies allows the elastic strains to recover completely (Fairhurst et al. 1990).

The impact of loading waveform (i.e. square or haversine) on equivalent modulus was also limited, and the equivalent modulus with square loading was smaller 11% (-30 MPa) than with haversine loading (Figure 4.11(d)). Previous research tended to show that the square loading could result in significant decrease in resilient modulus (around 10-60%) (Barksdale et al. 1997; Shafabakhsh and Tanakizadeh 2015). However, most of these results were obtained for hot mix asphalt (HMA), which behavior is more viscoelastic compared to CWR. In this case, and for elastic materials in general, stress-strain behavior for elastic materials (such as CWR) is usually less sensitive to loading features (Lekarp et al. 2000a).

The equivalent moduli measured in this study were not significantly affected by dry density either, and the average change of equivalent modulus between the maximum and minimum dry densities tested (i.e. 2039 and 2334 kg/m^3) was lower than 25 MPa (< 11%; Figure 4.11(e)). However, the interval of dry densities (induced by the changes of initial water contents and compaction energies) were relatively limited in this study (< 14.5%). In comparison, the resilient modulus of crushed rock increased significantly as the density increased by around 66% (Hicks and Monismith 1971). Some laboratory investigations also found that the effect of density on resilient modulus was limited and much lesser for fully crushed than for partially crushed (i.e. mixing both crushed and non-crushed materials) aggregates (Hicks and Monismith 1971). Further investigation should therefore be conducted to evaluate the resilient behavior of partially crushed waste rock.

Finally, soaking of CWR specimens had limited influence on the equivalent modulus (Figure 4.11(f)). The average variation observed between soaked and un-soaked specimens was smaller than 32 MPa (< 11%). The absence of expansive minerals (such as gypsum or montmorillonite) in the tested CWR material (Table 4.2) could be a reason for this observation (Kuttah and Sato 2015). On the other hand, drying had a marked effect on the measured equivalent modulus, with an average increase of around 200 MPa. Indeed, specimen drying in oven tends to create bonds between CWR particles, which tend to significantly increase CWR stiffness (Valdes and Cortes

2014).

Based on these results, it appears that drying of road materials in summer is also likely to be beneficial to the resilient behavior and the trafficability of the roads (even though they would also produce more dusts; (Thompson and Visser 2007)). The influence of CWR soaking caused by rainfall on the resilient behavior of haul roads seems, however, to be limited.

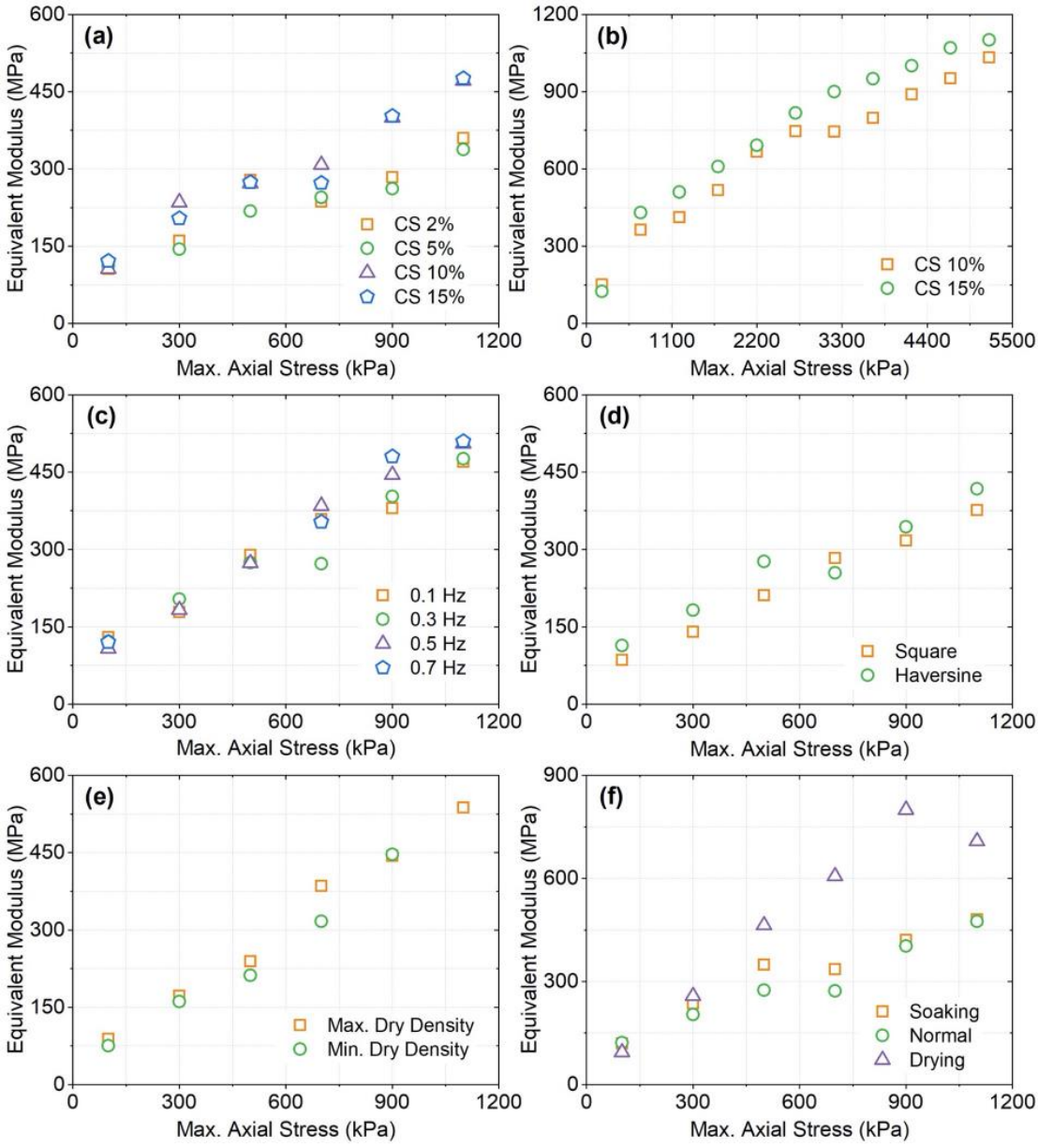

Figure 4.11: Influence of (a) contact stress (CS) for LSL RLCBR tests and (b) for HSL RLCBR tests, (c) frequency, (d) loading waveform, (e) dry density, and (f) specimen soaking and drying on CWR equivalent modulus.

4.5 Discussion and final remarks

Laboratory tests results indicated that RLCBR tests were able to estimate the resilient behavior of CWR satisfactorily through equivalent modulus calculations. The influence of loading frequency, waveform, specimen dry density, and soaking on equivalent modulus appeared limited, while the increase of contact stress and specimen drying resulted in a significant increase of the equivalent modulus. These results were, however, not validated for other types of waste rock. Mineralogy can have a marked effect on the resilient modulus of cohesive soils (Achampong et al. 1997), but was not investigated in this study.

The RLCBR tests results also depend on the accuracy of the loading actuator and nature of the software employed, and a high loading frequency generally gives less accurate load records for the minimum and maximum peaks of the loading cycle (Araya 2011). Similar limitations were also observed in this study. Also, the equipment used in this study was not designed specifically for RLCBR tests, and the plunger and mold were developed for static CBR tests, which could have affected the precision of the tests. The trends described are, however, considered representative of CWR resilient behavior. The RLCBR tests stability and repeatability under different loading frequency was evaluated by calculating the root mean squared error (RMSE) of equivalent modulus between duplicates. The 0.5 Hz frequency resulted in a significant increase of the RMSE (+65 MPa), which means the stability and precision of RLCBR test decreased significantly (Figure 4.12). The prediction for 0.7 Hz was even smaller (+160 MPa). However, these values were

significantly smaller than the loading frequencies caused by mining trucks (CAT 793F) on haul roads which typically are around 3 to 4 Hz (assuming a driving speed of 12 to 15 km/h and a payload rear tire contact radius of around 0.55 m). Therefore, the impact of higher loading frequency on CWR resilient behavior should be investigated.

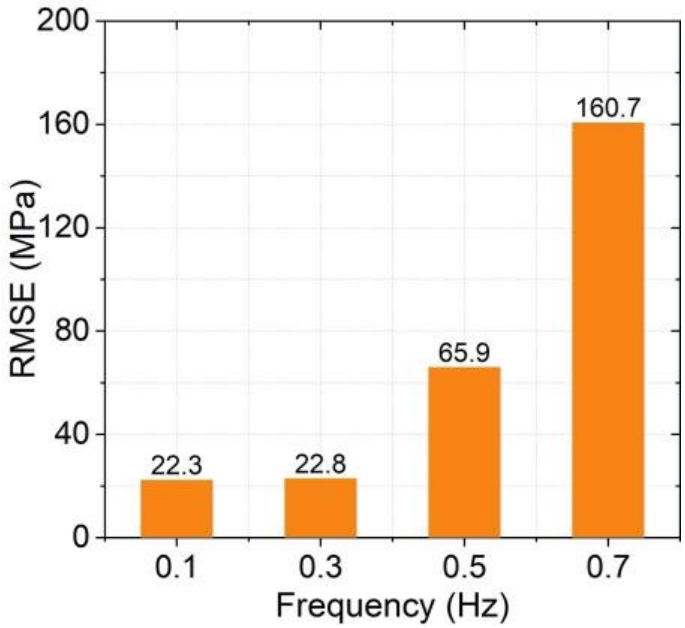

Figure 4.12: Root mean squared error (RMSE) of RLCBR equivalent modulus between duplicates for different test frequencies (0.1, 0.3, 0.5, and 0.7 Hz).

Poisson's ratio of CWR material was not measured in this study and was assumed to be constant and equal to 0.35. In practice, Poisson's ratio is not a constant and it may increase with a decrease in confining pressure and an increase in deviator stress (Hicks and Monismith 1971). The density, fines content, water content, aggregate type, and particle shape also affect the Poisson's ratio (Lekarp et al. 2000a). Poisson's ratio of CWR should therefore be measured in the laboratory to increase the accuracy of resilient and equivalent modulus estimation.

The effect of wetting and drying cycles on resilient behavior could be considered in a more realistic manner, for example, using wave propagation techniques as suggested by others (Said Razouki and Salem 2017). The freeze-thaw cycles were not considered in this study either, but can result in frost heave of pavement surface and a strength decrease of subgrade and base course in cold regions (Domitrović et al. 2019; Ishikawa et al. 2019). A more complete understanding of the mechanical behavior of the CWR material during freeze-thaw cycles would therefore be required for the mines located in cold regions (like in Canada).

Using a standard CBR mold limits the maximum particle size to 19 mm. In practice, even a wearing course should also have a maximum particle size (usually 40 mm) to provides a stronger matrix (Araya et al. 2012; Thompson et al. 2019). Larger diameters RLCBR or RLT tests are therefore recommended to evaluate the resilient behavior of coarser and more representative waste rocks.

Although a wide range of stress conditions (i.e., LSL and HSL) was applied in this study, the stress distribution and deformation in haul roads should also be determined using numerical simulations. In this case, non-linear elastic model should be used to accurately simulate the response of CWR layers under moving mining trucks (Coffey et al. 2018). However, the aim of this study was to evaluate the resilient behavior of CWR under low and high stress levels by using RLCBR and RLT tests. The evaluation of the performance (i.e. stress distribution and deformation) of the haul road constructed with the CWR exceeded the scope of this study.

The effect of principal stress reorientation on permanent deformation behavior of CWR was not taken into account in this study. In practice however, a reorientation of the principal stress can occur in real pavement structures under moving traffic load (Qian et al. 2016) which could result in large permanent strain, exceeding the deformation measured using RLT tests in the laboratory (Lekarp et al. 2000b; Qian et al. 2016). Such effect should be further investigated in the future studies.

The equation proposed in this study (Eq. 4.8) has the same structure as the existing NF, FF, and

WSOG equations (see Table 4.1), but with different parameters, which provides a more precise estimation of the CWR equivalent modulus under both low and high stress levels. Compared to the WSG equation, this new equation is easier to use since the horizontal and vertical stresses are not required. However, this equation needs to be validated before it can be applied to other materials.

4.6 Conclusions

In this study, the CWR resilient behavior was investigated under low and high stress level conditions by using RLCBR and RLT tests. The RLCBR equivalent modulus was compared to RLT resilient modulus, and the effect of loading features (frequency, contact stress, and waveform) and specimen properties (dry density, soaking, and drying) on CWR resilient behavior was investigated.

Based on the results of this study the following statements can be made:

1. The M_R-θ model showed good description for both RLCBR equivalent modulus and RLT resilient modulus. The prediction models calibrated from conventional RLT tests (e.g. AASHTO T307) could underestimate the resilient modulus of CWR used in mine haul roads.
2. The WOSG and NF equation were shown to yield satisfactory calculation of equivalent modulus for LSL and HSL RLCBR tests, respectively. A new equivalent modulus equation as a function of plunger stress and vertical resilient deformation was proposed to evaluate LSL and HSL RLCBR equivalent modulus with a coefficient of determination $R^2 > 0.93$.
3. The influence of loading frequency and waveform (haversine and square) on measured equivalent modulus was neglectable in the conducted tests. Equivalent modulus was, however, sensitive to contact stress, especially when the contact stress was lower than 10% of the maximum plunger stress.
4. The effect of dry density was limited since the change of dry density was relatively small in

this study. The influence of specimen soaking was insignificant because there is no expansive composition in this CWR material, while the specimen drying resulted in an obvious increase in equivalent modulus because of the cementation of particles.

This study was part of a more comprehensive research program which aimed at optimizing mine haul road design using waste rocks. The permanent deformation behavior of crushed waste rocks was also studied using repeated load triaxial and CBR tests, and the tests results will be presented in another article. Additional laboratory tests are ongoing to study the gradation effect on mechanical properties of crushed waste rocks.

Acknowledgements

This research was carried out with the financial support from FRQNT and the industrial partners of the Research Institute on Mines and the Environment (http://irme.ca/). The repeated load triaxial and CBR test equipment used in this study were acquired with a CFI grant.

4.7 References

AASHTO T307-99. Standard method of test for determining the resilient modulus of soils and aggregate materials. Washington, DC; 2017.

Achampong F, Usmen M, and Kagawa T. Evaluation of resilient modulus for lime- and cement-stabilized synthetic cohesive soils. Transportation Research Record 1997*;* 1589(1): 70-75.

Araya AA. Characterization of unbound granular materials for pavements. Delft University of Technology, 2011.

Araya AA, Huurman M, Molenaar AA, and Houben LJ. Investigation of the resilient behavior of

granular base materials with simple test apparatus. Materials and Structures 2012*;* 45(5): 695-705.

Araya AA, Huurman M, Molenaar AAA, and Houben LJM. Investigation of the resilient behavior of granular base materials with simple test apparatus. Materials and Structures 2011*;* 45(5): 695-705.

Araya AA, Molenaar AA, and Houben LJ. Characterization of unbound granular materials using repeated load CBR and triaxial testing. In: Paving Materials and Pavement Analysis; 2010.

ASTM D1557-12e1. Standard test methods for laboratory compaction characteristics of soil using modified effort (56,000 ft-lbf/ft^3 (2,700 kN-m/m^3)). ASTM International, West Conshohocken, PA; 2012.

ASTM D854-14. Standard test methods for specific gravity of soil solids by water pycnometer. ASTM International, West Conshohocken, PA; 2014.

ASTM C127-15. Standard test method for relative density (specific gravity) and absorption of coarse aggregate. ASTM International, West Conshohocken, PA; 2015.

ASTM D1883-16. Standard test method for California Bearing Ratio (CBR) of laboratory-compacted soils. ASTM International, West Conshohocken, PA; 2016.

ASTM D2487-17e1. Standard practice for classification of soils for engineering purposes (Unified Soil Classification System). ASTM International, West Conshohocken, PA; 2017.

ASTM C136/C136M-19. Standard test method for sieve analysis of fine and coarse aggregates. ASTM International, West Conshohocken, PA; 2019.

ASTM D698-12e2. Standard test methods for laboratory compaction characteristics of soil using standard effort (12 400 ft-lbf/ft^3 (600 kN-m/m^3)). ASTM International, West Conshohocken, PA; 2012.

Aubertin M. Waste rock disposal to improve the geotechnical and geochemical stability of piles. In: Proceedings of the world mining congress, Montreal, Canada; 2013.

Barksdale R, Alba J, Khosla N, Kim R, Lambe P, et al. Nchrp web doc 14 laboratory determination of resilient modulus for flexible pavement design. 1997.

Barksdale RD. Performance of crushed-stone base courses. Transp Res Record 1984*;* 954: 78-87.

Belaz-7571 series. BELAZ North America. http://belaz.ca/products/dumptrucks/7571.html, 2018.

Bhattacharjee S, and Bandyopadhyay K. Evaluation of elastic modulus of fly ash embankment by repeated load cbr test. Geotechnical Engineering for Infrastructure and Development 2015: 229-234.

Boyce J, Brown S, and Pell P. The resilient behaviour of a granular material under repeated loading. In: Australian Road Research Board Conference Proc; 1976.

Cetin A, Kaya Z, Cetin B, and Aydilek AH. Influence of laboratory compaction method on mechanical and hydraulic characteristics of unbound granular base materials. Road materials and pavement design 2014*;* 15(1): 220-235.

Coffey J, Ghadimi B, Nikraz H, and Rosano M. The modelling prediction of haul road surface deflection. Transp Geotech 2018*;* 14: 136-145.

Coronado O, Caicedo B, Taibi S, Gomes Correia A, Souli H, et al. Effect of water content on the resilient behavior of non standard unbound granular materials. Transp Geotech 2016*;* 7: 29-39.

Domitrović J, Rukavina T, and Lenart S. Effect of freeze-thaw cycles on the resilient moduli and permanent deformation of rap/natural aggregate unbound base mixtures. Transp Geotech 2019*;* 18: 83-91.

Dunlap WA. A report on a mathematical model describing the deformation characteristics of

granular materials: Texas Transportation Institute, Texas A & M University; 1963.

Ekblad J, and Isacsson U. Influence of water on resilient properties of coarse granular materials. Road materials and pavement design 2006*;* 7(3): 369-404.

Electric drive mining truck 960e-2k. KOMATSU. https://www.komatsuamerica.com/equipment/trucks/electric/960e-2k, 2020.

Elliott RP, and David L. Improved characterization model for granular bases. Transp Res Record 1989*;* (1227).

Evans MD, Bolton Seed H, and Seed RB. Membrane compliance and liquefaction of sluiced gravel specimens. Journal of Geotechnical Engineering 1992*;* 118(6): 856-872.

Evans MD, and Seed HB. Undrained cyclic triaxial testing of gravels: The effect of membrane compliance: College of Engineering, University of California; 1987.

Fairhurst C, Kosla N, and Kim Y. Resilient modulus testing of asphalt specimens in accordance with astm d4123-82. In: Mechanical Tests for Bituminous Mixes. Characterization, Design and Quality Control. Proceedings of the Fourth International Symposium held by RILEM, Budapest, Hungary; 1990.

Ferdosi B, James M, and Aubertin M. Effect of waste rock inclusions on the seismic stability of an upstream raised tailings impoundment: A numerical investigation. Can Geotech J 2015*;* 52(12): 1930-1944.

Haghighi H, Arulrajah A, Mohammadinia A, and Horpibulsuk S. A new approach for determining resilient moduli of marginal pavement base materials using the staged repeated load cbr test method. Road Materials and Pavement Design 2017*;* 19(8): 1848-1867.

Henkel D, and Gilbert G. The effect measured of the rubber membrane on the triaxial compression strength of clay samples. Geotechnique 1952*;* 3(1): 20-29.

Hicks RG, and Monismith CL. Factors influencing the resilient response of granular materials. Highway research record 1971*;* 345: 15-31.

Hu X, Zhou F, Hu S, and Walubita LF. Proposed loading waveforms and loading time equations for mechanistic-empirical pavement design and analysis. Journal of Transportation Engineering 2010*;* 136(6): 518-527.

IS 2386. Methods of test for aggregates for concrete, part I: Particle size and shape. 1963.

Ishikawa T, Lin T, Kawabata S, Kameyama S, and Tokoro T. Effect evaluation of freeze-thaw on resilient modulus of unsaturated granular base course material in pavement. Transp Geotech 2019*;* 21: 100284.

Kuttah D, and Sato K. Review on the effect of gypsum content on soil behavior. Transp Geotech 2015*;* 4: 28-37.

Laverdière A. Effet de la granulométrie sur le comportement géotechnique de roches stériles concassées utilisées comme surface de roulement sur des routes minières. École Polytechnique de Montréal, 2019.

Lekarp F, Isacsson U, and Dawson A. State of the art. I: Resilient response of unbound aggregates. Journal of Transportation Engineering 2000a*;* 126(1): 66-75.

Lekarp F, Isacsson U, and Dawson A. State of the art. Ii: Permanent strain response of unbound aggregates. Journal of transportation engineering 2000b*;* 126(1): 76-83.

Molenaar AA. Repeated load cbr testing, a simple but effective tool for the characterization of fine soils and unbound materials. 2008.

Molenaar AA, Araya AA, and Houben LJ. Characterization of unbound base materials for roads using a new developed repeated load cbr test. In: Eighth International Conference on Managing Pavement Assets, Santiago, Chile; 2011.

Moossazadeh J, and Witczak MW. Prediction of subgrade moduli for soil that exhibits nonlinear behavior. Transportation Research Record 810 1981: 9-17.

Ni B, Hopkins T, Sun L, and Beckham T. Modeling the resilient modulus of soils. In: Proceedings of the 6th international conference on the bearing capacity of roads and airfields, Lisbon, Portugal; 2002.

Opiyo T. A mechanistic approach to laterite-based pavements in transport and road engineering. (MSc Thesis). International Institute for Infrastructure, Hydraulics and Environment Engineering, Delft, the Netherlands. 1995.

Pezo R, and Hudson WR. Prediction models of resilient modulus for nongranular materials. Geotechnical Testing Journal 1994*;* 17(3): 349-355.

Qian JG, Wang YG, Yin ZY, and Huang MS. Experimental identification of plastic shakedown behavior of saturated clay subjected to traffic loading with principal stress rotation. Engineering Geology 2016*;* 214: 29-42.

Said Razouki S, and Salem BM. Gypsum sand resilient modulus during cyclic soaking and drying. International Journal of Pavement Engineering 2017*;* 18(2): 108-118.

Sas W, and Gluchowski A. Application of cyclic cbr test to approximation of subgrade displacement in road pavement. Acta Scientiarum Polonorum. Architectura 2013*;* 12(1).

Sas W, Głuchowski A, and Szymański A. Determination of the resilient modulus mr for the lime stabilized clay obtained from the repeated loading cbr tests. Annals of Warsaw University of Life Sciences-SGGW. Land Reclamation 2012*;* 44(2): 143-153.

Seed H, Mitry F, Monismith C, and Chan C. University of California, Berkeley. Prediction of pavement deflections from laboratory repeated load tests, report no. Te 65-6, soil mechanics and bituminous materials research laboratory. 1965.

Seed H, Mitry F, Monismith C, and Chan C. Prediction of flexible pavement deflections from

laboratory repeated-load tests (NCHRP report 35). 1967.

Shafabakhsh G, and Tanakizadeh A. Investigation of loading features effects on resilient modulus of asphalt mixtures using adaptive neuro-fuzzy inference system. Constr Build Mater 2015*;* 76: 256-263.

Sparsha N, Robinson R, and Murali J. Use of repeated load cbr test to characterize pavement granular materials. In: Functional Pavement Design; 2016.

Tannant D, and Regensburg B. Guidelines for mine haul road design. 2001.

Thach Nguyen B, and Mohajerani A. Possible simplified method for the determination of the resilient modulus of unbound granular materials. Road materials and pavement design 2016*;* 17(4): 841-858.

Thompson R, Peroni R, and Visser AT. Mining haul roads: Theory and practice: CRC Press; 2019.

Thompson RJ, and Visser AT. A mechanistic structural design procedure for surface mine haul roads. International Journal of Surface Mining, Reclamation and Environment 1997*;* 11(3): 121-128.

Thompson RJ, and Visser AT. Selection parameters for mine haul road wearing course materials. International Journal of Surface Mining, Reclamation and Environment 2007*;* 14(1): 1-17.

Tian P, Zaman MM, and Laguros JG. Gradation and moisture effects on resilient moduli of aggregate bases. Transp Res Record 1998*;* 1619(1): 75-84.

Titi HH, and Matar MG. Estimating resilient modulus of base aggregates for mechanistic-empirical pavement design and performance evaluation. Transp Geotech 2018*;* 17: 141-153.

Uzan J. Characterization of granular material. Transp Res Record 1985*;* 1022(1): 52-59.

Valdes JR, and Cortes DD. Heat-induced bonding of sands. In: Geo-Congress 2014: Geo-characterization and Modeling for Sustainability; 2014.

Witczak MW, and Uzan J. The universal airport pavement design system. Report I of V: granular material characterization, Department of Civil Engineering, University of Maryland, College Park, MD 1988.

Woodrooffe JH. Review of canadian experience with the regulation of large commercial motor vehicles (Vol. 671): Transportation Research Board; 2010.

CHAPTER 5 ARTICLE 2: ESTIMATION OF PERMANENT DEFORMATION BEHAVIOUR OF CRUSHED WASTE ROCKS USING MULTISTAGE REPEATED LOAD TRIAXIAL AND CBR TESTS

Shengpeng Hao and Thomas Pabst

This article was submitted to *International Journal of Pavement Engineering* in June 2021.

Abstract: Crushed waste rocks (CWR) are widely used to build mine haul roads. However, the permanent deformation in waste rocks layers can result in surface rutting. Realistic prediction of pavement rutting requires models that can accurately capture the permanent deformation behaviour under repeated loading. However, such models are usually based on advanced laboratory apparatus such as multistage (MS) repeated load triaxial (RLT) tests. In this study, a new approach, using MS repeated load CBR (RLCBR) tests, was proposed to estimate the permanent deformation behaviour of CWR. MS RLCBR tests are faster, easier and more often available than MS RLT tests. A series of MS RLCBR and MS RLT tests for different stress levels were therefore carried out on the same material to characterize CWR permanent deformation behaviour. Results showed that Rahman and Erlingsson model that modified by time hardening approach could satisfactorily capture CWR permanent deformation behaviour for MS RLT tests. A new model was proposed and fitted on MS RLCBR test results to predict CWR permanent deformation behaviour. This model performed well in describing MS RLCBR test results and predicting the CWR permanent deformation behaviour. Results indicate that MS RLCBR tests could be an effective alternative to MS RLT tests for estimating the permanent deformation behaviour of CWR.

Keywords: Crushed waste rocks, Mine haul roads, Permanent deformation, repeated load CBR tests, repeated load triaxial tests.

5.1 Introduction

Mining operations produce large quantities of waste rocks that can be valorized to build mine haul roads (Thompson 2011c). Pavements are typically subjected to cyclic stresses of varying magnitudes caused by the moving traffic loads, which can lead to resilient (or elastic) deformation and permanent (or plastic) deformation (Lekarp et al. 2000a). Permanent deformation can result from material compaction, crushing and particle migration (Tholen 1980; Lekarp 1999). The gradual accumulation of permanent deformation in pavement layers can result in rutting, one of the most common deteriorations in flexible pavements (Erlingsson 2012). Excess rutting can decrease the driving quality and safety because of hydroplaning and reduced skid resistance of the road surface (Rahman and Erlingsson 2015a; Salour and Erlingsson 2017). This phenomenon is particularly critical in mine haul roads because of the ultra-high weight of mining trucks. As a consequence, poor functional performance can lead to increased tire wear and damage and an accompanying loss of productivity, and result in an increase of overall vehicle operating and maintenance costs (Thompson and Visser 2007).

The development of permanent deformation in unbound granular material typically consists of two phases (Erlingsson et al. 2017). First, the permanent strain increases rapidly with loading cycles during the initial phase because of post-compaction. Post compaction is accompanied by densification, decrease in pore volume and volumetric change of the material (Werkmeister et al. 2004; El-Basyouny et al. 2005). In the second phase, the deformation rate becomes more or less constant and is dominated by volume change (Werkmeister et al. 2004). The shakedown concept is typically used to describe the behaviour of pavement materials under repeated loading (Werkmeister et al. 2001; Werkmeister et al. 2004; Mohammadinia et al. 2020). Based on the shakedown theory, the evolution of permanent strain with loading cycles can be classified into

three categories (A, B or C). Werkmeister (2003) suggested the following criteria to define the shakedown boundaries based on the repeated load triaxial (RLT) test results, and they have been adopted in the European standard Cyclic Load Triaxial Test for Unbound Mixtures (EN 13286 2004). The shakedown categories of unbound granular materials depend on the applied stress levels (Werkmeister et al. 2004):

Range A (plastic shakedown): $(\varepsilon_p^{5000}-\varepsilon_p^{3000})<0.045\times10^{-3}$

Range B (plastic creep): $0.045\times10^{-3}<(\varepsilon_p^{5000}-\varepsilon_p^{3000})<0.4\times10^{-3}$

Range C (incremental collapse): $(\varepsilon_p^{5000}-\varepsilon_p^{3000})>0.4\times10^{-3}$

Where ε_p^{5000} and ε_p^{3000}correspond to the accumulated permanent strains measured at the 5000^{th} and 3000^{th} loading cycles during the RLT tests.

In range A, the post-compaction is completed, and the material becomes stable with no further permanent strain after a finite number of load applications. In range B, the permanent strain rate decreases with the number of loads and progressively becomes very low and nearly constant. Yet, the permanent strain continues to accumulate but at a very slow rate. In range C, the permanent strain decreases very slowly compared to ranges A or B, and permanent strain continues to accumulate with load applications, ultimately leading to failure (Werkmeister 2003; EN 13286 2004; Werkmeister et al. 2004). The shakedown categories are often used in pavement analysis and design (Collins and Boulbibane 1998, 2000; Tao et al. 2010). For highway engineering, materials falling in range A can be used provided the total accumulated strain is sufficiently small, materials in range B may be permitted for a limited number of load cycles (e.g. short term roads) while materials in range C are not authorized (Werkmeister et al. 2004). However, the applicability of shakedown theory and the corresponding criteria to haul roads need further investigations because of the specificities of haul roads, such as high stress levels, low-volume traffic, short-service-life, and relatively low running speed of mining trucks.

Permanent deformation and shakedown categories of pavement materials are generally measured using multi stage (MS) RLT tests (EN 13286 2004). In these tests, the specimen is exposed to a series of consecutive stress paths of varying magnitudes to determine the maximum stress levels which should not be exceeded to avoid the development of excessive permanent deformations (EN 13286 2004). Applied stress levels in MS RLT tests should cover the stress range to which the material will be submitted in the field (EN 13286 2004). Various models were proposed for permanent strain prediction, which parameters are generally calibrated by fitting the permanent strains measured by RLT tests. These calibrated models can then be used to predict the permanent deformation behaviour of pavement materials caused by moving vehicles in the field. These models are usually a function of number of loading cycles and stress conditions (e.g., deviator stress q and mean bulk stress p) (Barksdale 1972; Sweere 1990; Wolff and Visser 1994; Lekarp et al. 2000b; Gidel et al. 2001; Korkiala-Tanttu 2005; Rahman and Erlingsson 2015a). The existing models were initially developed for highway engineering, but the applicability to mine haul roads with high stress levels should be evaluated. The size and capacity of mining trucks have, indeed, increased significantly over the past decades, and can now exceed 450 mt ("Belaz-7571 series", 2018). In comparison, the gross vehicle weight of three axles straight truck considered for highway design in Canada is 24.25 mt (Woodrooffe, 2010).

Also, MS RLT tests can be time consuming, sophisticated, and expensive, especially when up to 30 stress paths are used, each applied for 10 000 cycles (EN 13286 2004; Saberian et al. 2020). CWR tests also require larger and more specific equipment to accommodate larger particles and greater stresses (Mishra et al. 2013; Qian et al. 2014; Sun et al. 2014). MS repeated load CBR (RLCBR) tests were therefore proposed in this study as an alternative to evaluate permanent deformation behaviour of CWR used as pavement materials in haul roads. The principle of MS RLCBR test is similar to the standard CBR test, except that cyclic loads are applied (Opiyo 1995; Molenaar 2008; ASTM D1883 2016). MS RLCBR tests are frequently used to estimate the resilient modulus (Molenaar 2008; Molenaar et al. 2011; Araya et al. 2012; Sas et al. 2012; Bhattacharjee

and Bandyopadhyay 2015; Abid et al. 2017; Haghighi et al. 2017), but more rarely to evaluate permanent deformation behaviour. Therefore, it is necessary to identify the permanent deformation behaviour of CWR under MS RLCBR tests. Also, the existing permanent deformation models, which were primarily proposed for RLT tests, cannot be used directly for RLCBR tests (because of the completely different stress states within the specimens (Araya 2011).

The aim of this paper was, therefore, to evaluate the permanent deformation behaviour of CWR using MS RLT and RLCBR tests over a wide range of stress levels. The applicability of three constitutive models from the literature were evaluated. A model was then proposed to fit MS RLCBR test results, and to determine material parameters for Rahman and Erlingsson model to predict the permanent deformation behaviour of CWR. Finally, the Rahman and Erlingsson model parameters (a, b, and α) calibrated by the proposed new model and MS RLCBR tests were validated using MS RLT test data.

5.2 Methodology

5.2.1 Material characterization

The tested CWR were sampled on Canadian Malartic Mine, an open pit gold mine located in the Abitibi region, in Quebec province, Canada (Bussière 2007a; James et al. 2013). Particles larger than 19 mm were removed (sieved) to accommodate the specimen to the 152.4 mm diameter CBR mold. The particle size distribution of CWR was tested using sieving in the laboratory ((ASTM C136/C136M 2019); Figure 5.1(a)). The tested CWR had a small amount (< 4%) of fines (< 75 μm), and was classified as a well-graded gravel corresponding to the dual symbol GW-GM (ASTM D2487 2017). Maximum particle size was 25 mm and grading coefficient (Thompson 2010)) $G_c = 25.6$. Overall, the tested crushed waste rock was considered representative of materials typically used to build the surface layer of mine haul roads (Thompson 2010; Laverdière 2019).

The moisture-density relationship was measured using modified effort Proctor compaction tests (ASTM D1557 2012). The optimum water content was 5.6%, for a corresponding maximum dry density of 2334 kg/m^3 (Figure 5.1(b)). The maximum attainable degree of saturation was around 85%; above, water would leak out of the sample during compaction. Specific gravity (GS) of CWR particles finer and coarser than 4.75 mm was 2.75 and 2.71, respectively (ASTM D854 2014, C127 2015). Sample mineralogy was measured using X-ray diffraction (XRD) tests. CWR contained a small fraction of sulfides (1% of pyrite) but was considered non-acid generating because of a significant buffering capacity (Tremblay and Hogan 2001; Golder 2019). Additional properties of tested CWR are summarized in Table 5.1.

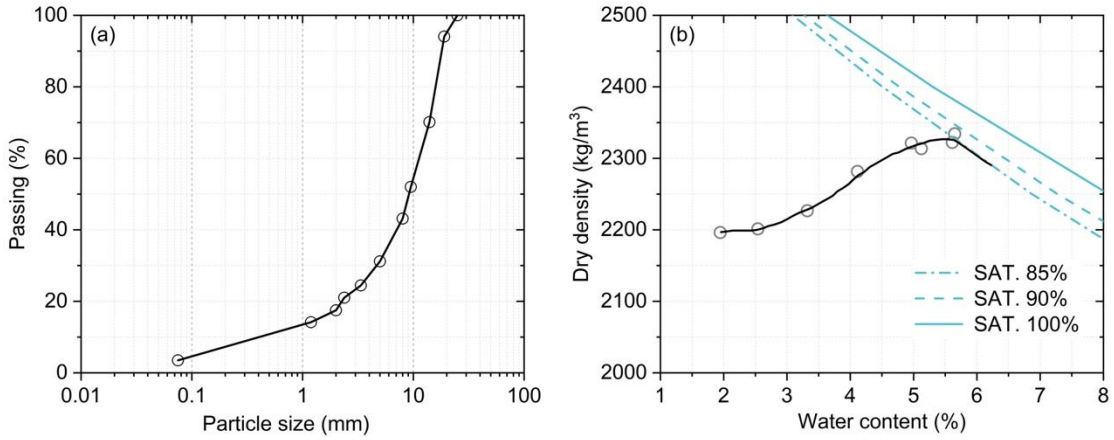

Figure 5.1: (a) Particle size distribution of tested crushed waste rocks, and (b) moisture-density relationship of crushed waste rocks measured by modified effort Proctor tests.

Table 5.1: Geotechnical and geochemical properties of tested crushed waste rocks. [a]: particle size smaller than 4.75 mm; [b]: particle size larger than 4.75 mm; coefficient of uniformity $C_U = D_{60}/D_{10}$ and coefficient of curvature $C_C = D_{30}^2/(D_{60}\times D_{10})$.

Mineralogy	Proportion	Properties		Standard
Quartz	26.08±2.46%	Specific gravity [a]	2.75	(ASTM D854 2014)

Albite	38.74±4.30%	Specific gravity [b]	2.71	(ASTM C127 2015)
Muscovite	10.87±1.42%	Water absorption [b]	0.41%	
Chlorite	7.12±0.97%	Elongation index	38.56±1.62%	(IS 2386 1963)
Corundum	6.80±1.33%	Flakiness index	34.95±2.08%	
Diopside	6.50±1.34%	Optimum water content	5.6%	(ASTM D1557 2012)
Anhydrite	2.42±0.48%	Maximum dry density	2334 kg/m^3	
Pyrite	1.08±0.15%	Coefficient of uniformity	7.98	(ASTM D2487 2017)
Rutile	1.18±0.79%	Coefficient of curvature	2.21	

Six static triaxial tests were also conducted under different confining pressures (i.e. 50 (duplicate), 100, 135, 200, and 300 kPa). The static test was carried out under drained condition. The testing specimens (300 mm in height and 150 mm in diameter) were prepared at 4% initial gravimetric water content using modified compaction effort (2700 kN-m/m^3). The deviator stress at failure (q_f) for each CWR specimen was plotted as a function of the mean bulk stress-deviator stress (i.e., *p*-*q*), and the Mohr-Coulomb envelope was estimated using linear regression. The slope (m) and intercept (s) of the Mohr-Coulomb failure line were 2.02 and 221.96 kPa, respectively (Figure 5.2).

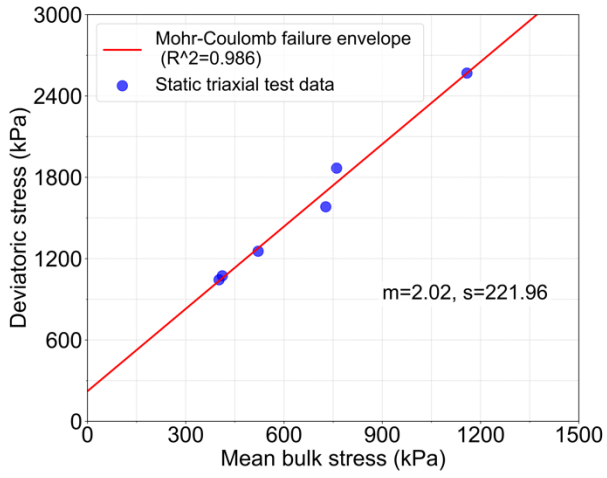

Figure 5.2: Mohr-Coulomb failure envelope in mean bulk stress-deviator stress space.

5.2.2 MS RLT tests

A total of three standard and modified MS RLT tests were carried out to measure the permanent deformation of CWR for different stress levels. MS RLT tests were conducted in load-controlled mode using a 100 kN loading frame and 1000 kPa stress controllers. A 50 kN load cell (error < 0.03% of applied load) recorded continuously the actual load applied on top of the specimens. The vertical deformation of the specimen was monitored using a linear variable differential transformer (LVDT) placed on the load cell. Specimens (300 mm in height and 150 mm in diameter) were prepared with 4% of initial gravimetric water content (w) using modified compaction effort (i.e. 2700 kN-m/m^3). MS RLT tests were conducted following the European Standard 13286-7 (2004) with two sets of stress levels (low stress level (LSL)) and high stress level (HSL)). Each stress level consisted of five sequences, and each sequence contained 5 or 6 stress paths with a constant confining pressure and different deviator stresses (Table 5.2). In this study, 10 000 loading cycles were applied in each stress path.

The tire pressure of mine trucks could reach 1000 kPa ("Electric drive mining truck 960e-2k" 2020), which is significantly higher than the deviator stress applied in LSL and HSL. Therefore, another high stress level was specifically defined in this study to represent typical stress conditions within mine haul roads and was referred to as HSLM (M standing for mining). HSLM was divided into 4 sequences, and each of these sequences contained 4 stress paths that had a constant confining pressure but different deviator stresses (Table 5.2). The confining pressure and deviator stress ranged from 80 to 550 kPa, and from 100 to 1500 kPa, respectively. In total, 6000 loading cycles were applied in each stress path.

In this study, MS RLT tests were carried out using haversine loading pulses with no rest period and with a 0.3 Hz loading frequency. The CWR specimens were tested under drained condition. The axial deformation of the CWR specimens was recorded during the MS RLT tests.

Table 5.2: Stress levels with different confining stress (CS) and deviator stress (DS) for MS RLT tests, LSL and HSL are prescribed by the European Standard (EN 13286 2004), and HSLM was defined in this study for mining applications (see text for details).

Sequence 1		Sequence 2		Sequence 3		Sequence 4		Sequence 5	
CS, kPa	DS, kPa	CS, kPa	DS, kPa	CS, kPa	DS, kPa	CS, kPa	DS, kPa	CS, kPa	DS, kPa
LSL									
20	20	45	60	70	80	100	100	150	100
20	40	45	90	70	120	100	150	150	200
20	60	45	120	70	160	100	200	150	300
20	80	45	150	70	200	100	250	150	400
20	100	45	180	70	240	100	300	150	500
20	120	45	210	70	280	100	350	150	600
HSL									
20	50	45	100	70	120	100	200	150	200
20	80	45	180	70	240	100	300	150	300
20	110	45	240	70	320	100	400	150	400
20	140	45	300	70	400	100	500	150	500
20	170	45	360	70	480	100	600	150	600
20	200	45	420	70	560				
HSLM									
80	100	200	300	350	400	550	600		
80	200	200	500	350	700	550	900		
80	300	200	700	350	1000	550	1200		
80	400	200	900	350	1300	550	1500		

5.2.3 MS RLCBR tests

A total of three MS RLCBR tests were performed in which each stress path was applied either 6000, 3000 or 1000 times (i.e. cycles), to evaluate the permanent deformation behaviour of CWR employing the same load frame than that for MS RLT tests.

A standard CBR mold (152.4 mm in diameter and 178 mm in height with a 51 mm compaction collar), and a 49.63 mm diameter plunger were used to prepare and penetrate CWR specimens. All

specimens for MS RLCBR tests were compacted using modified effort 2700 kN-m/m^3 (ASTM D1883 2016), and with an initial gravimetric water content of 4%.

Ten stress paths (noted SP1 to SP10) were defined in this paper (Table 3). MS RLCBR tests were carried out using haversine loading pulse with no rest period, and the loading frequency was 0.3 Hz. The deformation of the sample was monitored using a LVDT placed on the load cell.

Several transfer functions were proposed to estimate the stress state of CBR specimen under vertical plunger loading and are based on linear elastic theory to calculate the vertical and horizontal (or lateral) stresses, Poisson's ratio and elastic modulus (Araya et al. 2012). The estimation of stress state is generally based on the applied plunger stress, and corresponding vertical and lateral deformation of the specimen. However, the measurement of lateral deformation of CBR specimen is difficult, which limits the applicability of the existing functions. Therefore, the existing transfer functions were modified to calculate the vertical and horizontal stresses using the applied plunger stress and Poisson's ratio v of tested material (Eq. 5.1 and 5.2); (Hao and Pabst 2021)). The ratio of horizontal to vertical stress d varied linearly with the Poisson's ratio v (Eq. 5.3). The bulk stress p_c (Eq. 5.4) was calculated based on vertical and horizontal stresses (Eq. 5.1-5.3), and was used to propose a new model.

$$\sigma_H = 0.363 v \sigma_p e^{(0.072/v)} \quad 5.1$$

$$\sigma_V = 0.368 \sigma_p \quad 5.2$$

$$d = 0.986 v e^{(0.072/v)} \approx 0.9617\upsilon + 0.0919 \ (R^2 = 0.9996) \quad 5.3$$

$$p_c = (0.7078\upsilon + 0.4356)\sigma_p \quad 5.4$$

The Poisson's ratio v of granular material is typically between 0.3 and 0.5 (Tannant and Regensburg 2001). A Poisson's ratio of 0.35 was used here to estimate the stress state of MS RLCBR specimens (Thompson and Visser 1997b; Tannant and Regensburg 2001; Laverdière 2019).

The stress levels used for MS RLT and RLCBR tests were chosen so results would be comparable: the mean bulk stress used for MS RLT tests ranged from around 25 (LSL) to 1000 kPa (HSLM) (Table 5.2), and the maximum axial plunger stress for MS RLCBR tests varied from 100 to 4000 kPa which corresponded to a mean bulk stress between 23 and 900 kPa (Eq. 5.4; Table 5.3).

Table 5.3: Stress path (SP) for MS RLCBR tests with different maximum axial stress (MAS) and the corresponding maximum axial load (MAL).

SP	MAS, kPa	MAL, N	SP	MAS, kPa	MAL, N
1	100	193.4	6	2000	3867.1
2	200	386.7	7	2500	4833.9
3	500	966.8	8	3000	5800.7
4	1000	1933.6	9	3500	6767.5
5	1500	2900.3	10	4000	7734.2

5.3 Results

5.3.1 MS RLT test results

The influence of stress levels on accumulated permanent strains measured by MS RLT tests was significant (Figure 5.3). For most stress paths, permanent strain first rapidly increased during the first 500 loading cycles, and then reached an equilibrium state after post-compaction stabilization (i.e. after around 2000 cycles), and limited increase in permanent stain occurred during the following loading cycles. Stress path 16 (1500 kPa) in HSLM were slightly different and showed continuous increase of permanent strain for all cycles. The accumulated permanent strains during sequence 1 for LSL and HSL was similar, i.e. around 0.0025 after 60 000 cycles and for a maximum deviator stress of 120 kPa and 200 kPa, respectively. The difference of accumulated permanent strains between LSL and HSL then increased as the loading cycles and the difference in deviator stress increased. The final accumulated permanent strains were 0.007 and 0.008 for LSL and HSL,

respectively (Figure 5.3(a) and (b)).

The accumulated permanent strain for HSLM also increased with the stress paths, but the curve was steeper than for LSL and HSL because of the significantly greater deviator stress. The final accumulated permanent strain after four sequences and 96 000 cycles was around 0.012 that was much higher than LSL and HSL (Figure 5.3(c)).

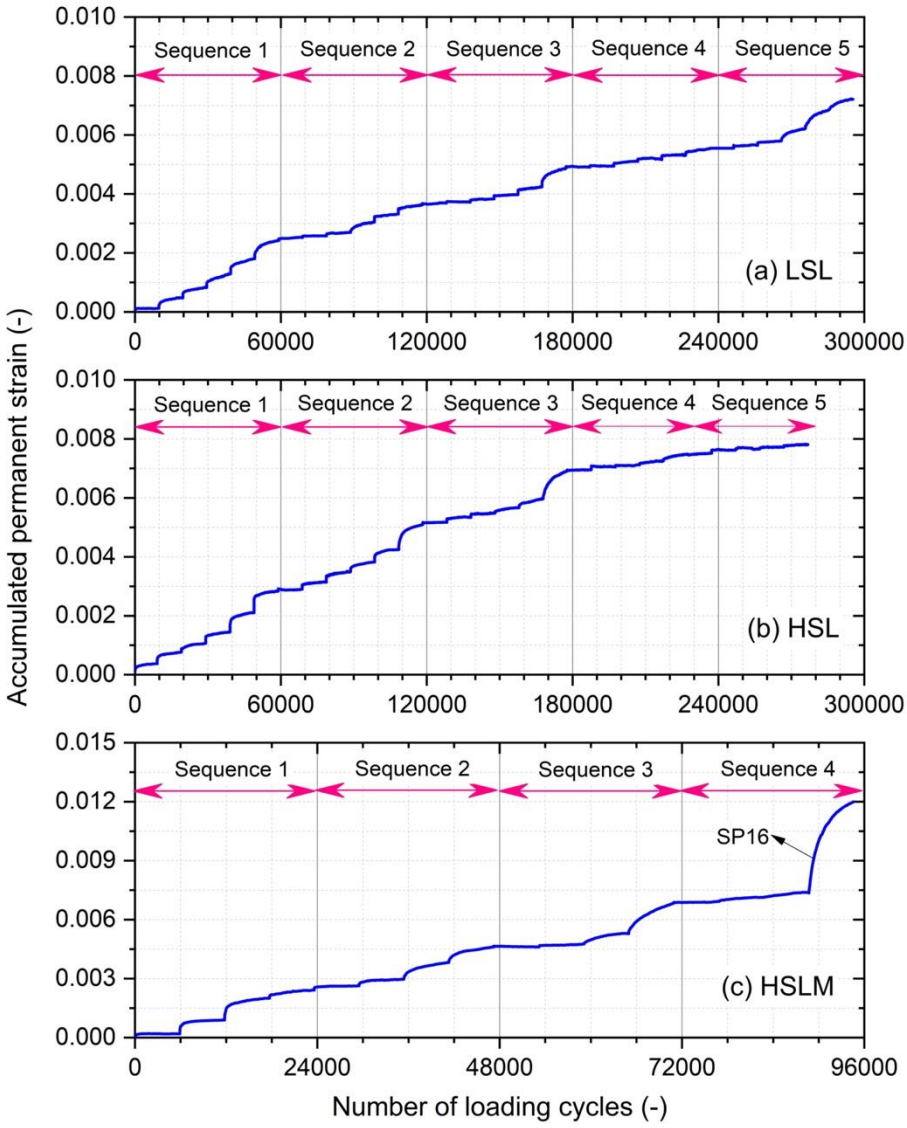

Figure 5.3: Accumulation of permanent strain of crushed waste rocks measured during MS RLT tests for different stress levels ((a) LSL: Low Stress Level, (b) HSL: High Stress Level, and (c)

HSLM: High Stress Level for Mining Engineering). SP: stress path (see Table 5.2).

The shakedown range was calculated for each stress path of the MS RLT tests (Werkmeister 2003; EN 13286 2004). The trace of the Mohr-Coulomb yield surface, the applied stress paths, and the shakedown ranges for each stress path were plotted in *p*-*q* space for each of the three MS RLT tests (Figure 5.4). The shakedown range increased gradually from A to B and from B to C as the applied deviator stress increased in each sequence (confining pressure remained constant). For HSL, shakedown range increased from A to B when the ratio of peak axial stress to confining pressure exceeded 9. For example, the shakedown range became B for the last two stress paths in sequence 1 and 2, as the ratio of peak axial stress to confining pressure was 9.5, 11, 9, and 10.3, respectively (Figure 5.4(b)). However, for LSL, shakedown range increased from A to B when the ratio of peak axial stress to confining pressure was greater than 5 in sequence 1 and 3, and greater than 3.5 for sequence 5. For HSLM, the limit ratio of peak axial to confining pressure for shakedown range B was around 4 for sequence 1, 2, and 3. In this case, however, the last stress path in sequence 4 (i.e. stress path 16 in Figure 5.3(c)) was in range C, corresponding to the rapid increase of permanent strain observed with loading cycles (also see above) although the ratio of peak axial stress to confining pressure was smaller than 4 (Figure 5.4(c)). One of the possible reasons for the inconsistent shakedown limit (i.e., ratio of peak axial stress to confining pressure) could be that the stress path history may affect the permanent deformation behaviour (Lytton et al. 1993; Zhou et al. 2010; Erlingsson and Rahman 2013).

Shakedown range C in stress path 16 in HSLM could lead to the failure of CWR and result in rutting (Werkmeister et al. 2004). However, in practice, the stress conditions within haul roads may be more complex than the applied stress paths in MS RLT tests, and a constitutive model should be determined to predict the permanent deformation behaviour of CWR in the field.

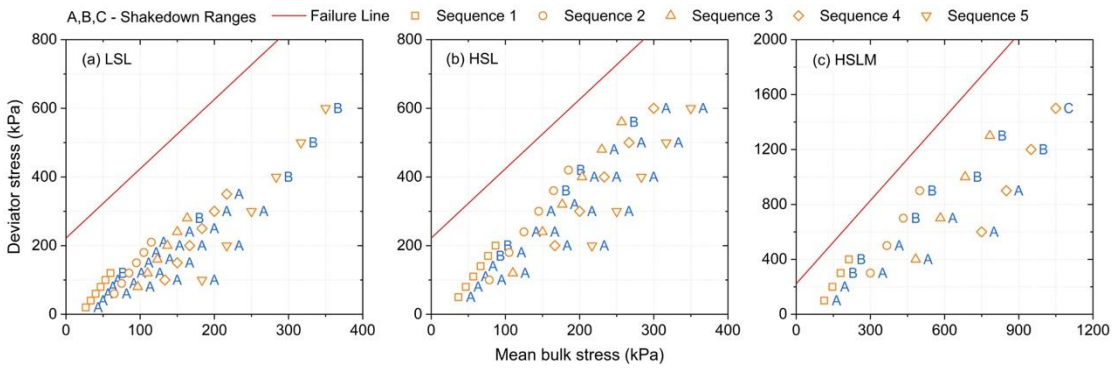

Figure 5.4: Trace of Mohr-Coulomb yield surface, applied stress paths and corresponding measured shakedown ranges for MS RLT tests for (a) LSL, (b) HSL, and (c) HSLM.

5.3.2 MS RLCBR test results

The accumulated permanent strain tended to increase with the number of loading cycles and the applied stress for all the three MS RLCBR tests, but the trends depended on the stress paths and the number of cycles for each stress path (Figure 5.5).

For the MS RLCBR test with 6000 cycles for each stress path, the accumulated permanent strain increased to around 0.02 after 10 stress paths corresponding to a maximum stress of 4000 kPa (also see Table 5.3). For the first five stress paths (i.e. maximum axial stress MAS < 1500 kPa), the trend of the permanent strain for each stress path was similar to MS RLT tests, i.e., the permanent strain increased rapidly during the first 2000 loading cycles, and then became more or less constant. However, the accumulated permanent strain kept increasing with cycles after stress path 5, especially for stress path 9 and 10, where the increase was almost linear (Figure 5.5).

The final accumulated permanent strains for the MS RLCBR tests with 1000 and 3000 cycles were 0.013 and 0.025 after10 stress paths, respectively (Figure 5.5). The slope of accumulated permanent strain increased significantly as the number of loading cycles for each stress path decreased from 6000 to 3000 and 1000. For the tests with 3000 and 1000 cycles, the permanent strain increased continuously for most stress paths above stress path 2. A probable explanation for the rapid increase

was that the permanent strains for these stress paths were still in the initial post-compaction phase and the CWR specimen was not able to reach a stable equilibrium state because of the insufficient loading cycles. This may explain the higher final accumulated permanent strain for the test with 3000 cycles per stress path than that for 6000 cycles.

The deviator stress applied for MS RLT test under HSLM and MS RLCBR test were similar, but the corresponding magnitude and trend of permanent strain were different. One of the possible reasons was that the confining pressure was different between these two tests. It indicates that MS RLCBR tests results cannot directly be used to characterize the permanent deformation behaviour of CWR under cyclic traffic loading. The existing permanent deformation models cannot be applied for RLCBR tests since the confining pressure (or horizontal stress) in RLCBR test specimen was inconstant with the vertical plunger stress during the cyclic loading.

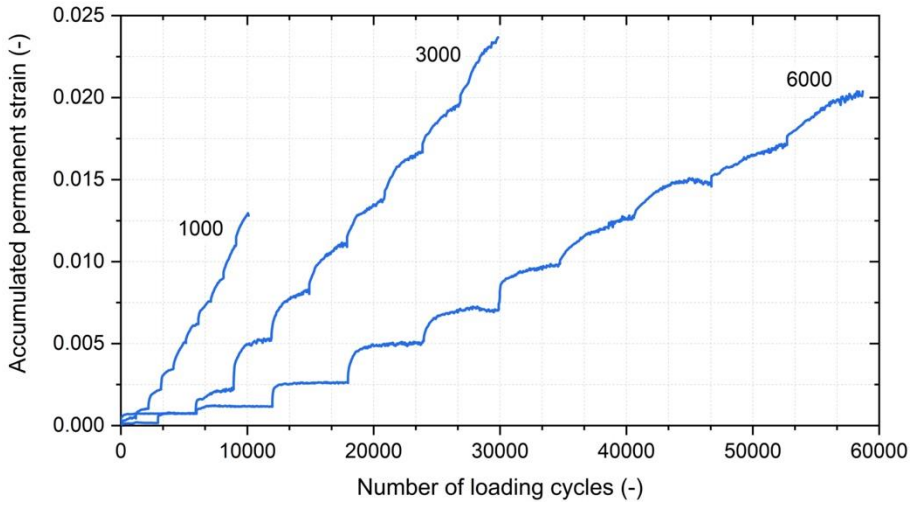

Figure 5.5: Accumulation of permanent strain of crushed waste rocks measured by MS RLCBR tests with 6000, 3000, and 1000 loading cycles for each stress path. Stress paths are defined in Table 3.

5.4 Results analysis and discussion

5.4.1 Applicability of existing permanent deformation models to CWR

Several models were proposed in the literature to describe the permanent strains measured during RLT tests and predict the permanent deformation behaviour of pavement materials in the field. These models are usually a function of the number of loading cycles and other parameters such as deviator stress and mean bulk stress (Lekarp et al. 2000b; Erlingsson et al. 2017). For example, Barksdale (1972), Sweere (1990), and Wolff and Visser (1994) developed permanent deformation models that relate the amount of permanent strain to the number of loading cycles and which have been widely used for unbound granular materials for single stage RLT tests. However, these models do not take into account the stress condition (which is one of the most important factors affecting the permanent deformation of granular materials; (Lekarp et al. 2000b), which limits their application and accuracy for MS RLT tests. Gidel et al. (2001) and Korkiala-Tanttu (2005) proposed models that relate the development of permanent strain to the shear strength characterization of materials and number of loading cycles. Rahman and Erlingsson (2015a) also developed a permanent deformation model for unbound granular materials that directly takes into account the stress level and the number of loading cycles. These models are usually more suitable to describe and predict coarse-grained materials strain (Rahman and Erlingsson 2015b; Erlingsson et al. 2017)

However, Gidel et al. (2001) model, Korkiala-Tanttu (2005) model, and Rahman and Erlingsson (2015a) model were initially proposed for single stress path RLT tests, and must be modified to describe MS RLT tests. Time hardening was proposed to take into account the stress history effect caused by previous loading stress paths. The approach consists in introducing the equivalent loading cycles N_i^{eq} (Lytton et al. 1993; Zhou et al. 2010; Erlingsson and Rahman 2013; Mohammadinia et al. 2020; Li et al. 2021) which is calculated based on the current *i*th stress condition and the accumulated permanent strain achieved by previous stress paths. The total

number of loading cycles N is then modified as $(N\text{-}N_{i\text{-}1}+N_i^{eq})$ in which $N_{i\text{-}1}$ is the total number of loading cycles at the end of the previous (i-1)th stress path.

In the present study, Gidel et al. (2001), Korkiala-Tanttu (2005), and Rahman and Erlingsson (2015a) models were modified to include time hardening. Model parameters were calibrated on experimental data (Figure 5.6 and Table 5.4) using the method of least squares, and the error between experimental and predicted accumulated permanent strains was assessed using coefficient of determination R^2.

Rahman and Erlingsson model was able to describe the accumulated permanent strains accurately for all the stress levels with $R^2 > 0.92$ (Figure 5.6 and Table 5.4). The fitted curves matched the measured accumulated permanent strain satisfactorily for LSL and HSL with $R^2 > 0.99$, although the model tended to slightly underestimate the strain for the last three stress paths in LSL (Figure 5.6). The performance of Rahman and Erlingsson model for HSLM was not as good as for LSL and HSL, but was still deemed satisfactorily with $R^2 = 0.92$. A possible reason for the relatively lower coefficient of determination may have been the shakedown range C for stress path 16 (Figure 5.6). Korkiala-Tanttu model fitted the accumulated permanent strain acceptably with $R^2 > 0.84$, but the fitting performance decreased with the increasing of stress levels. The fitting performance of Gidel et al. model was low for the three stress levels ($R^2 < 0$) in this study. One possible reason for the lower prediction accuracy of Gidel et al. and Korkiala-Tanttu models was the lack of significant correlation between the permanent deformation behaviour of CWR and the shear strength properties (which was also reported by Lekarp et al. (1996) for unbound granular materials).

The prediction accuracy of shakedown ranges for Rahman and Erlingsson model was also higher than that for Korkiala-Tanttu model and Gidel et al. model (Figure 5.7), and was greater than 80% for LSL and HSL. However, the model accuracy for HSLM was relatively low (around 70%) and the model failed to predict the shakedown range C of stress path 16 in HSLM. The relatively few stress paths available for HSLM probably affected negatively the accuracy of the calibrated model.

Despite these limitations, Rahman and Erlingsson model seemed more accurate to describe the accumulated permanent strains of CWR under different stress levels in this study.

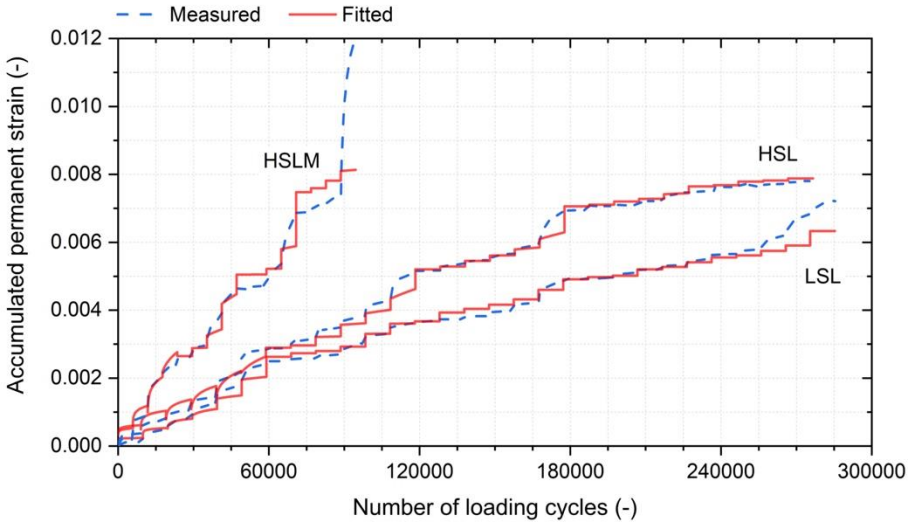

Figure 5.6: Measured and modelled accumulated permanent strain using Rahman and Erlingsson model as a function of number of loading cycles during MS RLT tests for LSL, HSL, and HSLM.

Table 5.4: Permanent deformation models and calibrated parameters for crushed waste rocks for different stress levels. Coefficient of determination R^2 are also presented. The Rahman and Erlingsson model parameter α was set as 0.75 according to the model author's recommendation (Rahman and Erlingsson 2015a). The Korkiala-Tanttu model parameter A=1.05 as recommended (Korkiala-Tanttu 2005).

Model	Calibrated Material Parameters			R^2		
Rahman and Erlingsson (2015a) Model	$a\times10^{-3}$	b	α	LSL	HSL	HSLM
$\varepsilon_p=aN^{bS_f}S_f \quad S_f=\frac{(q/p_a)}{(p/p_a)^{\alpha}}$	0.321	0.07	0.75	0.994	0.994	0.921
Gidel et al. (2001) Model	ε^0	B	u	LSL	HSL	HSLM

$\varepsilon_p=\varepsilon^0(1-(\frac{N}{100})^{-B})(\frac{L_{max}}{p_a})^u(m+\frac{s}{p_{max}}-\frac{q_{max}}{p_{max}})^{-1}$ $L_{max}=\sqrt{p_{max}^2+q_{max}^2}$	0.015	0.403	0.053	-0.193	-1.054	-3.372
Korkiala-Tanttu (2005) Model	$C\times10^{-3}$	b	A	LSL	HSL	HSLM
$\varepsilon_p=CN^b\frac{R}{A-R}$ $R=\frac{q}{q_f}$ $q_f=mp+s$	0.652	0.203	1.05	0.995	0.952	0.847

Where ε_p: permanent strain [-]; N: the number of loading cycles [-]; q: deviator stress [kPa]; p: mean bulk stress (one-third of the sum of the principle stresses) [kPa]; p_a: the reference stress taken equal to the atmospheric pressure (100 kPa); p_{max}: the maximum applied confining pressure [kPa]; q_{max}: the maximum deviator stress [kPa]; m and s: the slope and intercept of the Mohr-Coulomb failure line plotted in p-q space, respectively.

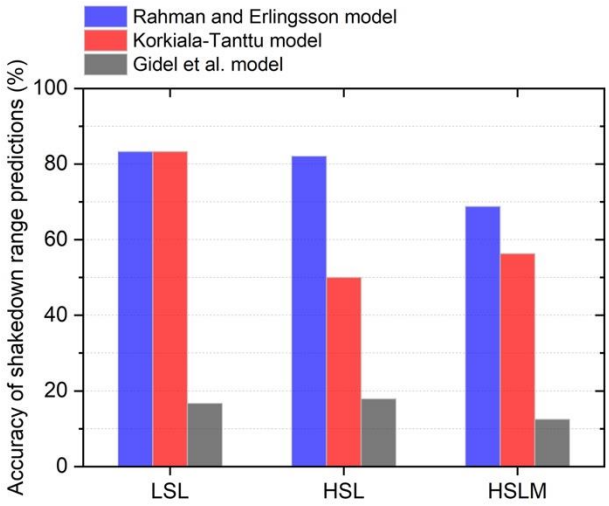

Figure 5.7: Prediction accuracy of the shakedown ranges for Rahman and Erlingsson model, Korkiala-Tanttu model, and Gidel et al. model on crushed waste rocks under LSL, HSL, and HSLM.

5.4.2 A new model for RLCBR test

Model development

The existing permanent deformation models (Table 5.4) were developed primarily to predict the

permanent deformation behaviour from RLT test results but cannot be used directly for RLCBR tests (see above). Therefore, a new model was proposed in this study to describe the RLCBR test results, and to determine the Rahman and Erlingsson model parameters (*a*, *b*, and α):

$$\varepsilon_p = aN^{b\beta S_f'}\beta S_f' \quad 5.5$$

$$S_f' = \frac{(\sigma_p/p_a)}{(p_c/p_a)^{\alpha}} = \frac{(\sigma_p/p_a)}{[(0.2359\upsilon+0.1452)\sigma_p/p_a]^{\alpha}} \quad 5.6$$

The new model was developed based on Rahman and Erlingsson model formulation. The increase of accumulated permanent strain with number of loading cycles was described as a power function like in the Sweere model, which was able to describe RLT test results well (Rahman and Erlingsson 2015a). A term S_f' was introduced in this new model to describe the effect of stress condition (similarly to S_f in Rahman and Erlingsson model). The amount of permanent strain was correlated with S_f' via multiplying it with the model parameter *a* (Eq. 5.5). S_f' was also incorporated as the exponent of the number of loading cycles with model parameter b, because the curve slope of permanent strain versus number of loading cycles was related to the applied stress condition (Rahman and Erlingsson 2015a). The maximum axial plunger stress σ_p and the mean bulk stress p_c (Eq. 5.4) were incorporated in the calculation of S_f' to account for the stress characteristics of RLCBR specimen (Eq. 5.6). The confining (horizontal) stress within RLCBR specimen caused by the plunger stress and rigid mold walls was not constant (contrary to RLT tests), so the mean bulk stress p_c was also linked with the confining stress in addition to the maximum principal stress (i.e. the vertical stress). Hence, a parameter β was introduced to regularize model parameter S_f' (Eq. (5)). In this study, β = 0.5 was chosen because it provided the best fitting to MS RLCBR tests results for CWR.

The time hardening approach was also applied for this new model to reflect the influence of stress history on permanent deformation in MS RLCBR test. At the beginning of any *i*th stress path of

the MS RLCBR test, the accumulated permanent strain from previous stress paths was used to determine the equivalent number of loading cycles N_i^{eq} that was required to achieve the same amount of accumulated permanent strain for the current *i*th stress path. The equivalent number of loading cycles N_i^{eq} for this new model can be calculated using Eq. 5.7. The permanent strain at loading cycles *N* in Eq. (5) therefore can be modified as $N\text{-}N_{i\text{-}1}+N_i^{eq}$ under the current stress path. The developed model therefore can be rewritten for fitting the accumulated permanent strain ε_{p_i} in the *i*th stress path in MS RLCBR test as shown in Eq. 5.8.

$$N_i^{eq} = \left(\frac{\varepsilon_{p_{i\text{-}1}}}{a\beta S_f'}\right)^{\frac{1}{b\beta S_f'}} \quad 5.7$$

$$\varepsilon_{p_i} = a(N\text{-}N_{i\text{-}1}+N_i^{eq})^{b\beta S_f'}\beta S_f' \quad 5.8$$

Calibration and validation of new model for CWR

The developed new model (Eqs. (6)~(8)) was used to fit the accumulated permanent strains of CWR measured by MS RLCBR tests (Figure 5.8). This model was able to fit relatively precisely ($R^2 > 0.99$) the accumulated permanent strains of CWR from MS RLCBR tests with 6000, 3000, and 1000 cycles for each stress path (Figure 5.8). The fitted model parameters for the different MS RLCBR tests varied slightly, but remained in the typical range for these parameters (Erlingsson et al. 2017). For example, the value of *a* varied from 0.330×10^{-3} to 0.382×10^{-3} and the model parameter *b* from 0.070 to 0.075 (Table 5). These variations indicate that the model may also be influenced by the number of loading cycles per stress path. The values of parameters *a* and *b* calibrated by new model and MS RLCBR tests were close to that calibrated by Rahman and Erlingsson model and MS RLT tests, particularly the MS RLCBR test with 6000 cycles performed better (see Table 5.4 and 5.5).

The precision of calibrated parameters in Table 5 was evaluated by comparing the predicted and measured accumulated permanent strain by MS RLT tests (Figure 5.9). The prediction performance of Rahman and Erlingsson model with the parameters calibrated using MS RLCBR tests with 6000 cycles per stress path (R^2=0.99) was better than that with 3000 and 1000 cycles per stress path (R^2=0.92). The accuracy of shakedown ranges predictions was greater than 80% for LSL and HSL, and above 70% for HSLM. The model calibrated with 1000 and 3000 cycles per stress path tended to overestimate the accumulated permanent strain for all the stress levels (Figure 5.9(a) and (b)), indicating that insufficient stress loading cycles could result in an overestimation of model parameters *a* and *b*. In other words, the number of loading cycles for each stress in MS RLCBR test should be at least 6000 to determine stable model parameters for Rahman and Erlingsson model and to predict adequately the permanent deformation behaviour of CWR.

Model parameters calibrated using MS RLCBR tests and the new model could reasonably predict the permanent deformation behaviour of CWR with $R^2 > 0.92$ for permanent strains and a prediction accuracy for shakedown ranges 70~80% in this study. It indicated that this new model for RLCBR tests was equivalent with Rahman and Erlingsson model for RLT tests.

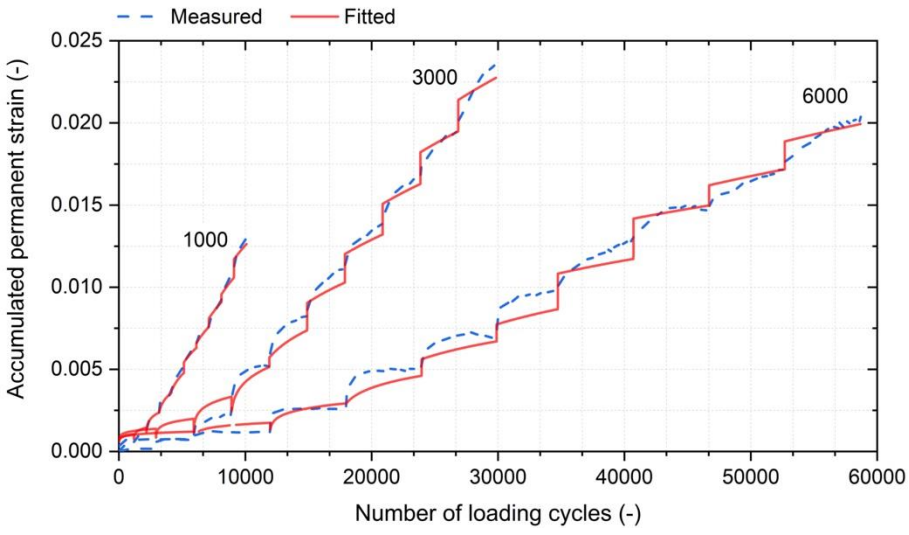

Figure 5.8: Experimental accumulated permanent deformation developed in MS RLCBR test with

6000, 3000, and 1000 cycles per stress path and the corresponding fitting curves by new model.

Table 5.5: Calibrated new model parameters and coefficient of determination R^2 by fitting the MS RLCBR test results with 6000, 3000, and 1000 cycles. The model parameter α was also set 0.75 which was same with Rahman and Erlingsson model for MS RLT tests in this study.

MS RLCBR tests	$a \times 10^{-3}$	b	α	β	R^2
6000	0.33	0.070	0.75	0.5	0.991
3000	0.382	0.075	0.75	0.5	0.990
1000	0.342	0.072	0.75	0.5	0.995

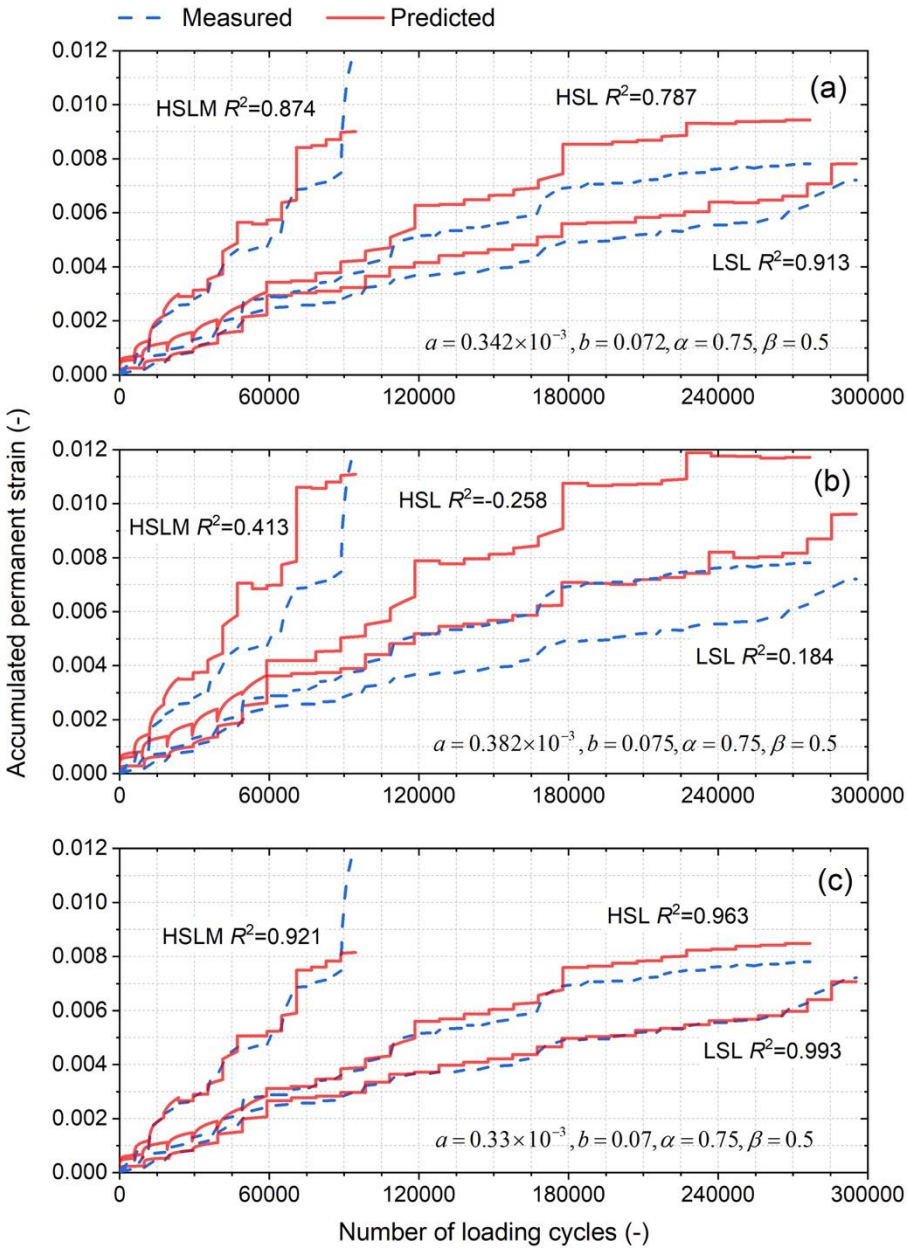

Figure 5.9: Measured and predicted accumulated permanent strain for LSL, HSL, and HSLM by Rahman and Erlingsson model with the parameters calibrated by new model and MS RLCBR tests, (a) 1000 cycles, (b) 3000 cycles, and (c) 6000 cycles per stress path.

5.5 Discussion

A new model was developed to fit RLCBR test data, and then this model was extended to fit MS

RLCBR test results through time hardening approach. This new model can be used to calibrate the Rahman and Erlingsson model parameters (i.e. a, b, and α) for which could then be used to predict the permanent deformation behaviour of CWR with a good precision. Although the CWR used in this study is representative of hard rock mines (Bussière 2007a; James et al. 2013), the new model developed for MS RLCBR tests should be validated for other materials.

The proposed new model in this paper was based on Rahman and Erlingsson model, and it is assumed that the material parameters (a, b, and α) used in these two models were equivalent. The good prediction of permanent deformation behaviour of CWR proved that the new model was effective. However, the parameter β (β = 0.5 in this study), which was introduced to regularize the stress condition within RLCBR specimen, need to be further studied with more data to establish reasonable ranges for its determination. Number of loading cycles in RLCBR test can affect the new model accuracy to calibrate the model parameters, and the insufficient loading cycles can result in overestimation in the parameters. The study results show that the more cycles applied in RLCBR test the better for this model to calibrate Rahman and Erlingsson model parameters, but it can lead to rapid increase in experimental time.

The apparatus that used to conduct RLCBR test is initially designed for static (or standard) CBR test, which may affect the test results precision in this study, especially considering the repeatability of cyclic load test is relatively low (Boudreau 2003). Zhang et al. (2019) showed that the cyclic loading frequency can influence the permanent deformation of on high-speed railway ballast. However, the applied loading frequency is 0.3 Hz which is relatively low because of the limitation of the laboratory apparatus in this study. The effect of loading frequency therefore cannot be taken into account in this paper. The permanent deformation response of granular materials is also affected by several factors, such as water content, dry density, and particle size distribution (Lekarp et al. 2000b; Touqan et al. 2020). Further research should therefore be concentrated on the effect of these factors on the material parameters of the model.

Poisson's ratio of CWR was not measured during RLCBR and RLT tests, and was assumed to be equal to 0.35 in the proposed model. However, Poisson's ratio is not a constant value and may increase as confining pressure decreases and deviator stress increases (Hicks and Monismith 1971). Measurement of Poisson's ratio by evaluating the radial strain (AASHTO T307 2017) could contribute to increase the accuracy of the permanent deformation model.

Finally, the models used in this study do not consider the reorientation of principal stress often observed in pavement structures for moving traffic loading (Qian et al. 2016). Such effect could, however, lead to large permanent deformation, exceeding the measured value using laboratory RLT tests (Lekarp et al. 2000b; Qian et al. 2016). The principal stress rotation therefore may affect the model parameters such as a in Rahman and Erlingsson model. Such effect should be further investigated and, if possible, implemented in the models to better predict deformation under field conditions.

5.6 Conclusions

In this study, a series of MS RLT and RLCBR tests with different stress levels and loading cycles were conducted to investigate the CWR permanent deformation behaviour. Three existing permanent deformation models modified using time hardening approach were evaluated to describe and predict permanent deformation of CWR measured by MS RLT tests results. A new model was also proposed to describe and predict permanent deformation of CWR based on MS RLCBR tests.

Based on the results of this study it was concluded that:

The effect of stress levels on accumulated permanent strains and shakedown ranges of CWR was significant. The accumulated permanent strain for HSLM increased much quicker than that for LSL and HSL conditions, and rang C appeared for high deviator stress path in HSLM.

Rahman and Erlingsson model appeared to be the most representative model to characterize the CWR permanent deformation behaviour ($R^2 > 0.92$). A model was proposed for MS RLCBR tests based on Rahman and Erlingsson model. This model was able to fit MS RLCBR tests results quite well ($R^2 > 0.99$).

The model parameters (i.e. a, b, and α for Rahman and Erlingsson model) calibrated by the new model and MS RLCBR test results were able to satisfactorily predict the permanent deformation behaviour of CWR with $R^2 > 0.92$, and the accuracy of the shakedown ranges was greater than 70%. The proposed model seemed therefore an effective alternative to predict the CWR permanent deformation behaviour from MS RLCBR tests.

The number of loading cycles for each stress path in MS RLCBR test could affect the calibration of model parameters (a, b, and α), and the insufficient loading cycles may result in overestimation in model parameters. Model parameters that calibrated from MS RLCBR test with 6000 cycles was more precise to predict the permanent deformation behaviour of CWR than with less loading cycles (i.e. 3000 and 1000). It would therefore be recommended to carry out MS RLCBR test with as many cycles as possible for each stress path.

The model developed in this paper should be validated for other materials and compared to field measurements. Additional MS RLT and RLCBR tests are ongoing to study the permanent deformation behaviour of CWR with different properties (e.g. gradation, water contents, and freeze-thaw cycles).

Acknowledgements

This work was carried out with the financial support from FRQNT and the industrial partners of Research Institute on Mines and the Environment (http://irme.ca/). The repeated load triaxial and CBR test equipment used in this study was acquired with a CFI grant.

5.7 References

AASHTO T307-99. Standard method of test for determining the resilient modulus of soils and aggregate materials. Washington, DC; 2017.

Abid AN, Salih AO, and Nawaf EA. The influence of fines content on the mechanical properties of aggregate subbase course material for highway construction using repeated load CBR test. Alnahrain Journal for Engineering Sciences 2017*;* 20(3): 615-624.

Araya AA. Characterization of unbound granular materials for pavements. Delft University of Technology, 2011.

Araya AA, Huurman M, Molenaar AA, et al. Investigation of the resilient behaviour of granular base materials with simple test apparatus. Materials and Structures 2012*;* 45(5): 695-705.

Araya AA, Huurman M, Molenaar AAA, et al. Investigation of the resilient behaviour of granular base materials with simple test apparatus. Materials and Structures 2011*;* 45(5): 695-705.

ASTM D1557-12e1. Standard test methods for laboratory compaction characteristics of soil using modified effort (56,000 ft-lbf/ft^3 (2,700 kN-m/m^3)). ASTM International, West Conshohocken, PA; 2012.

ASTM D854-14. Standard test methods for specific gravity of soil solids by water pycnometer. ASTM International, West Conshohocken, PA; 2014.

ASTM C127-15. Standard test method for relative density (specific gravity) and absorption of coarse aggregate. ASTM International, West Conshohocken, PA; 2015.

ASTM D1883-16. Standard test method for California Bearing Ratio (CBR) of laboratory-compacted soils. ASTM International, West Conshohocken, PA; 2016.

ASTM D2487-17e1. Standard practice for classification of soils for engineering purposes (Unified

Soil Classification System). ASTM International, West Conshohocken, PA; 2017.

ASTM C136/C136M-19. Standard test method for sieve analysis of fine and coarse aggregates. ASTM International, West Conshohocken, PA; 2019.

Barksdale RD. Laboratory evaluation of rutting in base course materials. In: Presented at the Third International Conference on the Structural Design of Asphalt Pavements, Grosvenor House, Park Lane, London, England, Sept. 11-15, 1972.; 1972.

Bhattacharjee S, and Bandyopadhyay K. Evaluation of elastic modulus of fly ash embankment by repeated load CBR test. Geotechnical Engineering for Infrastructure and Development 2015: 229-234.

Boudreau RL. (2003). Repeatability of the resilient modulus test procedure. In *Resilient modulus testing for pavement components*: ASTM International.

Bussière B. Colloquium 2004: Hydrogeotechnical properties of hard rock tailings from metal mines and emerging geoenvironmental disposal approaches. Can Geotech J 2007*;* 44(9): 1019-1052.

Collins I, and Boulbibane M. The application of shakedown theory to pavement design. Metals and materials 1998*;* 4(4): 832-837.

Collins I, and Boulbibane M. Geomechanical analysis of unbound pavements based on shakedown theory. Journal of Geotechnical and Geoenvironmental Engineering 2000*;* 126(1): 50-59.

El-Basyouny M, Witczak M, and Kaloush K. Development of the permanent deformation models for the 2002 design guide. In: 84th Annual Meeting of the Transportation Research Board, Available in TRB 2005 Annual Meeting CD-ROM; 2005.

Electric drive mining truck 960e-2k. KOMATSU. https://www.komatsuamerica.com/equipment/trucks/electric/960e-2k, 2020.

EN 13286-7. Unbound and hydraulically bound mixtures–cyclic load triaxial test for unbound

mixtures. 2004.

Erlingsson S. Rutting development in a flexible pavement structure. Road Materials and Pavement Design 2012*;* 13(2): 218-234.

Erlingsson S, and Rahman MS. Evaluation of permanent deformation characteristics of unbound granular materials by means of multistage repeated-load triaxial tests. Transp Res Record 2013*;* 2369(1): 11-19.

Erlingsson S, Rahman S, and Salour F. Characteristic of unbound granular materials and subgrades based on multi stage RLT testing. Transp Geotech 2017*;* 13: 28-42.

Gidel G, Hornych P, Breysse D, et al. A new approach for investigating the permanent deformation behaviour of unbound granular material using the repeated loading triaxial apparatus. Bulletin des laboratoires des Ponts et Chaussées 2001*;* (233).

Golder. Golder Associates Africa (Pty) Ltd. Environmental impact assessment and environmental management programme report for the proposed metsimaholo underground coal mine. Department of Mineral Resources; 2019.

Haghighi H, Arulrajah A, Mohammadinia A, et al. A new approach for determining resilient moduli of marginal pavement base materials using the staged repeated load cbr test method. Road Materials and Pavement Design 2017*;* 19(8): 1848-1867.

Hao S, and Pabst T. Estimation of resilient behaviour of crushed waste rocks using repeated load cbr tests. Transp Geotech 2021*;* 28: 100525.

Hicks RG, and Monismith CL. Factors influencing the resilient response of granular materials. Highway research record 1971*;* 345: 15-31.

IS 2386. Methods of test for aggregates for concrete, part i: Particle size and shape. 1963.

James, Aubertin M, and Bussière B. On the use of waste rock inclusions to improve the performance of tailings impoundments. In: Proceedings of the 18th International

Conference Soil Mechanics and Geotechnical Engineering, Paris, France; 2013.

Korkiala-Tanttu L. A new material model for permanent deformations in pavements. In: Proceedings of the international conferences on the bearing capacity of roads, railways and airfields; 2005.

Laverdière A. Effet de la granulométrie sur le comportement géotechnique de roches stériles concassées utilisées comme surface de roulement sur des routes minières. École Polytechnique de Montréal, 2019.

Lekarp F. Resilient and permanent deformation behaviour of unbound aggregates under repeated loading. Institutionen för infrastruktur och samhällsplanering, 1999.

Lekarp F, Isacsson U, and Dawson A. State of the art. I: Resilient response of unbound aggregates. Journal of Transportation Engineering 2000a*;* 126(1): 66-75.

Lekarp F, Isacsson U, and Dawson A. State of the art. II: Permanent strain response of unbound aggregates. Journal of transportation engineering 2000b*;* 126(1): 76-83.

Lekarp F, Richardson IR, and Dawson A. Influences on permanent deformation behaviour of unbound granular materials. Transp Res Record 1996*;* 1547(1): 68-75.

Li Y, Nie R, Yue Z, et al. Dynamic behaviours of fine-grained subgrade soil under single-stage and multi-stage intermittent cyclic loading: Permanent deformation and its prediction model. Soil Dyn Earthq Eng 2021*;* 142: 106548.

Lytton RL, Uzan J, Fernando EG, et al. Development and validation of performance prediction models and specifications for asphalt binders and paving mixes (Vol. 357): Strategic Highway Research Program Washington, DC; 1993.

Mishra D, Kazmee H, Tutumluer E, et al. Characterization of railroad ballast behaviour under repeated loading: Results from new large triaxial test setup. Transp Res Record 2013*;* 2374(1): 169-179.

Mohammadinia A, Naeini M, Arulrajah A, et al. Shakedown analysis of recycled materials as railway capping layer under cyclic loading. Soil Dyn Earthq Eng 2020; 139: 106423.

Molenaar AA. Repeated load CBR testing, a simple but effective tool for the characterization of fine soils and unbound materials. 2008.

Molenaar AA, Araya AA, and Houben LJ. Characterization of unbound base materials for roads using a new developed repeated load CBR test. In: Eighth International Conference on Managing Pavement Assets, Santiago, Chile; 2011.

Opiyo T. A mechanistic approach to laterite-based pavements in transport and road engineering. (MSc Thesis). International Institute for Infrastructure, Hydraulics and Environment Engineering, Delft, the Netherlands. 1995.

Qian JG, Wang YG, Yin ZY, et al. Experimental identification of plastic shakedown behaviour of saturated clay subjected to traffic loading with principal stress rotation. Engineering Geology 2016; 214: 29-42.

Qian Y, Tutumluer E, Hashash YM, et al. Effects of ballast degradation on permanent deformation behaviour from large-scale triaxial tests. In: ASME/IEEE Joint Rail Conference; 2014.

Rahman MS, and Erlingsson S. A model for predicting permanent deformation of unbound granular materials. Road Materials and Pavement Design 2015a; 16(3): 653-673.

Rahman MS, and Erlingsson S. Predicting permanent deformation behaviour of unbound granular materials. International Journal of Pavement Engineering 2015b; 16(7): 587-601.

Saberian M, Li J, Nguyen BT, et al. Experimental and analytical study of dynamic properties of ugm materials containing waste rubber. Soil Dyn Earthq Eng 2020; 130: 105978.

Salour F, and Erlingsson S. Permanent deformation characteristics of silty sand subgrades from multistage rlt tests. International journal of pavement engineering 2017; 18(3): 236-246.

Sas W, Głuchowski A, and Szymański A. Determination of the resilient modulus M_R for the lime

stabilized clay obtained from the repeated loading CBR tests. Annals of Warsaw University of Life Sciences-SGGW. Land Reclamation 2012*;* 44(2): 143-153.

Sun Q, Indraratna B, and Nimbalkar S. Effect of cyclic loading frequency on the permanent deformation and degradation of railway ballast. Géotechnique 2014*;* 64(9): 746-751.

Sweere GT. Unbound granular bases for roads. University of Delft, Delft, The Netherlands, 1990.

Tannant D, and Regensburg B. Guidelines for mine haul road design. 2001.

Tao M, Mohammad LN, Nazzal MD, et al. Application of shakedown theory in characterizing traditional and recycled pavement base materials. Journal of Transportation Engineering 2010*;* 136(3): 214-222.

Tholen O. Falling weight deflectometer. A device for bearing capacity measurements: Properties and performance. 1980.

Thompson RJ. Mine haul road design and management best practices for safe and cost-efficient truck haulage. In: Society for Mining, Metallurgy and Exploration 2010 Conference Proceedings Pre-print; 2010.

Thompson RJ. Mine haul road design, construction and maintenance management. Mining Roads 2011*;* 136.

Thompson RJ, and Visser AT. A mechanistic structural design procedure for surface mine haul roads. International Journal of Surface Mining, Reclamation and Environment 1997*;* 11(3): 121-128.

Thompson RJ, and Visser AT. Selection parameters for mine haul road wearing course materials. International Journal of Surface Mining, Reclamation and Environment 2007*;* 14(1): 1-17.

Touqan M, Ahmed A, El Naggar H, et al. Static and cyclic characterization of fouled railroad sub-ballast layer behaviour. Soil Dyn Earthq Eng 2020*;* 137: 106293.

Tremblay G, and Hogan C. Mend manual: Volume 1, summary. Ottawa, Ontario, Canada; 2001.

Werkmeister S. Permanent deformation behaviour of unbound granular materials. University of Technology, Dresden 2003.

Werkmeister S, Dawson A, and Wellner F. Pavement design model for unbound granular materials. Journal of Transportation Engineering 2004*;* 130(5): 665-674.

Werkmeister S, Dawson AR, and Wellner F. Permanent deformation behaviour of granular materials and the shakedown concept. Transp Res Record 2001*;* 1757(1): 75-81.

Wolff H, and Visser A. Incorporating elasto-plasticity in granular layer pavement design. In: Proceedings of the Institution of Civil Engineers-Transport; 1994.

Zhang X, Zhao C, and Zhai W. Importance of load frequency in applying cyclic loads to investigate ballast deformation under high-speed train loads. Soil Dyn Earthq Eng 2019*;* 120: 28-38.

Zhou F, Fernando E, and Scullion T. Texas Transportation Institute. Development, calibration, and validation of performance prediction models for the texas me flexible pavement design system. 2010.

CHAPTER 6 ARTICLE 3: EXPERIMENTAL STUDY OF GRADATION EFFECT ON THE MECHANICAL CHARACTERISTICS OF CRUSHED WASTE ROCKS

Shengpeng Hao and Thomas Pabst

This article was submitted to *Canadian Geotechnical Journal* in June 2021.

Abstract: Crushed waste rocks, generated from mining operations, have been widely used for mining infrastructure constructions such as haul roads because of their low-cost, high-strength, and availability. Crushed waste rocks gradation can, however, vary a lot, depending on blasting, mineralogy and crushing process, but is a key factor influencing the mechanical properties of crushed waste rocks (including resilient modulus, permanent deformation, and shear strength). Gradation should therefore be optimized to enhance their performance in the field. A series of repeated load and monotonic triaxial tests were carried out on crushed waste rocks with different gravel-to-sand ratios and fines contents. Results showed that the optimum gravel-to-sand ratio was between 1 and 1.5 and contributed to provide higher resilient modulus and shear strength, and lower permanent strain. An increase in fines content could, to the contrary, result in the decrease of resilient modulus and permanent strain but also to significant increase of shear strength. M_R-θ model and Rahman and Erlingsson model (extended using time hardening approach) were well adapted to describe resilient modulus and accumulated permanent strain, respectively, as a function of stress condition and number of loading cycles. Prediction models were therefore developed to predict the resilient modulus and permanent strain of crushed waste rocks based on correlation analysis results.

Keywords: Crushed waste rocks, Gradation, Resilient modulus, Permanent deformation, Shear

strength, Repeated load triaxial test.

6.1 Introduction

Mining operations generate large amounts of waste rocks that are often stored on the surface, in piles. However, the management and reclamation of waste rock piles can be challenging because of their large size and the risks for geotechnical and geochemical instabilities (Aubertin 2013). Waste rocks have been widely reused (or valorized) for the construction of various infrastructures such as dams (Bussière 2007a), waste rock inclusions (James et al. 2013), cover systems (Bussière et al. 2003; Aubertin et al. 2016), mine haul roads (Thompson et al. 2019), and highways (Ahmed and Abouzeid 2009; Amrani et al. 2019) because of their low cost, high strength, and availability. For example, most mines already use crushed waste rocks for the construction of haul road wearing courses (Thompson et al. 2019). The valorization of waste rocks for the construction of infrastructures helps to decrease the amounts of materials that need to be borrowed in the environment, so it also contributes to decrease environmental footprint and promote the circular economy.

The performance of these engineered infrastructures depends significantly on the mechanical properties of waste rocks such as their resilient modulus, permanent deformation, and shear strength (Tannant and Regensburg 2001; Aubertin 2013; Thompson et al. 2019). The resilient modulus and permanent deformation characteristics of unbound aggregates under traffic loading are, for example, important factors for road design, as they are strongly related to the rutting, cracking and other road diseases (Erlingsson 2012; Thompson et al. 2019). Unbound aggregates with low shear strength generally indeed show high lateral and vertical deformation accumulation under loading (Xiao and Tutumluer 2017; Byun et al. 2020). The deterioration of road layers can

result in reduced pavement performance and an increase of road maintenance and vehicle operation costs. Shear strength is a common index used for the design and safety assessment of infrastructures such as waste rock piles (Omraci et al. 2003; Zheng et al. 2005; Du et al. 2012), tailing dams (Blight 1969), and roads (Tannant and Regensburg 2001; Long et al. 2011; Byun et al. 2020). For example, low shear strength could lead to landslides at large piles, which would cause huge losses of lives and environmental degradation (Zheng et al. 2005; Bao et al. 2019). However, a previous survey suggests that up to 30% of active waste piles have the potential of geotechnical instability (Dawson et al. 1998).

Gradation of aggregates is a key factor that affects the mechanical properties including resilient modulus (Duong et al. 2016; Hatipoglu et al. 2020), permanent deformation (Wang et al. 2018), and shear strength (Xiao et al. 2012; Yang and Luo 2018; Qi, Cui, Chen, et al. 2020). Previous studies showed that well-graded aggregates generally provide good mechanical performance with respect to stiffness, rutting resistance, and shear strength (Thom and Brown 1988). The gravel-to-sand ratio is a practical and easy-to-use criterion which is often used to optimize aggregate gradations (Xiao et al., 2012). Fines content is another important factor influencing the mechanical properties of aggregates, but its effect varies depending on the authors. For example, some studies concluded that the resilient modulus increased with fines content (Thom and Brown 1988; Kamal et al. 1993), while Hicks and Monismith (1971), and Mishra and Tutumluer (2012) observed that the resilient modulus was decreasing as fines content increased. Excessive fines can also result in increasing permanent deformation (Tutumluer and Pan 2008).

Stress parameters also have a significant impact on the measured mechanical properties of granular materials. The stress-strain relationship should therefore be modeled as accurately as possible using constitutive models (Lekarp et al. 2000a, 2000b). Over the years, several researchers have proposed constitutive models for predicting resilient modulus and permanent strain of unbound aggregates. These models are generally expressed as a function of stress conditions (e.g. confining pressure,

deviator stress, and bulk stress) and number of loading cycles (especially for permanent deformation models) (Lekarp et al. 2000a, 2000b). The model coefficients are generally determined by fitting the repeated load triaxial test results (EN 13286 2004; AASHTO T307 2017). However, repeated load triaxial test is a relatively sophisticated test, and characterization can therefore be costly, and time-consuming, especially when multiple loading stages are applied. Prediction of model coefficient based on performance-related soil physical properties (e.g., water content, density, degree of compaction, coefficient of uniformity, and coefficient of curvature) can therefore be very useful in practice (Malla and Joshi 2007). Such method is much simpler and economical, especially considering the short-service-life of mine haul roads, because the evaluation of the physical properties is more straightforward and less expensive than conducting triaxial tests. Several researchers developed empirical regression models to predict the coefficients of resilient modulus and permanent deformation models (Drumm et al. 1990; Santha 1994; Mohammad et al. 1999; Rahim and George 2005; Malla and Joshi 2007, 2008). However, existing regression models were generally developed for fine-grained materials such as subgrade soils, which limits their applicability to waste rocks. Hence, developing regression models that can reflect the robust linkages between gradation and mechanical properties of waste rocks would be helpful for mining operators.

In this study, a series of multistage repeated load and monotonic triaxial tests were carried out on crushed waste rocks with different gradations. The mechanical properties characterized by resilient modulus, permanent deformation, and shear strength were compared to evaluate the effect of gravel-to-sand ratio and fines content. The measured resilient modulus and accumulated permanent strain were fitted using M_R-θ model and Rahman and Erlingsson model (extended using time-hardening approach), respectively. Coefficient prediction models were then developed using multiple linear regression for predicting the M_R-θ model and Rahman and Erlingsson model coefficients (k_1, k_2, a, and b) based on the physical properties of crushed waste rocks, including dry density and gradation parameters.

6.2 Materials and method

6.2.1 Studied materials

The tested crushed waste rocks were obtained from Canadian Malartic Mine, an open pit gold mine located in the Abitibi region (Quebec, Canada) and were typical of many hard rock mines (Bussière 2007a; James et al. 2013). The maximum particle size of crushed waste rocks on the mine site was 25 mm, but the particles larger than 19 mm (around 5% by weight) were removed by sieving to accommodate the triaxial test mold size (diameter = 150 mm). The original gradation of crushed waste rocks contained around 66% of gravel (> 4.75 mm), 30% of sand (< 4.75 mm) and 4% of fines (< 0.075 mm) (ASTM C136/C136M 2019). The material was classified as a poorly graded gravel (GP) based on Unified Soil Classification System (USCS; (ASTM D2487 2017)). The specific gravity measured using relative density (ASTM C127 2015) and water pycnometer (ASTM D854 2014) was 2.71 and 2.75 for particle size > 4.75 and < 4.75 mm, respectively. The optimum water content (measured using ASTM D1557) was 5.6% corresponding to a maximum density ρ_d = 2334 kg/m^3 for the original gradation (Hao and Pabst 2021). X-ray diffraction (XRD) test results showed that the studied crushed waste rocks were mainly composed of quartz (23-28%), albite (34-43%), muscovite (10-12%), and chlorite (6-8%), corundum (5-8%), and diopside (5-8%). Crushed waste rocks were considered non-acid generating (Tremblay and Hogan 2001; Golder 2019).

6.2.2 Specimen preparation

A total of 9 gradations (including the original material) were prepared to evaluate the effect of both the gravel-to-sand ratio and the fines content on crushed waste rock mechanical properties (Figure 6.1). The gravel-to-sand ratio (GS) is defined as the percentage retained on the No.4 sieve (i.e. 4.75 mm) divided by the percentage passing the No.4 sieve and retained on the No.200 sieve (i.e.

0.075 mm). Fines content (FC) is defined as the percentage passing the No.200 sieve. GS was varied from 0 to 3, and FC was increased from 3.75% to 12% based on typical gradations observed in the field (Laverdière 2019; Thompson et al. 2019). Each sample was named GS*x*FC*y*% corresponding to GS = *x* and FC = *y*%. The original gradation of sampled crushed waste rocks was named GS2.3FC3.75%, i.e. GS = 2.3 and FC = 3.75%. The crushed waste rocks named GS0FC3.75% did not contain gravel particles (> 4.75 mm).

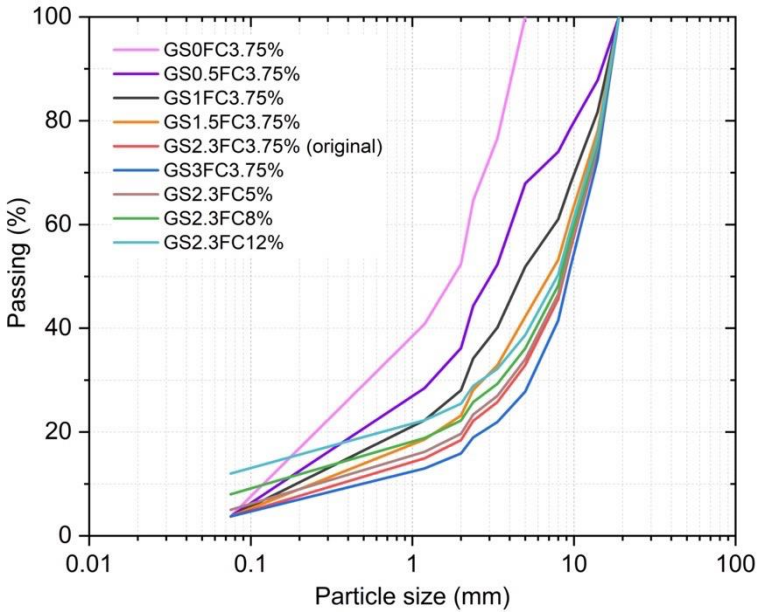

Figure 6.1: Particle size distribution of the different grading crushed waste rocks tested in this research; GS: gravel-to-sand ratio, FC (%): fines content.

6.2.3 Repeated load triaxial tests

Repeated load triaxial tests were conducted to evaluate the resilient behavior and the development of permanent deformation of crushed waste rocks under different stress levels. Monotonic triaxial tests (see below) were carried out to measure the shear strength. Both repeated load and monotonic

triaxial tests were conducted on 300 mm high and 150 mm diameter specimens under drained conditions. All specimens were prepared with an initial gravimetric water content $w = 4\%$ and compacted in ten layers using modified compaction effort 2700 kN-m/m^3 and 56 blows (ASTM D1557 2012). Specimens were sealed within two rubber membranes (0.304 mm and 0.635 mm thickness, respectively) to limit the risk to damage the thin membrane because of the angular particles and deep holes distributed on the specimen surface (especially under high confining pressures). A cuprum porous disc was placed on each end of the specimen.

Specimen characteristics are summarized in Table 1. For FC = 3.75%, the dry density varied with GS, and reached a peak value (2299 kg/m^3) for GS = 1; above, dry density started to decrease. For GS = 2.3, the dry density increased gradually from 2211 to 2311 kg/m^3 as FC increased from 3.75% to 8% but remained relatively constant for greater fines contents (Table 6.1).

Table 6.1: Physical properties of crushed waste rocks specimens for various gradations; ρ_d: dry density; D_{max}: maximum particle size; C_U: coefficient of uniformity; C_C: coefficient of curvature; D_{60}: 60% of the soil particles are finer than this size; D_{30}: 30% of the soil particles are finer than this size; D_{10}: 10% of the soil particles are finer than this size; PG: percentage of gravel; PS: percentage of sand; GS: gravel-to-sand ratio; FC: fines content.

Name	ρ_d	D_{max}	C_U	C_C	D_{60}	D_{30}	D_{10}	PG	PS	GS	FC
	kg/m^3	mm	-	-	mm	mm	mm	%	%	-	%
GS0FC3.75%	2108	4.75	16.92	0.98	2.2	0.53	0.13	0	96.25	0	3.75
GS0.5FC3.75%	2259	19	23.53	2.88	4.0	1.4	0.17	32.08	64.17	0.5	3.75
GS1FC3.75%	2299	19	39.47	3.09	7.5	2.1	0.19	48.13	48.13	1.0	3.75
GS1.5FC3.75%	2276	19	36.00	3.48	9.0	2.8	0.25	57.75	38.5	1.5	3.75
GS2.3FC3.75%	2211	19	27.63	4.42	10.5	4.2	0.38	67.08	29.17	2.3	3.75
GS3FC3.75%	2190	19	23.00	5.26	11.5	5.5	0.5	72.19	24.06	3.0	3.75
GS2.3FC5%	2240	19	76.92	12.31	10.0	4.0	0.13	66.21	28.79	2.3	5.0
GS2.3FC8%	2311	19	40.00	5.18	10.0	3.6	0.25	64.12	27.88	2.3	8.0
GS2.3FC12%	2304	19	237.50	20.632	9.5	2.8	0.04	61.33	26.67	2.3	12.0

Four successive stress sequences were applied for repeated load triaxial test, and each sequence included three stress paths that were combinations of confining pressure and deviator stress (Table 6.2). The confining pressure varied from 20 to 100 kPa and the deviator stress varied from 80 to 700 kPa. Each stress path was applied for 6000 cycles. All tests were performed in a load-controlled mode using haversine loading pulses with no rest period and a loading frequency of 0.2 Hz. Axial deformation and load were recorded during triaxial tests using a linear variable differential transformer (LVDT) and a 50 kN load cell, respectively. The resilient modulus M_R (MPa) of crushed waste rocks was defined as the ratio of the cyclic deviator stress σ_d (MPa) to the recoverable axial strain ε_r (-) (AASHTO T307 2017):

$$M_R = \frac{\sigma_d}{\varepsilon_r} \tag{6.1}$$

The variation of resilient modulus at the initial cycles (< 100) of each stress path was relatively significant since this phase corresponded to the stage where the permanent strain developed quickly, and the loading-unloading path did not form a close cycle in the stress-strain plane (Duong et al. 2016). Afterward, the cyclic loading led to a progressive stabilization of the particle arrangement and a relatively steady value of resilient modulus. The final value of resilient modulus after 6000 loading cycles was therefore considered as the representative for each stress path.

The permanent strain at each loading cycles was calculated as the ratio of permanent axial displacement to specimen height (EN 13286 2004):

$$\varepsilon_p(N) = \frac{L_p(N)}{L_0} \tag{6.2}$$

Where $\varepsilon_p(N)$: permanent strain at loading cycle N; $L_p(N)$: permanent axial displacement at loading cycle N, defined as the displacement accumulated from the beginning of the first cycles to the end of cycle N; L_0: the initial height of the tested specimen, i.e. 300 mm in this study.

Repeated load triaxial test results were also interpreted in terms of shakedown. The shakedown concept is generally used for ranking pavement materials on the basis of plastic deformability (EN 13286 2004). Permanent deformation tests can lead to three ranges of behavior including plastic shakedown (range A), plastic creep (range B), and incremental collapse (range C) (Werkmeister et al. 2001; Werkmeister et al. 2004). The shakedown range of crushed waste rocks for each stress path was assessed based on the value of $(\varepsilon_p^{5000}-\varepsilon_p^{3000})$ using following criteria (EN 13286 2004):

Plastic shakedown-range A: $(\varepsilon_p^{5000}-\varepsilon_p^{3000})<0.045\times10^{-3}$

Plastic creep-range B: $0.045\times10^{-3}<(\varepsilon_p^{5000}-\varepsilon_p^{3000})<0.4\times10^{-3}$

Incremental collapse-range C: $(\varepsilon_p^{5000}-\varepsilon_p^{3000})>0.4\times10^{-3}$

Where ε_p^{5000} and ε_p^{3000} correspond to the permanent strains measured at the 5000th and 3000th loading cycles in each stress path. Generally, materials in range C should not be authorized in a well-designed pavement (Werkmeister et al. 2004).

Table 6.2: Stress sequences for repeated load triaxial tests; σ_3: confining pressure, kPa; σ_d: deviator stress, kPa.

Sequence 1			Sequence 2			Sequence 3			Sequence 4		
Stress path	σ_3	σ_d	Stress path	σ_3	σ_d	Stress path	σ_3	σ_d	Stress path	σ_3	σ_d
1-1	20	80	2-1	45	180	3-1	70	240	4-1	100	300
1-2	20	140	2-2	45	300	3-2	70	400	4-2	100	500
1-3	20	200	2-3	45	420	3-3	70	560	4-3	100	700

6.2.4 Monotonic triaxial tests

Following the repeated load triaxial test, a consolidated drained (CD) monotonic triaxial test was carried out to evaluate the post-cyclic shear strength of crushed waste rocks specimens (AASHTO

T307 2017; ASTM D7181 2020). The consolidation was conducted by decreasing the confining pressure from 100 kPa (applied during the last sequence of the repeated load triaxial tests) to 50 kPa. The monotonic triaxial test was performed in a strain-controlled mode, and specimens were sheared at a constant axial rate of 0.015 mm/sec. The axial stress-strain curve for each specimen was recorded, and the peak deviator stress for different gradations was compared in this study. The shear test was stopped when the axial strain reached to 5%.

6.3 Test results

Stress condition was a critical factor influencing the resilient behavior of crushed waste rocks (Figure 6.2). Resilient modulus generally increased gradually with the applied deviator stress for a given confining pressure (i.e., different stress paths in one sequence). For example, for the specimen of GS2.3FC3.75% (original gradation), the resilient modulus increased from 150 MPa to 185 MPa when the deviator stress increased from 80 kPa to 200 kPa (i.e., from stress path 1-1 to 1-3). Resilient modulus also tended to increase with the stress sequence resulting from an increasing in stress level (or bulk stress here). In the following content, only the results for stress path 1-3, 2-3, 3-3, and 4-3 are presented to study the effect of gradation (GS and FC) on resilient modulus, but resilient modulus showed similar trend for the other stress paths. The measured stress-strain curves from monotonic triaxial tests on crushed waste rocks with different gradations can be found in APPENDIX B.

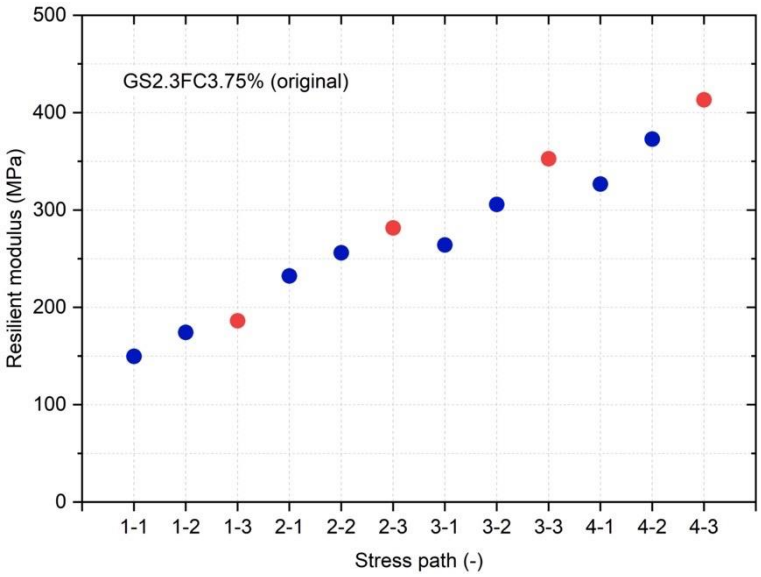

Figure 6.2: Evolution of resilient modulus of GS2.3FC3.75% (original gradation) with stress path (GS*x*FC*y*%: specimen prepared with a gravel-to-sand ratio GS = *x* and a fines content FC = *y*%). The red dots were the stress path 1-3, 2-3, 3-3, and 4-3 that were used to study the effect of GS and FC in the following sections. Similar trends were observed for the other specimens.

6.3.1 Effect of gravel-to-sand ratio (GS) on crushed waste rock mechanical properties

The GS ratio had a significant impact on the resilient modulus of crushed waste rocks (Figure 6.3(a)). Resilient modulus tended to increase significantly (+20 to 30%) when GS increased from 0 to 1.5. Above this value, the resilient modulus tended to decrease, but more slowly (< -10%) and somewhat stabilized for GS greater than 2.3. A GS of 1.5 seemed therefore optimum for the resilient behavior when FC was 3.75%.

The GS ratio also had a considerable influence on the shear strength of crushed waste rocks (Figure 6.3(b)). The peak deviator stress under 50 kPa confining pressure increased significantly from 1050 to 1280 kPa (+22%) as GS increased from 0 to 1. It then decreased gradually when GS exceeded

1, to around 1100 kPa for GS = 3. The trend between shear strength and GS was identical with the variation of dry density with GS. The dry density increased from 2108 to 2299 kg/m^3 when GS increased from 0 to 1, and then decreased to 2190 kg/m^3 for GS = 3. This confirmed that the dry density was one of the critical factors influencing the shear strength of crushed waste rocks (Hamidi et al. 2009). The optimum GS value of crushed waste rocks (FC = 3.75%) was 1 regarding to shear strength.

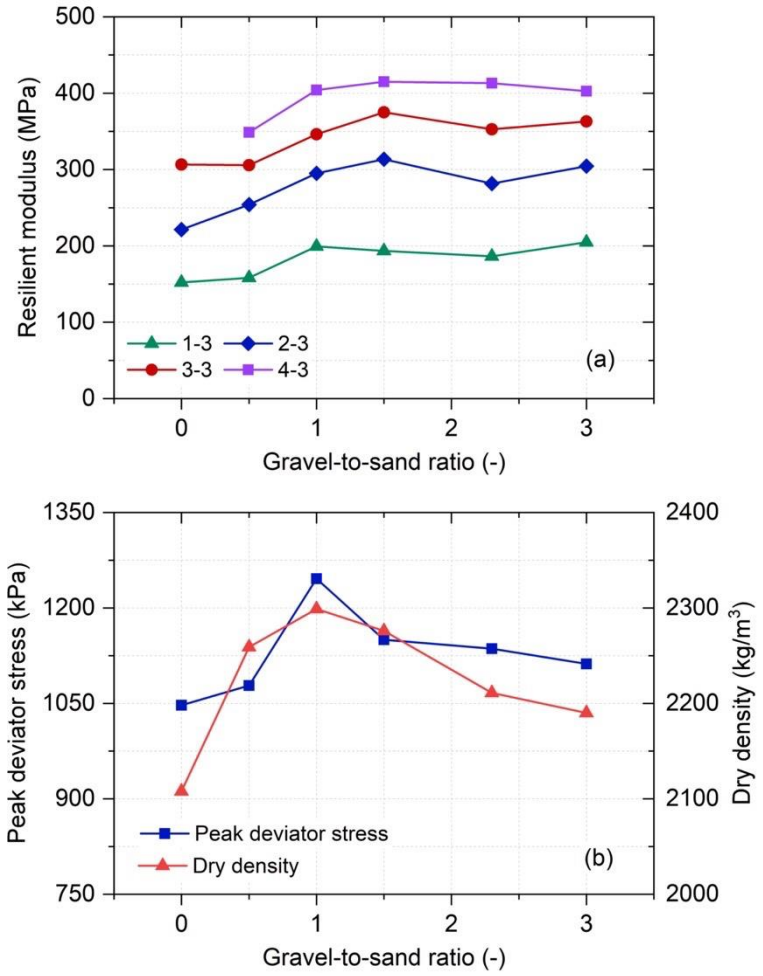

Figure 6.3: Measured mechanical properties of crushed waste rocks with different gravel-to-sand ratios (GS) (0, 0.5, 1, 1.5, 2.3, and 3); (a) resilient modulus (for stress path 1-3, 2-3, 3-3, and 4-3), and (b) shear strength (peak deviator stress under 50 kPa of confining pressure).

The accumulated axial permanent strain typically increased with the number of loading cycles, and depended on the gradation of crushed waste rocks (Figure 6.4). The permanent strain curves for GS = 0.5 and 1 were similar, and final accumulated permanent strain was around 0.013 after 72000 cycles (12 stress paths) for both specimens. When GS increased to 1.5, the strain increasing for stress path 3-3 was significantly lower than that for GS = 0.5 and 1. When GS increased to 2.3, the trend inversed, and the strain curve was significantly greater than that for GS = 1.5. As GS increased to 3, the permanent strain rapidly increased, especially in stress path 3-3 where the increasing in permanent strain was around 0.005.

The variation of permanent strain for various GS also influenced the shakedown range for the considered stress paths (Figure 6.4). The value of $(\varepsilon_p^{5000}-\varepsilon_p^{3000})$ in the first stress path for different specimens was very close although the shakedown range was different (A or B). Also, the permanent deformation behavior in the first stress path was more sensitive to the initial state of the tested specimen than to the GS ratio. Therefore, the shakedown range in stress path 1-1 was not taken into account in the analysis of gradation effect. The shakedown range in stress path 2-2 varied from B (plastic creep) to A (plastic shakedown) as GS increased from 0.5 to 1.5. Similarly to the trend of permanent strain observed when GS exceeded 1.5, the shakedown range also increased from A to B in stress path 3-2, and from B to C (incremental collapse) in stress path 3-3 and 4-3 for GS = 3. The optimum GS considering the permanent deformation behavior in this study was 1.5 for crushed waste rocks with FC = 3.75%.

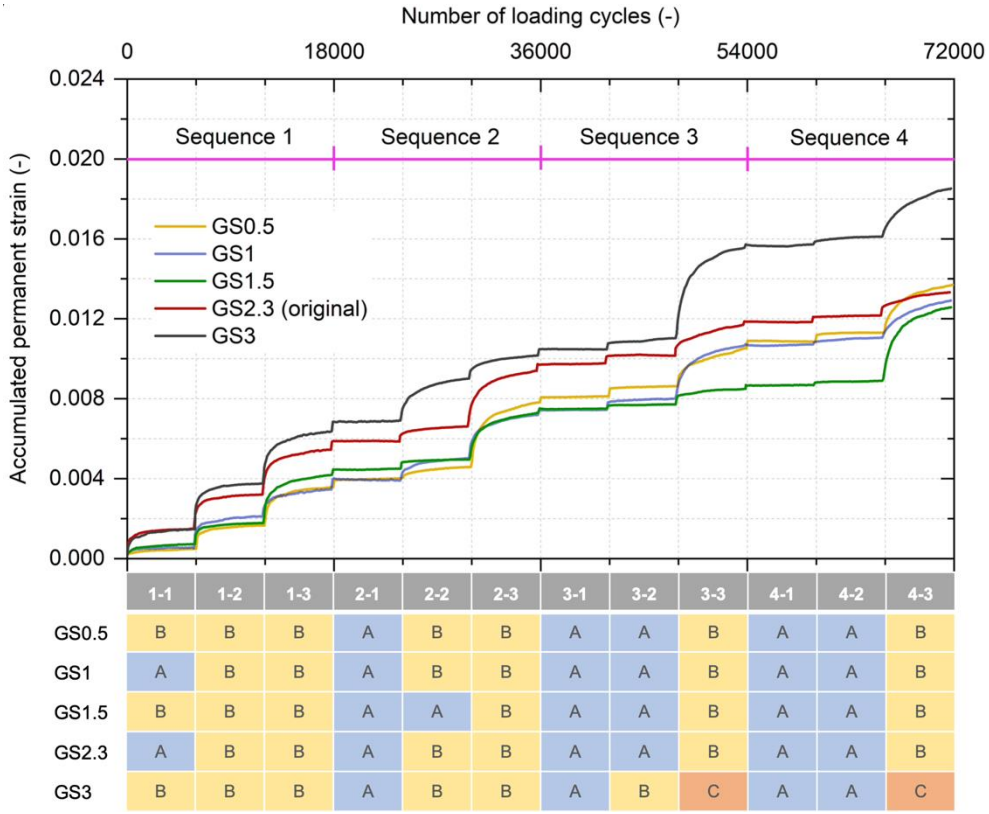

	1-1	1-2	1-3	2-1	2-2	2-3	3-1	3-2	3-3	4-1	4-2	4-3
GS0.5	B	B	B	A	B	B	A	A	B	A	A	B
GS1	A	B	B	A	B	B	A	A	B	A	A	B
GS1.5	B	B	B	A	A	B	A	A	B	A	A	B
GS2.3	A	B	B	A	B	B	A	A	B	A	A	B
GS3	B	B	B	A	B	B	A	B	C	A	A	C

Figure 6.4: Evolution of accumulated permanent strain with the number of loading cycles for crushed waste rocks with different gravel-to-sand ratios (GS) (0, 0.5, 1, 1.5, 2.3, and 3), and the corresponding shakedown range for each stress path.

6.3.2 Effect of fines content (FC) on crushed waste rock mechanical properties

The value of FC also affected the resilient modulus of crushed waste rocks (Figure 6.5(a)). For stress paths 1-3 and 2-3, the resilient modulus increased slightly (< 5%) when FC increased from 3.75% to 5%. As the stress level increased to 3-3 and 4-3, the resilient modulus change was not significant and was only slightly greater (< 5%) for FC = 3.75% than for FC = 5%. When FC > 5%, the increasing in FC resulted in a decrease of resilient modulus. For example, when FC increased from 5% to 12%, the resilient modulus decreased from 295 to 250 MPa, and from 395 to 375 MPa, for stress paths 2-3 and 4-3, respectively. Therefore, the optimum FC in terms of resilient modulus

appeared to be around 5% (with GS = 2.3). The shear strength of crushed waste rocks showed different trend with FC (Figure 6.5(b)). The peak deviator stress (under 50 kPa of confining pressure) increased from 1135 to 1410 kPa (+24%) as FC increased from 3.75% to 8%, and then decreased when FC exceeded 8%. The maximum shear strength measured for FC = 8% could be (mostly) attributed to the greater higher dry density (2311 kg/m^3) in this case.

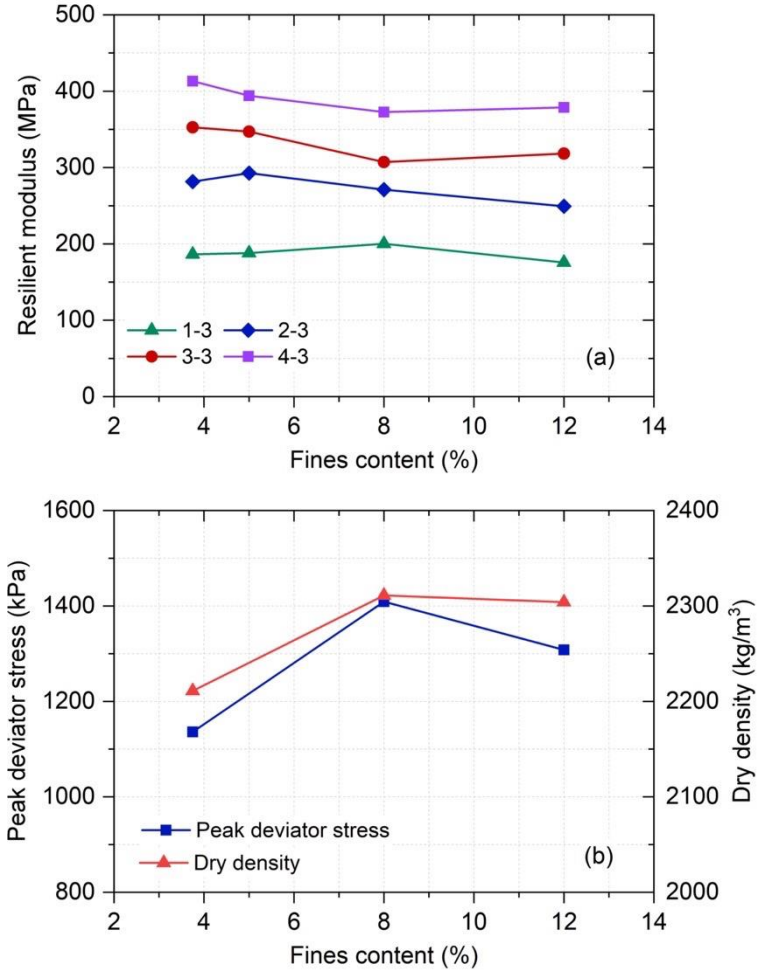

Figure 6.5: Measured mechanical properties of crushed waste rocks with different fines contents (FC) (3.75%, 8%, and 12%); (a) resilient modulus (for stress path 1-3, 2-3, 3-3, and 4-3), and (b) shear strength (peak deviator stress under 50 kPa of confining pressure).

Unlike the stiffness softening, an increasing FC from 3.75% to 12% resulted in a decrease of permanent strain (Figure 6.6). For example, the increasing of permanent strain for FC = 8% was around 0.001 in stress path 1-3, which was significantly lower than for FC = 3.75% where the increasing of permanent strain was around 0.003. When FC increased to 12%, the accumulated permanent strain curve was significantly lower than that for FC = 3.75% and 8%, and the final strain was around 0.01. On the other hand, the shakedown range in stress path 3-2 changed from A to B when FC exceeded 3.75%, but the values of $(\varepsilon_p^{5000}-\varepsilon_p^{3000})$ for different FC in this stress path were similar. Therefore, the increase of FC from 3.75 to 12% contributed to decrease the permanent deformation of crushed waste rocks (GS = 2.3).

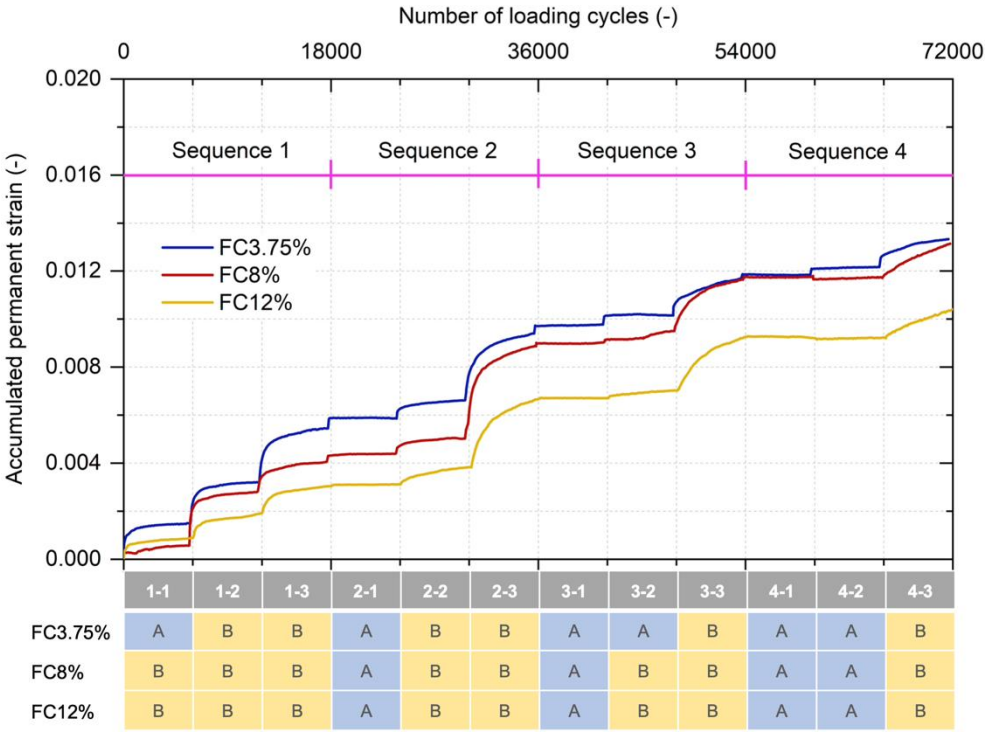

Figure 6.6: Evolution of accumulated permanent strain with the number of loading cycles for crushed waste rocks with different fines contents (FC) (3.75%, 8%, and 12%), and the corresponding shakedown range for each stress path.

6.4 Interpretation of test results

The impact of gradation (GS and FC) on the mechanical properties of crushed waste rocks can be attributed to the variation of specimen fabric. The fabric of crushed waste rocks consists of gravel, sand, and fines, in which the gravel particles form the skeleton that serves as a primary load-carrying network to transmit the major part of a axial load, while the fine particles (sand and fines) fill the void space enclosed by the gravel particles (Knight 1935; Xiao et al. 2012). The fine particles typically can have two effects, according to their location in the fabric: the fine particles between the gravel particles along the stress chain can weaken the interlocking of stress chain and promote sliding, while the fines in the pores can inhibit the gravel particle sliding (Qi, Cui, Dupla, et al. 2020).

6.4.1 Effect of gravel-to-sand ratio (GS)

The load-carrying network at low GS (i.e. GS < 1 in this study) cannot be formed, and the mechanical behavior of crushed waste rocks is primarily dominated by the fine particles. The low number of contacts between gravel particles reduces the load bearing capacity of crushed waste rocks (Xiao et al. 2012; Shi et al. 2021). Therefore, the resilient modulus and shear strength was relatively low in this case (Figure 6.3). The permanent deformation is primarily resulting from the compression of fine particles rather than the rearrangement of gravel particles for GS < 1, so the specimen is relatively stable and there was no rapid increasing in permanent strain although the stiffness and shear strength is low (Figure 6.4).

When GS increases to 1, a continuous load-carrying network can be developed in the specimen. The relatively higher dry density (2299 kg/m^3) compared other GS ratios (0-3) indicates the fine particles almost completely occupy the voids enclosed by gravel particles at GS = 1. Hence, the fine particles can provide adequate support to the load-carrying network in this case, and the

mechanical behavior of crushed waste rocks is dominated by both gravel and fine particles. The resilient modulus and shear strength therefore increased significantly, but the variation in permanent deformation was relatively low. When GS increases to 1.5, the number of contacts between gravel particles increases, which leads to an increase of resilient modulus. However, the decrease of fine particles content can also weaken the support to the load-carrying network, which becomes more significant at high axial strain and stress, resulting in the decrease in shear strength for GS = 1.5 in this study.

The support from fine particles would continue to decrease as GS exceeds 1.5, and the shear strength would decrease gradually with GS (Figure 6.3).The mechanical behavior of crushed waste rocks is primarily dominated by friction resistance between gravel particles for GS > 1.5 (Xiao et al. 2012). The resilient modulus decreased slightly with GS, and significantly less than shear strength, indicating that the impact of fine particles on resilient modulus of crushed waste rocks is limited for high GS ratio. The permanent deformation increased significantly and the shakedown range C (incremental collapse) observed for stress paths 3-3 and 4-3 for GS = 3 (Figure 6.4) could indicate gravel particle breakage or rearrangement (Werkmeister et al. 2001). It appears therefore that insufficient fine particles could fail to provide adequate support to the load-carrying network and material with high GS may not be very stable under high stress levels (Xiao et al. 2012).

In this study, the optimum GS for the resilient modulus, permanent deformation, and shear strength was between 1 and 1.5 with a FC = 3.75%. Xiao et al. (2012) proposed a method (Eq. 6.3) to approximate the optimum gradation of aggregates, which is derived from the maximum particle size in the specimen $D_{\max}$ and shape factor n from Talbot equation:

$$\frac{\text{Gravel}}{\text{Sand}} = \frac{p_{75\text{mm}} - p_{4.75\text{mm}}}{p_{4.75\text{mm}} - p_{0.075\text{mm}}} = \frac{1-\left(\frac{4.75}{D_{max}}\right)^n}{\left(\frac{4.75}{D_{max}}\right)^n - \left(\frac{0.075}{D_{max}}\right)^n} = \frac{(D_{max})^n - 4.75^n}{4.75^n - 0.075^n} \quad 6.3$$

Considering the maximum diameter $D_{\max}$ of crushed waste rocks was 19 mm, the optimum GS calculated with Eq. (3) was between 0.9 and 1.4 for porosities n comprised between 0.4 and 0.6.

This approximation method seems therefore acceptable to evaluate the optimum gradation of crushed waste rocks.

The above analysis of GS effect on mechanical properties can contribute to optimize the preparation and/or selection of waste rocks used on sites in various infrastructures. Modifying the gradation to get closer to the optimum GS could for example benefit the geotechnical stability of dams and piles that is significantly related to the shear strength (Blight 1969; Zheng et al. 2005). The choice of the optimum gradation also implies considering other properties and design constraints. For example, for mine haul roads, the water permeability of waste rock layers is one of the critical factors influencing the driving quality in humid regions with heavy rainfall (Tannant and Regensburg 2001). In this case, increasing the GS could contribute to increase significantly the permeability, while limiting the decrease of stiffness (as observed in Figure 6.3, resilient modulus decreased slightly, i.e. < -10%, with exceeding optimum GS).

6.4.2 Effect of fines content (FC)

The effect of fines on aggregates mechanical properties is multifactorial (Lekarp et al. 2000a, 2000b; Duong et al. 2016). On one side, an optimum fines content in voids between gravel particles can inhibit or slow down the rearrangement of gravel particles during shearing, while on the other side, fines between gravel particles can reduce the specimen stiffness. As a consequence, the shear strength increased significantly as FC increases from 3.75% to 8%, but the resilient modulus decreased slightly (see Figure 6.5). However, excessive fines content (12% in this study) would decrease the number of contacts between gravel particles, and break the load-carrying network in the material.

For GS = 2.3, the optimum FC was 5%, 12%, and 8% for resilient modulus, permanent deformation, and shear strength, respectively. In practice, the selection of optimum FC would, however, also

need to consider climate factors (Tannant and Regensburg 2001; AASHTO M-147 2008; Thompson et al. 2019). For example, when crushed waste rocks are used for the wearing course of mine haul roads, FC should not exceed 10% to prevent muddy and slippery conditions (Thompson et al. 2019). On the other hand, FC should also be greater than 5% to prevent raveling or loosening of crushed waste rocks in drier climates (Thompson et al. 2019). Finally, economy also influences the FC selection in practice (Hatipoglu et al. 2020). Optimization is indeed dependent of operation constraints. For example, the FC of an aggregate material is highly variable, and it dependents on the crushing process, transportation, and stockpiling in a quarry or mine site (Hatipoglu et al. 2020). The change in FC of aggregate base materials can therefore significantly affect the cost of valorization in haul, similarly to what is observed for highways (Hatipoglu et al. 2020). Also, decreasing the FC of crushed waste rocks implies sieving, which will raise the construction cost of infrastructures, especially for a massive project such as the large-scale network of haul roads at an open pit mine (10-40 km in length; (Thompson and Visser 2003)).

The gradation effect on the mechanical properties of crushed waste rocks was also quantified using the concept of structural model (Li and Wong 2016), and the detailed results can be found in APPENDIX D.

6.5 Prediction of resilient modulus and permanent deformation from gradation

Experimental results showed that the influence of gradation on the mechanical properties of crushed waste rocks was significant. However, the optimum gradation (GS and FC) measured in this study was only valid for crushed waste rocks with limited gradations. Also, conducting the repeated load triaxial test was time-consuming and required specific equipment. A predictive model

based on the gradation properties could therefore be useful in practice to estimate the mechanical properties efficiently (Rahim and George 2005; Malla and Joshi 2007).

6.5.1 Constitutive model fitting

Resilient modulus

The M_R-θ model was used to describe the measured resilient modulus. This model was proposed by Seed et al. (1967) for different kinds of pavement materials, and can be written:

$$M_R = k_1 p_a \left(\frac{\theta}{p_a}\right)^{k_2} \quad 6.4$$

Where k_1, and k_2: regression coefficients; θ: bulk stress [kPa]; and p_a: atmospheric pressure (100 kPa). The M_R-θ model is widely accepted because of its simplicity and efficiency, and is considered accurate as long as stresses remain below the static failure condition (Elliott and David 1989).

The model coefficients (k_1 and k_2) were calibrated for each gradation by minimizing the coefficient of determination R^2 calculated on the resilient modulus (Figure 6.7 and Table 6.3). The coefficient of determination R^2 was higher than 0.9 for all specimens and the fitting performance of M_R-θ model was therefore deemed acceptable. The model coefficient k_1 was affected significantly by gradation, and tended to increase with the stiffness of crushed waste rocks. Model coefficient k_2 tended to decrease with stiffness, and its variation was relatively small (between 0.42 and 0.64; Table 6.3) and little dependent on gradation.

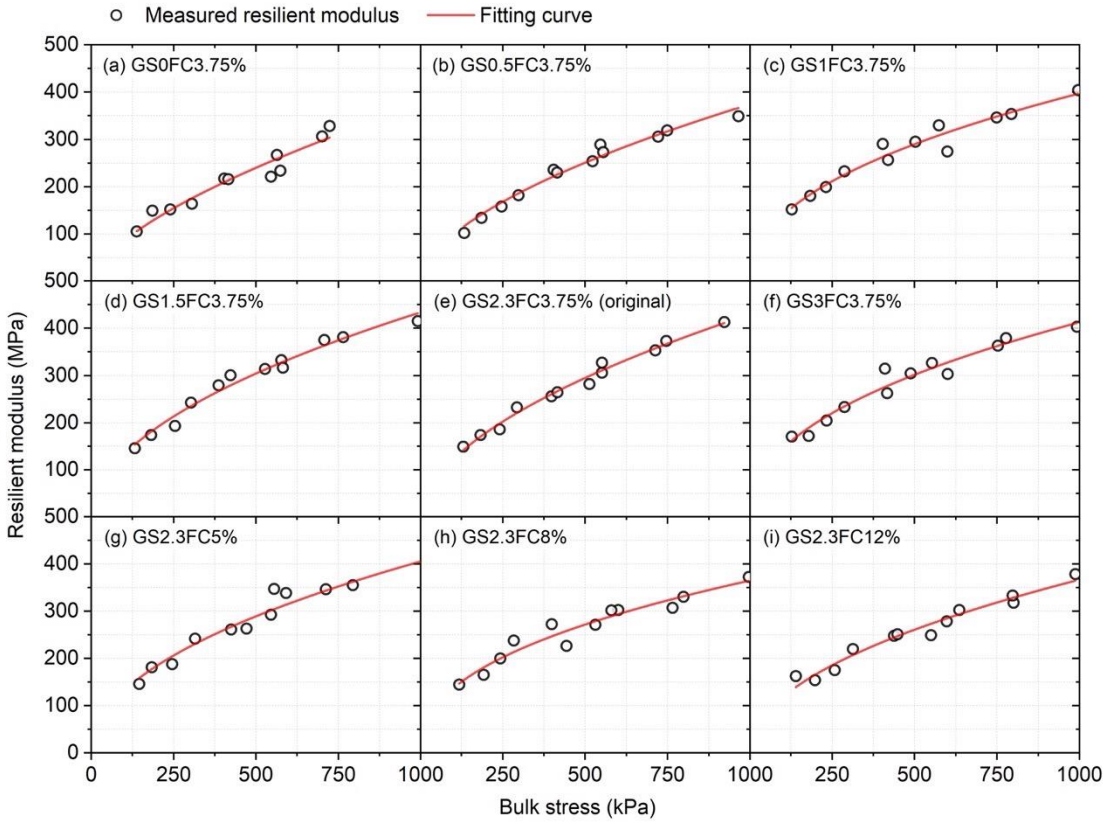

Figure 6.7: Model fitting (M_R-θ model) of measured resilient modulus for crushed waste rocks with different gradations (GS*x*FC*y*%: specimen prepared with a gravel-to-sand ratio GS = *x* and a fines content FC = *y*%); (a) GS0FC3.75%, (b) GS0.5FC3.75%, (c) GS1FC3.75%, (d) GS1.5FC3.75%, (e) GS2.3FC3.75% (original), (f) GS3FC3.75%, (g) GS2.3FC5%, (h) GS2.3FC8%, and (i) GS2.3FC12%.

Table 6.3: Calibrated model coefficients k_1 and k_2 and coefficient of determination R^2 for resilient modulus of crushed waste rocks with different gradations.

	k_1	k_2	R^2
GS0FC3.75%	0.861	0.636	0.933
GS0.5FC3.75%	0.989	0.578	0.981
GS1FC3.75%	1.394	0.455	0.945
GS1.5FC3.75%	1.335	0.512	0.977
GS2.3FC3.75%	1.232	0.542	0.993

GS3FC3.75%	1.456	0.452	0.954
GS2.3FC5%	1.322	0.487	0.940
GS2.3FC8%	1.373	0.425	0.931
GS2.3FC12%	1.185	0.491	0.968

Permanent deformation

The Rahman and Erlingsson model (Rahman and Erlingsson 2015a) was used to fit the measured accumulated permanent strain. Rahman and Erlingsson model is a function of mean bulk stress p, deviator stress q, and number of loading cycles N (Eq. 6.5 and 6.6). This model showed good fitting performance to unbound granular materials in previous studies (Rahman and Erlingsson 2015a; Erlingsson et al. 2017). It can be written:

$$\varepsilon_p = aN^{bS_f}S_f \tag{6.5}$$

$$S_f = \frac{(q/p_a)}{(p/p_a)^{\alpha}} \tag{6.6}$$

Where ε_p: permanent strain [-]; N is number of loading cycles [-]; q: deviator stress, [kPa]; p: mean bulk stress (one-third of the sum of the principal stresses), [kPa]; p_a: the reference stress taken equal to the atmospheric pressure (100 kPa); a, b, and α: model coefficients obtained from regression analysis.

However, Rahman and Erlingsson model was initially developed to fit permanent strain of a single stress path in repeated load triaxial tests. The model was therefore extended using time hardening approach to fit the accumulated permanent strain measured by multistage repeated load triaxial tests in this study. Time hardening approach has been widely used for fitting accumulated permanent strain through considering the effect of stress history (Lytton et al. 1993; Zhou et al. 2010; Erlingsson and Rahman 2013; Mohammadinia et al. 2020; Li et al. 2021). The extended Rahman and Erlingsson model can be written (Rahman and Erlingsson 2015a):

$$\varepsilon_{p_i} = a(N\text{-}N_{i\text{-}1}+N_i^{eq})^{bS_f}S_f \tag{6.7}$$

Where ε_{p_i} is the accumulated permanent strain in the *i*th stress path; the total number of loading cycles *N* from the beginning of the test is modified as $N\text{-}N_{i\text{-}1}+N_i^{eq}$, $N_{i\text{-}1}$ is the total number of loading cycles at the end of (*i*-1)th stress path, and N_i^{eq} is the equivalent number of loading cycles for *i*th stress path, which is required to develop the same amount of permanent strain that is accumulated from all the previous stress paths. Equivalent number of loading cycles N_i^{eq} can be calculated using Eq. 6.8 based on the accumulated permanent strain at the end of (*i*-1)th stress path $\varepsilon_{p_{i\text{-}1}}$.

$$N_i^{eq} = \left(\frac{\varepsilon_{p_{i\text{-}1}}}{aS_f}\right)^{\frac{1}{bS_f}} \tag{6.8}$$

Model coefficient α was relatively constant and close to 0.45 for all gradations. In the following, the value of α was therefore fixed to 0.45 to minimize the number of model coefficients in this study.

The extended Rahman and Erlingsson model was able to fit the accumulated permanent strain satisfactorily with coefficient of determination R^2 greater than 0.95 for all the cases (Figure 6.8 and Table 6.4). The model coefficient *a* was affected significantly by gradation, and tended to increase with the accumulated permanent strain. The value of *a* was lower than 1×10^{-3} for GS0.5FC3.75% and GS2.3FC12%, and it was relatively high ($> 1.5\times10^{-3}$) for GS2.3FC3.75% and GS3FC3.75%. Model coefficient *b* presented the opposite trend and tended to decrease with gradation (Table 6.4).

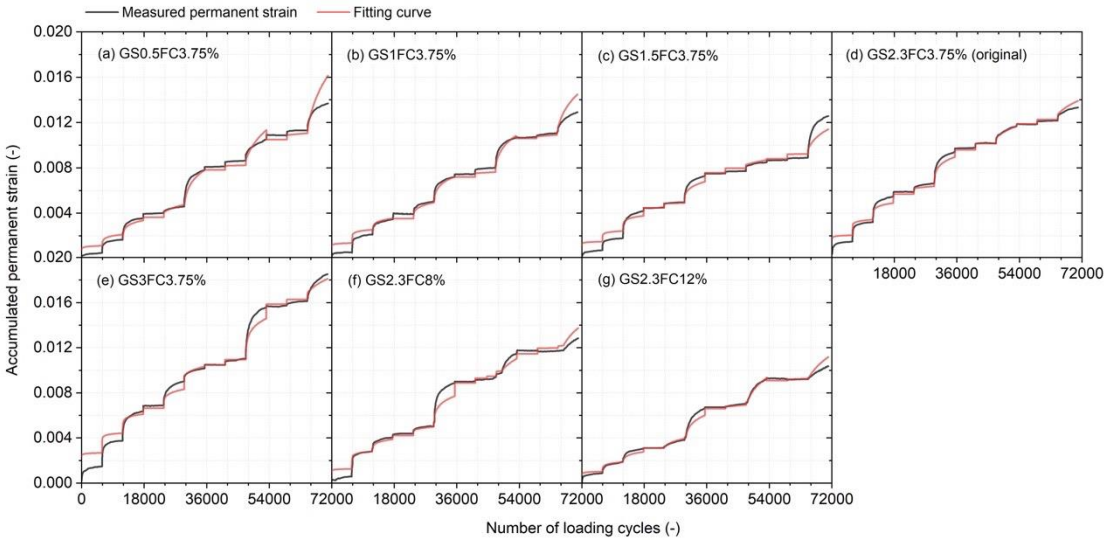

Figure 6.8: Model fitting (Rahman and Erlingsson model) of accumulated permanent strain for crushed waste rocks with different gradations (GS*x*FC*y*: specimen prepared with a gravel-to-sand ratio GS = *x* and a fines content FC = *y*%); (a) GS0.5FC3.75, (b) GS1FC3.75, (c) GS1.5FC3.75, (d) GS2.3FC3.75 (original), (e) GS3FC3.75, (f) GS2.3FC8, and (g) GS2.3FC12.

Table 6.4: Calibrated model coefficients a and b and coefficient of determination R^2 for accumulated permanent strain of crushed waste rocks with different gradations (α=0.45 in this study).

	a (10^{-3})	b	R^2
GS0.5FC3.75%	0.665	0.052	0.983
GS1FC3.75%	1.038	0.034	0.986
GS1.5FC3.75%	1.128	0.025	0.975
GS2.3FC3.75%	1.621	0.024	0.992
GS3FC3.75%	2.356	0.017	0.985
GS2.3FC8%	1.119	0.031	0.986
GS2.3FC12%	0.606	0.041	0.994

6.5.2 Correlation analysis

Model coefficients (k_1, k_2, a, and b) can be correlated with the physical properties of crushed waste rocks through regression. In this study, dry density (ρ_d) and gradation parameters were used as independent variables for the estimation of model coefficients. Gradation parameters included maximum particle size (D_{max}), coefficient of uniformity (C_U), coefficient of curvature (C_C), D_{60}, D_{30} and D_{10} (i.e., 60%, 30%, and 10% of the soil particles are finer than this size, respectively), percentage of gravel (PG), percentage of sand (PS), gravel-to-sand ratio (GS), and fines content (FC), parameters which are widely used to characterize soil gradation (Al-Hussaini 1983; Duong et al. 2016; Wang et al. 2017; Salam et al. 2018; Xu, Liu, et al. 2019; Hatipoglu et al. 2020; Qi, Cui, Chen, et al. 2020; Su et al. 2020; Shi et al. 2021). Correlation analysis was conducted using Pearson correlation coefficient (r). Pearson coefficient r is a statistical metric that measures the strength and direction of a linear relationship between two variables x and y (Eq. 6.9), which has been widely used for correlation analysis (Lee Rodgers and Nicewander 1988; Erzin and Turkoz 2016; Lee et al. 2021). It can be written:

$$r_{xy}=\frac{\sum(x_i-\bar{x})\sum(y_i-\bar{y})}{\sqrt{\sum(x_i-\bar{x})^2}\sqrt{\sum(y_i-\bar{y})^2}} \tag{6.9}$$

Where $\bar{x}=\frac{1}{n}\sum_{i=1}^{N}x_i$ denotes the mean of x, $\bar{y}=\frac{1}{n}\sum_{i=1}^{N}y_i$ denotes the mean of y.

Generally, two variables are considered strongly correlated when $|r| \geqslant 0.8$; an acceptable correlation exists when $0.2 < |r| < 0.8$; and the correlation is weak when $|r| \leqslant 0.2$ (Smith 1986).

The correlation results showed that eight properties had a medium to high correlation with M_R-θ model coefficient k_1 (i.e., $|r| \geqslant 0.2$). More particularly, there was a strong correlation between D_{60}, PG, and PS and k_1 with $|r| \geqslant 0.8$. Correlation with D_{30} (0.77), GS (0.74), D_{max} (0.71), ρ_d (0.51), and D_{10} (0.50) was slightly smaller but still acceptable (Figure 6.9(a)). Among all gradation

properties included in the correlation analysis, C_C, FC, and C_U had weak correlations with k_1 ($|r| \leqslant 0.2$). Properties D_{60}, PG, and PS also had a strong correlation with M_R-θ model coefficient k_2 ($|r| \geqslant 0.8$), but all the remaining eight physical properties also showed some correlation with coefficient > 0.2. The direction of the correlation (i.e., the sign of Pearson coefficient r) between the physical properties and k_1 and k_2 was inverse because of the reverse effects of gradation on k_1 and k_2 (Table 6.3).

Pearson correlation analysis showed that all the physical properties (ρ_d, D_{30}, FC, D_{10}, PG, D_{60}, GS, C_U, C_C, and PS) could affect Rahman and Erlingsson model coefficients a and b ($|r| \geqslant 0.2$; Figure 6.9(b)). Particularly, D_{10}, D_{30}, and ρ_d had strong correlation with coefficient a, and D_{60}, D_{30}, PG, D_{10} and GS had strong correlation with coefficient b ($|r| \geqslant 0.8$). The directions of the correlation between gradation properties and coefficients a and b were also inverse (Table 6.4).

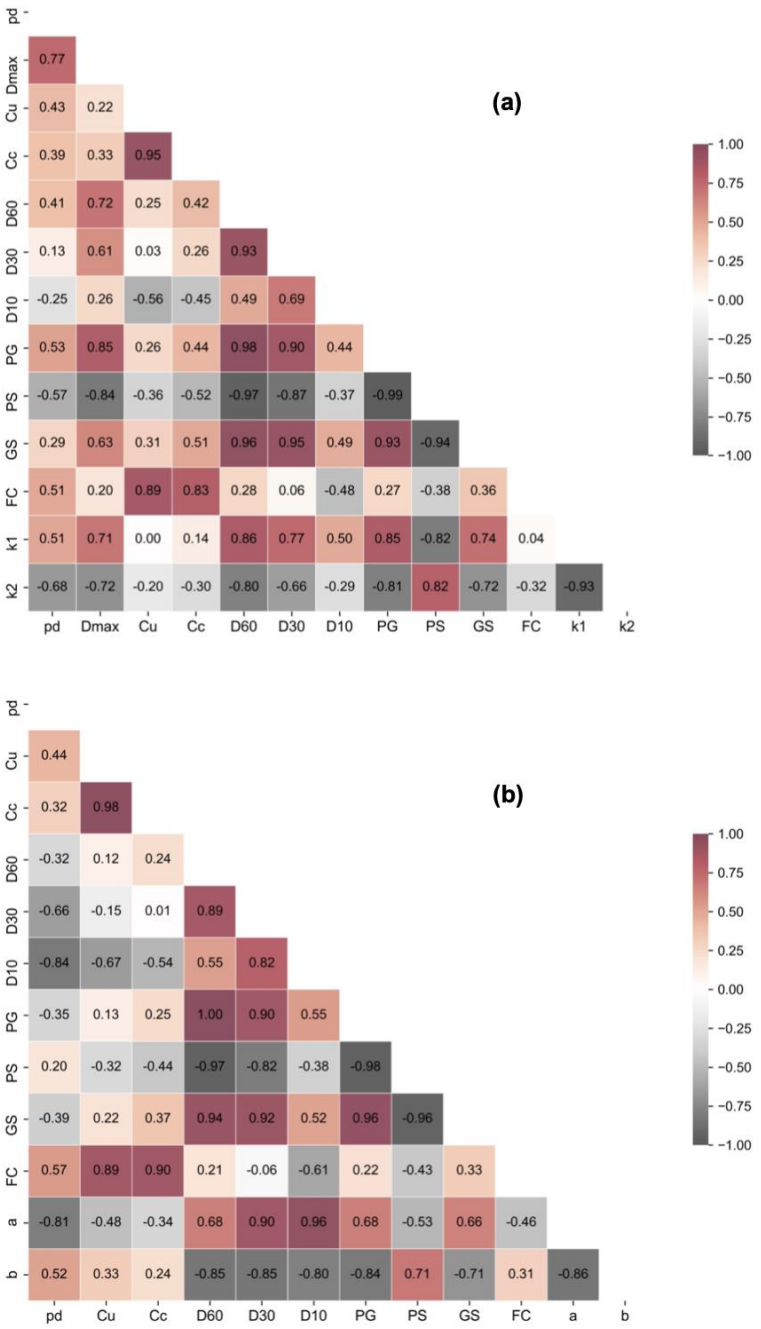

Figure 6.9: Pearson correlations between physical properties and model coefficients (a) k_1 and k_2 in M_R-θ model, and (b) a (10^{-3}) and b in Rahman and Erlingsson model.

6.5.3 Coefficient prediction

The model coefficients (k_1, k_2, a, and b) are generally determined through fitting experimental results, but repeated load triaxial test is relatively costly and time-consuming. The prediction models for k_1, k_2, a, and b, expressed as a function of gradation properties, were therefore developed in this study.

The number of independent variables in a model should generally be minimized to develop a robust link between the independent and dependent variables (Neter et al. 1989; Rahim and George 2005). On the other hand, using an insufficient number of independent variables could result in poor fitting. In this study, it was therefore decided to minimize the number of independent variables by eliminating the gradation properties with high correlations. Considering that most gradation parameters are mutually connected in practice (for example C_U and D_{60}), independent variables which were correlated with a factor $|r| > 0.95$ were eliminated. The correlation between C_U and C_C, between PG and D_{60}, between GS and D_{60}, between GS and D_{30}, between GS and PS, between GS and PG, between PS and PG, and between PS and D_{60} was higher than 0.95 (Figure 6.10), and therefore, only parameters D_{60}, D_{30}, D_{max}, ρ_d, and D_{10} were selected as the independent variables for predicting M_R-θ model coefficient k_1. Following the same reasoning, parameters PS, D_{max}, ρ_d, FC, C_C, and D_{10} were chosen as independent variables to predict coefficient k_2. Finally, D_{10}, D_{30}, D_{60}, C_U, ρ_d, and FC were used to predict Rahman and Erlingsson model coefficient a and b. The predictive models for k_1, k_2, a, and b were developed using multiple linear regression method (Eq. 6.10-6.13). The coefficient of determination R^2 was higher than 0.85 for k_1 and k_2, and was 0.99 for a and b.

$$k_1=0.0385D_{60}+0.0068D_{30}-0.0137D_{max}+0.0018\rho_d+0.5613D_{10}-3.0381 \quad (6.10)$$

$$k_2=0.0017\text{PS}+0.0252D_{max}-0.0021\rho_d+0.0212\text{FC}-0.0107C_C-0.4838D_{10}+4.7688 \quad (6.11)$$

$$a\ (\times 10^{-3})=-26.8692D_{10}+3.3927D_{30}+0.003\rho_d-0.4197D_{60}-0.0071C_U-0.5597\text{FC}-2.4021 \quad (6.12)$$

$$b=-0.0157D_{60}+0.12D_{30}-1.3028D_{10}-0.0003\rho_d-0.0006C_U-0.0145FC+0.9145 \quad (6.13)$$

6.5.4 Validation of the predictive models

The developed predictive models (Eq. 6.10-6.13) were verified using the literature (Table 6.5). The data on resilient modulus and permanent deformation from the literature were obtained from the same laboratory test used in this study, i.e., repeated load triaxial tests, but the tested materials were different and the gradation varied over a wide range. The prediction error was quantified using the root mean square error (RMSE) and a factor $(y_{pre}-y_{mea})/y_{mea}$, where y_{pre} and y_{mea} was predicted and measured mechanical property values (either resilient modulus M_R or permanent strain PS), respectively (Figure 6.10).

The prediction performance of the resilient modulus model was acceptable for results presented in Tutumluer et al. (2009), Araya (2011), Cetin et al. (2014), and Soliman and Shalaby (2016) with $(M_{Rpre}-M_{Rmea})/M_{Rmea}$ ranging from -0.5 to 0.5 and RMSE < 145 for most points (> 90%) (although the prediction performance was lower than that of data from this study (Figure 6.10(a)). However, the model tended to underestimate slightly the resilient modulus for Maghool et al. (2019) with $(M_{Rpre}-M_{Rmea})/M_{Rmea} \approx -0.5$ and RMSE = 211. On the other hand, the resilient modulus was overestimated for Gu, Ye, et al. (2020), and this overestimation tended to increase with bulk stress. The tested materials from Gu, Ye, et al. (2020) and Maghool et al. (2019) were mixed materials of crushed tuff and Kaolin clay, and mixed materials of electric arc and ladle furnace slags, respectively, and their mineralogy was very different from typical crushed waste rocks, which may be one of the possible reasons for observed discrepancies. However, the proposed model was relatively accurate for crushed waste rocks.

The proposed prediction models however tended to underestimate the permanent strain with $(PS_{pre}-PS_{mea})/PS_{mea} < -0.5$ and RMSE > 3×10^{-3} for all the literature results considered here (Figure 6.10(b)

(Lekarp et al. 1996; Tutumluer et al. 2009; Jing et al. 2018; Byun et al. 2020; Gu, Zhan, et al. 2020). This relatively low prediction performance can be attributed to the fact that permanent strain is more complex and sensitive to material properties than resilient modulus. For example, different materials with the same gradation often show different permanent deformation behavior (Tutumluer et al. 2009). Other properties such as compaction, saturation, and maximum particle size also could affect the permanent deformation behavior, but they were not taken into account in the developed model. Still, the proposed predictive model for permanent strain can remain useful but would require further work to improve its precision.

Table 6.5: The literature used for the validation of prediction models for resilient modulus (M_R) and permanent strain (PS), and the material information including material type, maximum particle size D_{max}, coefficient of curvature C_C, coefficient of uniformity C_U.

Reference	Property	Material	D_{max} (mm)	C_C (-)	C_U (-)
Tutumluer et al. (2009)	M_R, PS	Gravel, Dolomite	25	2.5-120	18-1500
Araya (2011)	M_R	Crushed rock, Ferricrete, Limestone gravel	32	1-4	12-40
Cetin et al. (2014)	M_R	Texas, Rockville, Churchville, Bladensburg	38	0.5-6	60-135
Soliman and Shalaby (2016)	M_R	Crushed limestone, Gravel	19	1.5-10	20-400
Maghool et al. (2019)	M_R	Electric arc furnace slag, Ladle furnace slag	20	1-4.5	5-60
Gu, Ye, et al. (2020)	M_R	Crushed tuff aggregates, Kaolin clay	30	4.8	30
Lekarp et al. (1996)	PS	Dolomitic magnesian limestone, Granidiorite, Slate waste, Sand and	1.5, 40, 75	0.2-1.5	2-110

		gravel, Leighton buzzard sand			
Jing et al. (2018)	PS	Missillac fine sand	4	1-2	3-9
Byun et al. (2020)	PS	Crushed aggregates (granite, basalt, and limestone)	25.4	0.5-3.5	30-155
Gu, Zhan, et al. (2020)	PS	Crushed tuff, Kaolin clay	30	2.8	20.6
This study	M_R, PS	Crushed waste rocks	19	0.9-21	16-240

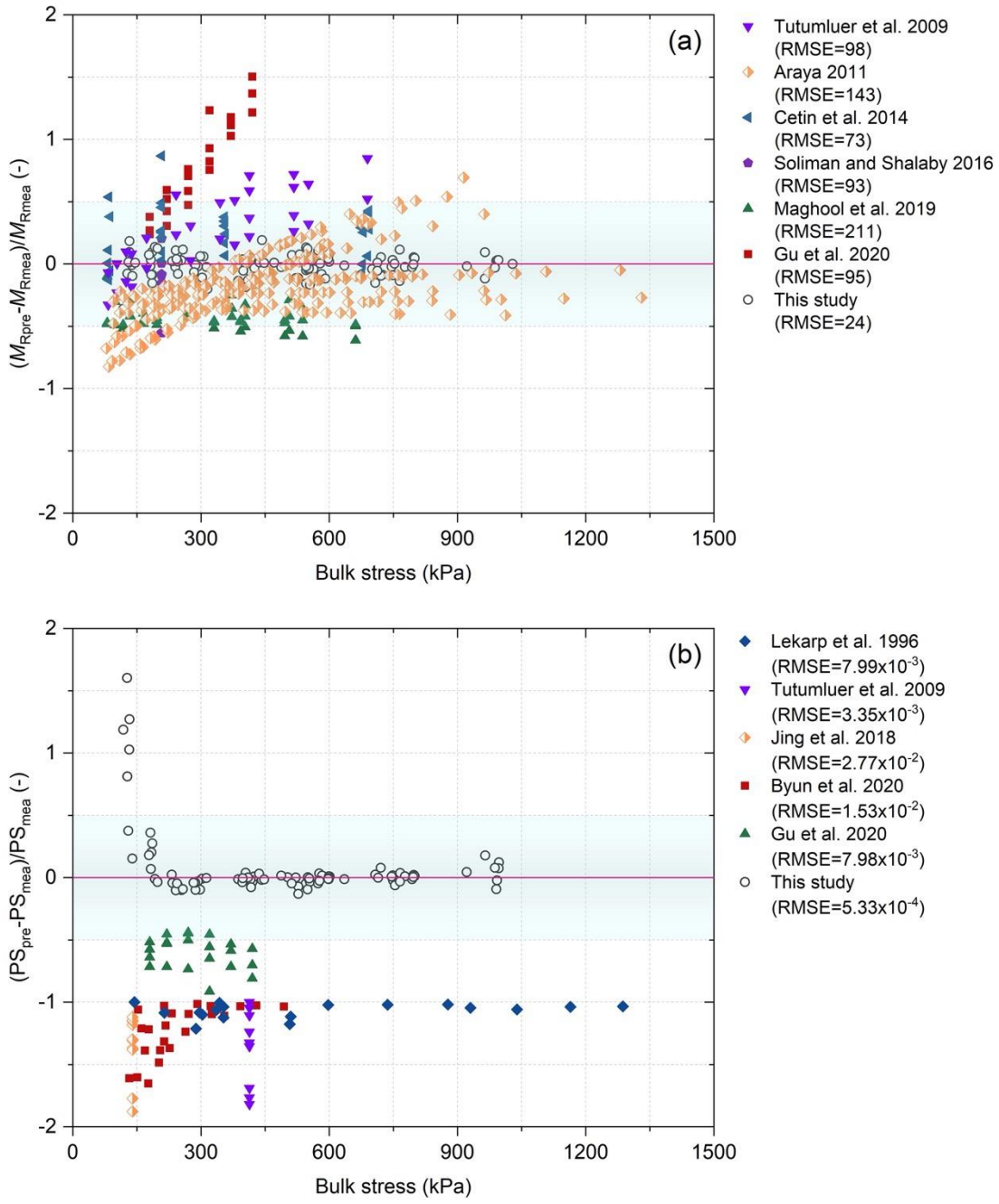

Figure 6.10: Prediction performance of the developed models on (a) resilient modulus (M_R) and (b) permanent strain (PS); the root mean square error (RMSE) and $(y_{pre}-y_{mea})/y_{mea}$ were used to describe the prediction error, where y_{pre} and y_{mea} were predicted and measured value, respectively; the blue zone represented the value of $(y_{pre}-y_{mea})/y_{mea}$ ranged from -0.5 to 0.5 that was deemed acceptable.

6.6 Discussion and final remarks

A series of repeated load and monotonic triaxial tests were carried out on crushed waste rocks to study the relationship between mechanical characteristics and gradation. Coefficient prediction models (k_1, k_2, a, and b), were also developed to estimate resilient modulus and permanent strain based on gradation properties. These models were validated using data from literature, indicating that the prediction performance for resilient modulus was relatively good while permanent strain tended to be somewhat underestimated. Although the crushed waste rocks used in this study were representative of hard rock mines (Bussière 2007a; James et al. 2013), the limited available database did influence the models' accuracy and generalization. Also, further would be required to extrapolate the trends observed and the proposed models to waste rocks which maximum particle size can exceed a meter (Williams and Walker 1983; James et al. 2013). In addition, this paper only focused on gradation, but other properties influence the soil mechanical properties, such as water content, degree of compaction, and particle shape (Al-Hussaini 1983; Duong et al. 2016; Yang and Luo 2018; Gu, Zhan, et al. 2020; Shi et al. 2021), and these should therefore be taken into account in future studies.

In this study, post-cyclic monotonic triaxial tests were conducted to assess the shear strength of crushed waste rocks. The cyclic loading causes additional compaction on the waste rock samples, which could result in a higher shear strength. The differences between experimental procedures make it difficult to compare the results with that from literature (Indraratna et al. 1998; Bray et al. 2009; Seif El Dine et al. 2010). Also, only one monotonic triaxial test was carried out on each sample to estimate the stress-strain curve of crushed waste rocks under 50 kPa of confining pressure, which limits the accuracy of the friction angle determination accurately (Xiao et al. 2014; Chen and Zhang 2016). Therefore, more monotonic triaxial tests should be carried out on crushed waste rocks without cyclic loading compression to study their shear behavior under different stress states.

Rahman and Erlingsson model (extended using time hardening approach) was able to accurately describe the measured accumulated permanent strain in this study. However, fitting performance of the extended model heavily relies on the initial values of the model coefficients (i.e., a, b, and α), and these are generally determined through trial and error method, which is time-consuming and complex especially when a large number of stress paths are applied in one multistage repeated load triaxial test. Although Rahman and Erlingsson (2015a) provided a detailed fitting process using Microsoft Excel, the engineer experience and judgement has a severe impact on the model fitting performance. This is one of the limitations of conventional regression models when dealing with complex and highly nonlinear data (Karlaftis and Vlahogianni 2011). One possible solution could consist in introducing machine learning to predict accumulated permanent strain (Ghorbani, Arulrajah, Narsilio, and Horpibulsuk 2020a).

6.7 Conclusions

A research study was undertaken to investigate the effect of gradation (i.e., gravel-to-sand ratio GS and fines content FC) on mechanical characteristics of crushed waste rocks from Canadian Malartic Mine using repeated load and monotonic triaxial tests. Predictive models were also developed for M_R-θ model coefficients k_1 and k_2 and Rahman and Erlingsson model coefficients a and b based on the gradation properties of crushed waste rocks. The results of the current study are summarized as follows:

1. An increasing in GS increased the resilient modulus and shear strength of crushed waste rocks until the optimum GS, and the optimum GS was 1.5 and 1 for stiffness and shear strength, respectively. The resilient modulus decreased slightly when exceeding optimum GS while the decrease of shear strength was more marked. The permanent strain decreased slowly as GS

increased from 0.5 to 1.5, but it increased very sharply (sometimes even reaching shakedown range C, i.e., incremental collapse) when GS increased to 3.

2. The resilient modulus tended to decrease with FC, and an optimum FC around 5% was recommended regarding stiffness. FC had a significant influence on shear strength, and a maximum shear strength was reached for FC = 8%. The variation of shear strength was directly correlated with the variation of dry density. Permanent strain tended to decrease when FC increased from 3.75% to 12% but selecting an optimum FC would require to consider other specifications in practice (e.g., AASHTO M-147 specifications for highway base layers and Guidelines for mine haul road design).

3. M_R-θ model and Rahman and Erlingsson model (extended using time hardening) performed well for fitting measured resilient modulus and accumulated permanent strain, respectively. Coefficient prediction models (k_1, k_2, a, and b), expressed as a function of gradation properties, were developed using multiple linear regression, and they were able to evaluate the effect of gradation on resilient modulus and permanent deformation of crushed waste rocks. The prediction performance of M_R-θ model was acceptable, the predicted permanent strain tended to be somewhat underestimated. The proposed models could be used to predict the mechanical properties of crushed waste rocks as a function of their gradation on other mines sites but would need to be improved using more test results to extend their generalization capacity.

Acknowledgements

This research was carried out with the financial support from FRQNT and the industrial partners of the Research Institute on Mines and the Environment (http://irme.ca/). The repeated load triaxial and CBR test equipment used in this study were acquired with a CFI grant.

6.8 References

AASHTO M-147. Standard specification for materials for aggregate and soil-aggregate subbase, base, and surface courses. Washington, DC; 2008.

AASHTO T307-99. Standard method of test for determining the resilient modulus of soils and aggregate materials. Washington, DC; 2017.

Ahmed A, and Abouzeid A. Potential use of phosphate wastes as aggregates in road construction. JES. Journal of Engineering Sciences 2009*;* 37(2): 413-422.

Al-Hussaini M. Effect of particle size and strain conditions on the strength of crushed basalt. Can Geotech J 1983*;* 20(4): 706-717.

Amrani M, Taha Y, Kchikach A, et al. Valorization of phosphate mine waste rocks as materials for road construction. Minerals-Basel 2019*;* 9(4): 237.

Araya AA. Characterization of unbound granular materials for pavements. Delft University of Technology, 2011.

ASTM D1557-12e1. Standard test methods for laboratory compaction characteristics of soil using modified effort (56,000 ft-lbf/ft^3 (2,700 kN-m/m^3)). ASTM International, West Conshohocken, PA; 2012.

ASTM D854-14. Standard test methods for specific gravity of soil solids by water pycnometer. ASTM International, West Conshohocken, PA; 2014.

ASTM C127-15. Standard test method for relative density (specific gravity) and absorption of coarse aggregate. ASTM International, West Conshohocken, PA; 2015.

ASTM D2487-17e1. Standard practice for classification of soils for engineering purposes (unified soil classification system). ASTM International, West Conshohocken, PA; 2017.

ASTM C136/C136M-19. Standard test method for sieve analysis of fine and coarse aggregates.

ASTM International, West Conshohocken, PA; 2019.

ASTM D7181-20. Standard test method for consolidated drained triaxial compression test for soils. ASTM International, West Conshohocken, PA; 2020.

Aubertin M. Waste rock disposal to improve the geotechnical and geochemical stability of piles. In: Proceedings of the world mining congress, Montreal, Canada; 2013.

Aubertin M, Bussière B, Pabst T, et al. Review of the reclamation techniques for acid-generating mine wastes upon closure of disposal sites. Proc., Geo-Chicago 2016 2016: 343-358.

Bao Y, Han X, Chen J, et al. Numerical assessment of failure potential of a large mine waste dump in panzhihua city, china. Engineering Geology 2019*;* 253: 171-183.

Blight GE. Shear stability of dumps and dams of gold mining waste. The Civil Engineering in South Africa 1969*;* (3): 49-54.

Bray JD, Zekkos D, Kavazanjian Jr E, et al. Shear strength of municipal solid waste. Journal of geotechnical and geoenvironmental engineering 2009*;* 135(6): 709-722.

Bussière B. Colloquium 2004: Hydrogeotechnical properties of hard rock tailings from metal mines and emerging geoenvironmental disposal approaches. Can Geotech J 2007*;* 44(9): 1019-1052.

Bussiere B, Aubertin M, and Chapuis RP. The behavior of inclined covers used as oxygen barriers. Can Geotech J 2003*;* 40(3): 512-535.

Byun Y-H, Feng B, Qamhia II, et al. Aggregate properties affecting shear strength and permanent deformation characteristics of unbound–base course materials. J Mater Civil Eng 2020*;* 32(1): 04019332.

Cetin A, Kaya Z, Cetin B, et al. Influence of laboratory compaction method on mechanical and hydraulic characteristics of unbound granular base materials. Road materials and pavement

design 2014; 15(1): 220-235.

Chen X, and Zhang J. Influence of relative density on dilatancy of clayey sand–fouled aggregates in large-scale triaxial tests. Journal of Geotechnical and Geoenvironmental Engineering 2016; 142(10): 06016011.

Dawson RF, Morgenstern NR, and Stokes AW. Liquefaction flowslides in rocky mountain coal mine waste dumps. Can Geotech J 1998; 35(2): 328-343.

Drumm E, Boateng-Poku Y, and Johnson Pierce T. Estimation of subgrade resilient modulus from standard tests. Journal of Geotechnical Engineering 1990; 116(5): 774-789.

Du J, Hou KP, and Liang W. Experimental research on strength characteristics of bulky rock material with different coarse grain content in waste pile of mine. In: Applied Mechanics and Materials; 2012.

Duong TV, Cui Y-J, Tang AM, et al. Effects of water and fines contents on the resilient modulus of the interlayer soil of railway substructure. Acta Geotechnica 2016; 11(1): 51-59.

Elliott RP, and David L. Improved characterization model for granular bases. Transp Res Record 1989; (1227).

EN 13286-7. Unbound and hydraulically bound mixtures–cyclic load triaxial test for unbound mixtures. 2004.

Erlingsson S. Rutting development in a flexible pavement structure. Road Materials and Pavement Design 2012; 13(2): 218-234.

Erlingsson S, and Rahman MS. Evaluation of permanent deformation characteristics of unbound granular materials by means of multistage repeated-load triaxial tests. Transp Res Record 2013; 2369(1): 11-19.

Erlingsson S, Rahman S, and Salour F. Characteristic of unbound granular materials and subgrades

based on multi stage rlt testing. Transp Geotech 2017*;* 13: 28-42.

Erzin Y, and Turkoz D. Use of neural networks for the prediction of the cbr value of some aegean sands. Neural Computing and Applications 2016*;* 27(5): 1415-1426.

Ghorbani B, Arulrajah A, Narsilio G, et al. Experimental and ann analysis of temperature effects on the permanent deformation properties of demolition wastes. Transp Geotech 2020*;* 24.

Golder. Golder Associates Africa (Pty) Ltd. Environmental impact assessment and environmental management programme report for the proposed metsimaholo underground coal mine. Department of Mineral Resources; 2019.

Gu C, Ye X, Wang J, et al. Resilient behavior of coarse granular materials in three-dimensional stress state. Can Geotech J 2020*;* 57(9): 1280-1293.

Gu C, Zhan Y, Wang J, et al. Resilient and permanent deformation of unsaturated unbound granular materials under cyclic loading by the large-scale triaxial tests. Acta Geotechnica 2020*;* 15(12): 3343-3356.

Hamidi A, Yazdanjou V, and Salimi N. Shear strength characteristics of sand-gravel mixtures. International Journal of Geotechnical Engineering 2009*;* 3(1): 29-38.

Hao S, and Pabst T. Estimation of resilient behavior of crushed waste rocks using repeated load cbr tests. Transp Geotech 2021: 100525.

Hatipoglu M, Cetin B, and Aydilek AH. Effects of fines content on hydraulic and mechanical performance of unbound granular base aggregates. Journal of Transportation Engineering, Part B: Pavements 2020*;* 146(1): 04019036.

Hicks RG, and Monismith CL. Factors influencing the resilient response of granular materials. Highway research record 1971*;* 345: 15-31.

Indraratna B, Ionescu D, and Christie H. Shear behavior of railway ballast based on large-scale

triaxial tests. Journal of geotechnical and geoenvironmental Engineering 1998*;* 124(5): 439-449.

James, Aubertin M, and Bussière B. On the use of waste rock inclusions to improve the performance of tailings impoundments. In: Proceedings of the 18th International Conference Soil Mechanics and Geotechnical Engineering, Paris, France; 2013.

Jing P, Nowamooz H, and Chazallon C. Permanent deformation behaviour of a granular material used in low-traffic pavements. Road Materials and Pavement Design 2018*;* 19(2): 289-314.

Kamal M, Dawson A, Farouki O, et al. Field and laboratory evaluation of the mechanical behavior of unbound granular materials in pavements. Transp Res Record 1993: 88-88.

Karlaftis MG, and Vlahogianni EI. Statistical methods versus neural networks in transportation research: Differences, similarities and some insights. Transportation Research Part C: Emerging Technologies 2011*;* 19(3): 387-399.

Knight J. Gradation of aggregate as applied to stabilization of gravel roads. Canadian Engineer 1935*;* 69(23): 9-10.

Laverdière A. Effet de la granulométrie sur le comportement géotechnique de roches stériles concassées utilisées comme surface de roulement sur des routes minières. École Polytechnique de Montréal, 2019.

Lee D-H, Cheon E, Lim H-H, et al. An artificial neural network model to predict debris-flow volumes caused by extreme rainfall in the central region of south korea. Engineering Geology 2020.

Lee Rodgers J, and Nicewander WA. Thirteen ways to look at the correlation coefficient. The American Statistician 1988*;* 42(1): 59-66.

Lekarp F, Isacsson U, and Dawson A. State of the art. I: Resilient response of unbound aggregates. Journal of Transportation Engineering 2000a*;* 126(1): 66-75.

Lekarp F, Isacsson U, and Dawson A. State of the art. Ii: Permanent strain response of unbound aggregates. Journal of transportation engineering 2000b*;* 126(1): 76-83.

Lekarp F, Richardson IR, and Dawson A. Influences on permanent deformation behavior of unbound granular materials. Transp Res Record 1996*;* 1547(1): 68-75.

Li, B, and Wong, R. Quantifying structural states of soft mudrocks. Journal of Geophysical Research: Solid Earth 2016; 121(5): 3324-3347.

Li Y, Nie R, Yue Z, et al. Dynamic behaviors of fine-grained subgrade soil under single-stage and multi-stage intermittent cyclic loading: Permanent deformation and its prediction model. Soil Dyn Earthq Eng 2021*;* 142: 106548.

Long W, Xiaoguang X, and Hai L. Influence of laboratory compaction methods on shear performance of graded crushed stone. J Mater Civil Eng 2011*;* 23(10): 1483-1487.

Lytton RL, Uzan J, Fernando EG, et al. Development and validation of performance prediction models and specifications for asphalt binders and paving mixes (Vol. 357): Strategic Highway Research Program Washington, DC; 1993.

Maghool F, Arulrajah A, Suksiripattanapong C, et al. Geotechnical properties of steel slag aggregates: Shear strength and stiffness. Soils and Foundations 2019*;* 59(5): 1591-1601.

Malla RB, and Joshi S. Resilient modulus prediction models based on analysis of ltpp data for subgrade soils and experimental verification. Journal of Transportation Engineering 2007*;* 133(9): 491-504.

Malla RB, and Joshi S. Subgrade resilient modulus prediction models for coarse and fine-grained soils based on long-term pavement performance data. International Journal of Pavement Engineering 2008*;* 9(6): 431-444.

Mishra D, and Tutumluer E. Aggregate physical properties affecting modulus and deformation characteristics of unsurfaced pavements. J Mater Civil Eng 2012*;* 24(9): 1144-1152.

Mohammad LN, Huang B, Puppala AJ, et al. Regression model for resilient modulus of subgrade soils. Transp Res Record 1999*;* 1687(1): 47-54.

Mohammadinia A, Naeini M, Arulrajah A, et al. Shakedown analysis of recycled materials as railway capping layer under cyclic loading. Soil Dyn Earthq Eng 2020*;* 139: 106423.

Neter J, Wasserman W, and Kutner MH. Applied linear regression models. 1989.

Omraci K, Merrien-Soukatchoff V, Tisot J-P, et al. Stability analysis of lateritic waste deposits. Engineering geology 2003*;* 68(3-4): 189-199.

Qi S, Cui Y, Dupla JC, et al. Investigation of the parallel gradation method based on the response of track-bed materials under cyclic loadings. Transp Geotech 2020*;* 24: 100360.

Qi S, Cui Y-J, Chen R-P, et al. Influence of grain size distribution of inclusions on the mechanical behaviours of track-bed materials. Géotechnique 2020*;* 70(3): 238-247.

Rahim A, and George K. Models to estimate subgrade resilient modulus for pavement design. International Journal of Pavement Engineering 2005*;* 6(2): 89-96.

Rahman MS, and Erlingsson S. A model for predicting permanent deformation of unbound granular materials. Road Materials and Pavement Design 2015*;* 16(3): 653-673.

Salam S, Osouli A, and Tutumluer E. Crushed limestone aggregate strength influenced by gradation, fines content, and dust ratio. Journal of Transportation Engineering, Part B: Pavements 2018*;* 144(1): 04018002.

Santha B. Resilient modulus of subgrade soils: Comparison of two constitutive equations. Transp Res Record 1994*;* (1462).

Seif El Dine B, Dupla JC, Frank R, et al. Mechanical characterization of matrix coarse-grained soils with a large-sized triaxial device. Can Geotech J 2010*;* 47(4): 425-438.

Shi XS, Liu K, and Yin J. Effect of initial density, particle shape, and confining stress on the critical

state behavior of weathered gap-graded granular soils. Journal of Geotechnical and Geoenvironmental Engineering 2021; 147(2): 04020160.

Smith GN. Probability and statistics in civil engineering. Collins professional and technical books 1986; 244.

Soliman H, and Shalaby A. Validation of long-term pavement performance prediction models for resilient modulus of unbound granular materials. Transp Res Record 2016; 2578(1): 29-37.

Su Y, Cui Y-J, Dupla J-C, et al. Effect of water content on resilient modulus and damping ratio of fine/coarse soil mixtures with varying coarse grain contents. Transp Geotech 2020: 100452.

Tannant D, and Regensburg B. Guidelines for mine haul road design. 2001.

Thom N, and Brown S. The effect of grading and density on the mechanical properties of a crushed dolomitic limestone. In: Australian Road Research Board (ARRB) Conference, 14th, 1988, Canberra; 1988.

Thompson R, Peroni R, and Visser AT. Mining haul roads: Theory and practice: CRC Press; 2019.

Thompson RJ, and Visser AT. Mine haul road maintenance management systems. J S Afr I Min Metall 2003; 103(5): 303-312.

Tremblay G, and Hogan C. Mend manual: Volume 1, summary. Ottawa, Ontario, Canada; 2001.

Tutumluer E, Mishra D, and Butt AA. Characterization of illinois aggregates for subgrade replacement and subbase (0197-9191). 2009.

Tutumluer E, and Pan T. Aggregate morphology affecting strength and permanent deformation behavior of unbound aggregate materials. J Mater Civil Eng 2008; 20(9): 617-627.

Wang H-L, Cui Y-J, Lamas-Lopez F, et al. Effects of inclusion contents on resilient modulus and damping ratio of unsaturated track-bed materials. Can Geotech J 2017; 54(12): 1672-1681.

Wang H-L, Cui Y-J, Lamas-Lopez F, et al. Permanent deformation of track-bed materials at various

inclusion contents under large number of loading cycles. Journal of Geotechnical and Geoenvironmental Engineering 2018*;* 144(8): 04018044.

Werkmeister S, Dawson A, and Wellner F. Pavement design model for unbound granular materials. Journal of Transportation Engineering 2004*;* 130(5): 665-674.

Werkmeister S, Dawson AR, and Wellner F. Permanent deformation behavior of granular materials and the shakedown concept. Transp Res Record 2001*;* 1757(1): 75-81.

Williams DJ, and Walker LK. Laboratory and field strength of mine waste rock. 1983.

Xiao Y, Liu H, Chen Y, et al. Strength and deformation of rockfill material based on large-scale triaxial compression tests. I: Influences of density and pressure. Journal of Geotechnical and Geoenvironmental Engineering 2014*;* 140(12): 04014070.

Xiao Y, and Tutumluer E. Gradation and packing characteristics affecting stability of granular materials: Aggregate imaging-based discrete element modeling approach. International Journal of Geomechanics 2017*;* 17(3): 04016064.

Xiao Y, Tutumluer E, Qian Y, et al. Gradation effects influencing mechanical properties of aggregate base–granular subbase materials in minnesota. Transp Res Record 2012*;* 2267(1): 14-26.

Xu D-s, Liu H-b, Rui R, et al. Cyclic and postcyclic simple shear behavior of binary sand-gravel mixtures with various gravel contents. Soil Dyn Earthq Eng 2019*;* 123: 230-241.

Yang J, and Luo XD. The critical state friction angle of granular materials: Does it depend on grading? Acta Geotechnica 2018*;* 13(3): 535-547.

Zheng H, Liu D, and Li C. Slope stability analysis based on elasto‐plastic finite element method. International Journal for Numerical Methods in Engineering 2005*;* 64(14): 1871-1888.

Zhou F, Fernando E, and Scullion T. Texas Transportation Institute. Development, calibration, and

validation of performance prediction models for the texas me flexible pavement design system. 2010.

CHAPTER 7 MECHANICAL CHARACTERIZATION OF COARSE-GRAINED WASTE ROCKS USING LARGE-SCALE REPEATED LOAD AND MONOTONIC TRIAXIAL TESTS

Abstract: Mining operations produce large quantities of waste rocks, which are usually disposed of in waste rock piles, but can also be valorized in various infrastructures on mine sites. For example, waste rocks are widely used to construct mine haul roads. The engineering performance of these haul roads significantly depends on the mechanical characteristics of the materials used for the construction. However, available experimental studies on coarse-grained waste rocks are relatively limited, mainly because of their large grain size and the scarcity of adapted testing equipment. In this study, a series of repeated load and monotonic triaxial tests (300 mm in diameter and 600 mm in height of specimen) were carried out to evaluate the resilient modulus, permanent deformation, and shear strength of coarse-grained waste rocks (up to 60 mm of maximum particle size) with different gradations. Results showed that an increasing in maximum particle size and compaction effort resulted in growth of resilient modulus and shear strength and decrease of permanent deformation. The optimal gravel-to-sand ratio to maximize resilient modulus and shear strength was around 5. Permanent strain was relatively constant when the gravel-to-sand ratio was between 1 and 5, but it decreased significantly when the ratio increased to 8. The impact of fines content and water content on the mechanical properties of coarse-grained waste rocks was relatively limited. The experimental findings in this study would be beneficial to the construction of haul roads using coarse-grained waste rocks in the field.

Keywords: Waste rocks, Physical properties, Resilient modulus, Permanent deformation, Shear strength, Repeated load triaxial test, Mine haul roads.

7.1 Introduction

Waste rocks, a by-product of mining, are typically produced in large quantities at open pit mines. The particle size distribution of waste rocks from hard rock mines generally varies from clay-size (0.002 m or less) to boulders fractions (1 m and above) (Williams and Walker 1983; James et al. 2013). Waste rocks are usually stored on the surface in piles, close to production sites. However, the management and reclamation of large size waste rock piles can be challenging both during the mine operation and after closure (Aubertin 2013), and an interesting alternative management approach therefore consists in valorizing them in various infrastructures on mine sites (Demers and Pabst, 2020). Waste rocks are for example widely reused for mine haul roads construction because of their low cost, high strength, and availability (Aubertin et al. 2016; Thompson et al. 2019; Hao and Pabst 2021). Waster rocks are generally crushed for the constructions of the surface layer, while the subbase can be built from waste rocks containing particles larger than 100 mm in some cases (Tannant and Regensburg 2001). Valorization of waste rocks in haul roads provides a number of environmental and geotechnical benefits and can, notably reduce the material demand, typically borrowed from the environment (Thompson et al. 2019).

The performance of haul roads significantly depends on the mechanical characteristics of waste rocks such as their shear strength, resilient modulus, and permanent deformation. In general, resilient modulus is used as the input parameter for the mechanistic design of haul roads, and shear strength is used to calculate the factor of safety (Thompson et al. 2019). The permanent deformation behavior of waste rocks is directly related to rutting, one of the most common deteriorations in flexible pavements (Erlingsson 2012). Excess rutting can decrease the driving quality and safety because of hydroplaning and reduced skid resistance of the haul road surface (Rahman and Erlingsson 2015a; Salour and Erlingsson 2017). The mechanical properties of unbound aggregates are affected by several factors such as stress condition, density, gravel-to-sand ratio, fines content,

maximum particle size, water content, and particle shape (Lekarp et al. 2000a, 2000b). Density plays an important effect on the mechanical properties of waste rocks, and the shear strength (Duncan et al. 2014) and resilient modulus (Lekarp et al. 2000a; Yao et al. 2016) generally increases with density (Lekarp et al. 2000a, 2000b). Compaction effort and water content for sample preparation are directly related to the dry density of aggregates. Gradation of waste rocks is another key factor that affects the shear strength (Ionescu 2004), resilient modulus (Duong et al. 2016; Hatipoglu et al. 2020), and permanent deformation (Thom and Brown 1988), and gravel-to-sand ratio and fines content are the critical gradation parameters that links to the mechanical properties of aggregates (Mishra and Tutumluer 2012; Xiao et al. 2012). The effect of these physical properties on the mechanical properties of waste rocks needs to be quantified to optimize the selection of waste rocks for haul roads construction.

However, the relevant research on the mechanical properties of coarse-grained waste rocks from hard rock mine is relatively limited, especially because large-scale testing equipment which is required to characterize materials are also relative scarce. This is particularly the case for the resilient modulus and permanent deformation which measurement typically require using repeated load triaxial tests (EN 13286 2004; AASHTO T307 2017). Repeated load triaxial test is sophisticated, costly, and time-consuming, especially when multi stages are applied in the tests (EN 13286 2004) and even more when large particle sizes must be accommodated.

In this study, a series of repeated load and monotonic triaxial tests were carried out on coarse-grained waste rocks with up to 60 mm maximum particle size. Various samples were prepared and tested to account for the naturally large variability and heterogeneity of waste rocks. The resilient modulus, permanent deformation, and shear strength were compared to evaluate the effect of these basic physical properties.

7.2 Experimental procedure

7.2.1 Large-scale triaxial apparatus

Repeated load and monotonic triaxial tests were carried out on large 600 mm high and 300 mm diameter waste rock samples (Figure 7.1(a) and (b)). The testing apparatus mainly consisted of a load frame (250 kN), a triaxial cell (2000 kPa), a water tank, a load cell (100 kN), a linear strain conversion transducer (LSCT, 100 mm of measurement range, < 0.2% error), a cell pressure controller (2000 kPa, < 5 kPa error), a back pressure controller (2000 kPa), and a control panel (including control valves for water supply system and a pressure indicator). The load cell and LSCT were used to record the axial load and axial deformation, respectively. The cell pressure controller was used to maintain the confining pressure during triaxial tests. In total, 12 tests were carried out; their preparation is described below.

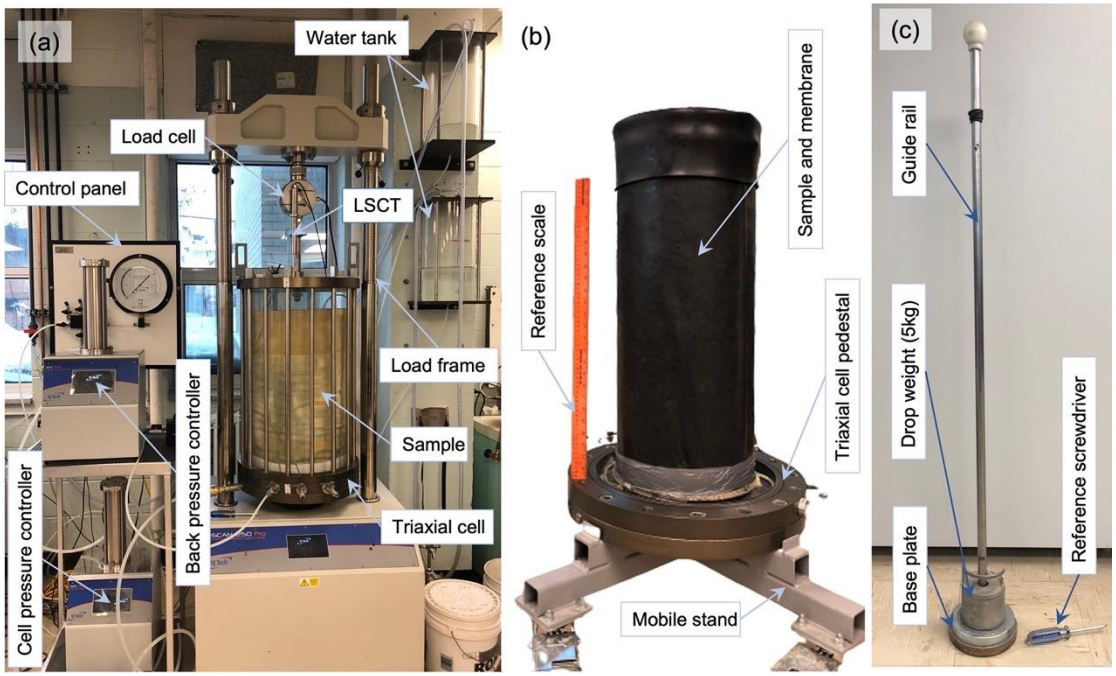

Figure 7.1: Laboratory devices used in this study; (a) large-scale triaxial apparatus; (b) one waste rock sample (300×600 mm); (c) hammer specifically designed for compacting large samples.

7.2.2 Test materials and samples preparation

Tested coarse-grained waste rocks were sampled at Canadian Malartic Mine, an open pit gold mine located in the Abitibi region, in Quebec province, Canada. Generally, the ratio between the diameter of the specimen and the largest particles in a triaxial test should be at least equal to 5 (EN 13286 2004), so the particles larger than 60 mm were removed (sieved). The sieved material was composed of around 80% of gravel (> 4.75 mm), 15% of sand (75 μm-4.75 mm), and 5% of fines (< 75 μm), and was classified as a poorly graded gravel corresponding to the symbol GP (ASTM D2487 2017). A hammer was especially designed for compacting the large waste rock samples in this study. The hammer was made of a 5 kg rammer dropped from a height of 1 m on a base plate with 160 mm diameter, and the compaction effort caused by one below of this hammer was 6.7 times the standard Proctor test hammer (ASTM D698 2012) (Figure 7.1(c)). All the waste rock samples were prepared with five layers of 12 cm, and each layer was compacted using 62 blows of the hammer except the samples for the study of compaction effort effect (see Table 1).

A total of 12 waste rock specimens were prepared with different physical properties, and the objective was to evaluate:

Effect of maximum particle size D_{max}: Three samples were prepared with different maximum particle sizes, i.e., 25, 40, and 60 mm (specimen $D_{max}25$, $D_{max}40$, and $D_{max}60$ in Figure 7.2 and Table 7.1). The initial water content for all the samples preparation was 5%.

Effect of gravel-to-sand ratio GS: Four samples were prepared using different gravel-to-sand ratios, i.e., 1, 3, 5, and 8 (specimen GS1, GS3, GS5, and GS8). The maximum particle size, fines content, and water content was 60 mm, 5%, and 2%, respectively, for all these four samples.

Effect of fines content FC: Three samples were prepared with different fines contents, i.e., 0%, 5%, and 10% (specimen FC0%, FC5%, and FC10%). The maximum particle size, gravel-to-sand ratio, and water content was 60 mm, 5, and 2%, respectively, for all the three samples.

Effect of compaction effort C: Three compaction efforts (C31, C62, and C93) was used to prepare waste rock samples, i.e., 31, 62, and 93 blows on each of the five layers of the samples (specimen C31, C62, and C93). The compaction effort C31, C62, and C93 were correspond to 180, 360, and 540 kJ/m^3, respectively. All the samples had the same maximum particle size (60 mm), gravel-to-sand ratio (5), fines content (5%), and water content (2%).

Effect of water content *w*: Three initial gravimetric water contents, i.e., 1%, 2%, and 4%, were used to prepare waste rock samples (specimen *w*1%, *w*2%, and *w*4%). The final water contents after test for *w*1%, *w*2%, and *w*4% were 0.9%, 1.8%, and 2.3%, respectively. The variation of compaction effort and water content for the sample preparation was directly related to the effect of density on the mechanical properties of waste rocks. The maximum particle size, gravel-to-sand ratio, fines content, and water content was 60 mm, 5, 5%, and 2%, respectively, for all the samples.

The particle size distributions of the samples are summarized in Figure 7.2. The original gradation of waste rocks was with D_{max}60, GS5, and FC5%. D_{max}60, GS5, FC5%, C62, and *w*2% were the same one sample in this study. The physical properties of tested samples are summarized in Table 7.2, including the corresponding grading parameters, compaction effort and water content.

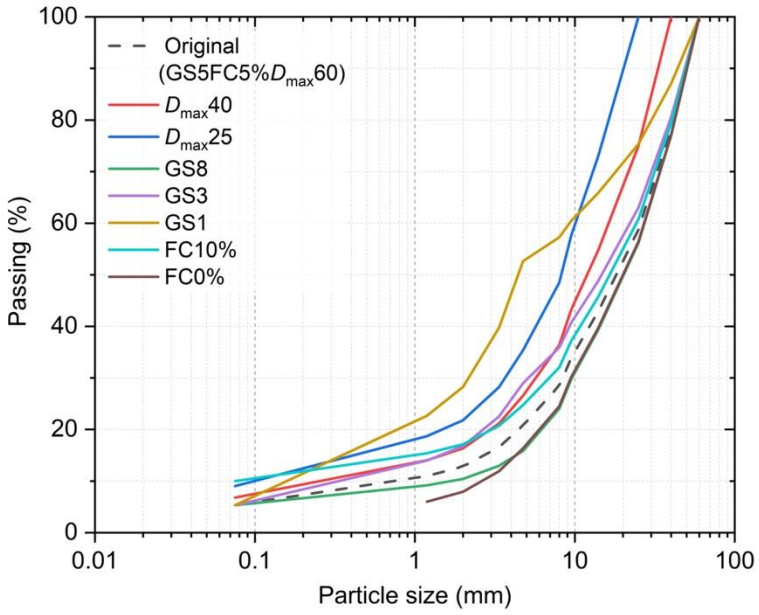

Figure 7.2: Particle size distribution of the different specimens tested (also see Table 7.1 for other specimen properties); D_{max}: maximum particle size, mm; GS: gravel-to-sand ratio, FC: fines content, %. Specimens not presented in this figure had the same particle size distribution curve as the original material.

Table 7.1: Tested waste rock samples with their physical properties including dry density ρ_d (kg/m^3), D_{10} (mm), D_{30} (mm), D_{60} (mm), coefficient of curvature C_C (-), coefficient of uniformity C_U (-), compaction effort C (kJ/m^3), maximum particle size D_{max} (mm), gravel-to-sand ratio GS (-), fines content FC (%), and water content w (%).

Name	ρ_d	D_{10}	D_{30}	D_{60}	C_C	C_U	C	D_{max}	GS	FC	w
	kg/m^3	mm	mm	mm	-	-	kJ/m^3	mm	-	%	%
Effect of maximum particle size D_{max}											
D_{max}25	2115	0.1	3.7	10	13.7	100.0	360	25	2.5	9	2
D_{max}40	1990	0.25	5.7	18	7.2	72.0	360	40	3.7	6.8	2
D_{max}60	2008	0.7	8.5	27	3.8	38.6	360	60	5	5	2
Effect of gravel-to-sand ratio GS											
GS1	2061	0.17	2.2	9	3.2	52.9	360	60	1	5	2

GS3	2037	0.25	5	22	4.5	88.0	360	60	3	5	2
GS5	2008	0.7	8.5	27	3.8	38.6	360	60	5	5	2
GS8	1939	1.8	9.5	28	1.8	15.6	360	60	8	5	2
Effect of fines content FC											
FC0%	1932	2.5	9.5	28	1.3	11.2	360	60	5	0	2
FC5%	2008	0.7	8.5	27	3.8	38.6	360	60	5	5	2
FC10%	2023	0.075	7	25	26.1	333.3	360	60	5	10	2
Effect of compaction effort C											
C31	1876	0.7	8.5	27	3.8	38.6	180	60	5	5	2
C62	2008	0.7	8.5	27	3.8	38.6	360	60	5	5	2
C93	2018	0.7	8.5	27	3.8	38.6	540	60	5	5	2
Effect of water content *w*											
*w*1%	2004	0.7	8.5	27	3.8	38.6	360	60	5	5	1
*w*2%	2008	0.7	8.5	27	3.8	38.6	360	60	5	5	2
*w*4%	2017	0.7	8.5	27	3.8	38.6	360	60	5	5	4

7.2.3 Repeated load and monotonic triaxial tests

Repeated load triaxial tests were carried on the prepared samples to measure resilient modulus and permanent deformation of waste rocks under drained conditions. A total of four successive stress paths were applied with increasing deviator stresses and confining pressures (Table 7.2). The confining pressure varied from 45 to 150 kPa and the deviator stress ranged from 120 to 320 kPa. Each stress path was applied for 3000 cycles with a frequency of 0.025 Hz with no rest period. All tests were performed in a stress-controlled mode using haversine loading pulses. The axial deformation and load were recorded during repeated load triaxial tests, and the resilient modulus (the ratio of deviator stress to recoverable axial strain; (AASHTO T307 2017)) and permanent strain were then calculated for each cycle.

Following the repeated load triaxial test, a consolidated drained (CD) monotonic triaxial test was carried out to evaluate the post-cyclic shear strength of crushed waste rocks specimens (AASHTO

T307 2017; ASTM D7181 2020). The consolidation was conducted by decreasing the confining pressure from 150 kPa (applied during the last sequence of the repeated load triaxial tests) to 50 kPa. The monotonic triaxial test was performed in a strain-controlled mode, and specimens were sheared at a constant axial rate of 0.02 mm/sec. The axial stress-strain curve for each specimen was recorded, and the peak deviator stress for different specimens was compared in this study. The shear test was stopped when the axial strain reached 12%.

Table 7.2: Stress paths applied in repeated load triaxial tests in this study.

Stress path	1	2	3	4
Confining pressure (kPa)	45	70	100	150
Deviator stress (kPa)	120	160	200	320

7.3 **Experimental results and interpretation**

The average resilient modulus of the last 100 cycles of each stress path was calculated as the representative modulus for each stress path. Only permanent strains measured at each 10 cycles from the 1st to 100th cycles, and at each 100 cycles from the 100th to 3000th loading cycles were presented in this paper. The effect of maximum particle size, gravel-to-sand ratio, fines content, compaction effort, and water content on the resilient modulus, permanent deformation, and shear strength of waste rocks were analyzed individually in the following, but some general observations could be made for all the tests carried out in this study. First, the resilient modulus of waste rocks always tended to increase with the stress path (i.e., the stress level), independently of the specimen physical properties (Figure 7.3-7.7). This was explained by the fact that the higher deviator stress and confining pressure contribute to higher compaction and particle interlocking (Leng et al. 2017). Also, the development of permanent strain in waste rocks typically consisted of two phases, which

was particularly noticeable during stress path 1 and 4 in this study (Figure 7.3-7.7). The permanent strain indeed increased rapidly with loading cycles in the initial phases. This phase was characterized as post-compaction, which was accompanied by densification of the material, reduction in pore volume and volumetric change of the material (Werkmeister et al. 2004; El-Basyouny et al. 2005). In the second phase, the deformation rate became more or less constant and was dominated by volume change (Werkmeister et al. 2004). Finally, the stress-strain curve under 50 kPa of confining pressure was similar for all the different samples (Figure 7.3-7.7). The deviator stress indeed increased first rapidly under the initial axial strain (< 1%), but then significantly more slowly. Also, there was no significant decline observed for any specimen as axial strain increased to 12%, and this was likely because the tested waste rocks were relatively loose.

7.3.1 Effect of maximum particle size

The resilient modulus increased gradually with the maximum particle size D_{max} increasing from 25 to 40 and 60 mm (Figure 7.3(a)). For the $D_{max}25$ sample, the resilient modulus was 114, 142, 165, and 221 MPa for stress path 1 (0-3000 cycles), 2 (3000-6000 cycles), 3 (6000-9000 cycles), and 4 (9000-12000 cycles), respectively. When D_{max} increased to 40 mm, the resilient modulus increased by 25 to 45% compared to $D_{max}25$ for each stress path. When D_{max} continued to increase to 60 mm, the resilient modulus also increased but at a slower rate became relatively low (around 5% compared to $D_{max}40$).

Maximum particle size also affected the permanent strain of waste rocks, and the final accumulated permanent strain of the three tested samples after four stress paths (12000 cycles) was between 0.005 and 0.007 (Figure 7.3(b)). During the stress path 1, the value of accumulated permanent strain of $D_{max}25$ was lower than that of $D_{max}40$ and $D_{max}60$, but this difference became relatively small during stress path 2 and 3. The strain curves of $D_{max}25$ and $D_{max}40$ were quite close during stress path 4, and were also higher than for $D_{max}60$, and this difference tended to increase with the

loading cycles. The slope of permanent strain curve for $D_{max}25$ was also steeper than that of $D_{max}40$ and $D_{max}60$, especially during the three first stress paths.

The stress-strain curves for $D_{max}25$ and $D_{max}40$ were very close when the axial strain was lower than 4% (Figure 7.3(c)). The peak deviator stress increased gradually with the maximum particle size D_{max}, and it was around 500, 600, and 700 kPa for $D_{max}25$, $D_{max}40$, and $D_{max}60$, respectively.

In general, the observed effects of maximum particle size on resilient modulus and permanent deformation were consistent with previous studies. For example, previous research also found that resilient modulus tended to increase and permanent deformation to decrease with maximum particle size (Gray 1962; Thom and Brown 1988; Kolisoja 1997). Coarser particles indeed contribute to transmit the major part of the load and the smaller number of particle contacts induces less deformation, which results in higher stiffness (Lekarp et al. 2000a). The higher dry density of $D_{max}25$ (2110 kg/m^3; see Table 7.1) resulted in a lower permanent strain during initial loading cycles, but the rate of permanent strain was higher because the smaller number of coarse particles reduced the sample load resistance, especially for high stress levels. Previous study also found that shear strength tended to increase with the maximum particle size (Bala and Bishnoi 2016). The most probably reason for this observation is that larger maximum particle size such as $D_{max}40$ and $D_{max}60$ could develop a stronger contact force network thus resulting in greater shear strength (Xu, Tang, et al. 2019).

The experimental results indicate that increasing the maximum particle size (25-60 mm) of waste rocks may be beneficial to the mechanical response of mine haul roads. However, the maximum particle size of waste rocks for the haul road construction in the field can be larger than 100 mm (Tannant and Regensburg 2001), which is significantly higher than 60 mm tested in this study.

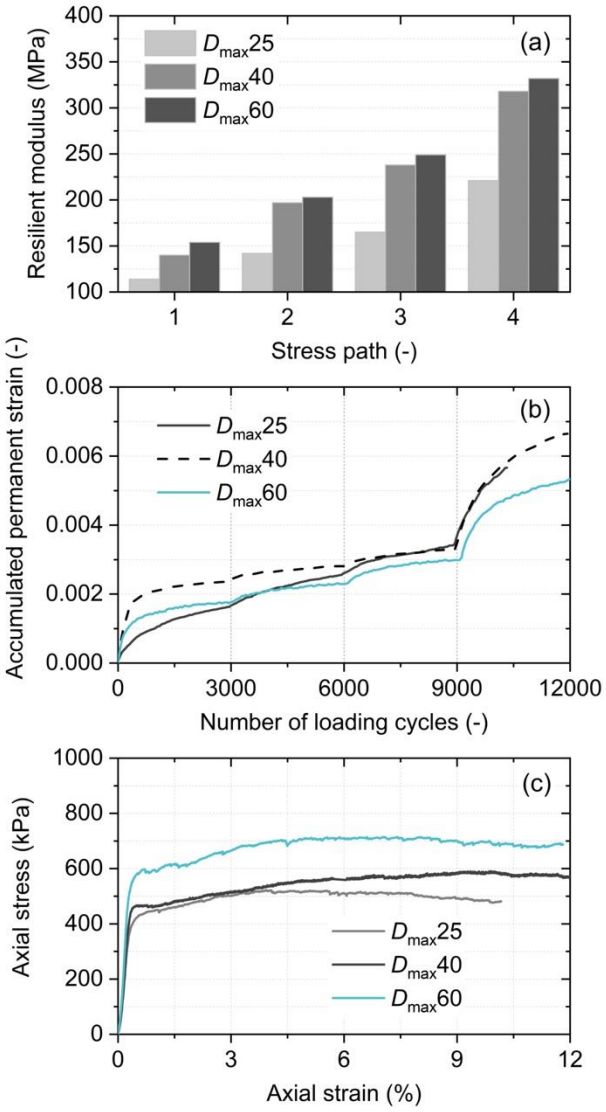

Figure 7.3: Mechanical characterization comparison of waste rocks with different maximum particle size D_{max} 25, 40, and 60 mm; (a) resilient modulus, (b) accumulated permanent strain, and (c) shear strength, i.e., stress-strain curves under 50 kPa of confining pressure.

7.3.2 Effect of gravel-to-sand ratio

The gravel-to-sand ratio GS only slightly affected the resilient modulus of waste rocks in this study (Figure 7.4(a)). For example, the difference of resilient modulus between specimens GS1 (gravel

to sand ratio = 1), GS3 and GS5 was relatively small and usually less than 5% for all stress paths. The resilient modulus of GS8 was around 10% lower than that of the other specimens.

The accumulated permanent strain of waste rocks also decreased for increasing GS, and this effect became more significant as the stress path increased (Figure 7.4(b)). Despite this general trend, the final accumulated permanent strain after four stress paths was relatively similar for all specimens and between 0.004 and 0.006.

The gravel-to-sand ratio effect on waste rocks shear strength was, however, significant, and the peak deviator stress under 50 kPa of confining pressure increased gradually from around 520 to 700 kPa as GS increased from 1 to 5 (Figure 7.4(c)). The trend tended to stabilize for greater gravel to sand ratio and the stress-strain curve for GS8 was slightly lower than that of GS5.

The gravel-to-sand ratio effect on the waste rocks mechanical properties can be attributed to the change induced to the waste rocks fabric (Thom and Brown 1988; Kolisoja 1997). Gravel particles usually enclose a void space that sand particles fill in, while fines fill the void space created by sand particles (Xiao et al. 2012). The amounts of coarse particles (gravel) in waste rocks could develop load-transferring chain that served to transmit the major part of a load, while the fine particles (sand and fines) were able to reinforce the load-carrying network of coarse particles and prevent buckling of the fabric network (Knight 1935). When the GS was greater than 5, the dry density decreased significantly (Table 7.1) indicating that the void space increased since fine particles could not fill the void space sufficiently anymore, which could explain that the resilient modulus for GS8 sample was relatively lower than for GS1, GS3, and GS5. However, the shear strength for GS5 and GS8 was higher than for GS1 and GS3 in this study. The most probably reason for this observation is that the interlocking of large angular particles plays a more important role than the density in the shear process of coarse-grained waste rocks. Although GS8 showed relatively low permanent strain in this study, it is expected that the sample with high GS value may not be very stable under high stress levels (Xiao et al. 2012).

Based on these results, the optimum gravel to sand ratio was therefore estimated around 5. The gravel-to-sand ratio is a practical parameter to modify the material gradation, and the finding in this study therefore can be used to guide the selection of waste rocks for the haul road construction in the field.

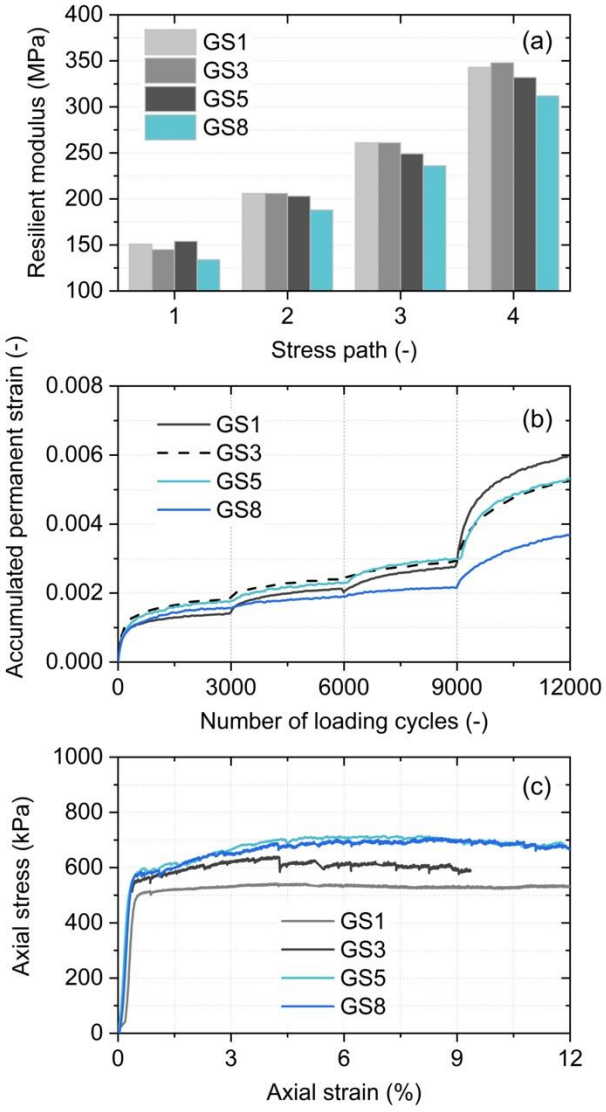

Figure 7.4: Mechanical characterization comparison of waste rocks with different gravel-to-sand ratio GS1 (gravel to sand = 1:1), GS3, GS5, and GS8; (a) resilient modulus, (b) accumulated permanent strain, and (c) shear strength, i.e., stress-strain curves under 50 kPa of confining pressure.

7.3.3 Effect of fines content

The impact of fines content FC on the resilient modulus of waste rocks was generally insignificant (Figure 7.5(a)). The resilient modulus for FC0% and FC10% was close, and around 155, 212, 262, and 350 MPa for stress path 1, 2, 3, and 4, respectively. The resilient modulus was slightly smaller (-15 MPa) for FC = 5% than to other tested fines contents tested, but this difference was not deemed significant.

The variation of FC in the range of 0-10% also had a limited influence on the waste rocks permanent strain (Figure 7.5(b)). The accumulated permanent strain curves for FC0%, FC5% and FC10% were also close, and the final permanent strain after four stress paths (12000 cycles) was around 0.005 in all cases.

The shear strength for FC5% was around 15% greater than that of FC0% and FC10% (Figure 7.5(c)), but the stress-strain curves under 50 kPa confining pressure were all very close, and the peak deviator stress was around 600 to 700 kPa in all cases.

In general, a proper fines content is existed to provide the optimal packing state of aggregates where the optimum mechanical properties can be obtained (Jehring and Bareither 2016). However, the effect of fines content was limited in this study. Similarly, Hicks (1970) also reported that the variation of fines content in the range of 2-10% had a minor influence on resilient modulus. This was probably explained by that the tested fines content was very limited (<10%), and the mechanical behavior of waste rocks was mainly dominated by the coarse-grained particles in this case (Jehring and Bareither 2016).

Waste rocks (at least in hard rock mines) are indeed usually characterized by a small amount of fines which rarely exceed 10% (Gamache-Rochette 2004; Bussière 2007b). The fines content therefore is not a critical parameter regarding to the mechanical properties of waste rocks for the haul road construction. However, in practice, the selection of fines content would also need to consider climate conditions (Tannant and Regensburg 2001; AASHTO M-147 2008; Thompson et

al. 2019). For example, when waste rocks are used for the surface layer of haul roads, fines content should not exceed 10% to prevent muddy and slippery conditions (Thompson et al. 2019). On the other hand, fines content should also be greater than 5% to prevent raveling or loosening of waste rocks in drier climates (Thompson et al. 2019).

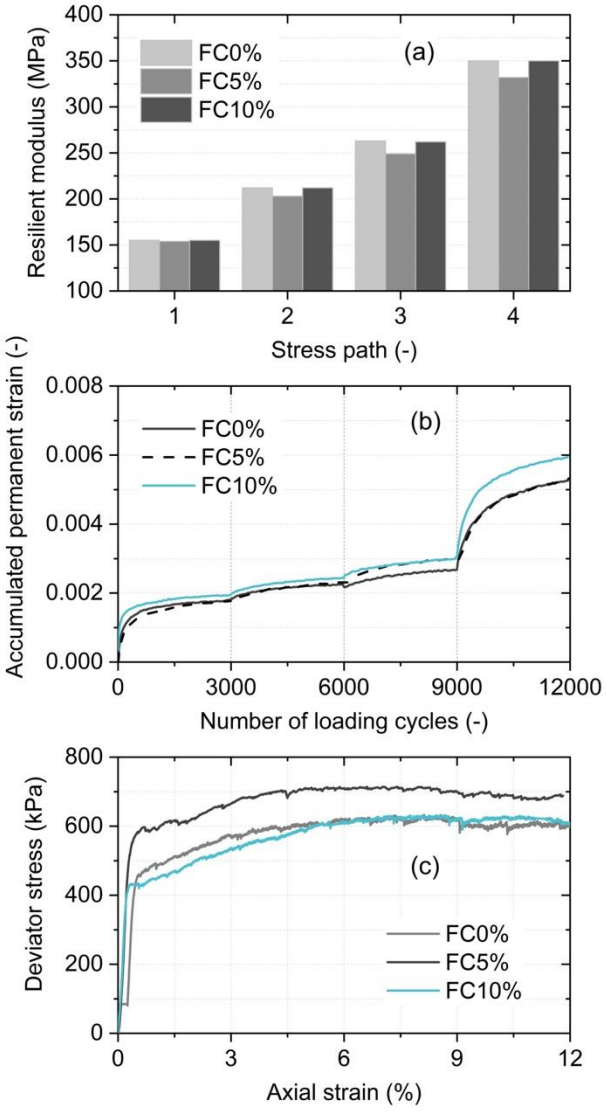

Figure 7.5: Mechanical characterization comparison of waste rocks with different fines content FC 0%, 5%, and 10%; (a) resilient modulus, (b) accumulated permanent strain, and (c) shear strength, i.e., stress-strain curves under 50 kPa of confining pressure.

7.3.4 Effect of compaction effort

The resilient modulus of waste rocks increased with dry density caused by different compaction efforts (Figure 7.6(a)). The resilient modulus for C31 (i.e., 31 blows applied for each layer of a sample, 180 kJ/m^3, 1876 kg/m^3 of dry density) was around 135, 185, 230, and 305 MPa for stress path 1, 2, 3, and 4, respectively. Resilient modulus increased by approximately 20 MPa as compaction effort increased to C62 (360 kJ/m^3, 2008 kg/m^3 of dry density), and an additional 20 MPa for compaction effort C93 (540 kJ/m^3, 2018 kg/m^3 of dry density).

The slope of accumulated permanent strain curve for C31 was significantly steeper than for the other specimens, and the final strain was around 0.0135 after four stress paths (Figure 7.6(b)). When the compaction effort increased to C62 and C93, the permanent strain decreased significantly, especially during stress path 4 (9000-12000 cycles). The strain curves for C62 and C93 were close, and the final strain was around 0.005 (between 2 and 3 times smaller than for C31).

The peak deviator stress under 50 kPa confining pressure for C31 was around 550 kPa (Figure 7.6(c)), but it increased significantly to 700 kPa (+27%) when the compaction effort increased to C62. Additional compaction contributed to increase the peak deviator stress only slightly to a maximum of 750 kPa.

The effect of compaction effect on the mechanical properties of waste rocks can be attributed to the increase of dry density (Table 7.1). The number of particle contacts per particle increases significantly when dry density increases, resulting from additional compaction effort, which in turn decreases the average contact stress corresponding to a certain external load. As a consequence, the deformation in particle contacts decreases and the resilient modulus increases (Kolisoja 1997). The effect of compaction effort became significant as the compaction effort increased from C31 (180 kJ/m^3) to C62 (360 kJ/m^3) because the increase of dry density was important (+7%), while the dry density increased only slightly (< 0.5%) when compaction effort increased from C62 (360 kJ/m^3) to C93 (540 kJ/m^3), and so the effect of compaction effort was also limited in this case.

The experimental results indicate that an increasing of compaction effort would be beneficial to the mechanical response of mine haul roads because of the growth of dry density. However, the effect of excessive compaction effort higher than a certain value (i.e., 360 kJ/m^3 in this study) would be limited for the road performance, but it can increase the cost of road construction. The reasonable compaction effort for the road construction needs further study to reach a balance between road performance and construction cost because the particle size used in the field can be different or larger than the tested materials in this study.

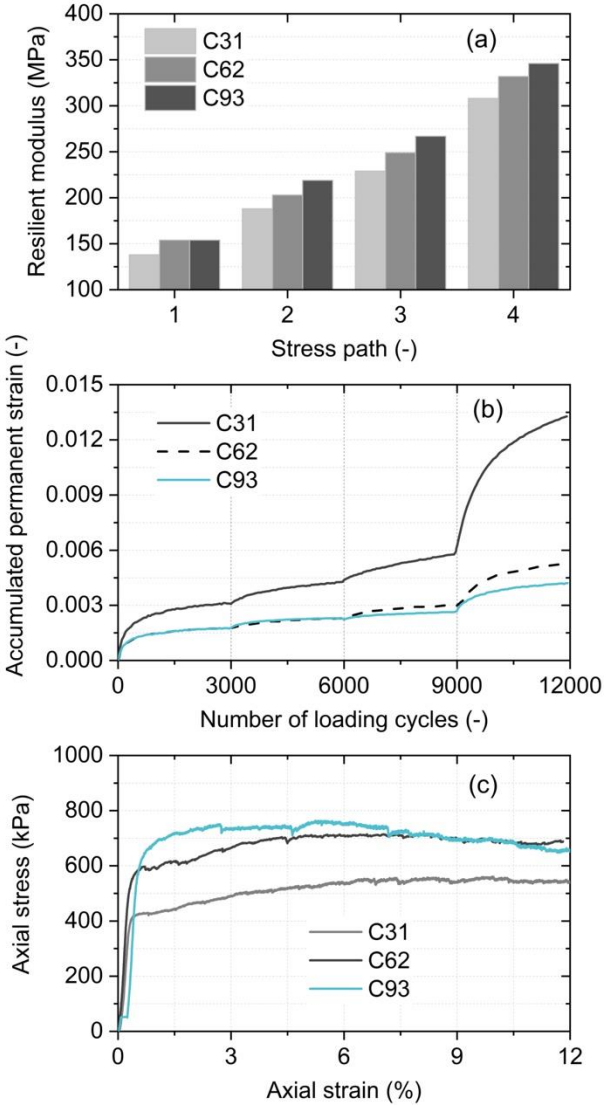

Figure 7.6: Mechanical characterization comparison of waste rocks under different compaction effort C, i.e., 31, 62, and 93 blows applied for each layer of a sample corresponding to 180, 360, and 540 kJ/m^3, respectively; (a) resilient modulus, (b) accumulated permanent strain, and (c) shear strength, i.e., stress-strain curves under 50 kPa of confining pressure.

7.3.5 Effect of water content

The influence of water content *w* on waste rocks resilient modulus was not significant for low stress levels (Figure 7.7(a)). The resilient modulus of specimens *w*1%, *w*2% and *w*4% was close and around 150, 200, and 250 MPa for stress path 1, 2, and 3, respectively. When the stress level increased to stress path 4 (150 kPa of confining pressure and 320 kPa of deviator stress), the resilient modulus of *w*4% increased to around 370 MPa that was around +40 MPa compared to other specimens.

There was no clear trend between the water content and the permanent deformation. The difference of permanent deformation for different water contents was limited in the initial three stress paths but increased slightly in the last stress path (150 kPa of confining pressure and 320 kPa of deviator stress) (Figure 7.7(b)). The final permanent strain was relatively similar around 0.006 for all samples.

The waste rocks with 4% water content showed slightly higher shear strength than specimen with lower water content, and the peak deviator stress was around 800 kPa under 50 kPa confining pressure (Figure 7.7(c)). The peak deviator stress for *w*1% and *w*2% was both around 700 kPa.

The main impact of the water content is the variation of the density of waste rocks which is probably explained by that adding water to the waste rocks enables fine particles to move past one another during the application of the compaction forces (Thompson 2011c). However, the increase of dry density caused by water content (1-4%) was limited in this study (2004-2017 kg/m^3; see

Table 7.1). This could explain the limited influence of water content. The maximum water content achievable in these tests was around 4% of initial water content (2.3% of final water content), and any additional water would leak out during the specimen preparation and cyclic loading. The impact of water content on the mechanical properties of coarse-grained waste rocks was therefore limited in the laboratory and similar behavior is also expected in the field.

The waste rocks, especially used in haul roads, are generally relatively dry and usually at their residual water content, for example, the measured gravimetric water content of waste rocks (< 25 mm) on mine haul roads at the site was between 2% and 4% (Laverdière 2019). The water contents used in this study therefore covered typical ranges observed in the field. The experimental results indicate that water content of coarse-grained waste rocks would not be a critical factor influencing the mechanical performance of haul roads, but it is directly related to the dust issues in the field, which would affect the trafficability and environment (Thompson et al. 2019).

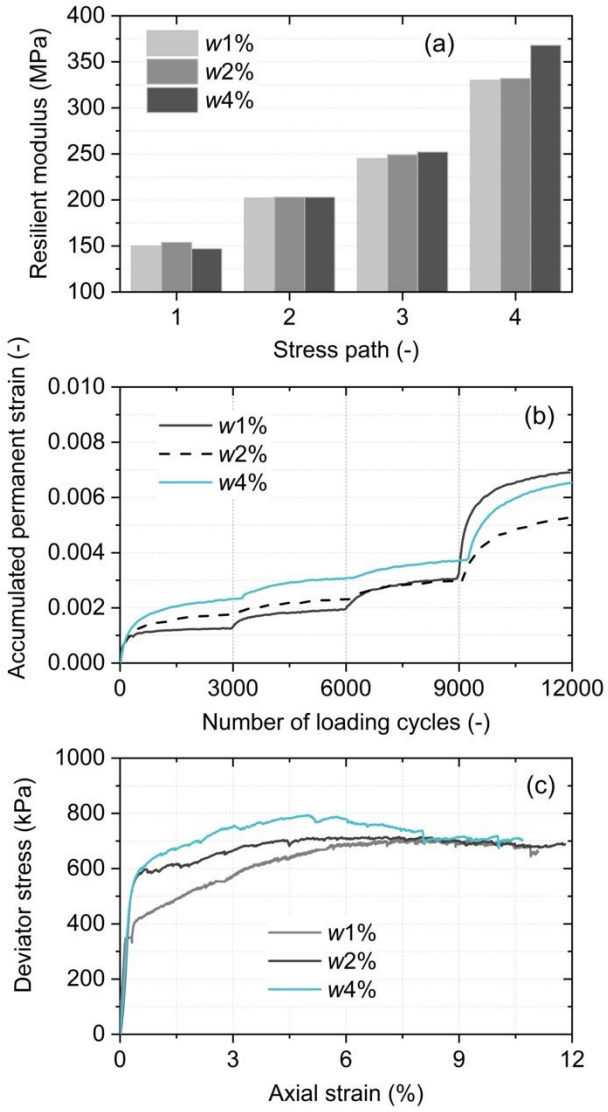

Figure 7.7: Mechanical characterization comparison of waste rocks samples prepared using different water content *w*, 1%, 2%, and 4%; (a) resilient modulus, (b) accumulated permanent strain, and (c) shear strength, i.e., stress-strain curves under 50 kPa of confining pressure.

For coarse-grained waste rocks (D_{max}60 mm), the optimum gravel-to-sand ratio is around 5 that is higher than that for crushed waste rocks (D_{max}19 mm; optimum ratio is around 3) measured in the previous study. The large angular particles can develop a strong and stable soil fabric and these particles would dominate the mechanical behavior of waste rocks, which also results in a high

porosity in this case. The effect of fines content and water content in coarse-grained waste rocks is therefore insignificant compared to crushed waste rocks. Also, the shear strength behavior for coarse-grained and crushed waste rocks is significantly different, i.e., there is no significant reduction occurred in shear strength with axial strain for coarse-grained waste rocks while an apparent peak deviator stress is observed during sample shearing for crushed waste rocks. It indicates that coarser waste rocks have higher resistance to shear stress.

Coarse-grained waste rocks are generally used for the base and subbase layers of haul roads, and these layers play the most important role in bearing the traffic loading of mining trucks while crushed waste rocks are generally used for the surface layer to provide safe ride (Tannant and Regensburg 2001; Thompson et al. 2019). Considering the difference of mechanical properties between coarse-grained and crushed waste rocks, waste rocks with relatively larger particles and higher content of gravel are recommended for the construction of base and subbase layers to carry heavy mining trucks in the field. However, the maximum particle size should be smaller than the 2/3 of the layer thickness (Tannant and Regensburg 2001).

7.4 **Discussion and final remarks**

The mechanical characterization of coarse-grained waste rocks from Canadian Malartic Mine was evaluated using a series of repeated load and monotonic triaxial tests. The influence of maximum particle size D_{max} (25, 40, and 60 mm), gravel-to-sand ratio GS (1, 3, 5, and 8), fines content FC (0%, 5%, and 10%), compaction effort C (180 kJ/m^3, 360 kJ/m^3, and 540 kJ/m^3), and water content w (1%, 2%, and 4%) on mechanical properties including resilient modulus, permanent deformation, and shear strength was quantified in this study. The experimental effects of D_{max}, GS, FC, C, and w on the mechanical properties are summarized in Figure 7.8.

Mechanical properties	D_{max}	GS	FC	C	w
Resilient modulus	↑	↓	=	↑	=
Shear strength	↑	↑	=	↑	=
Permanent deformation	↓	↓	=	↓	=

Figure 7.8: The measured effect of maximum particle size D_{max}, gravel-to-sand ratio GS, fines content FC, compaction effort C, and water content w on the mechanical properties of waste rocks including resilient modulus, shear strength, and permanent deformation; the symbol ↑ means the mechanical property increases with the physical property; the symbol ↓ means the mechanical property decreases with the physical property; and the symbol = means the effect of the physical property is insignificant.

The maximum particle size of waste rocks was 60 mm, but it was still much smaller than the large particles (up to 1 mm) in the field (Williams and Walker 1983; James et al. 2013). The ratio of specimen diameter to maximum particle size should be higher than 5 for repeated load triaxial test (EN 13286 2004; AASHTO T307 2017), and it generally should be higher than 6 for monotonic test (ASTM D6528 2017; Deiminiat et al. 2020). When the maximum particle size is very large, performing such tests in laboratory with field material size becomes difficult or impossible. The scaling-down techniques, including scalping, parallel, replacement, and quadratic, are often used to obtain a modeled sample excluding oversize particles (Deiminiat et al. 2020). However, it is unclear which of the four scaling-down techniques yields the most representative mechanical properties of waste rocks from hard rock mines.

Also, only four stress paths and 3000 cycles per stress path were applied for the repeated load triaxial tests in this study since the large-scale triaxial apparatus was only able to run at a low

loading frequency (0.025 Hz). In contrast, AASHTO standard T307 (AASHTO T307 2017) suggests to apply 15 stress paths to evaluate the resilient behavior of soils, and European standard EN 13286 (EN 13286 2004) recommend that at least 10000 loading cycles are applied for each stress path to evaluate the long-term permanent deformation of unbound mixtures. To better evaluate the resilient and permanent behavior of coarse-grained waste rocks and confirm the trends observed in this study, more stress paths and loading cycles should be applied in repeated load triaxial tests by using more advanced triaxial apparatus.

Post-cyclic monotonic triaxial tests were conducted to assess the shear strength of waste rocks in this study since the sample preparation of coarse-grained waste rocks is time-consuming and technologically sophisticated. The cyclic loading causes additional compaction on the waste rock samples, which could result in a higher shear strength. This difference in experimental procedure makes the comparison between test results in published literature difficult (Indraratna et al. 1998; Bray et al. 2009; Seif El Dine et al. 2010). Also, only one monotonic triaxial test was carried out on a specific sample to estimate the stress-strain curve of waste rocks under 50 kPa of confining pressure, and the friction angle of waste rocks could therefore not be determined accurately. Therefore, more monotonic triaxial tests should be carried out on coarse-grained waste rocks to study their shear behavior under different stress states.

7.5 **Conclusions**

In this study, the mechanical characterization of coarse-grained waste rocks from Canadian Malartic Mine was investigated by using large-scale repeated load and monotonic triaxial tests. The effects of maximum particle size, gravel-to-sand ratio, fines content, compaction effort, and water content on mechanical properties of waste rocks were analyzed. Based on the results of this

study the following statements can be made:

1. An increasing in maximum particle size (25-60 mm) resulted in growth of resilient modulus and shear strength and decrease of permanent deformation. The optimal gravel-to-sand ratio regarding to the resilient modulus and shear strength was around 5. Permanent strain was close when the gravel-to-sand ratio ranged between 1 and 5, but it decreased significantly when the ratio increased to 8.

2. The effect of compaction effort on the mechanical properties of coarse-grained waste rocks was significant. An increasing of compaction effort from 180 to 360 kJ/m^3 resulted in significant increase of resilient modulus and shear strength and decrease of permanent deformation because of the increase of dry density. However, the impact of more compaction effort (540 kJ/m^3) on the density and mechanical properties was limited.

3. The influence of fines content (0-10%) and water content (final value 0.9-2.3%) on the resilient modulus, shear strength, and permanent deformation of coarse-grained waste rocks was insignificant because the variation of these factors was relatively small, and the change of dry density caused by these factors was limited.

The mechanical behavior of coarse-grained waste rocks with 60 mm of maximum particle size was different to crushed waste rocks with 19 mm of maximum particle size. The experimental results in this study would be helpful for the construction of base/subbase layers using coarse-grained waste rocks in the field.

7.6 References

AASHTO M-147. (2008). Standard specification for materials for aggregate and soil-aggregate subbase, base, and surface courses. Washington, DC.

AASHTO T307-99. (2017). Standard method of test for determining the resilient modulus of soils and aggregate materials. Washington, DC.

ASTM D698-12e2. (2012). Standard test methods for laboratory compaction characteristics of soil using standard effort (12,400 ft-lbf/ft^3 (600 kN-m/m^3)). ASTM International, West Conshohocken, PA.

ASTM D2487-17e1. (2017). Standard practice for classification of soils for engineering purposes (unified soil classification system). ASTM International, West Conshohocken, PA.

ASTM D6528-17. (2017). Standard test method for consolidated undrained direct simple shear testing of fine grain soils. ASTM International, West Conshohocken, PA.

ASTM D7181-20. (2020). Standard test method for consolidated drained triaxial compression test for soils. ASTM International, West Conshohocken, PA.

Aubertin, M. (2013). *Waste rock disposal to improve the geotechnical and geochemical stability of piles.* Paper presented at the Proceedings of the world mining congress, Montreal, Canada.

Aubertin, M., Bussière, B., Pabst, T., James, M., and Mbonimpa, M. (2016). Review of the reclamation techniques for acid-generating mine wastes upon closure of disposal sites. In *Geo-chicago 2016* (pp. 343-358).

Bala, R., and Bishnoi, M. (2016). Shear strength characteristics of crushed limestone sandstone and gravel. *International Journal of Technical Research, 5*(3), 5-9.

Bray, J. D., Zekkos, D., Kavazanjian Jr, E., Athanasopoulos, G. A., and Riemer, M. F. (2009). Shear strength of municipal solid waste. *Journal of Geotechnical and Geoenvironmental Engineering, 135*(6), 709-722.

Bussière, B. (2007). Hydro-geotechnical properties of hard rock tailings from metal mines and subsoil characteristics and hydrogeology…… emerging geo-environmental disposal approaches. *Canadian Geotechnical Journal, 44*(9), 1019-1052.

Deiminiat, A., Li, L., Zeng, F., Pabst, T., Chiasson, P., and Chapuis, R. (2020). Determination of the shear strength of rockfill from small-scale laboratory shear tests: A critical review. *Advances in Civil Engineering, 2020*, 8890237.

Duncan, J. M., Wright, S. G., and Brandon, T. L. (2014). *Soil strength and slope stability*: John Wiley & Sons.

Duong, T. V., Cui, Y.-J., Tang, A. M., Dupla, J.-C., Canou, J., Calon, N., et al. (2016). Effects of water and fines contents on the resilient modulus of the interlayer soil of railway substructure. *Acta Geotechnica, 11*(1), 51-59.

El-Basyouny, M., Witczak, M., and Kaloush, K. (2005). *Development of the permanent deformation models for the 2002 design guide.* Paper presented at the 84th Annual Meeting of the Transportation Research Board, Available in TRB 2005 Annual Meeting CD-ROM.

EN 13286-7. (2004). Unbound and hydraulically bound mixtures–cyclic load triaxial test for unbound mixtures. British Standard Institute.

Erlingsson, S. (2012). Rutting development in a flexible pavement structure. *Road Materials and Pavement Design, 13*(2), 218-234.

Gamache-Rochette, A. (2004). *Une étude de caractérisation en laboratoire et sur le terrain des écoulements de l'eau dans les roches stériles*: École polytechnique.

Gray, J. (1962). Characteristics of graded base course aggregates determined by triaxial tests.

Hao, S., and Pabst, T. (2021). Estimation of resilient behavior of crushed waste rocks using repeated load cbr tests. *Transportation Geotechnics*, 100525.

Hatipoglu, M., Cetin, B., and Aydilek, A. H. (2020). Effects of fines content on hydraulic and mechanical performance of unbound granular base aggregates. *Journal of Transportation Engineering, Part B: Pavements, 146*(1), 04019036.

Hicks, R. (1970). *Factors in fluencing the resilient properties of granular materials.* Thesis submitted to the University of California.

Indraratna, B., Ionescu, D., and Christie, H. (1998). Shear behavior of railway ballast based on large-scale triaxial tests. *Journal of Geotechnical and Geoenvironmental Engineering, 124*(5), 439-449.

Ionescu, D. (2004). Evaluation of the engineering behaviour of railway ballast. University of Wollongong.

James, M., Aubertin, M., and Bussière, B. (2013). *On the use of waste rock inclusions to improve the performance of tailings impoundments.* Paper presented at the Proceedings of the 18th International Conference Soil Mechanics and Geotechnical Engineering, Paris, France.

Jehring, M. M., and Bareither, C. A. (2016). Tailings composition effects on shear strength behavior of co-mixed mine waste rock and tailings. *Acta Geotechnica, 11*(5), 1147-1166.

Knight, J. (1935). Gradation of aggregate as applied to stabilization of gravel roads. *Canadian Engineer, 69*(23), 9-10.

Kolisoja, P. (1997). *Resilient deformation characteristics of granular materials*: Tampere University of Technology Finland, Publications.

Laverdière, A. (2019). *Effet de la granulométrie sur le comportement géotechnique de roches stériles concassées utilisées comme surface de roulement sur des routes minières.* École Polytechnique de Montréal.

Lekarp, F., Isacsson, U., and Dawson, A. (2000a). State of the art. I: Resilient response of unbound aggregates. *Journal of Transportation Engineering, 126*(1), 66-75.

Lekarp, F., Isacsson, U., and Dawson, A. (2000b). State of the art. Ii: Permanent strain response of unbound aggregates. *Journal of Transportation Engineering, 126*(1), 76-83.

Leng, W., Xiao, Y., Nie, R., Zhou, W., and Liu, W. (2017). Investigating strength and deformation characteristics of heavy-haul railway embankment materials using large-scale undrained cyclic triaxial tests. *International Journal of Geomechanics, 17*(9), 04017074.

Mishra, D., and Tutumluer, E. (2012). Aggregate physical properties affecting modulus and deformation characteristics of unsurfaced pavements. *Journal of Materials in Civil Engineering, 24*(9), 1144-1152.

Rahman, M. S., and Erlingsson, S. (2015). A model for predicting permanent deformation of unbound granular materials. *Road Materials and Pavement Design, 16*(3), 653-673.

Salour, F., and Erlingsson, S. (2017). Permanent deformation characteristics of silty sand subgrades from multistage rlt tests. *International Journal of Pavement Engineering, 18*(3), 236-246.

Seif El Dine, B., Dupla, J. C., Frank, R., Canou, J., and Kazan, Y. (2010). Mechanical characterization of matrix coarse-grained soils with a large-sized triaxial device. *Canadian Geotechnical Journal, 47*(4), 425-438.

Tannant, D., and Regensburg, B. (2001). *Guidelines for mine haul road design*.

Thom, N., and Brown, S. (1988). *The effect of grading and density on the mechanical properties of a crushed dolomitic limestone.* Paper presented at the Australian Road Research Board (ARRB) Conference, 14th, 1988, Canberra.

Thompson, R., Peroni, R., and Visser, A. T. (2019). *Mining haul roads: Theory and practice*: CRC Press.

Thompson, R. J. (2011). Mine haul road design, construction and maintenance management. *Mining Roads, 136*.

Werkmeister, S., Dawson, A., and Wellner, F. (2004). Pavement design model for unbound granular materials. *Journal of Transportation Engineering, 130*(5), 665-674.

Williams, D. J., and Walker, L. K. (1983). Laboratory and field strength of mine waste rock. Transactions of the Institution of Engineers, Australia. Civil Engin, 27, 299-304.

Xiao, Y., Tutumluer, E., Qian, Y., and Siekmeier, J. A. (2012). Gradation effects influencing mechanical properties of aggregate base–granular subbase materials in minnesota. *Transportation Research Record, 2267*(1), 14-26.

Xu, D.-S., Tang, J.-Y., Zou, Y., Rui, R., and Liu, H.-B. (2019). Macro and micro investigation of gravel content on simple shear behavior of sand-gravel mixture. *Construction and Building Materials, 221*, 730-744.

Yao, H., Jia, S., Gan, W., Zhang, Z., and Lu, K. (2016). Properties of crushed red-bed soft rock mixtures used in subgrade. *Advances in Materials Science and Engineering, 2016*.

CHAPTER 8 ARTICLE 4: EFFECT OF FREEZE-THAW AND WETTING-DRYING CYCLES ON THE CBR, SHEAR STRENGTH, STIFFNESS, AND PERMANENT DEFORMATION OF CRUSHED WASTE ROCKS

Shengpeng Hao and Thomas Pabst

This article was submitted to *Cold Regions Science and Technology* in October 2021.

Abstract: Waste rocks produced from mining operations are widely reused for the construction of mine haul roads. However, seasonal changes expose mining facilities to repeated freeze-thaw and wetting-drying cycles which can significantly affect the geotechnical characteristics of the materials in situ. A better management and valorization of waste rocks therefore require a more detailed understanding of the geotechnical properties of waste rocks subjected to freeze-thaw and wetting-drying cycles. In this study, cyclic and monotonic triaxial and CBR tests were carried out to measure the stiffness, shear strength, CBR, and permanent deformation of crushed waste rocks subjected to freeze-thaw and wetting-drying cycles. Samples were prepared to simulate field conditions and were subjected to 16 freeze-thaw cycles and 15 wetting-drying cycles. Results showed that freeze-thaw cycles resulted in a reduction of the resilient modulus and shear strength, and an increase of the permanent deformation. A greater water content during freeze-thaw cycles also resulted in a significant increase of the permanent deformation. Results also showed that wetting-drying cycles could contribute to increase the stiffness, CBR, and permanent deformation of crushed waste rocks. Results were then used to develop predictive models based on MEPDG model and Rahman and Erlingsson model to estimate the effect of freeze-thaw cycles on resilient modulus and permanent deformation.

Keywords: Mine haul roads, Crushed waste rocks, Freeze-thaw cycles, Wetting-drying cycles,

Stiffness, Shear strength, CBR, Permanent deformation.

8.1 Introduction

Mine haul road network is a critical and vital component of the mining production process at open pit mines. Mine haul roads are generally constructed using local waste rocks available on site (Thompson et al. 2019), and their performance depends significantly on the geotechnical properties of waste rocks such as stiffness, California Bearing Ratio (CBR), shear strength, and permanent deformation (Tannant and Regensburg 2001; Thompson et al. 2019). The resilient modulus and permanent deformation characteristics of unbound aggregates under traffic loading are, for example, important factors for road design, because they are strongly related to the rutting, cracking and other road diseases (Erlingsson 2012; Thompson et al. 2019). CBR, meanwhile, is widely used to design mine haul roads in practice since this index is relatively easy and quick to measure (Tannant and Regensburg 2001; Thompson et al. 2019).

Durability of soils induced by the change of climatic conditions should be assessed because of their major factor influence on the performance of earthwork projects (Maalouf et al. 2012). Climatic factors to be considered are primarily temperature and moisture changes, especially for pavement design (AASHTO 1993; Mechanistic-Empirical Design Guide (MEPDG; (NCHRP 2004)). Pavements in cold regions are exposed to at least one freeze-thaw cycle every year (Kalkan 2009), and wetting-drying cycles may result from rainfall, snow- and ice-melt, and variations of water table position on site. According to several guides and research studies (Gullà et al. 2006; Bilodeau et al. 2011; Razouki and Salem 2015; Zou et al. 2020), freeze-thaw and wetting-drying cycles may result in significant decrease of shear strength (Gullà et al. 2006; Solanki and Zaman 2014) and stiffness (Liu et al. 2018; Lin et al. 2019), and increase of permanent deformation (Bilodeau et al.

2011). The degradation of geotechnical properties caused by freeze-thaw and wetting-drying cycles could then result in the deterioration of pavements, for example, the decrease of fatigue life of pavement may reach up to 80% caused by freeze-thaw and wetting-drying cycles (Ishikawa et al. 2019). Freeze-thaw cycles generally result in decrease of shear strength (Aldaood et al. 2016; Lu et al. 2019) and resilient modulus (Bozyurt et al. 2013), depending on climatic factors and material properties such as the availability of water (Aldaood et al. 2016), cooling rate (Broms and Yao 1964), particle size distribution (Miao et al. 2016), and fines content (Liu et al. 2016). The effect of freeze-thaw cycles on resilient modulus is more significant when larger percentage of fine particles are in aggregates (Simonsen et al. 2002). Dense materials tend to dilate under freeze-thaw cycles, while loose materials are densified under freeze-thaw cycles and may show an increase in resilient modulus (Liu et al. 2018). Permanent deformation generally increases gradually with the number of freeze-thaw cycles, and the first several cycles have the greatest impact (Li et al. 2013; Lu et al. 2019). A high water content in unbound granular materials subjected to freeze-thaw cycles can cause significant increase of permanent deformation (Bilodeau et al. 2011). The frost expansion of pore water can also lead to a redistribution of particles and porosity, therefore altering the mechanical properties of the material (Aldaood et al. 2016; Ishikawa et al. 2019; Lu et al. 2019). Wetting-drying cycles also can result in the decrease of the mechanical properties of soils, and this effect depends on the material minerology (Aldaood et al. 2014; Chittoori et al. 2018). A high content of gypsum in soil subjected to wetting-drying cycles can lead to pronounced reduction of mechanical strength (Aldaood et al. 2014). The resilient modulus of aggregates generally decreases as wetting-drying cycles increases, but conversely, the stiffness of some materials (e.g., sandstone-type aggregate with CKD stabilizing agents) may increase with wetting-drying cycles (Khoury et al. 2005; Khoury and Zaman 2007).

Although many research studies investigated the effect of freeze-thaw and wetting-drying cycles on geotechnical characteristics, they focused mainly on fine-grained soils both regarding freeze-thaw cycles (Othman and Benson 1993; Meiers et al. 2011; Tian et al. 2020; Kim et al. 2021), and

wetting-drying cycles (Khoury and Zaman 2007; Aldaood et al. 2014; ASTM D559/D559M 2015; Chittoori et al. 2018). Moreover, most of available research focused on the effect of freeze-thaw and wetting-drying cycles for civil engineering applications, such as for the construction of highways (Edil and Cetin 2018; Ishikawa et al. 2019). Studies for mine haul roads remain, however, relatively limited. One of the possible reasons is that the service life of haul roads are usually short, for example, their service life is generally 5-10 years which is significantly lower than highways (Tannant and Regensburg 2001). However, climate change and the increase of both the frequency and amplitude of extreme events (Dehn et al. 2000; Geertsema et al. 2006; Shou and Lin 2020), will expose mine haul roads to more frequent freeze-thaw and wetting-drying cycles (Hotton et al. 2020), even over short periods of time several freeze-thaw cycles could experience. A special consideration should therefore be paid to the degradation of waste rocks geotechnical properties including stiffness, CBR, shear strength, and permanent deformation caused by freeze-thaw and wetting-drying cycles.

In this study, a series of triaxial tests (both repeated load and monotonic tests) and CBR tests (both repeated load and standard tests) were carried out to evaluate the effect of freeze-thaw and wetting-drying cycles on the geotechnical characteristics of crushed waste rocks (i.e., stiffness, shear strength, CBR, and permanent deformation). The objective was also to develop models to describe and predict the degradation of crushed waste rocks properties depending on the number of freeze-thaw cycles.

8.2 Experimental program

8.2.1 Materials

Tested crushed waste rocks were obtained from Canadian Malartic Mine (48.11°N, 78.13°W), an

open pit gold mine in Abitibi region, Quebec, Canada. The nearest meteorological station, VAL-D'OR A (48.10°N, 77.80°W), indicates that the mean annual temperature in 2005 was 2.8 ℃, the total annual precipitation 719.0 mm, and the frost period around 5 months (from November to March) (data from Environment Canada). Crushed waste rocks were used for the construction of the entire mine haul road network on the site. The minerology of this material was mainly quartz (23-28%), albite (34-43%), muscovite (10-12%), and chlorite (6-8%) (Hao and Pabst 2021). The particles larger than 19 mm (around 5% by weight) were removed by sieving before the laboratory tests because of the limitation of the experimental setups (150 mm in diameter for triaxial tests, and 152 mm in diameter for CBR tests). The tested material contained around 4% of fines (< 0.075 mm), and the coefficient of uniformity C_U and the coefficient of curvature C_C were 27.6 and 4.4, respectively (Figure 8.1(a)). The crushed waste rocks were classified as a poorly graded gravel (GP) according to the Unified Soil Classification System (ASTM D2487 2017). The optimum water content was 5.6% corresponding to a maximum dry density $\rho_d = 2334$ kg/m^3 (ASTM D1557 2012) (Figure 8.1(b)).

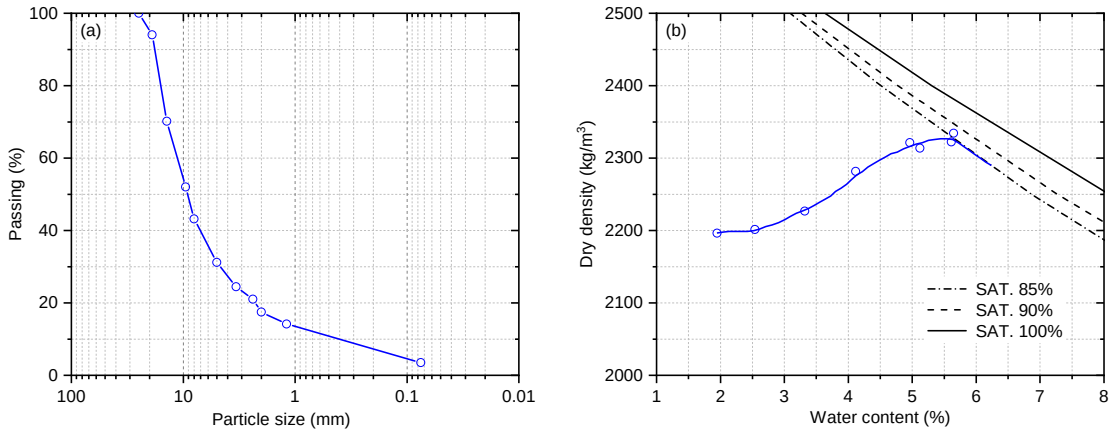

Figure 8.1: (a) Particle size distribution curve of tested crushed waste rocks, and (b) Proctor compaction test results using modified effort (w_{opt} = 5.6%).

8.2.2 Specimen preparation for triaxial tests

Eight specimens (Table 8.1) were prepared to study the effect of freeze-thaw cycles on the resilient modulus and permanent deformation using repeated load triaxial tests (EN 13286 2004; AASHTO M-147 2008), and on shear strength using consolidated drained (CD) monotonic triaxial tests (ASTM D7181 2020) (see below for test details). All the specimens (150 mm in diameter and 300 mm in height) were compacted in ten layers using modified effort 2700 kN-m/m^3 (ASTM D1557 2012) and 56 blows per layer. Six specimens (FT1 to FT6; Table 1) were prepared with an initial gravimetric water content w_0 = 4%, and were subjected to either 0, 2, 4, 7, 10, or 16 freeze-thaw cycles. An additional specimen (FT7) was prepared using an initial gravimetric water content w_0 = 2% and was subjected to 10 freeze-thaw cycles. Another specimen (FT8) was prepared using an initial gravimetric water content w_0 = 2%, and additional water was then added to reach a final water content of 5%. The specimen was then subjected to 10 freeze-thaw cycles.

One freeze-thaw cycle consisted in placing the specimen in an automatic temperature-controlled freezer with a constant temperature of -20 ℃ for 24 hours, and then moving it to a room with a temperature of 20 ℃ for 24 hours. A temperature of -20 ℃ is the common setting for freeze-thaw cycles in the literature (Tian et al. 2019; Zou et al. 2020) and was also considered representative of field conditions in Canada.

The preparation process of triaxial testing specimen consisted of six steps: (1) compaction of the specimen using modified effort hammer and steel mold (150 mm in diameter and 300 mm in height); (2) dismantling the mold and extracting the specimen; (3) enclosing the specimen into two latex membranes (0.304 mm and 0.635 mm thickness); (4) fixing the specimen using PVC mold to constraint the lateral deformation, and placing the top cap and plastic wrap on the surface of the specimen to prevent disturbance and moisture loss during freeze-thaw cycles; (5) subjecting the specimen to freeze-thaw cycles; and (6) placing the specimen after freeze-thaw cycles on the pedestal of the triaxial cell to conduct the repeated load and monotonic triaxial test.

The physical properties of the specimens subjected to triaxial tests in this study are summarized in Table 8.1. The dry density of triaxial testing specimens ranged from 2215 kg/m^3 to 2230 kg/m^3, which was deemed similar for all tests. The final water content of specimens with 4% of initial water content decreased from to 2.5% to 3.3% during the first 10 freeze-thaw cycles, and then remained constant during the subsequent cycles (Table 8.1).

Table 8.1: Physical properties of the specimens used for triaxial tests; w_0: initial gravimetric water content, w_f: final gravimetric water content after freeze-thaw (FT) cycles.

Name	No. of freeze-thaw cycles	w_0 (%)	w_f (%)	Dry density (kg/m^3)
FT1	0	4	3.3	2217
FT2	2	4	3.0	2220
FT3	4	4	2.7	2225
FT4	7	4	2.6	2226
FT5	10	4	2.5	2230
FT6	16	4	2.5	2226
FT7	10	2	1.9	2226
FT8	10	5	3.5	2223

8.2.3 Specimen preparation for CBR tests

A total of eight specimens (152.4 mm in diameter and 127 mm in height; Table 2) were prepared to evaluate the effect of wetting-drying cycles on equivalent modulus and permanent deformation using repeated load CBR tests (Molenaar 2008; Araya et al. 2012; Hao and Pabst 2021), and on CBR value using standard CBR tests (ASTM D1883 2016) (see details below). All the specimens were prepared with an initial gravimetric water content w_0 = 4%, and using modified compaction effort according to ASTM D1883 standard (ASTM D1883 2016). Four of the specimens (WD1 to WD4; Table 8.2) were subjected to 0, 5, 10, and 15 wetting-drying cycles, respectively, before repeated load CBR tests were conducted to measure equivalent modulus and permanent

deformation (Molenaar 2008; Araya et al. 2012; Hao and Pabst 2021). Another four specimens (WD5 to WD8) were also subjected to 0, 5, 10, and 15 wetting-drying cycles, but then submitted to standard CBR tests to measure the CBR value (ASTM D1883 2016). One wetting-drying cycle consisted first of immerging the specimen in water (allowing the free access of water to the top and bottom) at room temperature (20 °C) for 72 hours; after that, the specimen was dried at room temperature using a fan for 72 hours. The specimens were all subjected to the same surcharge load of 4.54 kg during wetting-drying cycles. The swelling of specimens during wetting-drying cycles was monitored. However, in this study, no notable swelling was observed during wetting-drying cycles, and there was no significant change observed on the specimen surface because of wetting-drying cycles. However, it was observed that, during sample dismantling, the coarse-grained particles in the specimen (14-19 mm) tended to be bonded together after drying.

The physical properties of the specimens prepared for the CBR tests are summarized in Table 8.2. The variation of dry density of CBR testing specimens was limited (2190-2235 kg/m^3) and therefore considered constant for all specimens. The dried specimens had a final gravimetric water content of only 0.05%.

Table 8.2: Physical properties of specimens for repeated load (RL) CBR tests, and standard (SD) CBR tests; all the specimens were prepared with 4% of initial gravimetric water content w_0, w_f: final gravimetric water content after wetting-drying (WD) cycles.

Name	Test	No. of wetting-drying cycles	w_f (%)	Dry density (kg/m^3)
WD1	RL CBR	0	3.3	2221
WD2	RL CBR	5	0.05	2219
WD3	RL CBR	10	0.05	2194
WD4	RL CBR	15	0.05	2235
WD5	SD CBR	0	3.3	2220
WD6	SD CBR	5	0.05	2232
WD7	SD CBR	10	0.05	2227
WD8	SD CBR	15	0.05	2197

8.2.4 Repeated load and monotonic triaxial tests

Repeated load triaxial tests were carried out to evaluate the resilient modulus and the accumulation of permanent strain of crushed waste rocks under traffic loading and subjected to freeze-thaw cycles (Figure 8.2(a)). Monotonic triaxial tests were conducted to measure the shear strength using the same triaxial test system. The triaxial tests were conducted on 300 mm high and 150 mm diameter specimens under drained conditions.

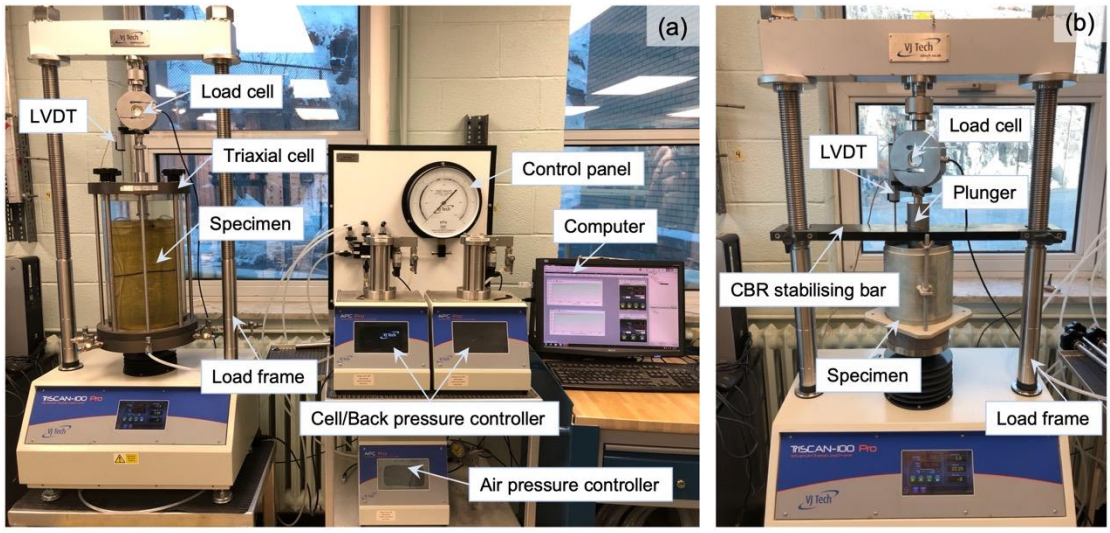

Figure 8.2: Laboratory apparatus used in this study; (a) triaxial tests setup, including a loading frame (100 kN), linear variable differential transformer (LVDT; 75 mm), load cell (50 kN), triaxial cell, pressure controllers, a waste rock specimen, and a computer; (b) CBR test setup, including a loading frame (100 kN), LVDT (75 mm), load cell (50 kN), plunger (or piston; 49.63 mm in diameter), a stabilizing bar, and a waste rock specimen.

Three successive stress sequences were applied for repeated load triaxial tests, and each sequences contained three stress paths (Table 8.3(a)). The confining stress was 45, 70, and 100 kPa for the

three sequences, respectively, and the deviator stress varied from 180 to 700 kPa. Each stress path was applied for 6000 cycles since mine haul roads are typical low-volume roads (Douglas 2016; Thompson et al. 2019). The haversine loading pulses with no rest period were applied to conduct the cyclic loading with 0.2 Hz of frequency. The tire (maximum payload rear tire) pressure of common-used mining trucks in the field generally varies from 400 to 600 kPa (data from *3D-Move Analysis_V2.1*). Although the tire pressure of few extra-heavy mining trucks can exceed 1000 kPa (e.g., Belaz-7571 series), the applied stress level in this study is considered to cover the most stress conditions in mine haul roads.

Table 8.3: Stress paths applied for cyclic tests in this study; (a) for repeated load triaxial tests, σ_3: confining pressure, kPa, σ_d: deviator stress, kPa; (b) for repeated load CBR tests.

(a)

Sequence 1			Sequence 2			Sequence 3		
Stress path	σ_3	σ_d	Stress path	σ_3	σ_d	Stress path	σ_3	σ_d
1-1	45	180	2-1	70	240	3-1	100	500
1-2	45	300	2-2	70	400	3-2	100	700

(b)

Stress path	1	2	3	4	5
Max. plunger stress (kPa)	100	300	500	800	1200

The resilient modulus M_R (MPa) of crushed waste rocks was defined as the ratio of the cyclic deviator stress σ_d (MPa) to the recoverable axial strain ε_r (-) (AASHTO T307 2017):

$$M_R = \frac{\sigma_d}{\varepsilon_r} \tag{8.1}$$

Resilient modulus from the last five cycles of each stress path were averaged to obtain the resilient modulus for each stress path. A summary resilient modulus (SM_R) was computed at a bulk stress of

208 kPa and an octahedral shear stress of 48.6 kPa, following the guidelines provided in NCHRP 1-28A Section 10.3.3.9. The effect of freeze-thaw cycles on resilient modulus was evaluated by comparing the SM_R of specimens subjected to a different number of freeze-thaw cycles.

The permanent strain at each loading cycle was calculated as the ratio of permanent axial displacement to specimen height (EN 13286 2004):

$$\varepsilon_p(N)=\frac{L_p(N)}{L_0} \quad 8.2$$

Where $\varepsilon_p(N)$: permanent strain at loading cycle N; $L_p(N)$: permanent axial displacement at loading cycle N, defined as the displacement accumulated from the beginning of the first cycles to the end of cycle N; L_0: the initial height of the tested specimen, i.e., 300 mm in this study.

Consolidated drained (CD) monotonic triaxial tests were carried out following repeated load triaxial tests to measure the post-cyclic shear strength of crushed waste rocks (AASHTO T307 2017; ASTM D7181 2020). The consolidation was conducted by decreasing the confining pressure from 100 kPa (applied during the last sequence of the repeated load triaxial tests) to 50 kPa. In monotonic triaxial tests, the specimens were sheared at a constant axial rate of 0.015 mm/sec. The axial stress-strain curve for each specimen was recorded, and the peak deviator stress of specimens was compared to study the effect of freeze-thaw cycles on shear strength.

8.2.5 Repeated load and standard CBR tests

Repeated load CBR tests were carried out to measure the stiffness and permanent strain of crushed waste rocks subjected to wetting-drying cycles using a 100 kN loading frame (Figure 8.2(b)). The vertical plunger load and deformation was recorded during the test to compute the stiffness and permanent strain. A standard CBR mold (152.4 mm in diameter, and 178 mm in height including a 51 mm compaction collar) and a plunger with 49.63 mm in diameter were used to prepare and penetrate the specimen, respectively (Figure 8.2(b)). Five stress paths were used for repeated load

CBR tests, and the maximum axial stress of plunger increased from 100 to 1200 kPa (Table 8.3(b)). Each stress path was also applied for 6000 cycles. The haversine loading pulses with no rest period were applied to conduct the cyclic loading with 0.2 Hz of frequency. Equivalent modulus ($E_{equ.}$) was used to characterize the stiffness of specimens subjected to wetting-drying cycles measured by repeated load CBR tests, and it can be calculated using the following equation (Hao and Pabst 2021):

$$E_{equ.}=\frac{2.432(1-v^{2.630})\sigma_p \cdot r}{u^{0.766}} \quad 8.3$$

Where $E_{equ.}$: equivalent modulus, kPa; v: Poisson's ratio, v=0.35 for crushed waste rocks in this study (Thompson and Visser 1997b; Tannant and Regensburg 2001; Laverdière 2019); σ_p: plunger stress, equal to total plunger load/plunger area, kPa; u: vertical elastic (resilient) deformation of materials under plunger, mm; r: the radius of plunger, 24.815 mm.

The axial deformation of plunger during cyclic loading was recorded, and the permanent strain (total strain minus recoverable strain) was then calculated to study the effect of wetting-drying cycles.

Standard CBR tests were also conducted to assess the effect of wetting-drying cycles on CBR value of crushed waste rocks according to the ASTM D1883 standard (ASTM D1883 2016). Standard CBR tests were carried out using the same apparatus (including load frame, mold, and plunger) with the repeated load CBR tests (Figure 8.2(b)).

8.3 Experimental results and interpretation

8.3.1 Effect of freeze-thaw cycles on resilient modulus, shear strength, and permanent deformation

The influence of freeze-thaw cycles was evaluated by comparing the summary resilient modulus, shear strength, and permanent deformation of waste rocks specimens subjected to different numbers of freeze-thaw cycles (Figure 8.3). Summary resilient modulus decreased from around 55 MPa to 50 MPa (-11%) after 4 freeze-thaw cycles (Figure 8.3(a)) and became relatively constant around 49 MPa for the subsequent freeze-thaw cycles. The freeze-thaw cycles therefore could result in 11% of reduction in resilient modulus in this case. The shear strength response, (i.e., the peak deviator stress under 50 kPa of confining pressure) to freeze-thaw cycles showed similar trend with stiffness (Figure 8.3(b)). The peak deviator stress decreased from around 1130 kPa to 1050 kPa (-7%) when the number of freeze-thaw cycles increased from 0 to 10; this influence was therefore deemed negligible. The stress-strain curves for crushed waste rocks subjected to freeze-thaw cycles can be found in APPENDIX C. The freeze-thaw cycles increased the permanent deformation of crushed waste rocks (Figure 8.3(c)). For the first two and last stress paths, the permanent strain generally increased rapidly during the first 500 loading cycles, and then reached an equilibrium state after post-compaction stabilization after around 2000 loading cycles, which was then followed by a very low rate of permanent strain. However, there was no rapid accumulation of permanent strain observed during the initial loading cycles for the other stress paths (12000-30000 loading cycles) because of the relatively low ratio of deviator stress to confining pressure. The accumulated permanent strain increased with freeze-thaw cycles and reached a stable state after 4 freeze-thaw cycles. The final accumulated permanent strain after 6 stress paths (36000 loading cycles) without freeze-thaw cycles was 0.0075, and it increased to 0.009 (+20%) when the specimen had been subjected to 4 freeze-thaw cycles. The accumulated permanent strains of the specimens subjected to 4 and 10 freeze-thaw cycles were close (0.009).

Experimental results indicated therefore that the first 4 freeze-thaw cycles had the greatest influence and could contribute to decrease the stiffness and shear strength, and to increase the permanent deformation of crushed waste rocks. Over 4 freeze-thaw cycles, the effect of more freeze-thaw cycles was insignificant. These results were similar to previous observations made for aggregate mixtures (Bozyurt et al. 2013; Miao et al. 2016; Domitrović et al. 2019). A similar effect of freeze-thaw cycles on permanent deformation for subgrade soil was also observed by Lu et al. (2019) which also showed that the accumulated permanent strain increases gradually with the number of freeze-thaw cycles, and that the first three cycles have the greatest impact. The variation of the geotechnical properties of crushed waste rocks could be attributed to some microstructural changes caused by freeze-thaw cycles (Gullà et al. 2006; Lu et al. 2019). The temperature gradient during freezing can, indeed, induce water movement from the inside of the sample to its surface, which would decrease the particle frictional coefficient (Ishikawa et al. 2019). In addition, the frost expansion of pore water could lead to an increase and redistribution of the porosity, and the samples can become less dense as soil particles get loose (Aldaood et al. 2016; Ishikawa et al. 2019; Lu et al. 2019).

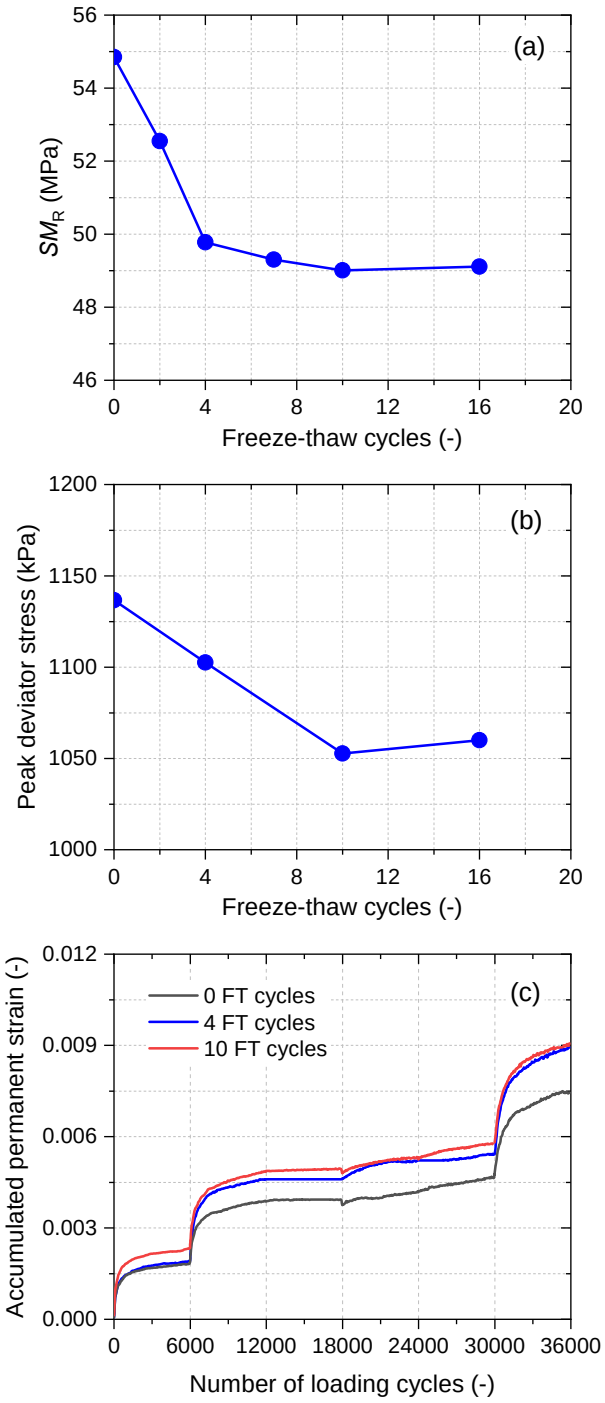

Figure 8.3: Influence of freeze-thaw (FT) cycles (0, 2, 4, 7, 10, 16) on the geotechnical properties of crushed waste rocks; (a) summary resilient modulus SM_R; (b) peak deviator stress under 50 kPa of confining pressure; (c) development of accumulated permanent strain with loading cycles.

8.3.2 Effect of water content during freeze-thaw cycles

The influence of water content on the geotechnical properties of specimens subjected to freeze-thaw cycles was investigated by comparing the summary resilient modulus, shear strength, and permanent deformation of crushed waste rocks specimens with various water contents and subjected to 10 freeze-thaw cycles (Figure 8.4). Three identical specimens were prepared, and water content was adjusted after compaction so that density was the same in all the samples and only water content changed (specimens FT5, FT7 and FT8 in Table 8.1). An increase of the water content contributed to decrease the summary resilient modulus and increased permanent deformation after 10 freeze-thaw cycles but had limited influence on the shear strength of crushed waste rocks (Figure 8.4). Summary resilient modulus decreased slightly from around 51 MPa to 49 MPa (-4%) when the water content increased from 1.9% to 2.5%, but then tended to stabilize around 49.5 MPa when the water content increased to 3.5% (Figure 8.4(a)). The peak deviator stress under 50 kPa confining pressure was nearly constant (1050-1080 kPa) when the water content was between 1.9% and 3.5% (Figure 8.4(b)). Permanent deformation was more significantly affected by water content during freeze-thaw cycles (Figure 8.4(c)), and an increase of the water content resulted in a significant increase of permanent deformation: the final accumulated permanent strain after 36000 loading cycles increased from 0.005 to 0.009 (+80%) when the water content increased from 1.9% to 2.5%; and it increased to 0.01 (+100%) for a water content of 3.5%. The influence of water content during freeze-thaw cycles on permanent strain was more remarkable during the first two stress paths (i.e., the first 12 000 loading cycles).

These observations could be explained by the changes in the microstructure caused by the freeze-thaw cycles: higher water content increases the frost expansion of pore water, which in turns promotes the particle rearrangement (Ishikawa et al. 2019). The sensitivity of the permanent deformation to water content during freeze-thaw cycles, was consistent with the conclusions from previous studies where it was shown that unbound granular materials at high water content

subjected to freeze-thaw cycles could fail after thousands of loading cycles (Bilodeau et al. 2011). A greater water content in the waste rock layers at the beginning of the winter (in cold regions) may therefore increase the permanent deformation of mine haul roads, and lead to rutting and slipperiness, which causes poor quality of roads and an increase of maintenance requirements (Thompson et al. 2019).

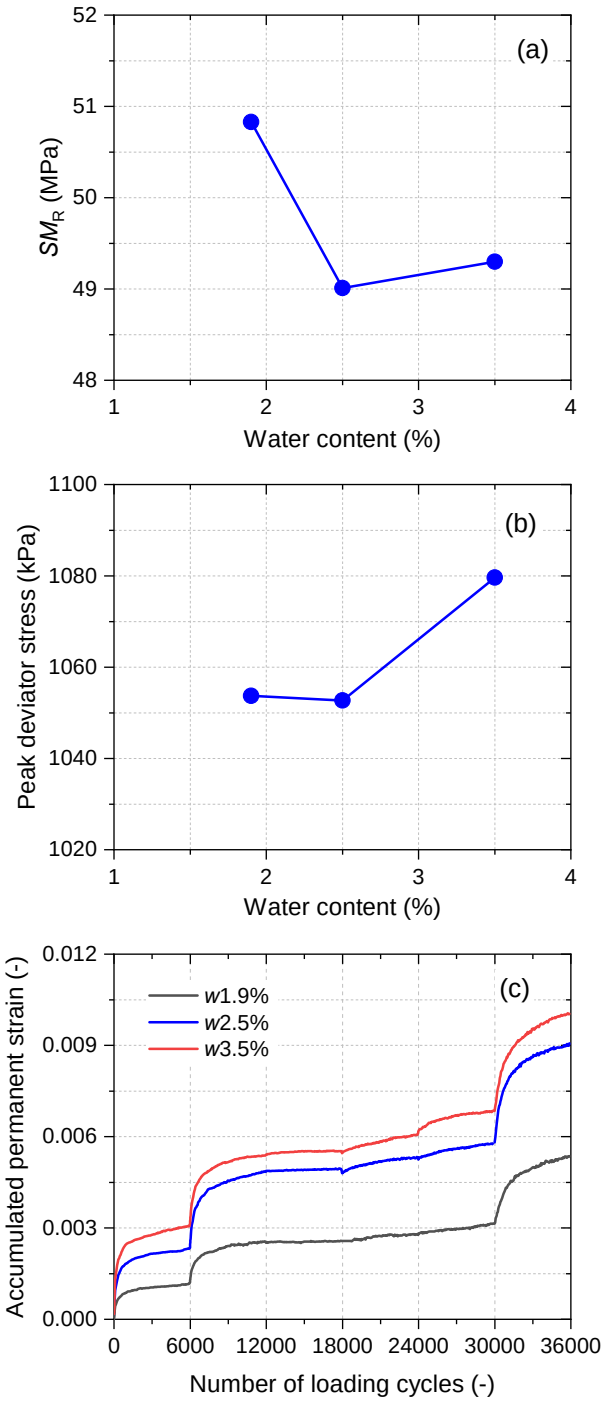

Figure 8.4: Influence of water content (1.9%, 2.5%, and 3.5%) within specimens subjected to 10 freeze-thaw (FT) cycles on the geotechnical properties of crushed waste rocks; (a) summary

resilient modulus SM_R; (b) peak deviator stress under 50 kPa of confining pressure; (c) development of accumulated permanent strain with loading cycles.

8.3.3 Effect of wetting-drying cycles on CBR, equivalent modulus, and permanent deformation

The impact of wetting-drying cycles on the geotechnical properties of crushed waste rocks was studied by comparing the CBR, equivalent modulus, and permanent deformation of specimens subjected to 0, 5, 10, and 15 wetting-drying cycles (Figure 8.5). The CBR of crushed waste rocks increased from 125 to 165 (+32%) after 5 wetting-drying cycles (Figure 8.5(a)). The effect of wetting-drying cycles on equivalent modulus was, however, neglectable, for low axial stress. As the axial stress increased to 800 and 1200 kPa, wetting-drying cycles increased the equivalent modulus by 9% and 18%, respectively (Figure 8.5(b)). The wetting-drying cycles also resulted in an increase of the permanent strain, especially at high axial stress (1200 kPa) (Figure 8.5(c)). For example, the final accumulated permanent strain after five stress paths increased from around 0.0035 to 0.007 (+100%) after 5 wetting-drying cycles. However, the final permanent strain remained relatively constant when the number of wetting-drying cycles exceeded 5. For example, the final permanent strain of the specimen subjected to 15 wetting-drying cycles 0.0075, i.e., very close to the 0.007 strain measured for 5 wetting-drying cycles. Overall, experimental results therefore indicated that wetting-drying cycles resulted in an increase in CBR, equivalent modulus, and permanent deformation, but that this effect was limited after 5 wetting-drying cycles.

Similar findings were observed by Khoury and Zaman (2007) who showed that wetting-drying cycles could result in an increase of resileint modulus for Sawyer aggregates with an additive of cement kiln dust. Several explanations were proposed in the litterature to explain this phenomenon. For example, some say that the drying process can induce the precipitation and crystallization of salts which tend to accumulate at particle contacts where water menisci dry out, and can therefore

create bonds between coarse particles, which result in the increase of the strength and stiffness of the material (Valdes and Cortes 2014; He and Chu 2017). The wetting-drying cycles may increase the porosity of samples, and so the permanent deformation would increase.

Drying process appears therefore beneficial to the CBR and stiffness of crushed waste rocks. However, low water content could also contribute to increase dust generation of mine haul roads which would reduce fleet productivity eventually (Thompson 2011c).

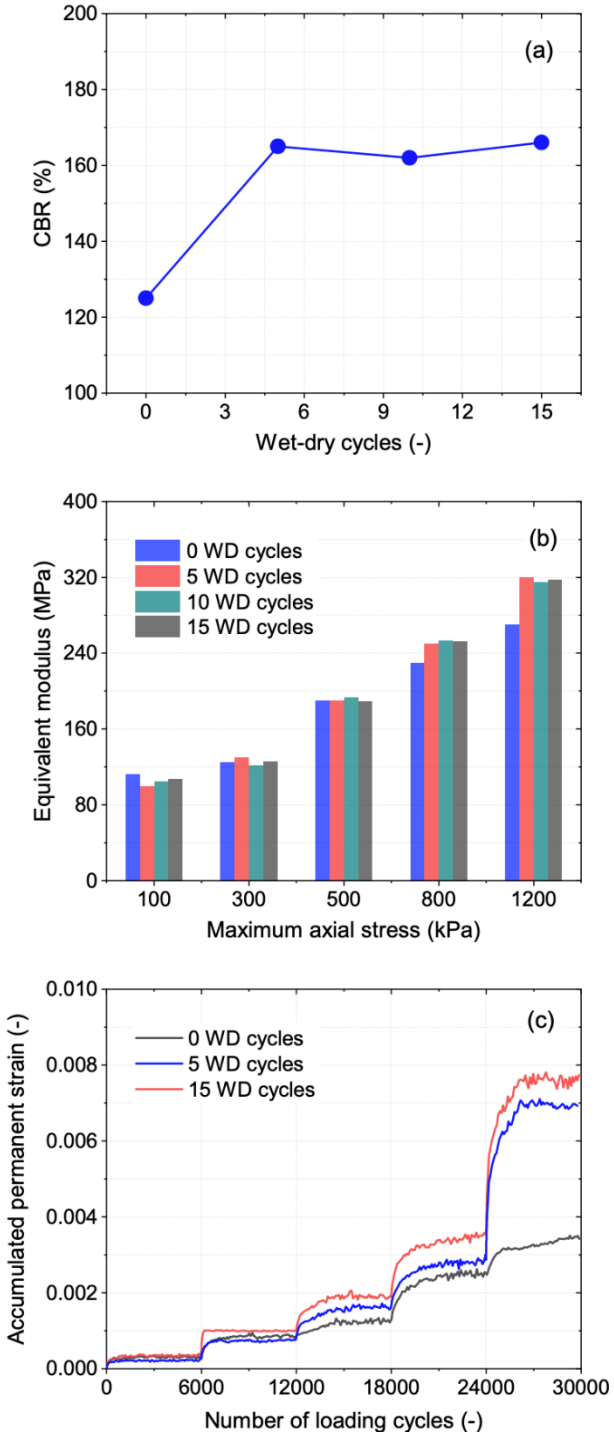

Figure 8.5: Influence of wetting-drying (WD) cycles (0, 5, 10, and 15) on the geotechnical properties of crushed waste rocks; (a) CBR; (b) equivalent modulus; (c) development of accumulated permanent strain with loading cycles.

8.4 Development of a model to predict resilient modulus and permanent deformation

Repeated load triaxial test on specimen subjected to 16 freeze-thaw cycles took around 40 days, and repeated load CBR test on specimen subjected to 15 wetting-drying cycles took around 90 days (including the specimen preparation). Conducting these tests is therefore very complex and time-consuming. Predictive models can therefore be an alternative tool to estimate the response of materials subjected to climatic factors when sufficient laboratory tests cannot be conducted or when such tests are not feasible for specific projects because of economic or time factors (Maalouf et al. 2012). For these reasons, the development of predictive models is pertinent to many engineering applications. In this case also, predictive models were proposed, based on the resilient modulus and permanent strain measured in this research. Laboratory data presented above were fitted by using regression models based on various material properties and climatic conditions. The following section describes the approach used and proposed models to predict the resilient modulus and the permanent strain of crushed waste rocks subjected to freeze-thaw cycles. Note that a similar approach could also be used to develop predictive models for wetting-drying cycles. However, such models were not developed here because the effect of wetting-drying cycles was too limited.

8.4.1 Resilient modulus

In this study, the nonlinear behavior of crushed waste rocks was characterized using the MEPDG (Mechanistic-Empirical Design Guide) model designed in NCHRP (NCHRP 2004):

$$M_R = k_1 p_a \left(\frac{\theta}{p_a}\right)^{k_2} \left(\frac{\tau_{oct}}{p_a} + 1\right)^{k_3} \quad 8.4$$

Where θ: bulk stress, kPa; τ_{oct}: octahedral shear stress (Eq. 8.5), kPa; p_a: atmospheric pressure (100 kPa); k_1, k_2, and k_3: model regression coefficients.

$$\tau_{oct}=\frac{1}{3}\sqrt{(\sigma_1-\sigma_2)^2+(\sigma_3-\sigma_2)^2+(\sigma_1-\sigma_3)^2} \quad 8.5$$

Regression analysis was conducted to fit the MEPDG model to the measured resilient modulus of specimens with different (final) water contents (1.9%, 2.5%, and 3.5%) and exposed to different numbers of freeze-thaw cycles (0, 2, 4, 7, 10, and 16) (Figure 8.6). The coefficient of determination R^2 for all cases was greater than 0.95, indicating that the MEPDG model was sufficiently reliable for fitting the measured resilient modulus. The regression coefficients k_2 and k_3 (Eq. 8.4) for the different specimens were close and seemed relatively independent of the number of freeze-thaw cycles. The values of k_2 and k_3 were therefore fixed to 1.038 and -0.312, respectively. Coefficient k_1, however, varied significantly with the number of freeze-thaw cycles, decreasing from 0.573 to 0.512 after 10 cycles (Figure 8.6(a)). Coefficient k_1 appeared to be proportional to the resilient modulus, and a lower k_1 values indicated a lower resilient modulus than a higher value of k_1. As discussed previously, the specimens tended to be less affected by freeze-thaw actions after 10 cycles and consequently, the k_1 value after 16 freeze-thaw cycles was close to that of the specimen after 10 freeze-thaw cycles. For the specimens exposed to 10 freeze-thaw cycles, an increasing of water content from 1.9% to 2.5% resulted in a decrease of k_1 value from 0.531 to 0.512 (Figure 8.6(b)). The k_1 values for the specimens with 2.5% to 3.5% of water content were close, and the influence of water content was considered negligible when water content was greater than 2.5%. Although the increase in water content resulted in a small decrease of resilient modulus, k_1 values and fitting surfaces indicated that the influence of the water content was relatively limited (Figure 8.6(b)).

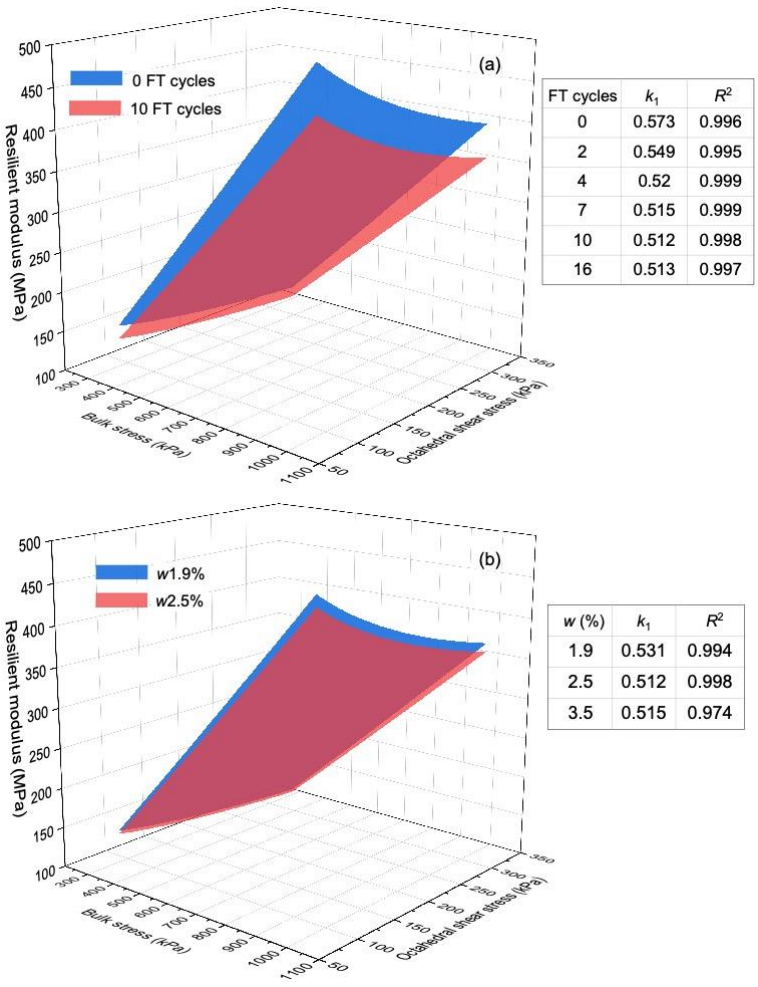

FT cycles	k_1	R^2
0	0.573	0.996
2	0.549	0.995
4	0.52	0.999
7	0.515	0.999
10	0.512	0.998
16	0.513	0.997

w (%)	k_1	R^2
1.9	0.531	0.994
2.5	0.512	0.998
3.5	0.515	0.974

Figure 8.6: Fitting surfaces of resilient modulus of crushed waste rocks using MEPDG model, the calibrated coefficient k_1 and the corresponding coefficient of determination R^2; (a) fitting results of specimens exposed to 0 and 10 freeze-thaw (FT) cycles with 2.5% of water content; (b) fitting results of specimens with 1.9% and 2.5% of water contents and exposed to 10 freeze-thaw (FT) cycles.

The correlation between MEPDG model coefficient k_1 and the number of freeze-thaw cycles was described using the following equation:

$$k_{1\text{-}n}=c_1\times k_{1\text{-}0}{}^{n}+c_2 \qquad 8.6$$

Where $k_{1\text{-}n}$: the k_1 value after n freeze-thaw cycles; $k_{1\text{-}0}$: the k_1 value without freeze-thaw cycles, it was 0.573 in this study; n: the number of freeze-thaw cycles; c_1 and c_2: regression coefficients.

Regression coefficients $c_1 = 0.062$ and $c_2 = 0.515$ were calibrated by fitting k_1 values (Figure 8.7). The coefficient of determination R^2 was greater than 0.9, indicating that the calibrated equation was relatively reliable to estimate k_1 value in MEPDG model and predict the resilient modulus of crushed waste rocks subjected to freeze-thaw cycles.

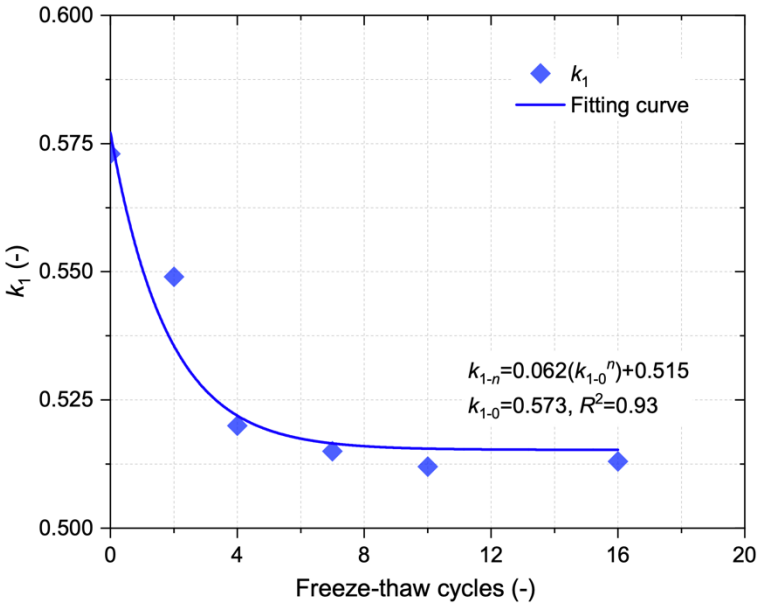

Figure 8.7: Fitting curve of determined MEPDG model coefficient k_1.

8.4.2 Permanent deformation

Previous studies have shown that Rahman and Erlingsson (2015) model performed well for fitting permanent strain of crushed waste rocks (Rahman and Erlingsson 2015a; Erlingsson et al. 2017). The same model (extended using time hardening approach) was therefore also used to fit the measured accumulated permanent strain after freeze-thaw cycles. The extended Rahman and

Erlingsson model can be written (Rahman and Erlingsson 2015a):

$$\varepsilon_{p_i} = a(N - N_{i-1} + N_i^{eq})^{bS_f} S_f \quad 8.7$$

$$S_f = \frac{(q/p_a)}{(p/p_a)^{\alpha}} \quad 8.8$$

$$N_i^{eq} = \left(\frac{\varepsilon_{p_{i-1}}}{aS_f}\right)^{\frac{1}{bS_f}} \quad 8.9$$

Where ε_{p_i}: the accumulated permanent strain in the *i*th stress path, -; N: number of loading cycles, -; q: deviator stress, kPa; p: mean bulk stress (one-third of the sum of the principal stresses), kPa; p_a: the reference stress taken equal to the atmospheric pressure (100 kPa); a, b, and α: model coefficients obtained from regression analysis; N_{i-1}: the total number of loading cycles at the end of (i-1)th stress path, -; N_i^{eq}: the equivalent number of loading cycles for *i*th stress path, -, which is required to develop the same amount of permanent strain that is accumulated from all the previous stress paths. Equivalent number of loading cycles N_i^{eq} can be calculated using Eq. 8.9 (Rahman and Erlingsson 2015a) based on the accumulated permanent strain at the end of (i-1)th stress path $\varepsilon_{p_{i-1}}$.

The measured accumulated permanent strains of crushed waste rocks subjected to different numbers of freeze-thaw cycles (0, 4, and 10 in this study) and with different water contents (1.9%, 2.5%, and 3.5%) were fitted using extended Rahman and Erlingsson model. The model fitting was deemed acceptable with coefficient of determination R^2 greater than 0.95 for all cases (Figure 8.8). Model coefficient α was relatively constant and close to 0.45 (±0.02) for all cases. It was therefore decided to fix α to 0.45 (also to minimize the number of model coefficients). Model coefficient a tended to increased slightly from 0.780×10^{-3} to 0.942×10^{-3} with the number of freeze-thaw cycles (with 2.5% of water content), while the variation of coefficient b was relatively limited (0.24 to 0.28) (Figure 8.8(a)). A greater value of coefficient a indicated a greater accumulation of permanent strain than a lower value of a. The impact of water content on the model coefficients a and b was more significant than the number of freeze-thaw cycles (Figure 8.8(b)). Coefficient a increased from 0.415×10^{-3} to 1.234×10^{-3} as the water content increased from 1.9% to 3.5%, while coefficient

b decreased from 0.033 to 0.020. Considering this significant effect of water content, it was deemed necessary to determine the correlation between Rahman and Erlingsson model coefficients *a* and *b* and the water content during freeze-thaw cycles.

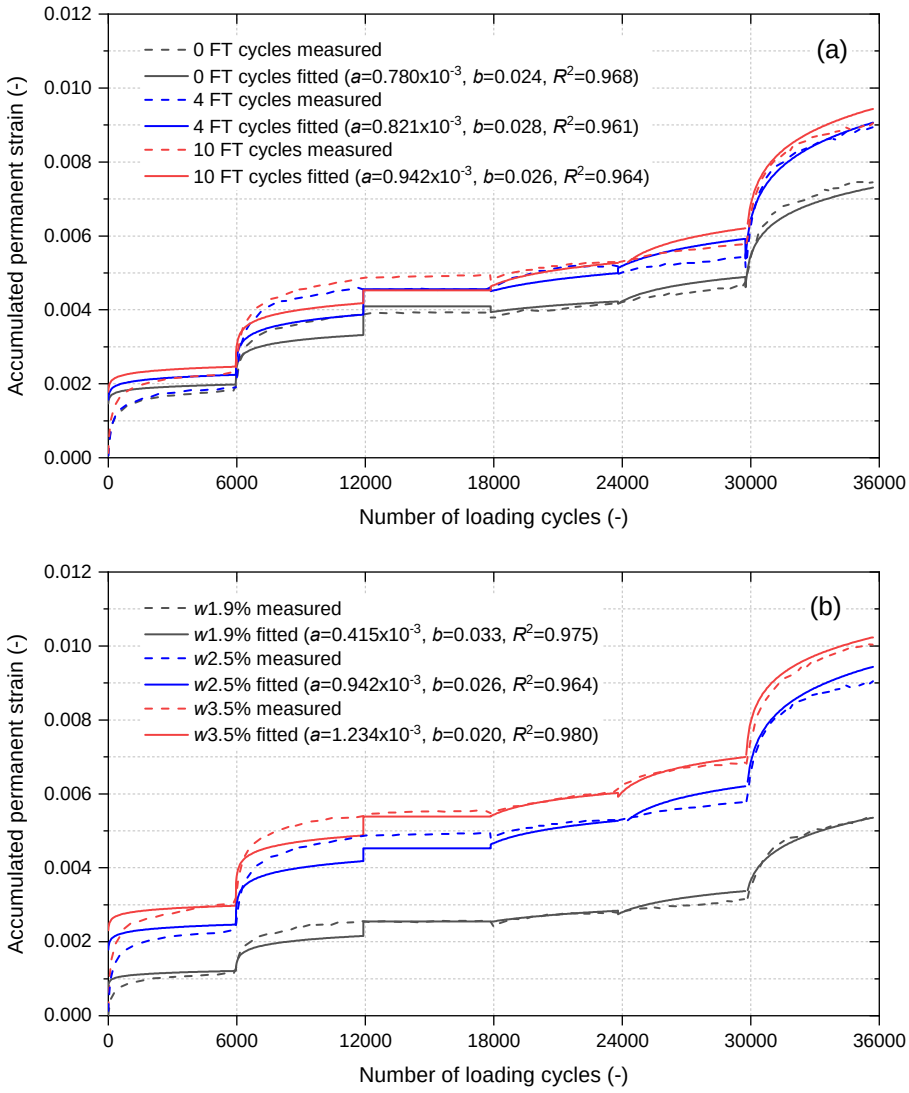

Figure 8.8: Measured and fitted (Rahman and Erlingsson model) accumulated permanent stain of crushed waste rocks, the corresponding calibrated model coefficients a and b and the coefficient of determination R^2; (a) fitting results for specimens with 2.5% of water content and subjected to 0, 4, and 10 freeze-thaw cycles; (b) fitting results for specimens with 1.9%, 2.5%, and 3.55% of water contents and subjected to 10 freeze-thaw cycles.

The calibrated coefficients a and b (see Figure 8.8(b)) were corelated with the water content w (Figure 8.9). Results showed that coefficients a and b linearly varied with the water content w (at least within the range of w tested in this study):

$$a=r_1\times w+r_2 \quad 8.10$$

$$b=r_3\times w+r_4 \quad 8.11$$

Where r_1, r_2, r_3 and r_4 were the regression coefficients depending on the water content. For a, r_1 and r_2 were 0.489 and -0.425, respectively; and for b, r_3 and r_4 were -0.008 and 0.047, respectively.

The coefficient of determination R^2 for the a and b functions was higher than 0.9, indicating these developed functions could be used to estimate the permanent deformation of crushed waste rocks with a certain water content and subjected to freeze-thaw cycles. The linear relation between coefficient a and water content w proposed in this study was similar with that developed by Rahman and Erlingsson (2015a), but with different values of regression coefficients r_1 and r_2. The value of r_1 and r_2 for the relation developed by Rahman and Erlingsson (2015a) varied from 0.1 to 4.7, and from -4 to 4.1, respectively, for different crushed rock aggregates.

The applicability of the proposed models in this study to other materials from the literature (Rahman and Erlingsson 2015a) was also evaluated, but the prediction accuracy was relatively low. One of the possible reasons was that the gradation of the aggregates in the literature was different with that of crushed waste rocks in this study, for example, the maximum particle size from the literature was 32 mm that was significantly higher than 19 mm of crushed waste rocks.

The highest gravimetric water content after freeze-thaw cycles in this study was 3.5%, which is relatively low compared to that of fine-grained pavement materials (Kalkan 2009; Han, Dong, et al. 2021). Waste rocks are, indeed, usually at their residual water content in the field, and as a matter of fact, the measured gravimetric water content on mine haul roads at the site was between 2% and

4% (Laverdière 2019). The water contents used in this study therefore covered typical ranges observed in the field. However, the validity of the proposed models to higher water contents was uncertain.

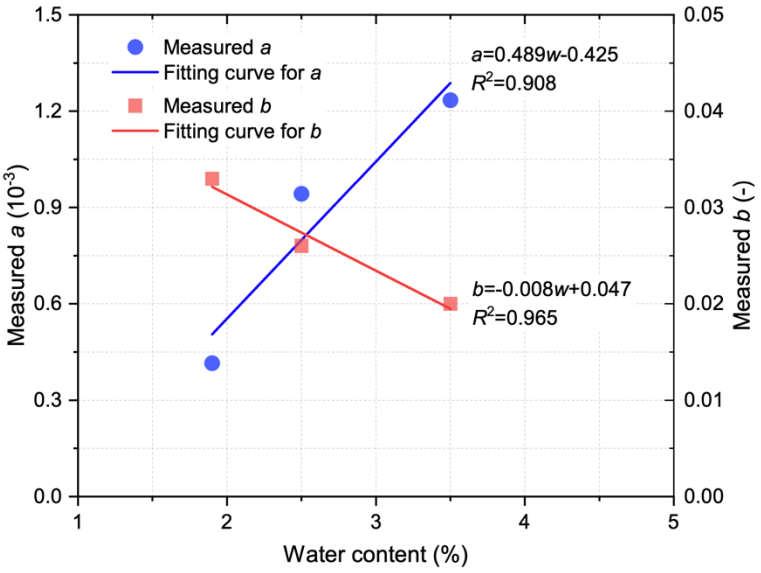

Figure 8.9: Rahman and Erlingsson model coefficients *a* and *b* as a function of the water content *w*.

8.5 Discussion and final remarks

In this study, the effect of freeze-thaw and wetting-drying cycles on the geotechnical characteristics of crushed waste rocks was studied, and the experimental results showed that these climatic factors influenced, sometimes significantly, the stiffness, shear strength, CBR, and permanent deformation. Although this study showed acceptable experimental results and similar findings with the literature (even though the tested materials were very different), their reproducibility could not be verified since the tests were so time-consuming. Considering the repeatability of repeated load triaxial test is relatively low (Boudreau 2003). Further study would be required to generalize the effect of

freeze-thaw and wetting-drying cycles more accurately on such materials.

The influence of freeze-thaw and wetting-drying cycles is also often affected by the particle size distribution. For example, Miao et al. (2016) reported that the stiffness and shear strength of gap and coarse graded unbound granular materials decreased with the freeze-thaw cycles, while a tiny increase in stiffness and a significant increase in shear strength were observer for continuous graded materials. Although the crushed waste rocks used in this study were representative of hard rock mines (Bussière 2007a; James et al. 2013), the observed results could not be extrapolated directly to other sites and materials. Additional tests and comparison are strongly recommended to validate the observed trends and the validity of the proposed model.

In the wetting-drying tests, even though the specimens were soaked in water, the approach used in this study could not completely and realistically simulate field condition such as the rainfall splash and water flows which would cause particle migration and change the fabric of waste rocks (Cui et al. 2017; Cui et al. 2019). Results in this study are therefore expected to have underestimate the effect of wetting-drying cycles compared to what would happen in the field. Alternative experimental approaches such as Scanning Electron Microscope (SEM) test are more and more frequently to examinate the microstructure change of the specimens subjected freeze-thaw cycles (Gullà et al. 2006; Aldaood et al. 2016; Zou et al. 2020) and wetting-drying cycles (Aldaood et al. 2014), and are therefore strongly recommended for further evaluating the effect of frost-thaw and wetting-drying on crushed waste rock.

The proposed models for the coefficients k_1, a, and b were deemed reliable to predict the resilient modulus and permanent deformation of crushed waste rocks after freeze-thaw cycles. These models can significantly decrease the laboratory work. However, the k_1 value for 0 freeze-thaw cycle is needed when use the predictive model for coefficient k_1, which means at least one repeated load triaxial test should be carried out. Also, the applicability of these models is relatively limited because these models take only one parameter (number of freeze-thaw cycles n or water content w)

into account. More physical properties of materials (e.g., gradation, mineralogy, and density) should be considered for the development of predictive models to improve their generalization.

8.6 Conclusions

The geotechnical characteristics of crushed waste rocks subjected to freeze-thaw and wetting-drying cycles were investigated through a series of triaxial tests and CBR tests. The following conclusions were found after the analysis of the experimental results:

1. The effect of freeze-thaw cycles on the geotechnical properties of crushed waste rocks was relatively significant during the first 4 cycles, and the material nearly reached an equilibrium state after 10 freeze-thaw cycles. The resilient modulus and shear strength of crushed waste rocks subjected to repeated freeze-thaw cycles were reduced by 11% and 7%, respectively, while the accumulated permanent strain increased by 20%.
2. The effect of water content on the permanent strain of crushed waste rocks during freeze-thaw cycles was significant (over 80% increase for less than 1% increase of water content. However, the influence of water content on the resilient modulus and shear strength was limited and usually smaller than 5%.
3. Wetting-drying cycles could result in a 32% increase of the CBR. The influence of wetting-drying cycles on stiffness (equivalent modulus) was negligible at low axial stress (<800 kPa) but caused an 18% increase at high axial stress. The permanent deformation increased by 100% following repeated wetting-drying cycles. Similarly to the freeze-thaw cycles, the effect of wetting-drying cycles on the geotechnical characteristics was limited after 5 cycles.
4. The MEPDG model and Rahman and Erlingsson model (extended using time hardening approach) were able to fit relatively well ($R^2 > 0.95$) the measured resilient modulus and accumulated permanent strain, respectively. Based on these results, coefficients (k_1, a, and b)

predictive models were developed to estimate the variation of resilient modulus and permanent deformation of crushed waste rocks as a function of number of freeze-thaw cycles and water content.

The results presented in this study should help to improve the design and evaluate the performance of mine haul roads affected by the climate change. The proposed coefficients predictive models also can decrease the laboratory work and increase the field work efficiency.

Acknowledgements

This research was carried out with the financial support from FRQNT and the industrial partners of the Research Institute on Mines and the Environment (http://irme.ca/). The repeated load triaxial and CBR test equipment used in this study were acquired with a CFI grant.

8.7 References

AASHTO M-147. (2008). Standard specification for materials for aggregate and soil-aggregate subbase, base, and surface courses. Washington, DC.

AASHTO T307-99. (2017). Standard method of test for determining the resilient modulus of soils and aggregate materials. Washington, DC.

Aldaood, A., Bouasker, M., and Al-Mukhtar, M. (2014). Impact of wetting–drying cycles on the microstructure and mechanical properties of lime-stabilized gypseous soils. *Engineering Geology, 174*, 11-21.

Aldaood, A., Bouasker, M., and Al-Mukhtar, M. (2016). Effect of water during freeze–thaw cycles on the performance and durability of lime-treated gypseous soil. *Cold Regions Science and*

Technology, 123, 155-163.

Araya, A. A., Huurman, M., Molenaar, A. A. A., and Houben, L. J. M. (2011). Investigation of the resilient behavior of granular base materials with simple test apparatus. *Materials and Structures, 45*(5), 695-705.

ASTM D1557-12e1. (2012). Standard test methods for laboratory compaction characteristics of soil using modified effort (56,000 ft-lbf/ft^3 (2,700 kN-m/m^3)). ASTM International, West Conshohocken, PA.

ASTM D559/D559M-15. (2015). Standard test methods for wetting and drying compacted soil-cement mixtures. ASTM International, West Conshohocken, PA.

ASTM D1883-16. (2016). Standard test method for California Bearing Ratio (CBR) of laboratory-compacted soils. ASTM International, West Conshohocken, PA.

ASTM D2487-17e1. (2017). Standard practice for classification of soils for engineering purposes (unified soil classification system). ASTM International, West Conshohocken, PA.

ASTM D7181-20. (2020). Standard test method for consolidated drained triaxial compression test for soils. ASTM International, West Conshohocken, PA.

Bilodeau, J.-P., Doré, G., and Schwarz, C. (2011). Effect of seasonal frost conditions on the permanent strain behaviour of compacted unbound granular materials used as base course. *International Journal of Pavement Engineering, 12*(5), 507-518.

Boudreau, R. L. (2003). Repeatability of the resilient modulus test procedure. *Resilient Modulus Testing for Pavement Components, ASTM International*.

Bozyurt, O., Keene, A., Tinjum, J., Edil, T., and Fratta, D. (2013). Freeze–thaw effects on stiffness of unbound recycled road base. In *Mechanical properties of frozen soil*: ASTM International.

Broms, B. B., and Yao, L. Y. (1964). Shear strength of a soil after freezing and thawing. *Journal of the Soil Mechanics and Foundations Division, 90*(4), 1-25.

Bussière, B. (2007). Colloquium 2004: Hydrogeotechnical properties of hard rock tailings from metal mines and emerging geoenvironmental disposal approaches. *Canadian Geotechnical Journal, 44*(9), 1019-1052.

Chittoori, B. C. S., Puppala, A. J., and Pedarla, A. (2018). Addressing clay mineralogy effects on performance of chemically stabilized expansive soils subjected to seasonal wetting and drying. *Journal of Geotechnical and Geoenvironmental Engineering, 144*(1), 04017097.

Cui, Y., Jiang, Y., and Guo, C. (2019). Investigation of the initiation of shallow failure in widely graded loose soil slopes considering interstitial flow and surface runoff. *Landslides, 16*(4), 815-828.

Cui, Y., Zhou, X., and Guo, C. (2017). Experimental study on the moving characteristics of fine grains in wide grading unconsolidated soil under heavy rainfall. *Journal of Mountain Science, 14*(3), 417-431.

Dehn, M., Bürger, G., Buma, J., and Gasparetto, P. (2000). Impact of climate change on slope stability using expanded downscaling. *Engineering Geology, 55*(3), 193-204.

Domitrović, J., Rukavina, T., and Lenart, S. (2019). Effect of freeze-thaw cycles on the resilient moduli and permanent deformation of rap/natural aggregate unbound base mixtures. *Transportation Geotechnics, 18*, 83-91.

Douglas, R. A. (2016). *Low-volume road engineering: Design, construction, and maintenance*: CRC Press.

Edil, T. B., and Cetin, B. (2018). Freeze-thaw performance of chemically stabilized natural and recycled highway materials. *Sciences in Cold and Arid Regions, 7*(5), 482-491.

EN 13286-7. (2004). Unbound and hydraulically bound mixtures–cyclic load triaxial test for

unbound mixtures. British Standard Institute.

Erlingsson, S. (2012). Rutting development in a flexible pavement structure. *Road Materials and Pavement Design, 13*(2), 218-234.

Erlingsson, S., Rahman, S., and Salour, F. (2017). Characteristic of unbound granular materials and subgrades based on multi stage rlt testing. *Transportation Geotechnics, 13*, 28-42.

Geertsema, M., Clague, J. J., Schwab, J. W., and Evans, S. G. (2006). An overview of recent large catastrophic landslides in northern british columbia, canada. *Engineering Geology, 83*(1), 120-143.

Gullà, G., Mandaglio, M. C., and Moraci, N. (2006). Effect of weathering on the compressibility and shear strength of a natural clay. *Canadian Geotechnical Journal, 43*(6), 618-625.

Han, C., Dong, Q., and Xu, X. (2021). Microstructural analysis on the variation of resilient modulus of lime modified soil under freezing–thawing action. *Road Materials and Pavement Design*, 1-15.

Hao, S., and Pabst, T. (2021). Estimation of resilient behavior of crushed waste rocks using repeated load cbr tests. *Transportation Geotechnics, 28*, 100525.

He, J., and Chu, J. (2017). Cementation of sand due to salt precipitation in drying process. *Marine Georesources & Geotechnology, 35*(3), 441-445.

Hotton, G., Bussière, B., Pabst, T., Bresson, É., and Roy, P. (2020). Influence of climate change on the ability of a cover with capillary barrier effects to control acid generation. *Hydrogeology Journal, 28*(2), 763-779.

Ishikawa, T., Lin, T., Kawabata, S., Kameyama, S., and Tokoro, T. (2019). Effect evaluation of freeze-thaw on resilient modulus of unsaturated granular base course material in pavement. *Transportation Geotechnics, 21*, 100284.

James, M., Aubertin, M., and Bussière, B. (2013). *On the use of waste rock inclusions to improve the performance of tailings impoundments.* Paper presented at the Proceedings of the 18th International Conference Soil Mechanics and Geotechnical Engineering, Paris, France.

Kalkan, E. (2009). Effects of silica fume on the geotechnical properties of fine-grained soils exposed to freeze and thaw. *Cold Regions Science and Technology, 58*(3), 130-135.

Khoury, N., Zaman, M., and Laguros, J. (2005). Behavior of stabilized aggregate bases subjected to cyclic loading and wet-dry cycles. In *Advances in pavement engineering* (pp. 1-10).

Khoury, N., and Zaman, M. M. (2007). Durability of stabilized base courses subjected to wet–dry cycles. *International Journal of Pavement Engineering, 8*(4), 265-276.

Kim, S. Y., Park, J., Cha, W., Lee, J.-S., and Santamarina, J. C. (2021). Soil response during globally drained and undrained freeze-thaw cycles under deviatoric loading. *Journal of Geotechnical and Geoenvironmental Engineering, 147*(2), 06020030.

Laverdière, A. (2019). *Effet de la granulométrie sur le comportement géotechnique de roches stériles concassées utilisées comme surface de roulement sur des routes minières.* École Polytechnique de Montréal.

Li, L., Saboundjian, S., Liu, J., and Zhang, X. (2013). Permanent deformation behavior of alaskan granular base materials. In *Iscord 2013: Planning for sustainable cold regions* (pp. 428-435).

Lin, T., Ishikawa, T., and Tokoro, T. (2019). Testing method for resilient properties of unsaturated unbound granular materials subjected to freeze-thaw action. *Japanese Geotechnical Society Special Publication, 7*(2), 576-581.

Liu, E., Lai, Y., Liao, M., Liu, X., and Hou, F. (2016). Fatigue and damage properties of frozen silty sand samples subjected to cyclic triaxial loading. *Canadian Geotechnical Journal, 53*(12), 1939-1951.

Liu, J., Zhang, X., Li, L., and Saboundjian, S. (2018). Resilient behavior of unbound granular materials subjected to a closed-system freeze-thaw cycle. *Journal of Cold Regions Engineering, 32*(1), 04017015.

Lu, Z., She, J., Wu, X., and Yao, H. (2019). Cumulative strain characteristics of compacted soil under effect of freeze-thaw cycles with water supply. *Transportation Geotechnics, 21*, 100291.

Maalouf, M., Khoury, N., Laguros, J. G., and Kumin, H. (2012). Support vector regression to predict the performance of stabilized aggregate bases subject to wet–dry cycles. *International Journal for Numerical and Analytical Methods in Geomechanics, 36*(6), 675-696.

Meiers, G. P., Barbour, S. L., Qualizza, C. V., and Dobchuk, B. S. (2011). Evolution of the hydraulic conductivity of reclamation covers over sodic/saline mining overburden. *Journal of Geotechnical and Geoenvironmental Engineering, 137*(10), 968-976.

Miao, Y., Huang, Y., Zhang, Q., and Wang, L. (2016). Effect of temperature on resilient modulus and shear strength of unbound granular materials containing fine rap. *Construction and Building Materials, 124*, 1132-1141.

Molenaar, A. A. (2008). *Repeated load cbr testing, a simple but effective tool for the characterization of fine soils and unbound materials*.

NCHRP. (2004). *Guide for mechanistic-empirical design of new and rehabilitated pavement structures* (Final Rep. No. 1-37A).

Othman, M. A., and Benson, C. H. (1993). Effect of freeze–thaw on the hydraulic conductivity and morphology of compacted clay. *Canadian Geotechnical Journal, 30*(2), 236-246.

Rahman, M. S., and Erlingsson, S. (2015). A model for predicting permanent deformation of unbound granular materials. *Road Materials and Pavement Design, 16*(3), 653-673.

Razouki, S. S., and Salem, B. M. (2015). Impact of soaking–drying cycles on gypsum sand roadbed soil. *Transportation Geotechnics, 2*, 78-85.

Shou, K.-J., and Lin, J.-F. (2020). Evaluation of the extreme rainfall predictions and their impact on landslide susceptibility in a sub-catchment scale. *Engineering Geology, 265*, 105434.

Simonsen, E., Janoo, V. C., and Isacsson, U. (2002). Resilient properties of unbound road materials during seasonal frost conditions. *Journal of Cold Regions Engineering, 16*(1), 28-50.

Solanki, P., and Zaman, M. (2014). *Effect of wet-dry cycling on the mechanical properties of stabilized subgrade soils.* Paper presented at the Geo-Congress 2014: Geo-characterization and Modeling for Sustainability.

Tannant, D., and Regensburg, B. (2001). *Guidelines for mine haul road design*.

Thompson, R., Peroni, R., and Visser, A. T. (2019). *Mining haul roads: Theory and practice*: CRC Press.

Thompson, R. J. (2011). Mine haul road design, construction and maintenance management. *Mining Roads, 136*.

Thompson, R. J., and Visser, A. T. (1997). A mechanistic structural design procedure for surface mine haul roads. *International Journal of Surface Mining, Reclamation and Environment, 11*(3), 121-128.

Tian, S., Indraratna, B., Tang, L., Qi, Y., and Ling, X. (2020). A semi-empirical elasto-plastic constitutive model for coarse-grained materials that incorporates the effects of freeze-thaw cycles. *Transportation Geotechnics, 24*, 100373.

Tian, S., Tang, L., Ling, X., Li, S., Kong, X., and Zhou, G. (2019). Experimental and analytical investigation of the dynamic behavior of granular base course materials used for china's high-speed railways subjected to freeze-thaw cycles. *Cold Regions Science and Technology, 157*, 139-148.

Valdes, J. R., and Cortes, D. D. (2014). *Heat-induced bonding of sands.* Paper presented at the Geo-Congress 2014: Geo-characterization and Modeling for Sustainability.

Zou, W.-l., Ding, L.-q., Han, Z., and Wang, X.-q. (2020). Effects of freeze-thaw cycles on the moisture sensitivity of a compacted clay. *Engineering Geology, 278*, 105832.

CHAPTER 9 ARTICLE 5: PREDICTION OF CBR AND RESILIENT MODULUS OF CRUSHED WASTE ROCKS USING ARTIFICIAL INTELLIGENCE MODELS

Shengpeng Hao and Thomas Pabst

This article was submitted to *Acta Geotechnica* in April 2021.

Abstract: California bearing ratio (CBR) and resilient modulus are critical factors for designing pavements. The optimal design of mine haul roads can significantly reduce the road maintenance costs and vehicle operating costs, but a lot of laboratory tests are needed to achieve it because of the large-scale network of haul roads at an open pit mine (10~40 km in length) and the heterogeneity of the used crushed waste rocks. However, the measurement of CBR and resilient modulus of crushed waste rocks can be costly and time-consuming which is often prohibitive, especially since service lifetime of haul roads is relatively short. Predictive models exist but typically are empirical regression-based models developed primarily for civil application and are not well adapted to mining applications. The recent development of artificial intelligence techniques makes it possible to develop more efficient models, but many approaches exist and it is not always clear to haul roads designers which to choose. The main objective of this study was therefore to develop, evaluate and compare the performance of multiple linear regression (MLR), k-nearest neighbors (KNN), decision tree (DT), random forest (RF), backpropagation neural network (BPNN), and neuroevolution of augmenting topologies (NEAT) for predicting CBR and resilient modulus of crushed waste rocks based on the experimental data. A series of CBR and repeated load triaxial tests were carried out to measure the CBR and resilient modulus of crushed waste rocks. Eight properties (dry density, compaction energy, fines content, maximum particle

size, C_C, C_U, D_{10}, and D_{60}) were selected as input variables for CBR models based on Pearson correlation analysis. Number of loading cycles, confining pressure, and deviator stress were chosen as the input variables for the resilient modulus models. The effect of model hyperparameters, including number of KNN neighbors, maximum DT depth, number of RF estimators, number of hidden neurons, and number of hidden layers, on prediction performance was also evaluated to determine the optimal architecture of artificial intelligence models. A comparison study showed that the DT and RF models provided better results with coefficient of determination R^2 greater than 0.91 and 0.99 for CBR and resilient modulus, respectively. The performance of MLR models was relatively low because of the limitation of simple linear relationship. The prediction accuracy of KNN and BPNN models for CBR was significantly influenced by the dataset size. The NEAT models showed good generalization and simple structure although their performance was lower than DT and RF models.

Keywords: Crushed waste rocks, CBR, Resilient modulus, Artificial intelligence, Neural network, Multiple linear regression, Decision tree, Random forest, K-nearest neighbors, Model hyperparameter.

9.1 Introduction

Waste rocks, produced by mining operations, have been widely used for road constructions because of their hardness, durability, low-cost and availability (Thompson 2011c). Crushed waste rocks are widely used for the construction of the wearing course of haul roads (Thompson et al. 2019), and the base/subbase layers of highways (Rahman and Erlingsson 2015b). California bearing ratio (CBR) and resilient modulus are fundamental engineering material properties that are widely used for the pavement design (Lekarp et al. 2000a; Coronado et al. 2016; Thompson et al. 2019). A mine

haul road network typically constitutes a length of 10~40 km, and it generally comprises a number of road segments, each with variable traffic volumes and construction and material qualities (Thompson and Visser 2003). Mine haul roads are often designed using empirical CBR method relying heavily on local experience because of short-service-life and low volume of traffic (Tannant and Regensburg 2001; Thompson et al. 2019). However, mechanistic design using resilient modulus is becoming more popular as it contributes to improve the road performance and to significantly reduce road maintenance costs and vehicle operating costs (Thompson et al. 2019). The AASHTO 1993 pavement design procedure and the mechanistic empirical pavement design guide (MEPDG) (NCHRP 2004) have adopted the resilient modulus as the main material property to characterize pavements.

CBR and resilient modulus of soils are generally measured using CBR test and repeated load triaxial (RLT) tests in the laboratory (ASTM D1883 2016; AASHTO T307 2017). However, laboratory experiments as direct approaches for measuring CBR and resilient modulus of waste rocks are costly, time-consuming and require specialized equipment (Seif El Dine et al. 2010; Yin et al. 2017; Ai et al. 2020; Gu, Zhan, et al. 2020; Qi, Cui, Dupla, et al. 2020; Hao and Pabst 2021). Therefore, predicting CBR and resilient modulus of crushed waste rocks accurately and efficiently can be useful to reduce costs and ensure optimal pavement performance.

Artificial intelligence (or machine learning) techniques have shown great promise in geoscience and geoengineering as an analytical alternative to conventional statistical method (Alavi et al. 2016; Lary et al. 2016; Shahin 2016; Wang et al. 2020; Díaz and Tomás 2021; Shen et al. 2021; Zhang et al. 2021) and were therefore considered here to predict CBR and resilient modulus from crushed waste rocks physical properties and stress conditions. Artificial intelligence techniques require less formal statistical training, and multiple different algorithms are available (Ceylan et al. 2014; Alavi et al. 2016). They also frequently require fewer hypotheses and constraints than usually necessary for statistical models, especially when dealing with complex and highly nonlinear data (Karlaftis

and Vlahogianni 2011). In recent years, a number of geotechnical studies have obtained satisfactory results using artificial intelligence techniques for the prediction of CBR and resilient modulus (see Table 9.1). Artificial neural network (ANN) with backpropagation algorithm, i.e. BPNN, was the most widely used technique in these studies because of its simple structure and high fitting accuracy (Ferreira 2017). The prediction performance of these models in the literature was acceptable in terms of coefficient of determination R^2 (> 0.85, Table 9.1). These models were developed for different materials such as cohesive subgrade soils, recycled aggregates, and sands. The input variables for these models are different, but mainly including dry density, water content, confining pressure, deviator stress, gradation parameters, liquid limit, and plastic index.

However, the forecasting performance of BPNN highly depends on the initial connection weights and biases, but the network generates the weights and biases randomly, which may result in poor forecasting (Pan et al. 2019). The architecture of BPNN is an important factor that can influence its computational efficiency and prediction accuracy (Pan et al. 2019). Hecht-Nielsen method (1987) was proposed to confirm the network architecture: if the number of input neurons is m, then the number of hidden neurons should be $2m+1$. However, the effect of number of hidden layers is not taken into account in this method, which limits the performance of the developed network. The determination of the BPNN architecture therefore mainly depends on trial and error methods based on the network performance, which is time-consuming and increases the workload. Although many studies have been conducted to predict CBR and resilient modulus using different artificial intelligence techniques (Table 9.1), some other techniques have not yet been used for this purpose or have rarely been used. It is not always clear which artificial intelligence technique to use and which one would give the best results. Therefore, the purpose of this paper was to propose a comparison of different techniques to make artificial intelligence techniques more accessible.

In this study, the CBR and resilient modulus of crushed waste rocks were measured using CBR and RLT tests, respectively. Six types of artificial intelligence techniques, including multiple linear

regression (MLR), k-nearest neighbors (KNN), decision tree (DT), random forest (RF), backpropagation neural network (BPNN), and neuroevolution of augmenting topologies (NEAT), were used to predict CBR and resilient modulus of crushed waste rocks. Pearson correlation analysis was used to select the suitable factors as the input variables of the artificial intelligence models for CBR. The effect of number of loading cycles and stress condition (i.e. confining pressure and deviator stress) on resilient modulus of crushed waste rocks was analyzed, and these factors were used as the input variables of the artificial intelligence models for resilient modulus. The prediction performance of the developed models for training and testing datasets was evaluated and compared using coefficient of determination R^2 and mean squared error MSE. The more reliable and accurate artificial intelligence models for CBR and resilient modulus of crushed waste rocks was specified and suggested for future studies.

Table 9.1: Some artificial intelligence models for predicting CBR and resilient modulus reported in the literature.

References	Technic	Input	Output	No. of datasets	Material	R^2
Oskooei et al. (2020)	BPNN	BR, DR, SR, OMC, q_u, σ_c, σ_d	Resilient modulus	645	Recycled aggregates	0.96
Ghorbani et al. (2020b)	BPNN	γ_d, w, q_c, f_s	Resilient modulus	124	Cohesive subgrade soils	0.99
Ghorbani et al. (2020a)	ANN-GA	LL, PI, P#200, w_{opt}, w, S_r, qu, σ_3, σ_d	Resilient modulus	283	Cohesive subgrade soils	0.97
Tenpe and Patel (2020)	BPNN	G, S, PI, w_{opt}, γ_{dmax}	CBR	389	Subgrade soil	0.89
Ghorbani et al. (2020b)	BPNN, SVR	N_{FT}, σ_3, σ_d, Mat	Resilient modulus	150	Demolition wastes	0.997
de Souza et al (2020)	BPNN	G, S, silt, clay, color	CBR	1790	Subgrade soil	0.997
Kaloop et al. (2019)	BPNN, LSSVM	RCM, θ/p_a, τ/p_a	Resilient modulus	128	Construction and demolition waste	0.887
Ren et al. (2019)	BPNN	PI, γ_{dmax}, w, No., σ_c, σ_d	Resilient modulus	2120	Subgrade soil	0.90

Saha et al. (2018)	BPNN	P#3/8, P#200, PL, PI, w_{opt}, γ_{dmax}, TMC, g_s, Ψ	Resilient modulus	779	Plastic and nonplastic base materials	0.90
Ghorbani and Hasanzadehshooiili (2018)	BPNN	lime, microsilica, curing days, curing conditions	CBR	90	lime and microsilica	0.99
Sadrossadat et al. (2016)	ANFIS	P#200, LL, PI, w_{opt}, w, S_r, q_u, σ_3, σ_d	Resilient modulus	418	Cohesive Ohio soils	0.973
Erzin and Turkoz (2016)	BPNN	G_s, C_U, C_C, ρ_d, w, Q, Fel, Ca, C, A	CBR	61	Sands	0.939
Kim et al. (2014)	BPNN	P#10, #40, #60, #200, Clay, Swell, Shrink, ρ_{dmax}, w_{opt}, LL, PI, EI, σ_1, σ_3, θ	Resilient modulus	27	Subgrade soils	0.86
Nazzal and Tatari (2013)	ANN-GA	P#4, P#40, w, P#200, w_{opt}, ρ_d, LL, ρ_{dmax}	Resilient modulus	-	Subgrade soils	0.92
Varghese et al. (2013)	BPNN	ρ_{dmax}, w_{opt}, PL, LL	CBR	112	Fine-grained soils	0.93
Taskiran (2010)	BPNN, GEP	LL, PI, ρ_d, w_{opt}, P#200, S, G	CBR	151	Base and subbase material	0.91
Park HI et al. (2009b)	BPNN	ρ_{dmax}, C_U, P#200, σ_3, σ_d	Resilient modulus	272	subgrade soils and subbase materials	0.982

Note: BPNN: backpropagation neural network; ANN: artificial neural network; GA: genetic algorithm; SVR: support vector regression; LSSVM: least square support vector machine; ANFIS: adaptive neuro-fuzzy inference system; GEP: gene expression programming; BR: binder ratio; q_u: unconfined compression strength; σ_c: confining pressure; σ_d: deviatoric stress; ρ_d: dry density; w: gravimetric water content; q_c: cone tip resistance; f_s: sleeve friction resistance; LL: liquid limit; PI: plastic index; P#4, #10, #40, #60, #200, and #3/8: percentage of soil particles passing through #4, #10, #40, #60, #200, and #3/8 sieve, respectively; w_{opt}: optimum water content; S_r: degree of saturation; G: gravel percentage; S: sand percentage; FC: fines content; γ_{dmax}: maximum dry density; RCM: recycled clay masonry; No.: number of F-T cycles; g_s: gradation scale parameter: Ψ: shape parameter; G_s: specific gravity; C_U: coefficient of uniformity; C_C: coefficient of curvature; Q, Fel, Ca, C, and A: the proportions of quartz, feldspar, calcite, corund, and amorphous minerals, respectively; EI: erosion index; θ: bulk stress.

9.2 Data preparation

9.2.1 Study material

The tested crushed waste rocks were obtained from Canadian Malartic Mine, an open pit gold mine

located in the Abitibi region, in Quebec province, Canada and were typical of most hard rock mines (Bussière 2007a; James et al. 2013). The maximum particle size was 25 mm, the material had around 65% of gravel (> 4.75 mm), 30% of sand (75 μm~4.75 mm), and very small amount (< 5%) of fines (< 75 μm), and was classified as a well-graded gravel corresponding to the dual symbols GW-GM (ASTM D2487 2017). Crushed waste rock particles were characterized by angular shape and rough surface texture. The elongation and flakiness index were 38.56±1.62% and 34.95±2.08%, respectively. Crushed waste rocks contained a small fraction of sulfides (<1% of pyrite) but was considered non-acid generating because of a significant buffering capacity (Tremblay and Hogan 2001; Golder 2019).

9.2.2 CBR database

The database used to train and test artificial intelligence models for CBR comprised 39 results from a study conducted by Laverdière (2019), on crushed waste rocks from Canadian Malartic Mine (see Table 9.2). The database was composed of ten properties, namely the dry density ρ_d, coefficient of uniformity C_U, coefficient of curvature C_C, D_{10}, D_{30}, D_{60}, compaction energy CE, fines content FC, maximum particle size D_{max}, water content WC, and the measured CBR (Table 9.2).

Correlation analysis was conducted between the ten specimen properties and CBR values of crushed waste rocks using Pearson correlation coefficient r analysis (Table 9.3). Pearson correlation coefficient r is a statistical metric that measures the strength and direction of a linear relationship between two variables, which is one of the most widely used measure of relationship for artificial intelligence models (Lee Rodgers and Nicewander 1988; Erzin and Turkoz 2016; Lee et al. 2021). Pearson correlation coefficient r ranges from +1 to -1. A value of +1 indicates that the two variables are completely linearly correlated. On the other hand, a value of 0 indicates not linearly correlated at all. A value of -1 implies that the two variables are completely negatively linearly correlated. The following criterion for values of $|r|$ between 0 and 1 proposed by Smith

(1986) were used in this study:

$|r| \geq 0.8$: strong correlation exists between the two variables;

$0.2 < |r| < 0.8$: correlation exists between the two variables;

$|r| \leq 0.2$: weak correlation exists between the two variables.

The results showed that eight properties (ρ_d, CE, FC, C_C, C_U, D_{10}, D_{60}, and D_{max}) had significant effects on CBR of crushed waste rocks. ρ_d had the highest r value (0.90), indicating there was a strong correlation between ρ_d and CBR. It was followed by CE (0.62), FC (0.49), C_C (0.48), C_U (0.44), D_{10} (-0.41), D_{60} (0.35), and D_{max} (0.35), which indicated that these properties could affect the CBR value of crushed waste rocks (Table 9.3). However, water content WC and D_{30} had relatively weak correlations with CBR ($|r| \leq 0.2$) indicating that the effect of these two properties on CBR was limited. Therefore, only the eight strongly correlated properties were selected as input variables of the CBR artificial intelligence models in this study.

Table 9.2: Database for the training and testing of artificial intelligence models for CBR of crushed waste rocks; ρ_d: dry density, kg/m^3; C_U: coefficient of uniformity, -; C_C: coefficient of curvature, -; D_{10}, D_{30}, D_{60}: effective size of particles corresponding to 10%, 30%, 60% finer in the particle size distribution, mm; CE: compaction energy, kN-m/m^3; FC: fines content, %; D_{max}: maximum particle size, mm; WC: water content, %; CBR: California bearing ratio, %.

ID	ρ_d	CE	FC	C_C	C_U	D_{10}	D_{60}	D_{max}	WC	D_{30}	CBR
-	kg/m^3	kN-m/m^3	%	-	-	mm	mm	mm	%	mm	%
1	2054	600	5.8	3.20	20.00	0.5	10	25	6	4	48
2	2100	600	5.8	3.20	20.00	0.5	10	25	6	4	68
3	2090	2700	5.8	3.20	20.00	0.5	10	25	3	4	67
4	2119	2700	5.8	3.20	20.00	0.5	10	25	3	4	78
5	2199	2700	5.8	3.20	20.00	0.5	10	25	5.5	4	104
6	2231	2700	5.8	3.20	20.00	0.5	10	25	5.5	4	125
7	2194	2700	5.8	3.20	20.00	0.5	10	25	7	4	89

8	2220	2700	5.8	3.20	20.00	0.5	10	25	7	4	128
9	2195	2700	5.8	3.20	20.00	0.5	10	25	7	4	125
10	2285	2700	5.8	3.20	20.00	0.5	10	25	7.3	4	119
11	2232	2700	5.8	3.20	20.00	0.5	10	25	7.3	4	95
12	2286	3900	5.8	3.20	20.00	0.5	10	25	6	4	205
13	2271	3900	5.8	3.20	20.00	0.5	10	25	6	4	230
14	2321	3900	5.8	3.20	20.00	0.5	10	25	6.3	4	159
15	2300	3900	5.8	3.20	20.00	0.5	10	25	6.3	4	115
16	2034	600	5.8	4.00	17.81	0.32	5.7	10	7	2.7	52
17	2049	600	5.8	4.00	17.81	0.32	5.7	10	7	2.7	47
18	2259	2700	5.8	4.00	17.81	0.32	5.7	10	8	2.7	122
19	2213	2700	5.8	4.00	17.81	0.32	5.7	10	8	2.7	92
20	2235	3900	5.8	4.00	17.81	0.32	5.7	10	6	2.7	132
21	2228	3900	5.8	4.00	17.81	0.32	5.7	10	6	2.7	126
22	2190	2700	2	1.95	12.20	0.82	10	25	6.5	4	142
23	2205	2700	2	1.95	12.20	0.82	10	25	6.5	4	127
24	2264	2700	4	2.29	14.29	0.7	10	25	6.5	4	138
25	2234	2700	4	2.29	14.29	0.7	10	25	6.5	4	149
26	2308	2700	6	3.40	21.28	0.47	10	25	6.5	4	170
27	2316	2700	6	3.40	21.28	0.47	10	25	6.5	4	160
28	2351	2700	8	5.48	40.00	0.25	10	25	6.5	3.7	197
29	2380	2700	8	5.48	40.00	0.25	10	25	6.5	3.7	170
30	2239	600	10	18.25	133.33	0.075	10	25	6.5	3.7	88
31	2209	600	10	18.25	133.33	0.075	10	25	6.5	3.7	110
32	2384	2700	10	18.25	133.33	0.075	10	25	6.5	3.7	197
33	2394	2700	10	18.25	133.33	0.075	10	25	6.5	3.7	225
34	2531	3900	10	18.25	133.33	0.075	10	25	6.5	3.7	267
35	2541	3900	10	18.25	133.33	0.075	10	25	6.5	3.7	250
36	2380	2700	12	36.30	333.33	0.03	10	25	6.5	3.3	174
37	2395	2700	12	36.30	333.33	0.03	10	25	6.5	3.3	217
38	2399	2700	14	39.20	500.00	0.02	10	25	6.5	2.8	180
39	2399	2700	14	39.20	500.00	0.02	10	25	6.5	2.8	205

Table 9.3: Pearson correlation coefficient between the specimen properties and CBR of crushed waste rocks.

Material properties	*r*

Dry density (ρ_d), kg/m^3	0.90
Compaction energy (CE), kN-m/m^3	0.62
Fines content (FC), %	0.49
Coefficient of curvature (C_C)	0.48
Coefficient of uniformity (C_U)	0.44
10 % of the soil particles finer than this size (D_{10}), mm	-0.41
60 % of the soil particles finer than this size (D_{60}), mm	0.35
Maximum particle size (D_{max}), mm	0.35
Water content (WC), %	0.13
30 % of the soil particles finer than this size (D_{30}), mm	0.04

9.2.3 Resilient modulus database

The resilient modulus of crushed waste rocks was measured using repeated load triaxial (RLT) tests. The tests followed the European Standard 13286-7 (2004) where two sets of stress levels (low stress level (LSL)) and high stress level (HSL)), are divided into five sequences, with each sequence containing 5 or 6 stress paths with a constant confining pressure and different deviator stresses. Each stress path was applied for 10000 cycles. Haversine loading pulses with a frequency of 0.3 Hz with no rest period were applied for RLT tests, and these tests were carried out under free drainage conditions. Specimens (300 mm in height and 150 mm in diameter) were prepared using modified compaction effort (i.e., 2700 kN-m/m^3) and an initial gravimetric water content w = 4%. A total of 2320 data sets were selected from the RLT test results to train and test the artificial intelligence models for resilient modulus. For each stress path, the measured resilient modulus was selected at each 300 cycles from the 100th to 10000th loading cycles in this study.

The effect of number of loading cycles and stress condition (confining pressure and deviator stress) on resilient modulus was studied to select the input variables of artificial intelligence models.

For some stress paths, the influence of number of loading cycles on resilient modulus was noteworthy, while its influence was relatively limited for other stress paths (Figure 9.1). The variation of resilient modulus with number of loading cycles was relatively higher for the sequence

1 for LSL than for other sequences. For example, the resilient modulus increased from around 112 to 135 MPa (+20%), from 100 to 138 MPa (+38%), from 133 to 165 MPa (+24%) when number of loading cycles increased from 100 to 10000 for stress path 1, 2, and 4 in sequence 1 for LSL, respectively. However, for stress path 3 in sequence 1, the resilient modulus decreased around 30% when the number of loading cycles increased from 100 to 10000. The variation of resilient modulus with number of loading cycles in sequence 1 for HSL was lower than 10%, which was relatively smaller than that for LSL. The high variation of resilient modulus with the number of loading cycles in sequence 1 in LSL could be attributed to the relatively high strain measurement errors under low amplitudes (Gu, Ye, et al. 2020), especially considering that only one LVDT was used to record vertical deformation. For some stress paths, such as stress path 6 in sequence 4 in LSL, the increase of the loading cycles led to a slight increase of the resilient modulus (+7%).

The resilient modulus of crushed waste rocks showed an increasing trend with the increase of confining pressure (Figure 9.1). For example, the resilient modulus for sequence 5 (150 kPa confining pressure) was around 15% greater than that for sequence 4 (100 kPa confining pressure) for HSL and under the same deviator stress. This finding was consistent with the conclusions of other researches, which have shown that the resilient modulus increases with confining pressure (Park et al. 2009a; Liu et al. 2019).

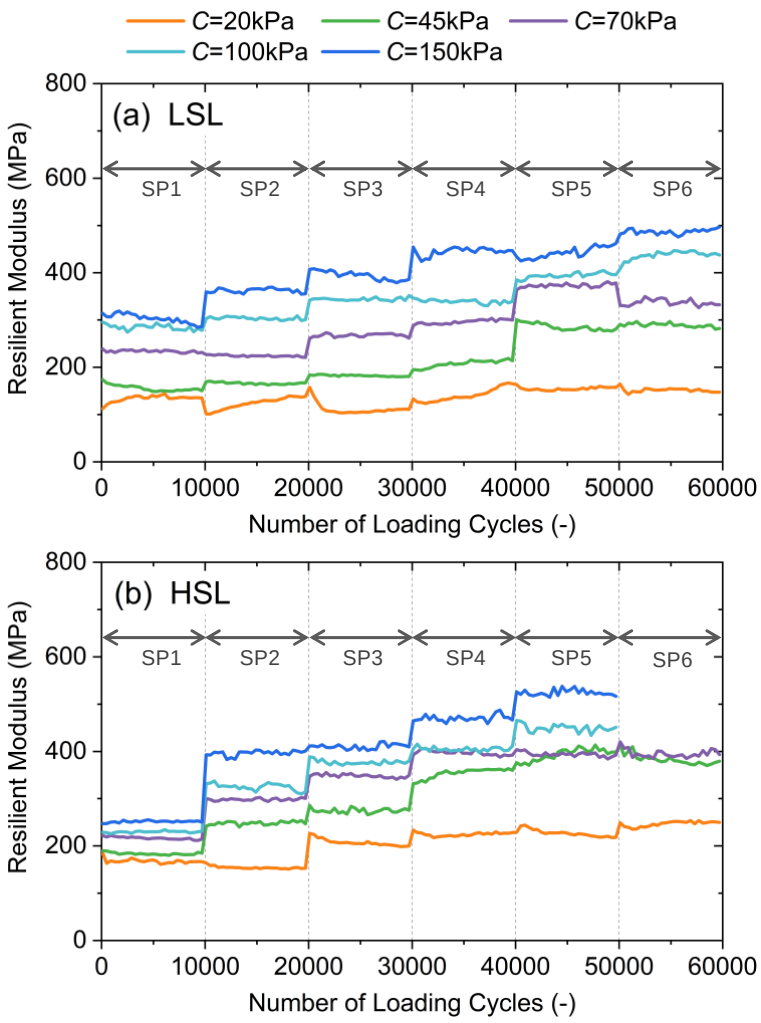

Figure 9.1: The evolution of resilient modulus with number of loading cycles for each stress path (SP) of five sequences with different confining pressures *C* for (a) LSL and (b) HSL.

An increase of deviator stress also resulted in the increase of the resilient modulus, for both low and high confining pressures (Figure 9.2). For example, the resilient modulus increased from around 130 to 250 MPa with the deviator stress increasing from 20 to 200 kPa when the confining pressure was 20 kPa (Figure 9.2(a)) and increased from around 300 to 520 MPa when the deviator stress increased from 100 to 600 kPa under 150 kPa confining pressure (Figure 9.2(e)). This also was observed by others, which showed an increase of resilient modulus of crushed limestone

aggregates with deviator stress (Khedr 1985).

Therefore, number of loading cycles *N*, confining pressure *C*, and deviator stress *D* were selected as the input variables of artificial intelligence models for resilient modulus. Other properties of crushed waste rocks such as gradation parameters, water content, and compaction energy could also influence resilient modulus but were not selected as input variables because they were identical for the repeated load triaxial tests conducted in this study.

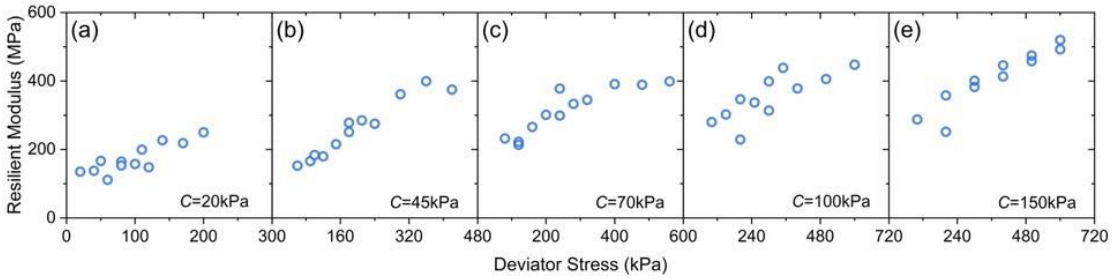

Figure 9.2: Resilient modulus versus deviator stress *D* under different confining pressure *C* (a) 20 kPa, (b) 45 kPa, (c) 70 kPa, (d) 100 kPa, and (e) 150 kPa; the resilient modulus point was the final value after 10000 loading cycles for each stress path.

9.2.4 Data preprocessing

The input variables were normalized to make learning easier for artificial intelligence models, especially for neural networks (BPNN and NEAT) (Sola and Sevilla 1997). The Z-Score normalization method was used in this study (Jain et al. 2005):

$$X_i^* = \frac{X_i - \mu}{\sigma} \tag{9.1}$$

Where X_i^* is the normalized input values; X_i is the experimental input values; μ is the mean value of the input feature and σ is the standard deviation of the input feature.

The experimental data were split into a training dataset and a testing dataset. The artificial intelligence models were trained on the training dataset and then tested on the testing dataset to verify its generalization capability. In this study, 70% of the total experimental data were selected randomly as the training dataset, while the remaining 30% data were used as the testing dataset.

9.3 Artificial intelligence techniques

Six different types of algorithms were used and compared to develop artificial intelligence models for predicting CBR and resilient modulus of crushed waste rocks, namely multiple linear regression (MLR), k-nearest neighbors (KNN), decision tree (DT), random forest (RF), backpropagation neural network (BPNN), and neuroevolution of augmenting topologies (NEAT). All these models were developed using Python.

9.3.1 Multiple linear regression (MLR)

Multiple linear regression (MLR) is one of the most popular techniques for predictive modeling (Tso and Yau 2007; Yilmazkaya et al. 2018) and can be used to predict an output as a linear function of input variables (Tso and Yau 2007). A MLR model with more than one independent variable can be written as:

$$y=a_1x_1+a_2x_2+\cdots+a_nx_n+b \tag{9.2}$$

Where y: the output variable; a_1~a_n:the regression parameters; x_1~x_n: the input variables; and b: the random error term.

The MLR model was fitted using the least squares method.

9.3.2 K-nearest neighbors (KNN)

K-nearest neighbors (KNN) is one of the most widely used machine learning techniques for classification and regression because of its simplicity, intuitiveness, and ease of implementation (Al-Qahtani and Crone 2013). KNN regression was used to predict CBR and resilient modulus of crushed waste rocks in this study. KNN regression is based on feature similarity, and new data points are assigned values according to how close it is to the training data (Mahmoodzadeh et al. 2020).

The Minkowski Distance Function was used for KNN regression model. The effect of the number of neighbors in KNN model was also investigated.

9.3.3 Decision tree (DT)

Decision tree (DT) is a technique that can stimulate trees for predicting both classification and regression targets (Pekel 2020). The objective of DT is to build the decision rules that can be used to predict the relations between the input variables and an objective variable. Generally, a DT structure is composed of a root node (containing all data), a set of internal nodes (splits) and a set of terminal nodes (leaves) (Xu et al. 2005). DT regression uses a fast divide and conquer greedy algorithm that recursively splits the data into smaller parts (Pekel 2020). The processing is carried out by moving down the tree until the terminal node is reached, which is known as top-down approach (Xu et al. 2005; Wang et al. 2016). The maximum DT depth determines how deep the tree can grow, which can influence the prediction performance significantly (Pekel 2020).

9.3.4 Random forest (RF)

Random forest (RF) has been successfully applied for both classification and regression in many

fields because of the ability of well approximating variables with nonlinear relationships (Li et al. 2018). RF consists of an ensemble of individual decision trees, which act as regression functions on their own, and the final output of the RF regression is the average of the outputs of all decision trees (Breiman et al. 1984; Breiman 1999). RF regression is therefore an extension of the DT regression with usually a better prediction performance.

9.3.5 Backpropagation neural network (BPNN)

The feedforward backpropagation neural network (BPNN) is one of the most widely used types of neural network in engineering applications because of the characteristics of simple structure and high fitting accuracy (Ferreira 2017). BPNN typically consists of input, hidden, and output layers (Ferentinou and Fakir 2018; Mukherjee et al. 2020). The backpropagation algorithm operates by propagating the input signal from the input layer through the output layer, while the error is propagated from the output layer to the input layer to calculate the weight correction and maximize the accuracy of the neural network (Sakellariou and Ferentinou 2005; Su and Fu 2020). The number of neurons in the input layer is equal to the number of the input variables. The rectified linear unit activation function (ReLU(x)=max(x,0)) was adopted for hidden layers in this study because of its simplicity of implementation and typically good performance (LeCun et al. 2015; Lin et al. 2020). The architecture of BPNN (i.e. the number of hidden neurons and hidden layers) has significant influence on the network performance (Sinha et al. 2010), and was therefore also evaluated in this study.

9.3.6 Neuroevolution of augmenting topologies (NEAT)

Stanley and Miikkulainen (2002) proposed neuroevolution of augmenting topologies (NEAT) approach to evolve neural networks using genetic algorithm (i.e. selection, crossover, and mutation

of neural networks). NEAT method has the ability to evolve and optimize the network's topology (i.e. architecture) and connection weights simultaneously and automatically (Stanley and Miikkulainen 2002). The topology of NEAT network can be mutated by either adding a new connection or adding a new neuron (Stanley and Miikkulainen 2002).

Some studies have proved that NEAT is a powerful and efficient technique to make neural network evolve to solve difficult control and sequential decision tasks (e.g., pole balancing, video games, and muscular-skeletal arm) (Stanley and Miikkulainen 2002; Stanley et al. 2005; Hausknecht et al. 2014; Poulsen et al. 2017; Wen et al. 2017; Yuksel 2018), but it has rarely been used in geotechnical engineering. In this study, NEAT initiated the topology only with input and output layers and complexified the network topology over 30000 generations. System configuration and parameters for the NEAT models are summarized in Appendix.

9.3.7 Evaluation of models' performance

Coefficient of determination R^2 (Eq. 9.3) and mean squared error MSE (Eq. 9.4) are widely used to assess the prediction accuracy of artificial intelligence models for regression tasks (Zhang and Goh 2013; Ghorbani, Arulrajah, Narsilio, and Horpibulsuk 2020a; Hanandeh et al. 2020; Lee et al. 2021), and were also used to evaluate the performance of the developed models in this study:

$$\mathrm{MSE}=\frac{1}{n}\sum_{i=1}^{n}(y_{\mathrm{expt}}-y_{\mathrm{pred}})^2 \tag{9.3}$$

$$R^2=1-\frac{\sum_{i=1}^{n}(y_{\mathrm{expt}}-y_{\mathrm{pred}})^2}{\sum_{i=1}^{n}(y_{\mathrm{expt}}-\overline{y_{\mathrm{expt}}})^2} \tag{9.4}$$

Where y_{expt}: value of CBR and resilient modulus measured from experimental results; y_{pred}: predicted value of CBR and resilient modulus from artificial intelligence models; $\overline{y_{\mathrm{expt}}}$: the mean value of experimental CBR and resilient modulus; n: the total number of data sets.

MSE value is always positive and the closer it is to zero, the more accurate the prediction is (Chen

2010; Chollet 2018; Vidal and Kristjanpoller 2020). Coefficient of determination R^2 is comprised between 0 and 1, and a value closer to 1 means that the prediction accuracy is higher.

9.4 Results

9.4.1 MLR model

MLR models were developed to predict CBR, and resilient modulus of crushed waste rocks based on eight and three inputs variables, respectively (Eq. 9.5 and 9.6). The MLR models were explicit equations, which make them convenient to use for predicting CBR and resilient modulus.

$$CBR=0.33\ \rho_d+1.426\ C_C-26.198\ FC+3.659\ D_{max}+1.049\ D_{60}-211.002\ D_{10}+0.116\ C_U+0.016\ CE-502.062 \quad 9.5$$

$$M_R=-4.791\times10^{-4}\ N+0.958\ C+0.368\ D+148.758 \quad 9.6$$

Where CBR: California bearing ratio, %; ρ_d: dry density, kg/m^3; C_C: coefficient of curvature, -; FC: fines content, %; D_{max}: maximum particle size, mm; D_{60}: effective size of particles corresponding to 60% finer in the particle size distribution, mm; D_{10}: effective size of particles corresponding to 10% finer in the particle size distribution, mm; C_U: coefficient of uniformity, -; CE: compaction energy, kN-m/m^3; M_R: resilient modulus, MPa; N: number of loading cycles, -; C: confining pressure, kPa ; D: deviator stress, kPa.

These models were developed based on a training dataset (70% of all experimental data), and their generalization capacity was validated using a testing dataset (remaining 30% of experimental data). The coefficient of determination R^2 of MLR model for CBR was 0.79 and 0.88 for training and testing datasets, respectively; and the MSE was lower than 600 for both training and testing datasets (Figure 9.3(a)). The prediction accuracy of MLR model for resilient modulus was higher than for

CBR, and the prediction performance for training and testing datasets was around 0.83 of coefficient of determination (Figure 9.3(b) and (c)). Relations between input and output variables are linear in MLR models, which is a limitation in this case (Yilmazkaya et al. 2018). Indeed, the relation between resilient modulus and stress variables is nonlinear (Lekarp et al. 2000a), which can explain the relatively low prediction performance ($R^2 < 0.85$).

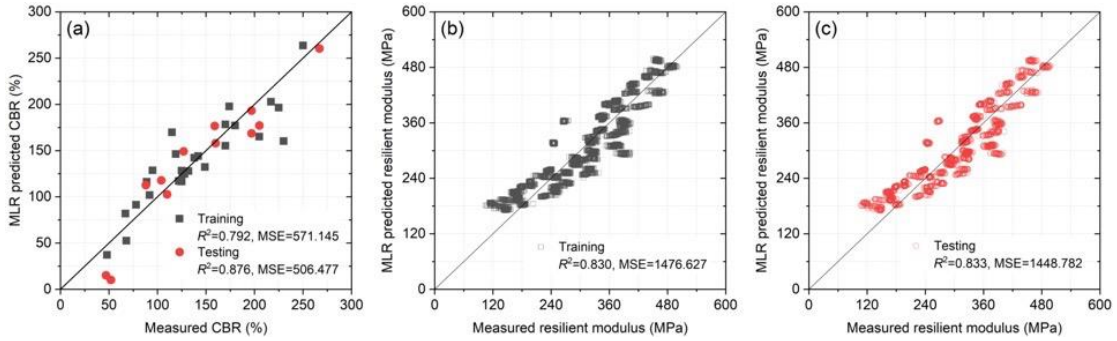

Figure 9.3: Comparison between measured and predicted (a) CBR and (b, c) resilient modulus M_R obtained using MLR model. Results for both training and testing are shown; R^2 and MSE indicate the model prediction performance.

9.4.2 KNN model

Number of neighbors affected the KNN model performance significantly for both CBR and resilient modulus (Figure 9.4(a) and (b)). When the neighbors in CBR KNN model increased from 1 to 4, the prediction error MSE increased from around 0 to 1100, and from around 450 to 1100 for training and testing datasets, respectively. When the neighbors increased to 5, MSE value decreased slightly (Figure 9.4(a)). For resilient modulus, MSE value increased with the number of KNN neighbors for training dataset, while the lowest MSE value was obtained when the number of neighbors was 2 (Figure 9.4(b)). In this study, the number of neighbors was therefore set as 1 and 2 for CBR and resilient modulus KNN models, respectively.

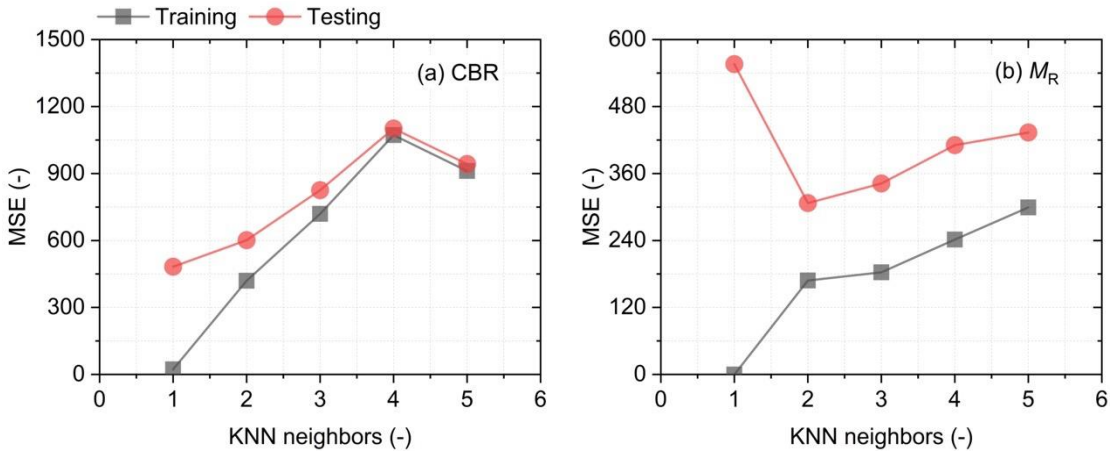

Figure 9.4: Effect of number of KNN neighbors on KNN model for (a) CBR and (b) resilient modulus M_R.

The developed KNN model could predict CBR very satisfactorily for training dataset ($R^2 > 0.99$, MSE < 25), but the accuracy for testing dataset was relatively lower ($R^2 = 0.86$, MSE < 500) (Figure 9.5(a)). The KNN model for resilient modulus showed well adapted for prediction with coefficients of determination R^2 greater than 0.95 for both training and testing datasets (Figure 9.5(b) and (c)). The proposed KNN model was therefore very suitable to compute resilient modulus as a function of number of loading cycles N, confining pressure C, and deviator stress D.

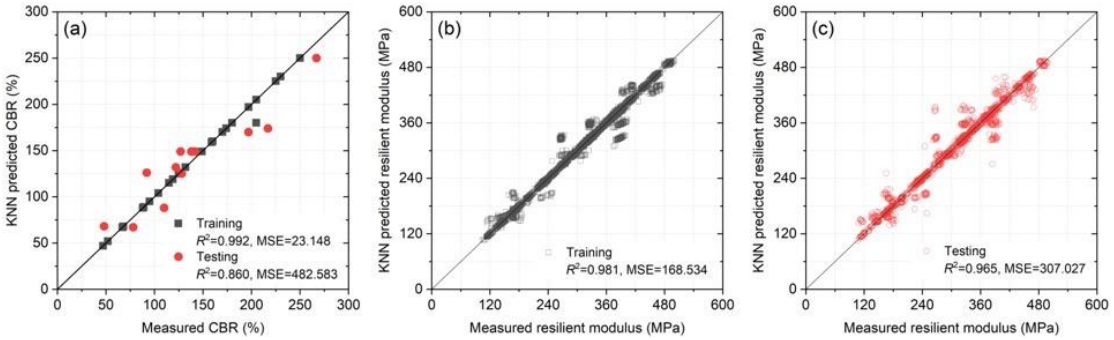

Figure 9.5: Comparison between measured and predicted (a) CBR and (b, c) resilient modulus M_R obtained using KNN model. Results for both training and testing are shown; R^2 and MSE indicate the model prediction performance.

9.4.3 DT model

The performance of DT model increased significantly with the maximum depth but tended to an optimum when the maximum depth reached 7 and 8 for CBR and resilient modulus, respectively (Figure 9.6(a) and (b)). Therefore, the maximum depth was 7 and 8 for CBR and resilient modulus DT models, respectively.

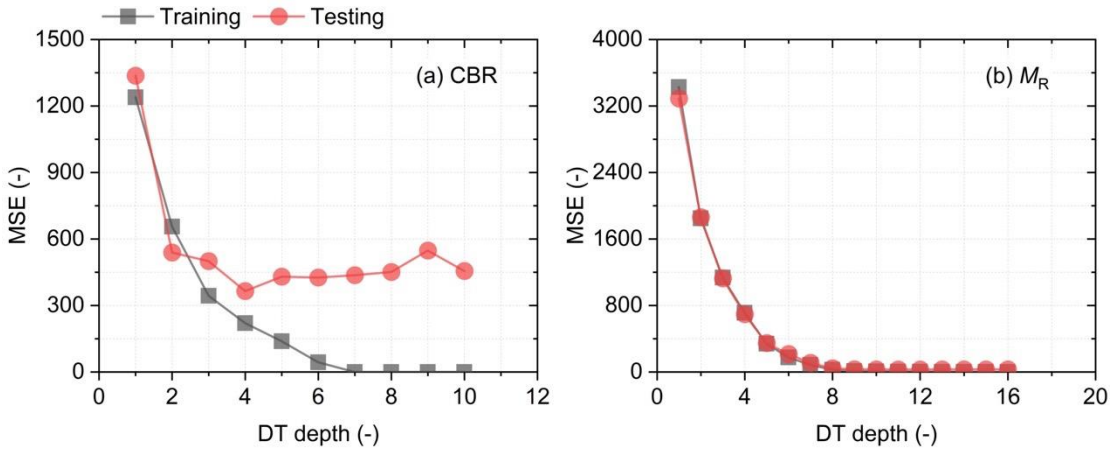

Figure 9.6: Effect of DT depth on DT model for (a) CBR and (b) resilient modulus M_R.

The developed DT model for CBR consisted of seven depths, including the root node (the topmost decision node), internal nodes (splits, i.e. middle decision nodes), and terminal nodes (leaves, i.e. the final decision node) (Figure 9.7). Density ρ_d was the most used criterion in the model, indicating that it was the most important factor influencing the CBR value of crushed waste rocks. The DT

model for resilient modulus, was characterized by a maximum depth of twelve. The deviator stress *D* and confining pressure *C* were the most important factors for predicting the resilient modulus. The DT model for resilient modulus is not presented in this paper because of its quite large size.

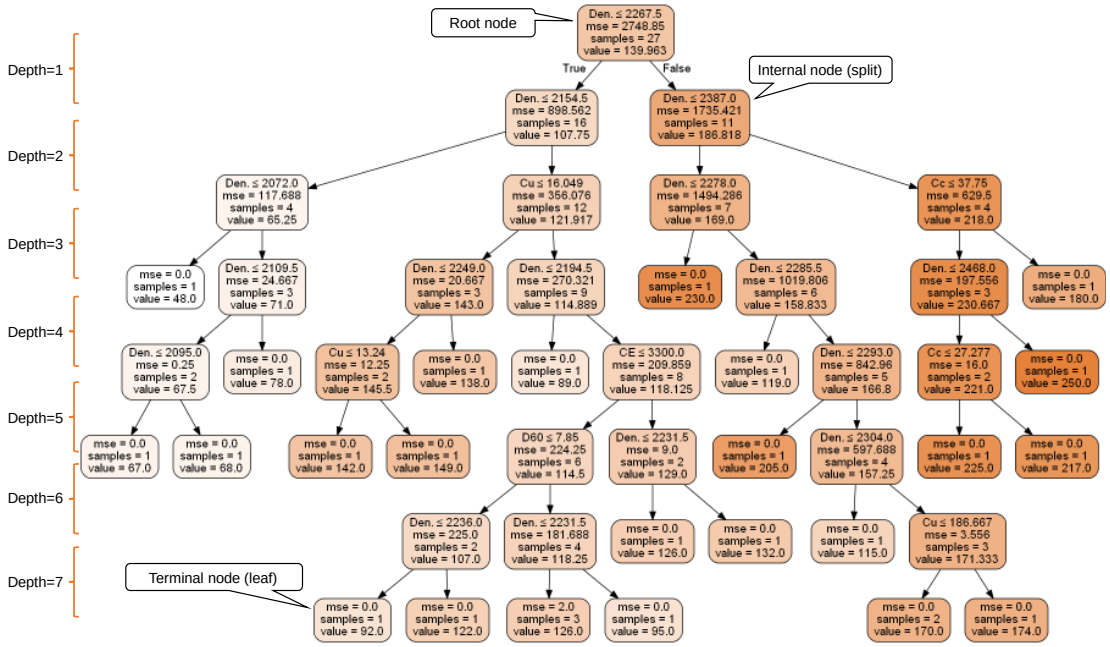

Figure 9.7: Structure of the developed DT model to predict CBR. The model consists of seven depths. The information in each box includes criterion, prediction error (MSE), number of samples which satisfied the criterion, and the corresponding predicted CBR. The deepness of orange color for each box corresponds to the CBR value.

The DT model showed good ability in CBR prediction for both training and testing datasets ($R^2 > 0.91$, MSE < 400, Figure 9.8(a)). The DT model could predict the resilient modulus of crushed waste rocks satisfactorily with $R^2 > 0.99$ and MSE < 35 (Figure 9.8(b) and (c)). The developed DT models for CBR and resilient modulus showed good generalization since the prediction accuracy for training and testing datasets were close.

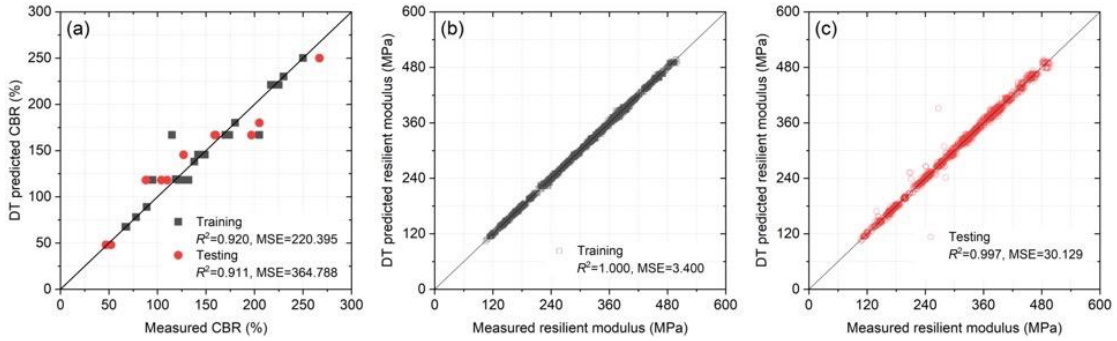

Figure 9.8: Comparison between measured and predicted (a) CBR and (b, c) resilient modulus M_R obtained using DT model. Results for both training and testing are shown; R^2 and MSE indicate the model prediction performance.

9.4.4 RF model

The number of estimators in RF model for CBR significantly affected prediction performance, and the prediction MSE decreased from around 450 to 350, and from 300 to 200 with estimators increasing from 1 to 70 for training and testing datasets, respectively (Figure 9.9(a)). However, this influence became limited when the number of estimators was higher than 70. The effect of number of estimators in RF model for resilient modulus showed similar trend and became insignificant when the number of estimators was greater than 100 (Figure 9.9(b)). In this study, the RF models consisted of 70 and 100 estimators for CBR and resilient modulus, respectively.

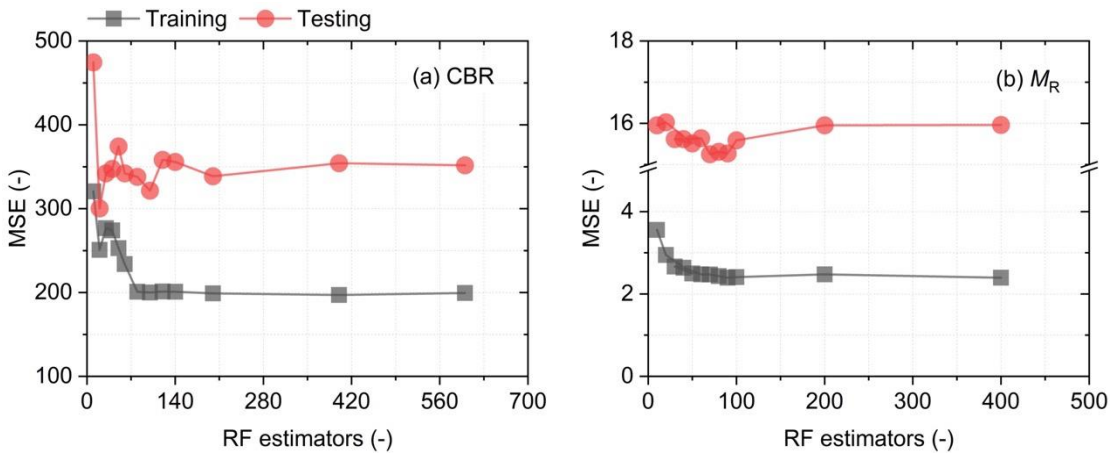

Figure 9.9: Effect of number of estimators on RF model for (a) CBR and (b) resilient modulus M_R.

The developed RF model for CBR had relatively high performance with coefficient of determination R^2 greater than 0.92 for both training and testing datasets (Figure 9.10(a)). The RF model for resilient modulus had superior performance with coefficient of determination R^2 higher than 0.99, and MSE lower than 20 for both training and testing datasets (Figure 9.10(b) and (c)). Therefore, the developed RF models could predict CBR and resilient modulus of crushed waste rocks with a high degree of accuracy. In addition, the model performance for training and testing datasets was close, indicating these RF models had satisfactorily generalization capacity.

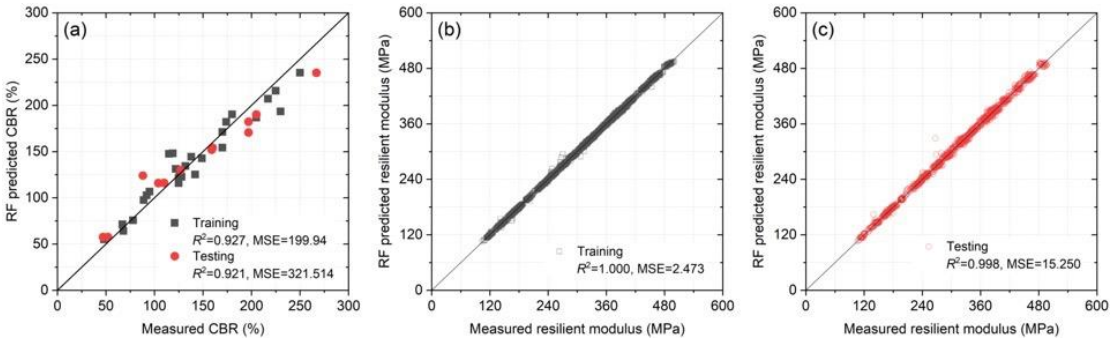

Figure 9.10: Comparison between measured and predicted (a) CBR and (b, c) resilient modulus M_R obtained using RF model. Results for both training and testing are shown; R^2 and MSE indicate the

model prediction performance.

9.4.5 BPNN model

The performance of BPNN model for both CBR and resilient modulus was affected by the number of hidden neurons and layers (Figure 9.11).

For CBR training dataset, the MSE fluctuated when the number of hidden neurons was smaller than 15 (one hidden layer), but MSE reached a relatively low and constant value (around 450) when the number of hidden neurons exceeded 15 (Figure 9.11(a)). For CBR testing dataset, the model performance showed similar trend, but the critical number of hidden neurons was 30. The MSE for training dataset decreased as the number of hidden layers increased until 6 (Figure 9.11(b)). However, the MSE for testing dataset variated significantly with the number of hidden layers, and it reached the lowest value of 700 when the model had 5 hidden layers. Therefore, the BPNN for CBR model was developed with 5 hidden layers and 30 hidden neurons per layer in this study.

For resilient modulus, the MSE value decrease from 1480 to 1450 (-2%) when the number of hidden neurons was smaller than 40, and then increased for greater number of neurons for both training and testing datasets (Figure 9.11(c)). The MSE decreased from around 400 to 100 as the number of hidden layers increased from 2 to 5 for both training and testing datasets. However, the performance difference between models with 5 or more hidden layers was very limited (Figure 9.11(d)), and the number of hidden neurons and hidden layers in resilient modulus model was therefore set as 40 and 5, respectively.

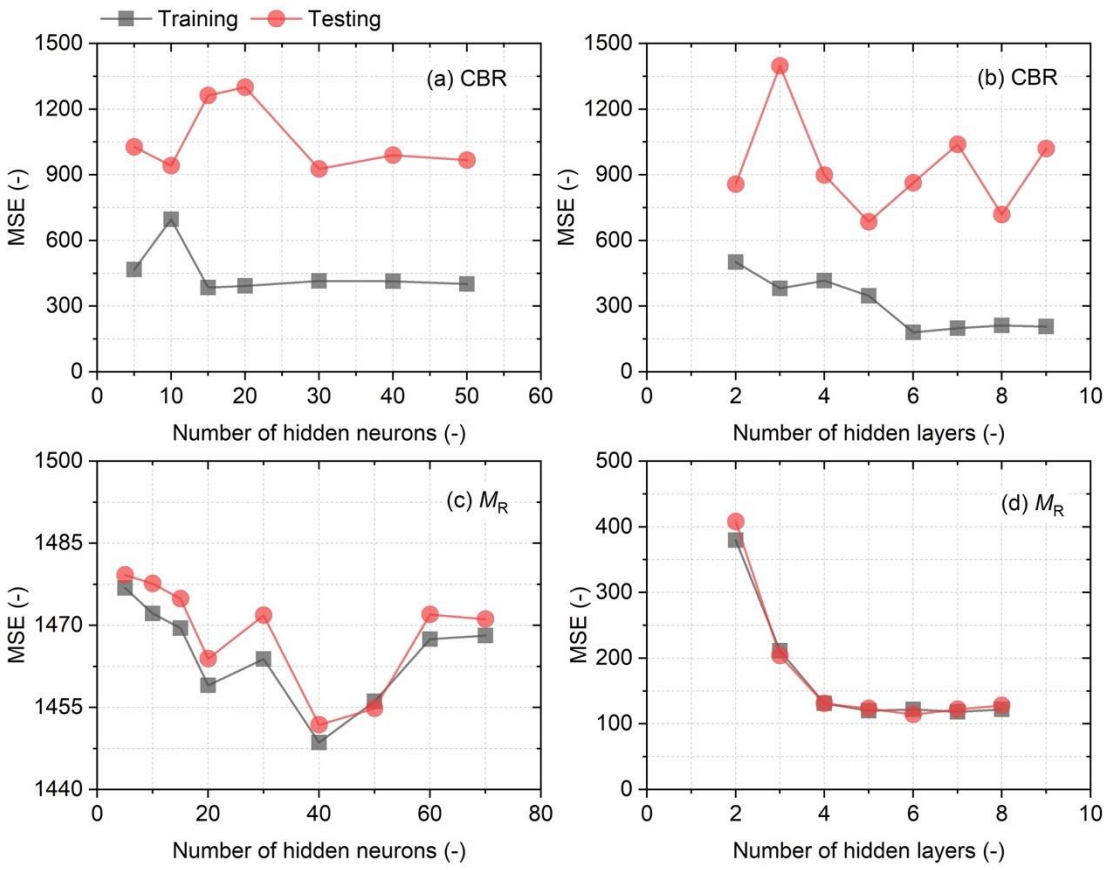

Figure 9.11: Effect of number of hidden neurons and hidden layers on BPNN model for (a, b) CBR and (c, d) resilient modulus M_R.

The developed BPNN model for CBR consisted of eight input neurons (ρ_d, CE, FC, C_C, C_U, D_{10}, D_{60}, and D_{max}), five hidden layers (30 neurons per layer), and one output neuron for CBR (Figure 9.12(a)). The architecture of BPNN model for resilient modulus M_R contained three input neurons (number of loading cycles N, confining pressure C, and deviator stress D), five hidden layers (40 neurons per layer), and one output neuron for resilient modulus M_R (Figure 9.12(b)).

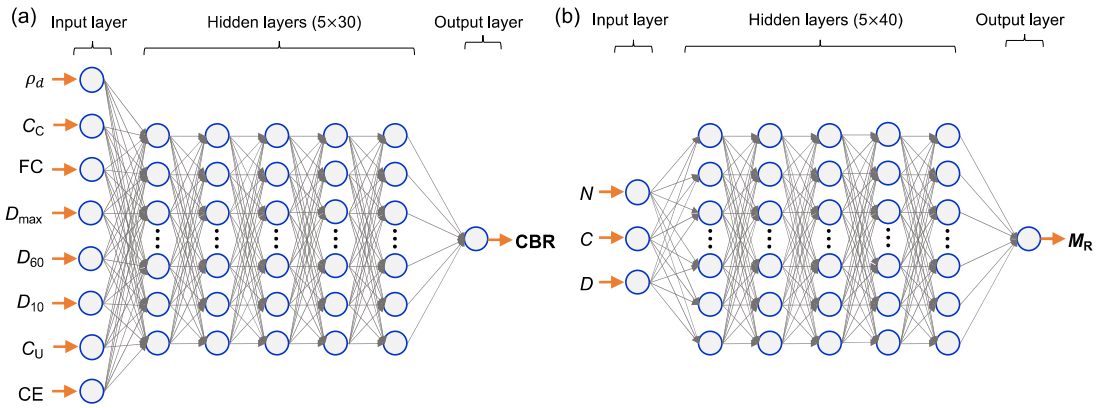

Figure 9.12: The architecture of the developed BPNN model for (a) CBR and (b) resilient modulus M_R of crushed waste rocks.

For CBR, the performance of BPNN model for testing dataset (R^2 = 0.60) was significantly lower than training dataset (R^2 = 0.84), indicating that the overfitting problem occurred in this model (Figure 9.13(a)). The measured and predicted resilient modulus from BPNN model exhibited strong correlation with $R^2 > 0.98$ and MSE < 155 for both training and testing datasets, and this model showed good generalization. However, there were still few scatters away from the best prediction line for training and testing datasets (Figure 9.13(b) and (c)).

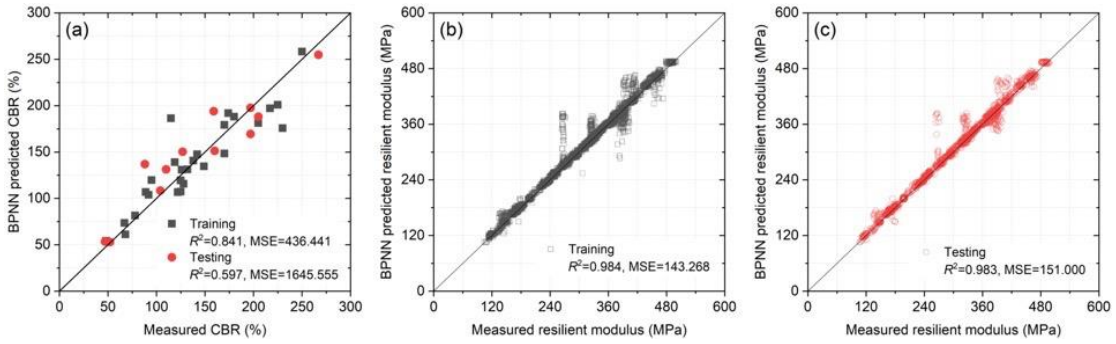

Figure 9.13: Comparison between measured and predicted (a) CBR and (b, c) resilient modulus M_R obtained using BPNN model. Results for both training and testing are shown; R^2 and MSE indicate

the model prediction performance.

9.4.6 NEAT model

The evolved best network by NEAT after 30000 generations progress was the one with eight hidden neurons, and four hidden neurons for CBR and resilient modulus, respectively (Figure 9.14). There was no obvious layer boundary in the NEAT models, and the input variables could be connected linearly/directly to the output neuron. In contrast to the stiff connection mode between layers and between neurons in BPNN models (see Figure 9.12), these NEAT models showed flexible connections between neurons (Figure 9.14). This advantage in network connections over the BPNN increases the efficiency and utilization of each neuron, which reduces the complexity of NEAT network. Number of loading cycles *N* as one of the input variables was not connected to the rest of the network (Figure 9.14(b)), implying that it was not particularly important for predicting resilient modulus of crushed waste rocks. However, it was still possible that given more time generations to evolve, the best performing network may connect the input variable *N* to other neurons.

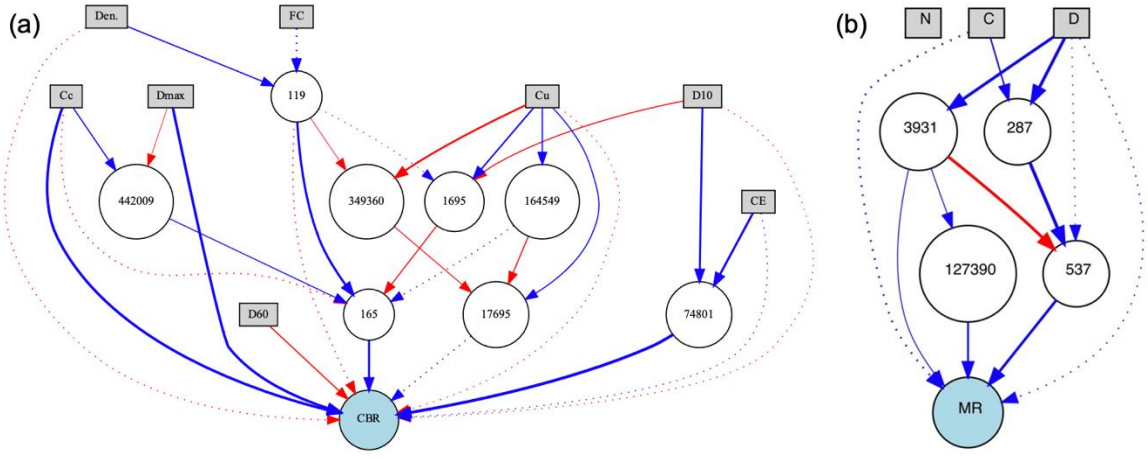

Figure 9.14: The architecture of the NEAT model for (a) CBR and (b) resilient modulus M_R of crushed waste rocks. Dark grey boxes represent input neurons; white circles represent hidden

neurons with the corresponding ID number; and the dark blue circle represents the output neuron (i.e. CBR and resilient modulus M_R). The thickness of the connection corresponds to the magnitude of the weight. Blue connections are positive, and red connections are negative of weight. The dotted lines represent disabled connections.

The NEAT model for CBR showed acceptable performance with coefficient of determination R^2 higher than 0.82 for both training and testing datasets (Figure 9.15(a)). The NEAT model also could predict resilient modulus with coefficient of determination R^2 higher than 0.90 and MSE lower than 850 for both training and testing datasets (Figure 9.15(b) and (c)). The close values of R^2 and MSE for training and testing datasets indicated that the developed NEAT models had satisfactory generalization capability.

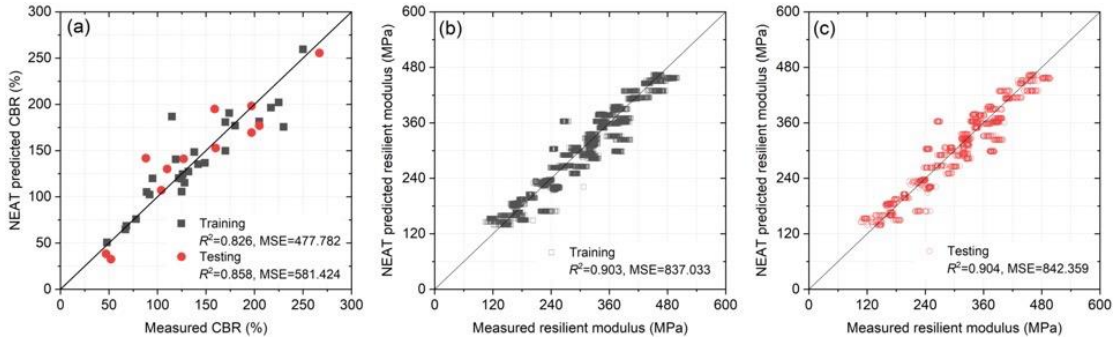

Figure 9.15: Comparison between measured and predicted (a) CBR and (b, c) resilient modulus M_R obtained using MLR model. Results for both training and testing are shown; R^2 and MSE indicate the model prediction performance.

9.5 Results analysis and discussions

9.5.1 Comparison of models' performance

The models' performance for CBR was generally lower than that for resilient modulus in this study (Table 9.4). The primary cause for this lower performance was the relatively small CBR dataset (39 tests in total), as also observed in the literature. For example, the BPNN model developed by Kim et al. (2014) based on 27 datasets was reported to have a relatively lower accuracy than others with larger database.

The results obtained using MLR exhibited relatively low performance for both CBR and resilient modulus in terms of coefficient of determination R^2 and MSE (Table 4). The stress-strain response of unbound aggregates under traffic loading is indeed quite complex, and granular materials usually show a nonlinear elastoplastic behavior (Lekarp et al. 2000a). Therefore, the MLR models, which are based on simple linear relationship, cannot accurately predict the mechanical properties (here, CBR and resilient modulus) of crushed waste rocks.

The KNN model performed satisfactorily for the CBR training dataset with $R^2 > 0.99$, but the prediction accuracy decreased to $R^2 = 0.86$ for testing dataset, indicating that this model was not reliable enough for broad applications. Similar limitations were observed with the BPNN model for CBR. DT and RF models for CBR showed better performance than other models, and the coefficient of determination R^2 was higher than 0.9 for both training and testing datasets.

For resilient modulus, KNN, DT, RF, BPNN, and NEAT models all showed good performance for both training and testing datasets ($R^2 > 0.9$ and MSE < 1000). Compared to the model performance for CBR, the relatively high prediction accuracy for resilient modulus could be attributed to the large dataset (2320 data sets in total) in this study. The performance of KNN and BPNN models ($R^2 > 0.95$) was almost equivalent with that from literature (Table 9.1). DT and RF models exhibited the highest performance for both training and testing datasets ($R^2 > 0.99$ and MSE < 50),

indicating that the DT and RF models provided the most reliable prediction results for resilient modulus among the developed models in this study. The accuracy of these two models was slightly higher than most models from the literature (see Table 9.1).

The performance of RF model was slightly higher than DT model for both CBR and resilient modulus in this study. A possible reason for this is that RF is an extension of DT, i.e., an ensemble of individual DTs (Breiman et al. 1984; Breiman 1999). A major advantage of DT over other modeling techniques is that it can represent interpretable rules or logic statements (Perner et al. 2001).

In general, BPNN model performs better for nonlinear data than DT and RF which are highly susceptible to noisy data (Curram and Mingers 1994; Tso and Yau 2007). Some researchers therefore recommend using BPNN to solve geotechnical problems (Adeli 2001; Shahin 2016). However, the model performance is also affected by the type and number of data, and the type and number of input variables (Mahmoodzadeh et al. 2020). Here, the small database for CBR was not sufficient to sufficiently train the BPNN model, which led to poorer model performance compared to recommendations from the literature.

In addition to the accuracy, other issues should also be considered when developing artificial intelligence models, such as the simplicity, suitability, required time and effort, and transferability of the results (Kirby et al. 1997; Karlaftis and Vlahogianni 2011). Although the prediction accuracy of the NEAT model for CBR and resilient modulus was not the highest in this study, its generalization capacity was the best among all the models, i.e., the model performance for testing dataset was not lower than that for training dataset (Table 9.4). It also proves that NEAT is an effective method to automatically evolve the topology of neural networks which would be unrealistic to create manually (see Figure 9.14). This characteristic of NEAT algorithm can significantly save effort and reduce user error. NEAT is also able to automatically select input variables, and thus reduce the complexity and running time of neural networks (Sohangir et al.

2013). Therefore, NEAT algorithm is worth further exploring in solving geotechnical problems.

Comparison results showed that the DT and RF models can be suggested for predicting CBR and resilient modulus of crushed waste rocks. This study provides similar results compared to other precious studies, in which the different parameters were considered to predict CBR and resilient modulus of different materials (see Table 9.1).

Table 9.4: A summary of the prediction performance of the developed artificial intelligence models for (a) CBR and (b) resilient modulus M_R.

	MLR	KNN	DT	RF	BPNN	NEAT
(a) CBR						
R^2 (training)	0.792	0.992	0.920	0.927	0.841	0.826
R^2 (testing)	0.876	0.860	0.911	0.921	0.597	0.858
MSE (training)	571	23.1	220	200	436	478
MSE (testing)	506	483	364	322	1646	581
(b) Resilient modulus M_R						
R^2 (training)	0.830	0.981	1.000	1.000	0.984	0.903
R^2 (testing)	0.833	0.965	0.997	0.998	0.983	0.904
MSE (training)	1477	169	3.4	2.5	143	837
MSE (testing)	1449	307	30.1	15.3	151	842

9.5.2 Discussion

Twelve artificial intelligence models (six for CBR and six for resilient modulus M_R) were developed and were compared in this study. As a result, it was confirmed that the DT and RF models exhibited better performance for predicting CBR and resilient modulus of crushed waste rocks than other models in terms of coefficient of determination R^2 and mean squared error MSE. However, the applicability of these models is limited to the crushed waste rocks from Canadian Malartic Mine. Therefore, these models may not be suitable for predicting CBR and resilient

modulus of materials from other regions. In addition, in comparison with the artificial intelligence models from the literature (Table 9.1), only three input variables (i.e., number of loading cycles *N*, confining pressure *C*, and deviator stress *D*) were used for resilient modulus models because of the limited data, which also restricts the applicability of the developed models. However, the characteristics of machine learning-based models allow further improvement of these models. The current models can be generalized and have higher performance through continuous verifications and updates made with more data for different tested materials.

For the BPNN models developed in this study, the number of neurons in each hidden layer was the same (i.e., 30 for CBR and 40 for resilient modulus) to simplify the process of model development. However, the number of neurons in the hidden layers could be different which could contribute to improve the neural network performance (Abdeen and Hodhod 2010; Vujicic et al. 2016). Further works could therefore contribute determine a better architecture of the BPNN model.

In general, the artificial intelligence models are difficult to express as explicit formula, which makes its application more complex in practice. Some studies tried to quantify the neural network model through connection weight-bias analysis (Mozumder and Laskar 2015; Hanandeh et al. 2020), but this method was unpractical when the size of the neural network model was relatively large. One possible solution would be to develop a user-friendly operation interface based on the proposed artificial intelligence models (Mata and Corchado 2009).

9.6 Conclusions

In recent years, artificial intelligence techniques have shown a significant degree of success in geotechnical engineering applications. In this study, six different types of artificial intelligence techniques including multiple linear regression (MLR), k-nearest neighbors (KNN), decision tree

(DT), random forest (RF), backpropagation neural network (BPNN), and neuroevolution of augmenting topologies (NEAT) were used to develop models for predicting CBR and resilient modulus of crushed waste rocks. The prediction performance of the developed models was compared in terms of coefficient of determination R^2 and mean squared error MSE. Based on the results of this study it was concluded that:

1. Dry density ρ_d, compaction energy CE, fines content FC, C_C, C_U, D_{10}, D_{60}, and maximum particle size D_{max} were selected as the input variables for the CBR models based on Pearson correlation analysis. The parameters in repeated load triaxial test, i.e., number of loading cycles N in each stress path, confining pressure C, and deviator stress D could affect the resilient modulus of crushed waste rocks, and they were therefore selected as the input variables for resilient modulus models.
2. The artificial intelligence models were trained on training dataset and verified on testing dataset. The performance of MLR models was relatively low because of the limitation of simple linear relationship. Other models showed good performance, particularly, the DT and RF models exhibited higher precision and satisfactory generalization capacity for both CBR ($R^2 > 0.91$) and resilient modulus ($R^2 > 0.99$) in this study. The prediction accuracy of KNN and BPNN models for CBR was influenced significantly by the dataset size. Although the NEAT models were not the best choice in terms of prediction accuracy, they are still worth to be considered in the following study because of their good generalization capacity and simple structure.
3. The model hyperparameters, including number of KNN neighbors, maximum DT depth, number of RF estimators, number of hidden neurons and hidden layers in BPNN, could affect the prediction performance significantly for both CBR and resilient modulus. These parameters should be studied and analyzed during the development of artificial intelligence models.

The limited data restricts the applicability of the developed artificial intelligence models. In order to generalize and update these models, additional RLT tests are ongoing to study the geomechanical

properties of waste rocks with more gradations, water contents, degree of compaction, and fines content.

Acknowledgements

This work was carried out with the financial support from FRQNT and the industrial partners of Research Institute on Mines and the Environment (http://irme.ca/). The repeated load triaxial and CBR test equipment used in this study was acquired with a CFI grant.

9.7 References

AASHTO T307-99. Standard method of test for determining the resilient modulus of soils and aggregate materials. Washington, DC; 2017.

Abdeen MAM, and Hodhod H. Experimental investigation and development of artificial neural network model for the properties of locally produced light weight aggregate concrete. Engineering 2010*;* 02(06): 408-419.

Adeli H. Neural networks in civil engineering: 1989–2000. Computer-Aided Civil and Infrastructure Engineering 2001*;* 16(2): 126-142.

Ai X, Yi J, Zhao H, et al. An empirical predictive model for the dynamic resilient modulus based on the static resilient modulus and california bearing ratio of cement-and lime-stabilised subgrade soils. Road Materials and Pavement Design 2020: 1-20.

Al-Qahtani FH, and Crone SF. Multivariate k-nearest neighbour regression for time series data—a novel algorithm for forecasting uk electricity demand. In: The 2013 international joint conference on neural networks (IJCNN); 2013.

Alavi AH, Gandomi AH, and Lary DJ. Progress of machine learning in geosciences: Preface. Geoscience Frontiers 2016*;* 7(1): 1-2.

ASTM D1883-16. Standard test method for california bearing ratio (CBR) of laboratory-compacted soils. ASTM International, West Conshohocken, PA; 2016.

ASTM D2487-17e1. Standard practice for classification of soils for engineering purposes (unified soil classification system). ASTM International, West Conshohocken, PA; 2017.

Breiman L. 1 Random forests--random features. 1999.

Breiman L, Friedman J, Stone CJ, et al. Classification and regression trees: CRC press; 1984.

Bussière B. Colloquium 2004: Hydrogeotechnical properties of hard rock tailings from metal mines and emerging geoenvironmental disposal approaches. Can Geotech J 2007*;* 44(9): 1019-1052.

Ceylan H, Bayrak MB, and Gopalakrishnan K. Neural networks applications in pavement engineering: A recent survey. International Journal of Pavement Research & Technology 2014*;* 7(6).

Chen L. A multiple linear regression prediction of concrete compressive strength based on physical properties of electric arc furnace oxidizing slag. International Journal of Applied Science and Engineering 2010*;* 7(2): 153-158.

Chollet F. Deep learning mit python und keras: Das praxis-handbuch vom entwickler der keras-bibliothek: MITP-Verlags GmbH & Co. KG; 2018.

Coronado O, Caicedo B, Taibi S, et al. Effect of water content on the resilient behavior of non standard unbound granular materials. Transp Geotech 2016*;* 7: 29-39.

Curram SP, and Mingers J. Neural networks, decision tree induction and discriminant analysis: An empirical comparison. Journal of the Operational Research Society 1994*;* 45(4): 440-450.

de Souza WM, Ribeiro AJA, and da Silva CAU. Use of ann and visual-manual classification for prediction of soil properties for paving purposes. 2020.

Díaz E, and Tomás R. Upgrading the prediction of jet grouting column diameter using deep learning with an emphasis on high energies. Acta Geotechnica 2021*;* 16(5): 1627-1633.

Erzin Y, and Turkoz D. Use of neural networks for the prediction of the cbr value of some aegean sands. Neural Computing and Applications 2016*;* 27(5): 1415-1426.

Ferentinou M, and Fakir M. Integrating rock engineering systems device and artificial neural networks to predict stability conditions in an open pit. Engineering Geology 2018*;* 246: 293-309.

Ferreira A. Application of ann in pavement engineering: State-of-art. 2017.

Ghorbani A, and Hasanzadehshooiili H. Prediction of ucs and cbr of microsilica-lime stabilized sulfate silty sand using ann and epr models; application to the deep soil mixing. Soils and Foundations 2018*;* 58(1): 34-49.

Ghorbani B, Arulrajah A, Narsilio G, et al. Experimental and ann analysis of temperature effects on the permanent deformation properties of demolition wastes. Transp Geotech 2020a*;* 24.

Ghorbani B, Arulrajah A, Narsilio G, et al. Experimental investigation and modelling the deformation properties of demolition wastes subjected to freezethaw cycles using ann and svr. Constr Build Mater 2020b*;* 258.

Ghorbani B, Arulrajah A, Narsilio G, et al. Development of genetic-based models for predicting the resilient modulus of cohesive pavement subgrade soils. Soils and Foundations 2020a*;* 60(2): 398-412.

Ghorbani B, Arulrajah A, Narsilio G, et al. Hybrid formulation of resilient modulus for cohesive subgrade soils utilizing cpt test parameters. J Mater Civil Eng 2020b*;* 32(9).

Golder. Golder Associates Africa (Pty) Ltd. Environmental impact assessment and environmental management programme report for the proposed metsimaholo underground coal mine. Department of Mineral Resources; 2019.

Gu C, Ye X, Wang J, et al. Resilient behavior of coarse granular materials in three-dimensional stress state. Can Geotech J 2020*;* 57(9): 1280-1293.

Gu C, Zhan Y, Wang J, et al. Resilient and permanent deformation of unsaturated unbound granular materials under cyclic loading by the large-scale triaxial tests. Acta Geotechnica 2020*;* 15(12): 3343-3356.

Hanandeh S, Ardah A, and Abu-Farsakh M. Using artificial neural network and genetics algorithm to estimate the resilient modulus for stabilized subgrade and propose new empirical formula. Transp Geotech 2020.

Hao S, and Pabst T. Estimation of resilient behavior of crushed waste rocks using repeated load cbr tests. Transp Geotech 2021: 100525.

Hausknecht M, Lehman J, Miikkulainen R, et al. A neuroevolution approach to general atari game playing. IEEE Transactions on Computational Intelligence and AI in Games 2014*;* 6(4): 355-366.

Hecht-Nielsen R. Kolmogorov's mapping neural network existence theorem. In: Proceedings of the international conference on Neural Networks; 1987.

Jain A, Nandakumar K, and Ross A. Score normalization in multimodal biometric systems. Pattern recognition 2005*;* 38(12): 2270-2285.

James, Aubertin M, and Bussière B. On the use of waste rock inclusions to improve the performance of tailings impoundments. In: Proceedings of the 18th International Conference Soil Mechanics and Geotechnical Engineering, Paris, France; 2013.

Kaloop MR, Gabr AR, El-Badawy SM, et al. Predicting resilient modulus of recycled concrete and

clay masonry blends for pavement applications using soft computing techniques. Frontiers of Structural and Civil Engineering 2019*;* 13(6): 1379-1392.

Karlaftis MG, and Vlahogianni EI. Statistical methods versus neural networks in transportation research: Differences, similarities and some insights. Transportation Research Part C: Emerging Technologies 2011*;* 19(3): 387-399.

Khedr S. Deformation characteristics of granular base course in flexible pavements. Transp Res Record 1985*;* 1043: 131-138.

Kim S-H, Yang J, and Jeong J-H. Prediction of subgrade resilient modulus using artificial neural network. KSCE Journal of Civil Engineering 2014*;* 18(5): 1372-1379.

Kirby HR, Watson SM, and Dougherty MS. Should we use neural networks or statistical models for short-term motorway traffic forecasting? International Journal of Forecasting 1997*;* 13(1): 43-50.

Lary DJ, Alavi AH, Gandomi AH, et al. Machine learning in geosciences and remote sensing. Geoscience Frontiers 2016*;* 7(1): 3-10.

Laverdière A. Effet de la granulométrie sur le comportement géotechnique de roches stériles concassées utilisées comme surface de roulement sur des routes minières. École Polytechnique de Montréal, 2019.

LeCun Y, Bengio Y, and Hinton G. Deep learning. Nature 2015*;* 521(7553): 436-444.

Lee D-H, Cheon E, Lim H-H, et al. An artificial neural network model to predict debris-flow volumes caused by extreme rainfall in the central region of south korea. Engineering Geology 2020.

Lee Rodgers J, and Nicewander WA. Thirteen ways to look at the correlation coefficient. The American Statistician 1988*;* 42(1): 59-66.

Lekarp F, Isacsson U, and Dawson A. State of the art. I: Resilient response of unbound aggregates. Journal of Transportation Engineering 2000*;* 126(1): 66-75.

Li Y, Zou C, Berecibar M, et al. Random forest regression for online capacity estimation of lithium-ion batteries. Applied Energy 2018*;* 232: 197-210.

Lin P, Ni P, Guo C, et al. Mapping soil nail loads using federal highway administration (fhwa) simplified models and artificial neural network technique. Can Geotech J 2020*;* 57(10): 1453-1471.

Liu X, Zhang X, Wang H, et al. Laboratory testing and analysis of dynamic and static resilient modulus of subgrade soil under various influencing factors. Constr Build Mater 2019*;* 195: 178-186.

Mahmoodzadeh A, Mohammadi M, Hashim Ibrahim H, et al. Artificial intelligence forecasting models of uniaxial compressive strength. Transp Geotech 2020: 100499.

Mata A, and Corchado JM. Forecasting the probability of finding oil slicks using a cbr system. Expert Systems with Applications 2009*;* 36(4): 8239-8246.

Mozumder RA, and Laskar AI. Prediction of unconfined compressive strength of geopolymer stabilized clayey soil using artificial neural network. Computers and Geotechnics 2015*;* 69: 291-300.

Mukherjee A, Jain DK, Goswami P, et al. Back propagation neural network based cluster head identification in mimo sensor networks for intelligent transportation systems. IEEE Access 2020*;* 8: 28524-28532.

Nazzal MD, and Tatari O. Evaluating the use of neural networks and genetic algorithms for prediction of subgrade resilient modulus. International Journal of Pavement Engineering 2013*;* 14(4): 364-373.

NCHRP. Guide for mechanistic-empirical design of new and rehabilitated pavement structures.

Final Rep. No. 1-37A 2004.

Oskooei PR, Mohammadinia A, Arulrajah A, et al. Application of artificial neural network models for predicting the resilient modulus of recycled aggregates. International Journal of Pavement Engineering 2020: 1-13.

Pan L, Feng X, Sang F, et al. An improved back propagation neural network based on complexity decomposition technology and modified flower pollination optimization for short-term load forecasting. Neural Computing and Applications 2019*;* 31(7): 2679-2697.

Park H, Kweon G, and Lee SR. Prediction of resilient modulus of granular subgrade soils and subbase materials using artificial neural network. Road Materials and Pavement Design 2009*;* 10(3): 647-665.

Park HI, Kweon GC, and Lee SR. Prediction of resilient modulus of granular subgrade soils and subbase materials using artificial neural network. Road Materials and Pavement Design 2009*;* 10(3): 647-665.

Pekel E. Estimation of soil moisture using decision tree regression. Theoretical and Applied Climatology 2020*;* 139(3): 1111-1119.

Perner P, Zscherpel U, and Jacobsen C. A comparison between neural networks and decision trees based on data from industrial radiographic testing. Pattern Recognition Letters 2001*;* 22(1): 47-54.

Poulsen AP, Thorhauge M, Funch MH, et al. Dlne: A hybridization of deep learning and neuroevolution for visual control. In: 2017 IEEE Conference on Computational Intelligence and Games (CIG); 2017.

Qi S, Cui Y-J, Dupla J-C, et al. Investigation of the parallel gradation method based on the response of track-bed materials under cyclic loadings. Transp Geotech 2020*;* 24: 100360.

Rahman MS, and Erlingsson S. Predicting permanent deformation behaviour of unbound granular

materials. International Journal of Pavement Engineering 2015*;* 16(7): 587-601.

Ren J, Vanapalli SK, Han Z, et al. The resilient moduli of five canadian soils under wetting and freeze-thaw conditions and their estimation by using an artificial neural network model. Cold Regions Science and Technology 2019*;* 168.

Sadrossadat E, Heidaripanah A, and Osouli S. Prediction of the resilient modulus of flexible pavement subgrade soils using adaptive neuro-fuzzy inference systems. Constr Build Mater 2016*;* 123: 235-247.

Saha S, Gu F, Luo X, et al. Use of an artificial neural network approach for the prediction of resilient modulus for unbound granular material. Transp Res Record 2018*;* 2672(52): 23-33.

Sakellariou MG, and Ferentinou MD. A study of slope stability prediction using neural networks. Geotechnical & Geological Engineering 2005*;* 23(4): 419.

Seif El Dine B, Dupla JC, Frank R, et al. Mechanical characterization of matrix coarse-grained soils with a large-sized triaxial device. Can Geotech J 2010*;* 47(4): 425-438.

Shahin MA. State-of-the-art review of some artificial intelligence applications in pile foundations. Geoscience Frontiers 2016*;* 7(1): 33-44.

Shen S-L, Atangana Njock PG, Zhou A, et al. Dynamic prediction of jet grouted column diameter in soft soil using bi-lstm deep learning. Acta Geotechnica 2021*;* 16(1): 303-315.

Sinha S, Singh T, Singh V, et al. Epoch determination for neural network by self-organized map (som). Computational Geosciences 2010*;* 14(1): 199-206.

Sohangir S, Rahimi S, and Gupta B. Optimized feature selection using neuroevolution of augmenting topologies (neat). In: 2013 Joint IFSA World Congress and NAFIPS Annual Meeting (IFSA/NAFIPS); 2013.

Sola J, and Sevilla J. Importance of input data normalization for the application of neural networks to complex industrial problems. IEEE Transactions on nuclear science 1997*;* 44(3): 1464-1468.

Stanley KO, Bryant BD, and Miikkulainen R. Real-time neuroevolution in the nero video game. IEEE transactions on evolutionary computation 2005*;* 9(6): 653-668.

Stanley KO, and Miikkulainen R. Evolving neural networks through augmenting topologies. Evolutionary computation 2002*;* 10(2): 99-127.

Su L, and Fu L. Regional land planning based on bpnn and space mining technology. Neural Computing and Applications 2020.

Tannant D, and Regensburg B. Guidelines for mine haul road design. 2001.

Taskiran T. Prediction of california bearing ratio (cbr) of fine grained soils by ai methods. Advances in Engineering Software 2010*;* 41(6): 886-892.

Tenpe AR, and Patel A. Application of genetic expression programming and artificial neural network for prediction of cbr. Road Materials and Pavement Design 2020*;* 21(5): 1183-1200.

Thompson R, Peroni R, and Visser AT. Mining haul roads: Theory and practice: CRC Press; 2019.

Thompson RJ. Mine haul road design, construction and maintenance management. Mining Roads 2011*;* 136.

Thompson RJ, and Visser AT. Mine haul road maintenance management systems. J S Afr I Min Metall 2003*;* 103(5): 303-312.

Tremblay G, and Hogan C. Mend manual: Volume 1, summary. Ottawa, Ontario, Canada; 2001.

Tso GKF, and Yau KKW. Predicting electricity energy consumption: A comparison of regression analysis, decision tree and neural networks. Energy 2007*;* 32(9): 1761-1768.

Varghese VK, Babu SS, Bijukumar R, et al. Artificial neural networks: A solution to the ambiguity in prediction of engineering properties of fine-grained soils. Geotechnical and Geological Engineering 2013*;* 31(4): 1187-1205.

Vidal A, and Kristjanpoller W. Gold volatility prediction using a cnn-lstm approach. Expert Systems with Applications 2020.

Vujicic T, Matijevic T, Ljucovic J, et al. Comparative analysis of methods for determining number of hidden neurons in artificial neural network. In: Central european conference on information and intelligent systems; 2016.

Wang L, Wu C, Tang L, et al. Efficient reliability analysis of earth dam slope stability using extreme gradient boosting method. Acta Geotechnica 2020*;* 15(11): 3135-3150.

Wang L-J, Guo M, Sawada K, et al. A comparative study of landslide susceptibility maps using logistic regression, frequency ratio, decision tree, weights of evidence and artificial neural network. Geosciences Journal 2016*;* 20(1): 117-136.

Wen R, Guo Z, Zhao T, et al. Neuroevolution of augmenting topologies based musculor-skeletal arm neurocontroller. In: 2017 IEEE International Instrumentation and Measurement Technology Conference (I2MTC); 2017.

Xu M, Watanachaturaporn P, Varshney PK, et al. Decision tree regression for soft classification of remote sensing data. Remote Sensing of Environment 2005*;* 97(3): 322-336.

Yilmazkaya E, Dagdelenler G, Ozcelik Y, et al. Prediction of mono-wire cutting machine performance parameters using artificial neural network and regression models. Engineering Geology 2018*;* 239: 96-108.

Yin Z-Y, Hicher P-Y, Dano C, et al. Modeling mechanical behavior of very coarse granular materials. J Eng Mech 2017*;* 143(1): C4016006.

Yuksel ME. Agent-based evacuation modeling with multiple exits using neuroevolution of

augmenting topologies. Advanced Engineering Informatics 2018; 35: 30-55.

Zhang W, Ching J, Goh ATC, et al. Big data and machine learning in geoscience and geoengineering: Introduction. Geoscience Frontiers 2021; 12(1): 327-329.

Zhang W, and Goh ATC. Multivariate adaptive regression splines for analysis of geotechnical engineering systems. Computers and Geotechnics 2013; 48: 82-95.

9.8 Appendix

System configuration and parameters in the NEAT models.

Startup parameters	Settings	Definition
Number of generations	30000	The number of generations to perform for a run.
Population size	150	The number of individuals in each generation.
Activation function	ReLU	The default activation function attribute assigned to hidden neurons.
Activation mutation rate	0.0	The probability that mutation will replace the neuron's activation function
Bias initial mean	0.0	The mean of the normal/gaussian distribution.
Bias initial standard deviation	1.0	The standard deviation of the normal/gaussian distribution.
Bias max. value	30.0	The maximum allowed bias value.
Bias min. value	-30.0	The minimum allowed bias value.
Bias mutation power	0.5	The standard deviation of the zero-centered normal/gaussian distribution from which a bias value mutation is drawn.
Bias mutation rate	0.7	The probability that mutation will change the bias of a neuron by adding a random value.
Bias replace rate	0.1	The probability that mutation will replace the bias of a neuron with a newly chosen random value.
Compatibility disjoint coefficient	1.0	The coefficient for the disjoint and excess gene counts' contribution to the network distance.
Compatibility weight coefficient	0.5	The coefficient for each weight, bias, or response multiplier difference's contribution to the network distance (for homologous neurons or connections).
Connection add probability	0.5	The probability that mutation will add a connection between existing neurons.

Connection delete probability	0.2	The probability that mutation will delete an existing connection.
Enabled default	True	The default enabled attribute of newly created connections.
Enabled mutation rate	0.03	The probability that mutation will replace the enabled status of a connection.
Feed forward	True	Generated networks will not be allowed to have recurrent connections.
Initial connection	Full	Each input neurons are connected to all output neurons.
Node add probability	0.3	The probability that mutation will add a new neuron.
Node delete probability	0.25	The probability that mutation will delete an existing neuron.
Number of hidden neurons	0	The number of hidden neurons to add to each genome in the initial population.
Number of input neurons	8 and 3	The number of input neurons, through which the network receives inputs.
Number of output neurons	1	The number of output neurons, to which the network delivers outputs.
Weight initial mean	0.0	The mean of the normal/gaussian distribution used to select weight attribute values for new connections.
Weight initial standard deviation	1.0	The standard deviation of the normal/gaussian distribution used to select weight values for new connections.
Weight max. value	30.0	The maximum allowed weight value.
Weight min. value	-30.0	The minimum allowed weight value.
Weight mutation power	0.5	The standard deviation of the zero-centered normal/gaussian distribution from which a weight value mutation is drawn.
Weight mutation rate	0.8	The probability that mutation will change the weight of a connection by adding a random value.
Weight replace rate	0.1	The probability that mutation will replace the weight of a connection with a newly chosen random value.

CHAPTER 10 ARTICLE 6: EXPERIMENTAL INVESTIGATION AND PREDICTION OF THE PERMANENT DEFORMATION OF CRUSHED WASTE ROCKS USING ARTIFICIAL NEURAL NETWORK MODEL

Shengpeng Hao and Thomas Pabst

This article was submitted to ASCE - *International Journal of Geomechanics* in February 2021.

Abstract: The gradual accumulation of permanent deformation in unbound granular material layers is one of the main reasons for flexible pavement rutting. The accurate determination of permanent deformation behavior of pavement materials is critical for the successful design of pavement systems. However, predicting the permanent deformation is complex and the available empirical regression models have limited accuracy and applicability. In this study, multi stage (MS) repeated load triaxial (RLT) tests were carried out under different stress levels to evaluate the permanent strain and shakedown ranges of crushed waste rocks. The plastic shakedown limit and plastic creep limit were determined to estimate the shakedown range of crushed waste rocks at certain stress conditions. Rahman and Erlingsson model (extended using time hardening approach) performed better than other models for fitting the accumulated permanent strains ($R^2 > 0.92$), but the prediction accuracy of shakedown range was relatively low (< 85%). An artificial neural network (ANN) model was therefore developed based on the experimental results to predict the permanent strain of crushed waste rocks. The ANN model consisted of three hidden layers (50 neurons per layer) with Tanh activation function and could predict the permanent strain ($R^2 > 0.97$) and shakedown ranges (accuracy > 93%) satisfactorily.

Keywords: Crushed waste rocks; Permanent deformation; Repeated load triaxial tests; Shakedown ranges; Rahman and Erlingsson model; Artificial neural network.

10.1 Introduction

Mining operations produce a large amount of waste rocks, which are usually disposed of in piles on the surface close to the production sites. The large size and the geochemical and geotechnical instability of waste rock piles make their management and reclamation difficult (Blowes 1997; Aubertin 2013). Reusing waste rocks for roads and pavement construction can therefore be a more sustainable strategy in terms of economics and environmental impacts (Vieira and Pereira 2015). Their high strength and durability (Thompson 2011c) and their availability on site make them particularly suitable for such applications.

Excess rutting can, however, decrease the quality and safety of ride because of hydroplaning and reduced skid resistance of the road surface (Rahman and Erlingsson 2015a; Salour and Erlingsson 2017). The gradual accumulation of permanent deformation in waste rocks layers and subgrade soils is one of the main reasons for rutting (Erlingsson 2012). The permanent deformation of waste rocks layers is principally caused by the cyclic stresses of varying magnitudes induced by the moving traffic loads (Lekarp et al. 2000b). Generally, multistage (MS) repeated load triaxial (RLT) tests are conducted to evaluate the permanent deformation behavior of pavement materials (EN 13286 2004). Pavement materials can be classified using shakedown concept based on the development of permanent deformation in MS RLT tests.

The shakedown concept has been widely applied to describe the deformation behavior of pavement materials under repeated loading (Werkmeister et al. 2004). Based on the shakedown theory, the permanent deformation behavior with loading cycles can be divided into three categories based on the value of ε_p^{5000}-ε_p^{3000}: plastic shakedown, plastic creep, and incremental collapse as shown in Figure 10.1 (Werkmeister 2003; EN 13286 2004). The ε_p^{5000} and ε_p^{3000} are the accumulated permanent strains measured at the 5000th and 3000th loading cycles during the RLT tests.

In range A (plastic shakedown), the accumulated permanent strain of materials increases significantly during initial load cycles until the material reaches a purely elastic behavior, after

which the permanent strain rate decreases rapidly; in range B (plastic creep), a large amount of permanent strain is accumulated during initial load cycles after which the strain continues to accumulate but at a slow rate; in range C (incremental collapse), the permanent strain rate decreases very slowly or not at all, accumulation of permanent strain continues with load applications, ultimately leading to failure (Werkmeister 2003; EN 13286 2004; Werkmeister et al. 2004). Similarly, in the Guide for Mechanistic-Empirical Design prepared by the Federal Highway Administration (FHWA), the permanent deformation behavior of pavement materials under a given load can be divided into three stages, i.e., primary stage (high initial level of rutting with a decreasing rate of plastic deformations), secondary stage (small rate of rutting associated with volumetric changes), and tertiary stage (high rate of rutting associated with shear deformations).

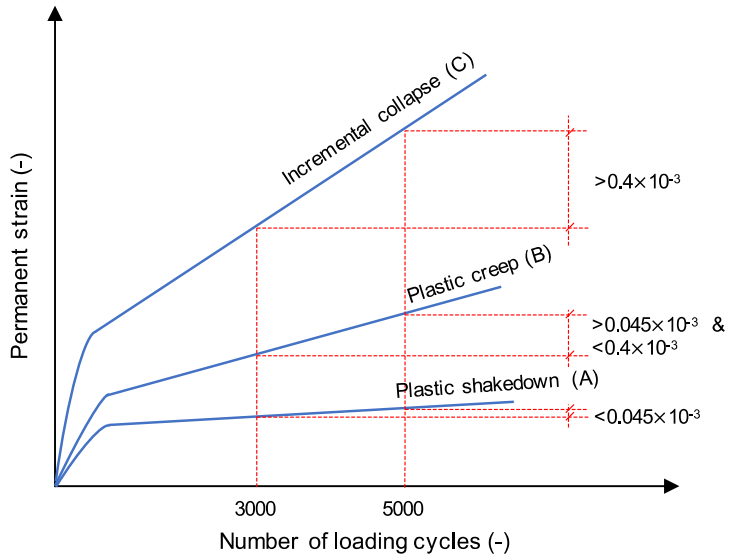

Figure 10.1: Different categories of permanent deformation development (after EN 13286-7 standard).

The adequate understanding of permanent deformation characterization of materials is necessary

for proper pavement design (Werkmeister et al. 2001; Pérez-González et al. 2020). However, pavement materials often exhibit complicated permanent deformation behavior under different stress conditions. Conducting MS RLT tests in the laboratory appears therefore necessary for material assessment and road design, but such tests can be complex, time-consuming and require adapted equipment (Yang and Han 2013). Therefore, various regression-based models were proposed to describe and predict the permanent deformation characterization of pavement materials (Barksdale 1972; Sweere 1990; Wolff and Visser 1994; Gidel et al. 2001; Korkiala-Tanttu 2005; Rahman and Erlingsson 2015a) (Table 10.1). These empirical models are usually a function of number of loading cycles and/or stress conditions (e.g., shear strength, deviator stress, and confining pressure). However, there are limited regression models capable of predicting the permanent deformation under multi-stress conditions, and these models have regression limitations and generally fail to cover the complexity of soil behavior (Alnedawi et al. 2019). Moreover, these models were developed for specific datasets, and their applicability and accuracy for crushed waste rocks used in mine haul roads may be limited.

Table 10.1: Commonly used empirical permanent deformation models.

Reference	Model
Barksdale model (1972)	$\varepsilon_p = a + b\log(N)$
Sweere model (1990)	$\varepsilon_p = aN^b$
Wolff and Visser model (1994)	$\varepsilon_p = (cN+a)(1-e^{-bN})$
Gidel et al. model (2001)	$\varepsilon_p = \varepsilon^0(1-(\frac{N}{100})^{-B})(\frac{L_{max}}{p_a})^u(m+\frac{s}{p_{max}}-\frac{q_{max}}{p_{max}})^{-1}$, $L_{max}=\sqrt{{p_{max}}^2+{q_{max}}^2}$
Korkiala-Tanttu model (2005)	$\varepsilon_p = CN^b\frac{R}{A-R}$, $R=\frac{q}{q_f}$, $q_f=mp+s$
Rahman and Erlingsson model (2015a)	$\varepsilon_p = aN^{bS_f}S_f$, $S_f=\frac{(q/p_a)}{(p/p_a)^\alpha}$

Where ε_p: permanent strain [-]; N: the number of loading cycles [-]; q: deviator stress [kPa]; p: mean bulk stress (one-third of the

sum of the principle stresses) [kPa]; p_a: the reference stress taken equal to the atmospheric pressure (100 kPa); p_{max}: the maximum applied confining pressure [kPa]; q_{max}: the maximum deviator stress [kPa]; m and s: the slope and intercept of the Mohr-Coulomb failure line plotted in p-q space, respectively, m=2.02 and s=221.96 in this study; other variables in the equations are the model coefficients that should be calibrated by fitting experiment results.

Artificial neural network (ANN) is more and more commonly used in geotechnical engineering applications such as rockburst prediction (Xue et al. 2020), tunnel convergence prediction (Mahdevari and Torabi 2012), structural health monitoring (Kang et al. 2019), slope stability analysis (Kang et al. 2017), and road layer modulus back calculation (Han, Ma, et al. 2021). The study and prediction of permanent deformation of unbound granular materials using ANN remains, however, relatively limited. Ghorbani et al. (2020a) developed an ANN model for predicting permanent strain of demolition wastes, but these materials are too different from crushed waste rocks to allow for a direct application of this model to mine sites.

The primary objective of this study was therefore to investigate the permanent deformation behavior of crushed waste rocks and then develop an ANN model for predicting the permanent strain. The permanent deformation under different stress levels was measured using MS RLT tests and fitted using different empirical regression models. An ANN model was also developed based on the experimental data. The effects of hyperparameters including epochs, number of hidden neurons and hidden layers, activation function, and regularization on ANN performance were also studied to determine the optimal ANN architecture.

10.2 Materials and methods

10.2.1 Material properties

The tested crushed waste rocks were obtained from Canadian Malartic Mine, an open pit gold mine

located in the Abitibi region, in Quebec province, Canada. This mine has been using crushed waste rocks for the construction of wearing course of mine haul roads. Sampled and tested crushed waste rocks were considered representative of the materials typically used for haul road wearing course construction at the mine. The particles larger than 19 mm were removed (sieved) because of the limitations of the equipment used (maximum specimen diameter = 150 mm).

The particle size distribution (PSD) was measured in the laboratory using sieving (ASTM C136, 2006) (Figure 10.2(a)). The material had very small amount (< 4%) of fines (< 75 μm). It was a poorly graded gravel with 3.72% fines and was classified as GP (ASTM D2487 2017). Proctor compaction tests were carried out on crushed waste rocks using modified effort (ASTM D1557, 2012) (Figure 10.2(b)). The optimum water content was 5.6% corresponding to a maximum dry density of 2334 kg/m^3. Mineralogy, specific gravity, water absorption, optimum water content, maximum dry density, shape index, uniformity coefficient, and curve coefficient are summarized in Table 10.2 and 10.3, and standards used for each test are also indicated.

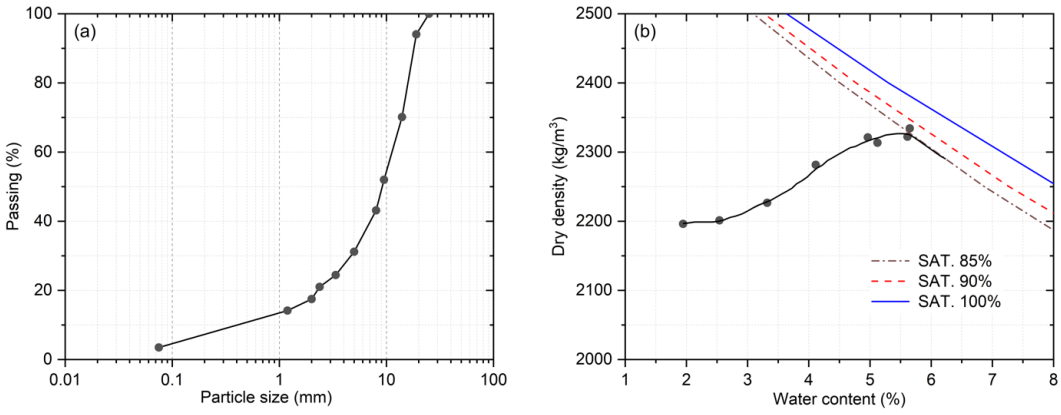

Figure 10.2: The physical properties of crushed waste rocks; (a) particle size distribution; (b) the relationship between dry density and water content obtained from Proctor compaction test using modified effort.

Table 10.2: The mineralogy of crushed waste rocks.

Mineralogy	Proportion
Quartz	26.08±2.46%
Albite	38.74±4.30%
Muscovite	10.87±1.42%
Chlorite	7.12±0.97%
Corundum	6.80±1.33%
Diopside	6.50±1.34%
Anhydrite	2.42±0.48%
Pyrite	1.08±0.15%
Rutile	1.18±0.79%

Table 10.3: The basic physical properties of crushed waste rocks.

Properties		Standard
Specific gravity (< 4.75 mm)	2.75	ASTM D854-14 (2014)
Specific gravity (>4.75 mm)	2.71	ASTM C127-15 (2015)
Water absorption (>4.75 mm)	0.41%	ASTM C127-15 (2015)
Elongation index	38.56±1.62%	IS 2386-1 (1963)
Flakiness index	34.95±2.08%	IS 2386-1 (1963)
Optimum water content	5.6%	ASTM D1557-12 (2012)
Maximum dry density	2334.29 kg/m^3	ASTM D1557-12 (2012)
Uniformity coefficient	7.98	ASTM D2487-17e1 (2017)
Curve coefficient	2.21	ASTM D2487-17e1 (2017)

10.2.2 MS RLT tests

The MS RLT tests were performed following the European standard EN-13286-7 (EN 13286 2004). This standard proposes two sets of stress levels, referred to as “low stress level” (LSL) and “high stress level” (HSL). Each set is divided into five sequences, and each of these sequences contains 5 or 6 stress paths with a constant confining pressure and different deviator stresses (Table 10.4). The deviator stress in HSL is higher than that in LSL with the same confining pressure. Each stress

path was applied for 10000 cycles according to EN 13286-7 standard.

LSL and HSL proposed in EN 13286-7 standard were initially developed for highways, and the stress levels were significantly lower than that observed on mine haul roads caused by extra heavy mining trucks. For example, the gross vehicle weight limit of three axles straight truck for highway in Canada is 24.25 mt, while the tire pressure of KOMATSU 960e-2k could exceed 1000 kPa. An additional high stress level for mining engineering applications (HSLM) was therefore defined in this study to simulate stress conditions more representatively in mine haul roads. HSLM was divided into four sequences, and each of these sequences contained 4 stress paths with a constant confining pressure and different deviator stresses (Table 10.4). The confining pressure and deviator stress in HSLM were significantly higher than that in LSL and HSL. The deviator stresses and confining pressures for HSLM were between 100 and 1500 kPa, and between 80 and 550 kPa, respectively, which covers the range of stress variations in the field, even for the heavier mining truck (e.g., BELAZ 75710 with 450 mt of payload capacity). Mine haul roads are typical low-volume roads compared with highways, and each stress path in HSLM was therefore applied for 6000 cycles. The number of loading cycles was also chosen to allow to calculate the shakedown range (i.e., the value of ε_p^{5000}-ε_p^{3000}).

Haversine loading pulses with a frequency of 0.3 Hz with no rest period were applied for MS RLT tests. The applied cyclic loading frequency was lower than that typically observed in the field (3-4 Hz) because of the limitation of the triaxial test equipment used in this study (Figure 10.3). However, Alnedawi et al. (2019) indicated that the influence of loading frequency on permanent deformation of unbound granular materials was negligible. All tests were carried out under free drainage conditions. Specimens were 300 mm high and 150 mm in diameter and were prepared using modified compaction effort (i.e., 2700 kN-m/m^3) with an initial gravimetric water content w = 4%. Vertical axial deformations were monitored using a LVDT (Linear Variable Displacement Transducers) from which the permanent strain was calculated. The shakedown ranges at each stress

path were evaluated based on the measured permanent strain.

MS RLT tests results were used to fit the empirical permanent deformation models, including Gidel et al. (2001) model, Korkiala-Tanttu (2005) model, and Rahman and Erlingsson (2015a) model because the stress condition is taken into account in these models (see Table 10.1), and to train and test the ANN model. Gidel et al. model, Korkiala-Tanttu model, and Rahman and Erlingsson model predict the permanent strain based on the applied stress and number of loading cycles, but these models were initially developed to fit permanent strain of a single stress path in RLT tests. These models were therefore extended using time hardening approach to fit the accumulated permanent strain measured by MS RLT tests in this study. In time hardening approach, the equivalent number of loading cycles N_i^{eq} (for the *i*th stress path) is introduced to take into account the effect of stress history, and the total number of loading cycles N from the beginning of the test is then modified as $N\text{-}N_{i\text{-}1}+N_i^{eq}$, where $N_{i\text{-}1}$ is the total number of loading cycles at the end of (i-1)th stress path (Lytton et al. 1993; Zhou et al. 2010). More details about the extended Gidel et al. model, Korkiala-Tanttu model, and Rahman and Erlingsson model can be found in Erlingsson et al. (2017).

Table 10.4: Stress levels with different confining pressure (C) and deviator stress (D) for MS RLT tests, LSL and HSL are prescribed by the EN-13286-7 standard, and HSLM was defined for mine haul roads (see text for details).

Sequence 1		Sequence 2		Sequence 3		Sequence 4		Sequence 5	
C, kPa	D, kPa	C, kPa	D, kPa	C, kPa	D, kPa	C, kPa	D, kPa	C, kPa	D, kPa
LSL									
20	20	45	60	70	80	100	100	150	100
20	40	45	90	70	120	100	150	150	200
20	60	45	120	70	160	100	200	150	300
20	80	45	150	70	200	100	250	150	400
20	100	45	180	70	240	100	300	150	500
20	120	45	210	70	280	100	350	150	600

HSL									
20	50	45	100	70	120	100	200	150	200
20	80	45	180	70	240	100	300	150	300
20	110	45	240	70	320	100	400	150	400
20	140	45	300	70	400	100	500	150	500
20	170	45	360	70	480	100	600	150	600
20	200	45	420	70	560				
HSLM (defined for mining engineering)									
80	100	200	300	350	400	550	600		
80	200	200	500	350	700	550	900		
80	300	200	700	350	1000	550	1200		
80	400	200	900	350	1300	550	1500		

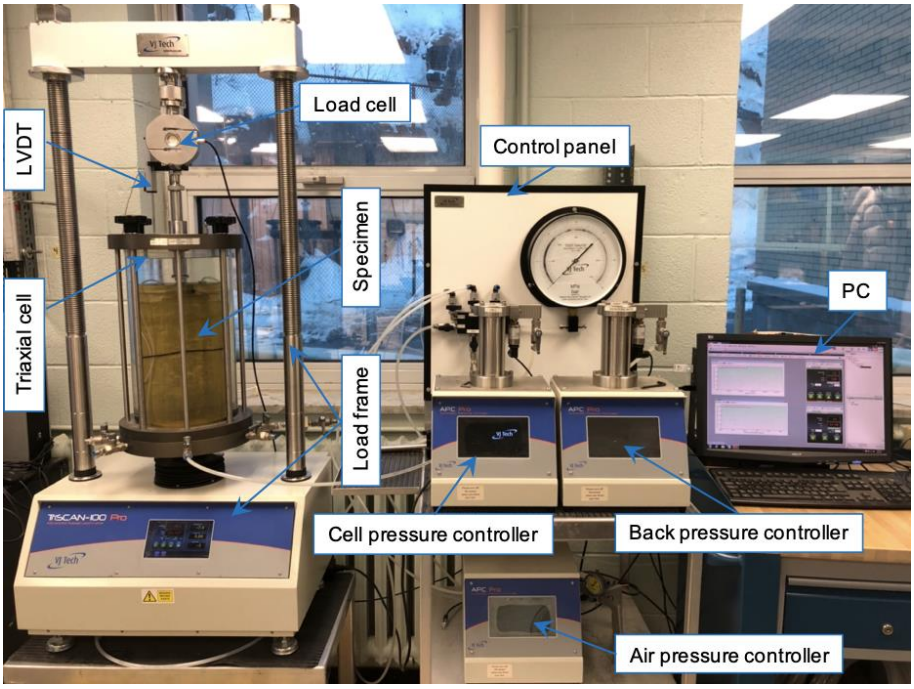

Figure 10.3: The triaxial test system used in this study.

10.3 Artificial neural network (ANN)

10.3.1 ANN algorithm

ANN typically consists of an input layer, an output layer and one or more hidden layers in between (Figure 10.4(a)). Each layer contains processing elements known as neurons (Tarawneh and Nazzal 2014; Xu, Chen, et al. 2019). The number of neurons in the input layer corresponds to the input features (or variables), i.e. number of loading cycles (N, -), confining pressure (C, kPa) and deviator stress (D, kPa) in this study. The output layer consisted of one neuron because regression problems only have one output value, i.e. permanent strain (PS, -) in this study (Figure 10.4(a)). Each neuron in an ANN is an independent processing element, having its own inputs X_i and output Y (Figure 10.4(b)). The inputs X_i are propagated to the output Y through an activation function by multiplying the value with an arbitrary weight and then adding a bias (Kim et al. 2014; Saha et al. 2018). The generated (output) permanent strain value is compared to the measured (target) permanent strain value by computing the error between the predicted output and the target value. The weight and bias values are modified iteratively (i.e. epochs) through the gradient descent method until the error is minimized. This iterative process is error backpropagation process that is widely used for training feedforward neural networks because of its significant efficiency in ANN training (Rumelhart et al. 1986). The backpropagation algorithm was employed to train the ANN model in this study. The ANN model for prediction of permanent strain of crushed waste rocks was developed in Python.

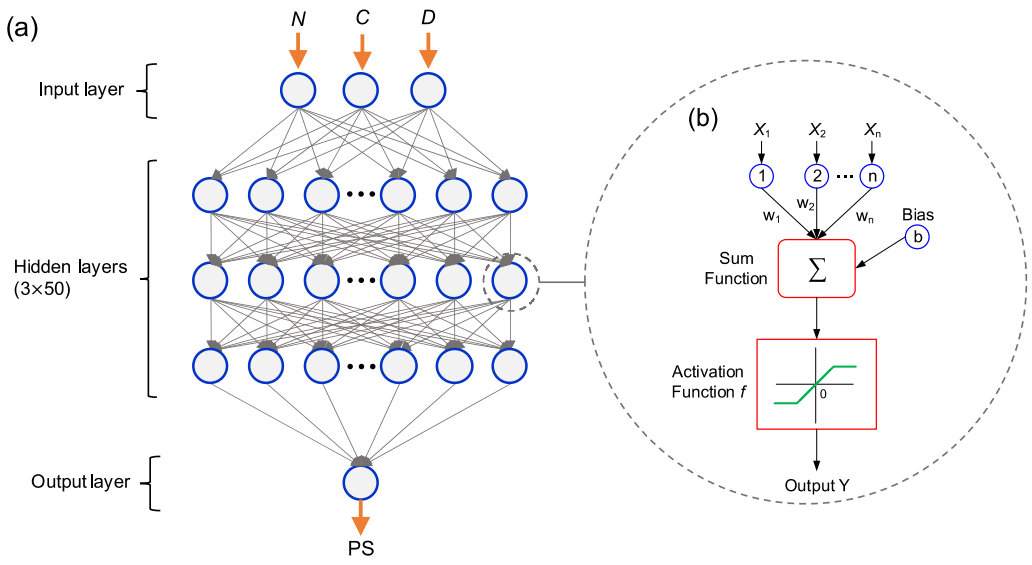

Figure 10.4: A typical neural network architecture; (a) the optimal neural network for prediction of permanent strain developed in this study; (b) the principles of each hidden neuron.

10.3.2 Data preprocessing and splitting

A total of 7500 data sets were selected from the MS RLT tests results to train and test the neural network and to fit the empirical permanent deformation models. For each stress path, the measured permanent strains were selected at each 10 cycles from the 1st to 100th loading cycles, and each 100 cycles from the 100th to 10000th (for LSL and HSL) and 6000th (for HSLM) loading cycles. Experimental data were preprocessed to remove the outliers that can strongly influence the output of a machine learning model. The difference of magnitude between the various experiment variables was significant which could reduce the training efficiency of neural networks (Chollet 2018; Lee et al. 2021). For example, number of loading cycles could reach 10000 while values of confining pressure and deviator stress did not exceed 1500. Therefore, input variables were normalized using the Z-Score normalization method (Jain et al. 2005):

$$X_i^* = \frac{X_i - \mu}{\sigma} \qquad 10.1$$

Where X_i^*: the normalized input values; X_i: the experimental input values; μ: the mean value of the input variable; and σ: the standard deviation of the input variable.

The normalized data were then split between a training dataset and a testing dataset (to verify the generalization capability of the trained ANN model). In this study, 80% of the total experimental data were selected randomly for the training dataset (for the training and validation of the ANN model), while the remaining 20% data were used as the testing dataset (to test the developed ANN model).

10.3.3 Hyperparameters study

The optimal ANN model, which can best predict permanent strain, is primarily dependent on the network hyperparameters which include epochs, number of hidden neurons, number of hidden layers, activation function, and regularization (Sinha et al. 2010). Literature does not provide specific guidelines in developing the hyperparameters, and their determination mainly depends on trial and error methods based on the neural network performance. In this study, the effect of hyperparameters was studied using 4-fold cross-validation technique (Chollet 2018), and then the optimal ANN model was selected based on the network performance. A 4-fold cross-validation technique was used in this study. This approach consists in dividing the training dataset was randomly divided into 4 partitions of equal size. The neural networks were trained on 3 partitions and evaluated on the remaining one. The training and validation process is repeated 4 times using different partitions, and the results are averaged to represent the global performance of the neural networks on the training dataset (Figure 10.5).

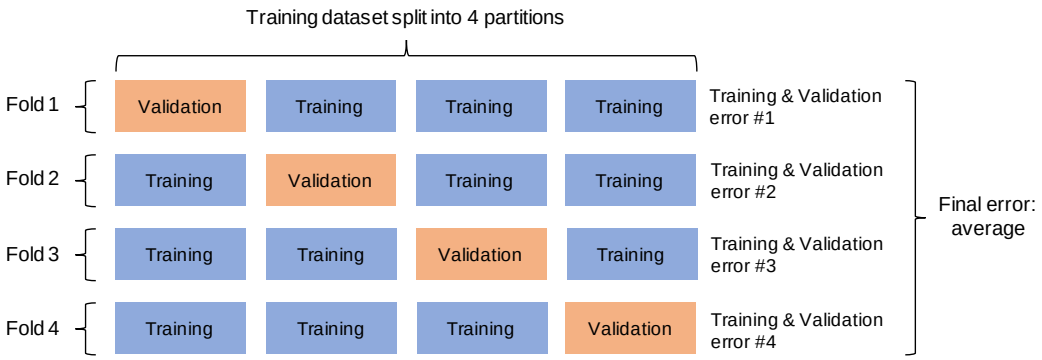

Figure 10.5: The sketch map of 4-fold cross-validation used for the study of ANN hyperparameters.

Epoch is the number of times a learning algorithm iterates the entire training dataset and the calculation of new weights and biases, and it plays a significant role on a network performance (Sinha et al. 2010). Epoch should be optimized for better performance: if epoch is too small then it will not be able to train the network completely and if epoch is too large, then the network training will take more time and an overfitting problem might occur. The effect of epoch on the network performance was evaluated in this study and an optimal value was selected for the proposed model.

Number of neurons (per hidden layer) and hidden layers significantly affect the neural network output and architecture (Panchal et al. 2011). In this study, number of neurons and hidden layers was varied between 2 and 300, and between 1 and 7, respectively, to study their effects on the performance of the neural network.

Finally, activation functions, which are used to transform an input signal into an output signal which in turn is fed as input to the next layer have a direct effect on the network prediction accuracy (Sharma 2017). Activation functions were used in hidden layers only, while output layer was a linear layer without any activation function (the prediction of permanent deformation was indeed a scalar regression issue). In total, four non-linear activation functions (i.e., Sigmoid, Tanh, ReLU, and Softmax functions) were evaluated in this study (Table 10.5).

Table 10.5: Activation functions used in hidden layers of the neural networks.

Sigmoid (Saul et al. 1996)	Tanh (Karlik and Olgac 2011)	ReLU (Li and Yuan 2017)	Softmax (Gold and Rangarajan 1996)
$\frac{1}{1+e^{-x}}$	$\frac{e^{x}-e^{-x}}{e^{x}+e^{-x}}$	$max(0,x)$	$\frac{e^{z_i}}{\sum_i^K e^{z_i}}$

Note: e: Euler's number; x: the summed weighted input from the neuron; z_i: the output of the i^{th} element or neuron; K: total number of categories.

The developed ANN model should have a good generalization potential to be able to accurately predict permanent deformation of crushed waste rocks. However, the complexity of the network and overfitting problems may reduce the generalization potential (Phaisangittisagul 2016). Two regularization techniques, i.e., L2 (also called weight decay) and dropout, were therefore evaluated to enhance the generalization capability. L2 regularization consists in adding a regularization term to an error function so that the total error function is minimized using following equation (Cortes et al. 2012):

$$\mathcal{L}_T(w)=\mathcal{L}_D(w)+\lambda\mathcal{L}_w(w) \quad 10.2$$

Where w: neural network weights; $\mathcal{L}_T(w)$: a total loss function; λ: a regularization parameter that controls the tradeoff between $\mathcal{L}_D(w)$ and $\mathcal{L}_w(w)$; $\mathcal{L}_D(w)$: a sum-of-squares error function between the target output and network output; $\mathcal{L}_w(w)$: a sum-of-squares of the weight parameters.

The regularization term in L2 was the sum of square of all feature weights (Eq. (2)). This regularization technique was chosen here because it performs better when all the input features influence the output with weights roughly equal (Cortes et al. 2012). The regularization parameter λ was set as 0.01 for hidden layers.

Dropout is another commonly used regularization approach which randomly drops out hidden neurons in the neural network during training (Hinton et al. 2012). The objective is to allow each

neuron to learn on its own without relying too much on other neurons and to reduce the risk of overfitting. Dropout regularization has proved to be an effective method to reduce overfitting and improve generalization for deep neural networks (Wager et al. 2013). In this study, the dropout rate was 0.5 for each hidden layer.

10.3.4 Performance assessment

Permanent strain was predicted using the ANN model and compared to the experimental permanent strain. Coefficient of determination (R^2) is widely used to assess the prediction accuracy of neural networks for regression tasks (Zhang and Goh 2013; Kang et al. 2019; Lee et al. 2021), and it was also used to evaluate the developed ANN model in this study:

$$R^2 = 1 - \frac{\sum_{i=1}^{n} (y_i^* - y_i)^2}{\sum_{i=1}^{n} (y_i - \bar{y})^2} \tag{10.3}$$

Where n: number of data sets; y_i and y_i^*: the experimental and predicted values of the i^{th} output, respectively; and $\bar{y}$: the mean of the experimental values. A value of R^2 closer to 1 means a better performance (Fan et al. 2019).

Mean squared error (MSE) is the average of the squared differences between prediction and experimental values. It was applied as the loss function to optimize connection weights and bias of the neural network during training:

$$\text{MSE} = \frac{1}{n}\left[\sum_{i=1}^{n} (y_i - y_i^*)^2\right] \tag{10.4}$$

MSE is widely used for loss function in regression problems (Zhang and Goh 2013; Lee et al. 2021). MSE value is always positive, and it is ideal to be close to zero (Chen 2010; Chollet 2018; Vidal and Kristjanpoller 2020).

Mean absolute error (MAE) was employed as the metric function to evaluate the performance of the neural network. Metric function is similar to loss function, except that the metric values are

calculated and recorded at the end of each epoch of the training and validation dataset, while loss values are calculated and recorded during each epoch.

$$\mathrm{MAE}=\frac{1}{n}\left(\sum_{i=1}^{n}\left|y_i-y_i^*\right|\right) \tag{10.5}$$

MAE is one of the most common regression metrics to measure accuracy for continuous variables (Kang et al. 2019). MAE value is always positive, and the smaller the value of MAE is, the better the model performs. MSE and MAE were used to evaluate the effects of the various hyperparameters on the neural network performance.

Huber loss L_δ was also used to evaluate the model performance (Eq. 10.6). Huber loss has been widely used in regression tasks because of its robustness for the noisy datasets (Meyer 2019; Gupta et al. 2020; Zheng 2020). The given constant δ in Huber loss controls the transitions from a quadratic function (for small values of $\left|y_i-y_i^*\right|$) to an absolute value function (when the value of $\left|y_i-y_i^*\right|$ exceeds δ) (Huber 1973, 1992). This feature allows it to combine analytical tractability of MSE and outlier-robustness of MAE (Yi and Huang 2017; Sun et al. 2020). In this study, δ was set as 5×10^{-5} for Huber loss.

$$L_\delta=\begin{cases}\frac{1}{2}(y_i-y_i^*)^2, & \text{if } \left|y_i-y_i^*\right|\leqslant\delta\\ \delta\left|y_i-y_i^*\right|-\frac{1}{2}\delta^2, & \text{otherwise}\end{cases} \tag{10.6}$$

10.4 Experimental results

10.4.1 Measured permanent strain

The accumulated permanent strain increased with number of loading cycles, and the final strain increased with the increasing of stress levels (Figure 10.6). The trends of accumulated permanent

strain for LSL and HSL were similar. LSL results showed the lowest final accumulated permanent strain (around 0.007) after 300000 loading cycles, but it was close to the strain measured with HSL after 280000 loading cycles. The accumulated permanent strain with HSLM, however, increased more sharply for some specific stress paths. For each stress path in LSL and HSL, permanent strain increased significantly during initial cycles, but then became almost constant for the rest of the cycles. Similar observations were also made for HSLM, except for the final stress path when the accumulated permanent strain continued to increase with loading cycles (Figure 10.6).

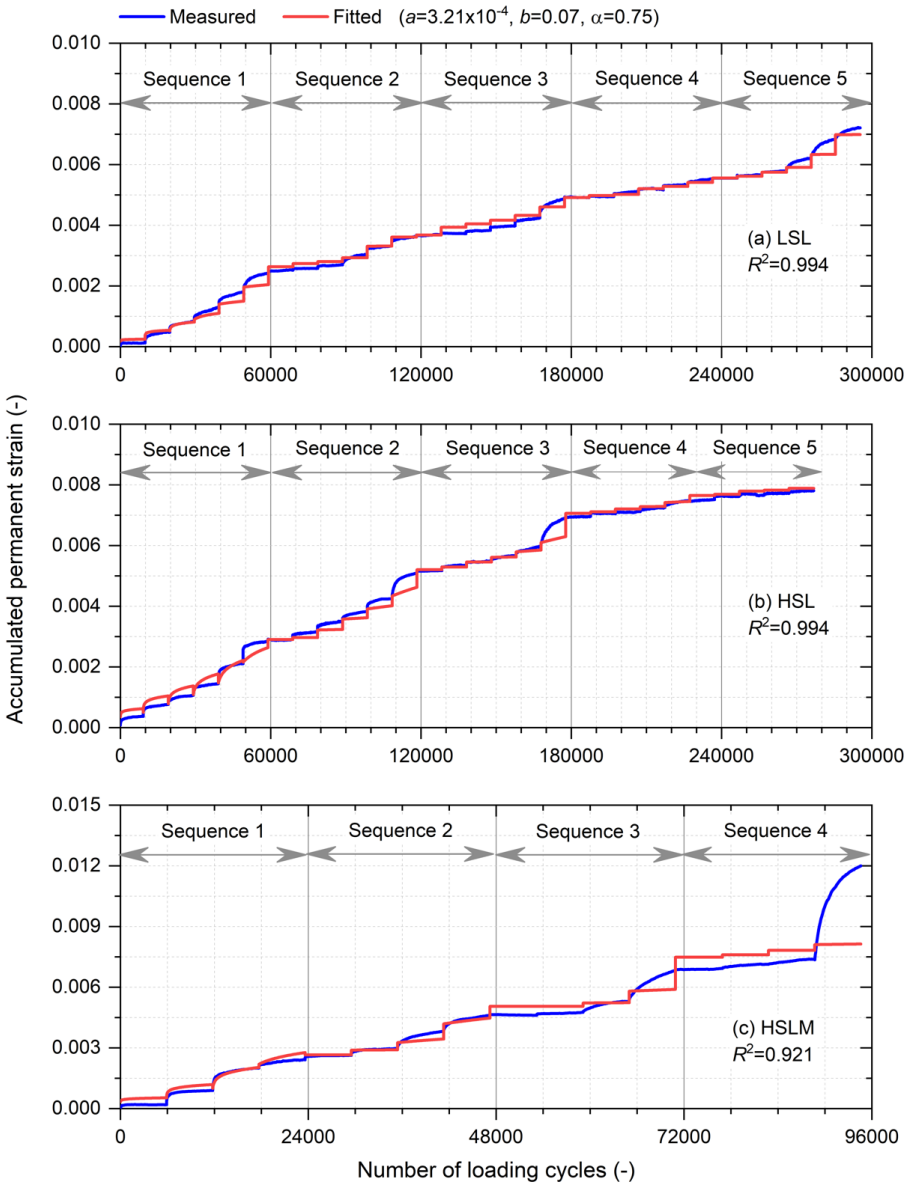

Figure 10.6: The accumulation of permanent strain with loading cycles for different stress levels; (a) low stress level LSL; (b) high stress level HSL; (c) high stress level for mining engineering HSLM.

The shakedown range was calculated for each stress path of the MS RLT tests (Werkmeister 2003; EN 13286 2004) and plotted as a function of the confining pressure-deviator stress space (Figure

10.7). The shakedown range increased gradually from A to B and from B to C when the applied deviator stress in each sequence increased (confining pressure remained constant). Most stress paths in LSL and HSL were in range A, except that some stress paths with a higher deviator stress were categorized in range B (Figure 10.7(a) and (b)). Half of the stress paths in HSLM were in range A, and others were in range B and C (Figure 10.7(c)). The shakedown range of the last stress path (the 16th stress path) was in range C (incremental collapse), corresponding to the rapid increase of permanent strain observed with loading cycles (also see above). In other words, the stress levels of the 16th stress path could therefore lead to the failure of crushed waste rocks and result in rutting (Werkmeister et al. 2004). The specimen seemed therefore to exhibit a stable behavior (i.e., either plastic shakedown or plastic creep) under LSL and HSL conditions but might become unstable (incremental collapse) for higher stress levels. Although the measured shakedown ranges can be used as a reference for the engineering practice, the stress conditions within haul roads may be more complex than the applied stress paths for MS RLT tests in the laboratory.

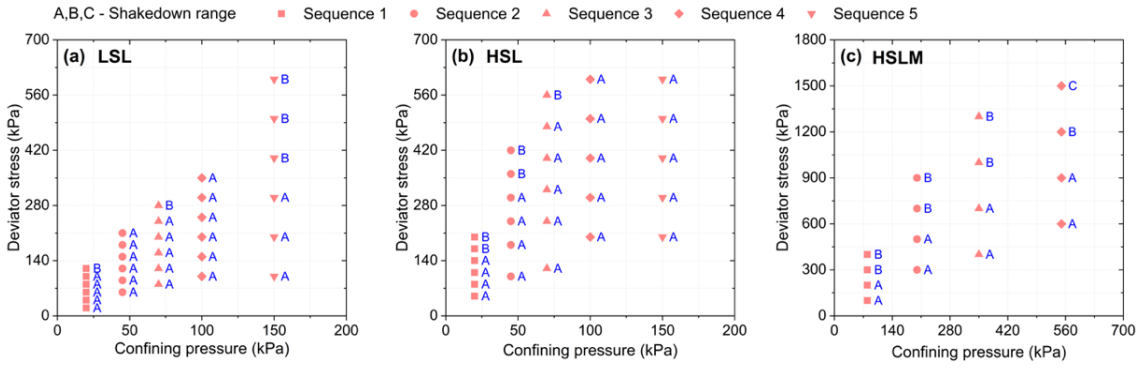

Figure 10.7: The measured shakedown range of each stress path in different stress levels, the red label of shakedown range represents an erroneous prediction; (a) shakedown range map in low stress level LSL; (b) shakedown range map in high stress level HSL; (c) shakedown range map in high stress level for mining engineering HSLM.

It can be seen that the shakedown range of crushed waste rocks changed accordingly with the variation of the stress state. Werkmeister (2004) found that certain limiting values exist to define the stress states at which the shakedown range changes. In general, the "plastic shakedown limit" is used to define the boundary of plastic shakedown A-plastic creep B, and the "plastic creep limit" is used to define the boundary of plastic creep B-incremental collapse C. The shakedown limit curves can be described by the following equation (Werkmeister 2004):

$$\sigma_{1max}=\alpha\left(\frac{\sigma_{1max}}{\sigma_3}\right)^{\beta} \quad 10.7$$

Where σ_{1max}: the peak axial stress (kPa), σ_{1max} was equal to the sum of confining pressure and deviator stress; σ_3: the confining pressure (kPa); α (kPa) and β were coefficients that depend on the type of shakedown limit and tested materials.

The shakedown limits for crushed waste rocks were approximated by fitting the shakedown range boundaries (Figure 10.8). For the plastic shakedown limit, the coefficients α and β were 9000 and -1.9, respectively; for the plastic creep limit, the coefficients α and β were 11000 and -1.35, respectively. These proposed shakedown limits could be used to estimate the shakedown range of crushed waste rocks at a certain stress state.

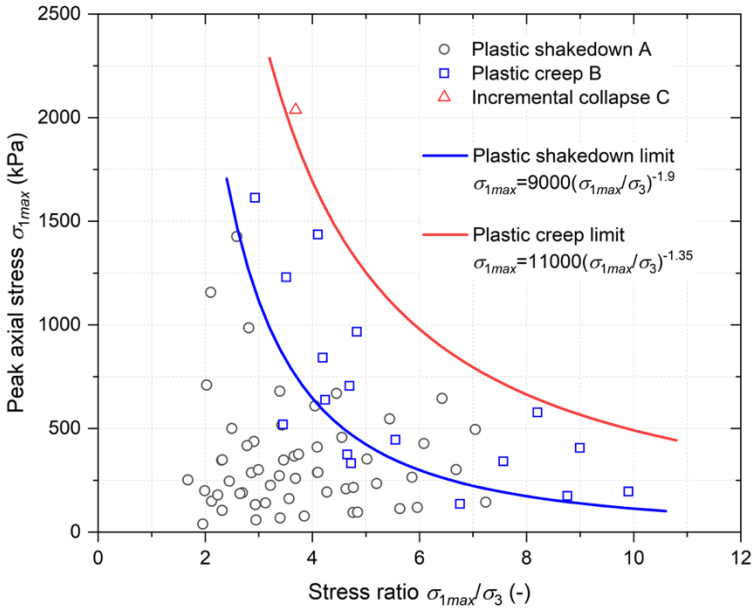

Figure 10.8: The plastic shakedown limit and plastic creep limit for crushed waste rocks.

10.4.2 Permanent strain modelling

Experimental accumulated permanent strains (for LSL, HSL, and HSLM) were fitted using the Gidel et al. (2001) model, Korkiala-Tanttu (2005) model, and Rahman and Erlingsson (2015a) model (all these models were extended using time hardening approach). Rahman and Erlingsson model showed better fitting accuracy with a coefficient of determination $R^2 > 0.92$ for all stress levels (Table 10.6). Korkiala-Tanttu model fitted the accumulated permanent strain relatively well with $R^2 > 0.84$, but the fitting performance decreased with the increasing of stress levels. The fitting performance of Gidel et al. model was low for the three stress levels ($R^2 < 0$). One possible reason for the lower prediction accuracy of Gidel et al. and Korkiala-Tanttu models was the lack of significant correlation between the permanent deformation behavior of crushed waste rocks and the shear strength properties, which was also pointed out by Lekarp et al. (1996) for unbound granular materials.

Table 10.6: The fitting performance of empirical permanent deformation models for different stress levels (LSL, HSL, and HSLM).

	Gidel et al. model	Korkiala-Tanttu model	Rahman and Erlingsson model
LSL	-0.913	0.995	0.994
HSL	-1.054	0.952	0.994
HSLM	-3.372	0.847	0.921

The calibrated Rahman and Erlingsson model coefficients a, b, and α were 3.21×10^{-4}, 0.07, and 0.75, respectively (Figure 10.6). Rahman and Erlingsson model was able to describe the accumulated permanent strains satisfactorily for LSL and HSL with $R^2 > 0.99$, although the model tended to slightly underestimate the strain for the last three stress paths in LSL (Figure 10.6(a) and (b)). The fitting performance for HSLM was relatively lower than that of LSL and HSL, especially in the sequence 4, but was still deemed acceptable with $R^2 = 0.92$ (Figure 10.6(c)).

The stress condition (mean bulk stress and deviator stress) is taken into account in Rahman and Erlingsson model, which makes it possible to describe the shakedown range of crushed waste rocks under different stress paths (Rahman and Erlingsson 2015a). The predicted shakedown range of each stress path was calculated based on the fitting curves and the shakedown criteria (Figure 10.9). The prediction accuracy of shakedown range was relatively low (< 85%). The shakedown range was tended underestimated from B to A for LSL (Figure 10.9(a)), while it was overestimated from A to B in the sequence 1 for HSL (Figure 10.9(b)). For HSLM, the shakedown range was also tended underestimated in sequence 3 and 4 (Figure 10.9(c)).

Rahman and Erlingsson model (extended using time hardening approach) seemed could describe the entire trend of accumulated permanent strains caused by numerous stress paths, but the fitting performance for the individual stress path was relatively poor, which resulted in the low prediction accuracy of shakedown ranges. Rahman and Erlingsson model showed satisfactory performance in

previous studies (Rahman and Erlingsson 2015a; Erlingsson et al. 2017). One of the possible reasons for the relatively low accuracy of shakedown range in this study was that multiple applied stress levels increased the fitting difficulty of permanent strain.

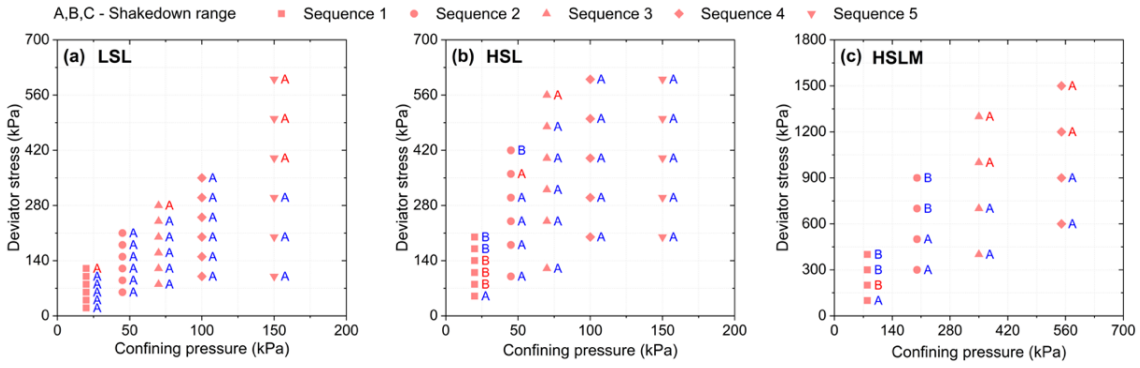

Figure 10.9: The predicted shakedown range of each stress path in different stress levels using Rahman and Erlingsson model, the red label of shakedown range represents an erroneous prediction; (a) shakedown range map in low stress level LSL; (b) shakedown range map in high stress level HSL; (c) shakedown range map in high stress level for mining engineering HSLM.

10.5 Development of ANN model

10.5.1 Determination of the optimal ANN architecture

The effect of hyperparameters on ANN performance was studied to determine the optimal ANN architecture using 4-fold cross-validation method on the training dataset. The influence of hyperparameters on the ANN performance was significant in this study.

The network performance was improved significantly with the number of epochs, and the prediction errors (MAE and MSE) for training and validation were close (Figure 10.10). MAE and

MSE decreased significantly from 25×10^{-5} to 1.5×10^{-5}, and from 20×10^{-12} to 0.1×10^{-12}, respectively, during the first 2000 epochs. The decrease rate of MAE and MSE became significantly slower after 2000 epochs, indicating the effect of epochs became limited in this case. In addition, the errors difference between training and validation tended to increase with the number of epochs since the excessive epochs would result in network overfitting on training but poor generalization on validation. The number of epochs for the ANN training was therefore set to 2000 in this study.

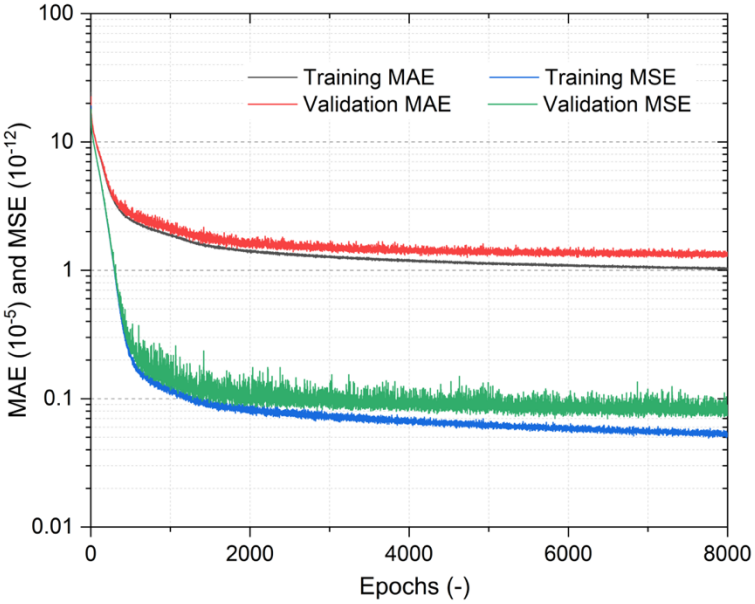

Figure 10.10: The development of ANN training and validation errors (MAE and MSE) with the number of epochs.

The effect of number of neurons per hidden layer on the neural network performance was investigated by varying number of the hidden neurons from 2 to 300 and fixing one hidden layer. The effect of number of hidden neurons on the neural network performance was significant in this study (Figure 10.11(a) and (b)). The errors MAE and MSE for training and validation were close independently of number of hidden neurons, while the Huber value for validation was lower than

that of training, which indicated that the generalization of the neural networks was acceptable. The increase of hidden neurons decreased MAE, MSE, and Huber significantly, especially when the number increased from 2 to 50: in this case, the error decreased from 16×10^{-5} to 6×10^{-5}, and from 600×10^{-10} to 80×10^{-10} for MAE and MSE, respectively; the Huber error decreased from 36×10^{-6} to 5×10^{-6}, and from 9×10^{-6} to 3×10^{-6} for training and validation, respectively. In other words, the network may not be powerful enough to accurately predict the permanent strain if the number of neurons was too small. However, the effect of increasing hidden neurons became insignificant when the number of hidden neurons was higher than 50. Similar observations were also reported in precious studies (Lee et al. 2021). In addition, large number of hidden neurons could increase the training and recalling time (Panchal et al. 2011; Vujicic et al. 2016). Hence, 50 neurons were applied in per hidden layer for the neural network in this study.

The effect of number of hidden layers on the neural network performance was studied by varying the number of the hidden layers from 1 to 7 and maintaining 50 neurons in each hidden layer. The effect of number of hidden layers on the neural network performance was significant, especially when the hidden layer increased from 1 to 3: the MAE and MSE decreased rapidly from 7×10^{-5} to 1×10^{-5}, and from 110×10^{-10} to 5×10^{-10}, respectively (Figure 10.11(c)); Huber decreased from 14×10^{-6} to 1.5×10^{-6}, and from 3.5×10^{-6} to 0.3×10^{-6} for training and validation, respectively (Figure 10.11(d)). However, the decreasing in errors was limited when the number of hidden layers was higher than 3. The errors (MAE and MSE) for training and validation were close when the number of hidden layers was lower than 3, and then it increased gradually, indicating overfitting occurred with the number of hidden layers higher than 3. Panchal et al. (2011) also reported that the overfitting problem may occur when unnecessary neurons are present in a neural network. Although some researchers suggest that a network with a single hidden layer is usually sufficient for solving complex problems (Mozumder and Laskar 2015; Hanandeh et al. 2020), the neural network with three hidden layers (50 neurons) was performing better in this study. One of the possible reasons was the relatively few input features (i.e. only three in this study) increasing the

complexity of the model learning process and architecture. Lee et al. (2021) also found that neural network with multiple hidden layers had higher accuracy than single hidden layer network in geotechnical engineering.

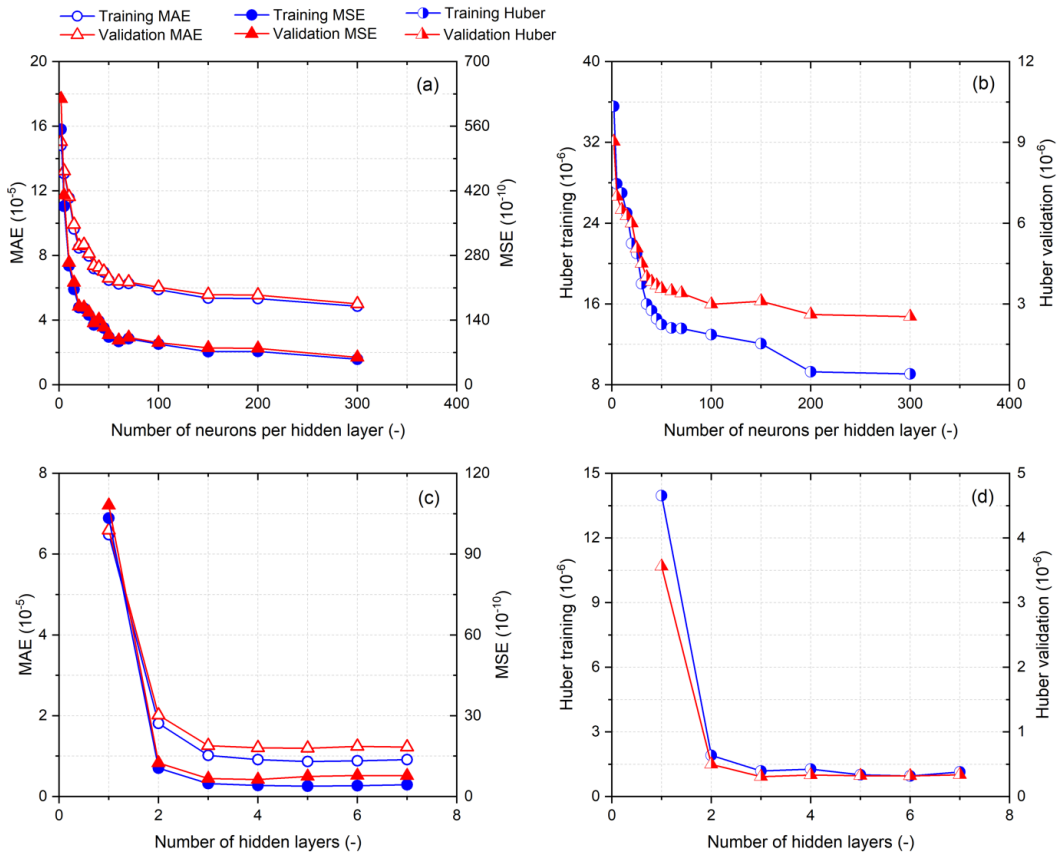

Figure 10.11: The effect of hyperparameters on the ANN prediction performance; (a) development of MAE and MSE for training and validation with the number of neurons in one hidden layer; (b) development of Huber error for training and validation with the number of neurons in one hidden layer; (c) development of MAE and MSE for training and validation with the number of hidden layers; (d) development of Huber error for training and validation with the number of hidden layers.

The influence of activation function (used in hidden layers) on the neural network performance

(with three hidden layers and 50 neurons per hidden layer) was studied by comparing the prediction errors of networks with different activation functions (i.e. Sigmoid, Tanh, ReLu, and Softmax). In this study, Tanh and ReLu functions performed better with relatively low MAE, MSE and Huber values compared to Sigmoid and Softmax functions. Particularly, the value of MAE, MSE, and Huber for Tanh were lower than 1.5×10^{-5}, 7×10^{-10}, and 1×10^{-6}, respectively, for both training and validation (Figure 10.12(a)-(c)). Tanh function therefore exhibited higher prediction accuracy (i.e. lower errors) than other activation functions, and it was therefore applied to the hidden layers for the ANN model in this study. The neural network with Softmax function showed relatively high errors, and one of the possible reasons was that this activation function is more suitable for classification issues rather than scalar regression (Gopalakrishnan et al. 2017).

Finally, the effect of regularization techniques on the neural network performance (with three hidden layers and 50 neurons per hidden layer) was studied by comparing the prediction errors of neural networks with none, one, and both two regularization techniques in this study (Figure 10.12(d)-(f)). The overfitting of neural networks with dropout and both dropout and L2 regularization was avoided adequately as the prediction error for the validation was significantly lower than that for training. However, the overall prediction performance in this case was poorer than for other networks. L2 could not completely avoid the overfitting problem as the MAE and MSE for validation was still higher than that for training but the neural network prediction accuracy was relatively high ($MAE < 2\times10^{-5}$ and $MSE < 15\times10^{-10}$). The network without regularization techniques occurred slight overfitting regarding to MAE and MSE errors, but the prediction accuracy was the highest in this case. The Huber error also showed that the network without regularization techniques had good prediction accuracy and generalization capacity, which could be attributed to the reasonable selection of the number of epochs, hidden neurons, and hidden layers. Dropout regularization could prevent overfitting efficiently for deep (or large) neural networks (Srivastava et al. 2014), but the size of the developed network in this study was relatively small, and the random dropout of hidden neurons therefore significantly decreased the prediction accuracy.

Therefore, the optimal ANN architecture for predicting permanent deformation consisted of three input features (number of loading cycles *N*, confining pressure *C*, and deviator stress *D*), one output neuron (permanent strain), and three hidden layers with 50 neurons per layer. Tanh activation function was used for the hidden neurons without regularization techniques.

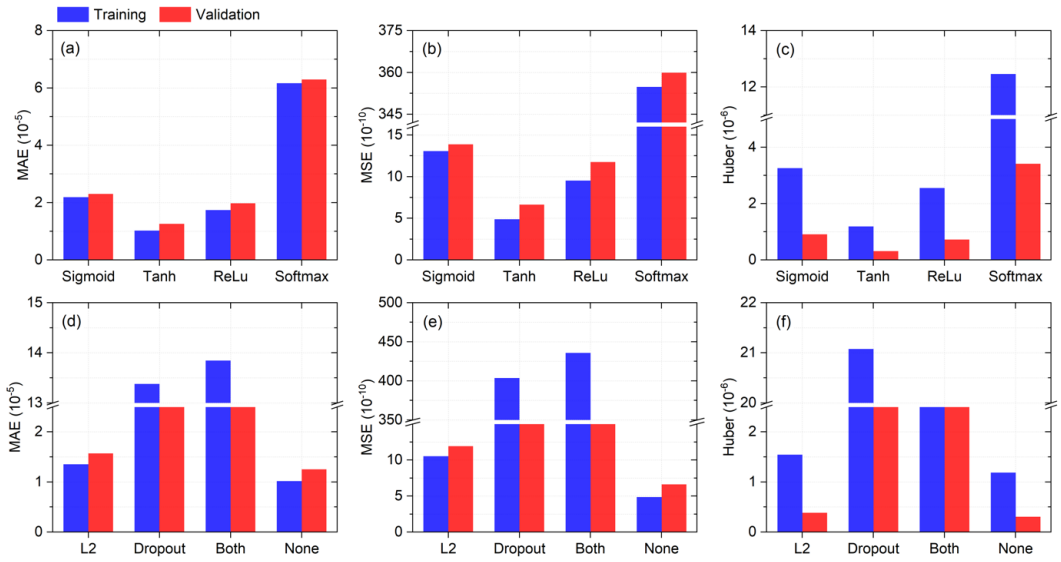

Figure 10.12: The effect of activation function and regularization technique on the ANN prediction performance; (a) MAE (b) MSE and (c) Huber for training and validation with different activation functions; (d) MAE (e) MSE and (f) Huber for training and validation with different regularization techniques.

10.5.2 Prediction of permanent strain

Here, 80% of the total experimental data were selected as the training dataset to generate the ANN model, while the remaining 20% data were used as the testing dataset to verify the developed model. The prediction errors (using MAE, MSE, and Huber) were close to or slightly lower than that of training, indicating the ANN model had a good generalization capacity (Table 10.7).

Table 10.7: The prediction errors (MAE, MSE, and Huber) of the developed ANN model for training and testing.

	MAE (10^{-6})	MSE (10^{-10})	Huber (10^{-7})
ANN training	9.76	4.67	8.26
ANN testing	10.92	4.79	2.43

The ANN model was used to predict the permanent strain of each stress path in the three stress levels, and the results showed the ANN model had a satisfactory prediction capacity (Figure 10.13). There was a strong correlation between the experimental and predicted permanent strain for both training and testing datasets ($R^2 > 0.97$), especially for HSLM where the predicted and measured permanent strains were quite close ($R^2 = 1.00$). However, there were still a few (less than 1% of total) scattered points that deviated from the best fit line for LSL and HSL (orange triangle in Figure 10.13(a) and (b)). The maximum difference between predicted and measured permanent strain was 3×10^{-4}, 2.5×10^{-4}, and 2×10^{-4} for LSL, HSL, and HSLM, respectively. The mean difference between predicted and measured permanent strain was 1.05×10^{-5} (10%), 1.25×10^{-5} (18%), and 0.85×10^{-5} (6%) for LSL, HSL, and HSLM, respectively. The prediction accuracy for the low permanent strains seemed relatively low for LSL and HSL.

The developed ANN model could predict the permanent strain accurately for both training and testing datasets since neural network can deal with nonlinearity and handle noisy data (Sinha et al. 2010). The relatively low prediction accuracy (scatter points in Figure 10.13(a) and (b)) could be attributed to the relatively large errors of strain measurement under low amplitudes (Gu, Ye, et al. 2020). Boudreau (2003) also reported that the repeatability of RLT tests is relatively low. In addition, only one LVDT was used to record the axial deformation, which could have decreased the precision of the measurements. In comparison, two LVDTs were used for RLT tests in other studies to minimize the deformation deviations (Erlingsson and Rahman 2013; AASHTO T307

2017). Considering these limitations, the accuracy of the ANN model is deemed very good.

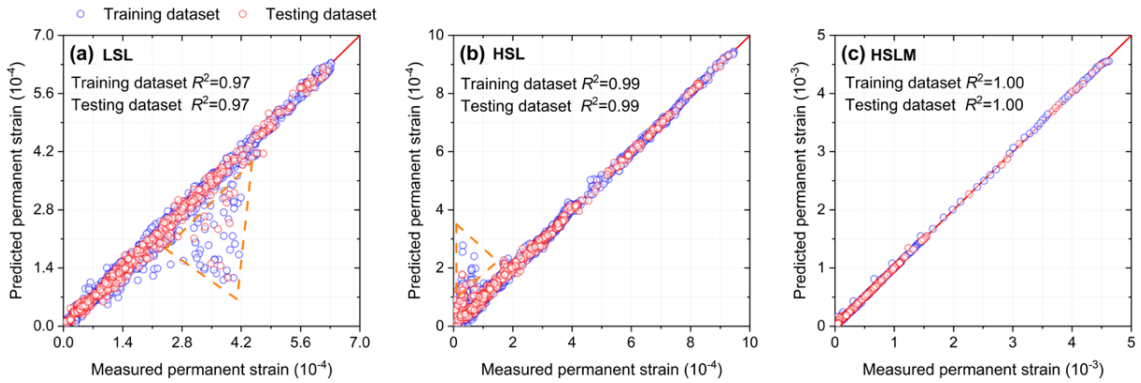

Figure 10.13: Comparison of experimental and predicted permanent strain using the ANN model for different stress levels; (a) ANN prediction performance for low stress level LSL; (b) ANN prediction performance for high stress level HSL; (c) ANN prediction performance for high stress level for mining engineering HSLM.

The shakedown ranges of each stress paths for LSL, HSL, and HSLM tests were calculated based on the predicted permanent strain values using the ANN model (Figure 10.14). There were only two erroneous predicted shakedown ranges for LSL and HSL, and one erroneous predicted shakedown range for HSLM. These errors could be explained by the fact that the measured values of ε_p^{5000}-ε_p^{3000} for these stress paths were close to 0.045×10^{-3} (i.e. the boundary between A and B ranges), and therefore more sensitive to the prediction accuracy of the permanent strain. The prediction accuracy of shakedown range for LSL, HSL, and HSLM was higher than 93% which was significantly higher than the accuracy of Rahman and Erlingsson model (65-85%; Table 10.8). The influence of the few scattered predicted points on the prediction of shakedown range was therefore limited, indicating the ANN model was reliable to predict the trend of permanent strain versus number of loading cycles for each stress path.

A Sobol (1990) sensitivity analysis was also conducted to determine the contribution and relative

importance of the input features (i.e., number of loading cycles *N*, confining pressure *C*, and deviator stress *D*) on the ANN model output (i.e. permanent strain). The sensitivity analysis was performed by assessing the response of the output permanent strain to the variation of *N*, *C*, and *D*. The deviator stress *D* showed the highest sensitivity value (0.92), indicating that deviator stress was the most significant variable affecting the permanent deformation of crushed waste rocks. The effect of confining pressure *C* and number of loading cycles *N* were also significant (Table 10.9). The results of sensitivity analysis indicated that all the input features were important and necessary for characterizing the permanent strain.

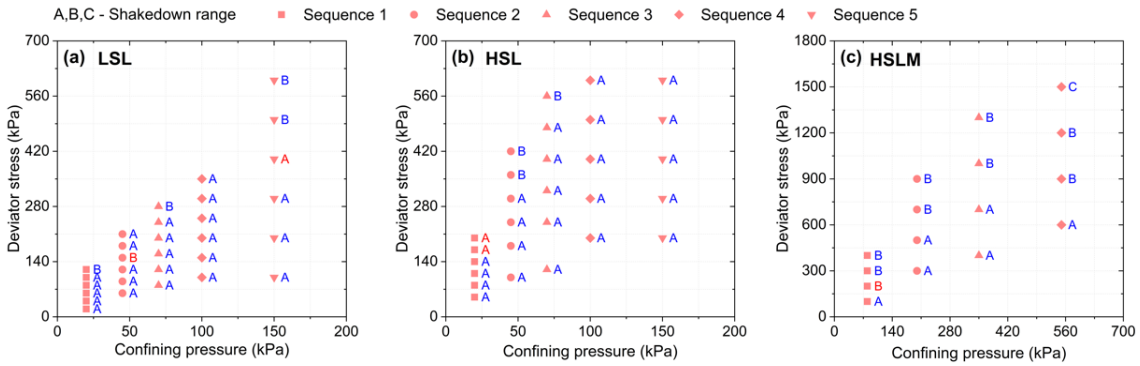

Figure 10.14: The predicted shakedown range of each stress path in different stress levels using ANN model, the red label of shakedown range represents an erroneous prediction; (a) shakedown range map in low stress level LSL; (b) shakedown range map in high stress level HSL; (c) shakedown range map in high stress level for mining engineering HSLM.

Table 10.8: Comparison of prediction accuracy of shakedown ranges between ANN model and Rahman and Erlingsson model for different stress levels (LSL, HSL, and HSLM).

	LSL	HSL	HSLM
ANN model	93%	93%	94%
Rahman and Erlingsson model	83%	82%	69%

Table 10.9: Sensitivity analysis of input features (number of loading cycles *N*, confining pressure *C*, and deviator stress *D*).

Input features	*N*	*C*	*D*
Sensitivity (-)	0.17±0.02	0.49±0.04	0.92±0.08

10.6 Discussion

ANN model was efficient to predict the permanent deformation of crushed waste rocks in this study. Some other widely used machine learning algorithms were also introduced, including k-nearest neighbors regression (KNN), decision tree regression (DT), random forest regression (RF), and support vector machine (SVM). All these machine learning models were trained on the same training dataset as the ANN (80% of total experimental data) and verified on the remaining testing dataset. Their prediction performance was assessed using MSE, MAE, and Huber (Table 10.10). Comparison results showed that ANN had the highest accuracy among all models. KNN also provided relatively good results, with prediction errors only slightly higher than ANN. Although the MSE and MAE of DT and RF models were slightly lower than that of ANN, the Huber error of DT and RF was significantly higher. Some researchers also recommend using ANN to solve geotechnical problems since it generally performs better for nonlinear data than DT and RF (Curram and Mingers 1994; Tso and Yau 2007). SVM had relatively poor performance predicting permanent deformation of crushed waste rocks compared with other models in this study.

Table 10.10: Comparison of prediction errors (MSE, MAE, and Huber) of permanent strain among different machine learning techniques including ANN, KNN, DT, RF, and SVM.

	ANN	KNN	DT	RF	SVM
MSE (training, 10^{-10})	4.67	8.02	0.26	2.24	994
MSE (testing, 10^{-10})	4.79	13.43	4.64	6.89	1182
MAE (training, 10^{-6})	9.76	11.60	2.78	3.21	125
MAE (testing, 10^{-6})	10.92	16.47	9.97	7.95	132
Huber (training, 10^{-7})	8.76	15.41	3.81×10^{6}	3.80×10^{6}	2.75×10^{6}
Huber (testing, 10^{-7})	2.43	5.82	0.25×10^{6}	0.25×10^{6}	0.18×10^{6}

The developed ANN model showed very high accuracy and generalization capacity ($R^2 > 0.97$) for predicting permanent deformation of the tested crushed wase rocks. The model was also tested to predict the permanent deformation of unbound granular materials from other studies (Rahman and Erlingsson 2015a), but the accuracy was not as good ($R^2 \approx 0.3$; detailed results not shown in this paper). The main reason for this lower performance was that only number of loading cycles N, confining pressure C, and deviator stress D were chosen as the independent input features, which limiting the model generalization to different materials. Other variables, such as gradation, mineralogy, water content and degree of compaction, which all affect the permanent deformation of unbound granular materials (Lekarp et al. 2000b), should therefore be taken into account to improve the ANN model generalization capacity. More MS RLT tests could be carried out on a wider range of materials and variables to develop a generalized prediction model.

Rahman and Erlingsson model (extended using time hardening approach) was able to fit relatively well the accumulated permanent strain caused by numerous stress paths, but the fitting accuracy for individual stress paths was limited, resulting in a relatively low prediction accuracy of shakedown ranges. Also, the fitting performance of the extended model largely relies on the initial values of the model coefficients (i.e. a, b, and α), which are generally determined through trial and error method, which can be time-consuming and complex. Although Rahman and Erlingsson (2015a) provided a detailed fitting procedure using Microsoft Excel, the engineer experience and judgement has a significant impact on the model fitting performance. This is one of the main

limitations of conventional regression models when dealing with complex and highly nonlinear data (Karlaftis and Vlahogianni 2011).

The number of neurons in the three hidden layers was the same (i.e. 50) to simplify the process of ANN development. However, the number of neurons in the hidden layers could be different which could contribute to improve the performance of the neural network (Abdeen and Hodhod 2010; Vujicic et al. 2016). Further works and a new algorithm (e.g., NeuroEvolution of Augmenting Topologies, (Stanley and Miikkulainen 2002)) would need to be conducted or applied to determine a better architecture of neural networks.

In general, the ANN model is difficult to be expressed as explicit formula, which makes its application by engineers more complex. Some studies tried to make the ANN model quantified through connection weight-bias analysis (Mozumder and Laskar 2015; Hanandeh et al. 2020), but this method was unpractical in this study because there were hundreds of neurons in the ANN model. One of the possible solutions would be to develop a user-friendly operation interface based on the proposed neural networks (Mata and Corchado 2009).

10.7 Conclusions

In this research, the permanent deformation of crushed waste rocks under three different stress levels was investigated using MS RLT tests. The empirical models extended using time hardening approach were used to fit the measured accumulated permanent strains. In addition, an ANN model was developed for the prediction of permanent strain and a sensitivity analysis was conducted to examine the influence of each input feature on the permanent strain. Based on the results of this study the following conclusions can be drawn:

1. The accumulated permanent strain increased from around 0.007 to 0.012 when the stress levels

increased from LSL to HSLM, and the slope of the accumulated permanent strain curve became steeper. Incremental collapse was observed at a high deviator stress in HSLM RLT test. The plastic shakedown limit and plastic creep limit were determined to estimate the shakedown range of crushed waste rocks at a certain stress condition.

2. Rahman and Erlingsson model (extended using time hardening approach) performed better than other empirical models for fitting the accumulated permanent strains caused by numerous stress paths ($R^2 > 0.92$), but the prediction accuracy of shakedown ranges was relatively low (< 85%) because of the relatively poor fitting for the individual stress path.

3. The optimal ANN architecture consisted of three input features (number of loading cycles N, confining pressure C, and deviator stress D), three hidden layers (50 neurons per layer) with Tanh activation function, and one output neuron for permanent strain. The ANN model was highly capable of predicting permanent strain of crushed waste rocks under different stress levels ($R^2 > 0.97$), and the prediction accuracy of shakedown ranges was higher than 93%. The ANN model appeared therefore reliable and efficient to predict the permanent strain of crushed waste rocks, but the ANN's generalization capacity for different materials should be enhanced in the future study.

4. The sensitivity analysis of input features showed that deviator stress was the most significant variable influencing the permanent strain of crushed waste rocks. The results also indicated that all the input features (N, C, and D) selected for ANN model were important and necessary for characterizing the permanent strain.

This study was part of a more comprehensive research program which aimed at optimizing mine haul road design using waste rocks. Additional laboratory tests are planned to study the effect of gradation and climatic conditions (freeze-thaw cycles and wet-dry cycles) on mechanical properties of waste rocks. These results will hopefully contribute to develop more generalized neural networks to predict the mechanical properties of waste rocks.

Acknowledgements

This work was carried out with the financial support from FRQNT and the industrial partners of Research Institute on Mines and the Environment (http://irme.ca/). The repeated load triaxial test equipment used in this study was acquired with a CFI grant.

10.8 References

AASHTO T307-99. Standard method of test for determining the resilient modulus of soils and aggregate materials. Washington, DC; 2017.

Abdeen MAM, and Hodhod H. Experimental investigation and development of artificial neural network model for the properties of locally produced light weight aggregate concrete. Engineering 2010*;* 02(06): 408-419.

Alnedawi A, Nepal KP, and Al-Ameri R. Effect of loading frequencies on permanent deformation of unbound granular materials. International Journal of Pavement Engineering 2019: 1-9.

ASTM D2487-17e1. Standard practice for classification of soils for engineering purposes (Unified Soil Classification System). ASTM International, West Conshohocken, PA; 2017.

Aubertin M. Waste rock disposal to improve the geotechnical and geochemical stability of piles. In: Proceedings of the world mining congress, Montreal, Canada; 2013.

Barksdale RD. Laboratory evaluation of rutting in base course materials. In: Presented at the Third International Conference on the Structural Design of Asphalt Pavements, Grosvenor House, Park Lane, London, England, Sept. 11-15, 1972.; 1972.

Blowes DW. The environmental effects of mine wastes. In: Proceedings of exploration; 1997.

Boudreau RL. (2003). Repeatability of the resilient modulus test procedure. In *Resilient modulus testing for pavement components*: ASTM International.

Chen L. A multiple linear regression prediction of concrete compressive strength based on physical properties of electric arc furnace oxidizing slag. International Journal of Applied Science and Engineering 2010*;* 7(2): 153-158.

Chollet F. Deep learning mit python und keras: Das praxis-handbuch vom entwickler der keras-bibliothek: MITP-Verlags GmbH & Co. KG; 2018.

Cortes C, Mohri M, and Rostamizadeh A. L2 regularization for learning kernels. arXiv preprint arXiv:1205.2653 2012.

Curram SP, and Mingers J. Neural networks, decision tree induction and discriminant analysis: An empirical comparison. Journal of the Operational Research Society 1994*;* 45(4): 440-450.

EN 13286-7. Unbound and hydraulically bound mixtures–cyclic load triaxial test for unbound mixtures. 2004.

Erlingsson S. Rutting development in a flexible pavement structure. Road Materials and Pavement Design 2012*;* 13(2): 218-234.

Erlingsson S, and Rahman MS. Evaluation of permanent deformation characteristics of unbound granular materials by means of multistage repeated-load triaxial tests. Transp Res Record 2013*;* 2369(1): 11-19.

Erlingsson S, Rahman S, and Salour F. Characteristic of unbound granular materials and subgrades based on multi stage rlt testing. Transp Geotech 2017*;* 13: 28-42.

Fan J, Wu L, Zhang F, et al. Evaluation and development of empirical models for estimating daily and monthly mean daily diffuse horizontal solar radiation for different climatic regions of china. Renewable and Sustainable Energy Reviews 2019*;* 105: 168-186.

Ghorbani B, Arulrajah A, Narsilio G, et al. Experimental and ann analysis of temperature effects on the permanent deformation properties of demolition wastes. Transp Geotech 2020*;* 24.

Gidel G, Hornych P, Breysse D, et al. A new approach for investigating the permanent deformation behaviour of unbound granular material using the repeated loading triaxial apparatus. Bulletin des laboratoires des Ponts et Chaussées 2001*;* (233).

Gopalakrishnan K, Khaitan SK, Choudhary A, et al. Deep convolutional neural networks with transfer learning for computer vision-based data-driven pavement distress detection. Constr Build Mater 2017*;* 157: 322-330.

Gu C, Ye X, Wang J, et al. Resilient behavior of coarse granular materials in three-dimensional stress state. Can Geotech J 2020*;* 57(9): 1280-1293.

Gupta D, Hazarika BB, and Berlin M. Robust regularized extreme learning machine with asymmetric huber loss function. Neural Computing and Applications 2020*;* 32(16): 12971-12998.

Han C, Ma T, Chen S, et al. Application of a hybrid neural network structure for fwd backcalculation based on ltpp database. International Journal of Pavement Engineering 2021: 1-14.

Hanandeh S, Ardah A, and Abu-Farsakh M. Using artificial neural network and genetics algorithm to estimate the resilient modulus for stabilized subgrade and propose new empirical formula. Transp Geotech 2020.

Hinton GE, Srivastava N, Krizhevsky A, et al. Improving neural networks by preventing co-adaptation of feature detectors. arXiv preprint arXiv:1207.0580 2012.

Huber PJ. Robust regression: Asymptotics, conjectures and monte carlo. Annals of statistics 1973*;* 1(5): 799-821.

Huber PJ. (1992). Robust estimation of a location parameter. In *Breakthroughs in statistics* (pp.

492-518): Springer.

Jain A, Nandakumar K, and Ross A. Score normalization in multimodal biometric systems. Pattern recognition 2005*;* 38(12): 2270-2285.

Kang F, Li J, and Dai J. Prediction of long-term temperature effect in structural health monitoring of concrete dams using support vector machines with jaya optimizer and salp swarm algorithms. Advances in Engineering Software 2019*;* 131: 60-76.

Kang F, Li J, and Xu Q. System reliability analysis of slopes using multilayer perceptron and radial basis function networks. Int J Numer Anal Met 2017*;* 41(18): 1962-1978.

Karlaftis MG, and Vlahogianni EI. Statistical methods versus neural networks in transportation research: Differences, similarities and some insights. Transportation Research Part C: Emerging Technologies 2011*;* 19(3): 387-399.

Kim S-H, Yang J, and Jeong J-H. Prediction of subgrade resilient modulus using artificial neural network. KSCE Journal of Civil Engineering 2014*;* 18(5): 1372-1379.

Korkiala-Tanttu L. A new material model for permanent deformations in pavements. In: Proceedings of the international conferences on the bearing capacity of roads, railways and airfields; 2005.

Lee D-H, Cheon E, Lim H-H, et al. An artificial neural network model to predict debris-flow volumes caused by extreme rainfall in the central region of south Korea. Engineering Geology 2020.

Lekarp F, Isacsson U, and Dawson A. State of the art. Ii: Permanent strain response of unbound aggregates. Journal of transportation engineering 2000*;* 126(1): 76-83.

Lekarp F, Richardson IR, and Dawson A. Influences on permanent deformation behavior of unbound granular materials. Transp Res Record 1996*;* 1547(1): 68-75.

Lytton RL, Uzan J, Fernando EG, et al. Development and validation of performance prediction models and specifications for asphalt binders and paving mixes (Vol. 357): Strategic Highway Research Program Washington, DC; 1993.

Mahdevari S, and Torabi SR. Prediction of tunnel convergence using artificial neural networks. Tunn Undergr Sp Tech 2012*;* 28: 218-228.

Mata A, and Corchado JM. Forecasting the probability of finding oil slicks using a cbr system. Expert Systems with Applications 2009*;* 36(4): 8239-8246.

Meyer GP. An alternative probabilistic interpretation of the Huber loss. arXiv preprint arXiv:1911.02088 2019.

Mozumder RA, and Laskar AI. Prediction of unconfined compressive strength of geopolymer stabilized clayey soil using artificial neural network. Computers and Geotechnics 2015*;* 69: 291-300.

Panchal G, Ganatra A, Kosta Y, et al. Behaviour analysis of multilayer perceptrons with multiple hidden neurons and hidden layers. International Journal of Computer Theory and Engineering 2011*;* 3(2): 332-337.

Pérez-González E, Bilodeau J-P, Doré G, et al. Assessment of the permanent deformation at the earth-core of a rockfill dam under heavy vehicle loading. Can Geotech J 2020*;* (999): 1-11.

Phaisangittisagul E. An analysis of the regularization between l2 and dropout in single hidden layer neural network. In: 2016 7th International Conference on Intelligent Systems, Modelling and Simulation (ISMS); 2016.

Rahman MS, and Erlingsson S. A model for predicting permanent deformation of unbound granular materials. Road Materials and Pavement Design 2015*;* 16(3): 653-673.

Rumelhart DE, Hinton GE, and Williams RJ. Learning representations by back-propagating errors. Nature 1986*;* 323(6088): 533-536.

Saha S, Gu F, Luo X, et al. Use of an artificial neural network approach for the prediction of resilient modulus for unbound granular material. Transportation Research Record: Journal of the Transportation Research Board 2018*;* 2672(52): 23-33.

Salour F, and Erlingsson S. Permanent deformation characteristics of silty sand subgrades from multistage rlt tests. International journal of pavement engineering 2017*;* 18(3): 236-246.

Sharma S. Activation functions in neural networks. Towards Data Science 2017*;* 6.

Sinha S, Singh T, Singh V, et al. Epoch determination for neural network by self-organized map (SOM). Computational Geosciences 2010*;* 14(1): 199-206.

Sobol' IyM. On sensitivity estimation for nonlinear mathematical models. Matematicheskoe modelirovanie 1990*;* 2(1): 112-118.

Srivastava N, Hinton G, Krizhevsky A, et al. Dropout: A simple way to prevent neural networks from overfitting. The journal of machine learning research 2014*;* 15(1): 1929-1958.

Stanley KO, and Miikkulainen R. Evolving neural networks through augmenting topologies. Evolutionary computation 2002*;* 10(2): 99-127.

Sun Q, Zhou W-X, and Fan J. Adaptive huber regression. Journal of the American Statistical Association 2020*;* 115(529): 254-265.

Sweere GT. Unbound granular bases for roads. University of Delft, Delft, The Netherlands, 1990.

Tarawneh B, and Nazzal MD. Optimization of resilient modulus prediction from fwd results using artificial neural network. Periodica Polytechnica Civil Engineering 2014*;* 58(2): 143-154.

Thompson RJ. Technical Report, Curtin University, Australia. Mine haul road design, construction and maintenance management. 2011.

Tso GKF, and Yau KKW. Predicting electricity energy consumption: A comparison of regression analysis, decision tree and neural networks. Energy 2007*;* 32(9): 1761-1768.

Vidal A, and Kristjanpoller W. Gold volatility prediction using a CNN-LSTM approach. Expert Systems with Applications 2020.

Vieira CS, and Pereira PM. Use of recycled construction and demolition materials in geotechnical applications: A review. Resources, Conservation and Recycling 2015*;* 103: 192-204.

Vujicic T, Matijevic T, Ljucovic J, et al. Comparative analysis of methods for determining number of hidden neurons in artificial neural network. In: Central european conference on information and intelligent systems; 2016.

Wager S, Wang S, and Liang PS. Dropout training as adaptive regularization. In: Advances in neural information processing systems; 2013.

Werkmeister S. Permanent deformation behavior of unbound granular materials. University of Technology, Dresden 2003.

Werkmeister S. Permanent deformation behaviour of unbound granular materials in pavement constructions. 2004.

Werkmeister S, Dawson A, and Wellner F. Pavement design model for unbound granular materials. Journal of Transportation Engineering 2004*;* 130(5): 665-674.

Werkmeister S, Dawson AR, and Wellner F. Permanent deformation behavior of granular materials and the shakedown concept. Transp Res Record 2001*;* 1757(1): 75-81.

Wolff H, and Visser A. Incorporating elasto-plasticity in granular layer pavement design. In: Proceedings of the Institution of Civil Engineers-Transport; 1994.

Xu J, Chen Y, Xie T, et al. Prediction of triaxial behavior of recycled aggregate concrete using multivariable regression and artificial neural network techniques. Constr Build Mater 2019*;* 226: 534-554.

Xue Y, Bai C, Qiu D, et al. Predicting rockburst with database using particle swarm optimization

and extreme learning machine. Tunn Undergr Sp Tech 2020*;* 98: 103287.

Yang X, and Han J. Analytical model for resilient modulus and permanent deformation of geosynthetic-reinforced unbound granular material. Journal of Geotechnical and Geoenvironmental Engineering 2013*;* 139(9): 1443-1453.

Yi C, and Huang J. Semismooth newton coordinate descent algorithm for elastic-net penalized huber loss regression and quantile regression. Journal of Computational and Graphical Statistics 2017*;* 26(3): 547-557.

Zhang W, and Goh ATC. Multivariate adaptive regression splines for analysis of geotechnical engineering systems. Computers and Geotechnics 2013*;* 48: 82-95.

Zheng C. A new principle for tuning-free huber regression. Statistica Sinica 2020.

Zhou F, Fernando E, and Scullion T. Texas Transportation Institute. Development, calibration, and validation of performance prediction models for the texas me flexible pavement design system. 2010.

CHAPTER 11 GENERAL DISCUSSION

11.1 Summary

11.1.1 Valorization of waste rocks

Literature review (Chapter 2) has shown that mining operations can generate large quantities of waste rocks, and that their management after their usual deposition in piles, can be a great challenge. The valorization of waste rocks in mining facilities such as waste rock inclusions, cover systems, backfills, and mine haul roads is therefore an attractive alternative to surface disposal, both economically and environmentally. This project research focused on the reuse of waste rocks in mine haul roads. The design of mine haul roads consists of geometric, structural, functional, and maintenance design, and the structural and functional design is the emphasis in this project. The mechanical properties of waste rocks, including CBR, shear strength, resilient modulus, and permanent deformation, are critical parameters for the design of mine haul roads. However, the literature review has shown that relevant research on the mechanical properties of waste rocks from hard rock mine were relatively limited, especially for mine haul roads that are subjected to significantly different traffic loading compared to highways. The applicability of laboratory test procedures and standards developed for highways to waste rocks should be assessed. Factors impacting the mechanical properties of waste rocks need to be quantified. The fitting performance of mathematical regression models to waste rock mechanical properties need to be evaluated. Machine learning, as an analytical alternative to conventional statistical method, is more and more commonly used in geotechnical engineering applications, and may also bring useful information to predicting waste rock mechanical properties.

11.1.2 Studied materials and laboratory tests

The studied waste rocks (including crushed and uncrushed materials) in this project were obtained from Canadian Malartic Mine. A thorough laboratory characterization program was conducted in Polytechnique Montreal laboratories to determine the physical properties of the waste rocks, including particle size distribution, particle shape, mineralogy, specific gravity, and compaction properties (Chapter 3). The maximum particle size of crushed and uncrushed waste rocks was 25 and 60 mm, respectively. The waste rocks contained more than 65% of gravel, and around 5% of fines, and were classified as poorly graded gravel. The elongation index and flakiness index of the studied crushed waste rocks were 38.56±1.62% and 34.95±2.08%, respectively. Waste rocks were mainly composed of quartz, albite, muscovite, and chlorite, corundum, and diopside, and they were considered non-acid generating materials. The specific gravity was 2.71 and 2.75 for particles larger and smaller than 4.75 mm, respectively. Following modified Proctor tests, the optimum water content of crushed waste rocks was 5.6%, for a corresponding maximum dry density of 2334 kg/m^3.

A total of 112 laboratory tests, including CBR and triaxial tests (both monotonic and cyclic load) were carried out to measure the CBR, shear strength, stiffness, and permanent deformation of crushed (19 mm of maximum particle size) and uncrushed (60 mm of maximum particle size) waste rocks in this study.

11.1.3 Applicability of the existing laboratory test standards

The existing laboratory test standards such as standard Proctor test (ASTM D698 2012), modified Proctor test (ASTM D1557 2012), AASHTO T307 standard (AASHTO T307 2017), and EN 13286 standard (EN 13286 2004) were initially proposed for usual soils or highways. These standards were therefore modified for waste rocks and mine haul roads in this project

Different compaction energies were used to prepare crushed waste rock specimens, i.e., standard effort (STD), 600 kN-m/m^3 (ASTM D698 2012) and modified effort (MOD), 2700 kN-m/m^3 (ASTM D1557 2012). An alternative compaction method (MOD 81) was also used in this study. MOD 81 compaction used a modified effort hammer (44.48 N), but with 81 blows per layer (instead of 56 blows; the rest of the test being identical to ASTM D1557). The objective was to simulate a higher compaction energy (3905 kN-m/m^3) which was more representative of field conditions where compaction is achieved using heavy mining trucks (Chapter 4). The dry density increased about 9% (i.e., from 2039 to 2227 kg/m^3) when the compaction energy increased from STD (600 kN-m/m^3) to MOD (2700 kN-m/m^3). The increase of dry density was, however, relatively limited when the compaction energy increased from MOD to MOD 81 (3905 kN-m/m^3; 2250 kg/m^3). The different compaction effort also changed the final particle size distribution after repeated load CBR tests. The proportion of coarse particles (14-19 mm) decreased between 3 and 8%, depending on compaction energy. The decrease was more pronounced for higher compaction energies (-8% for MOD 81 compaction) than for small energies (-4% for STD compaction). On the other hand, the fine content (< 0.075 mm) increased, by up to 7% for MOD 81. The in-situ dry density of surface layer of haul roads comprises between 2250 and 2375 kg/m^3 (Laverdière 2019). The dry density of crushed waste rocks compacted using MOD and MOD 81 was therefore closer to the density measured in the field and, to a certain extent, increasing the hammer blows could better simulate the in-situ compaction of haul roads.

The compaction standards, i.e., ASTM D698 (2012) and ASTM D1557 (2012), could not be used for uncrushed waste rocks since the hammers in these standards were too small to compaction the coarse-grained waste rocks (60 mm of maximum particle size). A hammer was therefore especially designed for compacting the large waste rock samples in this study (Chapter 7). The hammer was made of a 5 kg rammer dropped from a height of 1 m on a base plate with 160 mm diameter, and the compaction effort caused by one below of this hammer was 6.7 times the standard Proctor test hammer (ASTM D698 2012). There were three compaction efforts applied on uncrushed waste

rocks, i.e., 31, 62, and 93 blows on each of the five layers of the samples, corresponding to 180, 360, and 540 kJ/m^3, respectively. The dry density increased from 1872 to 2004 and 2014 kg/m^3 when the compaction effort increased from 180 to 360 and 540 kJ/m^3. The designed hammer in this study was therefore able to compact the coarse-grained waste rocks for laboratory tests, and it could be used in the future project.

AASHTO T307 (2017) standard is generally used to evaluate the resilient modulus of pavement materials, but it was initially proposed for highway design, with a maximum axial stress varying from 20.7 to 275.8 kPa and confining pressure from 20.7 to 137.9 kPa (for base/subbase materials). However, this stress level was significantly lower than the tire pressure of mining trucks, e.g., around 1000 kPa ("Electric drive mining truck 960e-2k"). High stress combinations of axial and confining stresses (HSL) were therefore proposed to evaluate the resilient behavior of crushed waste rocks under heavy mining trucks (Chapter 4). The maximum axial stress and confining pressure were between 80 and 2000 kPa, and between 100 and 1000 kPa, respectively, which could cover the range of stress variation in the field, even for the heavier mining truck (e.g., BELAZ 75710 with 450 mt of payload capacity). The resilient modulus of crushed waste rocks under high stress condition was significantly higher than for low stress conditions. The resilient modulus prediction model (M_R-θ model) calibrated from repeated load triaxial test results under low stress level (AASHTO T307 2017) tended to underestimate the resilient modulus of crushed waste rocks used in mine haul roads, as crushed waste rocks exhibited some “stiffening” with increasing stress levels. The experimental results indicated that the proposing high stress level (HSL) for measuring resilient modulus was necessary, and it was able to estimate the resilient behavior of waste rocks in haul roads more accurately.

EN 13286 standard (2004) is often used to evaluate the permanent deformation of pavement materials, and it proposed two sets of stress levels for highways with a deviator stress varying from 20 to 600 kPa and confining pressure from 20 to 150 kPa. The stress levels in European Standard

13286 (2004) were therefore significantly lower than the stress conditions in haul roads caused by mining trucks. Therefore, another high stress level (HSLM) was specifically defined in this study to represent typical stress conditions within mine haul roads. The confining pressure and deviator stress in the new stress level ranged from 80 to 550 kPa, and from 100 to 1500 kPa, respectively. The accumulated permanent strain for HSLM increased with the stress paths, but the curve was steeper than for the stress levels in EN 13286 standard (2004) because of the significantly greater deviator stress. The different stress levels resulted in the variation of permanent deformation behavior, indicating that the proposed HSLM was necessary and more accurate to estimate the permanent deformation behavior of waste rocks under heavy mining trucks.

The dry density of crushed waste rocks compacted using MOD and MOD 81 was similar and close to the in-situ density, indicating that modified Proctor (MOD) compaction effort or higher effort should be used for sample preparation to match the density in the field. The special designed big hammer could compact coarse-grained waste rocks sufficiently to simulate the field condition, and this hammer was therefore necessary for large-scale triaxial test. The proposed stress levels (HSL and HSLM) could better represent the stress states within haul roads, and therefore the existing laboratory standards for repeated load triaxial tests (i.e., AASHTO T307 and EN 13286) should be modified to estimate the resilient and permanent behavior of waste rocks under mining trucks.

11.1.4 Suitability of repeated load CBR test to characterize waste rocks

Repeated load CBR tests were setup to estimate the stiffness (equivalent modulus) and permanent deformation of crushed waste rocks under different stress levels in Chapter 4 and 5. The principle of repeated load CBR test is similar to the standard CBR test, except that cyclic loads are applied (Molenaar 2008; ASTM D1883 2016). The applicability of existing calculation equations of equivalent modulus to crushed waste rocks was evaluated. Experimental results showed that the impact of loading frequency and waveform was limited, while the measured equivalent modulus

increased significantly with contact stress. The effect of dry density and soaking on equivalent modulus was negligible, but specimen drying resulted in a marked increase of the equivalent modulus. An equation and a model were proposed for repeated load CBR tests to calculate the equivalent modulus and evaluate the permanent deformation of crushed waste rocks under different stress conditions, respectively. The stiffness and permanent deformation measured from repeated load CBR tests and repeated load triaxial tests were comparable, indicating that repeated load CBR tests could be used as an effective alternative to repeated load triaxial tests.

11.1.5 Effect of gravel-to-sand ratio and fines content

Gradation of aggregates is a key factor that affects the mechanical properties including resilient modulus (Duong et al. 2016; Hatipoglu et al. 2020), permanent deformation (Wang et al. 2018), and shear strength (Xiao et al. 2012; Yang and Luo 2018; Qi, Cui, Chen, et al. 2020), which can be attributed to the change of waste rocks fabric (Thom and Brown 1988; Kolisoja 1997). A series of repeated load and monotonic triaxial tests (150 mm and 300 mm of specimen diameter) were therefore carried out on crushed and uncrushed waste rocks to study the gradation effect by modifying the gravel-to-sand ratio and fines content (Chapter 6 and 7).

An increasing in gravel-to-sand ratio increased the resilient modulus and shear strength of crushed waste rocks until the optimum gravel-to-sand ratio, and the optimum gravel-to-sand ratio was 1.5 and 1 for stiffness and shear strength, respectively, exceeded, resilient modulus and shear strength decreased. The permanent strain decreased slowly as gravel-to-sand ratio increased from 0.5 to 1.5, but it increased very sharply when gravel-to-sand ratio increased to 3. The optimum gravel-to-sand ratio for crushed waste rocks was therefore 1 to 1.5. The optimum fines content for resilient modulus and shear strength of crushed waste rocks was around 5% and 8%, respectively, while the permanent strain tended to decrease when fines content increased from 3.75% to 12%. However, the selection of fines content for haul roads would require considering other specifications in

practice (e.g., AASHTO M-147 specifications for highway base layers and Guidelines for mine haul road design).

For uncrushed (coarse-grained) waste rocks, the optimal gravel-to-sand ratio regarding to the resilient modulus and shear strength was around 5. Permanent strain was close when the gravel-to-sand ratio ranged between 1 and 5, but it decreased significantly when the ratio increased to 8. The influence of fines content (0-10%) on the mechanical properties of uncrushed waste rocks was insignificant because the variation of fines content and dry density was limited.

Gravel-to-sand ratio was therefore a practical grading parameter to optimize the mechanical properties of both crushed and uncrushed waste rocks for haul roads in the field. The original gravel-to-sand ratio of crushed waste rocks was 2.3, and so the original materials should be crushed more to improve the mechanical characterization in the field. The original gravel-to-sand ratio of uncrushed waste rocks was 5 that was the optimum. Fines content was not recommended as a grading parameter for optimizing the mechanical properties of waste rocks considering the relevant specifications on fines content, the insignificant effect, and the limited amount in the field (< 10%; (Gamache-Rochette 2004; Bussière 2007b)).

11.1.6 Effect of other basic physical properties

The effect of other basic physical properties including maximum particle size, compaction effort, and water content on the mechanical properties of uncrushed waste rocks was studied using large-scale triaxial tests (Chapter 7).

An increasing in maximum particle size (25, 40, and 60 mm) resulted in growth of resilient modulus. The resilient modulus increased 25-45% when maximum particle size increased from 25 mm to 40 mm. The effect of maximum particle size was relatively low as it increased to 60 mm, i.e., around 5% increasing compared to 40 mm. The shear strength (peak deviator stress) increased

gradually with the maximum particle size, and it was around 500, 600, and 700 kPa under 50 kPa of confining pressure for maximum particle size 25 mm, 40 mm, and 60 mm, respectively. The permanent deformation of waste rocks with 60 mm maximum particle size was slightly lower than that of 25 mm and 40 mm maximum particle size.

The effect of compaction effort on the mechanical properties of coarse-grained waste rocks was significant. An increasing of compaction effort from 180 to 360 kJ/m^3 resulted in significant increase of resilient modulus and shear strength and decrease of permanent deformation because of the increase of dry density. However, the impact of more compaction effort (540 kJ/m^3) on the density and mechanical properties was limited.

The influence of water content (final value 0.9-2.3%) on the resilient modulus, shear strength, and permanent deformation of uncrushed waste rocks was insignificant because the variation of water content and dry density was limited.

Increasing the maximum particle size would be beneficial to the mechanical properties of waste rocks in the field. The maximum particle size for haul roads in practice actually can be higher than 100 mm (Tannant and Regensburg 2001), which is significantly higher than 60 mm tested in this study. However, the maximum particle size should be smaller than the 2/3 of the layer thickness, and larger particles should be removed or crushed (Tannant and Regensburg 2001). An increasing of compaction effort could increase the dry density and mechanical properties of waste rocks, but the effect of excessive compaction effort higher than a certain value (i.e., 360 kJ/m^3 in this study) would be limited. Considering the extreme heavy weight of mining trucks, it is considered sufficient to compact haul roads using mining trucks in the field. The influence of water content on the mechanical properties was insignificant (specially for uncrushed waste rocks), the rainy weather therefore has limited influence on the construction of base/subbase layers of haul roads.

11.1.7 Impact of freeze-thaw and wetting-drying cycles

Environmental conditions have a major factor influence on the performance of mine haul roads (Maalouf et al. 2012). A series of triaxial tests (monotonic and repeated load) and CBR tests (standard and repeated load) were therefore carried out to evaluate the impact of freeze-thaw cycles and wetting-drying cycles on the mechanical properties of crushed waste rocks (Chapter 8).

The effect of freeze-thaw cycles on the mechanical properties of crushed waste rocks was relatively significant during the first 4 cycles, and the material nearly reached an equilibrium state after 10 freeze-thaw cycles. The resilient modulus and shear strength of crushed waste rocks subjected to repeated freeze-thaw cycles were reduced by 11% and 7%, respectively, while the accumulated permanent strain increased by 20%.

In this study, the water content varied from 1.9% to 3.5% for the freeze-thaw tests, and the corresponding degree of saturation increased from around 5% to 10% which was considered relatively low. The impact of this limited increase of saturation on the resilient modulus and shear strength was insignificant (<5%). However, the increase of saturation resulted in a significant increase of permanent deformation (over 80% increase for less than 5% increase of water saturation).

Wetting-drying cycles could result in a 32% increase of the CBR. The influence of wetting-drying cycles on stiffness (equivalent modulus) was negligible at low axial stress (<800 kPa), but caused an 18% increase at high axial stress. The permanent deformation increased by 100% following repeated wetting-drying cycles. Similarly to the freeze-thaw cycles, the effect of wetting-drying cycles on the geotechnical characteristics was limited after 5 cycles.

Freeze-thaw cycles could reduce the mechanical performance of waste rocks and higher water content would increase this effect, which may increase the maintenance frequency of haul roads. For the haul roads in cold climate, the effect of freeze-thaw cycles should be considered during the haul road design. Although the impact of wetting-drying cycles on the mechanical properties of waste rocks was limited, it may decrease the road trafficability because of muddy surface (caused

by wetting such as rainfall) and dust (caused by drying in hot weather).

11.1.8 Existing mathematical models fitting

Several mathematical models were proposed in the literature to describe the resilient modulus of pavement materials. M_R-θ model and MEPDG model appeared to be more suitable to describe the stress dependency of waste rock resilient modulus (coefficient of determination R^2 higher than 0.9). The M_R-θ model coefficient k_1 was affected significantly by the physical properties of waste rocks and tended to increase with resilient modulus. Model coefficient k_2 tended to decrease with resilient modulus, and its variation was relatively small (Chapter 6 and 7). MEPDG model coefficient k_1 tended to decrease with the number of freeze-thaw cycles, while coefficients k_2 and k_3 for the different specimens were close for the different specimens (Chapter 8).

Several permanent deformation models were proposed to describe the permanent deformation with number of loading cycles. Rahman and Erlingsson model (extended using time hardening approach) was the most suitable model to fit the accumulated permanent strains of both crushed and uncrushed waste rocks in this project (coefficient of determination R^2 higher than 0.9). The Rahman and Erlingsson model coefficient α was usually relatively constant, and it was therefore fixed to 0.75 (Chapter 5), 0.45 (Chapter 6 and 8), and 0.3 (Chapter 7) to minimize the number of model coefficients. The model coefficient a was affected significantly by physical properties of waste rocks, and tended to increase with the accumulated permanent strain, while the variation of coefficient b was relatively limited.

Coefficient prediction models (k_1, k_2, a, and b), expressed as a function of gradation properties (Chapter 6) and climatic factors (Chapter 8), were also developed to evaluate the effect of gradation on resilient modulus and permanent deformation of waste rocks.

11.1.9 Development of machine learning models

Predicting CBR, resilient modulus, and permanent deformation of waste rocks accurately and efficiently can be useful to reduce costs and ensure optimal pavement performance. Although the fitting performance of conventional regression models was acceptable (section 11.1.8), the extrapolation performance of the calibrated models on new cases such as new stress states in the field was not certain. Also, the fitting process of permanent deformation model was complex and time-consuming. Different machine learning algorithms, including multiple linear regression (MLR), support vector machine (SVM), k-nearest neighbors (KNN), decision tree (DT), random forest (RF), backpropagation neural network (BPNN), and neuroevolution of augmenting topologies (NEAT), were therefore used to develop prediction models for CBR, resilient modulus, and permanent deformation of crushed waste rocks based on experimental data (Chapter 9 and 10).

Dry density, compaction energy, fines content, C_C, C_U, D_{10}, D_{60}, and maximum particle size were selected as the input variables for the CBR models based on Pearson correlation analysis. The parameters in repeated load triaxial test, i.e., number of loading cycles in each stress path, confining pressure, and deviator stress could affect the resilient modulus of crushed waste rocks, and they were therefore selected as the input variables for resilient modulus models and permanent strain. The machine learning models were trained on training dataset and verified on testing dataset.

For CBR and resilient modulus, the performance of MLR models was relatively low because of the limitation of simple linear relationship. Other models showed good performance, particularly, the DT and RF models exhibited higher precision and satisfactory generalization capacity for both CBR ($R^2 > 0.91$) and resilient modulus ($R^2 > 0.99$) (Chapter 9). The prediction accuracy of KNN and BPNN models for CBR was influenced significantly by the dataset size. Although the NEAT models were not the best choice in terms of prediction accuracy, they are still worth to be considered in the following study because of their good generalization capacity and simple structure. The model hyperparameters, including number of KNN neighbors, maximum DT depth,

number of RF estimators, number of hidden neurons and hidden layers in BPNN, could affect the prediction performance significantly for both CBR and resilient modulus. These parameters should be studied and analyzed during the development of artificial intelligence models.

For permanent deformation, BPNN model showed higher prediction accuracy than other machine learning models (Chapter 10). The optimal BPNN architecture consisted of three input features (number of loading cycles, confining pressure, and deviator stress), three hidden layers (50 neurons per layer) with Tanh activation function, and one output neuron for permanent strain. The BPNN model was highly capable of predicting permanent strain of crushed waste rocks under different stress levels ($R^2 > 0.97$), and the prediction accuracy of shakedown ranges was higher than 93%. The BPNN model appeared therefore reliable and efficient to predict the permanent strain of crushed waste rocks, but the model generalization capacity for different materials should be enhanced in the future study. The sensitivity analysis of input features showed that deviator stress was the most significant variable influencing the permanent strain of crushed waste rocks. The results also indicated that all the input features selected for BPNN model were important and necessary for characterizing the permanent strain.

The research results indicate that machine learning was a good alternative to regression method to predict the mechanical properties of waste rocks. The developed models can be extended via taking more physical properties into account (i.e., as the input features) in the future studies. However, machine learning model is difficult to be expressed as explicit formula, which makes its application by engineers more complex than other analytical models.

11.2 Discussion

This project presents an experimental study that evaluate the mechanical properties of waste rocks from hard rock mine used for haul roads. It also presents the mathematical description and machine learning prediction of the mechanical properties of waste rocks. The research results can help

improve the design of mine haul roads using waste rocks. However, it should be recalled here that the analyses in this project were based on some simplifying assumptions. The specific limitations associated with each sub-objective have been addressed in the "Discussion" of each chapter (Chapter 4-10). The main limitations of this project are summarized below.

Limited tested materials: Although the waste rocks used in this project were representative of hard rock mines (Bussière 2007a; James et al. 2013), they were obtained from one mine site (Canadian Malartic Mine), and the impact of mineralogy on the experimental results could not be studied. The applicability of obtained conclusions from the experimental results to other materials is therefore uncertain. The generalization of proposed descriptive and predictive models is therefore also limited to other materials.

Low cyclic loading frequency: The cyclic loading frequency applied in repeated load laboratory tests was lower than 1 Hz because of the limitation of the laboratory apparatus. However, it was significantly lower than the loading frequencies caused by mining trucks (CAT 793F) on haul roads which typically are around 3 to 4 Hz (assuming a driving speed of 12 to 15 km/h and a payload rear tire contact radius of around 0.55 m). This low loading frequency can limit the study of realistic mechanical response of waste rocks under mining trucks in the field.

Constant Poisson's ratio: Poisson's ratio of waste rocks was not measured in this research, and was assumed to be constant and equal to 0.35. In practice, Poisson's ratio is not a constant and it may increase with a decrease in confining pressure and an increase in deviator stress (Hicks and Monismith 1971). The density, fines content, water content, aggregate type, and particle shape also affect the Poisson's ratio (Lekarp et al. 2000a). An accurate Poisson's ratio of waste rocks is needed

for the mechanistic design of mine haul roads.

Effect of principal stress reorientation: The effect of principal stress reorientation on permanent deformation behavior of waste rocks was not considered in this study. In practice however, a reorientation of the principal stress can occur in real pavement structures under moving traffic load (Qian et al. 2016), which could result in large permanent strain, exceeding the deformation measured using repeated load triaxial tests in the laboratory (Lekarp et al. 2000b; Qian et al. 2016). The measured permanent deformation in this project therefore tends to underestimate the deformation occurred in the field.

Sample preparation of wetting-drying tests: In the wetting-drying study, even though the specimens were soaked in water in the wetting-drying tests, the approach used in this study could not completely and realistically simulate field condition such as the rainfall splash and water flows which would cause particle migration and change the fabric of waste rocks (Cui et al. 2017; Cui et al. 2019). Results in this study are therefore expected to have underestimated the effect of wetting-drying cycles compared to what would happen in the field.

Limited stress paths in large-scale triaxial tests: Only four stress paths and 3000 cycles per stress path were applied for the large-scale repeated load triaxial tests since the triaxial apparatus is only able to run at a low loading frequency (0.025 Hz). However, AASHTO T307 standard (2017), recommends 15 stress paths to evaluate the resilient behavior, and EN 13286 standard (2004) suggests at least 10000 loading cycles for each stress path to evaluate the long-term permanent deformation of unbound mixtures. More stress paths and loading cycles can help to better understand the resilient and permanent behavior of coarse-grained waste rocks in mine haul roads.

Reproducibility of laboratory tests: Although this study showed acceptable experimental results and similar findings with the literature (even though the tested materials were very different), their reproducibility could not always be verified since some tests were so time-consuming. Considering the repeatability of repeated load triaxial test is relatively low (Boudreau 2003), further study would be required to more accurately generalize the effect of material properties.

Mathematical model fitting: Rahman and Erlingsson model (extended using time hardening approach) was able to accurately describe the measured accumulated permanent strain of waste rocks. However, fitting performance of the extended model heavily relies on the initial values of the model coefficients (i.e. a, b, and α), and these are generally determined through trial and error method, which is time-consuming and complex especially when a large number of stress paths are applied in one multistage repeated load triaxial test. Although Rahman and Erlingsson (2015a) provided a detailed fitting process using Microsoft Excel, the engineer experience and judgement has a significant impact on the model fitting performance.

Limited input features of machine learning models: Although the developed machine learning predictive models showed satisfactory accuracy to the crushed waste rocks from Canadian Malartic Mine, only three input variables/features (i.e., number of loading cycles, confining pressure, and deviator stress) were used for the models because of the limited available data, which restricts the applicability of these models to other materials.

Some recommendations are presented below (Section 11.3) to answer some of the limitations or uncertainties raised during this research.

CHAPTER 12 CONCLUSION AND RECOMMENDATIONS

12.1 Conclusion

The primary objective of this project was to assess the mechanical properties of waste rocks under mining truck loading, and to improve the design of mine haul roads. Secondary objectives were to evaluate the applicability/suitability of laboratory test standards, repeated load CBR test and existing mathematical regression models to waste rocks, assess the impact of gravel-to-sand ratio and fines content, study the effect of basic properties and climatic factors, and develop machine learning models for predicting the mechanical properties. The main conclusions and contributions of this research can be summarized as follows:

- High stress levels for haul roads were proposed and used in repeated load triaxial tests, which were able to give more representative resilient and permanent behavior of waste rocks under mining truck loading.

- Repeated load CBR tests could be an effective alternative to repeated load triaxial tests to estimate resilient and permanent deformation behavior of waste rocks. Results showed that the impact of loading frequency and waveform in repeated load CBR tests was limited, while the measured equivalent modulus increased significantly with contact stress. The developed equation and model for repeated load CBR tests were reliable to describe the stiffness and permanent deformation of waste rocks, respectively.

- Gravel-to-sand ratio could be a practical grading parameter for optimizing the mechanical properties of waste rocks. The optimum gravel-to-sand ratio of crushed waste rocks was between 1 and 1.5 and contributed to provide higher resilient modulus and shear strength, and lower permanent strain. An increase in fines content could, to the contrary, result in the decrease of resilient modulus and permanent strain but also to significant increase of shear strength. The optimal gravel-to-sand ratio of uncrushed waste rocks regarding to the resilient modulus and shear

strength was around 5. Permanent strain was close when the gravel-to-sand ratio ranged between 1 and 5, but it decreased significantly when the ratio increased to 8. The influence of fines content (0-10%) on the resilient modulus, shear strength, and permanent deformation of uncrushed waste rocks was insignificant.

- Increasing maximum particle size and compaction effort would improve the mechanical response of haul roads. An increasing in maximum particle size (25, 40, and 60 mm) resulted in growth of resilient modulus and shear strength and decrease of permanent deformation. The effect of compaction effort on the mechanical properties of uncrushed waste rocks was significant, exceeded 360 kJ/m^3, this effect was limited. The influence of water content (final value 0.9-2.3%) on the resilient modulus, shear strength, and permanent deformation of uncrushed waste rocks was limited.

- Freeze-thaw cycles should be considered during the haul road design in cold regions. Freeze-thaw cycles resulted in a reduction of the resilient modulus and shear strength, and an increase of the permanent deformation. A greater water content during freeze-thaw cycles also resulted in a significant increase of the permanent deformation. Results also showed that wetting-drying cycles could contribute to increase the stiffness, CBR, and permanent deformation of crushed waste rocks, but further study should be conducted to evaluate the effect.

- M_R-θ model and MEPDG model were reliable to describe the resilient modulus behavior of waste rocks under different stress conditions. Rahman and Erlingsson model (extended using time hardening approach) was well adapted to fit the accumulation of permanent strain with number of loading cycles caused by numerous stress paths. The proposed models could be used to predict the mechanical properties of waste rocks in the field, but would need to be improved using more test results to extend their generalization capacity.

- A comparison study showed that the decision tree DT, random forest RF, and backpropagation neural network BPNN models provided better results for CBR, resilient modulus, and permanent

deformation, respectively. The NEAT models showed good generalization and simple structure although their performance was lower than DT and RF models. The developed models should be extended using more data to increase the generalization capability.

12.2 Recommendations

Following the limitations raised by this project, several recommendations are given below to better understand the mechanical properties of waste rocks and optimize mine haul road design:

- More laboratory tests with higher loading frequency, and more stress paths and loading cycles should be carried out in the future research to better understand the mechanical behavior of waste rocks in haul roads. The proposed descriptive and predictive models in this project should be validated using more experimental data and different materials. Also, more experimental data need to be used to train and test the machine learning models to extend the generalization capacity. It means more input variables/features should be used for the predictive models, such as gradation, density, and degree of compaction.

- The influence of particle size distribution on the environmental effect (freeze-thaw and wetting-drying cycles) needs further study, which will be helpful for the management and reclamation of waste rocks. A new wetting-drying process on specimen should be designed to simulate the realistic field condition such as the rainfall splash and water flows, which will be helpful to study the mechanical behavior of waste rocks under severe condition. Alternative experimental approaches such as Scanning Electron Microscope (SEM) test are more and more frequently to examinate the microstructure change of the specimens subjected freeze-thaw cycles (Gullà et al. 2006; Aldaood et al. 2016; Zou et al. 2020) and wetting-drying cycles (Aldaood et al. 2014), and are therefore strongly recommended for further evaluating the effect of freeze-thaw and

wetting-drying on waste rocks.

- Numerical simulations should be conducted to study the stress distribution in haul roads under mining trucks. Although high stress levels were proposed for haul roads based on the tire pressures of mining trucks in this study, more representative stress combinations of confining pressure and deviator stress should be proposed based on the numerical simulation results. The constitutive model for waste rocks, taking the resilient and permanent behavior into account, needs to be developed to simulate the response of haul roads subjected to mining trucks more accurately since the existing constitutive models for soils cannot match the mechanical behavior of waste rocks under traffic loading, for example, the most used Mohr-Coulomb model generally simulates soils at a constant elastic modulus for different stress conditions. Numerical simulation therefore would be beneficial to the laboratory test and haul road design.

- Field work, as an important part of road studies, are recommended in the future research. Although the density of surface layer of haul roads was measured by Laverdière (2019), the density of base/subbase layers also need to be measured in the field to help prepare the uncrushed waste rock samples that can match the in-situ density. However, the measurement of field density of base/subbase layers is difficult because it may need to excavate the haul roads, which would disrupt the transport of mining trucks. One of the possible solutions is to measure the field density of base/subbase layers during the road construction. Also, the field resilient modulus of haul roads should be measured using light falling weight deflectometer (LFWD), which can be used to verify the laboratory test results.

REFERENCES

AASHTO. (2008). *Mechanistic-empirical pavement design guide: A manual of practice*. AAoSHaT Officials, Editor.

AASHTO M-147. (2008). *Standard specification for materials for aggregate and soil-aggregate subbase, base, and surface courses*. Washington, DC.

AASHTO T307-99. (2017). *Standard method of test for determining the resilient modulus of soils and aggregate materials*. Washington, DC.

Abdeen, M. A. M., & Hodhod, H. (2010). Experimental Investigation and Development of Artificial Neural Network Model for the Properties of Locally Produced Light Weight Aggregate Concrete. *Engineering, 02*(06), 408-419. doi:10.4236/eng.2010.26054

Abid, A. N., Salih, A. O., & Nawaf, E. A. (2017). The Influence of Fines Content on the Mechanical Properties of Aggregate Subbase Course Material for Highway Construction using Repeated Load CBR Test. *Alnahrain Journal for Engineering Sciences, 20*(3), 615-624.

Achampong, F., Usmen, M., & Kagawa, T. (1997). Evaluation of resilient modulus for lime- and cement-stabilized synthetic cohesive soils. *Transportation research record, 1589*(1), 70-75. doi:10.3141/1589-12

Adamczyk, E. (2016). Landslide at Myanmar jade mine kills 12 people. In: United Press International.

Adeli, H. (2001). Neural networks in civil engineering: 1989–2000. *Computer-Aided Civil and Infrastructure Engineering, 16*(2), 126-142.

Ahmed, A., & Abouzeid, A. (2009). Potential use of phosphate wastes as aggregates in road construction. *JES. Journal of Engineering Sciences, 37*(2), 413-422.

Ai, X., Yi, J., Zhao, H., Chen, S., Luan, H., Zhang, L., & Feng, D. (2020). An empirical predictive

model for the dynamic resilient modulus based on the static resilient modulus and California bearing ratio of cement-and lime-stabilised subgrade soils. *Road Materials and Pavement Design*, 1-20.

Aiban, S. A., & Mohammed, O. E. H. (2002). *The effect of the CBR mould size and the maximum aggregate size on the load carrying capacity of base course materials.* Paper presented at the The 6th saudi Engineering Conference, KFUPM, Dhahran.

Al-Hussaini, M. (1983). Effect of particle size and strain conditions on the strength of crushed basalt. *Canadian Geotechnical Journal, 20*(4), 706-717. doi:10.1139/t83-077

Al-Obaydi, M. A., Abdulnafaa, M. D., Atasoy, O. A., & Cabalar, A. F. (2021). Improvement in Field CBR Values of Subgrade Soil Using Construction-Demolition Materials. *Transportation Infrastructure Geotechnology*, 1-21.

Al-Qahtani, F. H., & Crone, S. F. (2013). *Multivariate k-nearest neighbour regression for time series data—A novel algorithm for forecasting UK electricity demand.* Paper presented at the The 2013 international joint conference on neural networks (IJCNN).

Alavi, A. H., Gandomi, A. H., & Lary, D. J. (2016). Progress of machine learning in geosciences: Preface. *Geoscience Frontiers, 7*(1), 1-2. doi:https://doi.org/10.1016/j.gsf.2015.10.006

Albright, W. H., Benson, C. H., & Waugh, W. J. (2010). *Water balance covers for waste containment: Principles and practice*.

Aldaood, A., Bouasker, M., & Al-Mukhtar, M. (2014). Impact of wetting–drying cycles on the microstructure and mechanical properties of lime-stabilized gypseous soils. *Engineering Geology, 174*, 11-21. doi:https://doi.org/10.1016/j.enggeo.2014.03.002

Aldaood, A., Bouasker, M., & Al-Mukhtar, M. (2016). Effect of water during freeze–thaw cycles on the performance and durability of lime-treated gypseous soil. *Cold Regions Science and Technology, 123*, 155-163. doi:https://doi.org/10.1016/j.coldregions.2015.12.008

Alnedawi, A., Nepal, K. P., & Al-Ameri, R. (2019). Effect of loading frequencies on permanent deformation of unbound granular materials. *International Journal of Pavement Engineering, 22*(8), 1008-1016.

Alshameri, B., Bakar, I., Madun, A., Abdeldjouad, L., & Dahlan, S. H. (2016). *Effect of Coarse Materials Percentage in the Shear Strength.* Paper presented at the IOP Conference Series: Materials Science and Engineering.

Alshibli, K. A., Abu-Farsakh, M., & Seyman, E. (2005). Laboratory evaluation of the geogauge and light falling weight deflectometer as construction control tools. *Journal of Materials in Civil Engineering, 17*(5), 560-569.

Amos, R. T., Blowes, D. W., Bailey, B. L., Sego, D. C., Smith, L., & Ritchie, A. I. M. (2015). Waste-rock hydrogeology and geochemistry. *Applied Geochemistry, 57*, 140-156. doi:10.1016/j.apgeochem.2014.06.020

Amrani, M., Taha, Y., Kchikach, A., Benzaazoua, M., & Hakkou, R. (2019). Valorization of phosphate mine waste rocks as materials for road construction. *Minerals, 9*(4), 237.

Araya, A. A. (2011). *Characterization of unbound granular materials for pavements.* Delft University of Technology,

Araya, A. A., Huurman, M., Molenaar, A. A. A., & Houben, L. J. M. (2012). Investigation of the resilient behavior of granular base materials with simple test apparatus. *Materials and Structures, 45*(5), 695-705.

Araya, A. A., Molenaar, A. A., & Houben, L. J. (2010). *Characterization of unbound granular materials using repeated load CBR and triaxial testing.* Paper presented at the Paving Materials and Pavement Analysis.

Arulrajah, Piratheepan, J., Disfani, M., & Bo, M. (2012). Resilient moduli response of recycled construction and demolition materials in pavement subbase applications. *Journal of*

Materials in Civil Engineering, 25(12), 1920-1928.

Arulrajah, A., Disfani, M. M., Horpibulsuk, S., Suksiripattanapong, C., & Prongmanee, N. (2014). Physical properties and shear strength responses of recycled construction and demolition materials in unbound pavement base/subbase applications. *Construction and Building Materials, 58*, 245-257. doi:https://doi.org/10.1016/j.conbuildmat.2014.02.025

ASTM D1195-93. (1997). *Standard test method for repetitive static plate load tests of soils and flexible pavement components, for use in evaluation and design of airport and highway pavements*. ASTM International. West Conshohocken, PA.

ASTM D4429-04. (2004). *Standard test method for CBR (California Bearing Ratio) of soils in place*. ASTM International. West Conshohocken, PA.

ASTM D1557-12e1. (2012). *Standard test methods for laboratory compaction characteristics of soil using modified effort (56,000 ft-lbf/ft^3 (2,700 kN-m/m^3))*. ASTM International. West Conshohocken, PA.

ASTM D698-12e2. (2012). *Standard test methods for laboratory compaction characteristics of soil using standard effort (12,400 ft-lbf/ft^3 (600 kN-m/m^3))*. ASTM International, West Conshohocken, PA.

ASTM D854-14. (2014). *Standard test methods for specific gravity of soil solids by water pycnometer*. ASTM International, West Conshohocken, PA.

ASTM C127-15. (2015). *Standard test method for relative density (specific gravity) and absorption of coarse aggregate*. ASTM International, West Conshohocken, PA.

ASTM D2850-15. (2015). *Standard test method for unconsolidated-undrained triaxial compression test on cohesive soils*. ASTM International. West Conshohocken, PA.

ASTM D559/D559M-15. (2015). *Standard test methods for wetting and drying compacted soil-cement mixtures*. ASTM International. West Conshohocken, PA.

ASTM D1883-16. (2016). *Standard test method for california bearing ratio (CBR) of laboratory-compacted soils*. ASTM International, West Conshohocken, PA.

ASTM D2487-17e1. (2017). *Standard practice for classification of soils for engineering purposes (Unified Soil Classification System)*. ASTM International. West Conshohocken, PA.

ASTM D6528-17. (2017). *Standard test method for consolidated undrained direct simple shear testing of fine grain soils*. ASTM International. West Conshohocken, PA.

ASTM C136/C136M-19. (2019). *Standard test method for sieve analysis of fine and coarse aggregates*. ASTM International. West Conshohocken, PA.

ASTM D7181-20. (2020). *Standard test method for consolidated drained triaxial compression test for soils*. ASTM International, West Conshohocken, PA.

ASTM D4767-11. (2020). *Standard test method for consolidated undrained triaxial compression test for cohesive soils*. ASTM International. West Conshohocken, PA.

Atkinson, T. (1992). Design and layout of haul roads. *Chapter 13.4-SME Mining Engineering Handbook*, 1334-1342.

Aubertin, M. (2013). *Waste rock disposal to improve the geotechnical and geochemical stability of piles.* Paper presented at the Proceedings of the world mining congress, Montreal, Canada.

Aubertin, M., Bussière, B., Pabst, T., James, M., & Mbonimpa, M. (2016). Review of the reclamation techniques for acid-generating mine wastes upon closure of disposal sites. *Proc., Geo-Chicago 2016*, 343-358.

Ba, M., Nokkaew, K., Fall, M., & Tinjum, J. M. (2013). Effect of matric suction on resilient modulus of compacted aggregate base courses. *Geotechnical and Geological Engineering, 31*(5), 1497-1510.

Bagherzadeh-Khalkhali, A., & Mirghasemi, A. A. (2009). Numerical and experimental direct shear

tests for coarse-grained soils. *Particuology, 7*(1), 83-91. doi:https://doi.org/10.1016/j.partic.2008.11.006

Bala, R., & Bishnoi, M. (2016). Shear Strength Characteristics of Crushed Limestone Sandstone and Gravel. *International Journal of Technical Research, 5*(3), 5-9.

Bao, Y., Han, X., Chen, J., Zhang, W., Zhan, J., Sun, X., & Chen, M. (2019). Numerical assessment of failure potential of a large mine waste dump in Panzhihua City, China. *Engineering Geology, 253*, 171-183.

Barksdale, R., Alba, J., Khosla, N., Kim, R., Lambe, P., & Rahman, M. (1997). *NCHRP Web Doc 14 laboratory determination of resilient modulus for flexible pavement design*.

Barksdale, R. D. (1972). *Laboratory evaluation of rutting in base course materials.* Paper presented at the The Third International Conference on the Structural Design of Asphalt Pavements, Grosvenor House, Park Lane, London, England, Sept. 11-15, 1972.

Barksdale, R. D. (1984). Performance of crushed-stone base courses. *Transportation Research Record, 954*, 78-87.

Bassey, O. B., Attah, I. C., Ambrose, E. E., & Etim, R. K. (2017). Correlation between CBR values and index properties of soils: a case study of Ibiono, Oron and Onna in Akwa Ibom State. *Resour Environ, 7*(4), 94-102.

BELAZ-7571 Series. (2018). Retrieved from http://belaz.ca/products/dumptrucks/7571.html

Bhattacharjee, S., & Bandyopadhyay, K. (2015). Evaluation of elastic modulus of fly ash embankment by repeated load CBR test. *Geotechnical Engineering for Infrastructure and Development*, 229-234. doi:10.1680/ecsmge.60678.vol2.012

Bian, Z., Dong, J., Lei, S., Leng, H., Mu, S., & Wang, H. (2009). The impact of disposal and treatment of coal mining wastes on environment and farmland. *Environmental Geology, 58*(3), 625-634.

Bilodeau, J.-P., Doré, G., & Schwarz, C. (2011). Effect of seasonal frost conditions on the permanent strain behaviour of compacted unbound granular materials used as base course. *International Journal of Pavement Engineering, 12*(5), 507-518.

Blight, G. (2009). *Geotechnical engineering for mine waste storage facilities*: CRC Press.

Blight, G. E. (1969). Shear stability of dumps and dams of gold mining waste. *The Civil Engineering in South Africa*(3), 49-54. doi:doi:10.10520/AJA10212019_13800

Blowes, D., Ptacek, C., & Jambor, J. (1994). Short Course Handbook on Environmental Geochemistry of Sulfide Mine-Wastes. *Mineralogical Association of Canada, Nepean, 22*, 365.

Blowes, D. W. (1997). *The environmental effects of mine wastes.* Paper presented at the Proceedings of exploration.

Boudreau, R. L. (2003). Repeatability of the resilient modulus test procedure. *Resilient Modulus Testing for Pavement Components, ASTM International*.

Boyce, J., Brown, S., & Pell, P. (1976). *The resilient behaviour of a granular material under repeated loading.* Paper presented at the Australian Road Research Board Conference Proc.

Bozyurt, O., Keene, A., Tinjum, J., Edil, T., & Fratta, D. (2013). Freeze–thaw effects on stiffness of unbound recycled road base. In *Mechanical Properties of Frozen Soil*: ASTM International.

Bray, J. D., Zekkos, D., Kavazanjian Jr, E., Athanasopoulos, G. A., & Riemer, M. F. (2009). Shear strength of municipal solid waste. *Journal of Geotechnical and Geoenvironmental Engineering, 135*(6), 709-722.

Breiman, L. (1999). 1 Random forests--random features.

Breiman, L., Friedman, J., Stone, C. J., & Olshen, R. A. (1984). *Classification and regression trees*:

CRC press.

Broms, B. B., & Yao, L. Y. (1964). Shear strength of a soil after freezing and thawing. *Journal of the Soil Mechanics and Foundations Division, 90*(4), 1-25.

Brown, S., & Selig, E. (1991). *The design of pavement and rail track foundations.* Paper presented at the Cyclic loading of soils: from theory to design.

Bussière, B. (2007a). Colloquium 2004: Hydrogeotechnical properties of hard rock tailings from metal mines and emerging geoenvironmental disposal approaches. *Canadian Geotechnical Journal, 44*(9), 1019-1052.

Bussière, B. (2007b). Hydro-geotechnical properties of hard rock tailings from metal mines and Subsoil Characteristics and Hydrogeology…… emerging geo-environmental disposal approaches. *Canadian Geotechnical Journal, 44*(9), 1019-1052.

Bussière, B., Aubertin, M., & Chapuis, R. P. (2003). The behavior of inclined covers used as oxygen barriers. *Canadian Geotechnical Journal, 40*(3), 512-535. doi:10.1139/T03-001

Bussière, B., Aubertin, M., Mbonimpa, M., Molson, J. W., & Chapuis, R. P. (2007). Field experimental cells to evaluate the hydrogeological behaviour of oxygen barriers made of silty materials. *Canadian Geotechnical Journal, 44*(3), 245-265. doi:10.1139/T06-120

Byun, Y. H., Feng, B., Qamhia, I. I., & Tutumluer, E. (2020). Aggregate Properties Affecting Shear Strength and Permanent Deformation Characteristics of Unbound–Base Course Materials. *Journal of Materials in Civil Engineering, 32*(1), 04019332.

Cao, Z., Chen, J., Ye, X., Gu, C., Guo, Z., & Cai, Y. (2021). Experimental study on particle breakage of carbonate gravels under cyclic loadings through Large-scale triaxial tests. *Transportation Geotechnics*, 100632. doi:https://doi.org/10.1016/j.trgeo.2021.100632

Cerato, A. B., & Lutenegger, A. J. (2006). Specimen size and scale effects of direct shear box tests of sands. *Geotechnical Testing Journal, 29*(6), 507-516.

Cetin, A., Kaya, Z., Cetin, B., & Aydilek, A. H. (2014). Influence of laboratory compaction method on mechanical and hydraulic characteristics of unbound granular base materials. *Road Materials and Pavement Design, 15*(1), 220-235.

Ceylan, H., Bayrak, M. B., & Gopalakrishnan, K. (2014). Neural networks applications in pavement engineering: A recent survey. *International Journal of Pavement Research & Technology, 7*(6).

Chen, D. H., Zaman, M., Laguros, J., & Soltani, A. (1995). Assessment of computer programs for analysis of flexible pavement structure. *Transportation Research Record, 1482*(137), 123-133.

Chen, L. (2010). A multiple linear regression prediction of concrete compressive strength based on physical properties of electric arc furnace oxidizing slag. *International Journal of Applied Science and Engineering, 7*(2), 153-158.

Chen, X., & Zhang, J. (2016). Influence of Relative Density on Dilatancy of Clayey Sand–Fouled Aggregates in Large-Scale Triaxial Tests. *Journal of Geotechnical and Geoenvironmental Engineering, 142*(10), 06016011.

Chittoori, B. C. S., Puppala, A. J., & Pedarla, A. (2018). Addressing Clay Mineralogy Effects on Performance of Chemically Stabilized Expansive Soils Subjected to Seasonal Wetting and Drying. *Journal of Geotechnical and Geoenvironmental Engineering, 144*(1), 04017097. doi:doi:10.1061/(ASCE)GT.1943-5606.0001796

Chollet, F. (2018). *Deep Learning mit Python und Keras: Das Praxis-Handbuch vom Entwickler der Keras-Bibliothek*: MITP-Verlags GmbH & Co. KG.

Christensen, D., & O'Kane, M. (2005). The use of "enhanced" moisture store-and-release cover systems over reactive mine waste in cold and warm semi-arid climates. *Proceedings America Society of Mining and Reclamation*, 224-235.

Coffey, J., Ghadimi, B., Nikraz, H., & Rosano, M. (2018). The modelling prediction of haul road surface deflection. *Transportation Geotechnics, 14*, 136-145. doi:https://doi.org/10.1016/j.trgeo.2017.11.005

Collins, I., & Boulbibane, M. (1998). The application of shakedown theory to pavement design. *Metals and Materials, 4*(4), 832-837.

Collins, I., & Boulbibane, M. (2000). Geomechanical analysis of unbound pavements based on shakedown theory. *Journal of Geotechnical and Geoenvironmental Engineering, 126*(1), 50-59.

Coronado, O., Caicedo, B., Taibi, S., Gomes Correia, A., Souli, H., & Fleureau, J.-M. (2016). Effect of water content on the resilient behavior of non standard unbound granular materials. *Transportation Geotechnics, 7*, 29-39. doi:https://doi.org/10.1016/j.trgeo.2016.04.004

Cortes, C., Mohri, M., & Rostamizadeh, A. (2012). L2 regularization for learning kernels. *arXiv preprint arXiv:1205.2653*.

Cui, Y., Jiang, Y., & Guo, C. (2019). Investigation of the initiation of shallow failure in widely graded loose soil slopes considering interstitial flow and surface runoff. *Landslides, 16*(4), 815-828.

Cui, Y., Zhou, X., & Guo, C. (2017). Experimental study on the moving characteristics of fine grains in wide grading unconsolidated soil under heavy rainfall. *Journal of Mountain Science, 14*(3), 417-431.

Curram, S. P., & Mingers, J. (1994). Neural Networks, Decision Tree Induction and Discriminant Analysis: an Empirical Comparison. *Journal of the Operational Research Society, 45*(4), 440-450. doi:10.1057/jors.1994.62

Dagenais, A. M., Aubertin, M., & Bussière, B. (2006). *Parametric study on the water content profiles and oxidation rates in nearly saturated tailings above the water table.* Paper

presented at the Proceedings of the 7th International Conference on Acid Rock Drainage (ICARD).

Dawson, R. F., Morgenstern, N. R., & Stokes, A. W. (1998). Liquefaction flowslides in Rocky Mountain coal mine waste dumps. *Canadian Geotechnical Journal, 35*(2), 328-343. doi:10.1139/t98-009

de Souza, W. M., Ribeiro, A. J. A., & da Silva, C. A. U. (2020). Use of ANN and visual-manual classification for prediction of soil properties for paving purposes. doi:10.1080/10298436.2020.1807546

Dehn, M., Bürger, G., Buma, J., & Gasparetto, P. (2000). Impact of climate change on slope stability using expanded downscaling. *Engineering Geology, 55*(3), 193-204. doi:https://doi.org/10.1016/S0013-7952(99)00123-4

Deiminiat, A., Li, L., Zeng, F., Pabst, T., Chiasson, P., & Chapuis, R. (2020). Determination of the Shear Strength of Rockfill from Small-Scale Laboratory Shear Tests: A Critical Review. *Advances in Civil Engineering, 2020*, 8890237. doi:10.1155/2020/8890237

Díaz, E., & Tomás, R. (2021). Upgrading the prediction of jet grouting column diameter using deep learning with an emphasis on high energies. *Acta Geotechnica, 16*(5), 1627-1633. doi:10.1007/s11440-020-01091-8

Dobchuk, B., Nichol, C., Wilson, G. W., & Aubertin, M. (2013). Evaluation of a single-layer desulphurized tailings cover. *Canadian Geotechnical Journal, 50*(7), 777-792. doi:10.1139/cgj-2012-0119

Domitrović, J., Rukavina, T., & Lenart, S. (2019). Effect of freeze-thaw cycles on the resilient moduli and permanent deformation of RAP/natural aggregate unbound base mixtures. *Transportation Geotechnics, 18*, 83-91. doi:https://doi.org/10.1016/j.trgeo.2018.11.008

Douglas, R. A. (2016). *Low-volume road engineering: design, construction, and maintenance*:

CRC Press.

Drumm, E., Boateng-Poku, Y., & Johnson Pierce, T. (1990). Estimation of subgrade resilient modulus from standard tests. *Journal of Geotechnical Engineering, 116*(5), 774-789.

Du, J., Hou, K. P., & Liang, W. (2012). *Experimental Research on Strength Characteristics of Bulky Rock Material with Different Coarse Grain Content in Waste Pile of Mine.* Paper presented at the Applied Mechanics and Materials.

Du Plessis, L., Ulloa-Calderon, A., Harvey, J., & Coetzee, N. (2018). Accelerated pavement testing efforts using the Heavy Vehicle Simulator. *International Journal of Pavement Research and Technology, 11*(4), 327-338.

Duncan, J. M., Wright, S. G., & Brandon, T. L. (2014). *Soil strength and slope stability*: John Wiley & Sons.

Dunlap, W. A. (1963). *A report on a mathematical model describing the deformation characteristics of granular materials*: Texas Transportation Institute, Texas A & M University.

Duong, T. V., Cui, Y.-J., Tang, A. M., Dupla, J.-C., Canou, J., Calon, N., & Robinet, A. (2016). Effects of water and fines contents on the resilient modulus of the interlayer soil of railway substructure. *Acta Geotechnica, 11*(1), 51-59.

Edil, T. B., & Cetin, B. (2018). Freeze-thaw performance of chemically stabilized natural and recycled highway materials. *Sciences in Cold and Arid Regions, 7*(5), 482-491.

Ekblad, J., & Isacsson, U. (2006). Influence of water on resilient properties of coarse granular materials. *Road Materials and Pavement Design, 7*(3), 369-404.

El-Basyouny, M., Witczak, M., & Kaloush, K. (2005). *Development of the permanent deformation models for the 2002 design guide.* Paper presented at the 84th Annual Meeting of the Transportation Research Board, Available in TRB 2005 Annual Meeting CD-ROM.

Electric Drive Mining Truck 960E-2K. (2020). Retrieved from https://www.komatsuamerica.com/equipment/trucks/electric/960e-2k

Elliott, R. P., & David, L. (1989). Improved characterization model for granular bases. *Transportation Research Record* (1227).

EN. (2004). Unbound and Hydraulically Bound Mixtures–Cyclic Load Triaxial Test for Unbound Mixtures. In *13286-7*: British Standard Institute.

Erlingsson, S. (2012). Rutting development in a flexible pavement structure. *Road Materials and Pavement Design, 13*(2), 218-234.

Erlingsson, S., & Rahman, M. S. (2013). Evaluation of permanent deformation characteristics of unbound granular materials by means of multistage repeated-load triaxial tests. *Transportation Research Record, 2369*(1), 11-19.

Erlingsson, S., Rahman, S., & Salour, F. (2017). Characteristic of unbound granular materials and subgrades based on multi stage RLT testing. *Transportation Geotechnics, 13*, 28-42.

Erzin, Y., & Turkoz, D. (2016). Use of neural networks for the prediction of the CBR value of some Aegean sands. *Neural Computing and Applications, 27*(5), 1415-1426. doi:10.1007/s00521-015-1943-7

Evans, M. D., Bolton Seed, H., & Seed, R. B. (1992). Membrane compliance and liquefaction of sluiced gravel specimens. *Journal of Geotechnical Engineering, 118*(6), 856-872.

Evans, M. D., & Seed, H. B. (1987). *Undrained cyclic triaxial testing of gravels: the effect of membrane compliance*: College of Engineering, University of California.

Fairhurst, C., Kosla, N., & Kim, Y. (1990). *Resilient modulus testing of asphalt specimens in accordance with ASTM D4123-82.* Paper presented at the Mechanical Tests for Bituminous Mixes. Characterization, Design and Quality Control. Proceedings of the Fourth International Symposium held by RILEM, Budapest, Hungary.

Fala, O., Molson, J., Aubertin, M., Dawood, I., Bussière, B., & Chapuis, R. P. (2012). A numerical modelling approach to assess long-term unsaturated flow and geochemical transport in a waste rock pile. *International Journal of Mining, Reclamation and Environment, 27*(1), 38-55. doi:10.1080/17480930.2011.644473

Fan, J., Wu, L., Zhang, F., Cai, H., Ma, X., & Bai, H. (2019). Evaluation and development of empirical models for estimating daily and monthly mean daily diffuse horizontal solar radiation for different climatic regions of China. *Renewable and Sustainable Energy Reviews, 105*, 168-186.

Farias, I. G., Araujo, W., & Ruiz, G. (2018). Prediction of California bearing ratio from index properties of soils using parametric and non-parametric models. *Geotechnical and Geological Engineering, 36*(6), 3485-3498.

Farsangi, P. N. (1996). *Improving cemented rockfill design in open stoping*. McGill University.

Ferdosi, B., James, M., & Aubertin, M. (2015a). Effect of waste rock inclusions on the seismic stability of an upstream raised tailings impoundment: a numerical investigation. *Canadian Geotechnical Journal, 52*(12), 1930-1944. doi:10.1139/cgj-2014-0447

Ferdosi, B., James, M., & Aubertin, M. (2015b). Investigation of the Effect of Waste Rock Inclusions Configuration on the Seismic Performance of a Tailings Impoundment. *Geotechnical and Geological Engineering, 33*(6), 1519-1537. doi:10.1007/s10706-015-9919-z

Ferede, Z. W. (2010). Prediction of California Bearing Ratio (CBR) value from index properties of soil. *unpublished MS Thesis Submitted to School of Graduate Studies of Addis Ababa University, Ethiopia*.

Ferentinou, M., & Fakir, M. (2018). Integrating Rock Engineering Systems device and Artificial Neural Networks to predict stability conditions in an open pit. *Engineering Geology, 246*,

293-309. doi:https://doi.org/10.1016/j.enggeo.2018.10.010

Ferreira, A. (2017). Application of ANN in Pavement Engineering: State-of-Art. hal-02066889v2.

Ferry, C., Richon, P., Beneito, A., & Robe, M. C. (2002). Evaluation of the effect of a cover layer on radon exhalation from uranium mill tailings: transient radon flux analysis. *J Environ Radioact, 63*(1), 49-64. Retrieved from https://www.ncbi.nlm.nih.gov/pubmed/12230135

Gamache-Rochette, A. (2004). *Une étude de caractérisation en laboratoire et sur le terrain des écoulements de l'eau dans les roches stériles*: École polytechnique.

Geertsema, M., Clague, J. J., Schwab, J. W., & Evans, S. G. (2006). An overview of recent large catastrophic landslides in northern British Columbia, Canada. *Engineering Geology, 83*(1), 120-143. doi:https://doi.org/10.1016/j.enggeo.2005.06.028

George, V., Rao, N. C., & Shivashankar, R. (2009). PFWD, DCP and CBR correlations for evaluation of lateritic subgrades. *International Journal of Pavement Engineering, 10*(3), 189-199.

Ghorbani, A., & Hasanzadehshooiili, H. (2018). Prediction of UCS and CBR of microsilica-lime stabilized sulfate silty sand using ANN and EPR models; application to the deep soil mixing. *Soils and Foundations, 58*(1), 34-49. doi:10.1016/j.sandf.2017.11.002

Ghorbani, B., Arulrajah, A., Narsilio, G., & Horpibulsuk, S. (2020a). Experimental and ANN analysis of temperature effects on the permanent deformation properties of demolition wastes. *Transportation Geotechnics, 24*, 100365. doi:10.1016/j.trgeo.2020.100365

Ghorbani, B., Arulrajah, A., Narsilio, G., & Horpibulsuk, S. (2020b). Experimental investigation and modelling the deformation properties of demolition wastes subjected to freezethaw cycles using ANN and SVR. *Construction and Building Materials, 258*. doi:10.1016/j.conbuildmat.2020.119688

Ghorbani, B., Arulrajah, A., Narsilio, G., Horpibulsuk, S., & Bo, M. W. (2020a). Development of

genetic-based models for predicting the resilient modulus of cohesive pavement subgrade soils. *Soils and Foundations, 60*(2), 398-412. doi:10.1016/j.sandf.2020.02.010

Ghorbani, B., Arulrajah, A., Narsilio, G., Horpibulsuk, S., & Bo, M. W. (2020b). Hybrid Formulation of Resilient Modulus for Cohesive Subgrade Soils Utilizing CPT Test Parameters. *Journal of Materials in Civil Engineering, 32*(9). doi:10.1061/(ASCE)MT.1943-5533.0003329

Gidel, G., Hornych, P., Breysse, D., & Denis, A. (2001). A new approach for investigating the permanent deformation behaviour of unbound granular material using the repeated loading triaxial apparatus. *Bulletin des laboratoires des Ponts et Chaussées*(233), 5-21.

Gold, S., & Rangarajan, A. (1996). Softmax to softassign: Neural network algorithms for combinatorial optimization. *Journal of Artificial Neural Networks, 2*(4), 381-399.

Golder. (2019). *Environmental Impact Assessment and Environmental Management Programme Report for the Proposed Metsimaholo Underground Coal Mine.* Retrieved from Department of Mineral Resources:

Gopalakrishnan, K., Khaitan, S. K., Choudhary, A., & Agrawal, A. (2017). Deep Convolutional Neural Networks with transfer learning for computer vision-based data-driven pavement distress detection. *Construction and Building Materials, 157*, 322-330. doi:https://doi.org/10.1016/j.conbuildmat.2017.09.110

Gorakhki, M. H., & Bareither, C. A. (2017). Sustainable reuse of mine tailings and waste rock as water-balance covers. *Minerals, 7*(7), 128.

Gray, J. (1962). Characteristics of graded base course aggregates determined by triaxial tests.

Gray, R. E. (1990). Mining subsidence — past, present, future. *International Journal of Mining and Geological Engineering, 8*(4), 400-408. doi:10.1007/BF00920651

Gregory, G., & Cross, S. (2007). *Correlation of CBR with shear-strength parameters.* Paper

presented at the Proceedings of 9th Int. Conf. on Low-Volume Roads.

Gu, C., Ye, X., Wang, J., Cai, Y., Cao, Z., & Zhang, T. (2020). Resilient behavior of coarse granular materials in three-dimensional stress state. *Canadian Geotechnical Journal, 57*(9), 1280-1293.

Gu, C., Zhan, Y., Wang, J., Cai, Y., Cao, Z., & Zhang, Q. (2020). Resilient and permanent deformation of unsaturated unbound granular materials under cyclic loading by the large-scale triaxial tests. *Acta Geotechnica, 15*(12), 3343-3356. doi:10.1007/s11440-020-00966-0

Gu, F., Sahin, H., Luo, X., Luo, R., & Lytton, R. L. (2014). Estimation of resilient modulus of unbound aggregates using performance-related base course properties. *Journal of Materials in Civil Engineering, 27*(6), 04014188.

Gudishala, R. (2004). Development of resilient modulus prediction models for base and subgrade pavement layers from in situ devices test results.

Gullà, G., Mandaglio, M. C., & Moraci, N. (2006). Effect of weathering on the compressibility and shear strength of a natural clay. *Canadian Geotechnical Journal, 43*(6), 618-625.

Gupta, D., Hazarika, B. B., & Berlin, M. (2020). Robust regularized extreme learning machine with asymmetric Huber loss function. *Neural Computing and Applications, 32*(16), 12971-12998.

Haghighi, H., Arulrajah, A., Mohammadinia, A., & Horpibulsuk, S. (2017). A new approach for determining resilient moduli of marginal pavement base materials using the staged repeated load CBR test method. *Road Materials and Pavement Design, 19*(8), 1848-1867. doi:10.1080/14680629.2017.1352532

Hamidi, A., Yazdanjou, V., & Salimi, N. (2009). Shear strength characteristics of sand-gravel mixtures. *International Journal of Geotechnical Engineering, 3*(1), 29-38.

Han, C., Dong, Q., & Xu, X. (2021). Microstructural analysis on the variation of resilient modulus of lime modified soil under freezing–thawing action. *Road Materials and Pavement Design*, 1-15.

Han, C., Ma, T., Chen, S., & Fan, J. (2021). Application of a hybrid neural network structure for FWD backcalculation based on LTPP database. *International Journal of Pavement Engineering*, 1-14.

Hanandeh, S., Ardah, A., & Abu-Farsakh, M. (2020). Using artificial neural network and genetics algorithm to estimate the resilient modulus for stabilized subgrade and propose new empirical formula. *Transportation Geotechnics, 24*. doi:10.1016/j.trgeo.2020.100358

Hao, S., & Pabst, T. (2021). Estimation of resilient behavior of crushed waste rocks using repeated load CBR tests. *Transportation Geotechnics, 28*, 100525. doi:https://doi.org/10.1016/j.trgeo.2021.100525

Hassani, F., & Archibald, J. (1998). Mine Backfill, CD-ROM, Canadian Institute of Mine. *Metall. Petrol*.

Hatipoglu, M., Cetin, B., & Aydilek, A. H. (2020). Effects of Fines Content on Hydraulic and Mechanical Performance of Unbound Granular Base Aggregates. *Journal of Transportation Engineering, Part B: Pavements, 146*(1), 04019036. doi:doi:10.1061/JPEODX.0000141

Hausknecht, M., Lehman, J., Miikkulainen, R., & Stone, P. (2014). A neuroevolution approach to general atari game playing. *IEEE Transactions on Computational Intelligence and AI in Games, 6*(4), 355-366.

He, J., & Chu, J. (2017). Cementation of sand due to salt precipitation in drying process. *Marine Georesources & Geotechnology, 35*(3), 441-445. doi:10.1080/1064119X.2016.1168498

Hecht-Nielsen, R. (1987). *Kolmogorov's mapping neural network existence theorem.* Paper presented at the Proceedings of the international conference on Neural Networks.

Henkel, D., & Gilbert, G. (1952). The effect measured of the rubber membrane on the triaxial compression strength of clay samples. *Geotechnique, 3*(1), 20-29.

Hicks, R. (1970). *Factors influencing the resilient properties of granular materials.* Thesis submitted to the University of California.

Hicks, R. G., & Monismith, C. L. (1971). Factors influencing the resilient response of granular materials. *Highway research record, 345*, 15-31.

Hinton, G. E., Srivastava, N., Krizhevsky, A., Sutskever, I., & Salakhutdinov, R. R. (2012). Improving neural networks by preventing co-adaptation of feature detectors. *arXiv preprint arXiv:1207.0580*.

Hoffman, B. R., & Sargand, S. M. (2011). *Verification of Rut Depth Collected with the INO Laser Rut Measurement System (LRMS)* (No. FHWA/OH-2011/18). Ohio Research Institute for Transportation and the Environment.

Hotton, G., Bussière, B., Pabst, T., Bresson, É., & Roy, P. (2020). Influence of climate change on the ability of a cover with capillary barrier effects to control acid generation. *Hydrogeology Journal, 28*(2), 763-779.

Hu, X., Zhou, F., Hu, S., & Walubita, L. F. (2010). Proposed loading waveforms and loading time equations for mechanistic-empirical pavement design and analysis. *Journal of Transportation Engineering, 136*(6), 518-527. doi:doi:10.1061/(ASCE)TE.1943-5436.0000121

Huber, P. J. (1973). Robust regression: asymptotics, conjectures and Monte Carlo. *Annals of Statistics, 1*(5), 799-821.

Huber, P. J. (1992). Robust estimation of a location parameter. In *Breakthroughs in statistics* (pp. 492-518). New York, NY: Springer.

Hustrulid, W. A., McCarter, M. K., & Van Zyl, D. J. (2001). *Slope stability in surface mining*. SME.

Huurman, M. (1997). Permanent deformation in concrete block pavements.

Indraratna, B., Ionescu, D., & Christie, H. (1998). Shear behavior of railway ballast based on large-scale triaxial tests. *Journal of Geotechnical and Geoenvironmental Engineering, 124*(5), 439-449.

Ionescu, D. (2004). Evaluation of the engineering behaviour of railway ballast.

IS. 2386 (1963). Methods of test for aggregates for concrete, Part I: particle size and shape.

Ishikawa, T., Lin, T., Kawabata, S., Kameyama, S., & Tokoro, T. (2019). Effect evaluation of freeze-thaw on resilient modulus of unsaturated granular base course material in pavement. *Transportation Geotechnics, 21*, 100284. doi:https://doi.org/10.1016/j.trgeo.2019.100284

Jain, A., Nandakumar, K., & Ross, A. (2005). Score normalization in multimodal biometric systems. *Pattern recognition, 38*(12), 2270-2285.

James, M., & Aubertin, M. (2012). The use of waste rock inclusions to improve the seismic stability of tailings impoundments. In *GeoCongress 2012: State of the Art and Practice in Geotechnical Engineering* (pp. 4166-4175).

James, M., Aubertin, M., & Bussière, B. (2013). *On the use of waste rock inclusions to improve the performance of tailings impoundments.* Paper presented at the Proceedings of the 18th International Conference Soil Mechanics and Geotechnical Engineering, Paris, France.

James, M., Aubertin, M., Bussière, B., Pednault, C., Pépin, N., & Limoges, M. (2017). *A research project on the use of waste rock inclusions to improve the performance of tailings impoundments.* Paper presented at the GeoOttawa 2017, Ottawa, Ontario, Canada.

Janoo, V. C. (1998). Quantification of shape, angularity, and surface texture of base course materials.

Janoo, V. C., & Bayer II, J. J. (2001). The effect of aggregate angularity on base course performance.

Jehring, M. M., & Bareither, C. A. (2016). Tailings composition effects on shear strength behavior of co-mixed mine waste rock and tailings. *Acta Geotechnica, 11*(5), 1147-1166. doi:10.1007/s11440-015-0429-1

Jewell, R., & Wroth, C. (1987). Direct shear tests on reinforced sand. *Geotechnique, 37*(1), 53-68.

Jing, P., Nowamooz, H., & Chazallon, C. (2018). Permanent deformation behaviour of a granular material used in low-traffic pavements. *Road Materials and Pavement Design, 19*(2), 289-314.

Kalkan, E. (2009). Effects of silica fume on the geotechnical properties of fine-grained soils exposed to freeze and thaw. *Cold Regions Science and Technology, 58*(3), 130-135. doi:https://doi.org/10.1016/j.coldregions.2009.03.011

Kalonji-Kabambi, A., Bussière, B., & Demers, I. (2017). Hydrogeological Behaviour of Covers with Capillary Barrier Effects Made of Mining Materials. *Geotechnical and Geological Engineering, 35*(3), 1199-1220. doi:10.1007/s10706-017-0174-3

Kalonji-Kabambi, A., Bussière, B., & Demers, I. (2020a). Hydrogeochemical behavior of reclaimed highly reactive tailings, Part 1: Characterization of reclamation materials. *Minerals, 10*(7), 596.

Kalonji-Kabambi, A., Bussière, B., & Demers, I. (2020b). Hydrogeochemical behavior of reclaimed highly reactive tailings, Part 2: Laboratory and field results of covers made with mine waste materials. *Minerals, 10*(7), 589.

Kaloop, M. R., Gabr, A. R., El-Badawy, S. M., Arisha, A., Shwally, S., & Hu, J. W. (2019). Predicting resilient modulus of recycled concrete and clay masonry blends for pavement applications using soft computing techniques. *Frontiers of Structural and Civil Engineering, 13*(6), 1379-1392. doi:10.1007/s11709-019-0562-2

Kamal, M., Dawson, A., Farouki, O., Hughes, D., & Sha'at, A. (1993). Field and laboratory

evaluation of the mechanical behavior of unbound granular materials in pavements. *Transportation Research Record*, 88-88.

Kang, F., Li, J., & Dai, J. (2019). Prediction of long-term temperature effect in structural health monitoring of concrete dams using support vector machines with Jaya optimizer and salp swarm algorithms. *Advances in Engineering Software, 131*, 60-76. doi:https://doi.org/10.1016/j.advengsoft.2019.03.003

Kang, F., Li, J., & Xu, Q. (2017). System reliability analysis of slopes using multilayer perceptron and radial basis function networks. *International Journal for Numerical and Analytical Methods in Geomechanics, 41*(18), 1962-1978.

Karlaftis, M. G., & Vlahogianni, E. I. (2011). Statistical methods versus neural networks in transportation research: Differences, similarities and some insights. *Transportation Research Part C: Emerging Technologies, 19*(3), 387-399.

Karlik, B., & Olgac, A. V. (2011). Performance analysis of various activation functions in generalized MLP architectures of neural networks. *International Journal of Artificial Intelligence and Expert Systems, 1*(4), 111-122.

Katte, V. Y., Mfoyet, S. M., Manefouet, B., Wouatong, A. S. L., & Bezeng, L. A. (2019). Correlation of California bearing ratio (CBR) value with soil properties of road subgrade soil. *Geotechnical and Geological Engineering, 37*(1), 217-234.

Kaufman, W. W., & Ault, J. C. (1978). *Design of surface mine haulage roads: a manual* (Vol. 8758). Department of the Interior, Bureau of Mines.

Khedr, S. (1985). Deformation characteristics of granular base course in flexible pavements. *Transportation Research Record, 1043*, 131-138.

Khoury, N., Zaman, M., & Laguros, J. (2005). Behavior of stabilized aggregate bases subjected to cyclic loading and wet-dry cycles. In *Advances in Pavement Engineering* (pp. 1-10).

Khoury, N., & Zaman, M. M. (2007). Durability of stabilized base courses subjected to wet–dry cycles. *International Journal of Pavement Engineering, 8*(4), 265-276.

Kim, S.-H., Yang, J., & Jeong, J.-H. (2014). Prediction of subgrade resilient modulus using artificial neural network. *KSCE Journal of Civil Engineering, 18*(5), 1372-1379. doi:10.1007/s12205-014-0316-6

Kim, S. Y., Park, J., Cha, W., Lee, J.-S., & Santamarina, J. C. (2021). Soil Response during Globally Drained and Undrained Freeze-Thaw Cycles under Deviatoric Loading. *Journal of Geotechnical and Geoenvironmental Engineering, 147*(2), 06020030. doi:doi:10.1061/(ASCE)GT.1943-5606.0002464

Kin, M. W. (2006). California bearing ratio correlation with soil index properties. *Master degree Project, Faculty of Civil Engineering, University Technology Malaysia*.

Kirby, H. R., Watson, S. M., & Dougherty, M. S. (1997). Should we use neural networks or statistical models for short-term motorway traffic forecasting? *International Journal of Forecasting, 13*(1), 43-50.

Knapton, J. (1989). *The structural design of heavy duty pavements for ports and other industries*.

Knight, J. (1935). Gradation of aggregate as applied to stabilization of gravel roads. *Canadian Engineer, 69*(23), 9-10.

Kolisoja, P. (1997). *Resilient deformation characteristics of granular materials*: Tampere University of Technology Finland, Publications.

Korkiala-Tanttu, L. (2005). *A new material model for permanent deformations in pavements.* Paper presented at the Proceedings of the international conferences on the bearing capacity of roads, railways and airfields.

Kumar, V. (2000). *Design and construction of haul roads using fly ash.* University of Alberta.

Kurnaz, T. F., & Kaya, Y. (2019). Prediction of the California bearing ratio (CBR) of compacted soils by using GMDH-type neural network. *The European Physical Journal Plus, 134*(7), 326.

Kuttah, D., & Sato, K. (2015). Review on the effect of gypsum content on soil behavior. *Transportation Geotechnics, 4*, 28-37. doi:10.1016/j.trgeo.2015.06.003

L.Bolduc, F., & Aubertin, M. (2014). Numerical investigation of the influence of waste rock inclusions on tailings consolidation. *Canadian Geotechnical Journal, 51*(9), 1021-1032. doi:10.1139/cgj-2013-0137

Lakshmi, S. M., Subramanian, S., Lalithambikhai, M., Vela, A. M., & Ashni, M. (2016). Evaluation of soaked and unsoaked CBR values of soil based on the compaction characteristics. *Malaysian Journal of Civil Engineering, 28*(2).

Lary, D. J., Alavi, A. H., Gandomi, A. H., & Walker, A. L. (2016). Machine learning in geosciences and remote sensing. *Geoscience Frontiers, 7*(1), 3-10. doi:https://doi.org/10.1016/j.gsf.2015.07.003

Laverdière, A. (2019). *Effet de la granulométrie sur le comportement géotechnique de roches stériles concassées utilisées comme surface de roulement sur des routes minières.* École Polytechnique de Montréal,

LeCun, Y., Bengio, Y., & Hinton, G. (2015). Deep learning. *nature, 521*(7553), 436-444.

Lee, D.-H., Cheon, E., Lim, H.-H., Choi, S.-K., Kim, Y.-T., & Lee, S.-R. (2021). An artificial neural network model to predict debris-flow volumes caused by extreme rainfall in the central region of South Korea. *Engineering Geology, 281*. doi:10.1016/j.enggeo.2020.105979

Lee Rodgers, J., & Nicewander, W. A. (1988). Thirteen ways to look at the correlation coefficient. *The American Statistician, 42*(1), 59-66.

Lee, S. H., Lee, S. J., Park, J. G., & Choi, Y.-T. (2017). An experimental study on the characteristics

of polyurethane-mixed coarse aggregates by large-scale triaxial test. *Construction and Building Materials, 145*, 117-125. doi:https://doi.org/10.1016/j.conbuildmat.2017.03.107

Lekarp, F. (1999). *Resilient and permanent deformation behavior of unbound aggregates under repeated loading.* Institutionen för infrastruktur och samhällsplanering,

Lekarp, F., & Dawson, A. (1998). Modelling permanent deformation behaviour of unbound granular materials. *Construction and Building Materials, 12*(1), 9-18.

Lekarp, F., Isacsson, U., & Dawson, A. (2000a). State of the art. I: Resilient response of unbound aggregates. *Journal of Transportation Engineering, 126*(1), 66-75. doi:10.1061/(asce)0733-947x(2000)126:1(66)

Lekarp, F., Isacsson, U., & Dawson, A. (2000b). State of the art. II: Permanent strain response of unbound aggregates. *Journal of Transportation Engineering, 126*(1), 76-83.

Lekarp, F., Richardson, I. R., & Dawson, A. (1996). Influences on permanent deformation behavior of unbound granular materials. *Transportation Research Record, 1547*(1), 68-75.

Leng, W., Xiao, Y., Nie, R., Zhou, W., & Liu, W. (2017). Investigating strength and deformation characteristics of heavy-haul railway embankment materials using large-scale undrained cyclic triaxial tests. *International Journal of Geomechanics, 17*(9), 04017074.

Leps, T. M. (1970). Review of shearing strength of rockfill. *Journal of Soil Mechanics & Foundations Division,* 96(4), 1159-1170.

Li, B., & Wong, R. (2016). Quantifying structural states of soft mudrocks. *Journal of Geophysical Research: Solid Earth*, 121(5), 3324-3347.

Li, L., & Aubertin, M. (2003). A general relationship between porosity and uniaxial strength of engineering materials. *Canadian Journal of Civil Engineering, 30*(4), 644-658.

Li, L., Saboundjian, S., Liu, J., & Zhang, X. (2013). Permanent deformation behavior of alaskan

granular base materials. In *ISCORD 2013: Planning for Sustainable Cold Regions* (pp. 428-435).

Li, M., Zhang, J., Song, W., & Germain, D. M. (2019). Recycling of crushed waste rock as backfilling material in coal mine: effects of particle size on compaction behaviours. *Environmental Science and Pollution Research, 26*(9), 8789-8797.

Li, Y., Nie, R., Yue, Z., Leng, W., & Guo, Y. (2021). Dynamic behaviors of fine-grained subgrade soil under single-stage and multi-stage intermittent cyclic loading: Permanent deformation and its prediction model. *Soil Dynamics and Earthquake Engineering, 142*, 106548. doi:https://doi.org/10.1016/j.soildyn.2020.106548

Li, Y., & Yuan, Y. (2017). Convergence analysis of two-layer neural networks with relu activation. *Advances in neural information processing systems, 30*, 597-607.

Li, Y., Zou, C., Berecibar, M., Nanini-Maury, E., Chan, J. C. W., van den Bossche, P., . . . Omar, N. (2018). Random forest regression for online capacity estimation of lithium-ion batteries. *Applied Energy, 232*, 197-210. doi:https://doi.org/10.1016/j.apenergy.2018.09.182

Lin, P., Ni, P., Guo, C., & Mei, G. (2020). Mapping soil nail loads using Federal Highway Administration (FHWA) simplified models and artificial neural network technique. *Canadian Geotechnical Journal, 57*(10), 1453-1471.

Lin, T., Ishikawa, T., & Tokoro, T. (2019). Testing method for resilient properties of unsaturated unbound granular materials subjected to freeze-thaw action. *Japanese Geotechnical Society Special Publication, 7*(2), 576-581.

Ling, X. Z., Zhang, F., Li, Q. L., An, L. S., & Wang, J. H. (2015). Dynamic shear modulus and damping ratio of frozen compacted sand subjected to freeze–thaw cycle under multi-stage cyclic loading. *Soil Dynamics and Earthquake Engineering, 76*, 111-121. doi:https://doi.org/10.1016/j.soildyn.2015.02.007

Liu, E., Lai, Y., Liao, M., Liu, X., & Hou, F. (2016). Fatigue and damage properties of frozen silty sand samples subjected to cyclic triaxial loading. *Canadian Geotechnical Journal, 53*(12), 1939-1951.

Liu, J., Zhang, X., Li, L., & Saboundjian, S. (2018). Resilient behavior of unbound granular materials subjected to a closed-system freeze-thaw cycle. *Journal of Cold Regions Engineering, 32*(1), 04017015.

Liu, X., Zhang, X., Wang, H., & Jiang, B. (2019). Laboratory testing and analysis of dynamic and static resilient modulus of subgrade soil under various influencing factors. *Construction and Building Materials, 195*, 178-186.

Long, W., Xiaoguang, X., & Hai, L. (2011). Influence of laboratory compaction methods on shear performance of graded crushed stone. *Journal of Materials in Civil Engineering, 23*(10), 1483-1487.

Lu, Z., She, J., Wu, X., & Yao, H. (2019). Cumulative strain characteristics of compacted soil under effect of freeze-thaw cycles with water supply. *Transportation Geotechnics, 21*, 100291.

Lytton, R. L. (1996). *Foundations and pavements on unsaturated soils.* Paper presented at the Proceedings of the First International Conference on Unsaturated Soils/Unsat'95/Paris/France/6-8 September 1995. Volume 3.

Lytton, R. L., Uzan, J., Fernando, E. G., Roque, R., Hiltunen, D., & Stoffels, S. M. (1993). *Development and validation of performance prediction models and specifications for asphalt binders and paving mixes* (Vol. 357): Strategic Highway Research Program Washington, DC.

Maalouf, M., Khoury, N., Laguros, J. G., & Kumin, H. (2012). Support vector regression to predict the performance of stabilized aggregate bases subject to wet–dry cycles. *International Journal for Numerical and Analytical Methods in Geomechanics, 36*(6), 675-696.

Maghool, F., Arulrajah, A., Suksiripattanapong, C., Horpibulsuk, S., & Mohajerani, A. (2019). Geotechnical properties of steel slag aggregates: Shear strength and stiffness. *Soils and Foundations, 59*(5), 1591-1601.

Mahdevari, S., & Torabi, S. R. (2012). Prediction of tunnel convergence using Artificial Neural Networks. *Tunnelling and Underground Space Technology, 28*, 218-228. doi:https://doi.org/10.1016/j.tust.2011.11.002

Mahmoodzadeh, A., Mohammadi, M., Hashim Ibrahim, H., Nariman Abdulhamid, S., Ghafoor Salim, S., Farid Hama Ali, H., & Majeed, M. (2020). Artificial Intelligence Forecasting Models of Uniaxial Compressive Strength. *Transportation Geotechnics*, 100499. doi:https://doi.org/10.1016/j.trgeo.2020.100499

Maknoon, M. (2016). *Slope stability analyses of waste rock piles under unsaturated conditions following large precipitations.* Ecole Polytechnique, Montreal (Canada).

Maknoon, M., & Aubertin, M. (2020). On the Use of Bench Construction to Improve the Stability of Unsaturated Waste Rock Piles. *Geotechnical and Geological Engineering*, 1-25.

Malla, R. B., & Joshi, S. (2007). Resilient modulus prediction models based on analysis of LTPP data for subgrade soils and experimental verification. *Journal of Transportation Engineering, 133*(9), 491-504.

Malla, R. B., & Joshi, S. (2008). Subgrade resilient modulus prediction models for coarse and fine-grained soils based on long-term pavement performance data. *International Journal of Pavement Engineering, 9*(6), 431-444.

Mata, A., & Corchado, J. M. (2009). Forecasting the probability of finding oil slicks using a CBR system. *Expert Systems with Applications, 36*(4), 8239-8246. doi:https://doi.org/10.1016/j.eswa.2008.10.003

McCarter, M. (1990). Design and operating considerations for mine waste embankments. *Soc of*

Mining Engineers of Aime, 890-899.

McLemore, V. T., Fakhimi, A., van Zyl, D., Ayakwah, G. F., Anim, K., Boakye, K., . . . Gutierrez, L. A. (2009). Literature review of other rock piles: characterization, weathering, and stability. *New Mexico Bureau of Geology and Mineral Resources, Socorro, NM*.

Mehta, Y., & Roque, R. (2003). Evaluation of FWD data for determination of layer moduli of pavements. *Journal of Materials in Civil Engineering, 15*(1), 25-31.

Meiers, G. P., Barbour, S. L., Qualizza, C. V., & Dobchuk, B. S. (2011). Evolution of the Hydraulic Conductivity of Reclamation Covers over Sodic/Saline Mining Overburden. *Journal of Geotechnical and Geoenvironmental Engineering, 137*(10), 968-976. doi:doi:10.1061/(ASCE)GT.1943-5606.0000523

Meyer, G. P. (2019). An alternative probabilistic interpretation of the Huber loss. *arXiv preprint arXiv:1911.02088*.

Miao, Y., Huang, Y., Zhang, Q., & Wang, L. (2016). Effect of temperature on resilient modulus and shear strength of unbound granular materials containing fine RAP. *Construction and Building Materials, 124*, 1132-1141. doi:https://doi.org/10.1016/j.conbuildmat.2016.08.137

Mishra, D., Kazmee, H., Tutumluer, E., Pforr, J., Read, D., & Gehringer, E. (2013). Characterization of railroad ballast behavior under repeated loading: results from new large triaxial test setup. *Transportation Research Record, 2374*(1), 169-179.

Mishra, D., & Tutumluer, E. (2012). Aggregate physical properties affecting modulus and deformation characteristics of unsurfaced pavements. *Journal of Materials in Civil Engineering, 24*(9), 1144-1152.

Mohammad, L. N., Huang, B., Puppala, A. J., & Allen, A. (1999). Regression model for resilient modulus of subgrade soils. *Transportation Research Record, 1687*(1), 47-54.

Mohammadinia, A., Naeini, M., Arulrajah, A., Horpibulsuk, S., & Leong, M. (2020). Shakedown analysis of recycled materials as railway capping layer under cyclic loading. *Soil Dynamics and Earthquake Engineering, 139*, 106423. doi:https://doi.org/10.1016/j.soildyn.2020.106423

Molenaar, A. A. (2008). *Repeated load CBR testing, a simple but effective tool for the characterization of fine soils and unbound materials*. No. 08-0516.

Molenaar, A. A., Araya, A. A., & Houben, L. J. (2011). *Characterization of unbound base materials for roads using a new developed repeated load CBR test.* Paper presented at the Eighth International Conference on Managing Pavement Assets, Santiago, Chile.

Moossazadeh, J., & Witczak, M. W. (1981). Prediction of subgrade moduli for soil that exhibits nonlinear behavior. *Transportation Research Record 810*, 9-17.

Morgan, J. (1966). The response of granular materials to repeated loading. *Australian Road Research Board Proc*.

Morgan, J., Tucker, J., & McInnes, D. (1994). *A mechanistic design approach for unsealed mine haul roads.* Paper presented at the 17TH ARRB CONFERENCE, GOLD COAST, QUEENSLAND, 15-19 AUGUST 1994; PROCEEDINGS; VOLUME 17, PART 2.

Morin, K. A. (1991). *Critical literature review of acid drainage from waste rock* (Canadian MEND Report 1.11.1).

Mozumder, R. A., & Laskar, A. I. (2015). Prediction of unconfined compressive strength of geopolymer stabilized clayey soil using Artificial Neural Network. *Computers and Geotechnics, 69*, 291-300. doi:10.1016/j.compgeo.2015.05.021

Mukherjee, A., Jain, D. K., Goswami, P., Xin, Q., Yang, L., & Rodrigues, J. J. (2020). Back Propagation Neural Network Based Cluster Head Identification in MIMO Sensor Networks for Intelligent Transportation Systems. *IEEE Access, 8*, 28524-28532.

Nair, A. M., & Latha, G. M. (2012). Taming of large diameter triaxial setup. *Geomech. Eng, 4*(4), 251-262.

Nair, A. M., & Latha, G. M. (2015). Large Diameter Triaxial Tests on Geosynthetic-Reinforced Granular Subbases. *Journal of Materials in Civil Engineering, 27*(4), 04014148. doi:doi:10.1061/(ASCE)MT.1943-5533.0001088

Nazzal, M. D., & Tatari, O. (2013). Evaluating the use of neural networks and genetic algorithms for prediction of subgrade resilient modulus. *International Journal of Pavement Engineering, 14*(4), 364-373. doi:10.1080/10298436.2012.671944

NCHRP. (2004). *Guide for mechanistic-empirical design of new and rehabilitated pavement structures* (Final Rep. No. 1-37A). Retrieved from Washington, D.C.

Neter, J., Wasserman, W., & Kutner, M. H. (1989). Applied linear regression models.

Ni, B., Hopkins, T., Sun, L., & Beckham, T. (2002). *Modeling the resilient modulus of soils.* Paper presented at the Proceedings of the 6th international conference on the bearing capacity of roads and airfields, Lisbon, Portugal.

Omraci, K., Merrien-Soukatchoff, V., Tisot, J.-P., Piguet, J.-P., & Nickel-SLN, L. (2003). Stability analysis of lateritic waste deposits. *Engineering Geology, 68*(3-4), 189-199.

Opiyo, T. (1995). *A mechanistic approach to Laterite-based pavements in transport and road engineering.* (MSc Thesis). International Institute for Infrastructure, Hydraulics and Environment Engineering, Delft, the Netherlands.

Oskooei, P. R., Mohammadinia, A., Arulrajah, A., & Horpibulsuk, S. (2020). Application of artificial neural network models for predicting the resilient modulus of recycled aggregates. *International Journal of Pavement Engineering*, 1-13. doi:10.1080/10298436.2020.1791863

Othman, M. A., & Benson, C. H. (1993). Effect of freeze–thaw on the hydraulic conductivity and

morphology of compacted clay. *Canadian Geotechnical Journal, 30*(2), 236-246.

Ovalle, C., & Dano, C. (2020). Effects of particle size–strength and size–shape correlations on parallel grading scaling. *Géotechnique Letters, 10*(2), 191-197. doi:10.1680/jgele.19.00095

Ovalle, C., Frossard, E., Dano, C., Hu, W., Maiolino, S., & Hicher, P.-Y. (2014). The effect of size on the strength of coarse rock aggregates and large rockfill samples through experimental data. *Acta Mechanica, 225*(8), 2199-2216.

Ovalle, C., Linero, S., Dano, C., Bard, E., Hicher, P.-Y., & Osses, R. (2020). Data Compilation from Large Drained Compression Triaxial Tests on Coarse Crushable Rockfill Materials. *Journal of Geotechnical and Geoenvironmental Engineering, 146*(9), 06020013. doi:doi:10.1061/(ASCE)GT.1943-5606.0002314

Pabst, T. (2011). Etude expérimentale et numérique du comportement hydro-geochimique de recouvrement placé sur des résidus sulfureux partiellement oxydés. *These de doctorat. Département de génie civil, géologique et des mines. École Polytechnique de Montréal, Québec*.

Pabst, T., Aubertin, M., Bussière, B., & Molson, J. (2017). Experimental and numerical evaluation of single-layer covers placed on acid-generating tailings. *Geotechnical and Geological Engineering, 35*(4), 1421-1438. doi:10.1007/s10706-017-0185-0

Paige-Green, P. (2007). Improved material specifications for unsealed roads. *Quarterly Journal of Engineering Geology and Hydrogeology, 40*(2), 175-179.

Pan, L., Feng, X., Sang, F., Li, L., Leng, M., & Chen, X. (2019). An improved back propagation neural network based on complexity decomposition technology and modified flower pollination optimization for short-term load forecasting. *Neural Computing and Applications, 31*(7), 2679-2697.

Panchal, G., Ganatra, A., Kosta, Y., & Panchal, D. (2011). Behaviour analysis of multilayer

perceptrons with multiple hidden neurons and hidden layers. *International Journal of Computer Theory and Engineering, 3*(2), 332-337.

Pappas, D. M., & Mark, C. (1993). *Behavior of simulated longwall gob material* (Vol. 9458): US Department of the Interior, Bureau of Mines.

Park, H., Kweon, G., & Lee, S. R. (2009). Prediction of resilient modulus of granular subgrade soils and subbase materials using artificial neural network. *Road Materials and Pavement Design, 10*(3), 647-665.

Park, H. I., Kweon, G. C., & Lee, S. R. (2009). Prediction of resilient modulus of granular subgrade soils and subbase materials using artificial neural network. *Road Materials and Pavement Design, 10*(3), 647-665. doi:10.3166/rmpd.10.647-665

Patel, R. S., & Desai, M. (2010). *CBR predicted by index properties for alluvial soils of South Gujarat.* Paper presented at the Proceedings of the Indian geotechnical conference, Mumbai.

Pekel, E. (2020). Estimation of soil moisture using decision tree regression. *Theoretical and Applied Climatology, 139*(3), 1111-1119.

Pérez-González, E., Bilodeau, J.-P., Doré, G., & Doré-Richard, S. (2020). Assessment of the Permanent Deformation at the Earth-Core of a Rockfill Dam under Heavy Vehicle Loading. *Canadian Geotechnical Journal, 999*, 1-11.

Perner, P., Zscherpel, U., & Jacobsen, C. (2001). A comparison between neural networks and decision trees based on data from industrial radiographic testing. *Pattern Recognition Letters, 22*(1), 47-54. doi:https://doi.org/10.1016/S0167-8655(00)00098-2

Pezo, R., & Hudson, W. R. (1994). Prediction models of resilient modulus for nongranular materials. *Geotechnical Testing Journal, 17*(3), 349-355.

Phaisangittisagul, E. (2016). *An analysis of the regularization between L2 and dropout in single hidden layer neural network.* Paper presented at the 7th International Conference on

Intelligent Systems, Modelling and Simulation (ISMS).

Poisson, J., Chouteau, M., Aubertin, M., & Campos, D. (2009). Geophysical experiments to image the shallow internal structure and the moisture distribution of a mine waste rock pile. *Journal of Applied Geophysics, 67*(2), 179-192. doi:10.1016/j.jappgeo.2008.10.011

Poulsen, A. P., Thorhauge, M., Funch, M. H., & Risi, S. (2017). *DLNE: A hybridization of deep learning and neuroevolution for visual control.* Paper presented at the 2017 IEEE Conference on Computational Intelligence and Games (CIG).

Pyo, S. C. (2012). *Study of Non-Linear Stress Distribution and Permanent Deformation of Unbound Pavement Layers with Soft Subgrade under Various Stabilization Measures.* North Carolina State University,

Qi, S., Cui, Y., Dupla, J. C., Chen, R., Wang, H., Su, Y., . . . Canou, J. (2020). Investigation of the parallel gradation method based on the response of track-bed materials under cyclic loadings. *Transportation Geotechnics, 24*, 100360.

Qi, S., Cui, Y.-J., Chen, R.-P., Wang, H.-L., Lamas-Lopez, F., Aimedieu, P., . . . Saussine, G. (2020). Influence of grain size distribution of inclusions on the mechanical behaviours of track-bed materials. *Geotechnique, 70*(3), 238-247.

Qian, J. G., Wang, Y. G., Yin, Z. Y., & Huang, M. S. (2016). Experimental identification of plastic shakedown behavior of saturated clay subjected to traffic loading with principal stress rotation. *Engineering Geology, 214*, 29-42. doi:10.1016/j.enggeo.2016.09.012

Qian, Y., Tutumluer, E., Hashash, Y. M., & Ghaboussi, J. (2014). *Effects of ballast degradation on permanent deformation behavior from large-scale triaxial tests.* Paper presented at the ASME/IEEE Joint Rail Conference.

Rahim, A., & George, K. (2005). Models to estimate subgrade resilient modulus for pavement design. *International Journal of Pavement Engineering, 6*(2), 89-96.

Rahman, M. S., & Erlingsson, S. (2015a). A model for predicting permanent deformation of unbound granular materials. *Road Materials and Pavement Design, 16*(3), 653-673.

Rahman, M. S., & Erlingsson, S. (2015b). Predicting permanent deformation behaviour of unbound granular materials. *International Journal of Pavement Engineering, 16*(7), 587-601.

Razouki, S., & El-Janabi, O. (1999). Decrease in the CBR of a gypsiferous soil due to long-term soaking. *Quarterly journal of engineering geology and hydrogeology, 32*(1), 87-89.

Razouki, S. S., & Salem, B. M. (2015). Impact of soaking–drying cycles on gypsum sand roadbed soil. *Transportation Geotechnics, 2*, 78-85. doi:10.1016/j.trgeo.2014.11.003

Rehman, Z., Khalid, U., Farooq, K., & Mujtaba, H. (2017). Prediction of CBR value from index properties of different soils. *Technical journal university of engineering and technology Taxila, Pakistan, 22*.

Ren, J., Vanapalli, S. K., Han, Z., Omenogor, K. O., & Bai, Y. (2019). The resilient moduli of five Canadian soils under wetting and freeze-thaw conditions and their estimation by using an artificial neural network model. *Cold Regions Science and Technology, 168*. doi:10.1016/j.coldregions.2019.102894

Robinson, R. (1974). *Measurement of the elastic properties of granular materials using a resonance method*. Retrieved from

Rumelhart, D. E., Hinton, G. E., & Williams, R. J. (1986). Learning representations by back-propagating errors. *nature, 323*(6088), 533-536.

Saberian, M., Li, J., Nguyen, B. T., & Boroujeni, M. (2020). Experimental and analytical study of dynamic properties of UGM materials containing waste rubber. *Soil Dynamics and Earthquake Engineering, 130*, 105978. doi:https://doi.org/10.1016/j.soildyn.2019.105978

Sadrossadat, E., Heidaripanah, A., & Osouli, S. (2016). Prediction of the resilient modulus of flexible pavement subgrade soils using adaptive neuro-fuzzy inference systems.

Construction and Building Materials, 123, 235-247. doi:10.1016/j.conbuildmat.2016.07.008

Saha, S., Gu, F., Luo, X., & Lytton, R. L. (2018). Use of an Artificial Neural Network Approach for the Prediction of Resilient Modulus for Unbound Granular Material. *Transportation Research Record, 2672*(52), 23-33. doi:10.1177/0361198118756881

Said Razouki, S., & Salem, B. M. (2017). Gypsum sand resilient modulus during cyclic soaking and drying. *International Journal of Pavement Engineering, 18*(2), 108-118. doi:10.1080/10298436.2015.1039004

Sakellariou, M. G., & Ferentinou, M. D. (2005). A study of slope stability prediction using neural networks. *Geotechnical & Geological Engineering, 23*(4), 419. doi:10.1007/s10706-004-8680-5

Salam, S., Osouli, A., & Tutumluer, E. (2018). Crushed Limestone Aggregate Strength Influenced by Gradation, Fines Content, and Dust Ratio. *Journal of Transportation Engineering, Part B: Pavements, 144*(1), 04018002. doi:doi:10.1061/JPEODX.0000032

Saleh-Mbemba, F., Aubertin, M., & Boudrias, G. (2019). Drainage and consolidation of mine tailings near waste rock inclusions. In *Sustainable and Safe Dams Around the World* (pp. 3296-3305): CRC Press.

Salour, F., & Erlingsson, S. (2017). Permanent deformation characteristics of silty sand subgrades from multistage RLT tests. *International Journal of Pavement Engineering, 18*(3), 236-246.

Santha, B. (1994). Resilient modulus of subgrade soils: comparison of two constitutive equations. *Transportation Research Record* (1462).

Sas, W., & Gluchowski, A. (2013). Application of cyclic CBR test to approximation of subgrade displacement in road pavement. *Acta Scientiarum Polonorum. Architectura, 12*(1).

Sas, W., Głuchowski, A., & Szymański, A. (2012). Determination of the resilient modulus M_R for

the lime stabilized clay obtained from the repeated loading CBR tests. *Annals of Warsaw University of Life Sciences-SGGW. Land Reclamation, 44*(2), 143-153.

Saul, L. K., Jaakkola, T., & Jordan, M. I. (1996). Mean field theory for sigmoid belief networks. *Journal of artificial intelligence research, 4*, 61-76.

Sayida, M., Evangeline, S. Y., & Girish, M. (2019). Coir geotextiles for paved roads: A laboratory and field study using non-plastic soil as subgrade. *Journal of Natural Fibers*.

Seal II, R. R., & Shanks III, W. C. (2008). Sulfide oxidation: Insights from experimental, theoretical, stable isotope, and predictive studies in the field and laboratory. In: Pergamon.

Seed, H., Mitry, F., Monismith, C., & Chan, C. (1965). *Prediction of pavement deflections from laboratory repeated load tests, Report No. TE 65-6, soil mechanics and bituminous materials research laboratory*.

Seed, H., Mitry, F., Monismith, C., & Chan, C. (1967). *Prediction of flexible pavement deflections from laboratory repeated-load tests* (NCHRP report 35).

Seif El Dine, B., Dupla, J. C., Frank, R., Canou, J., & Kazan, Y. (2010). Mechanical characterization of matrix coarse-grained soils with a large-sized triaxial device. *Canadian Geotechnical Journal, 47*(4), 425-438.

Senadheera, S., Nash, P., & Rana, A. (1995). Characterization of the behavior of granular road material containing glass cullet. *Department of Civil Engineering, Texas Tech University, Lubbock, Texas, USA*.

Shafabakhsh, G., & Tanakizadeh, A. (2015). Investigation of loading features effects on resilient modulus of asphalt mixtures using Adaptive Neuro-Fuzzy Inference System. *Construction and Building Materials, 76*, 256-263. doi:https://doi.org/10.1016/j.conbuildmat.2014.11.069

Shahin, M. A. (2016). State-of-the-art review of some artificial intelligence applications in pile

foundations. *Geoscience Frontiers, 7*(1), 33-44. doi:https://doi.org/10.1016/j.gsf.2014.10.002

Sharma, S. (2017). Activation functions in neural networks. *Towards Data Science, 6*(12), 310-316.

Sheets, R., & Bates, E. (2008). Gold quarry North Waste Rock Facility slide investigation and stabilization. In *Tailings and Mine Waste'08* (pp. 421-434): CRC Press.

Shen, S., Atangana Njock, P. G., Zhou, A., & Lyu, H. M. (2021). Dynamic prediction of jet grouted column diameter in soft soil using Bi-LSTM deep learning. *Acta Geotechnica, 16*(1), 303-315. doi:10.1007/s11440-020-01005-8

Shi, E., Joseph, T. G., & Rasimarzabadi, R. (2017). Crushed rock pad capability under mining equipment operation. *International Journal of Geotechnical Engineering*, 1-9.

Shi, X. S., Liu, K., & Yin, J. (2021). Effect of Initial Density, Particle Shape, and Confining Stress on the Critical State Behavior of Weathered Gap-Graded Granular Soils. *Journal of Geotechnical and Geoenvironmental Engineering, 147*(2), 04020160. doi:doi:10.1061/(ASCE)GT.1943-5606.0002449

Shou, K., & Lin, J. (2020). Evaluation of the extreme rainfall predictions and their impact on landslide susceptibility in a sub-catchment scale. *Engineering Geology, 265*, 105434. doi:https://doi.org/10.1016/j.enggeo.2019.105434

Simonsen, E., Janoo, V. C., & Isacsson, U. (2002). Resilient properties of unbound road materials during seasonal frost conditions. *Journal of Cold Regions Engineering, 16*(1), 28-50.

Sinha, S., Singh, T., Singh, V., & Verma, A. (2010). Epoch determination for neural network by self-organized map (SOM). *Computational Geosciences, 14*(1), 199-206.

Siswosoebrotho, B. I., Widodo, P., & Augusta, E. (2005). *The influence of fines content and plasticity on the strength and permeability of aggregate for base course material.* Paper presented at the Proceedings of the Eastern Asia Society for Transportation Studies.

Skousen, J., Zipper, C. E., Rose, A., Ziemkiewicz, P. F., Nairn, R., McDonald, L. M., & Kleinmann, R. L. (2017). Review of Passive Systems for Acid Mine Drainage Treatment. *Mine Water and the Environment, 36*(1), 133-153. doi:10.1007/s10230-016-0417-1

Smith, G. N. (1986). Probability and statistics in civil engineering. *Collins professional and technical books, 244*.

Smith, L. J. D., Blowes, D. W., Jambor, J. L., Smith, L., Sego, D. C., & Neuner, M. (2013). The Diavik Waste Rock Project: Particle size distribution and sulfur characteristics of low-sulfide waste rock. *Applied Geochemistry, 36*, 200-209. doi:https://doi.org/10.1016/j.apgeochem.2013.05.006

Sobol', I. y. M. (1990). On sensitivity estimation for nonlinear mathematical models. *Matematicheskoe modelirovanie, 2*(1), 112-118.

Sohangir, S., Rahimi, S., & Gupta, B. (2013). *Optimized feature selection using NeuroEvolution of Augmenting Topologies (NEAT).* Paper presented at the 2013 Joint IFSA World Congress and NAFIPS Annual Meeting (IFSA/NAFIPS).

Sola, J., & Sevilla, J. (1997). Importance of input data normalization for the application of neural networks to complex industrial problems. *IEEE Transactions on nuclear science, 44*(3), 1464-1468.

Solanki, P., & Zaman, M. (2014). *Effect of wet-dry cycling on the mechanical properties of stabilized subgrade soils.* Paper presented at the Geo-Congress 2014: Geo-characterization and Modeling for Sustainability.

Soliman, H., & Shalaby, A. (2016). Validation of long-term pavement performance prediction models for resilient modulus of unbound granular materials. *Transportation Research Record, 2578*(1), 29-37.

Sparsha, N., Robinson, R., & Murali, J. (2016). *Use of repeated load CBR test to characterize*

pavement granular materials. Paper presented at the Functional Pavement Design.

Sreelekshmypillai, G., & Vinod, P. (2019). Prediction of CBR value of fine grained soils at any rational compactive effort. *International Journal of Geotechnical Engineering, 13*(6), 560-565.

Srivastava, N., Hinton, G., Krizhevsky, A., Sutskever, I., & Salakhutdinov, R. (2014). Dropout: a simple way to prevent neural networks from overfitting. *The Journal of Machine Learning Research, 15*(1), 1929-1958.

Stanley, K. O., Bryant, B. D., & Miikkulainen, R. (2005). Real-time neuroevolution in the NERO video game. *IEEE transactions on evolutionary computation, 9*(6), 653-668.

Stanley, K. O., & Miikkulainen, R. (2002). Evolving neural networks through augmenting topologies. *Evolutionary computation, 10*(2), 99-127.

Stefanow, D., & Dudziński, P. A. (2021). Soil shear strength determination methods – State of the art. *Soil and Tillage Research, 208*, 104881. doi:https://doi.org/10.1016/j.still.2020.104881

Su, L., & Fu, L. (2020). Regional land planning based on BPNN and space mining technology. *Neural Computing and Applications*. doi:10.1007/s00521-020-05316-5

Su, Y., Cui, Y.-J., Dupla, J.-C., & Canou, J. (2020). Effect of water content on resilient modulus and damping ratio of fine/coarse soil mixtures with varying coarse grain contents. *Transportation Geotechnics*, 100452. doi:https://doi.org/10.1016/j.trgeo.2020.100452

Sun, Q., Indraratna, B., & Nimbalkar, S. (2014). Effect of cyclic loading frequency on the permanent deformation and degradation of railway ballast. *Geotechnique, 64*(9), 746-751.

Sun, Q., Zhou, W.-X., & Fan, J. (2020). Adaptive huber regression. *Journal of the American Statistical Association, 115*(529), 254-265.

Sun, W., Wang, H., & Hou, K. (2018). Control of waste rock-tailings paste backfill for active

mining subsidence areas. *Journal of Cleaner Production, 171*, 567-579. doi:https://doi.org/10.1016/j.jclepro.2017.09.253

Sweere, G. T. (1990). *Unbound granular bases for roads.* University of Delft, Delft, The Netherlands.

Talukdar, D. K. (2014). A study of correlation between California Bearing Ratio (CBR) value with other properties of soil. *International Journal of Emerging Technology and Advanced Engineering, 4*(1), 559-562.

Tannant, D., & Regensburg, B. (2001). *Guidelines for mine haul road design*. Retrieved from

Tao, M., Mohammad, L. N., Nazzal, M. D., Zhang, Z., & Wu, Z. (2010). Application of shakedown theory in characterizing traditional and recycled pavement base materials. *Journal of Transportation Engineering, 136*(3), 214-222.

Tarawneh, B., & Nazzal, M. D. (2014). Optimization of resilient modulus prediction from FWD results using artificial neural network. *Periodica Polytechnica Civil Engineering, 58*(2), 143-154. doi:10.3311/PPci.2201

Taskiran, T. (2010). Prediction of California bearing ratio (CBR) of fine grained soils by AI methods. *Advances in Engineering Software, 41*(6), 886-892. doi:10.1016/j.advengsoft.2010.01.003

Tenpe, A. R., & Patel, A. (2020). Application of genetic expression programming and artificial neural network for prediction of CBR. *Road Materials and Pavement Design, 21*(5), 1183-1200. doi:10.1080/14680629.2018.1544924

Thach Nguyen, B., & Mohajerani, A. (2016). Possible simplified method for the determination of the resilient modulus of unbound granular materials. *Road Materials and Pavement Design, 17*(4), 841-858.

Tholen, O. (1980). *Falling weight deflectometer. A device for bearing capacity measurements:*

properties and performance. No. Monograph. 1980.

Thom, N., & Brown, S. (1988). *The effect of grading and density on the mechanical properties of a crushed dolomitic limestone.* Paper presented at the Australian Road Research Board (ARRB) Conference, 14th, 1988, Canberra.

Thompson, R., Peroni, R., & Visser, A. T. (2019). *Mining Haul Roads: Theory and Practice*: CRC Press.

Thompson, R. J. (1996). *The design and management of surface mine haul roads.* University of Pretoria.

Thompson, R. J. (2010). *Mine haul road design and management best practices for safe and cost-efficient truck haulage.* Paper presented at the Society for Mining, Metallurgy and Exploration 2010 Conference Proceedings Pre-print.

Thompson, R. J. (2011a). Building better haul roads. *Engineering and Mining Journal, 212*(5), 48-53.

Thompson, R. J. (2011b). Design, construction, and maintenance of haul roads. *SME mining engineering handbook, 1*, 957-977.

Thompson, R. J. (2011c). *Mine haul road design, construction and maintenance management.* Curtin University, Australia.

Thompson, R. J. (2015). *Principles of Mine Haul Road Design and Construction*.

Thompson, R. J., & Visser, A. T. (1996). An overview of the structural design of mine haulage roads. *Journal of the South African Institute of Mining and Metallurgy, 96*(1), 29-37.

Thompson, R. J., & Visser, A. T. (1997a). An introduction to the integrated design of surface mine haul roads. *International Journal of Surface Mining, Reclamation and Environment, 11*(3), 115-120. doi:10.1080/09208119708944074

Thompson, R. J., & Visser, A. T. (1997b). A mechanistic structural design procedure for surface mine haul roads. *International Journal of Surface Mining, Reclamation and Environment, 11*(3), 121-128. doi:10.1080/09208119708944075

Thompson, R. J., & Visser, A. T. (2000a). Designing and managing unpaved opencast mine haul roads for optimum performance. *Transactions-Society for Mining Metallurgy and Exploration Incorporated, 308*, 69-77.

Thompson, R. J., & Visser, A. T. (2000b). The functional design of surface mine haul roads. *Journal-South African Institute of Mining and Metallurgy, 100*(3), 169-180.

Thompson, R. J., & Visser, A. T. (2003). Mine haul road maintenance management systems. *Journal of the South African Institute of Mining and Metallurgy, 103*(5), 303-312.

Thompson, R. J., & Visser, A. T. (2007). Selection parameters for mine haul road wearing course materials. *International Journal of Surface Mining, Reclamation and Environment, 14*(1), 1-17. doi:10.1080/13895260008953294

Thompson, R. J., & Visser, A. T. (2013). Selection and maintenance of mine haul road wearing course materials. *Mining Technology, 115*(4), 140-153. doi:10.1179/174328606x155138

Thompson, R. J., Visser, A. T., Miller, R. E., & Lowe, N. T. (2003). Development of real-time mine road maintenance management system using haul truck and road vibration signature analysis. *Transportation Research Record: Journal of the Transportation Research Board*(1819), 305-312.

Tian, P., Zaman, M. M., & Laguros, J. G. (1998). Gradation and moisture effects on resilient moduli of aggregate bases. *Transportation Research Record, 1619*(1), 75-84.

Tian, S., Indraratna, B., Tang, L., Qi, Y., & Ling, X. (2020). A semi-empirical elasto-plastic constitutive model for coarse-grained materials that incorporates the effects of freeze-thaw cycles. *Transportation Geotechnics, 24*, 100373.

doi:https://doi.org/10.1016/j.trgeo.2020.100373

Tian, S., Tang, L., Ling, X., Li, S., Kong, X., & Zhou, G. (2019). Experimental and analytical investigation of the dynamic behavior of granular base course materials used for China's high-speed railways subjected to freeze-thaw cycles. *Cold Regions Science and Technology, 157*, 139-148.

Titi, H. H., & Matar, M. G. (2018). Estimating resilient modulus of base aggregates for mechanistic-empirical pavement design and performance evaluation. *Transportation Geotechnics, 17*, 141-153.

Touqan, M., Ahmed, A., El Naggar, H., & Stark, T. (2020). Static and cyclic characterization of fouled railroad sub-ballast layer behaviour. *Soil Dynamics and Earthquake Engineering, 137*, 106293. doi:https://doi.org/10.1016/j.soildyn.2020.106293

Tremblay, G., & Hogan, C. (2001). *MEND manual: volume 1, summary*. Retrieved from Ottawa, Ontario, Canada.

Tso, G. K. F., & Yau, K. K. W. (2007). Predicting electricity energy consumption: A comparison of regression analysis, decision tree and neural networks. *Energy, 32*(9), 1761-1768. doi:https://doi.org/10.1016/j.energy.2006.11.010

Tutumluer, E. (1995). *Predicting behavior of flexible pavements with granular bases.* Georgia Institute of Technology.

Tutumluer, E., Mishra, D., & Butt, A. A. (2009). *Characterization of Illinois aggregates for subgrade replacement and subbase* (0197-9191). Retrieved from

Tutumluer, E., & Pan, T. (2008). Aggregate morphology affecting strength and permanent deformation behavior of unbound aggregate materials. *Journal of Materials in Civil Engineering, 20*(9), 617-627.

ul Rehman, A., Farooq, K., Mujtaba, H., & Altaf, O. (2015). Estimation of california bearing ratio

(cbr) from index properties and compaction characteristics of coarse grained soil.

Ullah, S., Tanyu, B. F., & Zainab, B. (2020). Development of an artificial neural network (ANN)-based model to predict permanent deformation of base course containing reclaimed asphalt pavement (RAP). *Road Materials and Pavement Design*, 1-19.

Uthus, L. (2007). *Deformation properties of unbound granular aggregates*: Fakultet for ingeniørvitenskap og teknologi.

Uzan, J. (1985). Characterization of granular material. *Transportation Research Record, 1022*(1), 52-59.

Valdes, J. R., & Cortes, D. D. (2014). *Heat-induced bonding of sands.* Paper presented at the Geo-Congress 2014: Geo-characterization and Modeling for Sustainability.

Vallejo, L. E. (2001). Interpretation of the limits in shear strength in binary granular mixtures. *Canadian Geotechnical Journal, 38*(5), 1097-1104.

Vanapalli, S. K., Fredlund, D. G., Pufahl, D. E., & Clifton, A. W. (1996). Model for the prediction of shear strength with respect to soil suction. *Canadian Geotechnical Journal, 33*(3), 379-392. doi:10.1139/t96-060

Varghese, V. K., Babu, S. S., Bijukumar, R., Cyrus, S., & Abraham, B. M. (2013). Artificial Neural Networks: A Solution to the Ambiguity in Prediction of Engineering Properties of Fine-Grained Soils. *Geotechnical and Geological Engineering, 31*(4), 1187-1205. doi:10.1007/s10706-013-9643-5

Vidal, A., & Kristjanpoller, W. (2020). Gold Volatility Prediction using a CNN-LSTM approach. *Expert Systems with Applications*. doi:10.1016/j.eswa.2020.113481

Vieira, C. S., & Pereira, P. M. (2015). Use of recycled construction and demolition materials in geotechnical applications: A review. *Resources, Conservation and Recycling, 103*, 192-204.

Vujicic, T., Matijevic, T., Ljucovic, J., Balota, A., & Sevarac, Z. (2016). *Comparative analysis of methods for determining number of hidden neurons in artificial neural network.* Paper presented at the Central european conference on information and intelligent systems.

Wager, S., Wang, S., & Liang, P. S. (2013). *Dropout training as adaptive regularization.* Paper presented at the Advances in neural information processing systems.

Wang, H. (2005). *Development of laser system to measure pavement rutting*. University of South Florida.

Wang, H., Cui, Y., Lamas-Lopez, F., Dupla, J. C., Canou, J., Calon, N., . . . Chen, R. (2017). Effects of inclusion contents on resilient modulus and damping ratio of unsaturated track-bed materials. *Canadian Geotechnical Journal, 54*(12), 1672-1681.

Wang, H., Cui, Y., Lamas-Lopez, F., Dupla, J. C., Canou, J., Calon, N., . . . Chen, R. (2018). Permanent deformation of track-bed materials at various inclusion contents under large number of loading cycles. *Journal of Geotechnical and Geoenvironmental Engineering, 144*(8), 04018044.

Wang, L., Wu, C., Tang, L., Zhang, W., Lacasse, S., Liu, H., & Gao, L. (2020). Efficient reliability analysis of earth dam slope stability using extreme gradient boosting method. *Acta Geotechnica, 15*(11), 3135-3150. doi:10.1007/s11440-020-00962-4

Wang, L., Guo, M., Sawada, K., Lin, J., & Zhang, J. (2016). A comparative study of landslide susceptibility maps using logistic regression, frequency ratio, decision tree, weights of evidence and artificial neural network. *Geosciences Journal, 20*(1), 117-136.

Wen, R., Guo, Z., Zhao, T., Ma, X., Wang, Q., & Wu, Z. (2017). *Neuroevolution of augmenting topologies based musculor-skeletal arm neurocontroller.* Paper presented at the 2017 IEEE International Instrumentation and Measurement Technology Conference (I2MTC).

Werkmeister, S. (2003). Permanent deformation behavior of unbound granular materials.

University of Technology, Dresden.

Werkmeister, S. (2004). Permanent deformation behaviour of unbound granular materials in pavement constructions.

Werkmeister, S., Dawson, A., & Wellner, F. (2004). Pavement design model for unbound granular materials. *Journal of Transportation Engineering, 130*(5), 665-674.

Werkmeister, S., Dawson, A. R., & Wellner, F. (2001). Permanent deformation behavior of granular materials and the shakedown concept. *Transportation Research Record, 1757*(1), 75-81.

Wickland, B. E., & Wilson, G. W. (2005). Self-weight consolidation of mixtures of mine waste rock and tailings. *Canadian Geotechnical Journal, 42*(2), 327-339. doi:DOI 10.1139/t04-108

Wickland, B. E., Wilson, G. W., Wijewickreme, D., & Klein, B. (2006). Design and evaluation of mixtures of mine waste rock and tailings. *Canadian Geotechnical Journal, 43*(9), 928-945. doi:10.1139/T06-058

Williams, D. J., & Walker, L. K. (1983). Laboratory and field strength of mine waste rock.

Wilson, G. W., Miskolczi, J., Dagenais, A.-M., Levesque, I., Smith, Q., Lanteigne, L., . . . Landriault, D. (2006). *The application of blended waste rock and tailings for cover systems in mine waste management.* Paper presented at the Proceedings of the 7th International Conference on Acid Rock Drainage (ICARD). American Society of Mining and Reclamation (ASMR), Lexington, USA.

Witczak, M. W. (2004). *Laboratory determination of resilient modulus for flexible pavement design*: Transportation Research Board.

Witczak, M. W., & Uzan, J. (1988). The universal airport pavement design system. *Report I of V: granular material characterization, Department of Civil Engineering, University of Maryland, College Park, MD*.

Wolff, H., & Visser, A. (1994). *Incorporating elasto-plasticity in granular layer pavement design.* Paper presented at the Proceedings of the Institution of Civil Engineers-Transport.

Woodrooffe, J. H. (2010). *Review of Canadian experience with the regulation of large commercial motor vehicles* (Vol. 671): Transportation Research Board.

Xiao, Y., Liu, H., Chen, Y., & Jiang, J. (2014). Strength and deformation of rockfill material based on large-scale triaxial compression tests. I: Influences of density and pressure. *Journal of Geotechnical and Geoenvironmental Engineering, 140*(12), 04014070.

Xiao, Y., & Tutumluer, E. (2017). Gradation and packing characteristics affecting stability of granular materials: aggregate imaging-based discrete element modeling approach. *International Journal of Geomechanics, 17*(3), 04016064.

Xiao, Y., Tutumluer, E., Qian, Y., & Siekmeier, J. A. (2012). Gradation effects influencing mechanical properties of aggregate base–granular subbase materials in Minnesota. *Transportation Research Record, 2267*(1), 14-26.

Xu, D., Liu, H., Rui, R., & Gao, Y. (2019). Cyclic and postcyclic simple shear behavior of binary sand-gravel mixtures with various gravel contents. *Soil Dynamics and Earthquake Engineering, 123*, 230-241.

Xu, D., Tang, J., Zou, Y., Rui, R., & Liu, H. (2019). Macro and micro investigation of gravel content on simple shear behavior of sand-gravel mixture. *Construction and Building Materials, 221*, 730-744. doi:10.1016/j.conbuildmat.2019.06.091

Xu, J., Chen, Y., Xie, T., Zhao, X., Xiong, B., & Chen, Z. (2019). Prediction of triaxial behavior of recycled aggregate concrete using multivariable regression and artificial neural network techniques. *Construction and Building Materials, 226*, 534-554. doi:10.1016/j.conbuildmat.2019.07.155

Xu, M., Watanachaturaporn, P., Varshney, P. K., & Arora, M. K. (2005). Decision tree regression

for soft classification of remote sensing data. *Remote Sensing of Environment, 97*(3), 322-336. doi:https://doi.org/10.1016/j.rse.2005.05.008

Xu, W., Xu, Q., & Hu, R. (2011). Study on the shear strength of soil–rock mixture by large scale direct shear test. *International Journal of Rock Mechanics and Mining Sciences, 48*(8), 1235-1247. doi:https://doi.org/10.1016/j.ijrmms.2011.09.018

Xue, Y., Bai, C., Qiu, D., Kong, F., & Li, Z. (2020). Predicting rockburst with database using particle swarm optimization and extreme learning machine. *Tunnelling and Underground Space Technology, 98*, 103287. doi:https://doi.org/10.1016/j.tust.2020.103287

Yang, J., & Luo, X. D. (2018). The critical state friction angle of granular materials: does it depend on grading? *Acta Geotechnica, 13*(3), 535-547. doi:10.1007/s11440-017-0581-x

Yang, P. (2016). *Investigation of the geomechanical behavior of mine backfill and its interaction with rock walls and barricades.* Ecole Polytechnique, Montreal (Canada).

Yang, P., Li, L., Aubertin, M., Brochu-Baekelmans, M., & Ouellet, S. (2017). Stability analyses of waste rock barricades designed to retain paste backfill. *International Journal of Geomechanics, 17*(3), 04016079.

Yang, X., & Han, J. (2013). Analytical Model for Resilient Modulus and Permanent Deformation of Geosynthetic-Reinforced Unbound Granular Material. *Journal of Geotechnical and Geoenvironmental Engineering, 139*(9), 1443-1453. doi:doi:10.1061/(ASCE)GT.1943-5606.0000879

Yao, H., Jia, S., Gan, W., Zhang, Z., & Lu, K. (2016). Properties of Crushed Red-Bed Soft Rock Mixtures Used in Subgrade. *Advances in Materials Science and Engineering, 2016*.

Yazdanjou, V., Salimi, N., & Hamidi, A. (2008). *Effect of gravel content on the shear behavior of sandy soils.* Paper presented at the Proc. of 4th National Congress on Civil Engrg., Tehran University, Iran.

Yi, C., & Huang, J. (2017). Semismooth Newton coordinate descent algorithm for elastic-net penalized Huber loss regression and quantile regression. *Journal of Computational and Graphical Statistics, 26*(3), 547-557.

Yilmazkaya, E., Dagdelenler, G., Ozcelik, Y., & Sonmez, H. (2018). Prediction of mono-wire cutting machine performance parameters using artificial neural network and regression models. *Engineering Geology, 239*, 96-108. doi:https://doi.org/10.1016/j.enggeo.2018.03.009

Yin, Z.-Y., Hicher, P.-Y., Dano, C., & Jin, Y.-F. (2017). Modeling mechanical behavior of very coarse granular materials. *Journal of Engineering Mechanics, 143*(1), C4016006.

Yoder, E. J., & Witczak, M. W. (1991). *Principles of pavement design*: John Wiley & Sons.

Yu, T. (1989). Some factors relating to the stability of consolidated rockfill at Kidd Creek. *Innovations in Mining Backfill Technology*, 279-286.

Yuksel, M. E. (2018). Agent-based evacuation modeling with multiple exits using NeuroEvolution of Augmenting Topologies. *Advanced Engineering Informatics, 35*, 30-55. doi:https://doi.org/10.1016/j.aei.2017.11.003

Zhang, J., Peng, J., Zhang, A., & Li, J. (2020). Prediction of permanent deformation for subgrade soils under traffic loading in southern China. *International Journal of Pavement Engineering*, 1-10.

Zhang, J., Wang, X., Yin, Z., & Liang, Z. (2020). DEM modeling of large-scale triaxial test of rock clasts considering realistic particle shapes and flexible membrane boundary. *Engineering Geology, 279*, 105871. doi:https://doi.org/10.1016/j.enggeo.2020.105871

Zhang, W., Ching, J., Goh, A. T. C., & Leung, A. Y. F. (2021). Big data and machine learning in geoscience and geoengineering: Introduction. *Geoscience Frontiers, 12*(1), 327-329. doi:https://doi.org/10.1016/j.gsf.2020.05.006

Zhang, W., & Goh, A. T. C. (2013). Multivariate adaptive regression splines for analysis of geotechnical engineering systems. *Computers and Geotechnics, 48*, 82-95.

Zhang, X., Zhao, C., & Zhai, W. (2019). Importance of load frequency in applying cyclic loads to investigate ballast deformation under high-speed train loads. *Soil Dynamics and Earthquake Engineering, 120*, 28-38. doi:https://doi.org/10.1016/j.soildyn.2019.01.023

Zheng, C. (2020). A new principle for tuning-free Huber regression. *Statistica Sinica*.

Zheng, H., Liu, D., & Li, C. (2005). Slope stability analysis based on elasto-plastic finite element method. *International Journal for Numerical Methods in Engineering, 64*(14), 1871-1888.

Zhou, F., Fernando, E., & Scullion, T. (2010). *Development, calibration, and validation of performance prediction models for the Texas ME flexible pavement design system* (No. FHWA/TX-10/0-5798-2).

Zou, W.-l., Ding, L.-q., Han, Z., & Wang, X.-q. (2020). Effects of freeze-thaw cycles on the moisture sensitivity of a compacted clay. *Engineering Geology, 278*, 105832. doi:10.1016/j.enggeo.2020.105832

Zumrawi, M. M. (2014). *Prediction of in-situ CBR of subgrade cohesive soils from dynamic cone penetrometer and soil properties*. Paper presented at the 2014 APCBEES Shanghai Conferences Proceeding, Shanghai.

APPENDIX A X-RAY DIFFRACTION TESTS RESULTS

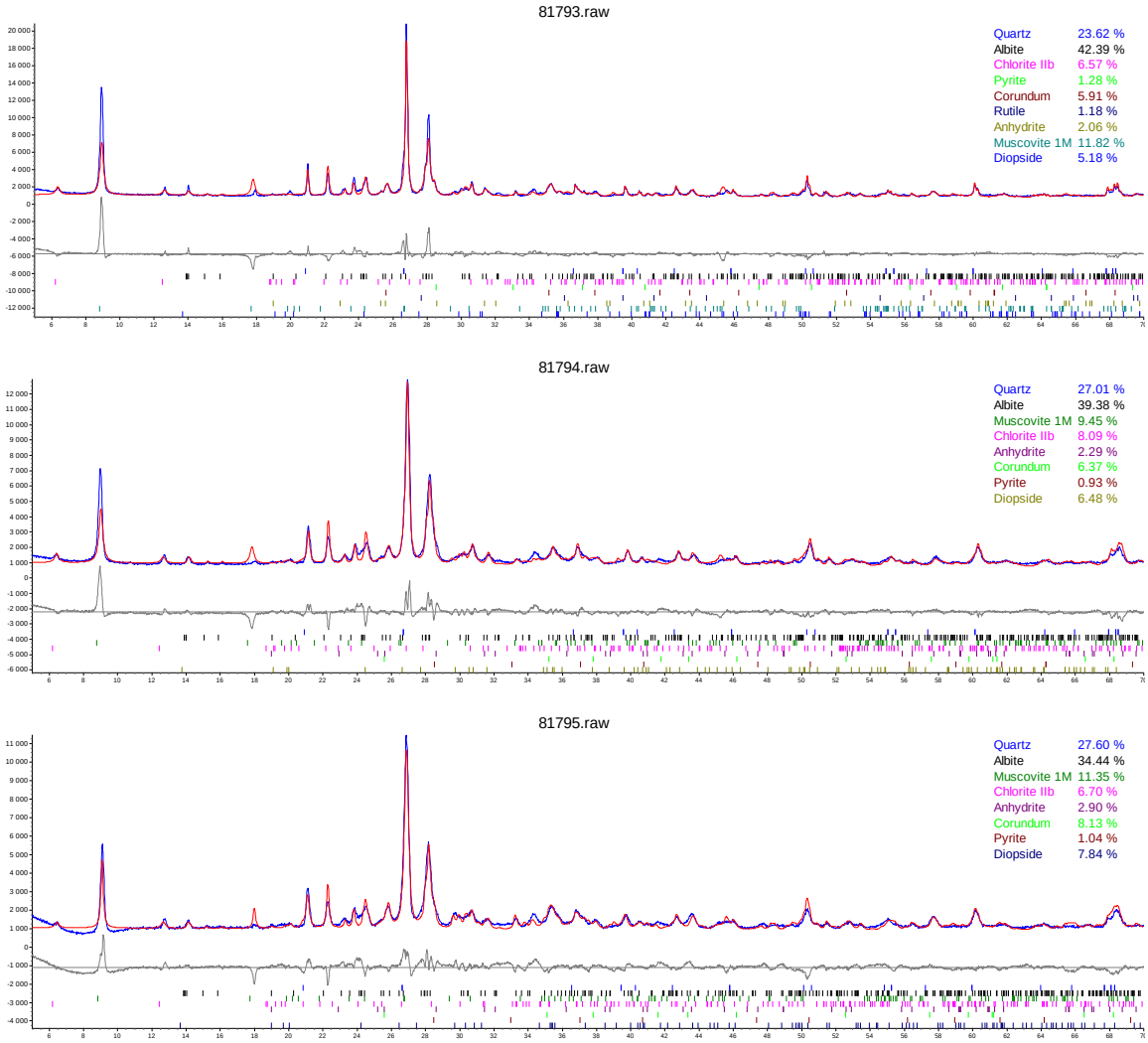

Figure A.1: X-ray diffraction test results for three samples of crushed waste rocks.

APPENDIX B STRESS-STRAIN CURVES FOR CRUSHED WASTE ROCKS WITH DIFFERENT GRADATIONS

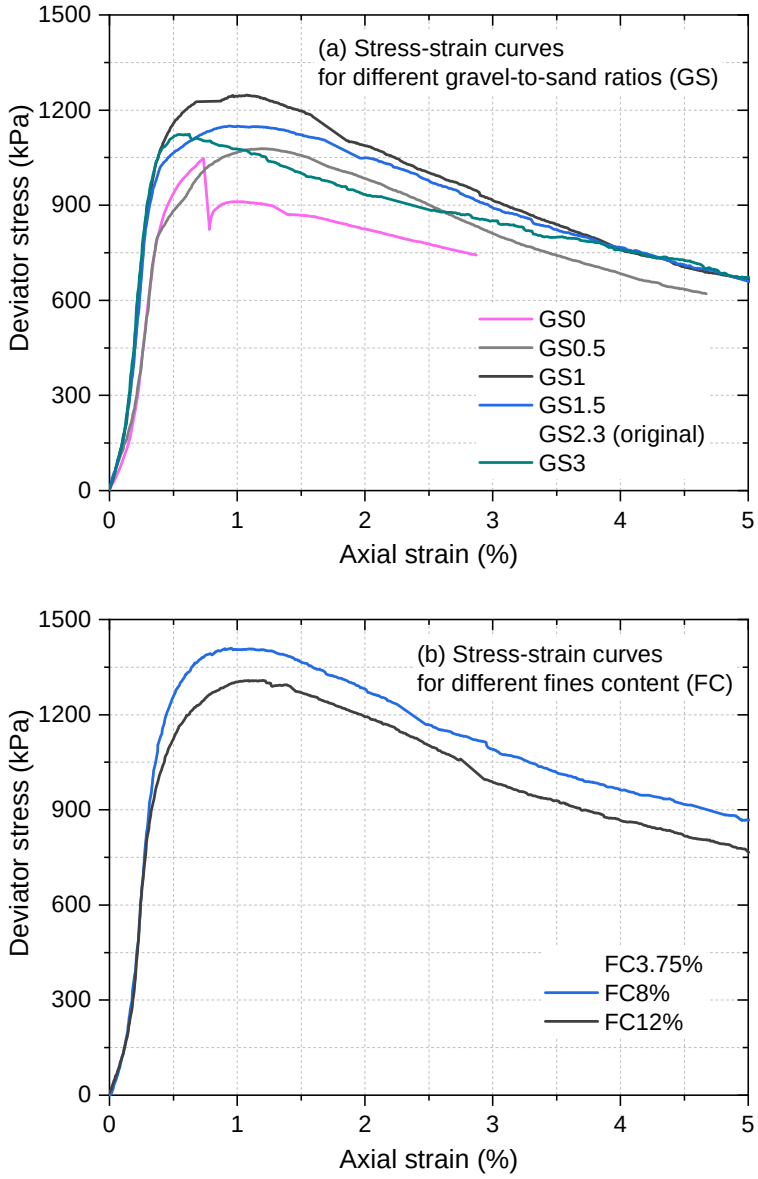

Figure B.1: The stress-strain curves from monotonic triaxial tests on crushed waste rocks with (a) different gravel-to-sand ratios GS and (b) fines contents FC.

APPENDIX C STRESS-STRAIN CURVES FOR CRUSHED WASTE ROCKS SUBJECTED TO FREEZE-THAW CYCLES

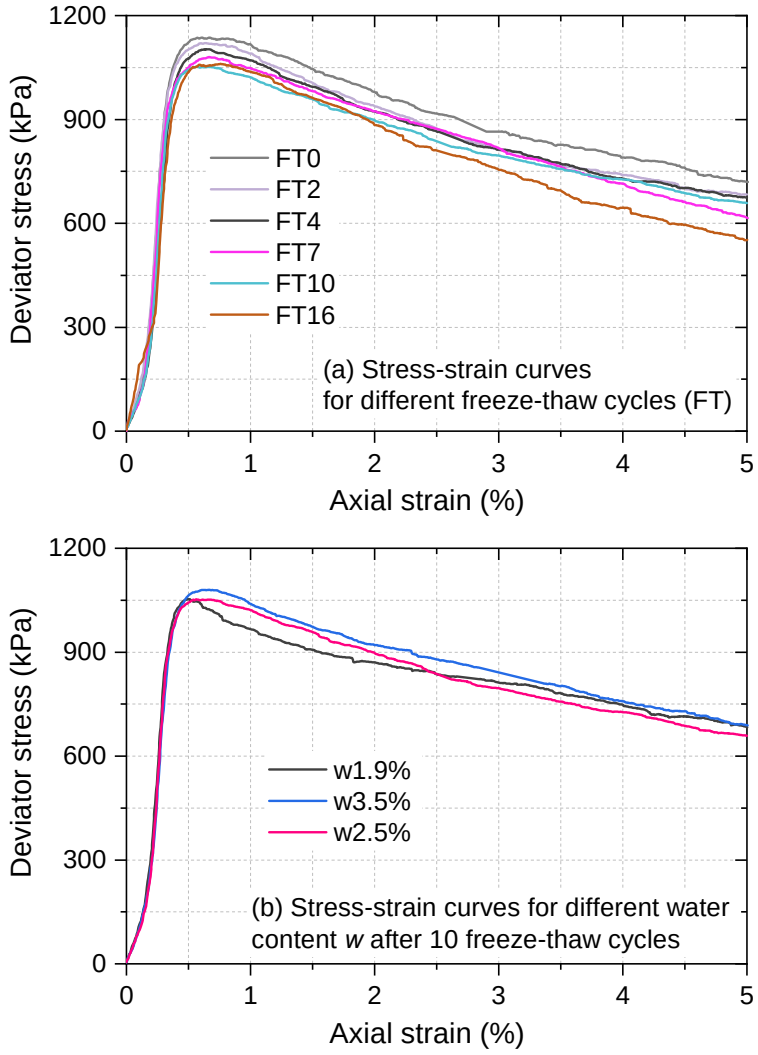

Figure C.1: The stress-strain curves from monotonic triaxial tests on crushed waste rocks (a) subjected to different freeze-thaw cycles FT and (b) with different final water content *w* after 10 freeze-thaw cycles.

APPENDIX D QUANTIFICATION OF GRADATION EFFECT USING THE CONCEPT OF STRUCTURAL MODEL

This section presents the quantification of the gradation effect on the mechanical properties (i.e., resilient modulus and shear strength) of crushed waste rocks using the concept of structural model. The gravel particles have a high stiffness and serve as a structural framework of crushed waste rocks when they have a high-volume fraction. Sand and fines contents are relatively compressible and occupy the voids among gravel particles, and they serve as an in-fill matrix. There is a transition in the structural state from the state of framework supported (dominated by gravel particles) to the state of matrix supported (dominated by sand and fines) with the increase of sand and fines contents. In this study, c_m model proposed by Li and Wong (2016) was applied to quantify the structural states. However, c_m model was developed for soft mdudrocks (a mixture of nonclay minerals and clay-water composites) that were significantly different to crushed waste rocks in terms of mineralogy and mechanical characteristics. The volume fraction of clay-water composites f_{cw} in c_m model was therefore replaced by the volume fraction of sand and fines contents f_{s+f}:

$$c_m = \frac{\tanh\left(\frac{f_{s+f}-A}{B}\right)+1}{2} \qquad \text{D.1}$$

Where *A* and *B* are two parameters of the c_m model, which values are affected by particle size and which can therefore change to accommodate for different geomaterials (Li and Wong 2016). Value of c_m tends to zero for low values of f_{s+f} for the state of framework supported, and c_m tends to one for high values of f_{s+f} for the state of matrix supported. The volume of sand and fines contents f_{s+f} is given by:

$$f_{s+f} = \frac{V_{s+f}}{V} \qquad \text{D.2}$$

Where V_{s+f}: the volume of sand and fines composites, -; and V: the total volume of a sample, -.

The c_m model indicates how actively sand and fines serve as the supporting matrix in crushed waste rocks. By considering the structural state, a geomechanical or physical property of crushed waste rocks M can be estimated by applying the mixture theory as follows (Li and Wong 2016):

$$M=M_{s+f}c_m+M_g(1-c_m) \quad \text{D.3}$$

Where M_{s+f}: the property when sand and fines are dominant; and M_g: the property when gravel contents are dominant.

A summary resilient modulus (SM_R) was computed at a bulk stress of 208 kPa (103 kPa of deviator stress and 35 kPa of confining pressure) based on test results, and following the guidelines provided in NCHRP 1-28A Section 10.3.3.9. The gradation effect on resilient modulus was evaluated by comparing the SM_R of samples with different sand and fines content. The summary resilient modulus and shear strength (i.e., peak deviator stress at 50 kPa of confining pressure) were fitted using equation D.1 and D.3 (Figure D.1). The c_m model parameters A and B were calibrated ($A = 0.712$ and $B = 0.018$). Model showed similar trend between resilient modulus and shear strength and the volume of sand and fines f_{s+f} that they decreased nonlinear with the increase of f_{s+f}. An increase or decrease of f_{s+f} showed very limited impact on the mechanical properties of crushed waste rocks when f_{s+f} was higher than 0.8 or lower than 0.6. Therefore, the mechanical properties of crushed waste rocks were dominated by sand and fines when $f_{s+f}>0.8$, while it was dominated by gravel particles when $f_{s+f}<0.6$. The fitting performance of c_m model for shear strength was, however, relatively low ($R^2 < 0.5$), indicating that the shear strength of crushed waste rocks showed no significant transition of structural states, which could result from the angular particles and the wide range of particle size distribution. In contrast, the soft mudrocks used for c_m model in previous study (Li and Wong 2016) showed a very large difference of particle size between nonclay mineral particles and clay particles. The structural states of crushed waste rocks

should be evaluated more accurately based on additional laboratory test results in the future study.

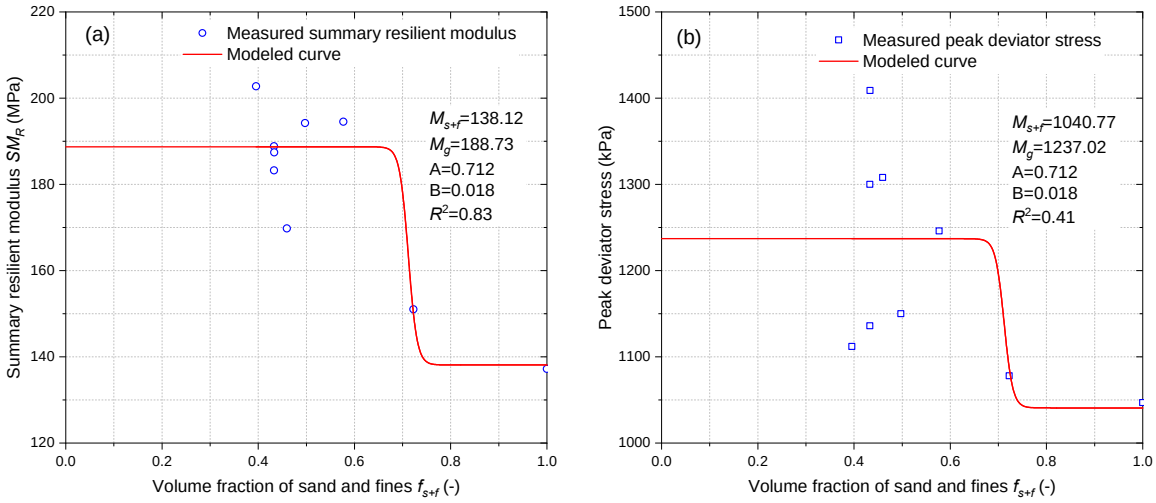

Figure D.1: Measured and modeled (c_m model) results of (a) summary resilient modulus SM_R and (b) shear strength (peak deviator stress at 50 kPa of confining pressure) of crushed waste rocks with different volumes fraction of sand and fines composites f_{s+f}. The model results and calibrated parameters M_{s+f}, M_g, A, and B are also shown in the figure.